JOURNAL OF Materials CHEMISTRY

A structural study of 2-amino-5-nitropyridine and 2-amino-3-nitropyridine: intermolecular forces and polymorphism

Christer B. Aakeröy,[a] Alicia M. Beatty,[a] Mark Nieuwenhuyzen[b] and Min Zou[a]

[a]*Department of Chemistry, Kansas State University, Manhattan, Kansas 66506, USA*
[b]*School of Chemistry, The Queen's University of Belfast, Belfast, Northern Ireland BT9 5AG*

The crystal structures of four compounds from a family of commonly used molecular building blocks of nonlinear optical materials, aminonitropyridines, have been determined. The structures of 2-amino-5-nitropyridine **1**, 2-amino-5-nitropyridine monohydrate **2**, and of two new polymorphs of 2-amino-3-nitropyridine **3,4**, are all stabilised by a combination of hydrogen bonds (including C—H···X interactions) and dispersive and electrostatic interlayer interactions. The balance between these intermolecular forces, and the way in which they influence the packing of these materials, are discussed.

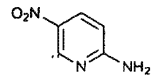
The principles that govern covalent synthesis are generally well understood, and thus an impressive array of molecules with specific molecular properties have been synthesized over the years.[1] From a materials perspective, however, unless individual molecules can be made to 'cooperate' through a favourable spatial arrangement within a 3D crystal, the molecular properties may not express themselves fully in the bulk material. In such cases, the efforts that go into the design and synthesis of the target molecule may be largely unrewarded. Unfortunately, the problems of controlling and predicting structures of molecular and ionic solids are still a long way from being solved. Such issues, which are addressed within the context of crystal engineering,[2] require considerable structural information coupled with a careful analysis of the balance between, and effects of, intermolecular forces.

One area where crystal engineering has an important role to play is in the continuous search for new nonlinear optical materials. A common and often productive route to such materials has been to utilise molecules with electron donating and accepting moieties attached to a conjugated system. The optical response of an SHG-active material is influenced both by the chemical purity and structural composition of the bulk sample. Consequently, the design and preparation of new NLO-materials can therefore be complicated by polymorphism (different crystalline forms of compounds with identical chemical composition). The presence of polymorphic structures is also of crucial importance to the pharmaceutical industry and in areas associated with specialty chemicals, since polymorphs can have significantly different physical properties. Despite this, the possibilities that new materials may appear in several polymorphic forms are often overlooked; a visual inspection of the sample does not always provide conclusive information about the bulk sample, since different polymorphs can display the same crystal habit.[3] However, polymorphic systems can provide excellent opportunities to study a chemical entity in more than one crystalline environment. By comparing thermodynamic quantities and trends displayed by calculated lattice energies for a series of solids, energy differences between molecular conformations can be estimated.[4]

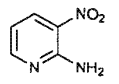
Model systems and objectives

As stated earlier, aromatic amino-nitro systems are potentially useful NLO materials and, typically, cations derived from such molecules have been used within hydrogen-bonded organic anionic networks, or as counterions in organic/inorganic salts.[5] Although several crystal structures of related molecules, *e.g.* 3-methyl-4-nitropyridine *N*-oxide[6] and 4-nitropyridine *N*-oxide,[7] have been published, few structure determinations have been reported on molecular solids containing the amino-nitro 'push–pull' system. In fact, a search of the Cambridge Structural Database[8,9] identified only four such structures,[10] one of them being 2-amino-3-nitropyridine.[11]

In order to study crystal packing and competition/complementarity between different hydrogen-bond interactions in amino-nitro compounds we have initiated a systematic structural study, starting with 2-amino-5-nitropyridine and 2-amino-3-nitropyridine. We have attempted to isolate polymorphic forms of these compounds by recrystallizing each sample from a variety of solvents and under a variety of conditions.[12] To the best of our knowledge, there have been no previous observations of polymorphs of 2-amino-3-nitropyridine.[13] In this paper we report the X-ray single-crystal determination of four structures; 2-amino-5-nitropyridine **1**, 2-amino-5-nitropyridine monohydrate **2**, and two new polymorphs of 2-amino-3-nitropyridine **3** and **4**.[14]



1
2 (monohydrate)



3,4 (polymorphs)

Results

Preparations of **1**–**4** are described in detail in the Experimental Section, and the relevant X-ray crystallographic information is presented in Table 1. Numbering schemes, molecular geometries and thermal ellipsoids of **1**–**4** are presented in Fig. 1(*a*)–(*d*). The structure determinations of **1**–**4** revealed that all four compounds crystallise in centrosymmetric space groups, with intramolecular bond lengths and angles of unremarkable values.

The crystal structure of **1** exhibits a flat, layered arrangement with five unique hydrogen-bond interactions within the layer, Table 2. In fact, every possible donor or acceptor is involved in a hydrogen bond (three of these interactions involve —CH moieties as donor functionalities), Fig. 2. Furthermore, since there are two more hydrogen-bond donors than acceptors, each oxygen atom of the nitro group is involved in two hydrogen bonds simultaneously. Somewhat surprisingly, the commonly observed $R_2^2(8)$ motif in 2-aminopyridine moieties involving symmetry related N—H···N hydrogen bonds, is absent in this structure.[15] Nevertheless, the hydrogen bonds in

UM00012820
NOVARTIS EXHIBIT 1017
Novartis v. Regents, IPR2023-01346
Page 1566 of 4460

Table 1 Data collection and refinement for 1–4

crystal data	1	2	3	4
empirical formula	$C_5H_5N_3O_2$	$C_5H_7N_3O_3$	$C_5H_5N_3O_2$	$C_5H_5N_3O_2$
M_w	139.12	157.14	139.12	139.12
crystal size/mm	0.74 × 0.33 × 0.09	0.58 × 0.31 × 0.26	0.92 × 0.38 × 0.06	0.64 × 0.44 × 0.12
crystal system	orthorhombic	monoclinic	monoclinic	monoclinic
space group	*Pnma*	*C2/c*	$P2_1/c$	$P2_1/n$
a/Å	15.357(3)	16.150(4)	4.917(1)	3.737(2)
b/Å	6.080(2)	11.135(2)	6.940(2)	7.445(2)
c/Å	6.099(2)	7.301(1)	17.507(3)	20.974(6)
β (°)		99.02(2)	95.63(2)	90.52(3)
V/Å^3	569.4(4)	1296.7(4)	594.5(2)	583.4(4)
Z	4	8	4	4
D_c/g cm^{-3}	1.623	1.610	1.554	1.584
F(000)	288	656	288	288
μ(Mo-Kα)/mm^{-1}	0.130	0.135	0.124	0.126
T/K	123	123	153	173
ω scans; *θ* range (°)	2.65–25.00	2.23–24.99	2.34–25.00	1.94–24.99
range *h*	−18 to 1	−1 to 19	−5 to 5	−1 to 4
range *k*	−7 to 7	−1 to 13	−5 to 8	−1 to 8
range *l*	−7 to 7	−8 to 8	−20 to 20	−24 to 24
refins. collected	2041	1425	1692	1772
unique/obs. refins.	552/406	1146/906	1051/568	1032/724
observed data : parameter ratio	6.5	8.2	6.2	7.9
refinement	full-matrix least-squares	full-matrix least-squares	full-matrix least-squares	full-matrix least-squares
R/R_w^2 (obs. data)	0.0399/0.0928	0.0554/0.1539	0.0575/0.0987	0.0716/0.1848
R/R_w^2 (all data)	0.0656/0.1061	0.0697/0.1689	0.1352/0.1256	0.1026/0.2052
$\Delta\rho_{max/min}$/e Å^{-3}	0.278/−0.315	0.305/−0.412	0.172/−0.205	0.249/−0.284
S	1.136	1.082	1.030	1.170

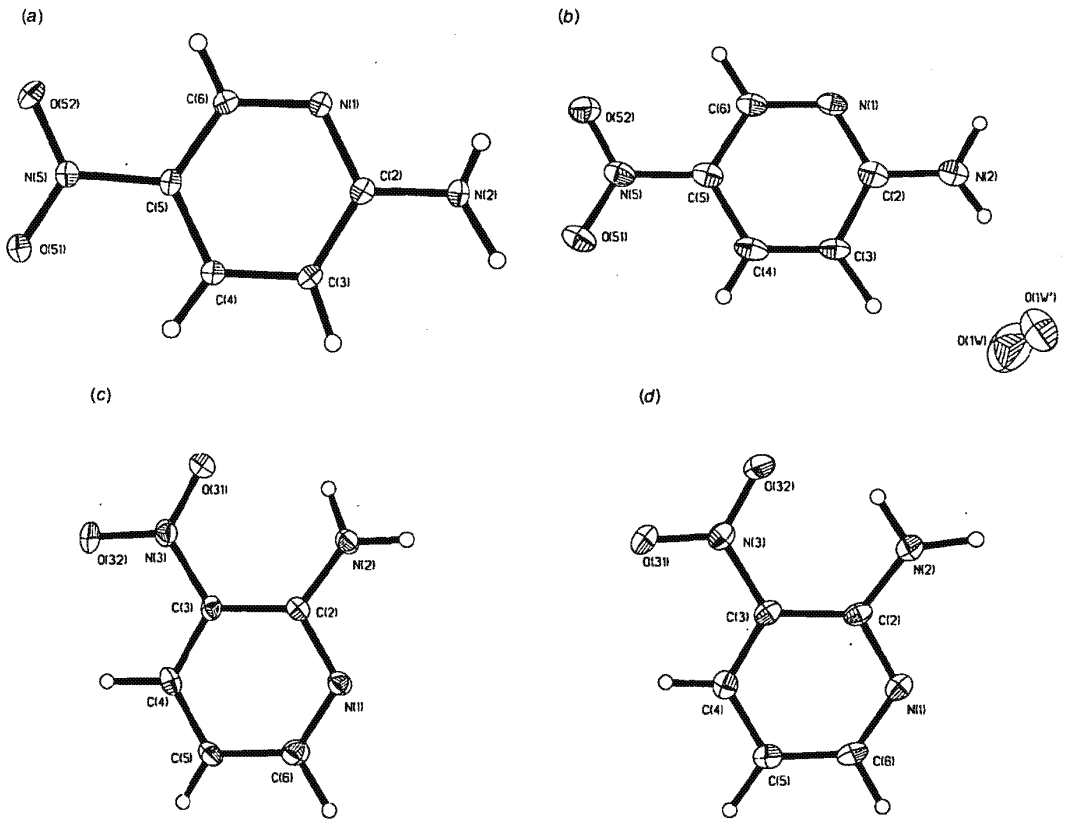


Fig. 1 Molecular geometry and numbering schemes for (*a*) 1, (*b*) 2, (*c*) 3 and (*d*) 4. Thermal ellipsoids at 30% probability.

UM00012821
NOVARTIS EXHIBIT 1017
Novartis v. Regents, IPR2023-01346
Page 1567 of 4460

Table 2 Geometry of the hydrogen bonds in 1[a]

D—H···A	r(H···A)/Å	r(D···A)/Å	∠(D—H···A) (°)
N(2)—H(21)···O(52)'	2.454(4)	3.035(4)	132.42(9)
N(2)—H(22)···O(51)"	1.906(2)	2.982(3)	177.8(1)
C(3)—H(3)···O(52)"	2.577(4)	3.497(4)	157.59(8)
C(6)—H(6)···O(51)""	2.639(4)	3.463(4)	151.36(8)
C(4)—H(4)···N(1)'''	2.426(4)	3.346(4)	157.0(1)

[a]Symmetry code: (') $-1/2+x, y, -z+1/2$; (") $-1/2+x, y, -z+11/2$; (''') $x, y, z+1$; ('''') $x, y, z-1$.

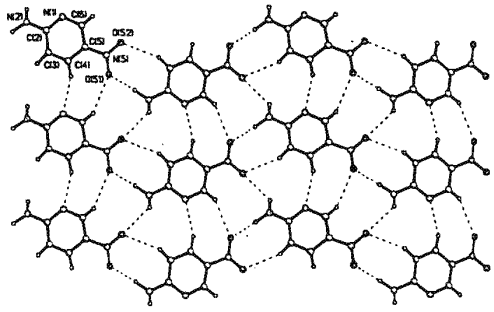


Fig. 2 Hydrogen-bond interactions within layers in 1

1 (including C—H···A, where A is an acceptor), are working in concert to produce a lamellar 2D structure. The interlayer separation is exceptionally short, approximately 3.035 Å (as a comparison, the interlayer separation in graphite is 3.35 Å). A recent theoretical study[16] of the intermolecular forces present in these crystal structures shows that this intralayer arrangement can be understood in terms of electrostatics and simple packing effects. Intermolecular interaction energies were calculated using ORIENT 3.2[17] and the distributed multipoles were obtained from the HF/6-31G* wave function of the single molecules using CADPAC.[18] The experimental interplanar distance in 1 is reproduced quite well (2.98 *vs.* 3.04 Å exp.), and the change in electrostatic energy as a function of interplanar distance is small, indicating that the separation results from a balance between repulsion and dispersion. Translational motion has a larger effect on the repulsive forces which means that the optimum packing is achieved when electrostatic forces are maximized, and when the layers are as close as possible (to maximize dispersion) without incurring a prohibitive repulsive energy penalty.[16] This balance can be achieved if the aromatic rings in one layer fit over nitrogen and oxygen atoms, which are smaller, in the neighbouring layer.

The water molecule in 2 is disordered and as a consequence, the 3D packing in this compound is rather more complex than in 1, and it is also influenced by several hydrogen bonds involving the water molecule, Table 3. However, even in the presence of one molecule of water, the 2-amino-5-nitropyridine molecules are arranged in a 2D network, Fig. 3, with three unique hydrogen bonds within each sheet (including two

Table 3 Geometry of the hydrogen bonds in 2[a]

D—H···A	r(H···A)/Å	r(D···A/Å	∠(D—H···A) (°)
N(2)—H(21)···N(1)'	2.087(3)	3.037(3)	171.50(8)
N(2)—H(22···O(1W)	2.203(9)	3.010(9)	153.8(2)
N(2)—H(22)···O(1W)'	2.20(2)	2.96(1)	145.6(6)
C(3)—H(3)···O(1W)	2.340(6)	3.266(6)	140.0(2)
C(3)—H(3)···O(1W)"	2.34(1)	3.37(1)	155.2(4)
C(4)—H(4)···O(52)"'	2.458(3)	3.208(3)	143.24(8)
C(6)—H(6)···O(51)""	2.618(3)	3.477(3)	147.05(7)

[a]Symmetry code: (') $-x, -y, -z$; (") $-x, 1-y, -z$; (''') $1/2-x, 1/2+y, -1/2-z$; ('''') $1/2-x, y-1/2, -1/2-z$.

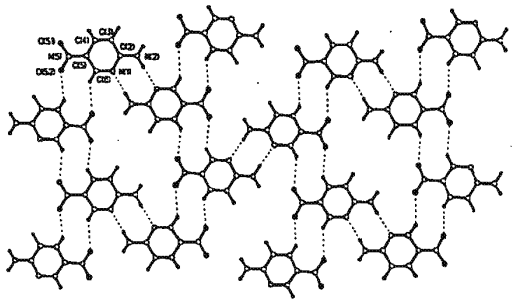


Fig. 3 Hydrogen-bond interactions within layers in 2. Water molecules not shown for clarity.

hydrogen bonds involving —CH donor functionalities), Table 3. These hydrogen bonds generate two different 'dimeric' interactions: an $R_2^2(8)$ motif *via* symmetry-related N—H···N interactions and two $R_2^2(10)$ motifs involving C—H···O hydrogen bonds. The water molecules are located within the 'holes' in the organic layer, and there is virtually no overlap between aromatic moieties in adjacent layers, indicating the absence of significant attractive π–π interactions.

An X-ray powder diffractogram was recorded for a bulk sample of 2-amino-5-nitropyridine recrystallized from water and compared with powder patterns simulated from single-crystal data for the two structures 1 and 2. All significant diffraction peaks present in the experimental pattern could be accounted for by combining the two simulated patterns. This, however, does not rule out the possibility of obtaining polymorphs of 2-amino-5-nitropyridine or its hydrated analogue through sublimation or recrystallization from other solvents or under different conditions.

Similarly, an experimental X-ray powder pattern of a bulk sample of 2-amino-3-nitropyridine was recorded and compared with the simulated pattern based on single crystal data for the previously reported crystal structure,[11] Fig. 4. The experimental pattern does show the presence of Form I, but there is also a number of peaks that are unaccounted for.

Since the chemical purity of the sample had been established by solution ^{1}H NMR, the additional peaks in the experimental powder pattern were thought to belong to a hitherto unknown polymorph of 2-amino-3-nitropyridine, and several recrystallization experiments were subsequently carried out. Upon recrystallisation from acetone, only the previously reported polymorph, Form I, was obtained (as determined by powder X-ray diffraction), but when the sample was recrystallised from ethanol, the recorded powder pattern displayed no similarities with the pattern expected for Form I, and thus indicated the presence of at least one new polymorph. We were able to isolate diamond-shaped crystals of 2-amino-3-nitropyridine

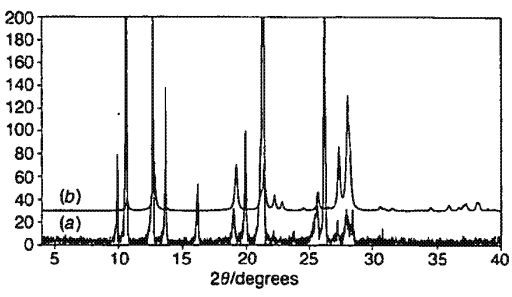


Fig. 4 (*a*) The experimental X-ray powder diffraction pattern of bulk 2-amino-3-nitropyridine and (*b*) the diffraction pattern simulated from the single-crystal data of Form I (ref. 11) of 2-amino-3-nitropyridine

UM00012822
NOVARTIS EXHIBIT 1017
Novartis v. Regents, IPR2023-01346
Page 1568 of 4460

through slow recrystallization from ethanol and the subsequent structure determination confirmed the existence of a new polymorph, 3 (Form II) of 2-amino-3-nitropyridine.

The molecule itself is planar with the two substituents coplanar with the aromatic ring. This is likely to be a result of the intramolecular N—H···O hydrogen bond that exists between the two functionalities, thereby restricting their torsional flexibility, Table 4. The structure contains infinite, staggered ribbons held together by two unique hydrogen bonds, N—H···N and N—H···O, each of which gives rise to ring-like dimeric interactions, $R_2^2(8)$ and $R_2^2(12)$, respectively, Fig. 5. Neighbouring ribbons are tilted, *ca.* 45° with respect to each other. As a comparison, Form I of 2-amino-3-nitropyridine also contains ribbon-like motifs, held together by two unique hydrogen bonds, but in this case the ribbon is generated *via* C—H···O, $R_2^2(10)$, and N—H···N, $R_2^2(8)$ dimeric interactions, resulting in a linear topology, Fig. 6.[11] Preliminary thermal microscopy data indicate that Form I undergoes a phase transformation at 120 °C. The melting point of the modification that appears after the phase transition is 166 °C, and these phases are probably enantiotropically related.[19]

We then made a serendipitous discovery of a third polymorph of 2-amino-3-nitropyridine during an attempt to cocrystallize 2-amino-3-nitroypyridine with maleic acid. We recovered pale yellow cuboid crystals which were suitable for X-ray single-crystal diffraction. The experiment revealed another monoclinic polymorph of 2-amino-3-nitropyridine, Form III. The structure is very similar to that observed for Form II and, indeed, all hydrogen-bond interactions show the same connectivity, Table 5, with identical graph-sets. The difference between the two polymorphs is most easily observed by comparing the topology of the infinite 1D ribbons in the two forms. Whereas the ribbon is flat in Form II, Fig. 7(*a*), it has a distinctive 'step' in Form III, Fig. 7(*b*). In all three polymorphs, the molecule is planar with an intramolecular N—H···O hydrogen bond between amino-nitro moieties.

Table 4 Geometry of the hydrogen bonds in 3[a]

D—H···A	r(H···A)/Å	r(D···A/Å	∠(D—H···A) (°)
N(2)—H(21)···N(1)'	2.071(5)	2.972(4)	166.5(4)
N(2)—H(22)···O(31)"	2.198(4)	3.044(4)	147.6(1)
N(2)—H(22)···O(31)	2.087(4)	2.663(4)	117.5(1)
C(4)—H(4)···O(32)"'	2.413(4)	3.177(4)	129.4(1)

Symmetry code: (') $2-x, 1-y, 2-z$; (") $1-x,-y, 2-z$; ("') $-x, 1/2+y, 11/2-z$; ("") $1+x, 1+y, z$.

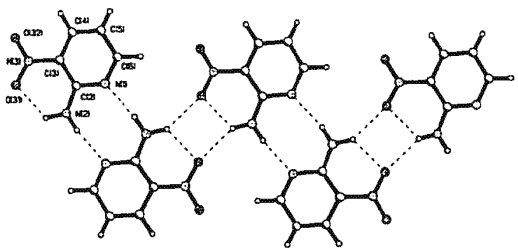


Fig. 5 Hydrogen-bonded molecular ribbon in 3

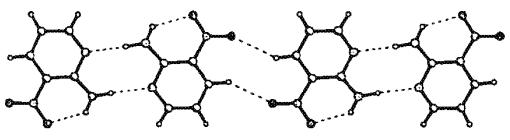


Fig. 6 Molecular ribbon in the first reported polymorph of 2-amino-3-nitropyridine (ref. 11)

Table 5 Geometry of the hydrogen bonds in 4[a]

D—H···A	r(H···A)/Å	r(D···A/Å	∠(D—H···A) (°)
N(2)—H(21)···O(32)	1.907(5)	2.672(5)	135.8(1)
N(2)—H(21)···O(32)"'	2.484(5)	3.055(5)	118.6(1)
N(1)—H(22)···N(2)'	1.970(5)	2.965(5)	156.9(1)
C(5)—H(5)···O(31)"	2.450(6)	3.278(6)	125.9(1)

Symmetry code: (') $-x+1, -y+2, -z+1$; (") $-x-1/2, y-1/2, -z+11/2$ ("') $-x, 1-y, 1-z$.

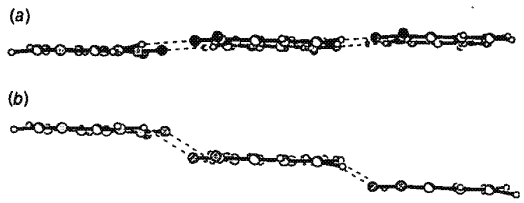


Fig. 7 Edge-on view of the molecular ribbons in (*a*) 3 and (*b*) 4

Discussion

The fact that all four crystal structures presented here are centrosymmetric obviously means that these aromatic amino-nitro compounds will not display second harmonic generation. It is tempting to conclude that these molecules crystallise in centrosymmetric structures simply to accommodate an antiparallel alignment of neighbouring dipoles, which in turn translates into an overall symmetric space group for the resulting 3D solid. However, such explanations have been contested based upon studies that have failed to find a correlation between high molecular dipole moments and centrosymmetric structures.[10] It is clear that the precise nature of the effects of a high molecular dipole moment upon the resulting crystal structure has yet to be fully understood, especially when stronger intermolecular forces, *e.g.* hydrogen bonding, are present.

From a practical point of view, it is important to note that there are at least three polymorphs of 2-amino-3-nitropyridine and a hydrated and non-hydrated structure of 2-amino-5-nitropyridine. Is it therefore possible to obtain non-centrosymmetric structures of these compounds by varying some of the experimental conditions? In the case of 2-amino-3-nitropyridine this would seem unlikely, as all three contain a dimeric N—H···N motif where participating molecules are related by an inversion centre. Such a dimer precludes packing in a non-centrosymmetric space group, and it would certainly seem that the odds are against obtaining an NLO-active polymorph of 2-amino-3-nitropyridine, based upon extant structural data. However, if the foundation for this dimer is destroyed, *i.e.* by replacing $-NH_2$ with $-N(Me)_2$ or $-NH(Me)$, then the chances of promoting a non-centrosymmetric packing arrangement should be enhanced, although there are several other ways in which neighbouring molecules or adjacent sheets can be aligned in an antiparallel manner. We are unaware of any reported structure determinations of such molecular solids, and are currently examining their crystal structures.

As for 2-amino-5-nitropyridine, there are no recurring 'dimeric' interactions between neighbouring molecules in 1 and 2, which may indicate a larger degree of flexibility in terms of the intermolecular motifs that are likely to appear in hitherto undiscovered polymorphs. Nevertheless, this molecule can also form the dimeric motif generated by symmetry related N—H···N hydrogen bonds which will preclude SHG-activity in the resulting material. However, it is possible to lower the symmetry and thereby increase the chances of obtaining non-centrosymmetric structures by cocrystallization reactions of molecules with complementary hydrogen-bond functionalities.

UM00012823
NOVARTIS EXHIBIT 1017
Novartis v. Regents, IPR2023-01346
Page 1569 of 4460

Experimental section

Preparation of single crystals of 1

2-Amino-5-nitropyridine was slowly recrystallized from ethanol to yield pale yellow, thin, plate-like crystals. Found: C, 43.0; H, 3.7; N, 30.1%. Calc. for $C_5H_5N_3O_2$: C, 43.18; H, 3.63; N, 30.20%. Mp 187–189 °C.

Preparation of single crystals of 2

2-Amino-5-nitropyridine was slowly recrystallized from water to yield yellow, needle-like crystals. Found: C, 38.4; H, 4.7; N, 26.5%. Calc. for $C_5H_7N_3O_3$: C, 38.22; H, 4.40; N, 26.75%. Mp 186–188 °C.

Preparation of single crystals of 3 (Form II)

2-Amino-3-nitropyridine was slowly recrystallized from ethanol to produce yellow, diamond-like crystals. Found: C, 43.1; H, 3.7; N, 30.0%. Calc. for $C_5H_5N_3O_2$: C, 43.18; H, 3.63; N, 30.20%. Mp 165–167 °C.

Preparation of single crystals of 4 (Form III)

2-Amino-3-nitropyridine was dissolved in water and added to an aqueous solution of maleic acid. Five drops of conc. HCl were then added, and the mixture was heated under reflux for 2 h. The solution was then left to cool to ambient temperature and left to stand. After two weeks crystals of two distinct morphologies appeared; yellow, elongated crystals (Form II, **3**, as determined by single-crystal X-ray diffraction), and irregular, cuboid yellow–brown crystals. Found: C, 42.9; H, 3.7; N, 29.9%. Calc. for $C_5H_5N_3O_2$: C, 43.18; H, 3.63; N, 30.20%. Mp 162–163 °C.

X-Ray crystallography

Crystal data were collected using a Siemens P4 four-circle diffractometer with graphite monochromated Mo-Kα radiation. Crystal stabilities were monitored by measuring standard reflections every 100 reflections, and there were no significant variations ($< \pm 1\%$). Cell parameters were obtained from 35 accurately centred reflections in the 2θ range 10–25°. ω scans were employed for data collection ($\theta/2\theta$ for **4**) and Lorentz and polarization corrections were applied. The structures were solved by direct methods and the non-hydrogen atoms were refined with anisotropic thermal parameters. Hydrogen-atom positions were located from difference Fourier maps and a riding model with fixed thermal parameters ($U_{ij} = 1.2U_{eq}$ for the atom to which they are bonded) was used for subsequent refinements. The function minimized was $\Sigma[\omega(|F_o|^2 - |F_c|^2)]$ with reflection weights $\omega^{-1} = [\sigma^2 |F_o|^2 + (g_1 P)^2 + (g_2 P)]$ where $P = [\max |F_p|^2 + 2|F_c|^2]/3$. The SHELXTL PC and SHELXL-93 packages were used for data reduction and structure solution and refinement.[21]

Hydrogen atoms could not be located for the disordered water molecules in **2**. Each water molecule is disordered over two sites and this disorder was refined to an occupancy of 80:20. It was also noted that crystals of **2** become opaque over a few days when removed from the solvent, which is presumably due to loss of water from the lattice.

Full crystallographic details, excluding structure factors, have been deposited at the Cambridge Crystallographic Data Centre (CCDC). See Information for Authors, *J. Mater. Chem.*, 1998, Issue 1. Any request to the CCDC for this material should quote the full literature citation and the reference number 1145/89.

Financial support from NSF-EPSCoR (OSR-9550487) and NIDevR (Northern Ireland) is gratefully acknowledged.

References

1 (*a*) E. J. Corey, *Pure Appl. Chem.*, 1967, **14**, 19; (*b*) E. J. Corey and X.-M. Cheng, *The Logic of Chemical Synthesis*, Wiley, New York, 1989.
2 (*a*) G. R. Desiraju, *Crystal Engineering: The Design of Organic Solids*, Elsevier, Amsterdam, 1989; (*b*) J. P. Mathias and J. F. Stoddart, *Chem. Soc. Rev.*, 1992, **21**, 215; (*c*) C. B. Aakeröy, *Acta Crystallogr., Sect. B*, 1997, **53**, 569.
3 T. L. Threlfall, *Analyst*, 1995, **120**, 2435.
4 J. Bernstein and A. T. Hagler, *Mol. Cryst. Liq. Cryst.*, 1979, **50**, 223.
5 J. Pecaut, J. P. Levy and R. Masse, *J. Mater. Chem.*, 1993, **3**, 999; J.-F. Nicoud, R. Masse, C. Bourgogne and C. Evans, *J. Mater. Chem.*, 1997, **7**, 35; R. Masse and J. Zyss, *Mol. Eng.*, 1991, **1**, 141; R. Masse, M. Bagieu-Beucher, J. Pecaut, J-P Levy and J. Zyss, *Nonlinear Optics*, 1993, **5**, 413; J. Pecaut and R. Masse, *Acta Crystallogr., Sect. C*, 1993, **49**, 277.
6 (*a*) F. Baert, P. Schweiss, G. Heger and M. Moore, *J. Mol. Struct.*, 1988, **178**, 29; (*b*) F. Hamzaoui, F. Baert and J. Zyss, *J. Mater. Chem.*, 1996, **6**, 1123.1.
7 M. Ziegelle, J. Zyss and R. Hierle, *J. Non-Cryst. Solids*, 1982, **47**, 287.
8 Cambridge Structural Database, version 5.14 (October 1997), F. H. Allen, O. Kennard and R. Taylor, *Acc. Chem. Res.*, 1983, **16**, 46.
9 The search fragments used were pyridine rings with all possible permutations of amino and nitro groups positioned around the ring. Only structures without disorder and with *R* values below 10% were considered.
10 R. A. Hollins, L. H. Merwin, R. A. Nissan, W. S. Wilson and R. Gilardi, *J. Heterocyclic Chem.*, 1996, **33**, 2883.
11 R. Destro, T. Pilati and M. Simonetta, *Acta Crystallogr., Sect. B*, 1975, **31**, 2883.
12 In order to probe the structural composition of each crystalline material presented here, X-ray powder diffraction patterns were simulated from single-crystal data using the diffraction-module in CERIUS2 (Molecular Simulations Inc. 9685 Scranton Road, San Diego, CA, 92121–3752) and compared with experimentally recorded powder data on the relevant bulk material. Powder diffraction data were recorded on a Siemens D5000.
13 (*a*) L. Deffet, *Repertoire de Composes organiques polymorphes*, Liege, 1942; (*b*) P. Pfeiffer, *Organische Molekulverbindungen*, 2nd edn., Verlag von Ferdinand Enke, Stuttgart, 1927; (*c*) P. Groth, *Chemische Krystallographie*, vol. III–V, Verlag von Wilhelm Engelman, Leipzig, 1910.
14 This form of 2-amino-3-nitropyridine was obtained serendipitously during an attempt to cocrystallize 2-amino-3-nitropyridine with maleic acid.
15 For information about graph-set notation, see J. Bernstein, R. E. Davis, L. Shimoni and N.-L. Chang, *Angew. Chem.*, 1995, **107**, 1687; *Angew. Chem., Int. Ed. Engl.*, 1995, **34**, 1555; M. C. Etter, J. C. MacDonald and J. Bernstein, *Acta Crystallogr., Sect. B.*, 1990, **46**, 256.
16 A. J. Stone and S. Tsuzuki, *J. Phys. Chem., B.*, 1997, **101**, 10178.
17 A. J. Stone, A. Dullweber, M. P. Hodges, P. L. P. Poperlier and D. J. Wales, *Orient: a program for studying interactions between molecules, Version 3.2*, University of Cambridge, 1995.
18 R. D. Amos, CADPAC: The Cambridge Analytic Derivatives Packagae, issue 6. Tech. rep., University of Cambridge, 1995.
19 J.-O. Henck, personal communication.
20 J. K. Whitesell, R. E. Davis, L. L. Saunders, R. J. Wilson and J. P. Feagins, *J. Am. Chem. Soc.*, 1991, **113**, 3267.
21 G. M. Sheldrick, SHELXL-93, University of Göttingen.

Paper 8/00073E; *Received 2nd January*, 1998

UM00012824
NOVARTIS EXHIBIT 1017
Novartis v. Regents, IPR2023-01346
Page 1570 of 4460

Supramolecular assembly of low-dimensional silver(I) architectures *via* amide–amide hydrogen bonds

Christer B. Aakeröy*† and Alicia M. Beatty

Department of Chemistry, Kansas State University, Manhattan, Kansas, 66506, USA

The ligand nicotinamide (L) is used to propagate the linear coordination geometry of AgL_2 into 1-D and 2-D assemblies *via* a combination of coordinate covalent bonds and specific intermolecular hydrogen-bond interactions; the precise nature of the resulting lamellar structures are also influenced by the nature of the counterion.

Some recent efforts in the field of crystal engineering have focused on the predictable assembly of organic molecular solids *via* intermolecular interactions,[1] and it has become clear that certain functional groups *e.g.* carboxylic acids and amides, are reliable, robust connectors for the formation of hydrogen-bonded organic networks.[2] However, relatively little work has been done in constructing predictable assemblies of coordination compounds *via* directional intermolecular interactions.[3] Ordered assemblies of transition metal complexes (*e.g.* 'coordination polymers'[4]) are being studied for their potential as useful conductive, porous and magnetic materials.[5] From a crystal engineering standpoint, the advantage of using transition metals is that the shape of the main building unit can be controlled by using a metal–ligand system that is known to exhibit a desired coordination geometry. A specific geometry can then be propagated throughout the crystal structure by attaching substituents (intermolecular connectors) to the ligands. In order to probe the strength and reliability of various intermolecular connectors, a low-dimensional metal–ligand system is a convenient starting point, as this may allow us to drive the assembly of linear coordination complexes into one or two dimensions in the crystal lattice *via* specific intermolecular interactions. Silver(I) is one of the few metal ions that commonly displays linear coordination, thus AgL_2 complexes of silver(I) with pyridine derivatives provide the required low-dimensional building blocks.[6] The amide functionality is an appropriate intermolecular connector for this study,[7] in part due to its well known ability to form hydrogen-bonding networks in organic molecular solids,[8] and also because it is unlikely that silver(I) ions will coordinate to either the amide carbonyl oxygen or amine nitrogen atoms in the presence of a pyridine nitrogen. In order to also investigate the influence of the steric requirements and hydrogen-bonding ability of the counter ion on the supramolecular assembly, we have initiated a systematic structural study of a family of silver complexes. We now report the X-ray single crystal structures of three new compounds,[9] $[Ag(C_5H_4NCONH_2)_2][O_3SCF_3]$ **1**, $[Ag(C_5H_4NCONH_2)_2][BF_4]$ **2** and $[Ag(C_5H_4NCONH_2)_2][PF_6]$ **3**, which contain infinite low-dimensional architectures, assembled through intermolecular hydrogen bonds.‡

The reaction of silver(I) triflate with nicotinamide leads to the formation of dinicotinamidesilver(I) triflate **1** (mp 183–185 °C), where the cationic complex contains a silver ion coordination to two nicotinamide ligands in a near-linear fashion, L–Ag–L 174.29(8)°. As expected, the coordination to the silver ion is through the ring nitrogen atoms. The 1-D geometry of the complex cation is propagated in the solid state through amide–amide hydrogen bonds [N···O 2.920(3) Å], leading to infinite $C_1^1(12)$ chains.[10] Neighbouring chains are linked through symmetry related hydrogen bonds, r(N···O) = 2.898(3) Å, forming a 'head-to-head' $R_2^2(8)$ motif. These two intermolecular interactions create an infinite ladder-like arrangement (Fig. 1). There are no further hydrogen-bond interactions between adjacent cationic ladders. The anion acts as a cross-link between two cationic ladders *via* weak hydrogen bonds to the two remaining amide hydrogen atoms, r(N···O) = 3.094(3) and 3.179(3) Å. Thus the presence of a triflate ion, which has oxygen atoms readily available as hydrogen-bond acceptors, does not disrupt the formation of the intended ligand–ligand hydrogen bonds, and the amide functionalities propagate a linear assembly of the silver complexes.

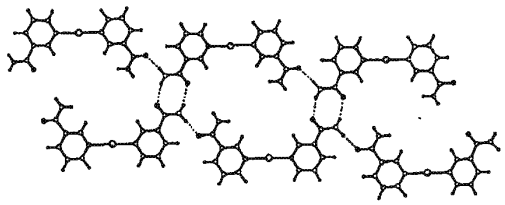


Fig. 1 Infinite 1D ladder motif in **1**, constructed *via* $C_1^1(12)$ and $R_2^2(8)$ hydrogen bonds between linear cationic moieties

Reaction of silver(I) tetrafluoroborate with nicotinamide yields the linear complex, dinicotinamidesilver(I) tetrafluoroborate **2** (mp 217–220 °C), where again the silver ion is coordinated to two ligands in a linear fashion, N–Ag–N [177.3(2)°]. However, in this structure, two unique amide–amide hydrogen bonds, r(N···O) = 2.966(7) and 2.863(7) Å, form two $C_1^1(4)$ chains, which generate infinite two-dimensional sheets (Fig. 2). The anions are sandwiched between cationic sheets, held there by two N–H···F; r(N···F) = 2.979(7) and 3.082(8) Å, and one C–H···F; r(C···F) = 3.138(7) Å, hydrogen bonds. The overall crystal packing displays an ...ABAABA...

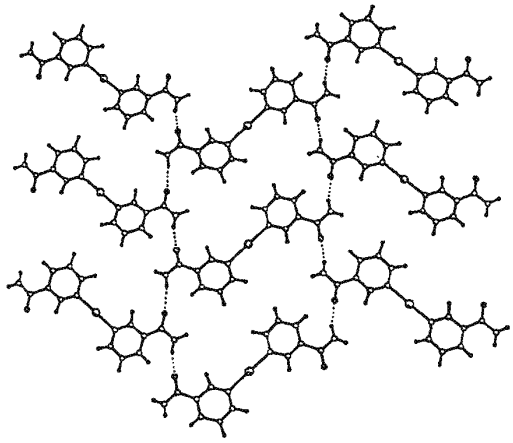


Fig. 2 2D cationic network in **2**, formed by $C_1^1(4)$ hydrogen bonds (the same 2D motif is found in the crystal structure of **3**

UM00012825
NOVARTIS EXHIBIT 1017
Novartis v. Regents, IPR2023-01346
Page 1571 of 4460

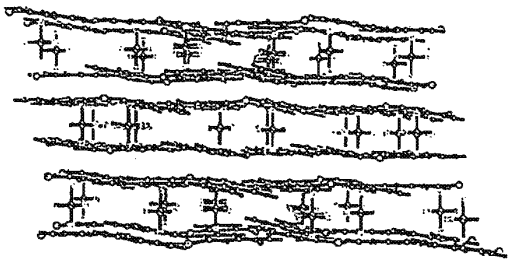


Fig. 3 Edge-on view of the lamellar crystal packing in 3; hexafluorophosphate counter ions are positioned between silver-containing cationic sheets

arrangement, where A is a cationic sheet and B is an anionic layer (Fig. 3). Within ABA units the distance between cationic sheets is *ca.* 3.6 Å, while the separation between ABA units is *ca.* 3.2 Å, with no hydrogen bonds between cationic layers.

The reaction of silver(I) hexafluorophosphate with nicotinamide yields dinicotinamidesilver(I) hexafluorophosphate 3 (mp 234–238 °C), which again contains the expected linear cationic complex, N–Ag–N 173.4(1)°. Neighboring cations are linked *via* two unique amide–amide hydrogen bonds, *r*(N···O) = 2.943(4) and 2.870(4) Å, leading to a 2D network that is virtually identical to the cationic sheet observed in **2** (Fig. 2). The anions are positioned between sheets through two N–H···F hydrogen bonding interactions, *r*(N···F) = 3.033(4) and 3.058(4) Å. The crystal structure displays an ...ABAABA... packing (Fig. 3), with cationic sheets separated by *ca.* 3.8 Å within ABA units and *ca.* 3.4 Å between ABA units.

The structures of **1**, **2** and **3** demonstrate that the silver ion provides the desired linear AgL_2 building unit, and neighboring amide functionalities assemble these complexes into either 1-D or 2-D supramolecular architectures *via* intermolecular hydrogen bonds. Although the precise geometries of the hydrogen-bond networks change in this series, amide–amide interactions persist in the presence of anions with widely differing geometries and coordinating abilities. Consequently, we have gained a level of control over the way in which adjacent linear silver(I) complexes are arranged within the 3-D lattice. However, a detailed comparison of the crystal structures of **1** *vs.* **2** and **3** indicates that the counter ion does play an important role in the assembly of these complexes, resulting in the formation of either 1-D or 2-D cationic motifs based on prevailing amide–amide interactions. For example, 2-D cationic sheets are observed in structures where the anion is approximately spherical and with relatively low-coordinating ability ($[BF_4]^-$ and $[PF_6]^-$), whereas cationic ladders arise in the presence of a more anisotropic counter ion with stronger hydrogen-bond acceptors. In the case of the lamellar 2-D assemblies displayed by **2** and **3**, we hope to specifically control inter-layer separations by altering the characteristics of the counterion. Moreover, we are also examining how changes to the position of the amide functionality (*e.g.* 4-carboxamidepyridine *vs.* 3-carboxamidepyridine) and the presence of other substituents on the ligand, influence the nature of the hydrogen-bond networks and the resulting 3-D packing.

The work presented here illustrates that directional hydrogen bonds can be used in assembly of transition-metal complexes even in competition with potentially disruptive counterion interactions. Consequently, we can expect that many principles of crystal engineering that have been developed and tested in organic solid-state chemistry will assume further relevance in supramolecular aspects of coordination chemistry.

We acknowledge financial support from Kansas State University, NSF-EPSCoR (OSR-9550487) and DuPont.

Notes and References

† E-mail: aakeroy@ksu.edu

‡ *Crystal data*: **1**: $C_{13}H_{12}AgF_3N_4O_5S$, triclinic, space group $P\bar{1}$, a = 7.4761(5), b = 10.8812(7), c = 11.1832(9) Å, α = 98.898(6), β = 106.639(6), γ = 99.406(5)°, U = 845.2(1) Å^3, Z = 2, D_c = 1.969 g cm^{-3}, μ = 1.383 mm^{-1}, R_1 (all data) = 0.0191, R^2 (all data) = 0.0460.

2: $C_{12}H_{12}AgBF_4N_4O_2$, monoclinic, space group $P2_1/c$, a = 9.9693(7), b = 9.7488(6), c = 15.5105(10) Å, β = 97.971(4)°, U = 1492.9(2) Å^3, Z = 4, D_c = 1.953 g cm^{-3}, μ = 1.410 mm^{-1}, R_1 (all data) = 0.0591, R_2 (all data) = 0.1185.

3: $C_{12}H_{12}AgF_6N_4O_2P$ monoclinic, space group $P2_1/c$, a = 8.1458(7), b = 9.9241(10), c = 20.1008(2) Å, β = 98.387(7)°, U = 1559.5(3) Å^3, Z = 4, D_c = 2.064 g cm^{-3}, μ = 1.442 mm^{-1}, R_1 (all data) = 0.0346, R_2 (all data) = 0.0566. CCDC 182/831.

1 G. R. Desiraju, *Crystal Engineering: The Design of Organic Solids*, Elsevier, Amsterdam, 1989; *Angew. Chem., Int. Ed. Engl.*, 1995, **34**, 2311; C. B. Aakeröy, *Acta Crystallogr., Sect. B*, 1997, **53**, 569; M. J. Zaworotko, *Nature*, 1997, **386**, 220; M. M. Conn and J. Rebek, Jr., *Chem. Rev.*, 1997, **97**, 1647.

2 S. Coe, J. J. Kane, T. L. Nguyen, L. M. Toledo, E. Wininger, F. W. Fowler and J. W. Lauher, *J. Am. Chem. Soc.*, 1997, **119**, 86; C. B. Aakeröy and M. Nieuwenhuyzen, *J. Am. Chem. Soc.*, 1994, **116**, 10983; K. E. Schwiebert, D. N. Chin, J. C. MacDonald and G. M. Whitesides, *J. Am. Chem. Soc.*, 1996, **118**, 4018; R. E. Melendez, C. V. Krishnamohan, M. J. Zaworotko, C. Bauer and R. D. Rogers, *Angew. Chem., Int. Ed. Engl.*, 1996, **35**, 2213; O. Felix, M. W. Hosseini, A. de Cian and J. Fischer, *Angew. Chem., Int. Ed. Engl.*, 1997, **36**, 102; P. Brunet, M. Simard and J. D. Wuest, *J. Am. Chem. Soc.*, 1997, **119**, 2737; A. Marsh, M. Silvestri and J.-M. Lehn, *Chem. Commun.*, 1996, 1527; W. T. S. Huck, R. Hulst, P. Timmerman, F. C. J. M. van Eggel and D. N. Reinhoudt, *Angew. Chem., Int. Ed. Engl.*, 1997, **36**, 1006.

3 A. D. Burrows, C.-W. Chan, M. M. Chowdhry, J. E. McGrady and D. M. P. Mingos, *Chem. Soc. Rev.*, 1995, 329; A. D. Burrows, D. M. P. Mingos, A. J. P. White and D. J. Williams, *Chem. Commun.*, 1996, 97; L. Carlucci, G. Ciani, D. M. Proserpio and A. Sironi, *J. Chem. Soc., Dalton Trans.*, 1997, 1801; A. Hassan and S. Wang, *J. Chem. Soc., Dalton Trans.*, 1997, 2009; C. M. Drain, K. C. Russel and J.-M. Lehn, *Chem. Commun.*, 1996, 337;

4 O. M. Yaghi, G. Li and H. Li, *Nature*, 1995, **378**, 703; A. J. Blake, N. R. Champness, S. S. M. Chung, W.-S. Li and M. Schröder, *Chem. Commun.*, 1997, 1005; S. Subramanian and M. J. Zaworotko, *Angew. Chem., Int. Ed. Engl.*, 1995, **34**, 2127; E. C. Constable, *Chem. Commun.*, 1997, 1073; M. Fujita, Y. J. Kwon, S. Washizu and K. Ogura, *J. Am. Chem. Soc.*, 1994, **116**, 1151.

5 J.-M. Lehn, *Angew. Chem., Int. Ed. Engl.*, 1990, **29**, 1342; J. S. Miller, A. J. Epstein and W. M. Reiff, *Acc. Chem. Res.*, 1988, **21**, 114; S. Subramanian and M. J. Zaworotko, *Coord. Chem. Rev.*, 1994, **137**, 357.

6 D. Venkataraman, S. Lee, J. S. Moore, P. Zhang, K. A. Hirsch, G. B. Gardner, A. C. Covey and C. L. Prentice, *Chem. Mater.*, 1996, **8**, 2030; L. Carlucci, G. Ciani, D. M. Proserpio and A. Sironi, *J. Am. Chem. Soc.*, 1995, **117**, 4562.

7 Hydrogen bonding in transition metal complexes containing nicotinamide has been noted previously, however not in the context of supramolecular design: B. L. Kindberg, E. H. Griffith and E. L. Amma, *Chem. Commun.*, 1977, 461; A. Vegas, A. Pérez-Salazar and F. Silió, *Acta Crystallogr., Sect. B*, 1981, **37**, 1916; J. Emsley, N. M. Reza, H. M. Dawes and M. B. Hursthouse, *J. Chem. Soc., Dalton Trans.*, 1986, 313; J. Skorsepa, K. Györyová, M. Melník, K. Smolander and M. Ahlgrèn, *Acta Crystallogr., Sect. C*, 1995, **51**, 1069.

8 Amide–amide interactions in organic molecular solids involve 'head-to-head' $R_2^2(8)$ or cetemer $C_4^4(4)$ hydrogen bonds: L. Leiserowitz and M. Tuval, *Acta Crystallogr., Sect. B*, 1978, **34**, 1230.

9 Suitable crystals of all compounds were grown from aqueous solutions containing 1:2 mixtures of the appropriate silver(I) salt and nicotinamide (3-pyridine carboxamide).

10 For information about graph-set notation, see: J. Bernstein, R. E. Davis, L. Shimoni and N.-L. Chang, *Angew. Chem., Int. Ed. Engl.*, 1995, **34**, 1555; M. C. Etter, J. C. MacDonald and J. Bernstein, *Acta Crystallogr., Sect. B*, 1990, **46**, 356.

Received in Cambridge, UK, 4th November 1997; 7/07919B

UM00012826
NOVARTIS EXHIBIT 1017
Novartis v. Regents, IPR2023-01346
Page 1572 of 4460

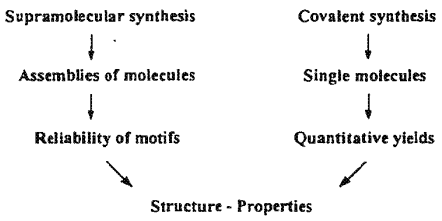
"Total Synthesis" Supramolecular Style: Design and Hydrogen-Bond-Directed Assembly of Ternary Supermolecules**

Christer B. Aakeröy,* Alicia M. Beatty, and Brian A. Helfrich

"Molecular chemistry, thus, has established its power over the covalent bond. The time has come to do the same for non-covalent intermolecular forces."[1]

Chemical synthesis, the making and breaking of covalent bonds, is a fundamental scientific discipline with consequences for all aspects of human existence. A vast number of reactions have been devised, discovered, and refined allowing more and more complicated molecules to be made using extraordinary multistep synthetic processes.[2] In contrast, crystal engineering, a new but rapidly expanding area of science concerned with the construction and properties of assemblies and extended networks of molecules, has yet to reach anywhere near the same level of sophistication.[3] Nevertheless, covalent *and* supramolecular (noncovalent) synthesis can be seen as having considerable overlap in terms of both methods and focus (Scheme 1).

"The consequences of directed and selective hydrogen-bond interactions on sets of molecules are to a solid-state chemist what a new synthesis is to a solution chemist."[4]



Scheme 1. Comparison between covalent and supramolecular synthesis.

In recent years many systematic and elegant studies have been witnessed that demonstrate how molecular assemblies of increasing complexity and dimensionality can be put together with complementary intermolecular interactions, for example, hydrogen bonds and $\pi-\pi$ interactions. Typically, these are homomeric architectures: "most crystals are built from identical (or enantiomeric) copies of the same molecule".[5] However, in order to bring crystal engineering to a higher level of refinement and versatility it is necessary to identify reliable supramolecular reactions and synthetic strategies that will allow us to build multicomponent heteromeric structures, such as binary and ternary supermolecules.[6]

Much of the important ground work regarding the preparation and utility of cocrystals was carried out by Etter and Frankenbach:[7] binary cocrystals were synthetic goals, but these cocrystallization reactions were also used as probes of the competition between different hydrogen-bonding interactions. An important rule of thumb resulted from this work: in a system with a multitude of hydrogen-bonding functionalities "the best hydrogen-bond donor and the best hydrogen-bond acceptor will preferentially form hydrogen bonds to one another".[8] From this it also follows that the second-best donor will form a hydrogen bond to the second-best acceptor, etc. It is still important to remember, however, that solid-state assembly is an enormously complex process governed by a subtle balance between relatively weak and often ill-defined intermolecular forces (in addition to possible complications posed by competition between kinetic and thermodynamic factors). This certainly helps to explain the fact that multistep intermolecular synthesis is not commonplace. In fact, to the best of our knowledge,[9–11] there is not a single example in the Cambridge Crystallographic Database[12] (amongst over 224000 entries) of a 1:1:1 ternary cocrystal containing supermolecules with well-defined and predictable connectivity that was synthesized using a deliberate supramolecular design strategy.[13]

Our approach to the design of ternary structures is based upon two simple principles: 1) Hydrogen bonds often form in a hierarchical fashion (best donor to best acceptor, second-best donor to second-best acceptor, etc.)[8] and 2) a small number of specific intermolecular interactions can provide a large part of the stabilization energy of molecular crystals.[14]

The centerpiece in our supramolecular systems is isonicotinamide. This molecule readily reacts with aromatic carboxylic acids to form 1:1 binary cocrystals that contain a robust and reproducible hydrogen-bonded motif (shown in Figure 1 for benzoic acid as the carboxylic acid (**1**)).[15]

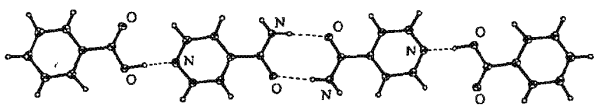


Figure 1. The supermolecule in the 1:1 cocrystal **1** of isonicotinamide and benzoic acid held together by acid···pyridine and amide···amide hydrogen-bonding interactions.

The best donor (carboxylic acid) and the best acceptor (pyridine nitrogen atom) form a short intermolecular N···O hydrogen bond, and the supermolecule is completed through a self-complementary amide···amide interaction. Isonicotinamide is a good example of a suitable building block for ternary cocrystals: it has two distinctly different, yet relatively strong, hydrogen-bonding moieties, and it shows good "structural flexibility" (it can form well-defined crystals with different components).[16] The primary hydrogen bond in this

[*] Dr. C. B. Aakeröy, B. A. Helfrich
Department of Chemistry
Kansas State University
Manhattan, KS 66506 (USA)
Fax: (+1) 785-532-6666
E-mail: aakeroy@ksu.edu
Dr. A. M. Beatty
Department of Chemistry and Biochemistry
University of Notre Dame, Notre Dame, IN 46556 (USA)

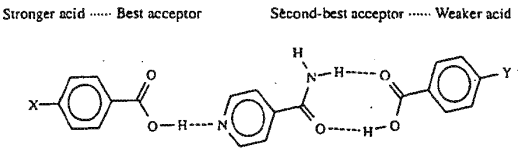
[**] We are grateful for financial support from the NSF (CHE-0078996) and Kansas State University.

 © WILEY-VCH Verlag GmbH, D-69451 Weinheim, 2001 1433-7851/01/4017-3240 $ 17.50+.50/0

UM00012827
NOVARTIS EXHIBIT 1017
Novartis v. Regents, IPR2023-01346
Page 1573 of 4460

system is the acid···pyridine interaction and, since hydrogen bonds have large electrostatic components, the strength of this interaction is governed by the acidity of the carboxylic acid donor. Of course, if the acid is too strong, the proton will be transferred to the nitrogen atom; this will result in an ionic compound and not in a cocrystal.[17]

The "weaker" link in the tetrameric motif in **1** is the amide···amide interaction. Since many reported structures contain heteromeric amide···acid hydrogen bonds (in preference to the corresponding homomeric options),[12, 18] our plan was to replace the amide···amide interaction with a more favorable heteromeric acid···amide interaction, thereby allowing the introduction of a third component in a specific manner. By offering two different carboxylic acids to the isonicotinamide molecule, we expected the stronger acid to interact preferentially with the best acceptor (the pyridine nitrogen atom) and the weaker acid to form a heteromeric motif with the remaining amide moiety (Scheme 2).



Scheme 2. Proposed scheme for the construction of a three-component supermolecule.

This supramolecular design strategy was put to the test by allowing equimolar amounts of a weaker acid, a stronger acid, and isonicotinamide to react in an aqueous solution. Herein we present the crystal structures of three different cocrystals obtained using this approach.[15, 19]

Compound **2** is a 1:1:1 ternary cocrystal of 3,5-dinitrobenzoic acid, isonicotinamide, and 3-methylbenzoic acid that contains the desired three-component supermolecule with the expected connectivity. The stronger acid ($pK_a = 2.8$)[20] interacts with the pyridine nitrogen atom, and the weaker acid ($pK_a = 4.3$)[20] competes successfully for the amide moiety and forms a heteromeric hydrogen-bonded motif (Figure 2). Compound **3** is a ternary cocrystal of 3,5-dinitrobenzoic acid, isonicotinamide, and 4-(dimethylamino)benzoic acid with the intended three-component supermolecule. Again, the strong acid···pyridine nitrogen atom interaction persists, and the weaker acid ($pK_a = 6.5$)[20] generates a heteromeric motif with the amide moiety (Figure 2). Finally, compound **4** is a 1:1:1 ternary cocrystal of 3,5-dinitrobenzoic acid, isonicotinamide, and 4-hydroxy-3-methoxycinnamic acid with the same primary supramolecular connectivity as in **2** and **3** (Figure 2). It is important to note that the desired trimer persists even in the presence of the potentially disrupting OH moiety on the weaker acid ($pK_a = 4.4$).[21]

Two important intermolecular synthons,[22] carboxylic acid···pyridine and carboxylic acid···carboxamide, have been utilized in the assembly of a family of 1:1:1 ternary cocrystals. All three structures contain a heteromeric, three-component supermolecule synthesized through the use of hierarchical (best donor/best acceptor, second-best donor/second-best acceptor) hydrogen-bonding interactions. None of the crystals incorporate solvent molecules in the lattice. There is no ambiguity about the classification of these compounds: they are molecular cocrystals, not ionic compounds. All the hydrogen atoms were located from difference density maps, and the C–O distances on each carboxylic acid moiety are distinctly different, and indicate the presence of one C–O and one C=O bond. In addition, the C-N-C angles on the isonicotinamide molecules are in the range of 117.7–118.5°, which is consistent with those exhibited by other nonprotonated pyridine derivatives.[23] All three structures (**2**–**4**) are also stabilized by additional π(weak acid)–π*(strong acid) charge-transfer interactions (see Figure 3).

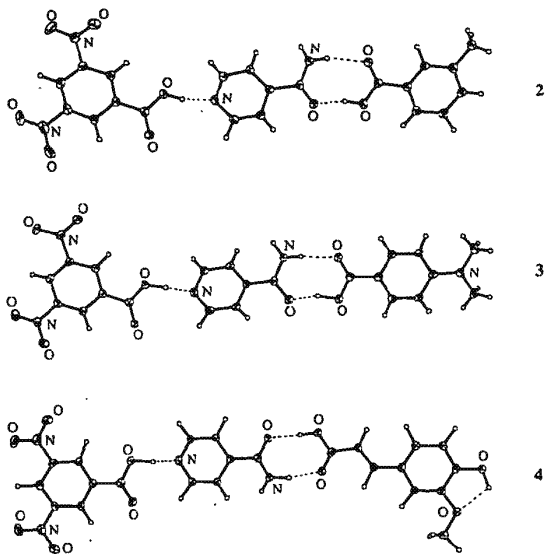


Figure 2. Structures of the ternary supermolecules in **2** (top), **3** (middle), and **4** (bottom) with the stronger acid···pyridine interaction being the "best" hydrogen bond and the weaker acid···amide interaction being the "second-best" hydrogen bond.

The ternary compounds are all colored whereas their constituent parts range from off-white to pale yellow in color. The colors of **2**–**4** reflect the changes in the resulting π–π* separation. The weakest acid, 4-(dimethylamino)benzoic acid, has the highest energy HOMO, and therefore the smallest π–π* separation, which results in the deep red color of **3**. Compound **4** is orange and **2** is yellow; these colors correspond to an expected increase in the energy of the π–π* charge-transfer interaction in these compounds.[24] It is unlikely that this charge transfer takes place through the isonicotinamide molecule from the weak acid (π) to the strong acid (π*). Instead, as the supermolecules are stacked in an antiparallel fashion (Figure 3) with considerable donor–acceptor overlap between neighboring weak and strong acids, it is reasonable to assume that the charge transfer is through space. The intrastack phenyl–phenyl separations are about 3.35 Å. Charge-transfer interactions are also known to be important for stabilizing 1:1 binary cocrystals containing weak and strong aromatic carboxylic acids.[25, 26] Of course it must be

UM00012828
NOVARTIS EXHIBIT 1017
Novartis v. Regents, IPR2023-01346
Page 1574 of 4460

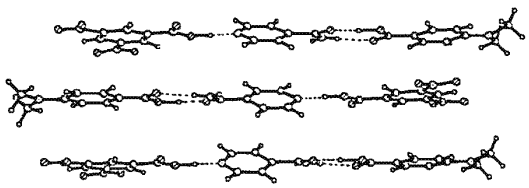


Figure 3. Side-on view of a stack of supermolecules arranged in an antiparallel fashion in 3 to illustrate the π(weak acid)–π^*(strong acid) charge-transfer interactions.

noted that we have presented a strategy for the construction of ternary supermolecules: real crystals are created through the three-dimensional assembly of such building blocks. Neighboring trimeric supermolecules are linked laterally through a variety of weaker N–H···O and C–H···O interactions, which lead to lamellar architectures in all three cases.

This work has demonstrated that three-component supermolecules can be constructed through the use of known intermolecular synthetic operations. Although these forces are weaker than covalent interactions, it is clearly possible to assemble more than two different building blocks in a preconceived manner. We have every reason to believe that more complex supermolecules can be readily synthesized through an improved awareness of the balance and competition between intermolecular interactions. In addition, supramolecular reactions of this type may have important ramifications for the pharmaceutical industry (circumventing patents, modifying crystal habit, and facilitating processing), and may also lead to new strategies for chiral separation.

Received: March 19, 2001
Revised: June 18, 2001 [Z16800]

[1] J.-M. Lehn, *Supramolecular Chemistry*, VCH, Weinheim, **1995**, p. 2.
[2] E. J. Corey, *Chem. Soc. Rev.* **1988**, *17*, 111; K. C. Nicolaou, E. J. Sorensen, *Classics in Total Synthesis*, Wiley-VCH, Weinheim, **1996**.
[3] a) C. B. Aakeröy, *Acta Crystallogr. Sect. B* **1997**, *53*, 569; b) "Crystal Engineering: From Molecules and Crystals to Materials": *NATO ASI Ser. Ser. C* **1999**, *538*.
[4] M. C. Etter, *J. Phys. Chem.* **1991**, *95*, 4601.
[5] J. D. Dunitz in *Perspectives in Supramolecular Chemistry, Vol. 2: The Crystal as a Supramolecular Entity* (Ed.: G. R. Desiraju), Wiley, New York, **1995**, p. 3.
[6] The term supermolecule used here indicates a discrete zero-dimensional species composed of molecular building blocks, assembled through directional noncovalent forces. Thus, ternary systems formed by ionic interactions (salts) or by incorporation of solvent molecules within a lattice (for example, clathrates, heterosolvates, or inclusion compounds) are distinctly different from the supermolecules that we discuss here.
[7] M. C. Etter, G. M. Frankenbach, *Chem. Mater.* **1989**, *1*, 10.
[8] M. C. Etter, *Acc. Chem. Res.* **1990**, *23*, 120.
[9] The well-known Koefler's complex is a solvate (pyridine), and its preparation was not based upon an explicit supramolecular strategy: J. Bernstein, H. Regev, F. H. Herbstein, *Acta Crystallogr. Sect. B* **1980**, *36*, 1170.
[10] A three-component cocrystal based on isomorphous replacement with acridine in a 2:3 2,2'-dihydroxybiphenylphenazine cocrystal has recently been reported. This approach also relies on molecular complementarity and recognition and may be effective in the future design of other ternary systems: T. Smolka, R. Boese, R. Sustmann, *Struct. Chem.* **1999**, *10*, 429.
[11] A three component 3:1:1 cocrystal has been reported previously although no explicit design strategy was evident: D. E. Lynch, G. Smith, K. A. Byriel, C. H. L. Kennard, *J. Chem. Soc. Chem. Commun.* **1992**, 300.
[12] F. H. Allen, O. Kennard, *Chem. Des. Automation News* **1993**, *8*(1), 31.
[13] Many binary cocrystals based on principles of molecular recognition have, however, been reported, see for example J. A. R. P. Sarma, G. R. Desiraju, *J. Chem. Soc. Perkin Trans. 2* **1985**, 1905; C. Huang, L. Leiserowitz, G. M. Schmidt, *J. Chem. Soc. Perkin Trans. 2* **1973**, 503; C. Tamura, N. Sakurai, S. Sato, *Bull. Chem. Soc. Jpn.* **1971**, *44*, 1473; F. Pan, M. S. Wong, V. Gramlich, C. Bosshard, P. Gunter, *Chem. Commun.* **1996**, 2; Y. LeFur, M. Bagieu-Beucher, R. Masse, J. F. Nicoud, J. P. Levy, *Chem. Mater.* **1996**, *8*, 8; J. A. Zerkowski, J. C. MacDonald, G. M. Whitesides, *Chem. Mater.* **1997**, *9*, 9; R.-F. Liao, J. W. Lauher, F. W. Fowler, *Tetrahedron* **1996**, *52*, 3153.
[14] P. Dauber, A. T. Hagler, *Acc. Chem. Res.* **1980**, *13*, 105.
[15] a) Crystal data for **1**: $C_{13}H_{12}N_2O_3$, $M_r = 244.25$, monoclinic, space group $C2/c$, $a = 22.379(4)$, $b = 5.1509(8)$, $c = 20.540(3)$ Å, $\beta = 96.927(2)°$, $V = 2350.3(6)$ Å^3, $Z = 8$, $\rho_{calcd} = 1.381$ g cm^{-3}, $\mu(Mo_{K\alpha}) = 1.133$ mm^{-1}. $T = 173(2)$ K, $R1 = 0.0365$, $wR2 = 0.1009$ for all data, 1693 independent reflections. b) Crystallographic data (excluding structure factors) for the structures reported in this paper have been deposited with the Cambridge Crystallographic Data Centre as supplementary publication nos. CCDC-160362–160365. Copies of the data can be obtained free of charge on application to CCDC, 12 Union Road, Cambridge CB2 1EZ, UK (fax: (+44) 1223-336-033; e-mail: deposit@ccdc.cam.ac.uk).
[16] C. B. Aakeröy, A. M. Beatty, B. Helfrich, unpublished results.
[17] There are of course many ternary supramolecular and host–guest systems built around ionic components, for example J. A. Swift, A. M. Pivovar, A. M. Reynolds, M. D. Ward, *J. Am. Chem. Soc.* **1998**, *120*, 5887; F. Xue, T. C. W. Mak, *J. Phys. Org. Chem.* **2000**, *13*, 405; P. Cudic, J.-P. Vigneron, J.-M. Lehn, M. Cesario, T. Prangé, *Eur. J. Org. Chem.* **1999**, 2479; C. V. K. Sharma, A. Clearfield, *J. Am. Chem. Soc.* **2000**, *122*, 4394.
[18] L. Leiserowitz, F. Nader, *Acta Crystallogr. Sect. B* **1977**, *33*, 2719.
[19] Crystal data for **2**: $C_{21}H_{18}N_4O_9$, $M_r = 470.39$, triclinic, space group $P\bar{1}$, $a = 7.1019(9)$, $b = 8.753(1)$, $c = 16.908(2)$ Å, $\alpha = 94.297(2)$, $\beta = 91.318(3)$, $\gamma = 95.192(3)°$, $V = 1043.3(2)$ Å^3, $Z = 2$, $\rho_{calcd} = 1.497$ g cm^{-3}, $\mu(Mo_{K\alpha}) = 1.133$ mm^{-1}. $T = 203(2)$ K, $R1 = 0.0431$, $wR2 = 0.1072$ for all data, 4624 independent reflections.[15b] Crystal data for **3**: $C_{22}H_{21}N_3O_9$, $M_r = 499.44$, triclinic, space group $P\bar{1}$, $a = 7.138(2)$, $b = 8.711(3)$, $c = 18.000(5)$ Å, $\alpha = 85.838(2)$, $\beta = 87.442(6)$, $\gamma = 83.897(5)°$, $V = 1109.2(9)$ Å^3, $Z = 2$, $\rho_{calcd} = 1.495$ g cm^{-3}, $\mu(Mo_{K\alpha}) = 1.133$ mm^{-1}, $T = 203(2)$ K, $R1 = 0.0652$, $wR2 = 0.2075$ for all data, 4859 independent reflections.[15b] Crystal data for **4**: $C_{23}H_{20}N_4O_{11}$, $M_r = 528.43$, monoclinic, space group $P2_1/c$, $a = 6.386(2)$, $b = 26.656(8)$, $c = 13.838(4)$ Å, $\beta = 96.647(5)°$, $V = 2340(1)$ Å^3, $Z = 4$, $\rho_{calcd} = 1.500$ g cm^{-3}, $\mu(Mo_{K\alpha}) = 1.133$ mm^{-1}, $T = 203(2)$ K, $R1 = 0.0448$, $wR2 = 0.1102$ for all data, 2870 independent reflections.[15b]
[20] G. Kartum, W. Vogel, K. Andrussov, *Dissociation Constants of Organic Acids in Aqueous Solution*, Butterworth, London, **1961**.
[21] Calculated using semi-empirical PM3 methods.
[22] G. R. Desiraju, *Angew. Chem.* **1995**, *107*, 2541; *Angew. Chem. Int. Ed. Engl.* **1995**, *34*, 2311.
[23] a) L. B. Jerzykiewicz, Z. Malarski, L. Sobczyk, T. Lis, E. Grech, *J. Mol. Struct.* **1998**, *440*, 175; b) I. Majerz, Z. Malarski, L. Sobczyk, *Chem. Phys. Lett.* **1997**, *274*, 361.
[24] Orbital energies for the individual components were calculated using semi-empirical (AM1 and PM3) and ab initio HF (3–21G) methods.
[25] D. E. Lynch, G. Smith, K. A. Byriel, C. H. L. Kennard, *Aust. J. Chem.* **1998**, *51*, 1019.
[26] C. V. K. Sharma, K. Panneerselvam, T. Pilati, G. R. Desiraju, *J. Chem. Soc. Perkin Trans. 2* **1993**, 2209.

 © WILEY-VCH Verlag GmbH, D-69451 Weinheim, 2001 1433-7851/01/4017-3242 $ 17.50+.50/0

UM00012829
NOVARTIS EXHIBIT 1017
Novartis v. Regents, IPR2023-01346
Page 1575 of 4460

DALTON COMMUNICATION

Two-fold interpenetration of 3-D nets assembled *via* three-co-ordinate silver(I) ions and amide–amide hydrogen bonds

Christer B. Aakeröy, Alicia M. Beatty and Brian A. Helfrich

Department of Chemistry, Kansas State University, Manhattan, Kansas 66506, USA

The combination of isonicotinamide with $AgBF_4$ or $AgClO_4$, respectively, led to isostructural compounds [tris(isonicotinamide)silver(I) tetrafluoroborate and tris(isonicotinamide)-silver(I) perchlorate], containing two 3-D interpenetrating nets of three-co-ordinate silver(I) ions linked by N–H···O hydrogen bonds between adjacent isonicotinamide ligands.

Crystal engineering is a rapidly developing field of structural and supramolecular chemistry, and a wide range of assemblies that are relevant to areas ranging from biochemistry to materials science has been conceived and characterized.[1] Although much of the inspiration for these efforts originates in organic solid-state chemistry,[2] the inorganic equivalent is quickly defining its own possibilities, strategies and boundaries. The most common approach to inorganic crystal engineering has been to propagate the co-ordination geometry of a specific metal ion into infinite architectures using co-ordinate–covalent bonds, leading to co-ordination polymers of varying dimensionality and topology.[3] The result has been a plethora of extended assemblies, *e.g.* squares,[4] ribbons,[5] grids,[6] helices,[7] and interpenetrating or porous diamondoid networks.[8] Far less common has been the use of non-covalent *intermolecular* interactions as a guide to the assembly of co-ordination complexes into extended networks.[9] Although such structures can be expected to have less rigid connectors (compared to strong co-ordinate–covalent bonds), the flexibility inherent in an assembly built upon, *e.g.* hydrogen bonds, may lead to materials with improved solubility and structural agility.

Employing a strategy using a combination of covalent and non-covalent synthesis, we now present two isostructural compounds, tris(isonicotinamide)silver(I) tetrafluoroborate **1**,* and tris(isonicotinamide)silver(I) perchlorate **2**,† where each structure is dominated by a three-dimensional network created by triligated silver(I) ions and short N–H···O hydrogen bonds between adjacent amide functionalities. Compound **1** was obtained by adding $AgBF_4$ (1.1 mmol) in ethanol–water (40 ml, 1:1 v/v) to isonicotinamide (2.2 mmol) in ethanol–water (40 ml, 1:1 v/v). Compound **2** was obtained by adding $AgClO_4$ (4.82 mmol) in water (10 ml) to an aqueous solution (30 ml) of isonicotinamide (9.82 mmol). Transparent colourless crystals (m.p. **1**: 238–240 °C, **2**: 230–235 °C) were obtained after several days through slow evaporation at ambient temperature.‡ These salts are stable in air and apparently do not decay upon continuous exposure to light.

As the two compounds are isostructural, the salient features of their molecular geometries and crystal structures will be discussed together. Although the co-ordination number and geometry of silver(I) complexes can vary considerably, the presence of a three-co-ordinate silver(I) ion is somewhat unexpected since there are relatively few reported crystallographically characterized examples of such complexes involving monodentate ligands [a recent survey found three trigonal planar silver(I) structures out of a total of 90 complexes examined].[10] The geometry of the complex ion is distorted trigonal planar with N–Ag–N bond angles of *ca.* 105, 120 and 135°, Fig. 1. The choice of isonicotinamide as a ligand was made for two reasons. First, silver(I) ions have a high affinity for softer, nitrogen-containing ligands, which encourages covalent–co-ordinate bonds between silver and the ring nitrogen atom in preference to co-ordination to the carbonyl oxygen. Secondly, amide moieties have a well established propensity to engage in complementary hydrogen bonds resulting either in infinite ribbons (through head-to-head interactions), or in infinite chains *via* equivalent N–H···O interactions.§ In the case of **1** and **2** the latter motif is observed, and the structures contain three short, near-linear crystallographically inequivalent N–H···O hydro-

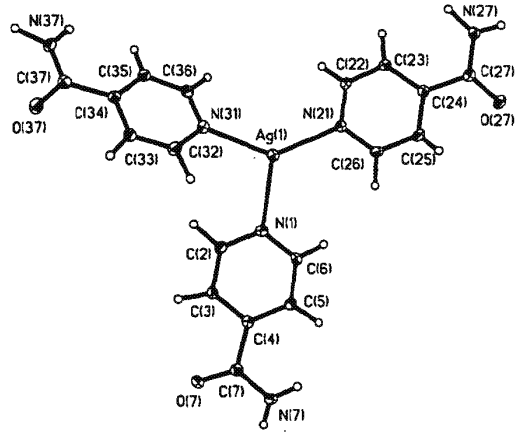


Fig. 1 The central silver(I) ions are co-ordinated by three isonicotinamide ligands in a distorted trigonal fashion in both complexes **1** and **2**

* Crystal data for **1**: $C_{18}H_{18}AgBF_4N_6O_3$, $M = 561.06$, monoclinic, $P2_1/n$, $a = 6.9461(6)$, $b = 18.108(2)$, $c = 16.897(2)$ Å, $\beta = 97.880(6)°$, $U = 2105.2(3)$ Å^3, $Z = 4$, $D_{calc} = 1.770$ g cm^{-3}, μ(Mo-Kα) = 1.027 mm^{-1}. Data were collected at 173(2) K and the structure was refined to $R1 = 0.0368$, $wR2 = 0.0837$ for all data, 3703 independent reflections.

† Crystal data for **2**: $C_{18}H_{18}AgClN_6O_7$, $M = 573.70$ monoclinic, $P2_1/n$, $a = 6.9240(5)$, $b = 18.199(2)$, $c = 16.988(2)$ Å, $\beta = 98.052(6)°$, $U = 2119.6(3)$ Å^3, $Z = 4$, $D_{calc} = 1.798$ g cm^{-3}, μ(Mo-Kα) = 1.133 mm^{-1}. Data were collected at 173(2) K and the structure was refined to $R1 = 0.0331$, $wR2 = 0.0808$ for all data, 2781 independent reflections. CCDC reference number 186/1012. See http://www.rsc.org/suppdata/dt/1943/ for crystallographic files in .cif format.

‡ Satisfactory elemental analyses were obtained, and X-ray powder diffraction showed that the single crystals were representative of the bulk materials.

§ Amide–amide interactions in organic molecular solids typically involve 'head-to-head' $R_2^2(8)$ or catemer $C_1^1(4)$ hydrogen bonds.[11]

UM00012830
NOVARTIS EXHIBIT 1017
Novartis v. Regents, IPR2023-01346
Page 1576 of 4460

BEST AVAILABLE COPY

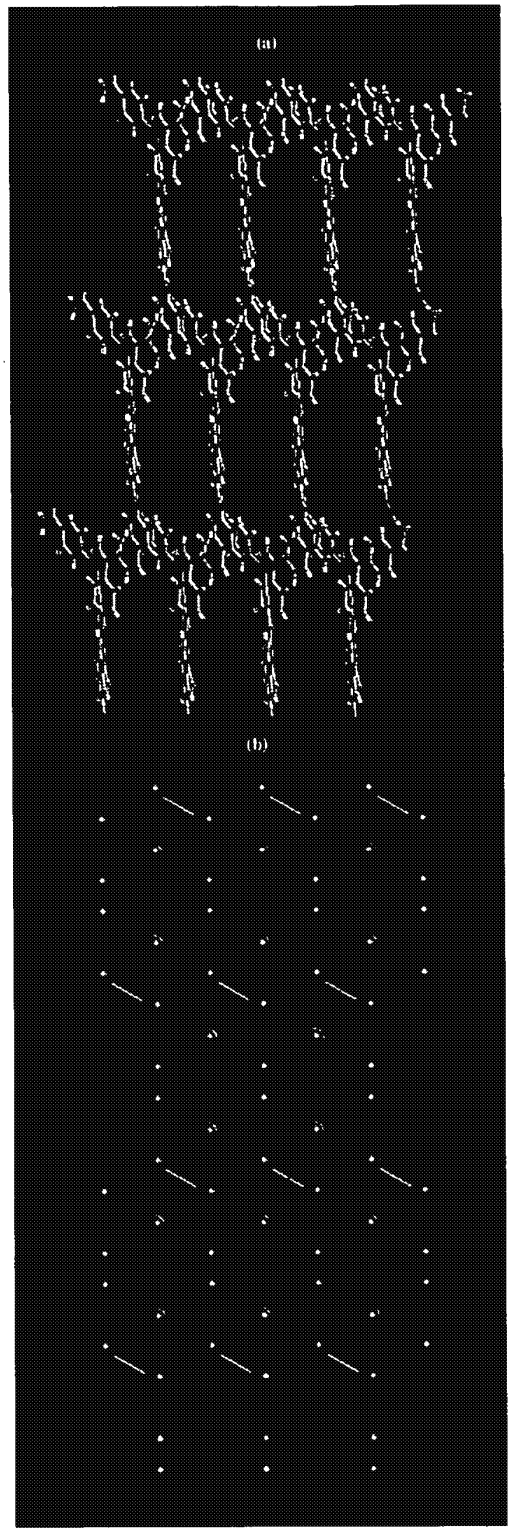


Fig. 2 (a) One of the 3-D cationic nets in the isostructural complexes 1 and 2. (b) The crystal lattice in α-$ThSi_2$

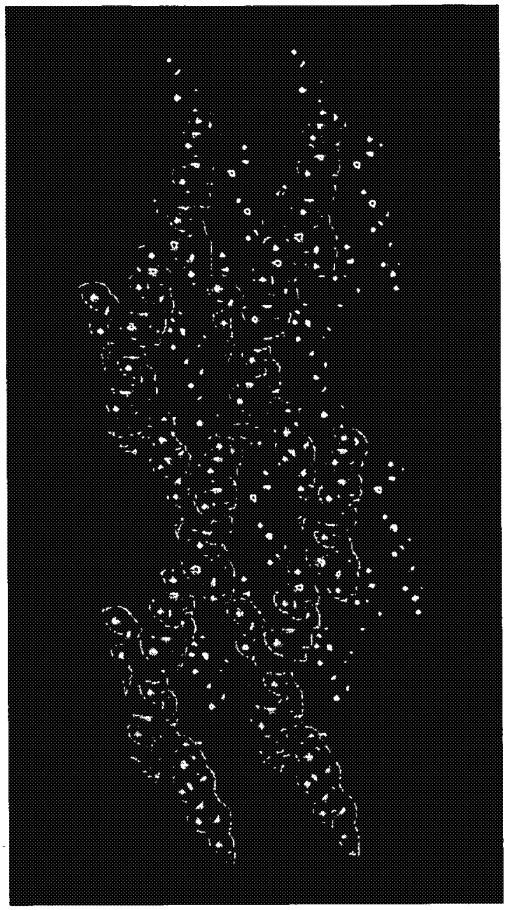


Fig. 3 The two-fold interpenetration of 3-D nets in complexes 1 and 2

gen bonds that connect neighbouring amide moieties.¶ It is possible to envisage how the pseudo three-fold symmetry of the complex ions can be propagated in several ways in the crystal structure, resulting in hexagonal sheets [analogous to molecules like trimesic acid, $C_6H_3(CO_2H_3)_3$-1,3,5], or the three-fold symmetry can be maintained within a spiraling arrangement of ions. The crystal structures of **1** and **2** contain a combination of both of these possibilities resulting in the formation of a net-like array, the topology of which is analogous to the silicon framework in α-$ThSi_2$,‖ Fig. 2. Each structure contains two interpenetrating 3-D nets, with each net being formed through amide–amide hydrogen bonds. While the holes created by the 10-membered chair-like assembly of the silicon framework in α-$ThSi_2$ are occupied by thorium atoms,[13] the corresponding holes in **1** and **2** are interwoven with the second net, resulting in a tight-fitting three-dimensional assembly, Fig. 3.

¶ Intermolecular N–H···O_{amide} hydrogen bond lengths (Å) and angles (°) for **1** [**2**]: N(7)···O(27) 2.869(4) [2.884(4)], N(7)–H(7A)···O(27) 157.9(1) [163.0(1)]; N(27)···O(37) 2.862(3) [2.874(4)], N(27)–H(27A)···O(37) 162.4(1) [176.9(1)]; N(37)···O(7) 2.817(3) [2.815(4)], N(37)–H(37A)···O(7) 167.08(1) [168.0(1)]. Amide–anion N–H···X hydrogen bond lengths (Å) and angles (°) for **1** (X = F) [**2** (X = O)]: N(27)···X(3) 2.947(4) [3.019(5)], N(27)–H(27B)···X(3) 159.5(1) [153.8(1)]; N(37)···X(1) 2.915(3) [2.970(5)], N(37)–H(37B)···X(1) 156.7(1) [152.4(1)].

‖ Frameworks of this type have been observed in silver(I)-containing co-ordination polymers.[12] Our thanks to the reviewer who drew our attention to this lattice type.

UM00012831
NOVARTIS EXHIBIT 1017
Novartis v. Regents, IPR2023-01346
Page 1577 of 4460

The formation of this framework may also be aided by the nature of the anions, which are contained within channels running through the structure. Each anion is anchored within these channels *via* two N–H · · · F or N–H · · · O interactions in **1** and **2**, respectively. There are no noteworthy close Ag · · · Ag contacts in these structures.

These structures represent relatively rare examples of 3-D metal-containing nets built around three-co-ordinate metal centers and propagated *via* intermolecular ligand–ligand hydrogen bonds. Thus, the crystal structures of **1** and **2** demonstrate how non-covalent intermolecular interactions can lead to architectures that mimic assemblies formed by both co-ordination polymers and by 'classic' inorganic lattices. We intend to further explore the supramolecular assembly of metal complexes *via* directional hydrogen bonds, and the possibilities of guiding pseudo-trigonal planar complex ions into alternate arrangements.

Acknowledgements

We acknowledge financial support from Kansas State University, NSF-EPSCoR (OSR-9550487) and DuPont.

References

1 C. B. Aakeröy, *Acta Crystallogr., Sect. B*, 1997, **53**, 569; J.-M. Lehn, *Supramolecular Chemistry*, VCH, Weinheim, 1995; S. Subramanian and M. Zaworotko, *Coord. Chem. Rev.*, 1994, **137**, 357; F. Vögtle, *Supramolecular Chemistry: An Introduction*, Wiley, Chichester, 1991; G. R. Desiraju, *Angew. Chem., Int. Ed. Engl.*, 1995, **34**, 2311; M. J. Zaworotko, *Nature (London)*, 1997, **386**, 220.

2 G. R. Desiraju, *Crystal Engineering: The Design of Organic Solids*, Elsevier, Amsterdam, 1989; G. R. Desiraju (Editor), *Perspectives in Supramolecular Chemistry, Vol. 2, The Crystal as a Supramolecular Entity*, Wiley, Chichester, 1995.

3 R. Robson, B. F. Abrahams, S. R. Batten, R. W. Gable, B. F. Hoskins and J. Liu, *Supramolecular Architectures*, ACS Publication, Washington, DC, 1992, pp. 256–273.

4 C.-Y. Duan, Z.-H. Liu, X.-Z. You and T. C. W. Mak, *Chem. Commun.*, 1997, 381; M. Fujita, Y. J. Kwon, S. Washizu and K. Ogura, *J. Am. Chem. Soc.*, 1994, **116**, 1151.

5 P. Losier and M. J. Zaworotko, *Angew. Chem., Int. Ed. Engl.*, 1996, **35**, 2779.

6 A. J. Blake, S. J. Hill, P. Hubberstey and W.-S. Li, *J. Chem. Soc., Dalton Trans.*, 1997, 913; O. M. Yaghi, H. Li and T. L. Groy, *Inorg. Chem.*, 1997, **36**, 4292.

7 T. M. Garrett, U. Koert, J.-M. Lehn, A. Rault, D. Meyer and J. Fischer, *J. Chem. Soc., Chem. Commun.*, 1990, 557.

8 L. Carlucci, G. Ciani, D. M. Proserpio and A. Sironi, *J. Chem. Soc., Chem. Commun.*, 1994, 2755; A. J. Blake, N. R. Champness, S. S. M. Chung, W.-S. Li and M. Schröder, *Chem. Commun.*, 1997, 1005; O. M. Yaghi and H. Li, *J. Am. Chem. Soc.*, 1996, **118**, 295; S. Subramanian and M. J. Zaworotko, *Angew. Chem., Int. Ed. Engl.*, 1995, **34**, 2127; G. B. Gardner, D. Venkataraman, J. S. Moore and S. Lee, *Nature (London)*, 1995, **374**, 792.

9 A. D. Burrows, D. M. P. Mingos, A. J. P. White and D. J. Williams, *Chem. Commun.*, 1996, 97; M. M. Chowdhry, D. M. P. Mingos, A. J. P. White and D. J. Williams, *Chem. Commun.*, 1996, 899; J.-C. Shi, B.-S. Kang and T. C. W. Mak, *J. Chem. Soc., Dalton Trans.*, 1997, 2171; C. M. Drain, K. C. Russel and J.-M. Lehn, *Chem. Commun.*, 1996, 337; L. Carlucci, G. Ciani, D. M. Proserpio and A. Sironi, *J. Chem. Soc., Dalton Trans.*, 1997, 1801; C. B. Aakeröy and A. M. Beatty, *Chem. Commun.*, 1998, 1067; C. B. Aakeröy and A. M. Beatty, *Crystal Engineering*, 1998, **1**, 39.

10 D. Venkataraman, S. Lee, J. S. Moore, P. Zhang, K. A. Hirsch, G. B. Gardner, A. C. Covey and C. L. Prentice, *Chem. Mater.*, 1996, **8**, 2030.

11 L. Leiserowitz and M. Tuval, *Acta Crystallogr., Sect. B*, 1978, **34**, 1230.

12 L. Carlucci, G. Ciani, D. M. Proserpio and A. Sironi, *J. Am. Chem. Soc.*, 1995, **117**, 4562.

13 G. Brauer and A. Mitius, *Z. Anorg. Allg. Chem*, 1942, **249**, 325.

Received 2*nd April* 1998; *Communication* 8/02520G

UM00012832
NOVARTIS EXHIBIT 1017
Novartis v. Regents, IPR2023-01346
Page 1578 of 4460

CRYSTAL GROWTH & DESIGN
2001
VOL. 1, NO. 2
107–111

Articles

Polymorphs of a 1:1 Cocrystal with Tunnel and Layer Structures: *p,p'*-Biphenol/Dimethyl Sulfoxide

Shinbyoung Ahn, Benson M. Kariuki, and Kenneth D. M. Harris*

School of Chemistry, University of Birmingham, Edgbaston, Birmingham B15 2TT, U.K.

Received September 10, 2000

ABSTRACT: Two polymorphs of the 1:1 cocrystal formed between *p,p'*-biphenol and dimethyl sulfoxide (DMSO) have been discovered. One polymorph has a tunnel type structure, which can be considered to comprise tunnels formed from *p,p'*-biphenol molecules accommodating the DMSO molecules as guests. The other polymorph has a layered structure, comprising layers of *p,p'*-biphenol molecules and layers of DMSO molecules. In both structures, there is direct hydrogen bonding between the *p,p'*-biphenol and DMSO components of the cocrystal. The general utility of the *p,p'*-biphenol molecule as a component in crystal engineering strategies is discussed.

1. Introduction

The successful development of crystal engineering strategies relies first on developing an understanding and rationalization of intermolecular interactions in the context of crystal packing, followed by the subsequent utilization and exploitation of this understanding in the design of new solids with specific desired structural properties.[1–7] Clearly much of the impetus for progress in this field is driven by the need to design crystalline solids with optimal structural properties for specific materials applications.

In general, rationalization of the structural properties of organic molecular crystals is rendered difficult by the fact that crystal structures arise from the interplay of several different intermolecular interactions that are often of comparable importance. However, for cases in which one specific intermolecular interaction (or a small number of interactions) is clearly dominant, it may be possible to develop a reliable rationalization of the observed molecular packing arrangement in the crystal. In this regard, studies of hydrogen-bonded crystals have been particularly prominent in view of the fact that the hydrogen bond[8–10] is generally stronger and more directional than the other types of intermolecular interactions that are typically present in organic molecular crystals, such that the formation of optimal hydrogen-bonding patterns can often be recognized as the main determinant of the observed crystal structures. Thus, the structures of hydrogen-bonded crystals can often be rationalized by identifying the preferred modes of interaction of the hydrogen bond donor and hydrogen bond acceptor groups present.[11–24]

The phenomenon of polymorphism[25–27] (i.e., when a given type of molecule is able to form different crystal structures) is of considerable interest in the field of organic solid state chemistry, in part because comparison of the properties of different polymorphs provides an ideal basis for understanding relationships between solid-state properties and crystal structure. Furthermore, in the development of reliable strategies for the prediction, rationalization, and design of the crystal structure(s) formed by a given type of organic molecule, studies of polymorphic systems provide fertile grounds for exploring and testing our understanding of crystal-packing arrangements. In the case of molecular cocrystals (i.e., crystals containing more than one type of molecule), true polymorphism (in which the different polymorphs have precisely the same stoichiometry) has been relatively rarely reported (see refs 28–32 for examples). In contrast, pseudo-polymorphism (i.e., the case of cocrystals comprising the same molecules but with different stoichiometries and different crystal structures) has been much more widely reported.

In this paper, we report a case of true polymorphism of a cocrystal—the 1:1 cocrystal formed between *p,p'*-biphenol ($HOC_6H_4C_6H_4OH$, abbreviated PBP; Figure 1) and dimethyl sulfoxide ($O{=}S(CH_3)_2$, DMSO)—in which the two polymorphs differ substantially in their structural properties. These structural differences may be understood on the basis of conformational differences in one component of the cocrystal promoting different geometric opportunities for intermolecular hydrogen bonding. In a broader context, the structural properties

* To whom correspondence should be addressed. Fax: +44-121-414-7473. E-mail: K.D.M.Harris@bham.ac.uk.

10.1021/cg000010b CCC: $20.00 © 2001 American Chemical Society
Published on Web 01/05/2001

UM00012833
NOVARTIS EXHIBIT 1017
Novartis v. Regents, IPR2023-01346

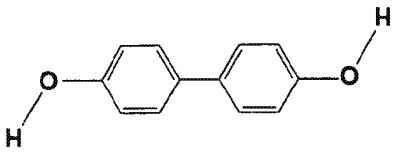


Figure 1. Molecular structure of *p,p'*-biphenol (PBP).

of these polymorphs provide a basis for assessing the utilization of the PBP molecule as a component for inducing different packing arrangements within the context of crystal engineering strategies.

2. Experimental Section

One polymorph (denoted form I) of the PBP/DMSO (1:1) cocrystal was prepared by slow evaporation of solvent from a solution of PBP in DMSO. The crystals have prismatic shape. As discussed below, this polymorph has a tunnel type structure in which tunnels formed from PBP molecules accommodate the DMSO molecules as guests. On obtaining this result, we next explored the possible formation of other cocrystals (inclusion compounds) of PBP containing other appropriate guest molecules in the same tunnel structure (i.e., to replace the DMSO component in this structure). These molecules typically either contained one or two hydrogen bond acceptor groups and/or were based on a long alkane chain (the latter feature chosen with the aim of assisting the templating of tunnel structures). However, most of the experiments involving crystallization of these potential guest molecules together with PBP in DMSO produced only crystals of pure PBP or the PBP/DMSO cocrystal (form I) discussed above. When other solvents (DMF, ethyl acetate, acetone, and cyclopentanone) were used instead of DMSO, only crystals of the pure phase of PBP were produced.

However, a second polymorph (denoted form II) of the 1:1 cocrystal of PBP and DMSO was obtained while exploring the cocrystallization of PBP and 1,10-dibromodecane from DMSO/ethanol (4:1) solution at −4 °C. The crystals of form II were obtained together with crystals of form I but were readily distinguished on the basis of crystal morphology (form I, prismatic; form II, thin plates). Crystals of both forms I and II tend to be unstable with respect to the loss of DMSO over a period of about 1 day under ambient conditions, with form II probably less stable than form I.

Crystals of forms I and II were studied by single-crystal X-ray diffraction, using graphite-monochromated Mo Kα radiation (λ = 0.710 69 Å) on a Rigaku R-Axis II single-crystal X-ray diffractometer equipped with an image plate detector and rotating anode X-ray source. Each data collection comprised a total crystal rotation of 180°, in 30 frames for form I and 60 frames for form II. The crystal-to-detector distance was 80 mm in both cases. In the course of data collection for form II, some extent of deterioration of the crystal was observed, yielding small amounts of polycrystalline material. This decomposition undoubtedly contributes to the comparatively poor quality of the diffraction data and, hence, of the refined structure for form II.

The crystal structures of both forms I and II were solved by direct methods (SIR92 program[33]) and difference Fourier techniques and refined using full-matrix least-squares analysis (SHELXL program[34]). All calculations were performed using the TEXSAN crystallographic software package.[35]

For form I, the positions of all non-hydrogen atoms and the hydrogen atoms of the hydroxyl groups were refined freely. The hydrogen atoms of the aryl rings were placed in standard positions relative to the aryl rings. Anisotropic displacement parameters were refined freely for all non-hydrogen atoms, and isotropic displacement parameters were refined freely for all hydrogen atoms.

For form II, the positions and anisotropic displacement parameters of all non-hydrogen atoms were refined, with the geometry of each aryl ring of the PBP molecule constrained to be a regular hexagon. The positions of the hydrogen atoms of the hydroxyl groups (which were located by difference Fourier synthesis) were refined freely, with the isotropic displacement parameter of each of these hydrogen atoms taken to be 1.2 times the equivalent isotropic displacement parameter of the oxygen atom to which it is bonded. The hydrogen atoms of the aryl rings were placed in standard positions relative to the aryl rings, with the isotropic displacement parameter of each of these hydrogen atoms taken to be 1.2 times the equivalent isotropic displacement parameter of the carbon atom to which it is bonded. It became clear during the refinement that the DMSO molecule is disordered between two orientations, with the relative occupancies refined. As the

Table 1. Crystal Data for Forms I and II of the PBP/DMSO Cocrystal ($C_{12}H_{10}O_2 \cdot C_2H_6SO$)

	form I	form II
PBP:DMSO	1:1	1:1
cryst syst	orthorhombic	orthorhombic
cryst size/mm^3	0.17 × 0.3 × 0.1	0.15 × 0.12 × 0.1
temp/K	248(2)	293(2)
a/Å	10.4405(11)	8.153(2)
b/Å	10.3493(8)	24.106(5)
c/Å	12.3209(14)	7.1794(7)
space group	$P2_12_12_1$	$P2_12_12_1$
cell vol/Å^3	1331.3(3)	1411.1(5)
calcd density/g cm^{-3}	1.319	1.244
Z	4	4
data/params	2350/187	1731/165
final *R* indices ($I > 2\sigma(I)$)		
R	0.041	0.15
R_w	0.095	0.34

Table 2. Fractional Atomic Coordinates and Equivalent Isotropic Displacement Parameters for Form I of the PBP/DMSO Cocrystal[a]

	x	*y*	*z*	U_{eq}/Å^2
S(1)	−1.2831(1)	0.1576(1)	−0.4517(1)	0.046(1)
O(1)	−1.0584(2)	−0.2915(2)	−0.1444(2)	0.051(1)
O(2)	−0.8707(2)	−0.0523(2)	−0.8979(2)	0.046(1)
O(3)	−1.1608(2)	0.2314(2)	−0.4763(2)	0.054(1)
C(1)	−1.0303(2)	−0.2521(3)	−0.2483(2)	0.038(1)
C(2)	−1.1002(2)	−0.3065(3)	−0.3319(2)	0.041(1)
C(3)	−1.0748(2)	−0.2707(2)	−0.4376(2)	0.041(1)
C(4)	−0.9793(2)	−0.1803(2)	−0.4622(2)	0.033(1)
C(5)	−0.9121(3)	−0.1255(2)	−0.3763(2)	0.041(1)
C(6)	−0.9377(2)	−0.1599(3)	−0.2700(2)	0.042(1)
C(7)	−0.9495(2)	−0.1464(2)	−0.5762(2)	0.033(1)
C(8)	−0.9595(2)	−0.2389(2)	−0.6577(2)	0.037(1)
C(9)	−0.9330(3)	−0.2106(2)	−0.7647(2)	0.038(1)
C(10)	−0.8957(2)	−0.0867(2)	−0.7928(2)	0.033(1)
C(11)	−0.8846(2)	0.0069(2)	−0.7138(2)	0.035(1)
C(12)	−0.9107(2)	−0.0224(2)	−0.6067(2)	0.035(1)
C(13)	−1.2467(3)	0.0615(3)	−0.3369(3)	0.061(1)
C(14)	−1.2910(4)	0.0328(3)	−0.5502(3)	0.070(1)
H(2)	−1.1646(2)	−0.3673(3)	−0.3168(2)	0.052(8)
H(3)	−1.1225(2)	−0.3078(2)	−0.4943(2)	0.054(8)
H(5)	−0.8482(3)	−0.0639(2)	−0.3907(2)	0.049(8)
H(6)	−0.8925(2)	−0.1208(3)	−0.2128(2)	0.047(8)
H(8)	−0.9852(2)	−0.3231(2)	−0.6392(2)	0.038(7)
H(9)	−0.9403(3)	−0.2750(2)	−0.8182(2)	0.059(9)
H(11)	−0.8592(2)	0.0910(2)	−0.7329(2)	0.035(7)
H(12)	−0.9022(2)	0.0421(2)	−0.5535(2)	0.035(6)
H(13A)	−1.3172(10)	0.0029(15)	−0.3226(11)	0.086(12)
H(13B)	−1.2335(20)	0.1169(4)	−0.2744(5)	0.086(12)
H(13C)	−1.1695(12)	0.0121(16)	−0.3508(7)	0.074(11)
H(14A)	−1.3637(15)	−0.0226(15)	−0.5348(13)	0.128(18)
H(14B)	−1.2129(11)	−0.0178(16)	−0.5479(15)	0.098(14)
H(14C)	−1.3009(25)	0.0705(3)	−0.6218(4)	0.087(12)
H(15)	−0.9861(34)	−0.2704(39)	−0.1031(30)	0.079(12)
H(16)	−0.8548(38)	−0.1237(40)	−0.9365(32)	0.095(14)

[a] For atoms with anisotropic displacement parameters, U_{eq} is defined as one-third of the trace of the orthogonalized U_{ij} tensor. For atoms with isotropic displacement parameters, U_{eq} is equal to U_{iso}. Estimated standard deviations are given in parentheses.

UM00012834
NOVARTIS EXHIBIT 1017
Novartis v. Regents, IPR2023-01346
Page 1580 of 4460

Table 3. Fractional Atomic Coordinates and Equivalent Isotropic Displacement Parameters for Form II of the PBP/DMSO Cocrystal[a]

	x	*y*	*z*	U_{eq}/Å²	occ
S(1)	0.6684(12)	0.2426(4)	0.2796(8)	0.102(3)	0.63(2)
O(1)	0.8124(10)	−0.1630(4)	0.2230(13)	0.089(3)	1
O(2)	0.1638(11)	0.1834(5)	0.2770(14)	0.097(3)	1
O(3)	0.7504(4)	0.2404(2)	0.4684(5)	0.090(3)	1
C(1)	0.7198(4)	−0.1137(2)	0.2262(5)	0.085(4)	1
C(2)	0.7662(4)	−0.0709(2)	0.3446(5)	0.091(4)	1
C(3)	0.6715(4)	−0.0231(2)	0.3559(5)	0.099(5)	1
C(4)	0.5302(4)	−0.0181(2)	0.2488(5)	0.079(4)	1
C(5)	0.4838(4)	−0.0609(2)	0.1303(5)	0.077(4)	1
C(6)	0.5785(4)	−0.1087(2)	0.1190(5)	0.082(4)	1
C(7)	0.4292(4)	0.0365(2)	0.2620(5)	0.071(4)	1
C(8)	0.4651(4)	0.0761(2)	0.3969(5)	0.081(4)	1
C(9)	0.3764(4)	0.1253(2)	0.4035(5)	0.072(4)	1
C(10)	0.2520(4)	0.1350(2)	0.2752(5)	0.071(3)	1
C(11)	0.2162(4)	0.0954(2)	0.1404(5)	0.102(5)	1
C(12)	0.3048(4)	0.0462(2)	0.1338(5)	0.106(6)	1
C(13)	0.7956(35)	0.2903(12)	0.1675(30)	0.129(9)	0.63(2)
C(14)	0.7393(43)	0.1868(10)	0.1600(28)	0.118(7)	0.63(2)
C(13A)	0.5966(34)	0.2659(17)	0.1772(37)	0.130(9)	0.37(2)
C(14A)	0.7719(69)	0.1670(7)	0.2196(42)	0.129(11)	0.37(2)
S(1A)	0.7749(17)	0.2365(6)	0.2546(11)	0.108(5)	0.37(2)
H(2)	0.8607(4)	−0.0742(2)	0.4163(5)	0.109	1
H(3)	0.7025(4)	0.0056(2)	0.4352(5)	0.119	1
H(5)	0.3893(4)	−0.0576(2)	0.0586(5)	0.092	1
H(6)	0.5474(4)	−0.1374(2)	0.0398(5)	0.098	1
H(8)	0.5483(4)	0.0696(2)	0.4827(5)	0.097	1
H(9)	0.4004(4)	0.1518(2)	0.4937(5)	0.086	1
H(11)	0.1329(4)	0.1019(2)	0.0545(5)	0.122	1
H(12)	0.2808(4)	0.0197(2)	0.0435(5)	0.127	1
H(13A)	0.8505(168)	0.3128(49)	0.2588(32)	0.155	0.63(2)
H(13B)	0.7308(43)	0.3137(48)	0.0879(191)	0.155	0.63(2)
H(13C)	0.8755(136)	0.2709(12)	0.0942(189)	0.155	0.63(2)
H(14A)	0.8570(43)	0.1869(38)	0.1611(197)	0.142	0.63(2)
H(14B)	0.7009(176)	0.1885(38)	0.0337(68)	0.142	0.63(2)
H(14C)	0.6999(170)	0.1534(10)	0.2175(141)	0.142	0.63(2)
H(13D)	0.5967(169)	0.2667(117)	0.0435(38)	0.156	0.37(2)
H(13E)	0.5881(176)	0.3030(45)	0.2244(343)	0.156	0.37(2)
H(13F)	0.5050(40)	0.2444(70)	0.2202(355)	0.156	0.37(2)
H(14D)	0.6739(177)	0.1516(18)	0.2730(350)	0.154	0.37(2)
H(14E)	0.8661(190)	0.1505(16)	0.2777(339)	0.154	0.37(2)
H(14F)	0.7740(364)	0.1594(8)	0.0884(42)	0.154	0.37(2)
H(15)	0.7479(86)	−0.1836(18)	0.1407(150)	0.107	1
H(16)	0.1841(159)	0.2072(72)	0.3774(232)	0.116	1

[a] For atoms with anisotropic displacement parameters, U_{eq} is defined as one-third of the trace of the orthogonalized U_{ij} tensor. For atoms with isotropic displacement parameters, U_{eq} is equal to U_{iso}. Estimated standard deviations are given in parentheses. Note that the DMSO molecule is disordered between two orientations, but with the same position of the oxygen atom in each orientation.

molecular geometry of the minor orientation tended to distort during refinement, the geometry of this component was restrained to standard geometry.

Data concerning the crystal structures are reported in Table 1, and fractional atomic coordinates are given in Table 2 (form I) and Table 3 (form II).

3. Results and Discussion

Form I of PBP/DMSO (1:1) has a helical tunnel structure along the crystallographic *c* axis, as shown in Figure 2. In projection on the plane perpendicular to the tunnel axis, four PBP molecules complete a given host tunnel around the DMSO guest molecules. The DMSO molecules in a given tunnel adopt two different orientations, which alternate along the tunnel, and the same orientation of both the PBP and DMSO molecules is repeated every 12.32 Å along the tunnel (the periodic repeat distance along the *c* axis). In the PBP molecule, the dihedral angle between the two aryl rings is 33.6° and the dihedral angles around the two C−O bonds are

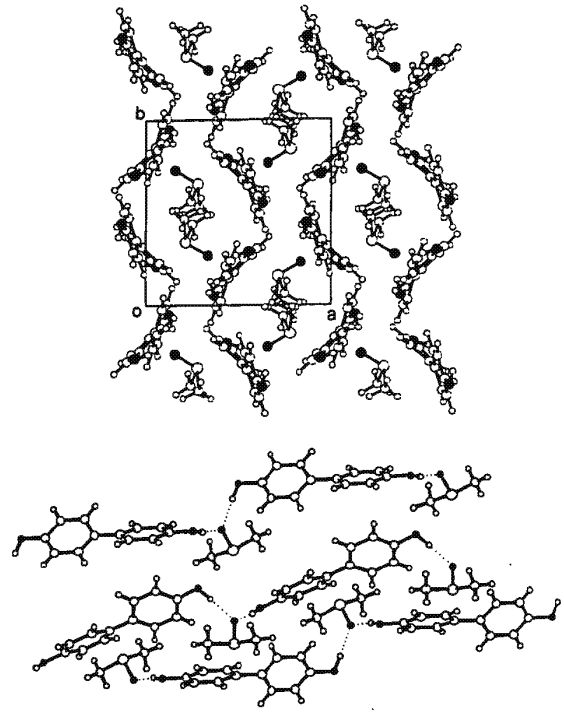


Figure 2. (a, top) Crystal structure of form I of the PBP/DMSO cocrystal viewed along the tunnel axis (*c* axis) and (b, bottom) a section of the crystal structure showing the hydrogen-bonding arrangement.

such that the H−O···O−H dihedral angle is 105.0°. The actual angle between the two O−H vectors is 107.3° (see section 4). The hydrogen atom of each hydroxyl group lies significantly out of the plane of the aryl ring to which it is bonded (H−O−C−C dihedral angles ca. 20 and 21°). As shown in Figure 2b, the crystal structure contains S=O···H−O hydrogen bonds between the DMSO and PBP molecules, representing a helical hydrogen-bonded chain of alternating PBP and DMSO molecules. In these chains, a given DMSO molecule accepts hydrogen bonds from two different PBP molecules, and the graph set description[36,37] is $C_2^1(13)$. For one of the hydrogen bonds formed to the DMSO molecule, the O···H distance is 1.82 Å, the O···O distance is 2.74 Å, and the O−H···O angle is 167.0°. For the other hydrogen bond, the O···H distance is 1.85 Å, the O···O distance is 2.74 Å, and the O−H···O angle is 173.7°. There is no direct hydrogen bonding between PBP molecules. Under ambient conditions, DMSO is lost from the cocrystal over a period of time and the tunnel structure collapses, producing the pure phase of PBP (as shown by powder X-ray diffraction).

The crystal structure of form II of PBP/DMSO (1:1) is a layered structure, comprising alternating layers of PBP and DMSO molecules, as shown in Figure 3. The layers are perpendicular to the crystallographic *b* axis. The asymmetric unit comprises one PBP molecule and one DMSO molecule. In this structure, the DMSO molecule is disordered between two orientations (occupancies 0.63 and 0.37), with the same position of the oxygen atom in each case. The two orientations differ

UM00012835
NOVARTIS EXHIBIT 1017
Novartis v. Regents, IPR2023-01346
Page 1581 of 4460

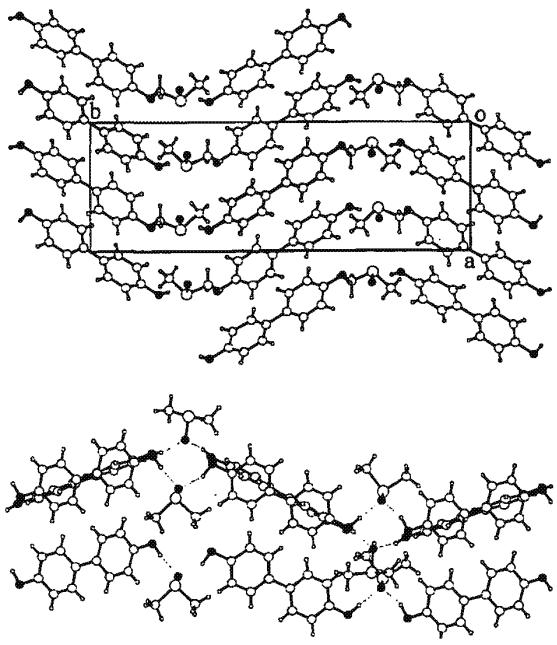


Figure 3. (a, top) Crystal structure of form II of the PBP/DMSO cocrystal viewed along the *c* axis and (b, bottom) a section of the crystal structure showing the hydrogen-bonding arrangement. Only the major orientation of the disordered DMSO molecule in this structure is shown.

in terms of reorientation about an axis almost parallel to the O=S bond; therefore, the disorder mainly involves different positions of the methyl groups. In the PBP molecule, the dihedral angle between the two aryl rings is 9.7° and the dihedral angles around the two C–O bonds are such that the H–O···O–H dihedral angle is 161.8°. The actual angle between the two O–H vectors is 155.9° (see section 4). The hydrogen atoms of the hydroxyl groups lie virtually within the plane of the aryl rings (H–O–C–C dihedral angles ca. 1 and 7°). The conformation of the PBP molecule in form II is substantially closer to the conformation in the pure crystalline phase of PBP[38,39] than is the conformation in form I (in the pure phase of PBP, the molecule is strictly centrosymmetric, with the two aryl rings coplanar and an angle of 180° between the two O–H vectors). As shown in Figure 3b, the DMSO molecule interacts through S=O···H–O hydrogen bonds with a PBP molecule in each of the two adjacent layers, forming essentially linear hydrogen-bonded chains that run along the *b* axis (i.e., perpendicular to the layers). The graph set description of these chains is $C_2^1(13)$. For one of these hydrogen-bonds, the O···H distance is 1.85 Å, the O···O distance is 2.66 Å, and the O–H···O angle is 144.5°. For the other hydrogen bond, the O···H distance is 1.76 Å, the O···O distance is 2.69 Å, and the O–H···O angle is 167.5°. Thus, as in form I, the S=O group of the DMSO molecule acts as a bifurcated hydrogen bond acceptor. Recalling that the DMSO molecule is orientationally disordered in this structure, we note that the geometric features of the hydrogen-bonding arrangement discussed above are actually the same for the major and minor orientations of the molecule, as the position of the oxygen atom is the same in both orientations (however, the orientation of specific orbitals of the DMSO molecule relative to the hydrogen bond donor (hydroxyl) groups of the PBP molecules clearly differs for the two orientations of the DMSO molecule). There is no direct hydrogen bonding between PBP molecules; however, within the layer of PBP molecules, the aryl rings of neighboring molecules interact through recognizable edge-to-face interactions.

We now highlight some comparisons between the structures of forms I and II of the PBP/DMSO cocrystal. In form II, the conformation of the PBP molecule is such that the aryl rings are close to coplanar (dihedral angle between the aryl rings is 9.7°), whereas in form I the corresponding dihedral angle is substantially larger (33.6°). Importantly, in form I the angle between the O–H vectors of the molecule is 107.3°, whereas in form II the corresponding angle is 155.9°. This angle is critically important in determining the directionality of the hydrogen-bonding arrangement around a given PBP molecule, and it is clear that the different molecular conformations in forms I and II lead to different intermolecular hydrogen-bonding schemes. As discussed in more general terms in section 4, the large value (155.9°) of this angle in form II is completely consistent with the propagation of essentially linear hydrogen-bonded chains of alternating PBP and DMSO molecules running perpendicular to the planes of the layers in this structure. In contrast, the substantially smaller angle of 107.3° in form I is consistent with the formation of an extended hydrogen-bonded array with significant curvature (rather than linear), as observed with the helical hydrogen-bonded chains of alternating PBP and DMSO molecules in this tunnel type structure.

The calculated densities of the two polymorphs of PBP/DMSO are 1.32 g cm^{-3} for form I and 1.24 g cm^{-3} for form II. It is noteworthy that the polymorph (form I) that apparently has the greater stability is the polymorph of higher density.

4. Concluding Remarks

The PBP molecule has considerable potential as a building block to construct a variety of hydrogen-bonded structures, as demonstrated in the crystal structures of the two polymorphs of the PBP/DMSO cocrystal reported in this paper and in the structures of other cocrystals involving PBP reported previously.[40–43] Much of the potential for using PBP as a versatile component in the construction of hydrogen-bonded arrays in crystals originates from the compromise that it offers in terms of rigidity and flexibility, with regard to both molecular conformation and intermolecular hydrogen-bonding capacity. Thus, while the biphenyl component of the molecule represents an essentially rigid linear unit, the molecule nevertheless has flexibility in terms of (i) the dihedral angles around the C–O bonds of the two hydroxyl groups and (ii) the dihedral angle around the C–C bond that links the two aryl rings.

First, as discussed in section 3, the flexibility of the dihedral angles around the C–O bonds leads to a wide range of possible relative orientations of the two O–H bond vectors within the molecule, giving very wide scope for the PBP molecule to propagate extended hydrogen-bonded arrays of differing geometries. In principle, the angle between the two O–H bond vectors may range

UM00012836
NOVARTIS EXHIBIT 1017
Novartis v. Regents, IPR2023-01346
Page 1582 of 4460

from ca. 39° (for the case with the hydroxyl groups cis; H−O···O−H dihedral angle 0°) to 180° (for the case with the hydroxyl groups trans; H−O···O−H dihedral angle 180°). Clearly form I of the PBP/DMSO cocrystal lies between these extremes, whereas form II of the PBP/DMSO cocrystal is close to the upper limit of this range. The consequences in terms of the differing geometries of the extended hydrogen-bonded arrays formed in each case is readily apparent from the comparison of the structures of these polymorphs discussed in section 3, with form I exhibiting an extended hydrogen-bonded array (helical chain) of significantly greater curvature than the extended hydrogen-bonded array (essentially linear) in form II.

Second, variation of the dihedral angle around the C−C bond that links the two aryl rings does not alter the geometric requirements of the PBP molecule for intermolecular hydrogen bonding but, rather, alters the steric nature of the molecule, which is clearly also an important factor influencing crystal packing. The provision of this flexibility in the steric character of the molecule is potentially advantageous within a component used for crystal engineering purposes, as it provides the molecule with some opportunity to find an optimal shape to facilitate the relative packing of extended hydrogen-bonded chains (formed by interactions of the hydroxyl groups). Furthermore, as illustrated in the structure of form II of the PBP/DMSO cocrystal, interactions between the aryl rings of neighboring PBP molecules may also influence the crystal packing arrangement—this structure exhibits recognizable edge-to-face interactions between aryl rings, which may promote the observed aggregation of the hydrogen-bonded chains into layers of PBP molecules and layers of DMSO molecules.

In view of the features discussed above, it is not surprising that, in addition to the two polymorphs of the PBP/DMSO cocrystal reported in this paper, other crystal structures containing PBP exhibit a variety of different types of hydrogen-bonding networks, including one-dimensional chains (for example, PBP/1,4-diazabicyclo-[2.2.2]octane (1:1)[40] and PBP/hexamethylenetetramine (1:1)[42]), two-dimensional layers (for example, PBP/1,2-diaminoethane/methanol (2:1:1)[40]), and three-dimensional diamondoid structures (for example, PBP/1,2-diaminoethane (1:1),[40] PBP/*p*-phenylenediamine (1:1),[43] and PBP/benzidine (1:1)[43]).

Acknowledgment. We are grateful to the EPSRC for general support and to the University of Birmingham for providing a studentship (to S.A.).

Supporting Information Available: X-ray crystallographic information files (CIF) are available for forms I and II of the PBP/DMSO cocrystal. This material is available free of charge via the Internet at http://pubs.acs.org.

References

(1) Desiraju, G. R. *Crystal Engineering: the Design of Organic Solids*; Elsevier: Amsterdam, 1989.
(2) Aakeröy, C. B.; Seddon, K. R. *Chem. Soc. Rev.* **1993**, *22*, 397.
(3) Desiraju, G. R. *Angew. Chem., Int. Ed. Engl.* **1995**, *34*, 2311.
(4) Aakeröy, C. B. *Acta Crystallogr.* **1997**, *B53*, 569.
(5) Desiraju, G. R. *Chem. Commun.* **1997**, 1475.
(6) Dunitz, J. D.; Gavezzotti, A. *Acc. Chem. Res.* **1999**, *32*, 677.
(7) Harris, K. D. M.; Hollingsworth, M. D. *Nature* **1989**, *341*, 19.
(8) Pimentel, G. C.; McClellan, A. C. *The Hydrogen Bond*; Freeman: San Francisco, 1960.
(9) Hamilton, W. C.; Ibers, J. A. *Hydrogen Bonding in Solids*; Benjamin: New York, 1968.
(10) Jeffrey, G. A.; Saenger, W. *Hydrogen Bonding in Biological Structures*; Springer-Verlag: Berlin, 1994.
(11) Leiserowitz, L. *Acta Crystallogr.* **1976**, *B32*, 775.
(12) Leiserowitz, L.; Tuval, M. *Acta Crystallogr.* **1978**, *B34*, 1230.
(13) Berkovitch-Yellin, Z.; Leiserowitz, L. *J. Am. Chem. Soc.* **1980**, *102*, 7677.
(14) Leiserowitz, L.; Hagler, A. T. *Proc. R. Soc. London, Ser. A* **1983**, *A388*, 133.
(15) Etter, M. C. *Acc. Chem. Res.* **1990**, *23*, 120.
(16) Etter, M. C.; Urbanczyk-Lipkowska, Z.; Zia-Ebrahimi, M.; Panunto, T. W. *J. Am. Chem. Soc.* **1990**, *112*, 8415.
(17) Stainton, N. M.; Harris, K. D. M.; Howie, R. A. *J. Chem. Soc., Chem. Commun.* **1991**, 1781.
(18) Etter, M. C.; Reutzel, S. M. *J. Am. Chem. Soc.* **1991**, *113*, 2586.
(19) Garcia-Tellado, F.; Geib, S. J.; Goswami, S.; Hamilton, A. D. *J. Am. Chem. Soc.* **1991**, *113*, 9265.
(20) Harris, K. D. M.; Stainton, N. M.; Callan, A. M.; Howie, R. A. *J. Mater. Chem.* **1993**, *3*, 947.
(21) MacDonald, J. C.; Whitesides, G. M. *Chem. Rev.* **1994**, *94*, 2383.
(22) Brown, M. E.; Chaney, J. D.; Santarsiero, B. D.; Hollingsworth, M. D. *Chem. Mater.* **1996**, *8*, 1588.
(23) Desiraju, G. R. *Acc. Chem. Res.* **1996**, *29*, 441.
(24) Krische, M. J.; Lehn, J. M.; Kyritsakas, N.; Fisher, J. *Helv. Chim. Acta* **1998**, *81*, 1909.
(25) Dunitz, J. D. *Pure Appl. Chem.* **1991**, *63*, 177.
(26) Caira, M. R. *Top. Curr. Chem.* **1998**, *198*, 164.
(27) Bernstein, J.; Davey, R. J.; Henck, J.-O. *Angew. Chem., Int. Ed.* **1999**, *38*, 3441.
(28) Coppens, P.; Sabine, T. M. *Acta Crystallogr.* **1969**, *B25*, 2442.
(29) Agmon, I.; Herbstein, F. H. *Eur. Cryst. Meeting* **1982**, *7*, 50.
(30) Sletten, J.; Daraghmeh, H.; Lloret, F.; Julve, M. *Inorg. Chim. Acta* **1998**, *279*, 127.
(31) Lovell, S.; Subramony, P.; Kahr, B. *J. Am. Chem. Soc.* **1999**, *121*, 7020.
(32) Bosshard, C.; Pan, F.; Wong, M. S.; Manetta, S.; Spreiter, R.; Cai, C.; Günter, P.; Gramlich, V. *Chem. Phys.* **1999**, *245*, 377.
(33) Altomare, A.; Cascarano, G.; Giacovazzo, C.; Guagliardi, A.; Barla, M. C.; Polidori, G.; Camalli, M. *J. Appl. Crystallogr.* **1994**, *27*, 435.
(34) Sheldrick, G. M. SHELXL93, Program for the Refinement of Crystal Structures; University of Göttingen, Göttingen, Germany, 1993.
(35) TEXSAN, Single-Crystal Structure Analysis Software, Molecular Structure Corporation, 3200 Research Forest Drive, The Woodlands, TX 77381, 1993.
(36) Etter, M. C. *Acc. Chem. Res.* **1990**, *23*, 120.
(37) Bernstein, J.; Davis, R. E.; Shimoni, L.; Chang, N. L. *Angew. Chem., Int. Ed. Engl.* **1995**, *34*, 1555.
(38) Akhmed, N. A.; Farag, M. S.; Amin, A. *Zh. Strukt. Khim.* **1971**, *12*, 738.
(39) Jackisch, M. A.; Fronczek, F. R.; Geiger, C. C.; Hale, P. S.; Daly, W. H.; Butler, L. G. *Acta Crystallogr.* **1990**, *C46*, 919.
(40) Ferguson, G.; Glidewell, C.; Gregson, R. M.; Meehan, P. R.; Patterson, I. L. J. *Acta Crystallogr.* **1998**, *B54*, 151.
(41) Ferguson, G.; Coupar, P. I.; Glidewell, C. *Acta Crystallogr.* **1997**, *B53*, 513.
(42) Coupar, P. I.; Glidewell, C.; Ferguson, G. *Acta Crystallogr.* **1997**, *B53*, 521.
(43) Ermer, O.; Eling, A. *J. Chem. Soc., Perkin Trans. 2* **1994**, 925.

CG000010B

UM00012837
NOVARTIS EXHIBIT 1017
Novartis v. Regents, IPR2023-01346
Page 1583 of 4460

Enantioselective Inclusion of Methyl Phenyl Sulfoxides and Benzyl Methyl Sulfoxides by (*R*)-Phenylglycyl-(*R*)-phenylglycine and the Crystal Structures of the Inclusion Cavities

Motohiro Akazome, Yuki Ueno, Haruko Ooiso, and Katsuyuki Ogura*

Department of Materials Technology, Faculty of Engineering, Chiba University, 1-33 Yayoicho, Inageku, Chiba 263-8522, Japan

Received June 30, 1999

Crystalline (*R*)-phenylglycyl-(*R*)-phenylglycine [(*R,R*)-**1**] includes methyl phenyl sulfoxides (**2** and **3**) and benzyl methyl sulfoxides (**4**) with high enantioselectivity. The dipeptide exhibited different stereoselectivity depending on four structural isomers of methyl tolyl sulfoxide ($C_8H_{10}OS$): *R* for methyl 2-tolyl sulfoxide, *S* for methyl 3-tolyl sulfoxide, and racemic for methyl 4-tolyl sulfoxide. A structural isomer, benzyl methyl sulfoxide, was included in racemic form. Chlorophenyl methyl sulfoxides **3** (C_7H_7ClOS) with a similar volume showed the same enantioselectivity for their recognition. By single-crystal X-ray analyses of these inclusion compounds, it was elucidated that (*R,R*)-**1** molecules self-assembled to form layer structures and included the sulfoxides between these layers and that the origin of the enantioselectivity based on chiral cavities was induced by conformation of the C-terminal phenyl group of the dipeptide. The relative position between the ammonio proton and the C-terminal phenyl group in one molecule of the dipeptide determined the stereochemistry of the methyl sulfinyl groups to be recognized. Various positional isomers of methyl xylyl sulfoxide having the formula of $C_9H_{12}OS$ were subjected to the enantioselective inclusion by (*R,R*)-**1** crystals and these results are also discussed.

Introduction

In many inclusion systems, host molecules change their conformation more or less to include guest molecules.[1,2] As for inclusion of various guest molecules, it is more important for relatively large host molecules to possess flexibility. Herbstein has reported conformational isomerism of the flexible host as a factor for molecular recognition of the tripod host molecule, that is, tris(5-acetyl-3-thienyl)methane.[3]

Our attention has been focused on dipeptide molecules that have a straight glycylglycine backbone to construct a two-dimensional layer by means of intermolecular salt formation between COOH and NH_2 groups.[4,5] To date, we have reported that (*R*)-phenylglycyl-(*R*)-phenylglycine [(*R,R*)-**1**] effectively affords inclusion crystals of alkyl phenyl sulfoxides with high enantioselectivity.[4,6,7] Single-crystal X-ray analyses revealed that (*R,R*)-**1** molecules self-assemble to form layer structures, between which the sulfoxide molecules are accommodated. Ethyl, isopropyl, and *tert*-butyl phenyl sulfoxides were included with high *S* enantioselectivity, while the stereochemistry of the preferably included methyl phenyl sulfoxide was *R*. All of these inclusion crystals have a quite similar hydrogen bonding network of the dipeptide molecules to construct a layer. The sulfoxide molecules are in the channel between the walls of the dipeptide phenyl groups which stand on the layer. There are schematically represented in Figures 1 and 2.

The central ammonio proton of the channel binds to the sulfinyl oxygen, and the phenyl groups of the wall are rotatable to create a specific cavity suitable for the inclusion of the sulfoxide. It is noteworthy that the methyl group of methyl phenyl sulfoxide is located on the right side of the inclusion void (motif A), while ethyl, isopropyl, and *tert*-butyl groups are on the left side (motif B). Hence we have investigated the inclusion of various methyl phenyl sulfoxides (**2** and **3**) and benzyl methyl sulfoxides (**4**) in (*R,R*)-**1** crystals from the following viewpoints: (1) whether their methyl group is always located on the right side of the void or not and (2) how the shape of the sulfoxide influences the rotation of the phenyl wall to determine the enantioselectivity.

Results and Discussion

Inclusion of Structural Isomers of Sulfoxide ($C_8H_{10}OS$ 2a−d,4a, and C_7H_7ClOS 3a−d). An inclusion compound was prepared by three methods: (a) (*R,R*)-**1**

(1) Molecular Inclusion and Molecular Recognition-Clathrates I and II, *Topics in Current Chemistry*, Weber, E., Ed.;. Springer-Verlag: Berlin-Heidelberg, **1987** and **1988**; Vol. 140 and 149.

(2) *Comprehensive Supramolecular Chemistry*, NacNicol, D. D., Toda, F.; Bishop, R., Eds.; Pergamon: U.K., 1996; Vol. 9.

(3) Herbstein, F. H. *Acta Crystallogr.* **1997**, *B53*, 168.

(4) (a) Akazome, M.; Noguchi, M.; Tanaka, O.; Sumikawa, A.; Uchida, T.; Ogura, K. *Tetrahedron* **1997**, *53*, 8315. (b) Ogura, K.; Uchida, T.; Noguchi, M.; Minoguchi, M.; Murata, A.; Fujita, M.; Ogata, K. *Tetrahedron Lett.* **1990**, *31*, 3331.

(5) (a) Akazome, M.; Takahashi, T.; Ogura, K. *J. Org. Chem.* **1999**, *64*, 2293. (b) Akazome, M.; Yanagita, Y.; Sonobe, R.; Ogura K. *Bull. Chem. Soc. Jpn.* **1997**, *70*, 2823. (c) Akazome, M.; Sumikawa, A.; Sonobe, R.; Ogura, K. *Chem. Lett.* **1996**, 995.

(6) Optical resolution of sulfoxides using inclusion phenomena has been already reported by Toda et al. (a) Toda, F.; Tanaka, K.; Nagamatsu, S. *Tetrahedron Lett.* **1984**, *25*, 4929. (b) Toda, F.; Tanaka, K.; Mak, T. C. W. *Chem. Lett.* **1984**, 2085.

(7) As application for molecular recognition of sulfoxides, several NMR chiral shift reagents have been designed and reported for determination of the stereochemistry of sulfoxides and their enantiomeric excess: (a) Drabowicz, J.; Duddeck, H. *Sulfur Lett.* **1989**, *10*, 37. (b) Buist, P. H.; Marecak, D.; Holland, H. L.; Brown, F. M. *Tetrahedron: Asymmetry* **1995**, *6*, 7. (c) Charpin, P.; Duñach, E.; Kagan, H. B.; Theobald, F. R. *Tetrahedron Lett.* **1986**, *27*, 2989. (d) Deshmukh, M.; Duñach, E.; Juge, S.; Kagan, H. B. *Tetrahedron Lett.* **1984**, *25*, 3467.

10.1021/jo9910511 CCC: $19.00 © 2000 American Chemical Society
Published on Web 12/09/1999

UM00012838
NOVARTIS EXHIBIT 1017
Novartis v. Regents, IPR2023-01346
Page 1584 of 4460

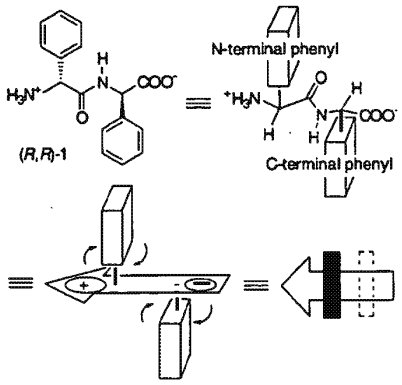


Figure 1. Structure of (*R*)-phenylglycyl-(*R*)-phenylglycine [(*R,R*)-**1**].

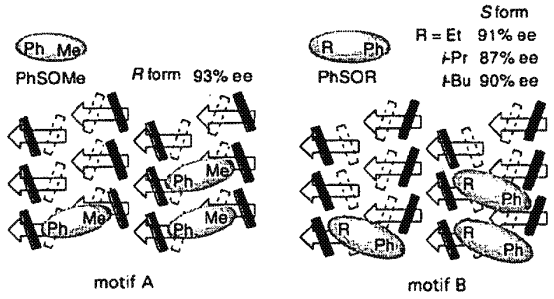


Figure 2. Schematic representation of the chiral cavities for alkyl phenyl sulfoxides.

was crystallized in the presence of the sulfoxide (method A, "crystallization"); (b) insoluble (*R,R*)-**1** was simply stirred in the presence of an alkyl phenyl sulfoxide and water for 24 h (method B, "sorption"); and (c) a mixture of a sulfoxide and solid (*R,R*)-**1** was coground in an agate mortar for 30 min (method C, "cogrinding").[8]

Results for the present inclusion are summarized in Table 1. The stereochemistry of inclusion in the dipeptide framework changes with the shape of the guest. Even if the CH_3 unit in the sulfoxides is replaced by a chlorine atom, the resulting sulfoxide isomers **3** (C_7H_7ClOS) seem to have a molecular volume comparable to that of **2** ($C_8H_{10}OS$).[9] In fact, a similar tendency was observed in their molecular recognition. The efficiency is the mole percentage of the guest molecule based on (*R,R*)-**1** molecule in the inclusion compound. Layer distances (L.D. in the tables) were determined by powder X-ray diffraction (PXRD). A series of the present inclusion

(8) Recently, it is known that inclusion compound could be obtain by directed cogrouding in the absence of solvent: (a) Scheffer, J. R.; Wohg, Y.-F.; Patil, A. O.; Curtion, D. Y.; Paul, I. C. *J. Am. Chem. Soc.* **1985**, *107*, 4898. (b) Toda, F.; Tanaka, K.; Sekikawa, A. *J. Chem. Soc., Chem. Commun.* **1987**, 279. (c) Etter, M. C.; Frankenbach, G. M. *Chem. Mater.* **1989**, *1*, 10. (d) Hollingworth, M. D.; Brown, M. E.; Santarsiero, B. D.; Huffman, J. C.; Goss, C. R. *Chem. Mater.* **1994**, *6*, 1227. (e) Caira, M. R.; Nassimbeni, L. R.; Wildervanck, *J. Chem. Soc., Perkin Trans. 2* **1995**, 2213. (f) Pedireddi, V. R.; Jones, W.; Chorlton, A. P.; Docherty, R. *Chem. Commun.* **1996**, 987. (g) Toda, F.; Miyamoto, H.; Kanemoto, K. *J. Org. Chem.* **1996**, 61, 6490.

(9) (a) Substiuent volumes of CH_3 and Cl are 13.67 and 12.00 cm^3/mol, respectively: Bond, A. *Physical Properties of Molecular Crystals, Liquids & Glasses*; Wiley: New York, 1968. (b) Substiuent radii of CH_3 and Cl are 2.00 and 1.80, respectively: Pauling, L. *The Nature of the Chemical Bond*; Oxford: London, 1940.

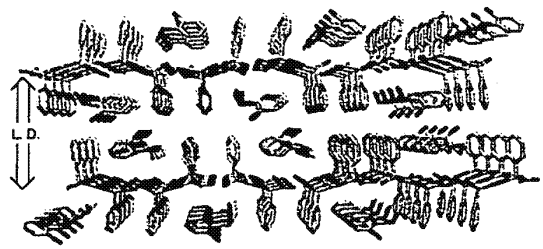


Figure 3. Perspective view of the inclusion compound of (*R*)-**3a** along the *c* axis.

compounds has a strong diffraction peak at lower 2θ range. Assignment of these layer distances was confirmed by the single-crystal structure (vide infra), because the strong peak of PXRD corresponds to the diffraction plane of the peptide backbones in the crystals.

Both 2-tolyl and 2-chlorophenyl sulfoxides (**2a** and **3a**) were recognized with high enantioselectivity of the *R* form (entries 1 and 2). In a previous paper, we reported that methyl phenyl sulfoxide is also recognized with the same enantioselectivity.[4a] Interestingly, substitution of the methyl group at the 3-position of the phenyl ring resulted in a drastic inversion of stereoselectivity. Both 3-tolyl and 3-chlorophenyl sulfoxides (**2b** and **3b**) were recognized with high *S* enantioselectivity (entries 3 and 4). However, 4-tolyl and 4-chlorophenyl sulfoxides (**2c** and **3c**) were included without the recognition of their chirality (entries 5 and 6). This phenomenon was also observed in the inclusion of benzyl methyl sulfoxide **4a** (entry 9).

Although ethyl phenyl sulfoxide **2d** was included by method A with high *S* enantioselectivity, chloromethyl phenyl sulfoxide **3d** was not included by any method (entries 7 and 8). It is likely that the terminal chlorine atom would electrically repel the π-face of the phenyl group of (*R,R*)-**1**,[4a] suggesting that alkyl−phenyl interaction (CH/π interaction[10]) is important for the inclusion of alkyl phenyl sulfoxides.

Irrespective of the three preparative methods, the obtained inclusion crystals showed the same PXRD pattern. Some sulfoxides were included by crystallization method A, but not by sorption method B or cogrinding method C. In the low efficiency of inclusion, especially by method C, the PXRD of the resulting crystals showed a pattern similar to that of the starting (*R,R*)-**1** crystal and the corresponding inclusion crystal. These results excluded the presence of other inclusion crystals.

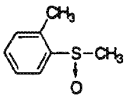
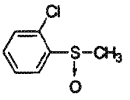
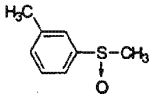
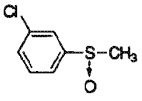
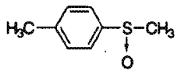
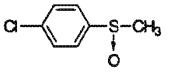
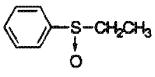
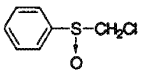
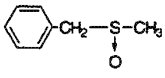
Crystal Structures of (*R,R*)-1 Dipeptide Sheets in Inclusion Compounds. The crystal structures of the inclusion compounds of (*R*)-**3a** and (*S*)-**2b** were determined by single-crystal X-ray analyses. The perspective views of the inclusion compounds are shown in Figures 3 and 4. The layer distance is half of the *b* axial length of the unit cell, which corresponds to diffraction from the (020) plane.

In the inclusion of **2c**, **3c**, and **4a**, optical resolution of the sulfoxide did not occur. Fortunately, we were able to obtain single crystals of the inclusion compound of **4a**. X-ray crystallographic analysis confirmed that both (*R*)- and (*S*)-enantiomers of **4a** were included in a crystal

(10) (a) Umezawa, Y.; Tsuboyama, S.; Honda, K.; Uzawa, J.; Nishio, M. *Bull. Chem. Soc. Jpn.* **1998**, *71*, 1207. (b) For a review of CH/π interaction: Nishio, M.; Umezawa, Y.; Hirota, M.; Takeuchi, Y. *Tetrahedron* **1995**, *51*, 8665 and references therein.

UM00012839
NOVARTIS EXHIBIT 1017
Novartis v. Regents, IPR2023-01346
Page 1585 of 4460

Table 1. Enantioselective Inclusion of Structural Isomers ($C_8H_{10}OS$ and C_7H_7ClOS) by (*R*,*R*)-1

Entry	Sulfoxide		A(crystallization) ee/%	Ef.[a]/%	B(sorption) ee/%	Ef.[a]/%	C(cogrinding) ee/%	Ef.[a]/%	L.D.[b]/ Å
1		2a	94(*R*)	98	92(*R*)	54	N. I.[c]		12.3
2		3a	99(*R*)	97	48(*R*)	100	N. I.[c]		12.4
3		2b	93(*S*)	98	92(*S*)	78	75(*S*)	87	13.3
4		3b	97(*S*)	100	92(*S*)	87	N. I.[c]		13.4
5		2c	Rac.[d]	93	18(*R*)	98	15(*R*)	88	12.4
6		3c	Rac.[d]	96	Rac.[d]	27	N. I.[c]		12.5
7[e]		2d	91(*S*)	95	N. I.[c]		N. I.[c]		13.3
8		3d	N. I.[c]		N. I.[c]		N. I.[c]		—
9		4a	Rac.[d]	100	Rac.[d]	100	Rac.[d]	42	12.8

[a] Ef. is the abbreviation for "efficiency" and is the mol % of guest based on (*R*,*R*)-**1** in the inclusion complex. [b] L.D. is a layer distance measured by XRD. [c] N.I. means no inclusion complex formed. [d] Rac. means enantioselectivity within 10%. [e] In ref 4a.

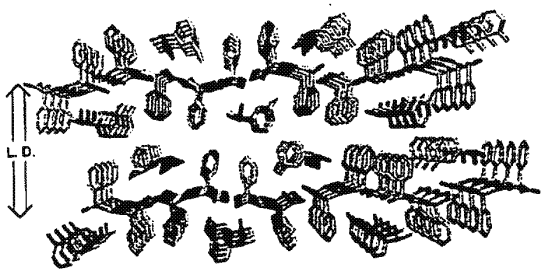


Figure 4. Perspective view of the inclusion compound of (*S*)-**2b** along the *c* axis.

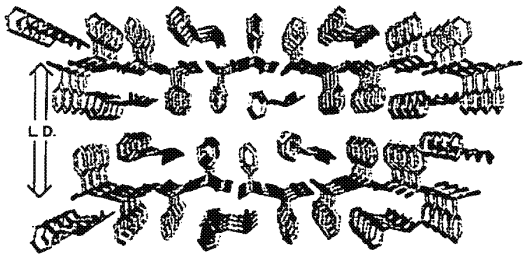


Figure 5. Perspective view of the inclusion compound of racemic **4a** along the *c* axis.

lattice of (*R*,*R*)-**1** (Figure 5). Interestingly, there are two conformers of (*R*,*R*)-**1** which construct a layer (vide infra). The *S* form of **4a** was included in the upper side cavity of the layer and the *R* form of **4a** in the lower side cavity of the same layer, but the side view is very similar to that of the two inclusion compounds mentioned above. In the PXRD analysis, this crystal also shows a layer distance that corresponds to a strong peak from the (010) plane, since this crystal has a *P*1 space group. The dipeptide sheets of the inclusion compound pile up to form a stacked layer structure in parallel.

To compare these methyl sulfoxides (**3a**, **2b**, and **4a**), the previously reported inclusion compound of (*S*)-ethyl phenyl sulfoxide (**2d**) is also shown in Figure 6.[4a] This arrangement of the dipeptide is very similar to the

UM00012840
NOVARTIS EXHIBIT 1017
Novartis v. Regents, IPR2023-01346
Page 1586 of 4460

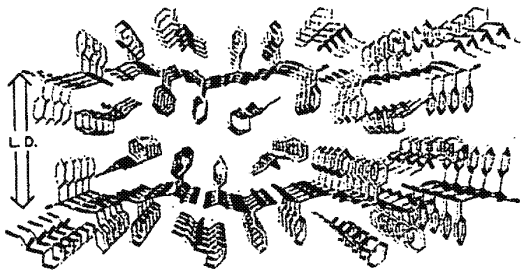
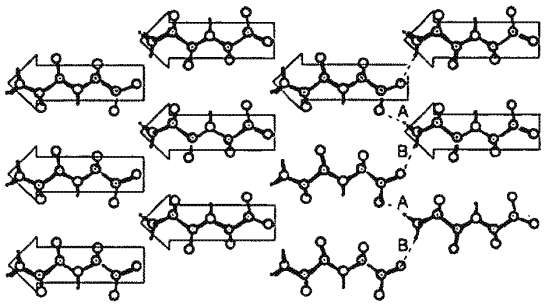


Figure 6. Perspective view of the inclusion compound of (*S*)-**2d** along the *c* axis.



		A N···O	B N···O	H-G N···O
2-ClC$_6$H$_4$SOMe	**3a**	2.72	2.79	2.77
3-TolSOMe	**2b**	2.67	2.79	2.75
BnSOMe	**4a**	2.75	2.73	2.78
		2.73	2.73	2.73
PhSOEt	**2d**	2.74	2.75	2.76

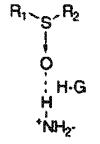


Figure 7. Dipeptide backbone and atomic distances between hydrogen bonds.

inclusion compound of (*S*)-**2b**, but the phenyl and the ethyl groups of (*S*)-**2d** replaced each other in position to realize *S* chirality. Judging from the inclusion of various methyl sulfoxides in (*R,R*)-**1** crystals, the methyl groups were always close to the C-terminal phenyl groups of (*R,R*)-**1**, which constructed the right wall of the void.

The hydrogen-bonding distances between $^+NH_3$ group and COO^- groups are summarized in Figure 7. In all of these inclusion crystals, the dipeptide backbones are very similar to each other. As for hydrogen-bonding distances between the sulfinyl oxygen and the ammonio group, these values are almost the same as the reported distances: 2.758(2) and 2.781(1) Å for SO···O of binaphthol[6] and 2.85(2) Å for SO(sulfinyl)···N(amide).[7c]

Crystal Structures of Chiral Cavities of (*R,R*)-1 for Enantioselective Inclusion. CPK models of the inclusion cavities are illustrated in Figures 8–10. Sheet structures are colored in black, guest sulfoxides in gray, and the phenyl groups of dipeptides in white. One molecule of the sulfoxide was deleted to clarify the inclusion cavity and the position of the ammonio group. These cavities are four motifs (A, B, pseudo-B, and C), which were characterized by the conformation of the phenyl groups of (*R,R*)-1.

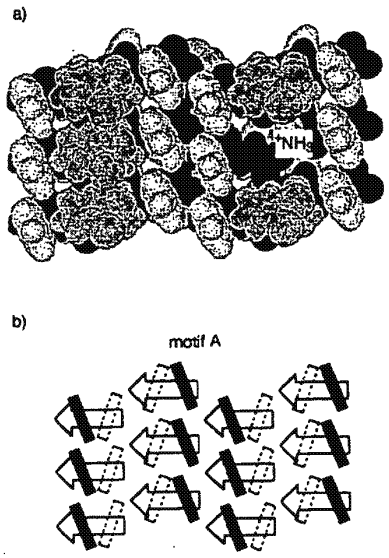


Figure 8. (a) CPK model of recognition site of (*R*)-**3a**. (b) Schematic representation of the chiral cavity (motif A).

As shown in Figure 8, (*R*)-2-chlorophenyl methyl sulfoxide **3a** is accommodated in a channel between the phenyl groups of (*R,R*)-**1**. It is notable that the phenyl–phenyl stacking mode of (*R,R*)-**1** was a "parallel stacking and displaced" mode (motif A)[11] and the methyl group of the sulfinyl was directed to the C-terminal phenyl group of the dipeptide. The 2-chlorophenyl group of **3a** was directed to the N-terminal phenyl group of the dipeptide, where "T"-mode phenyl–phenyl stacking occurred[11] (the distance between the hydrogen at the 4-position of the 2-chlorophenyl group of (*R*)-**3a** and the center of one phenyl ring of (*R,R*)-**1** is 2.56 Å). This motif A was also observed in the inclusion of (*R,R*)-bis[2-(methylsulfinyl-)benzyl] ether.[4a]

Figure 9a shows that (*S*)-methyl 3-tolyl sulfoxide **2b** was accommodated in a channel between the phenyl groups of (*R,R*)-**1**. These phenyl groups on the dipeptide layer interact in the "tilted T"-shaped mode and construct motif B. The methyl group of **2b** was directed to the C-terminal phenyl group of the dipeptide and the 3-tolyl group of **2b** to the N-terminal phenyl group. This cavity is very close to that of (*S*)-**2d**, but the guest molecule is arranged in a quite different manner: the ethyl group and phenyl group are directed to the phenyl groups of N-terminal and C-terminal, respectively (Figure 9b). Hence, the difference in volume between methyl and ethyl groups seems to be a crucial factor in positioning the guest sulfoxide in the cavity.

In the inclusion of racemic **4a**, there are two different recognition cavities on the upper side for its *S* enantiomer and on the lower side for its *R* enantiomer as mentioned above (Figure 5). The upper side cavity can be illustrated by motif pseudo-B, and the lower side one by motif C in

(11) Three types of interaction between two molecules of benzene ("tilted T", "T", and "parallel stacked and displaced" modes) must be taken into consideration. Jorgensen and Severance calculated these benzene dimers by the Monte Carlo method to show that they have comparable energies: Jorgensen, W. L.; Severance, D. L. *J. Am. Chem. Soc.* **1990**, *112*, 4768.

UM00012841
NOVARTIS EXHIBIT 1017
Novartis v. Regents, IPR2023-01346
Page 1587 of 4460

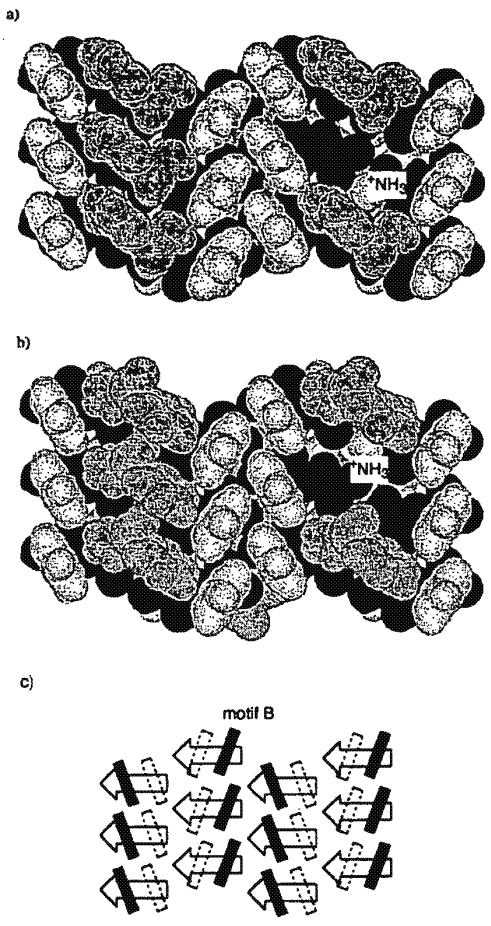


Figure 9. (a) CPK models of recognition site of (*S*)-**2b**. (b) CPK models of recognition site (*S*)-**2d**. (c) Schematic representation of the chiral cavity (motif B).

Figure 10. These cavities are just like a mirror image to each other in shape. In these cases, (*R*)- and (*S*)-benzyl methyl sulfoxides directed the methyl group and benzyl groups to the C-terminal phenyl group and to the N-terminal phenyl group, respectively. This arrangement makes the phenyl groups of (*R*,*R*)-**1** and **4a** pack tightly in the usual herringbone motif.[12,13]

From the CPK models of Figure 10, it can be assumed that, when a methyl group is introduced into the α-position of the benzyl group, the inclusion is not retarded if the methyl is located at the front site. Therefore, the (α*R**,S*S**)-isomer of methyl α-methylbenzyl sulfoxide **4b** is expected to be preferentially recognized by (*R*,*R*)-**1** crystals. According to the literature, oxidation of α-methylbenzyl methyl sulfides affords a mixture of sulfoxides, and the ratio is (α*R**, S*S**):(α*R**, S*R**) = 1:3.[14] The guest molecule (**4b**) was included by method A, but not by method B. As for the variation of the guest amount, the results of crystallization are summarized in Scheme 1. The stereochemisrty of the products was determined by comparison with authentic samples synthesized by other routes,[15] and the distributions of the diastereomers were determined by the chiral shift reagent (*S*)-MPAA.[7b]

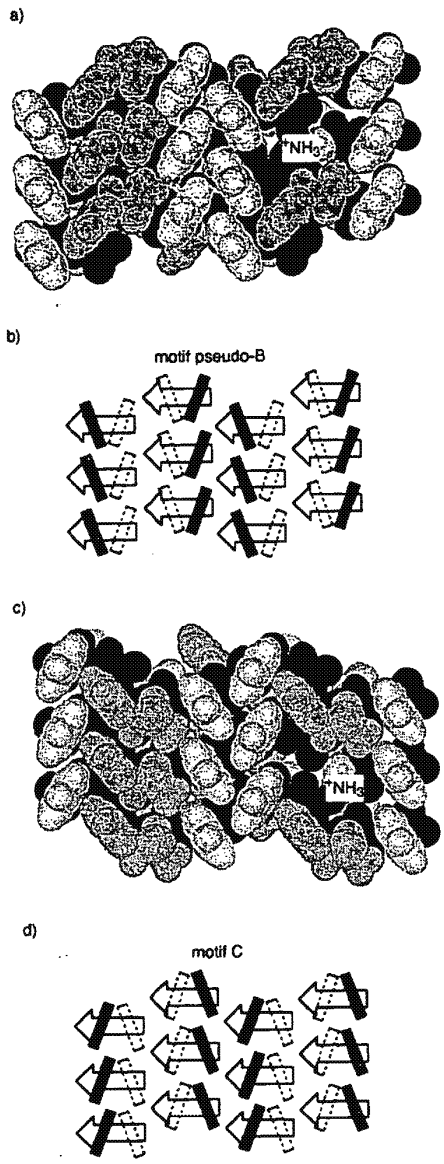


Figure 10. (a and c) CPK models of recognition sites of racemic **4a**. Recognition sites for (*S*)-**4a** (a) and (*R*)-**4a** (c). (b and d) Schematic representation of the corresponding chiral cavities (motifs pseudo-B and C).

(12) (a) Swift, J. A.; Pal, R.; McBride, J. M. *J. Am Chem. Soc.* **1998**, *120*, 96. (b) Lewis, F. D.; Yang, J.-S.; Stern, C. L. *J. Am Chem. Soc.* **1996**, *118*, 12029. (c) Hunter, C. A.; Sanders, J. K. M. *J. Am Chem. Soc.* **1990**, *112*, 5525. (d) Desiraju, G. R.; Gavezzotti, A *J. Chem. Soc., Chem. Commun.* **1989**, 621. (e) Gavezzotti, A *Chem. Phys. Lett.* **1989**, *161*, 67.

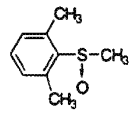
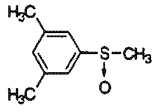
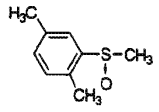
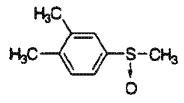
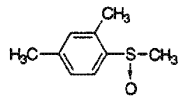
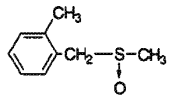
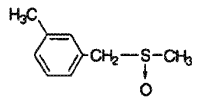
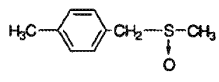
(13) In proteins, $\pi-\pi$ interactions on their side chains have already been investigated to reveal the edge-to-face interaction between two benzene rings to be important: (a) Burley, S. K.; Petsko, G. A. *Science* **1985**, *229*, 23. (b) Gould, R. O.; Gray, A. M.; Taylor, P.; Walkinshaw, M. D. *J. Am. Chem. Soc.* **1985**, *107*, 5921. (c) Burley, S. K.; Petsko, G. A. *J. Am. Chem. Soc.* **1986**, *108*, 7995.

(14) (a)Nishihata, K.; Nishio, M. *Tetrahedron Lett.* **1977**, *12*, 1041.

(15) (a) Nishihata, K.; Nishio, M. *Chem. Commun.* **1971**, 958. (b) Hoffmann, H. M.; Hughes, E. D. *J. Chem. Soc.* **1964**, 1244. (c) Burwell, R. L.; Shields, A. D.; Hart, H. *J. Am. Chem. Soc.* **1954**, 908.

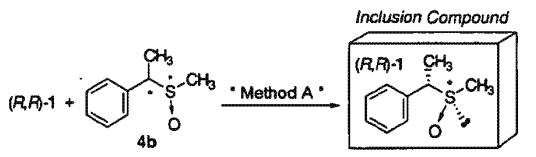
UM00012842
NOVARTIS EXHIBIT 1017
Novartis v. Regents, IPR2023-01346
Page 1588 of 4460

Table 2. Inclusion of Structural Isomers with Methylsulfinyl Group ($C_9H_{12}OS$) by (*R*,*R*)-1

Entry	Sulfoxide		A(crystal.) ee/%	A(crystal.) Ef.[a]/%	B(sorption) ee/%	B(sorption) Ef.[a]/%	L.D.[b]/ Å
1		**2e**	87(*R*)	99	72(*R*)	67	14.0
2		**2f**	91(*S*)	99	77(*S*)	100	13.7
3		**2g**	73(*S*)	100	58(*S*)	85	13.6
4		**2h**	85(*S*)	91	79(*S*)	99	13.4
5		**2i**	30(*R*)	80	N. I.[c]		12.3
6		**4c**	Rac.[d]	100	Rac.[d]	100	13.0
7		**4d**	82(*R*)	100	88(*R*)	90	12.7
8		**4e**	N. I.[c]		N. I.[c]		—

[a] Ef. is the abbreviation for "efficiency" and is the mol % of guest based on (*R*,*R*)-**1** in the inclusion complex. [b] L.D. is a layer distance measured by XRD. [c] N.I. means no inclusion complex formed. [d] Rac. means enantioselectivity within 10%.

Scheme 1



Sulfoxide / mol equiv	Ef. /%	Distribution of diastereomers / % (αS, SR)	(αR, SS)	(αR, SR)	(αS, SS)
Starting material		13	13	37	37
2	69	40	33	17	10
4	87	47	32	13	8
8	100	63	21	10	6

As expected, two enantiomers (α*R**,*SS**) could be recognized and included preferably from the diastereomeric mixture in the presence of 2−4 mol equiv of **4b**. Using an 8-fold amount of **4b**, the (α*S*,*SR*)-enantiomer is recognized more predominantly than the (α*R*,*SS*)-enamtiomer. Since the stereochemistry on the sulfur atom of recognized (α*S*,*SR*)-**4b** was the *R* form, (*R*,*R*)-**1** would construct a cavity similar to that for (*R*)-**4a**.

Inclusion of Structural Isomers of One-Carbon Homologous Sulfoxides ($C_9H_{12}OS$). Results for methyl xylyl sulfoxides **2e**−**i** and methyl tolylmethyl sulfoxides **4c**−**e** ($C_9H_{12}OS$), one-carbon homologues of $C_8H_{10}OS$, are summarized in Table 2.

We examined how substitution of two methyl groups on the phenyl group of methyl phenyl sulfoxide influences the inclusion stereoselectivity. In the case of **2e**, two methyl groups at the ortho positions of the phenyl group were shown to be tolerant to the present inclusion, because its *R* form was included in the cavity with expansion of the layer distance to 14.0 Å (entry 1). In a similar manner to methyl 3-tolyl sulfoxide (**2b**), methyl 3,5-, 2,5-, or 3,4-xylyl sulfoxides (**2f**, **2g**, or **2h**) was recognized as their *S* forms (entries 2−4). Therefore, it was suggested that the methyl group at the meta position

UM00012843
NOVARTIS EXHIBIT 1017
Novartis v. Regents, IPR2023-01346
Page 1589 of 4460

of the phenyl group was crucial for its *S* selectivity. Since 4-tolyl sulfoxide **2c** was not enantiomerically recognized at all, the *R* enantioselectivity of 2,4-xylyl sulfoxide **2i** seems to be attributable to some degree to the 2-methyl group (entry 5).

The sulfoxides having a benzyl skeleton (**4c–e**) were also examined. The substitution on the 2-position did not affect the enantioselectivity of **4c**, but that of the 3-position drastically induced the enantiomeric inclusion for the *R* form of **4d** (entries 6 and 7). Two possible origins of the high *R* enantioselective inclusion can be rationalized: first, the 3-methylbenzyl group of **4d** might have a conformation like the 2,6-xylyl group of (*R*)-**2e**; second, (*R,R*)-**1** would construct only the *R* site of the inclusion compound of **4a**, and (*R*)-**4d** was included in it. The latter is more plausible, because the inclusion compound of (*R*)-**4d** shows a shorter layer distance (12.7 Å), which is rather comparable to that of **4a** (12.8 Å) than that of (*R*)-**2e** (14.0 Å). It should be noted that the substitution at the 4-position disturbed the inclusion of **4e** (entry 8). This is probably because **4e** is too large to be included in the void.

Conclusion Remarks

(*R*)-Phenylglycyl-(*R*)-phenylglycine [(*R,R*)-**1**] molecules self-assemble through intermolecular salt formation to form layers, on which an enantiomeric cavity is produced between the walls of the phenyl groups of (*R,R*)-**1** to recognize various sulfoxide guests. In this paper, we demonstrated the flexibility of the inclusion cavity on the lattice of crystalline (*R,R*)-**1** to have high potential for molecular recognition of structurally isomeric sulfoxides which have a similar volume. It was also shown that a slight difference in molecular shape induced a drastic change of conformation of (*R,R*)-**1** and the stereoselectivity of recognized sulfoxide molecules.

In sharp contrast to ethyl or isopropyl phenyl sulfoxide, methyl sulfoxides bearing a phenyl or benzyl group are structurally different when included: the methyl groups of sulfoxides were always directed to the C-terminal phenyl groups of (*R,R*)-**1**. It is important for the conformation of the C-terminal phenyl group to determine which binds to the ammonio proton via hydrogen bonding, the *R* or *S* form of the methyl sulfinyl group (Figure 11). In other words, the methyl sulfoxide induces the conformation of the dipeptide to make the shape of the recognition cavity fit for its sulfinyl group.

Experimental Section

General. (*R*)-Phenylglycine (99% ee) was purchased from Tokyo Chemical Industry. Chiral shift reagents, (*S*)-α-methoxyphenylacetic acid [(*S*)-MPAA] and (*R*)-(+)-2,2′-dihydroxy-1,1′-binaphthyl [(*R*)-BINOL], were purchased from Aldrich and Kankyo Kagaku Center, respectively.

Synthesis of (*R*)-Phenylglycyl-(*R*)-phenylglycine [(*R,R*)-1].[16] As for protection of the carboxylic group of (*R*)-phenylglycine, the benzyl ester *p*-toluenesulfonate was prepared in 98% yield according to a literature:[17] colorless powder; mp 191–192 °C; $[\alpha]^{25}_D = -35.3$ ($c = 2.00$, MeOH); ^{1}H NMR (300 MHz, $CDCl_3$) δ 2.29 (s, 3H), 4.93 (d, 1H, 12.4 Hz), 4.96 (d, 1H, 12.4 Hz), 5.13 (s, br, 1H), 6.97 (d, 2H, 8.1 Hz), 7.00–7.28 (m, 10H), 7.51 (d, 2H, 8.1 Hz), 8.70 (s, br, 3H); IR (KBr) 3220, 3360, 1749, 1597, 1497 cm^{-1}. Anal. Calcd for $C_{22}H_{22}NO_5S$: C, 63.91; H, 5.61; N, 3.39. Found: C, 63.78; H, 5.59; N, 3.40.

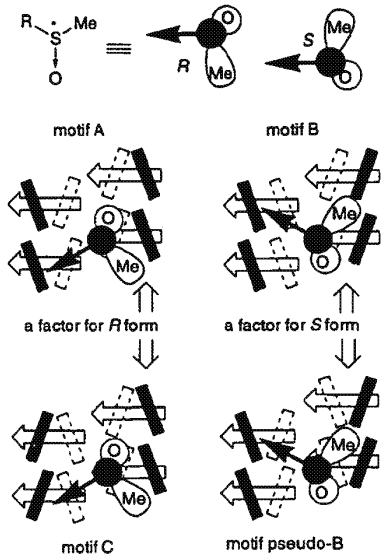


Figure 11. Schematic representation of C-terminal phenyl groups as a factor to determine the stereochemistry of the sulfoxides.

According to the DCC–HOBt method,[18] coupling between (*R*)-*N*-(benzyloxycarbonyl)phenylglycine[19] (12.8 g, 45.0 mmol) and (*R*)-phenylglycine benzyl ester *p*-toluenesulfonate (18.6 g, 45.0 mmol) provided the protected dipeptide (20.8 g, 40.9 mmol, yield 91%): mp 193.5–195 °C; $[\alpha]^{25}_D = -93.2$ ($c = 2.1$, $CHCl_3$); ^{1}H NMR (300 MHz, CD_3OD) δ 5.09 (s, 4H), 5.40 (s, 1H), 5.53 (s, 1H), 7.13–7.45 (m, 20H); IR (KBr) 3320, 3040, 1732, 1718, 1690, 1654, 1526 cm^{-1}.

The protected dipeptide (8.50 g, 16.7 mmol) was dissolved in a mixture of MeOH (80 mL), AcOH (20 mL), and water (10 mL) and treated with hydrogen in the presence of Pd black (prepared from $PdCl_2$, 0.76 g, 4.3 mmol) overnight. The catalyst was removed by filtration, and concentration of the filtrate gave a solid. The solid was dissolved in 0.2 M aqueous HCl, the pH was adjusted to about 6.5 by the addition of 5 M aqueous NaOH. The solution was concentrated until a small amount of a solid was deposited. Then the solution was stored to precipitate crystalline (*R,R*)-**1** in a refrigerator overnight. Colorless powder (*R,R*)-**1** was collected, washed with water, and dried in vacuo (4.27 g, 15.0 mmol, yield 88%). (*R,R*)-**1**: mp 220–223 °C, (dec) $[\alpha]^{25}_D = -137.2$ ($c = 0.99$, 0.2 M HCl); ^{1}H NMR (300 MHz, DCl + D_2O) δ 5.24 (s, 1H), 5.50 (s, 1H), 7.41–7.46 (m, 5H), 7.53 (s, br, 5H); IR (KBr) 3370, 3300, 1676, 1560, 1508 cm^{-1}. Anal. Calcd for $C_{16}H_{16}N_2O_3$: C, 67.59; H, 5.67; N, 9.85. Found: C, 67.36; H, 5.81; N, 9.81.

Synthesis of Sulfoxide 2, 3, and 4. Sulfides were prepared from corresponding halides and thiols by Williamson-type sulfide synthesis, except for **3d**.[20] Oxidation of sulfide was proceeded by hydrogen peroxide in acetic acid or sodium metaperiodate.[21] In the case of **3d**, methyl phenyl sulfoxide was chlorinated by our procedure.[22]

(16) Akazome, M.; Matsuno, H.; Ogura, K. *Tetrahedron: Asymmetry* **1997**, *8*, 2331.

(17) Zervas, L.; Winitz, M.; Greenstein, J. P. *J. Org. Chem.* **1957**, *22*, 1515.

(18) König, W.; Geiger, R. *Chem. Ber.* **1970**, *103*, 788.

(19) Doyle, F. P.; Fosker, G. R.; Nayler, J. H. C.; Smith, H. *J. Chem. Soc.* **1962**, 1440.

(20) Sandler, S. R.; Karo, W. *Organic Functional Group Preparations*, 2nd ed.; Academic Press: San Diego, 1989; Vol. I, Chapter 18, p 585.

(21) Sandler, S. R.; Karo, W. *Organic Functional Group Preparations*, 2nd ed.; Academic Press: San Diego, 1989; Vol. I, Chapter 19, p 603.

(22) Tsuchihashi, G.; Ogura, K.; Iriuchijima, S.; Tomisawa, S. *Synthesis* **1971**, 91.

UM00012844
NOVARTIS EXHIBIT 1017
Novartis v. Regents, IPR2023-01346
Page 1590 of 4460

Preparation of Inclusion Compounds of Alkyl Phenyl Sulfoxide and (*R,R*)-1. Method A. (*R,R*)-**1** (1.0 mmol) was dissolved in 0.1 M aqueous HCl, then the pH was adjusted to about 6.5 by the addition of 0.1 M aqueous NaOH.[4a] After the addition of a racemic sulfoxide (**2**, **3**, or **4**) (2.0 mmol) to the aqueous solution of (*R,R*)-**1**, the resulting mixture was allowed to stand at an ambient temperature for several days. The deposited inclusion compound was collected by filtration and washed with water (20 mL) and $CHCl_3$ (20 mL).

Method B. Crystals of (*R,R*)-**1** are essentially insoluble in organic solvents and water. A suspension of (*R,R*)-**1** (1.0 mmol) in water (2 mL) was stirred together with a racemic sulfoxide (**2**, **3**, or **4**) (2.0 mmol) at ambient temperature for 1 day. The formed inclusion compound was collected by filtration and washed with water (20 mL) and $CHCl_3$ (20 mL).

Method C. An agate mortar and (*R,R*)-**1** were dried in a desiccator. A mixture of (*R,R*)-**1** (1.0 mmol) and a racemic sulfoxide (**2**, **3**, or **4**) (2.0 mmol) was often grounded in an agate mortar at ambient temperature for 30 min. To keep dry, the mortar was stored in a desiccator when not being used. The formed inclusion compound was washed with water (20 mL) and $CHCl_3$ (20 mL).

Determination of Efficiency, Stereochemistry, and Enantiomeric Excess in the Inclusion. After decomposition of the inclusion compound with diluted DCl in D_2O, inclusion efficiency was determined by NMR measurement. The included sulfoxide was isolated by dissolution of the inclusion compound in 0.1 M aqueous HCl (40 mL) and extraction with $CHCl_3$. The absolute stereochemistry of recognized sulfoxides was determined by comparison of the optical rotation to the value of the literature and/or by chiral shift reagents [(*R*)-(+)-2,2′-dihydroxy-1,1′-binaphthyl[7a] ((*R*)-BINOL, 1 mol equiv for the sulfoxide) and (*S*)-α-methoxyphenyl acetic acid[7b] ((*S*)-MPAA, 3 mol equiv for the sulfoxide)]. Enantiomeric excess of the sulfoxide was determined by a chiral HPLC (Daicel Chiralcel OB).

2c, **3c**, **4a**, and **4c** were not recognized enantiomerically, and **3d** and **4e** were not included at all.

2a $[\alpha]^{25}_D$ = +190.5 (*c* = 1.3, acetone); 92% ee *R* by [α];[23] HPLC eluent, hexane/2-propanol (4:1), flow rate = 0.6 mL/min, $t_R(S)$ = 11.0 min, t_R (*R*) = 22.8 min); ^{1}H NMR (with (*R*)-BINOL in $CDCl_3$) δ 2.64 (s, 2.6H, *R* major), 2.65 (s, 0.4H, *S* minor), 2.36 (s, 3H), 7.19−7.61 (m, 4H).

2b: $[\alpha]^{25}_D$ = −120.4 (*c* = 1.0, EtOH); 92% ee *S* by [α],[6b] HPLC eluent, hexane/2-propanol (4:1), flow rate = 0.6 mL/min, $t_R(S)$ = 10.7 min, $t_R(R)$ = 15.4 min); ^{1}H NMR (with (*R*)-BINOL in $CDCl_3$) δ 2.41 (s, 3H), 2.67 (s, 0.1H, *R* minor), 2.68 (s, 2.9H, *S* major), 7.45 (s, 1H). Aromatic 3H could be not identified because of the binaphthyl group.

2c: $[\alpha]^{25}_D$ = +21.0 (*c* = 2.2, acetone); 18% ee *R* by [α],[24] HPLC eluent, hexane/2-propanol (4:1), flow rate = 0.6 mL/min, $t_R(S)$ = 11.6 min, $t_R(R)$ = 22.9 min); ^{1}H NMR (with (*R*)-BINOL in $CDCl_3$) δ 2.67 (s, 1.8H, *R* major), 2.68 (s, 1.2H, *S* minor), 2.41 (s, 3H), 7.32 (d, 2H 8.2 Hz), 7.52 (d, 2H, 8.2 Hz).

2d: $[\alpha]^{25}_D$ = −143.1 (*c* = 1.4 EtOH); 74% ee *S* by [α],[25a,b] HPLC eluent, hexane/2-propanol (4:1), flow rate = 0.7 mL/min, $t_R(S)$ = 11.3 min, $t_R(R)$ = 20.5 min).

3a: $[\alpha]^{25}_D$ = +140.6 (*c* = 1.0, acetone); 48% ee *R* by HPLC; HPLC eluent, hexane/2-propanol (9:1), flow rate = 0.7 mL/min, $t_R(S)$ = 18.5 min, $t_R(R)$ = 23.6 min); ^{1}H NMR (with (*R*)-BINOL in $CDCl_3$) δ 2.78 (s, 2.2H, *R* major), 2.79 (S, 0.8H, *S* minor). Aromatic 4H could be not identified because of the binaphthyl group.

3b: $[\alpha]^{25}_D$ = −85.2 (*c* = 0.87, acetone); 92% ee *S* by HPLC; HPLC eluent, hexane/2-propanol (9:1), flow rate = 0.7 mL/min, $t_R(S)$ = 18.3 min, $t_R(R)$ = 27.0 min); ^{1}H NMR (with (*R*)-BINOL in $CDCl_3$) δ 2.69 (s, 0.1H, *R* minor), 2.70 (s, 2.9H, *S* major), 7.43−7.48 (m, 3H), 7.64−7.64 (m, 1H).

2e: $[\alpha]^{25}_D$ = +177.9 (*c* = 1.1, acetone); 72% ee *R* by HPLC; HPLC eluent, hexane/2-propanol (20:1), flow rate = 0.6 mL/min, $t_R(S)$ = 25.7 min, $t_R(R)$ = 28.2 min); ^{1}H NMR (with (*R*)-BINOL in $CDCl_3$) δ 2.84 (s, 2.6H, *R* major), 2.84 (s, 0.4H, *S* minor), 2.58 (s, 6H), 7.04 (d, 2H, 7.6 Hz), 7.22 (t, 1H, 7.6 Hz)

2g: $[\alpha]^{25}_D$ = −87.8 (*c* = 1.3, acetone); 73% ee *S* by NMR, ^{1}H NMR (with (*R*)-BINOL in $CDCl_3$) δ 2.63 (s, 2.60H, *R* minor), 2.64 (s, 0.40H, *S* major), 2.31 (s, 3H), 2.39 (s, 3H), 7.08 (d, 1H, 7.8 Hz), 7.14 (d, 1H, 7.8 Hz), 7.73 (s, 1H). HPLC showed no baseline separation (eluent, hexane/2-propanol (20:1), flow rate = 0.5 mL/min, $t_R(S)$ = 38.3 min, $t_R(R)$ = 40.9 min).

2i: $[\alpha]^{25}_D$ = +57.86 (*c* = 0.59, acetone), 30% ee *R* by NMR; ^{1}H NMR (with (*R*)-BINOL in $CDCl_3$,) δ 2.63 (s, 1.95H *R* major), 2.64 (s, 1.05H, *S* minor), 2.33 (s, 3H), 2.36 (s, 3H), 7.01 (s, 1H), 7.23 (d, 1H, 8.0 Hz), 7.80 (d, 1H, 8.0 Hz). HPLC showed no baseline separation (eluent, hexane/2-propanol (20:1), flow rate = 0.5 mL/min, $t_R(S)$ = 32.3 min, $t_R(R)$ = 34.8 min).

2f: $[\alpha]^{25}_D$ = −102.59 (*c* = 0.925, acetone); 77% ee *S* by HPLC; HPLC eluent, hexane/2-propanol (9:1), flow rate = 0.6 mL/min, $t_R(S)$ = 16.8 min, $t_R(R)$ = 23.5 min); ^{1}H NMR (with (*R*)-BINOL in $CDCl_3$) δ 2.37 (s, 6H), 2.67 (s, 0.3H, *R* minor), 2.68 (s, 2.7H, *S* major), 7.11 (s, 1H), 7.23 (s, 2H).

2h: $[\alpha]^{25}_D$ = −111.33 (*c*=0.98, acetone); 79% ee *S* by HPLC; HPLC eluent, hexane/2-propanol (9:1), flow rate = 0.6 mL/min, $t_R(S)$ = 20.8 min, $t_R(R)$ = 41.3 min); ^{1}H NMR (with (*R*)-BINOL in $CDCl_3$, 75% ee *S*) δ 2.304 (s, 3H), 2.309 (s, 3H), 2.648 (s, 0.4H, *R* minor), 2.662(s, 2.6H, *S* major). Aromatic 3H could be not identified because of the binaphthyl.

4b starting material (major/minor = 3:1):[15a] ^{1}H NMR ($CDCl_3$) (major, α*R**,*SR**) δ 1.75 (d, 3H, 7.1 Hz), 2.30 (s, 3H), 3.76 (q, 1H, 7.1 Hz), 7.08−7.44 (m, 5H), (minor, α*R**,*SS**) δ 1.73 (d, 3H, 7.1 Hz), 2.18 (s, 3H), 3.86 (q, 1H, 7.1 Hz), 7.08−7.44 (m, 5H). ^{1}H NMR (with (*S*)-MPAA in $CDCl_3$) (major, α*S,SS*) δ 1.72 (d, 3H, 7.1 Hz), 2.34 (s,3H), 3.93 (q, 1H, 7.1 Hz), (major, α*R,SR*) 1.69 (d, 3H, 7.1 Hz), 2.35 (s, 3H), 3.95 (q, 1H, 7.1 Hz), (minor, α*R,SS*) 1.69 (d, 3H, 7.1 Hz), 2.24 (s,3H), 3.99 (q, 1H, 7.1 Hz), (minor, α*S,SR*) 1.68 (d, 3H, 7.1 Hz), 2.26 (s, 3H), 4.12 (q, 1H, 7.1 Hz). Aromatic H could be not identified because of (*S*)-MPAA.

4d: $[\alpha]^{25}_D$ = −55.7 (*c* = 1.1, acetone), 81% ee *R* by NMR; ^{1}H NMR (with (*S*)-MPAA in $CDCl_3$) δ 2.33 (s, 3H), 2.49 (s, 0.27H, *S* minor), 2.51 (s, 2.72H, *R* major), 3.94 (d, 0.91H *J* = 12.7 Hz, *R* major), 3.95 (d, 0.09H, *J* = 12.7 Hz, S minor), 4.17 (d, 1H, *J* = 12.6 Hz), 7.23 (t, 1H 7.6 Hz), 7.14 (d, 1H, 7.6 Hz), 7.06 (s, 1H), 7.04 (d, 1H, 7.6 Hz). HPLC showed no baseline separation (eluent, hexane/2-propanol (9:1), flow rate = 0.6 mL/min, $t_R(S)$ = 29.4 min, $t_R(R)$ = 33.4 min).

X-ray Analyses. X-ray powder diffractions were obtained with a MAC Science MXP diffractometer using graphite-monochromated Cu Kα radiation (40 kV, 300 mA). The spectra were measured at room temperature between 2° and 50° in the 2θ scan mode with steps of 0.01° in 2θ and 4°/min.

Crystallographic Data for the Inclusion Compounds. To the solution of (*R,R*)-**1** was added a methanol solution of the guest (**3a**, **2b**, or **4a**) directly in a vial, then the lid of the vial was loosely closed for evaporation of the solvent. The samples were allowed to stand for several days to form the desirable single crystals. Data of an inclusion complex with **2d** were already reported in our previous paper.[4a] Data collection was performed on a Mac Science MXC18 four-circle diffractometer with graphite-monochromated Cu Kα (λ = 1.541 78) radiation using the 2θ−ω scan technique, and the X-ray intensities were measured up to 2θ = 140° at 298 K. The structures were solved by a direct method SIR 92[26] and refined by a computer program package, CRYSTAN-GM ver. 6.2.1 or maXus ver. 1.1 from MAC Science Co. Ltd. Hydrogen atoms are calculated in the appropriate position.

The inclusion compound of 3a (2-chlorophenyl methyl sulfoxide): $C_{23}H_{23}ClN_2O_4S$, *M* = 459.00, crystal dimensions 0.15 × 0.10 × 0.05 mm, orthorhombic, $P2_12_12_1$, *a* = 16.226(4) Å, *b* = 24.679(6) Å, *c* = 5.635(2) Å, *V* = 2256.5(9) Å^3, *Z* = 4,

(23) Duñach, E.; Kagan, H. B. *Nouv. J. Chim.*, **1985**, *9*, 1.
(24) Brunel, J.-M.; Diter, P.; Duetsch, M.; Kagan, H. B. *J. Org. Chem.* **1995**, *60*, 8086.
(25) (a) Mikolajczyk, M.; Drabowicz, J. *J. Am. Cem. Soc.* **1978**, *100*, 2510. (b) Rebiere, F.; Samuel, O.; Ricard, L.; Kagan, H. B. *J. Org. Chem.* **1991**, *56*, 5991.

(26) Altomare, A.; Cascarano, G.; Giacovazzo, C.; Guagliardi, A.; Burla, M. C.; Polidori, G.; Camalli, M. *J. Appl. Crystallogr.* **1994**, *27*, 435.

UM00012845
NOVARTIS EXHIBIT 1017
Novartis v. Regents, IPR2023-01346
Page 1591 of 4460

ρ_{calcld} = 1.35 g cm^{-3}, 2594 reflections measured, 2268 independent, R = 0.085 (1291 reflections with $I > 1.00\sigma(I)$), R_w = 0.068, 297 parameters, with heavy atoms refined anisotropically, residual electron density 0.44/−0.36.

The inclusion compound of 2b (methyl 3-tolyl sulfoxide): $C_{24}H_{26}N_2O_4S$, M = 438.55, crystal dimensions 0.10 × 0.05 × 0.05 mm, orthorhombic, $P2_12_12_1$, a = 15.953(4) Å, b = 26.586(6) Å, c = 5.628(2) Å, V = 2234.2(9) Å^3, Z = 4, ρ_{calcld} = 1.30 g cm^{-3}, 4911 reflections measured, 3951 independent, R = 0.131 (2251 reflections with $I > 1.00\sigma(I)$), R_w = 0.077, 150 parameters. This very small crystal afforded weak diffraction, so heavy atoms refined isotropically except for the sulfur atom, residual electron density 0.41/−0.42.

The inclusion compound of 4a (benzyl methyl sulfoxide): $C_{24}H_{26}N_2O_4S$, M = 438.55, crystal dimensions 0.40 × 0.15 × 0.05 mm, triclinic, $P\bar{1}$, a = 5.446(2) Å, b = 13.908(3) Å, c = 16.164(3) Å, α = 69.815(15), β = 88.028(22), γ = 79.457(21), V = 1129.2(5) Å^3, Z = 2, ρ_{calcld} = 1.29 g cm^{-3}, 4911 reflections measured, 3951 independent, R = 0.067 (2251 reflections with $F > 3.00\sigma(F)$); R_w = 0.074, 632 parameters, with heavy atoms refined anisotropically, residual electron density 0.33/−0.41.

Acknowledgment. This work was supported by Grant-in-Aids for Research for the Future Program (JSPS-RFTF96P00304) and Encouragement of Young Scientists (No. 11750733) from The Japan Society for the Promotion of Science.

Supporting Information Available: Tables of atomic coordinates and thermal parameters, bond lengths and angles, and ORTEP views of inclusion compounds of (*R*)-**3a**, (*S*)-**2b**, and racemic **4a**. This material is available free of charge via the Internet at http://pubs.acs.org.

JO991051L

UM00012846
NOVARTIS EXHIBIT 1017
Novartis v. Regents, IPR2023-01346
Page 1592 of 4460

Acta Crystallographica Section E
Structure Reports Online
ISSN 1600-5368

One-dimensional hydrogen-bonded molecular tapes in 1,4-bis[(4-pyridinio)ethynyl]benzene chloranilate

Md. Akhtaruzzaman,[a] Masaaki Tomura[b]* and Yoshiro Yamashita[c]

[a]Department of Structural Molecular Science, The Graduate University for Advanced Studies, Myodaiji, Okazaki 444-8585, Japan, [b]Institute for Molecular Science, Myodaiji, Okazaki 444-8585, Japan, and [c]Department of Electronic Chemistry, Interdisciplinary Graduate School of Science and Engineering, Tokyo Institute of Technology, Nagatsuta, Midori-ku, Yokohama 226-8502, Japan

Correspondence e-mail: tomura@ims.ac.jp

Key indicators

Single-crystal X-ray study
T = 296 K
Mean σ(C–C) = 0.005 Å
R factor = 0.053
wR factor = 0.161
Data-to-parameter ratio = 12.0

For details of how these key indicators were automatically derived from the article, see http://journals.iucr.org/e.

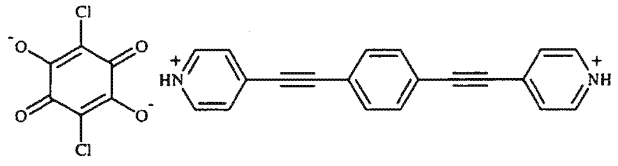
© 2001 International Union of Crystallography
Printed in Great Britain – all rights reserved

Received 8 March 2001
Accepted 15 March 2001
Online 23 March 2001

The structure of the title compound, $C_{20}H_{14}N_2^{2+}\cdot C_6Cl_2O_4^{2-}$, contains one-dimensional hydrogen-bonded molecular tapes along the [113] direction. The molecular tapes are connected *via* two N—H···O hydrogen bonds in $R_1^2(5)$ patterns.

Comment

We have recently shown that the simple combination of chloranilic acid and dipyridyl-type ligands can create a variety of supramolecular architectures involving infinite one-dimensional molecular tape structures (Zaman *et al.*, 1999, 2000). In the course of our crystal engineering studies on chloranilic acid, we have obtained the title compound, (I), a 1:1 co-crystal of chloranilic acid and 1,4-bis[(4-pyridyl)-ethynyl]benzene. A long rigid and conjugated bridging ligand has received much current interest for the construction of self-assembling macrocyclic architectures (Lehn, 1995; Fujita, 1999) and the development of molecular wires (Tour, 1996). However, we have found only two examples (Lin *et al.*, 1995, 1998) of structures containing a 1,4-bis[(4-pyridyl)ethynyl]-benzene unit in the Cambridge Structural Database (Allen & Kennard, 1993). We report here the structure of (I) with hydrogen-bonded molecular tapes.



(I)

The molecular structure of (I) is shown in Fig. 1, and both molecules are located on inversion centers. A one-dimensional molecular tape is observed in the structure of (I), as shown in Fig. 2. The molecular tape is nearly flat. The angles between the molecular planes of the chloranilate and the pyridinium ring, and of the pyridinium ring and the benzene ring are 7.3 (2) and 11.8 (4)°, respectively. The molecular tapes are connected *via* $R_1^2(5)$ couplings with two intermolecular N—H···O hydrogen bonds (Table 1), where both H atoms of chloranilic acid have transfered to the pyridine rings. In previous work (Zaman *et al.* 2000), we have shown that the flat molecular tapes form segregated stacks of each molecule. However, overlaps between the chloranilate–pyridinium ring–benzene ring–pyridinium ring–chloranilate are observed in the stacks of the molecular tapes of (I). A short C—Cl···π interaction [Cl1···(C7≡C8) 3.440 (7), Cl1···C7 3.503 (4), Cl1···C8 3.480 (4) Å; Cl1···C7≡C8 79.1 (3) and

UM00012847
NOVARTIS EXHIBIT 1017
Novartis v. Regents, IPR2023-01346
Page 1593 of 4460

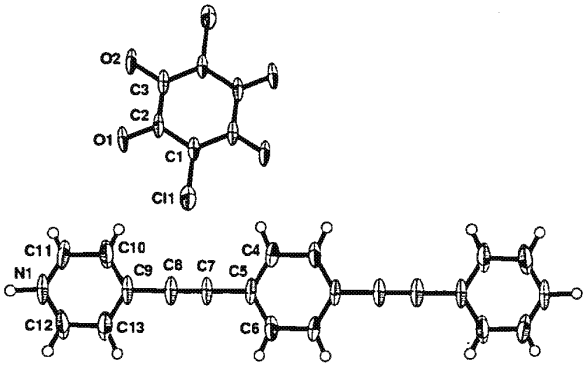


Figure 1
The molecular structure of (I) with the atomic numbering scheme. Displacement ellipsoids are drawn at the 50% probability level.

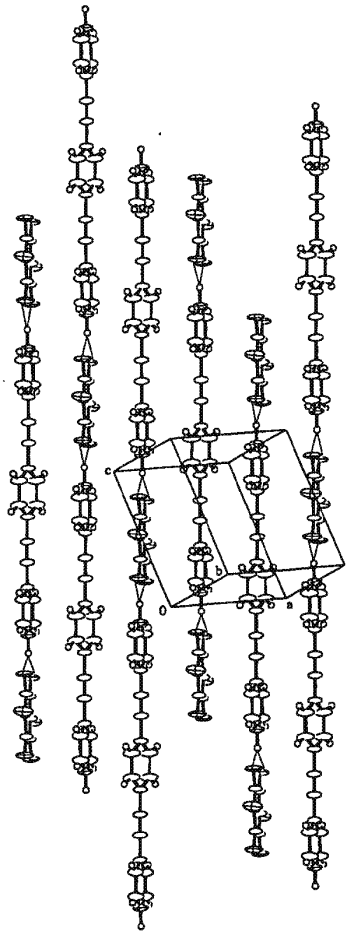


Figure 2
Packing diagram of (I). Dotted lines show the intermolecular N—H···O hydrogen bonds.

Cl1···C8≡C7 81.3 (3)°] exists between the stacks of the molecular tapes (Reddy *et al.*, 1996; Prasanna & Row, 2000). It is 1.7% shorter than the sum of the van der Waals radii of Cl and Csp^2 (Pauling, 1960).

Experimental

1,4-Bis[(4-pyridyl)ethynyl]benzene was prepared according to the literature (Lin *et al.*, 1995). Chloranilic acid was commercially available and purified by the usual method. A diffusion method for a solution of 1,4-bis[(4-pyridyl)ethynyl]benzene (0.02 mmol) and chloranilic acid (0.02 mmol) in acetonitrile (5 ml) using an H-tube gave crystals of (I) suitable for X-ray analysis.

Crystal data

$C_{20}H_{14}N_2^{2+}\cdot C_6Cl_2O_4^{2-}$
M_r = 489.29
Triclinic, $P\overline{1}$
a = 7.6279 (9) Å
b = 8.4019 (10) Å
c = 8.6291 (4) Å
α = 97.171 (6)°
β = 99.673 (6)°
γ = 95.728 (10)°
V = 536.76 (9) Å^3
Z = 1
D_x = 1.514 Mg m^{-3}
Cu $K\alpha$ radiation
Cell parameters from 23 reflections
θ = 5.9–43.0°
μ = 3.05 mm^{-1}
T = 296 (2) K
Needle, dark red
0.7 × 0.1 × 0.1 mm

Data collection

Enraf–Nonius CAD-4 diffractometer
ω–2θ scans
Absorption correction: ψ scan (North *et al.*, 1968)
T_{min} = 0.224, T_{max} = 0.750
2340 measured reflections
2187 independent reflections
1213 reflections with $I > 2\sigma(I)$
R_{int} = 0.041
θ_{max} = 74.3°
$h = -9 \rightarrow 9$
$k = -10 \rightarrow 10$
$l = 0 \rightarrow 10$
3 standard reflections
every 120 reflections
intensity decay: 2.5%

Refinement

Refinement on F^2
$R[F^2 > 2\sigma(F^2)]$ = 0.053
$wR(F^2)$ = 0.161
S = 0.99
2187 reflections
182 parameters
All H-atom parameters refined
$(\Delta/\sigma)_{max} < 0.001$
$\Delta\rho_{max}$ = 0.29 e Å^{-3}
$\Delta\rho_{min}$ = −0.37 e Å^{-3}

Table 1
Hydrogen-bonding geometry (Å, °).

D—H···A	D—H	H···A	D···A	D—H···A
N1—H1···O1^{i}	1.05 (7)	2.23 (6)	2.897 (4)	120 (5)
N1—H1···O2^{i}	1.05 (7)	1.62 (7)	2.609 (3)	154 (5)

Symmetry code: (i) $-x, 1-y, -z$.

All H atoms were located in the Fourier map and were refined isotropically.

Data collection: *CAD-4 EXPRESS* (Enraf–Nonius, 1992); cell refinement: *CAD-4 EXPRESS*; data reduction: *HELENA* (Spek, 1997); program(s) used to solve structure: *SHELXS97* (Sheldrick, 1997); program(s) used to refine structure: *SHELXL97* (Sheldrick, 1997); molecular graphics: *ORTEPIII* (Burnett & Johnson, 1996); software used to prepare material for publication: *SHELXL97*.

This work was supported by a Grant-in-Aid for Scientific Research on Priority Areas from the Ministry of Education, Culture, Sports, Science and Technology, Japan.

UM00012848
NOVARTIS EXHIBIT 1017
Novartis v. Regents, IPR2023-01346
Page 1594 of 4460

References

Allen, F. H. & Kennard, O. (1993). *Chem. Des. Autom. News*, **8**, 1, 31–37.
Burnett, M. N. & Johnson, C. K. (1996). *ORTEP*III. Report ORNL-6895. Oak Ridge National Laboratory, Tennessee, USA.
Enraf–Nonius (1992). *CAD-4 EXPRESS*. Version 5.1. Enraf–Nonius, Delft, The Netherlands.
Fujita, M. (1999). *Acc. Chem. Res.* **32**, 53.
Lehn, J.-M. (1995). In *Supramolecular Chemistry*. Weinheim: VCH.
Lin, J. T., Sun, S.-S., Wu, J. J., Lee, L., Lin, K.-J. & Huang, Y. F. (1995). *Inorg. Chem.* **34**, 2323.
Lin, J. T., Yang, M.-F., Tsai, C. & Wen, Y. S. (1998). *J. Organomet. Chem.* **564**, 257.
North, A. C. T., Phillips, D. C. & Mathews, F. S. (1968). *Acta Cryst.* A**24**, 351–359.
Prasanna, M. D. & Row, T. N. G. (2000). *Cryst. Eng.* **3**, 135–154.
Pauling, L. (1960). In *The Nature of the Chemical Bond*. Ithaca: Cornell University Press.
Reddy, D. S., Craig, D. C. & Desiraju, G. R. (1996). *J. Am. Chem. Soc.* **118**, 4090–4093.
Sheldrick, G. M. (1997). *SHELXS*97 and *SHELXL*97. University of Göttingen, Germany.
Spek, A. L. (1997). *HELENA*. University of Utrecht, The Netherlands.
Tour, J. M. (1996). *Chem. Rev.* **96**, 537–553.
Zaman, M. B., Tomura, M. & Yamashita, Y. (1999). *Chem. Commun.* pp. 999–1000.
Zaman, M. B., Tomura, M. & Yamashita, Y. (2000). *Org. Lett.* **2**, 273–275.

UM00012849
NOVARTIS EXHIBIT 1017
Novartis v. Regents, IPR2023-01346
Page 1595 of 4460

Systematic Analysis of Structural Data as a Research Technique in Organic Chemistry

FRANK H. ALLEN, OLGA KENNARD,* and ROBIN TAYLOR

Crystallographic Data Centre, University Chemical Laboratory, Cambridge CB2 1EW, Great Britain

Received April 20, 1982 (Revised Manuscript Received November 1, 1982)

Crystallography is the most powerful method available for studying molecular structures. It has become increasingly important in recent years with the introduction of automatic diffractometers and new methods of structure solution and refinement. There are now more than 30 000 organocarbon structures (i.e., organics, organometallics, and metal complexes) in the literature, a number that is likely to double within 5–7 years. Unfortunately, this wealth of information has not been greatly exploited; detailed discussions of individual crystal structures are commonplace, but systematic studies of large numbers of related structures are rarely undertaken.

The purpose of this Account is to illustrate how the systematic analysis of crystallographic data can be a versatile research technique in organic chemistry.[1] Examples are taken from many areas, including studies of bonding theories, conformational analysis, reaction pathways and hydrogen bonding. Many of the studies were carried out with the aid of the Cambridge Structural Database (CSD),[2] which is described briefly below.

Cambridge Structural Database (CSD)

CSD contains results of X-ray and neutron diffraction studies of organics, organometallics, and metal complexes. The information stored for each entry (Table I) may be divided into three categories: bibliographic information (BIB),[3] chemical connectivity information (CONN), and crystallographic data (DATA). CSD is fully comprehensive from 1935 onward, and is also a depository for unpublished atomic coordinates.[4] The database is available in 22 countries and on January 1, 1982, contained 31 631 studies of 28 978 different compounds. About 4000 new entries are added each year.

The information in CSD is searched and analyzed by a system of computer programs;[2] examples of program input and output are given in Figure 1. The two main search programs are BIBSER and CONNSER. BIBSER uses the bibliographic information fields italicized in Table I to locate entries on the basis of their chemical name, molecular formula, chemical class, etc. (e.g., Figure 1a). CONNSER is used to search for compounds containing specific chemical fragments. Program input consists of a coded representation of the desired fragment (e.g., the coding in Figure 1c would be used to find compounds containing the substructure shown in Figure 1b).

Output from both BIBSER and CONNSER consists of a listing of all structures in the database that satisfy the search criteria, together with the corresponding literature references (e.g., Figure 1, parts d and e). The RETRIEVE program may now be used to create a file of crystallographic data for entries located by the search. This DATA subfile can be processed by the programs PLUTO78, which produces plots and illustrations (e.g., Figure 1f), and GEOM78, which is used for geometrical analysis. GEOM78 will calculate the intra- and/or intermolecular geometries of all entries in a DATA subfile or provide systematic tabulations of selected geometrical parameters for a specific chemical fragment. Figure 1g is a tabulation of R factor, five independent bond lengths, and the torsion angle O(1)–C(2)–C(3)–X (X = midpoint of C(4)–C(5)) for the fragment shown

Table I
Principal Information Held in the Cambridge Structural Database (CSD)

Bibliographic (BIB)
Compound name(s); *qualifying phrase(s)* [e.g., neutron study, low-temperature study, absolute configuration determined]; *molecular formula, literature citation; chemical class(es)* [e.g., 15 = benzene nitro compounds, 51 = steroids, 58 = alkaloids, etc.]
Chemical Connectivity (CONN)
Chemical structural diagrams are coded in terms of *atom* and *bond properties*. Atom properties: atom sequence number (*n*); element symbol (*el*); no. of connected non-H atoms (*nca*); no. of terminal H atoms (*nh*); net charge (*ch*). Bond properties: pair of atom sequence numbers ($n = i, j$); bond type for bond i–j (*bt*); [see Figure 1, b and c].
Crystallographic Data (DATA)
Unit-cell Parameters; space group; symmetry operators; atomic coordinates; accuracy indicators [mean estimated standard deviation of C–C bonds, R factor]; evaluation flags [indicating: presence of disorder, presence of errors, method used for data collection, etc.]; comment text [e.g., describing any disorder, or errors in the original reference].

After graduating from Cambridge University, Olga Kennard worked at the Cavendish Laboratory and subsequently joined the Medical Research Council in London. She returned to Cambridge in 1981, as a member of M. R. C. External Staff, to build up an X-ray crystallographic unit in the University Chemical Laboratory. The Cambridge Crystallographic Data Centre (CCDC) was established there, under her direction, in 1965. Olga Kennard's research is concerned with biological structures, particularly oligonucleotides and their interaction with drugs and proteins. She was awarded an Sc.D. (Cantab) in 1971 and the Structural Chemistry Prize of the Chemical Society in 1980.

Frank Allen obtained a Ph.D. from London University and did postdoctoral crystallographic work at the University of British Columbia. He joined the CCDC in 1970 and has been involved in many aspects of its development; he is a member of the Data Commission of the International Union of Crystallography. Current research interests involve applications of the Structural Database in physical organic chemistry.

Robin Taylor obtained a B.A. from Oxford and a Ph.D. in chemical crystallography from Cambridge University. He held postdoctoral positions in York and Pittsburgh before joining the CCDC in 1980. His research interests include the structure and energy of hydrogen-bonded systems and the application of statistical methods to crystallographic data.

(1) This Account complements an earlier paper that was primarily concerned with the chemical interpretation of *individual* structures: Wilson, S. R.; Huffman, J. C. *J. Org. Chem.* 1980, *45*, 560–566.

(2) Allen, F. H.; Bellard, S.; Brice, M. D.; Cartwright, B. A.; Doubleday, A.; Higgs, H.; Hummelink, T.; Hummelink-Peters, B. G.; Kennard, O.; Motherwell, W. D. S.; Rodgers, J. R.; Watson, D. G. *Acta Crystallogr. Sect. B* 1979, *B35*, 2331–2339 and references therein.

(3) Bibliographic information is also published annually in: "Molecular Structures and Dimensions", Kennard, O., Watson, D. G., Allen, F. H., Bellard, S., Eds.; D. Reidel: Dordrecht, The Netherlands.

(4) Journals involved in this scheme since 1977 include *Chemical Communications*, *Tetrahedron*, and *Tetrahedron Letters*.

0001-4842/83/0116-0146$01.50/0 © 1983 American Chemical Society

UM00012850
NOVARTIS EXHIBIT 1017
Novartis v. Regents, IPR2023-01346
Page 1596 of 4460

(a) BIBSER : Sample Questions

(i) Find all steroids :

```
Q *CLASS '51'
```

Note : Chemical class 51 = steroids

(ii) Find all penicillins published between 1970 and 1980 inclusive :

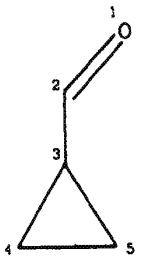
```
Q *COMPND 'PENICILL' and *YEAR '70-80'
```

Note : The string PENICILL will locate penicillin, penicillanic, penicilloic, etc.

(iii) Find all compounds for which absolute configuration has been established by X-ray methods :

```
Q *COMPND 'ABSOLUTE CONFIGURATION'
```

(b) CONNSER : Search Fragment



(c) CONNSER : Search Query (for fragment in (b))

```
Q Cyclopropyl-carbonyls
C
C Atom properties:
C only nca is specified :
C
AT1  O  1
AT2  C  2
AT3  C  3
AT4  C  2
AT5  C  2
C
C Bond properties :
C node numbers, bond-type,
C and Acyclic/Cyclic flag :
C
BO  1  2  2  A
BO  2  3  1  A
BO  3  4  1  C
BO  4  5  1  C
BO  3  5  1  C
END
```

(d) BIBSER : Sample Output from Question (a,i)

```
AAMAND   16alpha-Acetyl-3beta-methoxy-CD-cis-D-
         norandrostane
         C21 H34 O2; Class 51
         J.Meinwald,A.J.Taggi,P.A.Luhan,
         A.T.McPhail
         Proc.Nat.Acad.Sci.U.S.A., 71, 78, 1974

ABAXES   2alpha-Bromo-17beta-acetoxy-9-methyl-
         5alpha,9beta,10alpha-estran-3-one
         C21 H31 Br1 O3; Class 51
         J.C.A.Boeyens,J.R.Bull,J.Floor,
         A.Tuinman
         J.Chem.Soc.,Perkin 1, 808, 1978
```

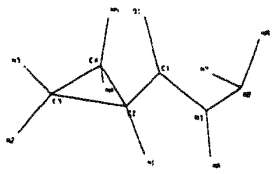
(e) CONNSER : Sample Bibliographic Listing for Search Query (c)

```
CORAMA   (-)-Coronamic acid N-acetate
         (absolute configuration)
         C8 H13 N1 O3; Class 48,20
         A.Ichihara,K.Shirashi,S.Sakamura,
         A.Furusaki,N.Hashiba,T.Matsumoto
         Tetrahedron Lett., 365, 1979

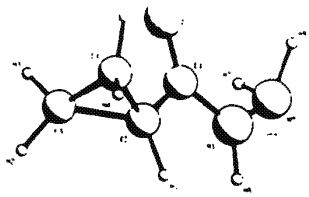
CPCOHA   Cyclopropanecarbohydrazide
         C4 H8 N2 O1; Class 20,9
         D.B.Chesnut,R.E.Marsh
         Acta Crystallogr., 11, 413, 1958

CPRPCX10 Cyclopropanecarboxamide
         C4 H7 N1 O1; Class 20,1
         R.E.Long,H.Maddox,K.N.Trueblood
         Acta Crystallogr.,Sect.B, 25, 2083, 1969
```

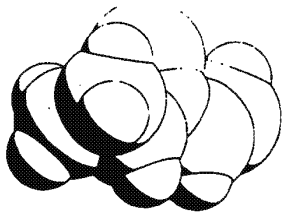
(f) PLUTO78 : Sample Plots for Cyclopropanecarbohydrazide (CPCOHA in (e))



(i) 'stick' diagram



(ii) 'ball-and-spoke' style with shading and perspective



(iii) 'space-filling' model with shading and perspective

(g) GEOM78 : Example of Geometry Tabulation for Fragment (b)

Notes :

Distances in Angstroms, angle (TAU) in degrees.

TAU is the torsion angle : O(1) - C(2) - C(3) - X(1), where X(1) is the mid-point of the bond C(4) - C(5).

STD. DEVN. is the standard deviation of each sample. The standard deviations of the means are 0.004, 0.006, 0.003, 0.005 and 0.006.

CSD code	*RFACT	C4-C5	C3-C4	C3-C5	C3-C2	C2=O1	TAU
CORAMA	0.059	1.491	1.534	1.503	1.502	1.216	28.04
CPCOHA	0.130	1.478	1.520	1.493	1.478	1.213	4.52
CPRPCX10	0.087	1.467	1.485	1.501	1.484	1.238	-7.74
CPRPCX10	0.087	1.450	1.489	1.493	1.470	1.249	-4.67
DCPEDO	0.047	1.475	1.515	1.510	1.456	1.213	3.19
DMCPRC	0.085	1.477	1.521	1.510	1.456	1.246	-7.30
MBCPCX	0.062	1.488	1.531	1.508	1.480	1.210	30.07
NPCPMK	0.092	1.474	1.513	1.488	1.469	1.235	8.64
PMCPRC10	0.037	1.490	1.548	1.505	1.484	1.205	-21.17
SDPPCX	0.042	1.482	1.533	1.510	1.470	1.201	-5.47
MEAN		1.477	1.519	1.502	1.475	1.223	
STD. DEVN.		0.012	0.020	0.008	0.014	0.018	

Figure 1. Examples of input and output for the CSD program system.

in Figure 1b. The DATA subfile may also be processed by the user's own programs.

Systematic Analysis of Intramolecular Geometry

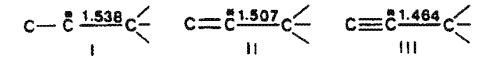
Mean Geometries. The results of early X-ray analyses were used to derive mean bond lengths,[5] covalent radii, etc., which were important in the development of structural chemistry and bonding theories. As the number of structural studies increased, it became possible to determine the mean geometries of complete

(5) Sutton, L. E., Ed., "Tables of Interatomic Distances and Configuration in Molecules and Ions"; The Chemical Society: London; Special Publication 11 (1958) and 18 (1965).

UM00012851
NOVARTIS EXHIBIT 1017
Novartis v. Regents, IPR2023-01346
Page 1597 of 4460

chemical residues. Thus, the average dimensions of furanose,[6] pyranose,[7] and nucleic acid base residues[8] have all been determined. Given these mean values, together with their standard deviations, it is easy[8] to derive orthogonal coordinates for "standard residues". Apart from a variety of crystallographic uses, standard geometries are invaluable in model building, parameterization of empirical force fields, and interpretation of new structural data.

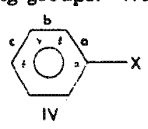
Substituent and Hybridization Effects. Early bond length tabulations[6] were subdivided on the basis of gross differences in hybridization and environment. For example, hybridization changes at C* in I–III cause



I II III

appreciable bond length alterations, which are easily recognized in any individual crystal structure. Smaller changes in electron distribution—due, perhaps, to substitution and slight rehybridization—produce correspondingly smaller geometric variations, which are often close to the error limits of individual structure determinations. These are only discovered by the systematic analysis of many related structures. Studies of this type provide results that can be correlated with theoretical calculations, reactivity, spectral properties, and other physical phenomena. Two examples are discussed below.

Substituent-Induced Ring Deformations in Benzene. Early microwave and X-ray investigations showed that the regular hexagonal geometry of benzene is perturbed when the ring is substituted by strong electron-withdrawing or -donating groups. With reference to IV,



IV

deformations due to electron-withdrawing groups involve an increase in the ipso angle α, a decrease in the ortho angles β, and shortening of bonds a with respect to bonds b. Deformations due to electron-donating groups are in the opposite sense. Only groups with strong electronic effects produce deformations that are consistently larger than the error limits of individual structure determinations.

The angular deformations ($\Delta\alpha$, $\Delta\beta$, $\Delta\gamma$, $\Delta\delta$ from 120°; see IV) in more than 100 mono- and para-disubstituted benzenes have been analyzed. Early results[9,10] showed that $\Delta\alpha$ is the largest deformation, and that its value for a particular substituent X is unaffected by para-substitution; $\Delta\beta$ was found to be $\simeq -\Delta\alpha/2$. Values of α were determined for a variety of substituents (Table II) by averaging relevant fragment geometries. It was recognized that σ-effects predominate in determining $\Delta\alpha$ values.[10,11] This is consistent with the observed correlation between α and the electronegativity (χ) for

Table II
Angular Deformations in Substituted Benzenes (IV)[a,b]

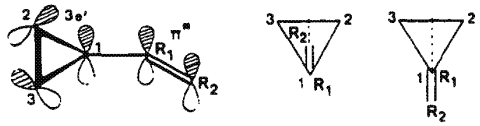
X	α(mean), deg[c]	Linear regression values, deg[d] Δα	Δβ	Δγ	Δδ
$N(Me)_2$	117.2	−2.4 (3)	0.6 (2)	1.4 (2)	−1.7 (3)
Ph	117.6	−2.3 (2)	1.0 (1)	0.6 (1)	−0.9 (2)
Me	118.1	−1.9 (2)	1.0 (1)	0.4 (1)	−0.8 (2)
CH=CHR	118.0	−1.8 (2)	0.8 (1)	0.3 (1)	−0.4 (2)
COMe	118.8	−1.0 (2)	0.4 (1)	0.2 (1)	−0.3 (2)
COOH	119.8	0.1 (2)	−0.2 (1)	0.1 (1)	0.2 (2)
OMe	119.9	0.2 (2)	−0.6 (1)	1.1 (1)	−1.1 (2)
CN	121.8	1.1 (2)	−0.8 (1)	0.3 (1)	−0.1 (2)
Cl	121.4	1.9 (2)	−1.4 (1)	0.6 (1)	−0.2 (2)
NO_2	122.1	2.9 (2)	−1.9 (1)	0.3 (1)	0.4 (1)
F	123.4	3.4 (2)	−2.0 (1)	0.5 (1)	−0.4 (2)

[a] Standard deviations in α (mean) are in the range 0.1–0.2°. [b] Substitution reduces perfect D_{6h} ring symmetry to C_{2v}; hence $\Delta\alpha + 2\Delta\beta + 2\Delta\gamma + \Delta\delta = 0$. [c] Reference 11. [d] Reference 13.

first-row functional groups[11] and second-row elements[10] (Figure 2a,b). Later,[12] it was realized that substituents that interact with the benzene π-system also produce significant deformations ($\Delta\gamma$, $\Delta\delta$). Factor analysis showed that *all* substituent-induced deformations can be ascribed to two independent effects, which were interpreted as σ- and π-interactions.[13] Values of $\Delta\alpha$, $\Delta\beta$, $\Delta\gamma$, $\Delta\delta$ for 21 functional groups were derived by linear regression, the geometries of 71 mono- and para-disubstituted benzenes (Table II)[14] being used.

The marked sensitivity of α to σ-effects, evidenced by the α–χ plots, is confirmed by the plot[11,13] of $\Delta\alpha$ against the Taft[15] inductive parameter, σ_I (Figure 2c). The sensitivity of γ to π-effects is shown by the $\Delta\gamma$–σ_R° plot[13] in Figure 2d (σ_R° = Taft resonance parameter[15]). These correlations suggest that Δ-values may be a useful addition to traditional reactivity parameters, since they measure substituent effects on the ring in the ground state, do not depend on the choice of a suitable reaction series, are independent of solvent effects, and can be related to conformational changes.

Conjugation and Hybridization in Three-Membered Rings. Cyclopropane is unusual among cycloalkanes in that it conjugates with π-acceptor substituents,[16] as is shown by spectroscopic results[17] and the stabilization of carbonium ions by cyclopropane. Molecular orbital theory suggests[18] that conjugation involves transfer of electron density from the cyclopropane 3e′ orbitals to the π^* orbitals of the substituent (V). This would be



V VI VII

(6) Arnott, S.; Hukins, D. W. L. *Biochem. J.* 1972, *130*, 453–465.
(7) Arnott, S.; Scott, W. E. *J. Chem. Soc., Perkin Trans. II* 1972, 324–335.
(8) Taylor, R.; Kennard, O. *J. Mol. Struct.* 1982, *78*, 1–28. Taylor, R.; Kennard, O. *J. Am. Chem. Soc.* 1982, *104*, 3209–3212.
(9) Domenicano, A.; Vaciago, A.; Coulson, C. A. *Acta Crystallogr., Sect. B* 1975, *B31*, 221–234.
(10) Domenicano, A.; Vaciago, A.; Coulson, A. A. *Acta Crystallogr., Sect. B* 1975, *B31*, 1630–1641.
(11) Domenicano, A.; Mazzeo, P.; Vaciago, A. *Tetrahedron Lett.* 1976, 1029–1032.
(12) Domenicano, A.; Vaciago, A. *Acta Crystallogr., Sect. B* 1979, *B35*, 1382–1388.
(13) Domenicano, A.; Murray-Rust, P. *Tetrahedron Lett.* 1979, 2283–2286.
(14) A similar independent analysis is described by: Norrestam, R.; Schepper, L. *Acta Chem. Scand. Sec. A* 1981, *A35*, 91–103. The two sets of angle deformations have a correlation coefficient of 0.966 and a root mean square deviation of 0.22°.
(15) Ehrenson, S.; Brownlee, R. T. C.; Taft, R. W. *Prog. Phys. Org. Chem.* 1973, *10*, 1–80.
(16) Charton, M. "The Chemistry of Alkenes"; Zabicky, J., Ed.; Interscience, London, 1970; Vol. II, pp 511–610.
(17) Pete, J.-P. *Bull. Soc. Chim. Fr.* 1967, 357–370.
(18) Hoffmann, R. *J. Chem. Phys.* 1964, *40*, 2480–2488. Hoffmann R.; Stohrer, W.-D. *J. Am. Chem. Soc.* 1971, *93*, 6941–6948.

UM00012852
NOVARTIS EXHIBIT 1017
Novartis v. Regents, IPR2023-01346
Page 1598 of 4460

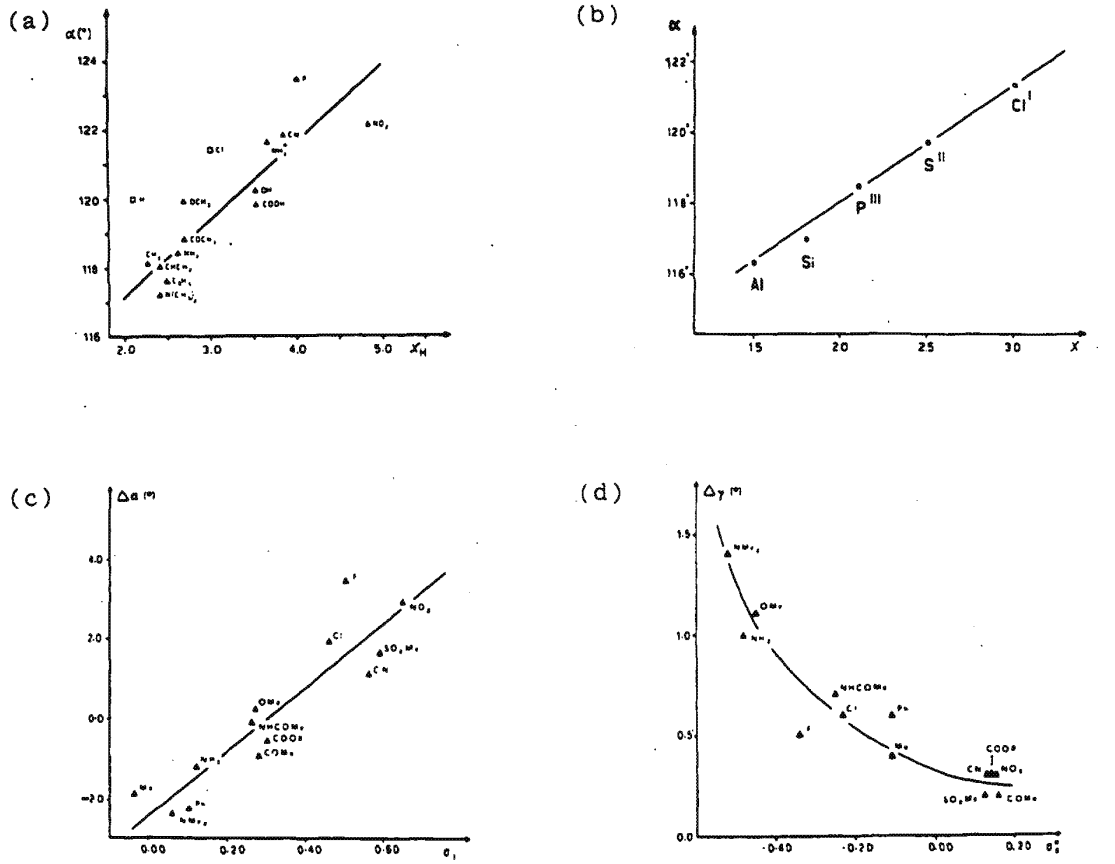
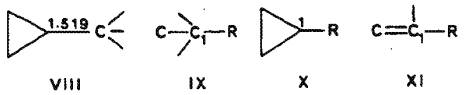


Figure 2. Correlation of substituent-induced angular deformations in benzene with electronegativity (χ) and Taft parameters (σ). The ipso angle (α in IV) is plotted (a) against χ for first-row functional groups (Reprinted with permission from ref 11. Copyright 1976, Pergamon Press Ltd.) and (b) against χ for second-row elements (Reprinted with permission from ref 10. Copyright 1975, International Union of Crystallography). In (c) the deformation $\Delta\alpha$ is plotted against the inductive parameter σ_I (Reprinted with permission from ref 13. Copyright 1979, Pergamon Press Ltd.), while in (d) the deformation $\Delta\gamma$ is plotted against σ_R° (Reprinted with permission from ref 13. Copyright 1979, Pergamon Press Ltd.). We gratefully acknowledge permission to reproduce these plots from Dr. Aldo Domenicano and the copyright holders.

expected to shorten the distal (2–3) bond by δ and increase the vicinal (1–2,1–3) bonds by $\sim\delta/2$. However, the degree of conjugation will depend on the extent of orbital overlap, which is maximized in the cis- and trans-bisected conformations (Newman projections VI and VII, respectively).[19]

In order to quantify these effects, Allen[20] analyzed results from 146 X-ray studies of cyclopropane derivatives. The mean geometry of nonconjugated cyclopropanes was established by using purely C(sp^3) derivatives (VIII). Substituent-induced bond length



VIII IX X XI

asymmetries were consistently observed in the geometries of derivatives involving the π-acceptor substituents —C=O (ketones, acids, esters; see Figure 1g for a typical geometrical tabulation), —C=C, and —CN. It was found that multiple substitution produces net distortions that can be approximated by simple sums of individual substituent effects. The bond length asymmetry parameters (δ in the preceding paragraph) due to some representative substituents are given in Table III. The variation of bond length asymmetries with conformation suggests[20,21] that conjugative overlap of ring and acceptor orbitals is effective for —C=O and C=C conformations within 30° of the bisected positions (VI, VII). These results are in agreement with ultraviolet spectral data.[17]

Cyclopropane is also unusual because its protons exhibit vinylic properties.[16] This is consistent with the

Table III
Asymmetry Parameter[a] for Cyclopropane Rings Having π-Acceptor Substituents

subst.	δ, A	subst.	δ, A
C=O	−0.026 (5)	N=C	−0.018 (-)
C=C	−0.022 (4)	CN	−0.017 (2)
Ph	−0.018 (-)	N=N	−0.014 (-)

[a] Reference 20.

(19) Hoffmann, R. *Tetrahedron Lett.* 1970, 2907–2909. Hoffmann, R.; Davidson, R. B. *J. Am. Chem. Soc.* 1971, *93*, 5699–5705.
(20) Allen, F. H. *Acta Crystallogr., Sect. B* 1980, *B36*, 81–96.
(21) Allen, F. H. In "Molecular Structure and Biological Activity"; Griffin, J. F., Duax, W. L., Eds.; Elsevier Biomedical: New York, 1982; 105–116.

UM00012853
NOVARTIS EXHIBIT 1017
Novartis v. Regents, IPR2023-01346
Page 1599 of 4460

Table IV
Variation in the C(1)–R Bond Length[a] in IX–XI due to Changes in Hybridization (h) and to Conjugative Effects (c)

R		fragment IX	X	XI	$h(\Delta)$[b]	$h(sp^2)$[b]
C sp^3	h	1.538	1.519	1.507	−0.019	−0.031
C=C	h	1.507	1.480	1.472	−0.027	−0.035
	$h + c$		1.470	1.458		
	c		−0.010	−0.014		
C=O	h	1.512	1.489	1.482	−0.023	−0.030
(keto)	$h + c$		1.474	1.460		
	c		−0.015	−0.022		
C=O	h	1.514	1.504	1.497	−0.010	−0.017
(acids,	$h + c$		1.484	1.470		
esters)	c		−0.020	−0.027		

[a] Reference 22. [b] $h(\Delta) = h(X) - h(IX)$, $h(sp^2) = h(XI) - h(IX)$ for each substituent R (see text).

abnormally short exocyclic C–C bond in derivatives of the type VIII (cf. I, II).[20,22] Theoretical models[23] indicate that the C(ring) hybrid involved in the exocyclic C–C bond in VIII is ~sp^2, whereas those involved in the ring σ-bonds are ~sp^5. Hybridization in cyclopropane was studied in detail[22] by comparing the C–R distances in the related fragments IX–XI (R = C(sp^3), vinyl, keto, acid, ester). In those cases where conjugation can occur (i.e., X and XI with R = —C=C or —C=O), two C–R distances were obtained, for (i) conformations outside the ranges established for effective conjugation (this is a measure of hybridization effects (h)) and (ii) conjugative conformations, where C–R is further shortened by π-effects (c). Representative results are given in Table IV. The relative bond length contractions due to hybridization, defined by

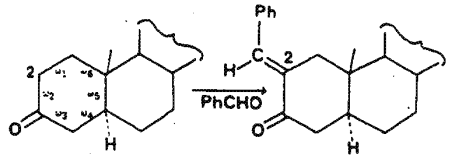
$$h(\Delta) = [\text{R–C(cyclopropane)}]_h - [\text{R–C}(sp^3)]$$

$$h(sp^2) = [\text{R–C}(sp^2)]_h - [\text{R–C}(sp^3)]$$

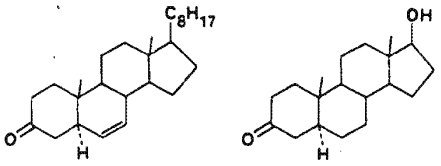
can be used to infer the hybridization of the cyclopropane ring atoms. Values of $h(\Delta)/h(sp^2)$ range from 59 to 77%. The mean, 69%, corresponds to $sp^{2.25}$ hybridization (30.8% s character) in exocyclic bonds; hence, ring σ-hybrids are $sp^{4.20}$ (19.2% s). Table IV also permits comparison of the relative conjugative abilities of cyclopropane and the vinyl group.[16] The ratios $c(\Delta)/c(sp^2)$ average to 71%, which compares well with a UV bathochromic shift ratio of ~60%.[17]

Conformational Analysis. Comparative reviews of steroids,[24] alkaloids and terpenes,[25] and medium rings[26] illustrate the extensive application of crystallographic data to conformational analysis.[27] In the present review, we are particularly concerned with the *systematic* analysis of solid-state conformations. Although some molecules are known to adopt different conformations in solution and in the crystalline state, it has been shown that solid-state conformational data can be successfully related to solution properties, provided that a sufficient number of crystal structures are studied. This is illustrated by the following example.

The relative rates of condensation with benzaldehyde of a series of 3-keto-5α steroids (XII) were determined



XII XIII



XIV XV

by Barton et al.[28] The 2-benzylidene ketone XIII is exclusively formed by elimination of OH^-, the reaction involving rehybridization of C(2) from sp^3 to sp^2. The presence of ethylenic links and/or substituents at positions remote from the reaction center was found to produce large differences in reaction rates. It was therefore inferred that gross conformational changes at remote sites produce small changes—here at C(2)—by "conformational transmission". This influences the rate of condensation, r, which may be expressed as[28]

$$r = r_0 \Pi f_i$$

where r_0 is the rate for saturated XII and the f_i are "group rate factors" for remote substituents or double bonds.

The crystal structure[29] of cholest-6-en-3-one (XIV), which has the highest reaction rate (r = 645), shows an unusually flat A ring, with a mean ring torsion angle $\bar{\omega}$ ($=\sum_i \omega_i/6$ in XII) of only 50.4°. The flattening is especially pronounced at C(2), where ω_{12} ($=(\omega_1 + \omega_2)/2$ in XII) is 42.2°. The ring bond angle at C(2), υ, is correspondingly high at 114.4 (8)°. In contrast, the structure[30] of 17β-hydroxyandrostan-3-one (XV), which has a much lower reaction rate (r = 188), shows $\bar{\omega}$ = 54.1°, ω_{12} = 51.7°, and υ = 110.7°. Clearly, C(2) is more prepared to undergo rehybridization in XIV than in XV.[29] An analysis[21] of several other A-ring conformations confirmed that the reaction rate tends to increase as the ring becomes flattened at C(2). The parameter $\alpha = \omega_{12} - \bar{\omega}$ was used to express the relative puckering in each ring (negative α represents flattening at C(2)). For steroids with r = 33, 188, 235, and 645, the corresponding mean values of α were 2.6, −2.8, −3.3, and −8.3°. Although the data are limited, the r–α correlation is qualitatively acceptable.

Systematic Analysis of Intermolecular Interactions

Hydrogen-Bonding Studies. Systematic analyses of crystal structures have made a significant contribution to our knowledge of hydrogen bonding. Studies of O–H···O and C–H···O bonds are discussed below.

(22) Allen, F. H. *Acta Crystallogr., Sect. B* 1981, *B37*, 890–900.
(23) Bernett, W. A. *J. Chem. Educ.* 1967, *44*, 17–24 and references therein.
(24) Altona, C.; Geise, H. J.; Romers, C. *Tetrahedron* 1968, *24*, 13–32. Duax, W. L.; Norton, D. A. "Atlas of Steroid Structures"; Plenum: London, 1975. Duax, W. L.; Weeks, C. M.; Rohrer, D. C. *Recent Prog. Horm. Res.* 1976, *32*, 81–116.
(25) Mathieson, A. McL. *Perspect. Struct. Chem.* 1967, *1*, 41–108.
(26) Dunitz, J. D. *Perspect. Struct. Chem.* 1968, *2*, 1–70.
(27) The correlation of crystal structure conformations with pharmaceutical activity cannot be covered adequately here. Interested readers are referred to: Griffin, J. F.; Duax, W. L., Eds., "Molecular Structure and Biological Activity"; Elsevier Biomedical: New York, 1982.
(28) Barton, D. H. R.; Head, A. J.; May, P. J. *J. Chem. Soc.* 1957, 935–944. Barton, D. H. R.; McCapra, F.; May, P. J.; Thudium, F. *J. Chem. Soc.* 1960, 1297–1311.
(29) Guy, J. J.; Allen, F. H.; Kennard, O.; Sheldrick, G. M. *Acta Crystallogr., Sect. B* 1977, *B33*, 1236–1244.
(30) Courseille, C.; Precigoux, G.; Leroy, F.; Busetta, B. *Cryst. Struct. Commun.* 1973, *2*, 441–446.

UM00012854
NOVARTIS EXHIBIT 1017
Novartis v. Regents, IPR2023-01346
Page 1600 of 4460

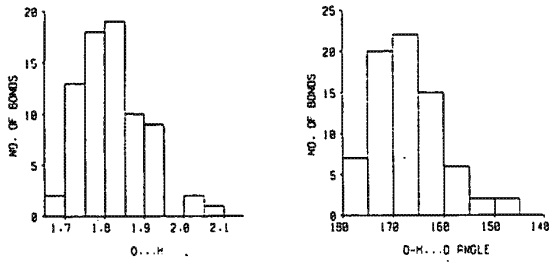
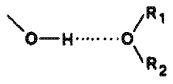


Figure 3. Distribution of O–H distances (Å) and O–H···O angles (°) in O–H···O hydrogen bonds (ref 31).

O–H···O Hydrogen Bonds. The distributions of O···H distances and O–H···O angles were determined in a survey of the neutron diffraction geometries of 74 O–H···O< bonds (Figure 3).[31] The mean values are 1.818 (9) Å and 167.1 (8)°, respectively. The latter is in good agreement with the most probable value predicted by molecular orbital calculations (163°).[32] For hydrogen bonds with O···H < 1.812 Å (the median O···H distance of the sample) the mean O–H···O angle was 168.4 (9)°, compared with 165.8 (12)° for bonds with O···H > 1.812 Å. The difference between these means is statistically significant at the 92.5% level, which suggests that short hydrogen bonds tend to be more linear than long ones. This can be ascribed to the unfavorable van der Waals interaction between the oxygen atoms in short, nonlinear O–H···O bonds.[33]

In the same study,[31] it was found that the proton in XVI tends to lie in, or near to, the plane containing the



XVI

lone-pair orbitals of the acceptor atom (assumed to be the plane bisecting the R_1–O–R_2 angle). However, there was no evidence of a preferred direction within the plane. Apparently, hydrogen bonding does not occur preferentially along the directions which correspond to idealized sp^3 lone-pair orbitals. This finding is consistent with charge density studies,[34] which show the lone-pair electron density of sp^3 oxygen atoms to be rather diffuse, bearing little resemblance to the simple "rabbit-ear" model. The directional influence of the lone pairs may be more important in hydrogen bonds that involve carbonyl acceptors[35] because the angular separation of sp^2 lone pairs is greater than that of sp^3 lone pairs.

Theoretical calculations[36] suggest that the length of an O–H···O bond should be dependent on its environment. Specifically, hydrogen bonds belonging to infinite ···O–H···O–H··· chains should be stronger, and therefore shorter, than isolated O–H···O bonds (the so-called "cooperative effect"). This is due to the changes that occur in the electron densities at the oxygen and hydrogen atoms upon hydrogen-bond formation. The mean O···H distance of hydrogen bonds belonging to infinite chains was found[31] to be 1.805 (9) Å, compared with 1.869 (23) Å for isolated hydrogen bonds. The difference between these means is statistically significant at the 99.5% level, thus confirming the theoretical prediction. Many of the hydrogen-bond patterns observed in carbohydrate crystal structures can be rationalized by the cooperative effect.[37] For example, all of the hydrogen bonding in sugar alcohol structures is of the favorable infinite chain variety. These structures are ideally suited to this type of arrangement because they possess only hydroxyl groups; i.e., there is a 1:1 ratio of hydrogen-bond donor and acceptor atoms. Thus, it is possible for infinite ···O–H···O–H··· chains to incorporate all of the oxygen atoms in the structure. This is not the case in cyclic pyranoses, where the ring oxygen atom can accept but not donate hydrogen bonds. It therefore acts as a chain stopper and is often completely excluded from the hydrogen-bonding schemes in pyranose crystal structures.[37]

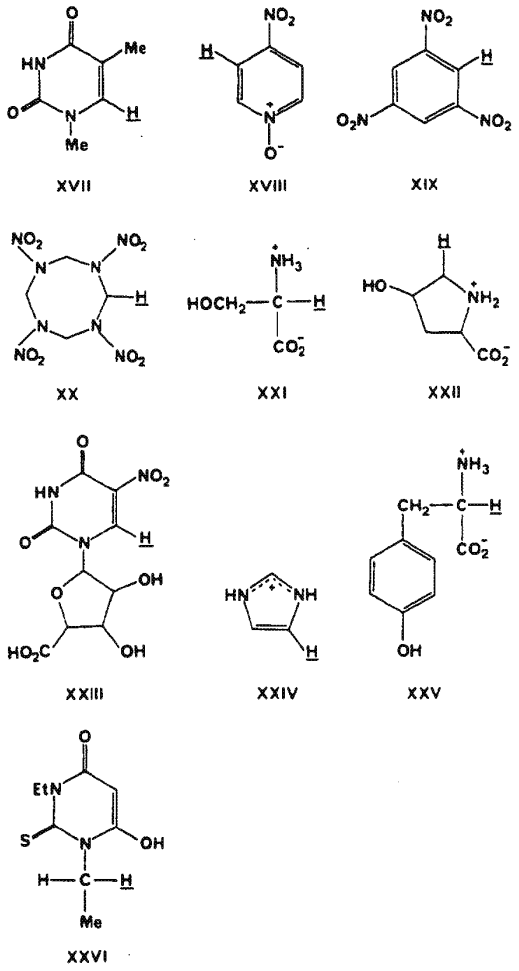
C–H···O Hydrogen Bonds. The hydrogen-bonding schemes observed in the structures of other biologically important molecules (e.g., amino acids, nucleosides) are more difficult to interpret. Nevertheless, some useful results were obtained in a recent survey of hydrogen-bond patterns in amino acid structures.[38] Among these was the observation that short C–H···O contacts are relatively common in amino acid crystal structures, particularly when the C–H group is adjacent to a $^+NH_3$ group. Thus, C–H···O hydrogen bonding may be a significant factor in determining the conformations and crystal-packing arrangements of amino acids. This conclusion was supported by an analysis[39] of the crystallographic environments of 661 (C–)H atoms (i.e., hydrogen atoms covalently bonded to carbon), observed by neutron diffraction in 113 organic crystal structures. Fifty-nine C–H···O contacts (of which 41 were intermolecular) were found with H···O < 2.4 Å and C–H···O > 90°; 2.4 Å is 0.3 Å shorter than the sum of the van der Waals radii of H and O, using the values of Bondi and Kitaigorodsky.[40] In contrast, short C–H···C and C–H···H contacts were found to be extremely rare: it was established that (C–)H atoms have a statistically significant (> 99.9%) tendency to form short intermolecular contacts to oxygen rather than carbon or hydrogen. The proton in the majority of short C–H···O contacts lies within 30° of the plane containing the oxygen lone pairs.[39]

The (C–)H atoms involved in the 10 shortest C–H···O contacts found in the above survey are underlined in XVII–XXVI. Eight of them are immediately adjacent to nitrogen; the other two belong to nitrogen-containing aromatic molecules. Presumably, the inductive effect of nitrogen decreases the electron density at nearby (C–)H atoms, thereby enhancing their ability to form short C–H···O contacts.

Inference of Reaction Pathways. The use of crystallographic information for the inference of reac-

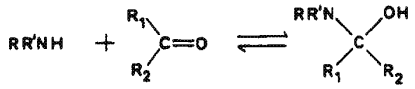
(31) Ceccarelli, C.; Jeffrey, G. A.; Taylor, R. *J. Mol. Struct.* 1981, *70*, 255–271.
(32) Newton, M. D.; Jeffrey, G. A.; Takagi, S. *J. Am. Chem. Soc.* 1979, *101*, 1997–2002.
(33) Taylor, R. *J. Mol. Struct.* 1981, *73*, 125–136.
(34) For example, Diercksen, G. H. F. *Theor. Chim. Acta* 1971, *21*, 335–367.
(35) Olovsson, I.; Jönsson, P.-G. In "The Hydrogen Bond—Recent Developments in Theory and Experiments"; Schuster, P., Zundel, G., Sandorfy, C., Eds.; Elsevier North-Holland: Amsterdam, 1976; Vol II 416–420.
(36) Del Bene, J. E.; Pople, J. A. *J. Chem. Phys.* 1973, *58*, 3605–3608.
(37) Jeffrey, G. A.; Lewis, L. *Carbohydr. Res.* 1978, *60*, 179–182. Jeffrey, G. A.; Takagi, S. *Acc. Chem. Res.* 1978, *11*, 264–270.
(38) Jeffrey, G. A.; Maluszynska, H. *Int. J. Biol. Macromol.* 1982, *4*, 173–185.
(39) Taylor, R.; Kennard, O. *J. Am. Chem. Soc.*, 1982, *104*, 5063–5070.
(40) Bondi, A. *J. Phys. Chem.* 1964, *68*, 441–451. Kitaigorodsky, A. I. "Molecular Crystals and Molecules"; Academic Press: New York and London, 1973; 10–18.

UM00012855
NOVARTIS EXHIBIT 1017
Novartis v. Regents, IPR2023-01346
Page 1601 of 4460



XVII XVIII XIX XX XXI XXII XXIII XXIV XXV XXVI

tion pathways is illustrated by an early application:[41] the addition of a nitrogen nucleophile to a carbonyl group (XXVII). N···C–O contacts in six crystal



XXVII

structures were examined, the N···C distances ranging from 2.91 Å (i.e., nonbonded N···C=O contact) to 1.49 Å (i.e., covalent N–C–O linkage). It was assumed that each contact represents a point on, or near to, the minimum-energy pathway followed by a nitrogen nucleophile as it approaches a carbonyl group. The longest contact represents the incipient addition reaction, while the shortest contact corresponds to the completed reaction. Between them, the contacts should map out the minimum-energy reaction pathway, provided that the perturbing effects of crystal-packing forces are small enough to average out over the 6 structures.

The N···C–O geometries were described[41] by parameters shown in Figure 4 and tabulated in Table V. The N···C distance (d_1) is inversely correlated with the C–O

(41) Bürgi, H. B.; Dunitz, J. D.; Shefter, E. *J. Am. Chem. Soc.* 1973, *95*, 5065–5067.

Table V
Geometries of N···C-O Contacts[a]

compound	d_1, Å	d_2, Å	Δ, Å	N···C-O, deg
methadone	2.910	1.214	0.064	105.0
cryptopine	2.581	1.209	0.102	102.2
protopine	2.555	1.218	0.115	101.6
clivorine	1.993	1.258	0.213	110.2
retusamine	1.64	1.38	0.36	110.9
N-brosylmitomycin A	1.49	1.37	0.42	113.7

[a] Reference 41. Parameters are illustrated in Figure 4.

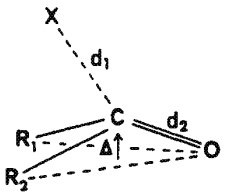


Figure 4. Parameters used to describe geometry of N···C=O and O···C=O contacts (ref 41, 42, 44). X = N or O.

distance (d_2), and the deviation of the carbon atom from the R_1,R_2,O plane (Δ). Thus, as the nitrogen atom approaches the carbonyl group, the C–O distance increases and the carbon atom is progressively displaced from the R_1,R_2,O plane. This can be related to the changes that occur in the molecular orbitals as the reaction proceeds: the π and π^* carbonyl group orbitals develop into an oxygen lone-pair orbital and an empty sp^n orbital on the carbon atom, which overlaps with the nitrogen lone-pair orbital. The N···C–O angles suggest that the nitrogen atom approaches from a constant direction, at ~107° to the C–O bond, i.e., the approach direction is *not* perpendicular to the C–O bond.

These conclusions were supported by a subsequent analysis[42] in which eight more structures were studied. It was found that the deviation of the carbon atom from the R_1,R_2,O plane depends on the nature of the nitrogen atom. Weak nucleophiles (e.g., anilines) induce smaller deviations than strong nucleophiles (e.g., aliphatic amines). Thus, a 2.76 Å (C—aryl)N···C=O contact in 1-*p*-tolyl-1-azacyclooctan-5-one[43] induces a deviation of only 0.016 Å (cf. Table V). Presumably, the energy required to displace the carbon atom from the R_1,R_2,O plane is offset by the attractive N···C interaction, which becomes weaker as the nucleophilicity of the nitrogen atom is reduced.[42] The same principles govern the interaction between oxygen nucleophiles and carbonyl groups.[44]

The crystallographic environments of divalent sulfur groups (R_1–S–R_2) have also been investigated.[45] These groups form short nonbonded contacts to both electrophiles and nucleophiles. The majority of S···electrophile contacts are approximately perpendicular to the R_1,S,R_2 plane. However, most S···nucleophile contacts lie in, or near to, this plane, and at an angle of ~180° to one of the S–R bonds. This suggests that approaching electrophiles interact preferentially with

(42) Dunitz, J. D. "X-Ray Analysis and the Structure of Organic Molecules"; Cornell University Press: Ithaca and London, 1979; 366–379.
(43) Kaftory, M.; Dunitz, J. D. *Acta Crystallogr., Sect. B* 1975, *B31*, 2912–2914.
(44) Bürgi, H. B.; Dunitz, J. D.; Shefter, E. *Acta Crystallogr., Sect. B* 1974, *B30*, 1517–1527.
(45) Rosenfield, R. E.; Parthasarathy, R.; Dunitz, J. D. *J. Am. Chem. Soc.* 1977, *99*, 4860–4862.

UM00012856
NOVARTIS EXHIBIT 1017
Novartis v. Regents, IPR2023-01346
Page 1602 of 4460

the highest occupied molecular orbital, i.e., a sulfur lone-pair orbital nearly perpendicular to the R_1,S,R_2 plane. Conversely, nucleophiles tend to approach along the direction of the lowest unoccupied molecular orbital, i.e., σ^* (S–R_1) or σ^* (S–R_2).[46]

Concluding Remarks

This Account illustrates the variety of chemical phenomena that can be investigated by systematic examination of published crystallographic results. Such analyses can now be carried out with comparative ease by both crystallographers and chemists. Although there is much scepticism about the relevance of crystallographic results to molecular properties in solution, this Account shows that this reservation has only limited justification. The reaction pathway studies, in particular, demonstrate that crystal-packing effects are small enough to permit meaningful analysis of very weak interactions, such as N···C=O and O···C=O.

(46) For other reaction pathway studies, see: Bürgi, H. B. *Inorg. Chem.* **1973**, *12*, 2321–2325. Bürgi, H. B. *Angew. Chem., Int. Ed. Engl.* **1975**, *14*, 460–473. Britton, D.; Dunitz, J. D. *Helv. Chim. Acta* **1980**, *63*, 1068–1073.

The 30 000 organocarbon crystal structures currently available cover an enormous chemical range and include many novel and unusual compounds (since these are the ones most likely to be examined by crystallographic methods). By the end of the century, there will be over 100 000 structures in the public domain. The importance of this information to organic chemistry can scarcely be overstated, because the results of most crystal structure determinations are precise, detailed, and unambiguous. However, studies of individual structures are often of limited value: if an unexpected structural feature is observed, it may not be statistically significant and may well be ascribed to experimental errors or packing effects. When the same feature is consistently observed in a series of related structures, these explanations become untenable and the observation must be rationalized in physicochemical terms. Thus, the *systematic* analysis of large numbers of related structures is a powerful research technique, capable of yielding results that could not be obtained by any other method.

We thank Professors Aldo Domenicano and Jack Dunitz for reading the manuscript prior to submission.

From Crystal Statics to Chemical Dynamics

HANS BEAT BÜRGI*

Laboratory for Chemical and Mineralogical Crystallography, University of Berne, CH-3012 Berne, Switzerland

JACK D. DUNITZ*

Organic Chemistry Laboratory, Swiss Federal Institute of Technology, CH-8092 Zürich, Switzerland

Received May 19, 1982 (Revised Manuscript Received October 6, 1982)

The study of molecular structure involves both static and dynamic aspects, the static aspects dealing with equilibrium arrangements of atoms in molecules, the dynamic ones with the relative motion of atoms during molecular vibrations or transformations, i.e., chemical reactions. The contribution of X-ray crystallography to the static aspects is well-known; in fact, for many years now, crystallography has been the main source of our information about the three-dimensional structure of molecules.[1] Automatic diffractometers and fast, powerful methods for interpreting the diffraction measurements have led to an unprecedented increase in the amount of structural information available.[2] Fortunately, for organic structures at least, this information is stored in computer-readable form in the Cambridge Structural Database (CSD), which has established itself as an essential instrument for answering questions about the systematics of atomic arrangements in molecules.[3]

It is not so well-known that crystallography can also provide important information about the dynamic aspects of molecular structure. Of course, we cannot observe the actual motion of the atoms; an X-ray diffraction experiment takes roughly 10^{-5}–10^{-6} s, whereas dynamic processes on the molecular level occur on a time scale of 10^{-12} s or less. Thus, diffraction measurements provide at best averaged information, in the form of mean-square vibration amplitudes for the individual atoms (expectation values of the square of the atomic displacements from equilibrium). This is the kind of information that is expressed in vivid, pictorial fashion by the thermal ellipsoids in the computer-drawn ORTEP diagrams that adorn many crystallographic publications.[4] At a given temperature, large extension

Hans-Beat Bürgi was born in Switzerland in 1942. He studied chemistry and received his Ph.D. degree at the ETH, Zürich, working with Jack D. Dunitz at the Laboratory for Organic Chemistry. After 2 years as a postdoctoral student of Larry S. Bartell at the University of Michigan, he joined the Laboratory for Inorganic Chemistry, ETH, Zürich. In 1979 he became Professor of X-ray crystallography at the University of Berne, Switzerland.

Jack D. Dunitz was born in Glasgow in 1923 and studied chemistry at Glasgow University, where he received his B.Sc. and Ph.D. degrees. Following a decade of postdoctoral studies at Oxford, Caltech, NIH, and the Royal Institution, London, he moved in 1957 to the ETH, Zürich, where he has been ever since and where he is Professor of Chemical Crystallography.

(1) J. D. Dunitz, "X-Ray Analysis and the Structure of Organic Molecules", Cornell University Press, Ithaca, NY, 1979.

(2) As of early 1982 the number of published organic crystal structures was more than 30 000 and increasing at the rate of about 4000 per year. Corresponding figures for inorganic structures are not known to us.

(3) For a recent authoritative review, see F. H. Allen, O. Kennard, and R. Taylor, *Acc. Chem. Res.*, preceding paper in this issue. See also the editorial by J. P. Glusker, *Acc. Chem. Res.*, 15, 231 (1982).

0001-4842/83/0116-0153$01.50/0 © 1983 American Chemical Society

UM00012857
NOVARTIS EXHIBIT 1017
Novartis v. Regents, IPR2023-01346
Page 1603 of 4460

FEATURE ARTICLE

www.rsc.org/crystengcomm

Crystal engineering of the composition of pharmaceutical phases. Do pharmaceutical co-crystals represent a new path to improved medicines?

Örn Almarsson*[a] and Michael J. Zaworotko*[b]

[a] *TransForm Pharmaceuticals, Inc., 29 Hartwell Avenue, Lexington, MA 02421, USA. E-mail: almarsson@transformpharma.com; Fax: +781 863 6519; Tel: +781 674 7894*

[b] *Department of Chemistry, University of South Florida, SCA400, 4202 E. Fowler Avenue, Tampa, FL 33620, USA. E-mail: xtal@usf.edu; Fax: +813 974 3203; Tel: +813 974 4129*

Received (in Columbia, MO, USA) 11th February 2004, Accepted 26th May 2004
First published as an Advance Article on the web 5th August 2004

The evolution of crystal engineering into a form of supramolecular synthesis is discussed in the context of problems and opportunities in the pharmaceutical industry. Specifically, it has become clear that a wide array of multiple component pharmaceutical phases, so called pharmaceutical co-crystals, can be rationally designed using crystal engineering, and the strategy affords new intellectual property and enhanced properties for pharmaceutical substances.

1 Introduction

"Benzoic acid and other carboxylic acids have been shown to be associated to double molecules in solution in certain solvents, such as benzene, chloroform, carbon tetrachloride and carbon disulfide...Benzoic acid exists in the monomeric form in solution in acetone, acetic acid, ethyl ether, ethyl alcohol, ethyl acetate and phenol; in these solutions the single molecules are stabilized by hydrogen bond formation with the solvent." (Linus Pauling in *The Nature of the Chemical Bond*, 2nd edition, Cornell University Press, 1948.)

Dr Örn Almarsson is senior director of Pharmaceutical Chemistry at TransForm Pharmaceuticals, Inc. Prior to joining TransForm in December of 2000, he was a research fellow in the department of Pharmaceutical Research and Development at Merck Research Laboratories in West Point, Pennsylvania. He received his BS degree in chemistry from the University of Iceland in 1988 and his PhD in physical-organic chemistry from the University of California at Santa Barbara in 1994. His PhD thesis work, performed under Prof. Thomas C. Bruice, is in the field of bio-organic mechanisms of nicotinamide co-factor redox reactions in dehydrogenases and the mechanisms of O–O bond cleavage in peroxidase model systems. At TransForm, Dr Almarsson has focused on development and application of high-throughput crystallization technologies for pharmaceutical compounds. His current work involves optimizing crystal forms for formulation of drug development candidates with the aim of enhancing biopharmaceutical performance and drug delivery properties.

Dr Mike Zaworotko is Professor and Chair of the Department of Chemistry at the University of South Florida, USF. He was born in Wales in 1956 and received his BSc and PhD degrees from Imperial College (1977) and the University of Alabama (1982), respectively. He joined USF in 1999. Current research interests include the following: crystal engineering, nanotechnology, supramolecular chemistry, X-ray crystallography. Particular emphasis is currently placed upon applications of crystal engineering in the context of nanoscale structures, magnetism, porosity and compositions of active pharmaceutical ingredients. Dr Zaworotko has published over 210 peer reviewed papers and he currently serves on the editorial boards of J. Chemical Crystallography and Crystal Growth & Design.

In terms of intrinsic value, active pharmaceutical ingredients (API's) are among the most valuable materials on the planet. It is therefore surprising that the growing field of crystal engineering[1–3] and its ability to produce new and potentially valuable materials has only addressed API's within the last two years.[4–9] Pharmaceuticals are generally comprised of an API, a formulation containing inactive ingredients as a carrier system, and a package for market performance and appeal. The vast majority of API's occur as solids. Crystalline API's are strongly preferred due to their relative ease of isolation, the rejection of impurities inherent to the crystallization process and the physico-chemical stability that the crystalline solid state affords. The problems that arise with the use of crystalline material are usually related to poor solubility properties and the existence of more than one crystalline form of an API. In terms of regulatory approval crystalline forms of an API have traditionally been limited to polymorphs, salts and stoichiometric solvates (pseudopolymorphs).[10] However, crystal engineering affords a paradigm for rapid development of a fourth class of API's, that of pharmaceutical co-crystals.

Crystal engineering can be defined as application of the concepts of supramolecular chemistry to the solid state with particular emphasis upon the idea that crystalline solids are *de facto* manifestations of self-assembly. Crystal structures can therefore be regarded as the result of a series of weak but directional molecular recognition events. With understanding comes the possibility of design and it is the advent of supramolecular synthesis[1–3] that facilitates the rational design of new structures and compositions. The roots of crystal engineering can be traced at least as far back as the 1930's, when Pauling defined the chemical bond in both covalent and noncovalent terms.[11] The term "crystal engineering" was coined by Pepinsky in 1955[12] but was not implemented until Schmidt studied a series of solid state reactions in crystalline solids.[13] Indeed, solvent free synthesis continues to represent an active area of research in the context of crystal engineering.[14,15] Based upon literature citations,† it is apparent that crystal engineering enjoyed rapid growth during the 1990's, especially in terms of organic solids and metal-organic solids but also in terms of organometallic[16] and inorganic structures.[17]

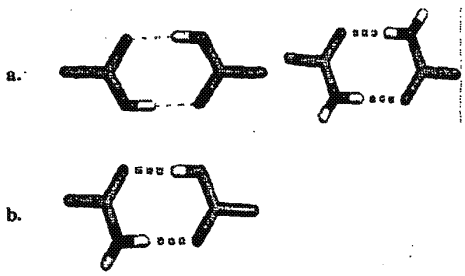
What are pharmaceutical co-crystals? Herein we define pharmaceutical co-crystals as being a subset of a broader group of multi-component crystals that also includes salts, solvates (pseudopolymorphs), clathrates, inclusion crystals and hydrates. In a supramolecular context, solvates and pharmaceutical co-crystals are related to one another in that at least two components of the crystal interact by hydrogen bonding and, possibly, other non-covalent interactions rather than by ion-pairing. Neutral compounds and salt forms alike have the potential to be solvated (*i.e.* interact with solvent molecules) or co-crystallized (*i.e.* interact with a co-crystal former). Solvate molecules and co-crystal formers can include organic acids or bases that remain in their neutral form within the multi-component crystal. The primary difference is the physical state of the isolated pure components: if one component is a liquid at room temperature, the crystals are referred to as solvates; if both components are solids at room temperature, the products are

DOI: 10.1039/b402150a

UM00012858
NOVARTIS EXHIBIT 1017
Novartis v. Regents, IPR2023-01346
Page 1604 of 4460

referred to as co-crystals. While at first glance these differences may seem inconsequential, they have profound impact on the preparation, stability, and ultimately on developability of products. Furthermore, whereas solvates are commonplace because they often occur as a serendipitous result of crystallization from solution, co-crystals, especially pharmaceutical co-crystals, represent a relatively unexplored class of compounds. On the other hand, as will become clear herein, pharmaceutical co-crystals can be rationally designed and there are many more potential co-crystal formers than there are solvents or counterions.

The complex nature of API structures means that they inherently contain exterior functional groups that engage in molecular recognition events. Indeed, it is the very presence of these functional groups that affords biological activity but also provides an ability to engage in more than one supramolecular event with itself, a solvent molecule or co-crystal former, thereby forming polymorphs, solvates or co-crystals, respectively. It is important to note that there are two basic types of molecular recognition that facilitate the formation of polymorphs, solvates and co-crystals. Functional groups that are self-complementary are capable of forming *supramolecular homosynthons*. For example, as revealed by Scheme 1a, carboxylic acid moieties and amide moieties can



Scheme 1 The formation of supramolecular synthons between acids and amides: (a) supramolecular homosynthons as exhibited by acid–acid and amide–amide dimers; (b) supramolecular heterosynthons as exhibited by acid–amide dimers.

form homodimers *via* a two-point donor-acceptor molecular recognition path. However, it is also possible for functional groups to engage with a different but complementary functional group, as noted by Pauling. Indeed, carboxylic acids and amides are complementary with each other and can interact through formation of a *supramolecular heterosynthon* (Scheme 1b). This particular motif has been studied for some time in the context of co-crystals.[18]

In this contribution we detail the current and potential impact of crystal engineering on our understanding of polymorphs, solvates and co-crystals with particular emphasis upon API's. Carboxylic acid and amide moieties are widely encountered in API's and studied in model compounds. They will therefore be used extensively in this contribution even though it should be remembered that they represent just a microcosm of the functional group diversity that exists in API's.

2 Crystal engineering in the context of polymorphs

"A solid crystalline phase of a given compound resulting from the possibility of at least two different arrangements of the molecules of that compound in the solid state" (W.C. McCrone in *Physics and Chemistry of the Organic Solid State*, Vol II, Wiley Interscience, New York, 725–726, 1965.)

McCrone's definition of a polymorph as presented above is particularly appropriate in the context of drugs, since the existence of highly functional API's invites multiple modes of self-organization and amounts to promiscuity in self-assembly. It is this feature and conformational flexibility that are the primary driving forces for the existence of crystal polymorphism. It is therefore not surprising that it is well and long documented that API's can exist in several polymorphic, solvated and/or hydrated forms.[10,18] This tendency for polymorphism represents both a problem and an opportunity in pharmaceutical research. Lack of reliability of manufacturing and physical (and sometimes chemical) instability of a given polymorph can be an issue for a drug developer, while a novel polymorph in the hands of a competitor can provide options for generic pharmaceutical competition.

We shall focus upon polymorphism from a supramolecular perspective with emphasis upon two functional groups that are commonly encountered in API's: carboxylic acids and amides.

2.1 Structures in which carboxylic acids are involved in self-organization.

Carboxylic acid moieties represent perhaps the longest and most widely studied functional group in terms of our understanding of hydrogen bonding in both solution and the solid state.[11] In the context of crystal structures, carboxylic acids exhibit a remarkable range of diversity in their supramolecular chemistry and this in turn leads to observation of polymorphs in even the most simple of chemical structures. There are two primary modes for carboxylic acids to self-organize in the form of supramolecular homosynthons: the dimer and the catemer. Such "supramolecular isomerism" is the origin of polymorphism exhibited by the two polymorphs of chloroacetic acid (Fig. 1). Fig. 1a illustrates the dimer motif which

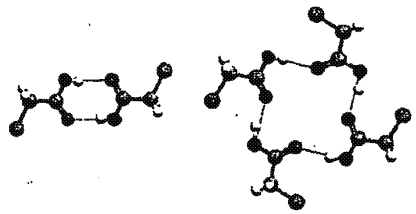


Fig. 1 The self-organization modes seen in the two reported polymorphs of chloroacetic acid: (a) centrosymmetric dimer; (b) catemer motif, which leads to a tetrameric assembly.

occurs in one polymorph[19] whereas Fig. 1b presents the second form, in which a catemer supramolecular synthon results in the formation of a tetrameric supramolecular assembly.[20] It should be noted that carboxylic acid polymorphs are not always a consequence of isomerism in supramolecular homosynthons. For example, they can result from factors such as different crystal packing arrangements of dimer motifs or, if appropriate, torsional flexibility, which can afford conformational polymorphism.[21] Nevertheless, there are other simple carboxylic acids that exhibit polymorphism because of dimer/catemer supramolecular isomerism (*e.g.* hydroxybenzoic acid,[22] oxalic acid[23] and tetrolic acid[24]).

The story does not end there: whereas there are over 4000 entries in the Cambridge Structural Database[25] (CSD) of crystal structures in which at least one carboxylic acid moiety is present, 1179 exhibit the dimer motif (29.4%) and only 86 exhibit the catemer motif (2.1%). In other words, the formation of supramolecular homosynthons is not the dominant supramolecular event in the solid state even if it might be in solution. An analysis of the remaining carboxylic acid containing crystal structures reveals that they typically form supramolecular structures that involve a carboxylic acid and a different functional group, *i.e.* they form *supramolecular heterosynthons*. The ability of a molecule to engage in either supramolecular homosynthons or supramolecular heterosynthons represents another avenue for the existence of polymorphism.

UM00012859
NOVARTIS EXHIBIT 1017
Novartis v. Regents, IPR2023-01346
Page 1605 of 4460

Polymorphism in molecules which contain multiple functional groups is exemplified by Fig. 2, which presents the monoclinic and

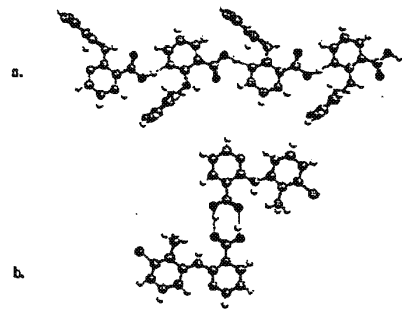
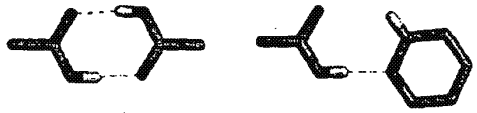


Fig. 2 The monoclinic (a) and triclinic (b) forms of 2-(2-methyl-3-chloroanilino)-nicotinic acid, an analgesic/anti-inflammatory molecule.

triclinic forms of 2-(2-methyl-3-chloroanilino)-nicotinic acid,[26] a molecule that exhibits analgesic and anti-inflammatory properties. Fig. 2 reveals that 2-(2-methyl-3-chloroanilino)-nicotinic acid can self-organize *via* either supramolecular homosynthons or supramolecular heterosynthons: (a) generation of head-to-tail chains sustained by a carboxylic acid–pyridine supramolecular heterosynthon; (b) formation of centrosymmetric dimers sustained by the carboxylic acid supramolecular homosynthon.

It is important to emphasize the distinction between supramolecular homosynthons and supramolecular heterosynthons since the latter represent a possible entry into the realm of multiple-component crystals and a diverse range of compositions of matter and physical properties. That carboxylic acids represent such a large subset of the CSD makes it possible to ask an important question: are supramolecular heterosynthons not just rational but also predictable? In the context of the pyridine–carboxylic supramolecular heterosynthon the CSD reveals that there are 424 compounds that contain both a carboxylic acid and an aromatic nitrogen base. 198 of these compounds (46.7%) exhibit the supramolecular heterosynthon rather than one of the carboxylic acid supramolecular homosynthons (Scheme 2). When one considers that many of the compounds in this dataset contain multiple functional groups this is a remarkably high rate of occurence.



a. homosynthon **vs.** **b. heterosynthon**

Scheme 2 The homosynthon *vs.* heterosynthon motifs observed in crystal structures of compounds in which both carboxylic acids and pyridine moieties are present. The heterosynthon dominates, occurring in 119/245 crystal structures whereas the homosynthon occurs in only 10 crystal structures.

2.2 Structures in which primary amides are involved in self-organization

Primary amides are also well represented in the CSD, with 1152 entries. The dominant supramolecular homosynthon is the centrosymmetric dimer as presented in Scheme 1. This homosynthon contains complementary hydrogen bond donors and acceptors and is capable of further self-assembly, thereby generating supramolecular tapes or sheets. Fig. 3a illustrates how chloroacetamide forms a tape network based upon self-organization of homodimers.[27–30] Interestingly, chloroacetamide also exhibits polymorphism and for the same fundamental reason as chloroacetic acid: it exhibits a catemer structure as well as a homodimer structure.[31] The

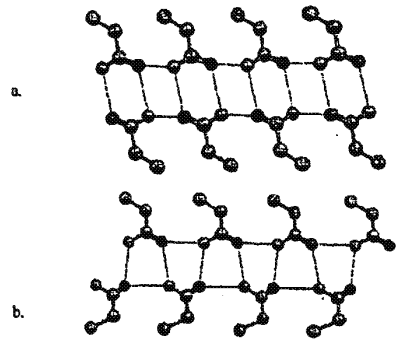


Fig. 3 The self-organization modes seen in two polymorphs of chloroacetamide: (a) centrosymmetric dimer that self-assembles as 1-D tapes; (b) catemer motif, which also forms 1-D tapes.

polymorphic form of chloroacetamide that is the result of catemer motifs is illustrated in Fig. 3b. It reveals that the superstructure is also that of a tape. The two forms of chloroacetamide crystallize in the same space group with almost identical cell parameters. This is an extremely unusual situation and is presumably related to the fact that the two tapes are similar in terms of dimensions and exterior features.

Chloroacetic acid and chloroacetamide serve as illustrations of how even small molecules with only one hydrogen bonding group can generate polymorphs based upon supramolecular isomerism. A similar analogy can be found in API's that contain acid and amide moieties. Piracetam, a learning process drug, is an amide-containing API that exemplifies the type of polymorphism that occurs when supramolecular isomerism occurs in supramolecular homosynthons. There are three forms of Piracetam reported in the CSD.[32,33] Two of these forms exist as tapes that are sustained by the amide homodimer and NH···O=C(carboxamide) hydrogen bonds (Fig. 4a).[32] The third form is sustained by catemer chains that are crosslinked by N–H···O=C(carboxamide) hydrogen bonds (Fig. 4b).[33] The superstructure can therefore be described as hydrogen bonded sheets.

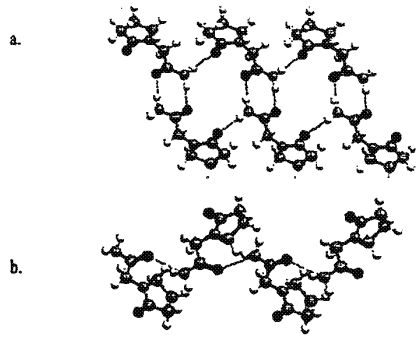


Fig. 4 The network structures formed by Piracetam: (a) homodimers form supramolecular tapes two forms; (b) 1-D chains sustained by the catemer motif are found in the third form.

To summarize the points made thus far:

- Single component crystals that contain carboxylic acid or amide moieties are prone to polymorphism even if only one hydrogen bonding moiety is present and supramolecular homosynthons are the primary molecular recognition events.
- In the case of API's, the situation is further complicated by the presence of additional hydrogen bonding moieties, which can lead to the formation of supramolecular heterosynthons.

UM00012860
NOVARTIS EXHIBIT 1017
Novartis v. Regents, IPR2023-01346
Page 1606 of 4460

• Carboxylic acid and amide groups were chosen as examples, because they are prevalent in the CSD and in API's. However, the points made thus far can be regarded as being generally relevant. For example, we recently reported[34] how alcohol–ether heterosynthons can afford polymorphic forms of butylated hydroxy anisole, an antioxidant that is commonly used in solid dosage forms of API's.[35,36] The difference between the two forms is striking: form I exists as the result of 4-fold helical chains: form II contains discrete hexamers.

How one might exploit supramolecular heterosynthons for the crystal engineering of new compositions of matter will form the basis of the remainder of this contribution.

3 Crystal engineering in the context of co-crystals

"Supramolecular synthons are structural units within supermolecules that can be formed and/or assembled by known or conceivable synthetic operations involving intermolecular interactions". (Gautam R. Desiraju *Angew. Chem. Int. Ed. Engl.*, 34, 2311, 1995.)

How does one develop a strategy for the preparation of co-crystals? Solvates are frequently encounted but are typically the result of serendipity rather than design and are often found as by-products of polymorph and salt screens. Co-crystals, on the other hand, are less ubiquitous but are more prone to rational design. Co-crystals have been prepared by melt-crystallization, by grinding[37] and by recrystallization from solvents.[14,15] Pharmaceutical co-crystals have the potential to be much more useful in pharmaceutical products than solvates or hydrates. First, the number of pharmaceutically acceptable solvents is very small. Secondly, solvents tend to be more mobile and have higher vapour pressures than small molecule co-crystal formers. It is not unusual to observe dehydration/desolvation of hydrates/solvates in solid dosage forms, depending on storage conditions. Solvent loss frequently leads to amorphous compounds, which are generally less chemically stable and can crystallize into less soluble forms. In contrast to solvents, most co-crystal formers are unlikely to evaporate from solid dosage forms, making phase separation less likely.

3.1 Co-crystals based upon acids or amides

As suggested earlier, an effective approach to understanding and designing co-crystals is to apply the paradigm of supramolecular synthesis, in particular exploitation of supramolecular heterosynthons. The ubiquity of acids and amides in the CSD makes them appropriate foci for design and synthesis. Indeed, the acid–amide supramolecular heterosynthon illustrated in Scheme 1a has been exploited by several groups for the generation of co-crystals[18,38–41] and the CSD reveals that there are 118 crystal structures in which both an acid and an amide moiety are present. Remarkably, 58 of these structures exhibit the acid–amide supramolecular heterosynthon whereas only 11 structures exhibit the acid homodimer and only 28 exhibit the amide homodimer. Fig. 5 presents two

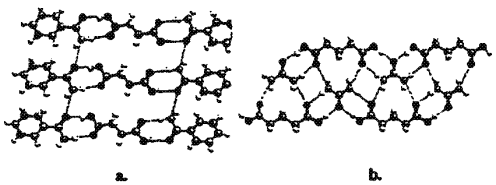


Fig. 5 Two examples of co-crystals that are sustained by the acid–amide supramolecular heterosynthon: (a) succinic acid : benzamide (1:2); (b) urea : glutaric acid (1:1).

prototypal examples of co-crystals that are sustained by the acid–amide supramolecular heterosynthon: succinic acid : benzamide[18] and urea : glutaric acid.[38] Acid–amide supramolecular heterosynthons are not the only examples of robust heterosynthons that are favored over the parent homosynthons. Acid–pyridine supramolecular heterosynthons, a subset of the acid–aromatic amine set described earlier, occur in 119 of the 245 crystal structures that contain both functional groups. Remarkably, only 10 of these 245 structures contain acid–acid homosynthons (Scheme 2).

Representative examples of co-crystals that are sustained by the pyridine–carboxylic acid supramolecular synthon are presented in Fig. 6. Maleic acid : 4,4′-bipyridine forms a discrete 2:1 adduct[42]

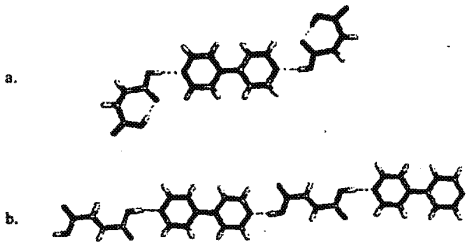


Fig. 6 Two examples of co-crystal structures formed by the acid–pyridine supramolecular heterosynthon: (a) maleic acid: 4,4′-bipyridine; (b) fumaric acid : 4,4′-bipyridine.

whereas fumaric acid : 4,4′-bipyridine forms in 1:1 stoichiometry and thereby generates a 1-D chain.[42]

3.2 Functional co-crystals

Examples of co-crystals have existed in conductive organic crystals, non-linear optical crystals, dyes, pigments and agrochemicals for some time[43] but have only recently been applied to API's. Several recent papers emphasize the importance of understanding supramolecular heterosynthons in the synthesis of pharmaceutical co-crystals. For example, the ability to insert 4,4′-bipyridine and related molecules between the carboxylic acid dimers of aspirin, *rac*-ibuprofen, and *rac*-flurbiprofen was recently reported.[6] Fig. 7 illustrates two of these structures, which further demonstrate the ability of the pyridine–carboxylic acid heterosynthon to compete with a carboxylic acid dimer homosynthon (Scheme 2).

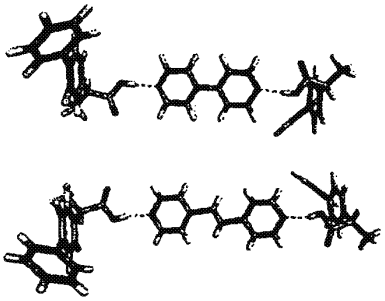


Fig. 7 The 2:1 supramolecular adducts formed by flurbiprofen and 4,4′-bipyridine (top) and 4,4′-dipyridylethane (bottom). Similar structures occur for ibuprofen and aspirin.

A second study focused on finding multiple solvates and co-crystals of carbamazepine.[5] Carbamazepine represents an excellent test case since four polymorphs and two solvates of carbamazepine have been reported in the literature. In all of the compounds for which structural data is available, carbamazepine molecules crystallize as amide dimers (Fig. 8). The crystal structures illustrate that each dimer contains a peripheral H-bond donor and acceptor pair that is unsatisfied due to geometric constraints imposed by the drug molecule. Simple H-bond acceptor solvents like acetone and DMSO insert themselves to fill voids between the adjacent pairs of dimers. Multiple co-crystal formers having hydrogen bonding

UM00012861
NOVARTIS EXHIBIT 1017
Novartis v. Regents, IPR2023-01346
Page 1607 of 4460

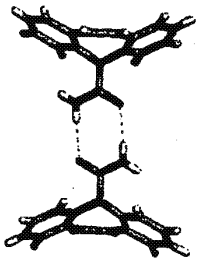
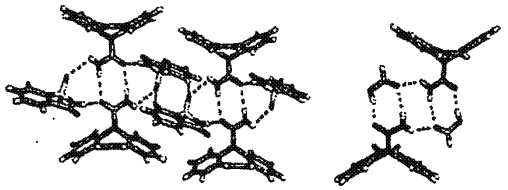


Fig. 8 The carbamazepine dimers that exist in all previously reported solvates and polymorphs of carbamazepine.

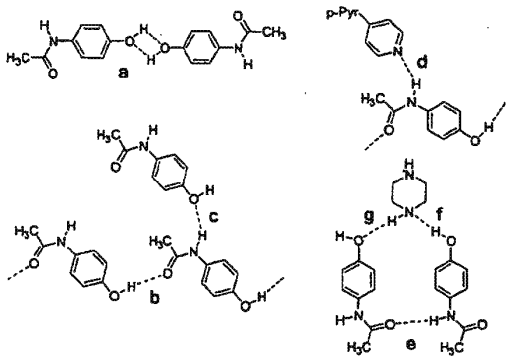
groups likewise insert themselves into the void, including saccharin and nicotinamide. The amide homosynthon can also be broken to form heterosynthon Ib. This was achieved to form solvates with acetic, formic, and butyric acids and co-crystals with trimesic and nitroisophthalic acid. The crystal structures of the carbamazepine : saccharin co-crystal and the formic acid solvate are illustrated in Fig. 9.



a. b.

Fig. 9 Examples of the supramolecular adducts formed in the crystal structures of co-crystals and solvates of carbamazepine: (a) saccharin co-crystal; (b) carbamazepine:formic acid solvate.

A study of adducts of acetaminophen (paracetamol) with ethers and amines provides additional examples of supramolecular synthons for co-crystal formation (Scheme 3).[9] While supramo-



Scheme 3 The supramolecular synthons observed in co-crystals of acetaminophen (paracetamol): IIIa–c occur in polymorphs whereas IIId and IIIe occur in co-crystals.

lecular homosynthon IIIa could have formed, both known forms of the pure material consist of linear head-to-tail chains held together through motif IIIb; the chains are cross-linked through synthon IIIc. The linear chain structure is preserved in co-crystals with 4,4′-bipyridine, but the cross-linking interaction IIIc is replaced by IIId, in which the 4,4′-bipyridine is hydrogen bonded to the amide hydrogen. The chains remain cross-linked but only through pi-stacking interactions between 4,4′-bipyridine pairs on neighboring chains. In co-crystals with piperazine, the acetaminophen forms head-to-head chains through IIIe. Each chain is joined to the next through a layer of piperazine molecules that interact through heterosynthons IIIf and IIIg. The paper also includes many solvates that will not be reviewed here, but their supramolecular synthons should also be applicable in the context of co-crystal design and formation.

The analysis of molecules for complementarity of supramolecular synthons represents a valuable approach to screening that a knowledgeable scientist can exploit to narrow the search for co-crystals. However, an early study of 1:1 molecular complexes between the antibacterial agents trimethoprim (TMP) and sulfamethoxypyridazine (SMP) highlights the need to explore the space beyond those leading to expected interactions.[44] Each complex contains an 8-membered, hydrogen-bonded ring joining the two molecules as shown in Fig. 10. The specific ring structures formed

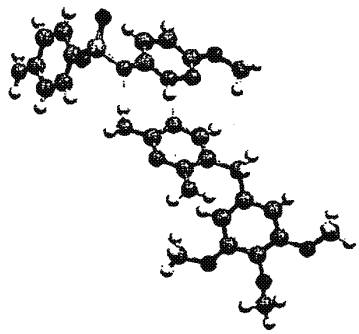


Fig. 10 The 8-membered hydrogen-bonded ring that links antibacterial agents trimethoprim (TMP) and sulfamethoxypyridazine (SMP).

are not those that might have been predicted by inspection of the structures of the neutral molecules. Instead, the synthons are derived from the 2-aminopyridine of TMP and the zwitterionic form of SMP involving the sulfonamide (pK_a ~ 7) and pyridazine (pK_a ~ 2). The zwitterion is a thermodynamically unfavorable form of SMP in aqueous solution. This example of assembly through an unstable intermediate underscores the limitation of the approach of analyzing co-crystal formation solely on the basis of pK_a arguments. A more comprehensive approach is needed. HT crystallization offers the possibility to uncover unexpected interactions by screening against a full library of pharmaceutically acceptable molecules instead of limiting the studies to co-crystal formers with perceived complementarity.

The more comprehensive approach to study expected and unexpected co-crystal formation events is high-throughput (HT) crystallization. The discovery of pharmaceutically acceptable co-crystals consisting of hydrogen-bonded trimers of two molecules of *cis*-itraconazole, a triazole anti-fungal agent, and a molecule of a 1,4-dicarboxylic acid resulting from a HT crystallization screen was recently reported.[8] The crystal structure of the succinic acid co-crystal (Fig. 11) reveals a supramolecular heterosynthon between the triazole of each pair of drug molecule and carboxylic acid moieties on a single diacid molecule. The extended succinic acid molecule fills a pocket, while bridging the triazole groups. The interaction between the 1,4-diacid and the strongest base on itraconazole (piperazine) is not observed in the co-crystal structure. Other 1,4-diacids capable of extended (anti-) conformations also yielded co-crystals with itraconazole, while co-crystals could not be made from maleic acid with *Z*-regiochemistry, or from 1,3- or 1,5-dicarboxylic acids. Hence, structural fit appears to be far more important than acid–base strength complementarity for co-crystallization of itraconazole with 1,4-dicarboxylic acids.

The structures presented herein demonstrate that pharmaceutical co-crystals represent an interesting and emerging class of pharma-

CrystEngComm, 2004, 6, 489–493 | 493

UM00012862
NOVARTIS EXHIBIT 1017
Novartis v. Regents, IPR2023-01346
Page 1608 of 4460

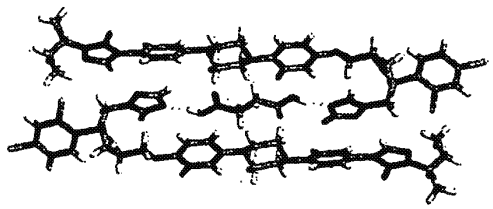


Fig. 11 The 2:1 supramolecular adduct formed by itraconazole and succinic acid.

ceutical materials in terms of rational design, projected diversity and applicability. Furthermore, the study of pharmaceutical co-crystals, along with polymorphs, solvates, salts and hydrates, is perfectly suited to HT crystallization experimentation and could in the future be considered an integral part of form selection processes in pharmaceutical research and development.

4 Conclusions and future directions

"What would the properties of materials be if we could really arrange the atoms the way we want them?...we will get an enormously greater range of possible properties that substances can have, and of different things that we can do." (Richard P. Feynman, December 29, 1959).

In the world of pharmaceuticals, the opportunity presented by co-crystals appears to be significant. Published examples of pharmaceutical co-crystals are few as yet, but we now believe the approach can be applied broadly to API's. The design and selection of optimal pharmaceutical materials based on supramolecular synthesis is a relatively low-risk strategy, because the approach employs principles of molecular recognition and self-assembly rather than creating covalent bonds. Therefore, there are no covalent modifications of the API in question. Nevertheless, some big questions remain:

4.1 How large is the space of pharmaceutical co-crystals?

Compared with the space of salt forms, solvates and polymorphs, how large is the space of pharmaceutical co-crystals? Polymorphism tendency of pharmaceutical substances varies greatly, but the general observation is that most compounds are at some time or another going to display polymorphic behavior. Typically, the extent of polymorphism of pharmaceuticals is limited to a handful of different crystal forms. A recent review classifies highly polymorphic materials as having 4 or more forms.[45] Solvates (including hydrates) can be more numerous, and in certain cases very large numbers of solvates can be observed. Indeed, one study suggests that sulfathiazole is inordinately promiscuous in terms of solvate formation, with over one hundred solvates found.[46] Salt forms can be numerous as well, with over 90 acids and 30 bases being considered suitable for pharmaceutical salt selection.[47] Examples of compounds possessing a dozen or more crystalline salt forms have been published.[48,49] It is important to remember that salt formation is generally directed at one acidic or basic functional group. In contrast, co-crystals can simultaneously address multiple functional groups (synthons) in a single drug molecule. In addition, the space is not limited to binary combinations (such as acid–base pairs) since tertiary and quaternary co-crystals are realistic possibilities. Co-crystal formers for pharmaceutical use remain to be enumerated fully, but we argue that well over a hundred solid materials with GRAS status (including food additives and other well-accepted substances) can be employed. Even more provocatively, one might consider using sub-therapeutic amounts of eminently safe drug substances, such as aspirin and acetaminophen, as legitimate co-crystal formers, thus expanding the arsenal even further. Taken together with the high dimensionality and resulting combinatorial nature of supramolecular assembly, the space of pharmaceutical co-crystals would appear to be extremely large: one can easily envision thousands of possibilities for any given drug with at least two synthons present in the molecule. Such diversity will probably be best addressed with combinatorial methodologies, such as high-throughput crystallization.

4.2 Can there be rational, directed design of pharmaceutical co-crystal phases?

This is another question which relates to the prospect for design. Crystal structures are inherently unpredictable, but the interactions that occur prior to a crystal forming or growing are predictable. An analogy can be drawn to salt selection,[47,50] in which pK_a arguments are used to select acid–base pairs that can be converted to salt compounds. The prediction of the proton transfer event is based on solution data, but the occurrence of a crystalline salt form cannot be predicted *a priori*. Based on the examples of rational synthon selection presented here, it follows that strategies of rational design of co-crystal experimentation are viable.

4.3 Are pharmaceutical co-crystals more or less prone to polymorphism than other pharmaceutical phases?

This question will not have a direct answer, because to prove the absence of polymorphism is tantamount to "proving the negative". But if one considers the argument that compounds have a lower degree of self-complementarity than complementarity to a rationally selected co-crystal former, one might suspect that a compound polymorphic in the pure state could display a decreased tendency to polymorphism as a co-crystal relative to the pure phase. Support for or defeat of this argument will involve significant research. Initial indications are that polymorphic substances may provide good candidates for co-crystal formation.[39a] As an example, carbamazepine can exist as four well characterized polymorphs[51] and a dihydrate.[52] This drug was recently converted to many co-crystals.[5] In terms of assessing polymorphism, one co-crystal of carbamazepine and saccharin has only displayed one packing arrangement, despite testing *via* HT crystallization in over 2000 experiments.[53] In contrast, two co-crystal structures of a *N,N'*-bis(para-bromophenyl)melamine-diethylbarbital demonstrate how a specific heterosynthon between the two molecules is robust, but packing of the tapes into a crystalline arrangement can lead to two discrete polymorphs.[54] Hence, there may be opportunity to reduce the practical extent of polymorphism of drug compounds specifically by co-crystal formation although there may be exceptions.

4.4 What opportunities exist for tuning physico-chemical properties by pharmaceutical co-crystal formation?

This is perhaps the most important question, because it is after all the complex interplay of form, function and performance attributes that determine success (or failure) of a particular pharmaceutical formulation.[55] Issues ranging from *poor solubility* and inadequate dissolution properties to lack of crystallinity and attendant instability plague the industry.[56] Poor aqueous solubility is a growing problem in the industry and it is having an impact on the productivity of drug research. The solubility issue hampers preclinical study of a new drug candidate, and can limit dosing and bioavailability. New strategies to deal with these problems are badly needed. Why are API's increasingly found to be of low solublility? There are varying ways to speculate around this question, but some would point to the methodologies that are now employed to discover pharmacologically active compounds. *In*

UM00012863
NOVARTIS EXHIBIT 1017
Novartis v. Regents, IPR2023-01346
Page 1609 of 4460

vitro assays have largely replaced *in vivo* animal screens as means to discover active compounds. The challenge of drug delivery is not addressed until there is a real desire to advance a compound into the development process. In addition, combinatorial chemistry and application of genomics have generated molecular targets for which the most potent lead compounds are inherently poorly soluble. Attempts to engineer compounds *via* medicinal chemistry avenues often lead to frustration, as the *in vitro* activity is frequently lost with increased water solubility. In the end, a discovery project may end up advancing a compound for which the stable crystal form exhibits inadequate aqueous solubility or dissolution rate that leads to poor oral absorption or inability to deliver by other routes (*e.g.* injection or inhalation). The most common strategy currently employed for improving bioavailability and optimizing drug delivery is to prepare salt forms of ionizable compounds, using pharmaceutically acceptable acids and bases. However, in the case of compounds that cannot form stable salts in aqueous medium, pharmaceutical scientists are left with few good options for material design, and must resort to particle size reduction to the nanometer range, deliberate amorphization, or solubilization in non-aqueous vehicles. These processes lead to formulations that have more physico-chemical problems than crystalline preparation.[55]

In terms of addressing the *stability issue*, one of the most important challenges presently is crystallization of compounds that are amorphous. In general, amorphs are undesirable forms due to physical instability (at the very least, there is the theoretical possibility of the material crystallizing at some point). Chemical reactivity can be significantly increased in amorphous states relative to crystalline forms.[57] In addition, amorphous forms tend to be hygroscopic and have low powder densities, giving rise to significant processing challenges. One reason for the resistance to crystallization is undoubtedly the mismatch that can occur in the number of hydrogen bond donors and acceptors in a molecule. In such cases, a solvate (or series of solvates) that leads to more satisfied hydrogen bond arrangements may be produced, while the pure, desolvated substance remains amorphous. An example of this situation is the HCl salt of the ACE inhibitor quinapril HCl.[57b] The opportunity exists to use co-crystallization to replace the solvate, while taking advantage of the supramolecular synthons that are suggested by the solvate structures. Given a co-crystal form thus obtained, one can expect the crystallinity of the material to result in greater stability and other desirable properties as compared with the amorphous form. In terms of solubility, amorphous compounds can have significant advantage over crystalline forms.[58,59] Though this advantage could find use in isolated cases, the lack of a crystalline form and concern over phase changes make the use of amorphous drugs in market formulations undesirable. When a crystalline form of a pure phase exhibits poor solubility or slow dissolution rate in aqueous media that translates to inadequate bioperformance, the strategies of salt selection and co-crystal formation should be considered. While salts can be made of acidic and basic drugs, the large space of non-ionizable compounds are generally candidates for co-crystal exploration. The *in vitro* dissolution profile of carbamazepine-saccharin co-crystal[60] illustrates the superior dissolution of the drug molecule in that context as compared with one of the pure anhydrous polymorphs. While the polymorph transiently supersaturates in the aqueous medium and subsequently precipitates to eventually form the known dihydrate, the co-crystal supersaturates to a sustained two-fold equilibrium solubility of the dihydrate. Such supersaturation behavior has been found to influence the bioavailability of carbamazepine.[61] While equilibrium solubility of drug compounds in co-crystals may be less affected than in the context of salt forms, the kinetic aspects of solubilization provide the key to many successful formulation strategies, such as oral immediate or controlled release. Co-crystals clearly open up a vast space of possibilities for exploring the range of dissolution characteristics, and facilitate co-optimization with other parameters, such as stability and processability.

To summarize, despite the need for a greater understanding and control of the crystalline phases for pharmaceutical development, the concepts of supramolecular synthesis and crystal engineering have remained underexploited in the world of drugs. As presented herein, applying the concept of supramolecular synthesis to the development of pharmaceutical co-crystals would seem to represent a new paradigm that would address both intellectual and property issues related to drug development and delivery, especially when supramolecular synthesis is coupled with HT screening technologies.

Notes and references

† There has been steady growth in occurrence of the term "crystal engineering" in titles, keywords or abstracts as follows for 1989–2003, respectively: 4, 6, 6, 14, 26, 22, 19, 45, 59, 67, 96, 93, 129, 129, 133. The actual number of papers addressing the general subject of crystal engineering is much larger.

1 (*a*) G. R. Desiraju, *Crystal Engineering—The Design of Organic Solids*, Elsevier, Amsterdam, 1989; (*b*) G. R. Desiraju, *Angew. Chem., Int. Ed. Engl.*, 1995, **34**, 2311–2327.
2 M. C. Etter, *J. Chem. Phys.*, 1991, **95**, 4601–4610; M. C. Etter, *Acc. Chem. Res.*, 1990, **23**, 120–126.
3 B. Moulton and M. J. Zaworotko, *Chem. Rev.*, 2001, **101**, 1629.
4 Ö. Almarsson, M. B. Hickey, M. L. Peterson, S. L. Morissette, C. McNulty, S. Soukasene, M. Tawa, M. MacPhee and J. F. Remenar, *Cryst. Growth Des.*, 2003, **3**, 927–933.
5 S. G. Fleischman, S. S. Kuduva, J. A. McMahon, B. Moulton, R. B. Walsh, N. Rodriguez-Hornedo and M. J. Zaworotko, *Cryst. Growth Des.*, 2003, **3**, 909–919.
6 S. G. Fleischman, L. Morales, B. Moulton, N. Rodríguez-Hornedo, R. B. Walsh and M. J. Zaworotko, *Chem. Commun.*, 2003, 186–187.
7 S. Datta and D. J. W. Grant, *Nat. Rev. Drug Discovery*, 2004, **3**, 42–57.
8 J. F. Remenar, S. L Morissette, M. L. Peterson, B. Moulton, J. M. MacPhee, H. R. Guzman and Ö. Almarsson, *J. Am. Chem. Soc.*, 2003, **125**, 8456–8457.
9 I. D. H. Oswald, D. R. Allen, P. A. McGregor, W. D. S. Motherwell, S. Parsons and C. R. Pulham, *Acta Crystallogr.*, 2002, **B58**, 1057–1066.
10 (*a*) J. K. Haleblian, *J. Pharm. Sci.*; 1975, **64**, 1269; (*b*) J. Bernstein, *Polymorphism in Molecular Crystals*, Clarendon Press, Oxford, 2002.
11 L. Pauling, *The Nature of the Chemical Bond*, Cornell University Press, New York, 2nd edn., 1948.
12 R. Pepinsky, *Phys. Rev.*, 1955, **100**, 971.
13 G. M. Schmidt, *Pure Appl. Chem.*, 1971, **27**, 647.
14 F. Toda, *Chem. Rev.*, 2000, **100**, 1025–1074.
15 T. Friscic and L. R. MacGillivray, *Chem. Commun.*, 2003, 1306–1307.
16 D. Braga, F. Grepioni and G. R. Desiraju, *Chem. Rev.*, 1998, **98**, 1375–1405.
17 R. C. Finn, J. Zubieta and R. C. Haushalter, *Prog. Inorg. Chem.*, 2003, **51**, 421–601.
18 (*a*) L. Leiserowitz and F. Nader, *Angew. Chem.*, 1972, **84**, 536; (*b*) C. M. Huang, L. Leiserowitz and G. M. J. Schmidt, *J. Chem. Soc. Perkins Trans. 2*, 1973, **5**, 503; (*c*) Z. Berkovitch-Yellin, L. Leiserowitz and F. Nader, *Acta Cryst.*, 1977, **B33**, 3670.
19 J. A. Kanters, G. Roelofsen and T. Feenstra, *Acta. Cryst. B.*, 1976, **32**, 3331.
20 J. A. Kanters and G. Roelofsen, *Acta. Cryst. B.*, 1976, **32**, 3328.
21 J. Bernstein and A. T. Hagler, *J. Am. Chem. Soc.*, 1978, **100**, 673–681.
22 G. V. Gridunova, *Kristallografiya*, 1982, **27**, 267.
23 J. L. Derissen and P. H. Smit, *Acta Cryst. B*, 1974, **30**, 2240.
24 V. Benghiat and L. Leiserowitz, *J. Am. Chem. Soc. Perkins Trans. 2*, 1972, **12**, 1763.
25 F. H. Allen and O. Kennard, *Chem. Des. Automation News*, 1993, **8**, 31.
26 M. Takasuka, H. Nakai and M. Shiro, *J. Chem. Soc. Perkins Trans. 2*, 1982, **9**, 1061.
27 J. Dejace, *Acta. Cryst.*, 1955, **8**, 851.
28 B. R. Penfold and W. S. Simpson, *Acta. Cryst.*, 1956, **9**, 831.
29 B. Kalyanaraman, L. D. Kispert and J. L. Atwood, *J. Cryst. Mol. Struct.*, 1978, **8**, 175.

UM00012864
NOVARTIS EXHIBIT 1017
Novartis v. Regents, IPR2023-01346
Page 1610 of 4460

30 Y. Kato and N. Oguro, *Mem. Osaka Kyoiku Univ. Ser. 3*, 1982, 30, 155.
31 M. Katayama, *Acta. Cryst.*, 1956, 9, 986.
32 G. Admiraal, J. C. Eikelenboom and A. Vos, *Acta. Cryst. B.*, 1982, 38, 2600.
33 D. Louer, M. Louer, V. A. Dzyabchenko, V. Agafonov and R. Ceolin, *Acta. Cryst. B.*, 1995, 51, 182.
34 J. A. McMahon, M. J. Zaworotko and J. F. Remenar, *Chem. Commun.*, 2004, 278.
35 H. Verhagen, P. A. E. L. Schilderman and J. C. S Kleinjans, *Chem-Biol. Interactions*, 1991, 80, 109.
36 J. W. Finley and P. Given Jr, *Food Chem. Toxicol.*, 1986, 24, 999.
37 A. V. Trask, S. W. D. Motherwell and W. Jones, *Chem. Commun.*, 2004, 890–891.
38 V. Videnova-Adrabinska and M. C. Etter, *J. Chem. Cryst.*, 1995, 25, 823.
39 (*a*) C. B. Aakeroy, A. M. Beatty and B. A. Helfrich, *Angew. Chem. Int. Ed. Engl.*, 2001, 40, 3240; (*b*) C. B. Aakeroy, A. M. Beatty and B. A. Helfrich, *J. Am. Chem. Soc.*, 2002, 124, 14425.
40 (*a*) S. Ohba, H. Hosomi and Y. Ito, *J. Am. Chem. Soc.*, 2001, 123, 6349; (*b*) Y. Ito, H. Hosomi and S. Ohba, *Tetrahedron*, 2000, 56, 6833; (*c*) H. Hosomi, S. Ohba and Y. Ito, *Acta. Cryst. C.*, 2000, 56, 507.
41 (*a*) G. Smith, K. E. Baldry, K. A. Byriel and C. H. L. Kennard, *Aust. J. Chem.*, 1997, 50, 727; (*b*) R. C. Bott, G. Smith, V. D. Wermuth and N. C. Dwyer, *Aust. J. Chem.*, 2000, 53, 767; (*c*) G. Smith, M. G. Coyne and J. M. White, *Aust. J. Chem.*, 2000, 53, 203; (*d*) T. J. M. Luo and G. T. R. Palmore, *Cryst. Growth Des.*, 2002, 2, 337; (*e*) P. Vishweshwar, A. Nangia and V. M. Lynch, *Cryst. Growth Des.*, 2003, 3, 783–790; (*f*) L. S. Reddy, A. Nangia and V. M. Lynch, *Cryst. Growth Des.*, 2004, 4, 89–94.
42 S. Chatterjee, V. R. Pedireddi and C. N. R. Rao, *Tetrahedron Lett.*, 1998, 39, 2843.
43 (*a*) J. Fabian, H. Nakazumi and M. Matsuoka, *Chem. Rev.*, 1992, 92, 1197; (*b*) G. de la Torre, P. Vazquez, F. Agullo-Lopez and T. Torres, *J. Mater. Chem.*, 1998, 8, 1671.
44 G. Bettinetti, M. R. Caira, A. Callegari, M. Marcello, M. Sorrenti and C. Tadini, *J. Pharm. Sci.*, 2000, 89, 478–489.
45 S. Morissette, Ö. Almarsson, M. Peterson, J. Remenar, M. Read, A. Lemmo, S. Ellis, M. Cima and C. Gardner, *Adv. Drug Deliv. Rev.*, 2004, 56(3), 275–300.
46 A. L. Bingham, D. S. Hughes, M. B. Hursthouse, R. W. Lancaster, S. Tavener and T. L. Threlfall, *Chem. Comm.*, 2001, 603.
47 P. H. Stahl and M. Nakano, Pharmaceutical Aspects of the Drug Salt Form, in *Handbook of Pharmaceutical Salts: Properties, Selection, and Use*, ed. P. H. Stahl and C.G. Wermuth, Wiley-VCH/VCHA, New York, 2002.
48 S. M. Berge, L. D. Bighley and D. C. Monkhouse, *J. Pharm. Sci.*, 1977, 66, 1–19.
49 J. F. Remenar, J. M. MacPhee, B. K. Larson, V. A. Tyagi, J. H. Ho, D. A. McIlroy, M. B. Hickey, P. B. Shaw and O. Almarsson, *Org. Process. Res. Dev.*, 2003, 7, 990–996 and references therein.
50 P. L. Gould, *Int. J. Pharm.*, 1986, 33, 201.
51 A. L. Grzesiak, M. Lang, K. Kim and A. J. Matzger, *J. Pharm. Sci.*, 2003, 92, 2260.
52 F. U. Krahn and J. B. Mielck, *Pharm. Acta Helv.*, 1987, 62, 247.
53 M. B. Hickey, personal communication.
54 J. A. Zerkowski, J. C. MacDonald and G. M. Whitesides, *Chem. Mater.*, 1997, 9, 1933.
55 S.-D. Clas, *Curr. Opin. Drug Disc. Dev.*, 2003, 6, 550.
56 Ö. Almarsson and C. R. Gardner, *Current Drug Discovery*, 2003, pp. 21–26.
57 (*a*) S. R. Byrn, R. R. Pfeiffer and J. G. Stowell, *Solid-State Chemistry of Drugs*, SSCI, Inc., West Lafayette, IN, 1999; (*b*) S. R. Byrn, A. W. Newman and W. Xu, *Adv. Drug Deliv. Rev.*, 2000, 48, 115.
58 B. C. Hancock and M. Parks, *Pharm. Res.*, 2000, 17, 397–404.
59 S.-D. Clas, M. Cotton, E. Moran, S. Spagnoli, G. Zografi and E. B. Vadas, *Thermochim. Acta.*, 1996, 288, 83.
60 N. Rodriguez-Hornedo, personal communication.
61 Y. Kobayashi, S. Ito, S. Itai and K. Yamamoto, *Int. J. Pharm.*, 2000, 193, 137.

UM00012865
NOVARTIS EXHIBIT 1017
Novartis v. Regents, IPR2023-01346
Page 1611 of 4460

The work was supported in part by a grant from the Israeli Ministry of Science and Technology.

Supplementary data for this paper are available from the IUCr electronic archives (Reference: CF1132). Services for accessing these data are described at the back of the journal.

References

Bondi, A. (1964). *J. Phys. Chem.* **68**, 441–445.

Bulgarovskaya, I. V., Sobolev, A. N., Zavodnik, V. E., Khodorkovsky, V. Yu. & Neiland, O. Ya. (1988). *Proc. Acad. Sci. Latv. SSR Chem.* **3**, 349–354.

Bulgarovskaya, I. V., Zavodnik, V. E. & Vozzhennikov, V. M. (1990). *Khim. Fiz.* **9**, 224–227.

Campaign, E. & Jacobsen, N. W. (1964). *J. Org. Chem.* **29**, 1703–1708.

Klingsberg, E. (1963). *J. Am. Chem. Soc.* **85**, 3244–3246.

Ried, W. & Conte, R. (1971). *Chem. Ber.* **104**, 1573–1579.

Sheldrick, G. M. (1990). *Acta Cryst.* A**46**, 467–473.

Sheldrick, G. M. (1993). *SHELXL93. Program for the Refinement of Crystal Structures.* University of Göttingen, Germany.

Siemens (1990). *P3 Diffractometer Control Program.* Version 4.01. Siemens Analytical X-ray Instruments Inc., Madison, Wisconsin, USA.

Siemens (1992). *SHELXTL.* Siemens Analytical X-ray Instruments Inc., Madison, Wisconsin, USA.

Vega, D. R. & Baggio, R. F. (1989). *Acta Cryst.* C**45**, 1612–1618.

Watson, W. H., Galloy, J., Grossie, D. A. & Nakajama, J. (1984). *Acta Cryst.* C**40**, 190–201.

Acta Cryst. (1998). C**54**, 1367–1369

1:1 Complex of Octadecanoic Acid and 3-Pyridinecarboxamide

MAKOTO AMAI,[a] TOMOHIRO ENDO,[a] HIROMASA NAGASE,[a] HARUHISA UEDA[a] AND MASAYUKI NAKAGAKI[b]

[a]*Department of Physical Chemistry, Hoshi University, 4-41 Ebara 2-Chome, Shinagawa-ku, Tokyo 142, Japan, and* [b]*Tokyo Institute of Colloid Science, 502 Higashi-Nakano 4-4-3, Nakano-ku, Tokyo 164, Japan. E-mail: ueda@hoshi.ac.jp*

(*Received 9 June 1997; accepted 11 December 1997*)

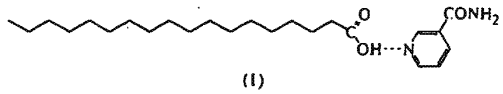
Abstract

An equimolar mixture of stearic acid (octadecanoic acid) and nicotinamide (3-pyridinecarboxamide) in acetone yields crystals of a 1:1 complex, $C_{18}H_{36}O_2.C_6H_6N_2O$. In this structure, the 1:1 complexes form dimers through hydrogen bonds between the amide groups, thus forming a lamellar structure. The alkyl chain of stearic acid has an all-*trans* conformation.

© 1998 International Union of Crystallography
Printed in Great Britain – all rights reserved

Comment

The title compound, (I), has the bitter taste of nicotinamide and the pharmaceutical advantage of improved hygroscopicity (Ayukawa *et al.*, 1986). Nicotinamide is released from (I) at a certain temperature and pH level depending on the number of C atoms contained in the fatty acid. The applicability of a pH- and thermo-responsive drug delivery system has been reported (Yokoyama *et al.*, 1993; Yokoyama, Sunohara *et al.*, 1994; Yokoyama, Miyamura & Fujie, 1994). However, the crystal structures of these complexes have not been determined. Therefore, we report here the structure of the title compound, (I).



(I)

The numbering scheme for the equimolar complex of stearic acid and nicotinamide is given in Fig. 1. The equimolar complex forms a hydrogen-bonded dimer, thus forming a lamellar structure. As is apparent from Table 2, which gives geometric details of the hydrogen bonds, and also from Fig. 2, which shows a projection of the title compound along the *a* axis, three types of hydrogen bonding occur in this structure. One hydrogen bond forms between the N1 atom of the pyridine ring of the nicotinamide (acceptor) and the O2 atom of the stearic acid (donor), with an N1···O2 distance of 2.693 (1) Å. Another hydrogen bond forms between the O3 atom of the amide group of the nicotinamide (acceptor) and the N2 atom of the amide group of the other nicotinamide (donor), with an O3···$N2^{i}$ distance of 2.939 (1) Å, thus forming the dimer. The third hydrogen bond is formed between two amide groups, between atoms O3 (acceptor) and N2 (donor), with an O3···$N2^{ii}$ distance of 2.904 (1) Å, being parallel to the lamellar structures (the symmetry codes are as in Table 2).

As is apparent from Table 1, which gives bond lengths and torsion angles, the C1—O1 bond length of 1.199 (2) Å and the C1—O2 length of 1.321 (2) Å are characteristic of C=O and C—O bonds.

The amide group in the title compound is twisted out of the plane of the pyridine ring. The torsion angles N2—C24—C20—C21 and O3—C24—C20—C19 are 26.0 (2) and 25.3 (2)°, respectively; these angles are considerably different from the torsion angles of 179 and −168° calculated by Wright & King (1954). Compared with the crystal structure of nicotinamide alone, the amide group of the title compound is rotated in a counterclockwise direction by about 150° around C20—C24. That is to say, in the case of nicotinamide alone, two N atoms of the amide group and the pyridine ring are present on the same side, but in the title compound, the two N atoms are present on opposite sides.

UM00012866
NOVARTIS EXHIBIT 1017
Novartis v. Regents, IPR2023-01346
Page 1612 of 4460

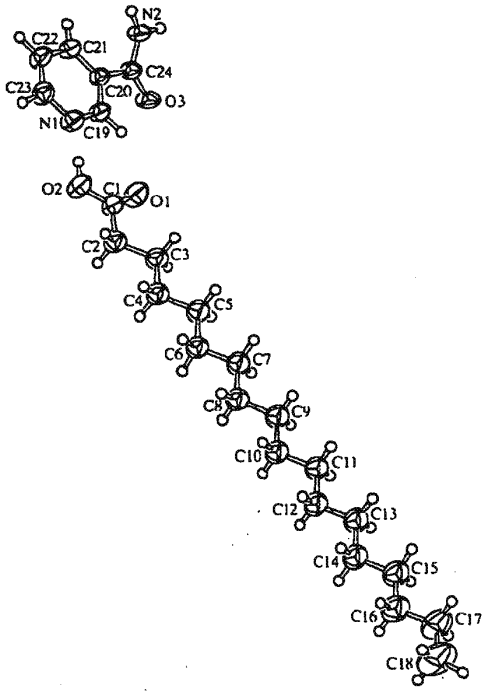


Fig. 1. Drawing of title compound showing the numbering scheme. Displacement ellipsoids are drawn at the 50% probability level.

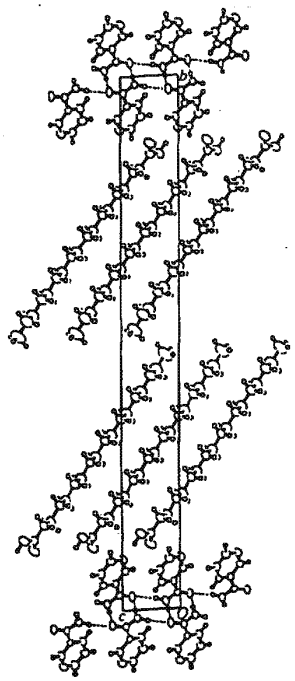


Fig. 2. A view of the title compound projected along the *a* axis. Intermolecular hydrogen bonds are represented by dashed lines.

The crystal structure of stearic acid has polymorphs; the *B*, *C* and *E* forms have been described in detail (Goto & Asada, 1978; Kaneko *et al.*, 1994*a*,*b*; Malta *et al.*, 1971; Kaneko & Kobayashi, 1990). The *E* form is metastable and is transformed into the *B* form, which is stable at room temperature. The *E* and *B* forms of stearic acid are transformed into the *C* form at about 315 K. The alkyl chains of the *E* and *C* forms have all-*trans* conformations, while the C2—C3 bond in the *B* form of stearic acid takes a *gauche* conformation. In the title complex, the alkyl chain of the stearic acid has an all-*trans* conformation, as in the *C* and *E* forms of stearic acid.

Experimental

Crystals of the title compound were grown from an equimolar mixture of stearic acid and nicotinamide in acetone at 308 K.

Crystal data

$C_{18}H_{36}O_2.C_6H_6N_2O$
M_r = 406.607
Triclinic
$P\bar{1}$
a = 5.4313 (5) Å
b = 45.180 (3) Å
c = 5.0355 (5) Å
α = 92.924 (6)°
β = 92.317 (8)°
γ = 92.088 (6)°
V = 1232.1 (2) Å^3
Z = 2
D_x = 1.096 Mg m^{-3}
D_m not measured

Cu $K\alpha$ radiation
λ = 1.5418 Å
Cell parameters from 25 reflections
θ = 27.8–28.5°
μ = 0.559 mm^{-1}
T = 293.2 K
Needle
0.50 × 0.04 × 0.02 mm
Colorless

Data collection

Rigaku AFC-7*R* diffractometer
ω–2θ scans
Absorption correction: none
5966 measured reflections
4193 independent reflections
3231 reflections with $I > 1.5\sigma(I)$

R_{int} = 0.018
θ_{max} = 65°
$h = -6 \rightarrow 6$
$k = -51 \rightarrow 51$
$l = 0 \rightarrow 5$
3 standard reflections every 150 reflections
intensity decay: none

Refinement

Refinement on F
R = 0.042
wR = 0.053
S = 2.428
4193 reflections
431 parameters
All H atoms refined
$w = 1/[\sigma^2(F_o) + 0.00002|F_o|^2]$
$(\Delta/\sigma)_{max}$ = 0.004

$\Delta\rho_{max}$ = 0.24 e Å^{-3}
$\Delta\rho_{min}$ = −0.24 e Å^{-3}
Extinction correction: Zachariasen (1967) type 2, Gaussian isotropic
Extinction coefficient: 0.179 (5)
Scattering factors from *International Tables for X-ray Crystallography* (Vol. IV)

UM00012867
NOVARTIS EXHIBIT 1017
Novartis v. Regents, IPR2023-01346
Page 1613 of 4460

Table 1. *Selected geometric parameters (Å, °)*

O1—C1	1.199 (2)	C9—C10	1.513 (2)
O2—C1	1.321 (2)	C10—C11	1.518 (2)
O3—C24	1.237 (1)	C11—C12	1.513 (2)
N1—C19	1.333 (2)	C12—C13	1.513 (2)
N1—C23	1.336 (2)	C13—C14	1.515 (2)
N2—C24	1.331 (2)	C14—C15	1.511 (2)
C1—C2	1.498 (2)	C15—C16	1.510 (2)
C2—C3	1.508 (2)	C16—C17	1.511 (3)
C3—C4	1.519 (2)	C17—C18	1.494 (3)
C4—C5	1.512 (2)	C19—C20	1.384 (2)
C5—C6	1.515 (2)	C20—C21	1.388 (2)
C6—C7	1.513 (2)	C20—C24	1.489 (2)
C7—C8	1.514 (2)	C21—C22	1.377 (2)
C8—C9	1.506 (2)	C22—C23	1.376 (2)
C19—N1—C23	118.0 (1)	C12—C13—C14	114.1 (1)
O1—C1—O2	122.4 (1)	C13—C14—C15	114.0 (2)
O1—C1—C2	125.7 (1)	C14—C15—C16	114.7 (2)
O2—C1—C2	111.8 (1)	C15—C16—C17	114.1 (2)
C1—C2—C3	115.7 (1)	C16—C17—C18	114.4 (2)
C2—C3—C4	111.6 (1)	N1—C19—C20	123.3 (1)
C3—C4—C5	114.9 (1)	C19—C20—C21	117.9 (1)
C4—C5—C6	113.4 (1)	C19—C20—C24	118.99 (10)
C5—C6—C7	114.6 (1)	C21—C20—C24	123.1 (1)
C6—C7—C8	114.6 (1)	C20—C21—C22	119.1 (1)
C7—C8—C9	114.5 (1)	C21—C22—C23	119.0 (1)
C8—C9—C10	114.5 (1)	N1—C23—C22	122.7 (1)
C9—C10—C11	114.4 (1)	O3—C24—N2	122.0 (1)
C10—C11—C12	114.3 (1)	O3—C24—C20	120.67 (10)
C11—C12—C13	114.2 (1)	N2—C24—C20	117.32 (9)

Table 2. *Hydrogen-bonding geometry (Å, °)*

D—H···*A*	*D*—H	H···*A*	*D*···*A*	*D*—H···*A*
O2—H1···N1	1.02 (1)	1.67 (1)	2.693 (1)	174 (1)
$N2^{i}$—H41^{i}···O3	0.96 (1)	1.98 (1)	2.939 (1)	172 (1)
$N2^{ii}$—H42^{ii}···O3	0.94 (1)	2.04 (2)	2.904 (1)	153 (1)

Symmetry codes: (i) $-1-x,-y,-z$; (ii) $x,y,z-1$.

Data collection: *MSC/AFC Diffractometer Control Software* (Molecular Structure Corporation, 1988). Cell refinement: *MSC/AFC Diffractometer Control Software*. Data reduction: *TEXSAN* (Molecular Structure Corporation, 1995). Program(s) used to solve structure: *MULTAN*88 (Debaerdemaeker *et al.*, 1988). Program(s) used to refine structure: *TEXSAN*. Software used to prepare material for publication: *TEXSAN*.

We wish to thank Dr S. Shiro of the Rigaku Corporation for his helpful assistance in the diffractometry measurements. We also thank Mr M. Usuda for his continued assistance in this investigation.

Supplementary data for this paper are available from the IUCr electronic archives (Reference: OA1032). Services for accessing these data are described at the back of the journal.

References

Ayukawa, K., Azuma, T. & Ueda, F. (1986). Japanese Patent No. 289078.

Debaerdemaeker, T., Germain, G., Main, P., Refaat, L. S., Tate, C. & Woolfson, M. M. (1988). *MULTAN*88. *A System of Computer Programs for the Automatic Solution of Crystal Structures from X-ray Diffraction Data*. University of York, England.

Goto, M. & Asada, E. (1978). *Bull. Chem. Soc. Jpn.* 51, 2456–2459.

Kaneko, F. & Kobayashi, M. (1990). *Acta Cryst.* C46, 1490–1492.

Kaneko, F., Sakashita, H., Kobayashi, M., Kitagawa, Y., Matsuura, Y. & Suzuki, M. (1994*a*). *Acta Cryst.* C50, 245–247.

Kaneko, F., Sakashita, H., Kobayashi, M., Kitagawa, Y., Matsuura, Y. & Suzuki, M. (1994*b*). *Acta Cryst.* C50, 247–250.

Malta, V., Celotti, G., Zannetti, R. & Martelli, A. F. (1971). *J. Chem. Soc. B*, pp. 548–553.

Molecular Structure Corporation (1988). *MSC/AFC Diffractometer Control Software*. MSC, 3200 Research Forest Drive, The Woodlands, TX 77381, USA.

Molecular Structure Corporation (1995). *TEXSAN. Single Crystal Structure Analysis Software*. MSC, 3200 Research Forest Drive, The Woodlands, TX 77381, USA.

Wright, W. B. & King, G. S. D. (1954). *Acta Cryst.* 7, 283–288.

Yokoyama, S., Miyamura, Y. & Fujie, T. (1994). *Chem. Pharm. Bull.* 42, 422–424.

Yokoyama, S., Sunohara, M. & Fujie, T. (1993). *Chem. Pharm. Bull.* 41, 1674–1676.

Yokoyama, S., Sunohara, M., Fujie, T., Hasegawa, M. & Abe, M. (1994). *Chem. Lett.* pp. 445–448.

Zachariasen, W. H. (1967). *Acta Cryst.* 23, 558–564.

© 1998 International Union of Crystallography
Printed in Great Britain – all rights reserved

Acta Cryst. (1998). C54, 1369–1372

6,6′-Dimethylbiphenyl-2,2′-dicarboxylic Acid (6,6′-Dimethyldiphenic Acid)

ROGER E. GERKIN

Department of Chemistry, The Ohio State University, Columbus, Ohio 43210, USA. E-mail: gerkin@chemistry.ohio-state.edu

(Received 2 March 1998; accepted 6 April 1998)

Abstract

The title compound, $C_{16}H_{14}O_4$, crystallized in the centrosymmetric space group $P2_1/c$ with a single molecule in the asymmetric unit. The two carboxyl H atoms are ordered and are involved in hydrogen bonds whose $O_d\cdots O_a$ distances are 2.660 (2) and 2.641 (2) Å. Each of the hydrogen bonds forms a cyclic hydrogen-bonded dimer about a center of symmetry. Thus, each molecule is linked to two others to form a chain. The structure comprises two sets of such chains linked, not by conventional hydrogen bonds, but by one significantly attractive C—H···O interaction. The intramolecular dihedral angle between the ring planes (twist angle) is 84.9 (1)°. The dihedral angles between the carboxyl-group planes and the planes of the rings to which they are attached are 36.7 (1) and 21.4 (1)°. A number of comparisons are made with the structure of the 'parent' compound, biphenyl-2,2′-dicarboxylic acid.

Comment

This report on 6,6′-dimethylbiphenyl-2,2′-dicarboxylic acid, (I), is one of a series on hydrogen bonding in biphenylcarboxylic acids which includes biphenyl-

UM00012868
NOVARTIS EXHIBIT 1017
Novartis v. Regents, IPR2023-01346
Page 1614 of 4460

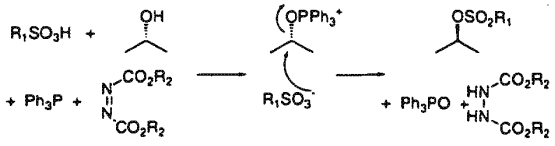
Sulfonation with Inversion by Mitsunobu Reaction: An Improvement on the Original Conditions

Neal G. Anderson,* David A. Lust, Kay A. Colapret,[†] James H. Simpson, Mary F. Malley,[‡] and Jack Z. Gougoutas[‡]

Chemical Process Technology, Pharmaceutical Research Institute, Bristol-Myers Squibb Co., P.O. Box 191, New Brunswick New Jersey 08903-0191, and Department of Solid State Chemistry, Pharmaceutical Research Institute, Bristol-Myers Squibb Co., P.O. Box 4000, Princeton New Jersey 08543-4000

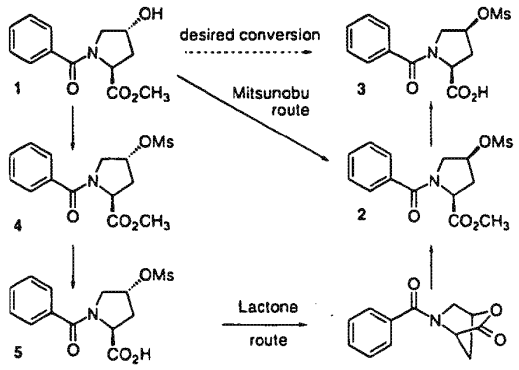
Received May 23, 1996

Sulfonation of a secondary alcohol with stereochemical inversion using Mitsunobu conditions was first described by Galynker and Still, using zinc tosylate.[1] The sulfonates produced have been displaced with inversion, resulting in new bond formation with net retention of stereochemistry.[2] The covalent nature of the zinc salts has been claimed as essential for clean sulfonation and similar displacements using Mitsunobu-like chemistry.[3] Typically the redox byproducts (triphenylphosphine oxide and the hydrazinedicarboxylate) are removed by chromatography,[4,5] which complicates scale-up operations.



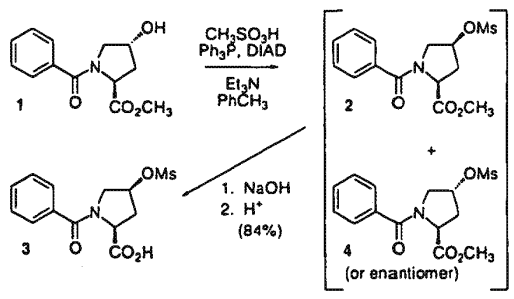
Results and Discussion

The *cis*-mesyloxy proline derivative **3** is a key intermediate for the marketed ACE inhibitor Fosinopril Sodium,[6] and the naturally occurring L-hydroxyproline derivative **1** was selected as starting material for the preparation of this bulk drug substance.[7] The lactone route below was initially used for the preparation of **3**, but was abandoned in favor of a more efficient process for eventual scale-up.



The Mitsunobu approach to **3** was viewed as an efficient alternative to the lengthy lactone approach. Several goals were set for cost-productive development of a suitable process: minimize the number of equivalents of the azodicarboxylate,[8] simplify conditions by avoiding the preparation of a zinc salt, and optimize isolation conditions to avoid purifying **3** by column chromatography.

Mesylation of **1** with clean inversion could be readily conducted with triphenylphosphine (1.2 equiv) methanesulfonic acid (1.2 equiv), diisopropyl azodicarboxylate (DIAD, 1.4 equiv), and triethylamine (0.4 equiv) in toluene. DIAD has been preferred to diethyl azodicarboxylate on scale-up, for safety reasons.[1d,9] The use of triethylamine was found to eliminate the need to prepare the zinc salt of methanesulfonic acid, and increasing the triethylamine charge led to increased levels of dehydroproline byproducts.[10] Typically the condensation was complete after about 3 h at 60–70 °C. Stereochemical inversion to **2** was clean, producing only 3% of the undesired *trans*-mesylate ester **4**.[11] To minimize byproduct formation, the optimal charging sequence was found to be triphenylphosphine, methanesulfonic acid, and DIAD, followed by **1** and triethylamine.[1d]



For economy of operations on scale, mesylate **2** was not isolated. (For analytical purposes a reference sample

[†] Current address: Texaco, Inc., P.O. Box 1608, Port Arthur, TX 77641.

[‡] Department of Solid State Chemistry.

(1) (a) Galynker, I.; Still, W. C. *Tetrahedron Lett.* **1982**, *23*, 4461. For scope and mechanistic details on the Mitsunobu reaction, see: (b) Mitsunobu, O. *Synth.* **1981**, *1*, 1. (c) Hughes, D. L. The Mitsunobu Reaction. *Organic Reactions*; John Wiley and Sons, Inc.: 1992; Vol. 42, p 335. (d) Hughes, D. L.; Reamer, R. A.; Bergan, J. J.; Grabowski, E. J. J. *J. Am. Chem. Soc.* **1988**, *110*, 6487. (e) Hughes, D. L. *Org. Prep. Proc. Int.* **1996**, *28*, 129. (f) Hughes, D. L.; Reamer, R. A. *J. Org. Chem.* **1996**, *61*, 2967.

(2) (a) Emmer, G.; Grassberger, M. A.; Meingassner, J. G.; Schulz, G.; Schaude, M. *J. Med. Chem.* **1994**, *37*, 1908. (b) Keinan, E.; Sinha, S. C.; Sinha-Bagchi, A. *J. Org. Chem.* **1992**, *57*, 3631. (c) Ladouceur, G.; Mais, D. E.; Jakubowski, J. A.; Utterback, B. G.; Robertson, D. W. *Biomed. Lett.* **1991**, *1*, 173. (d) Salomon, R. G.; Basu, B.; Roy, S.; Sachinvala, N. D. *J. Am. Chem. Soc.* **1991**, *113*, 3096. (e) Iguchi, S.; Miyata, Y.; Miyake, H.; Arai, Y.; Okegawa, T.; Kawasaki, A. *Adv. Prostaglandin, Thromboxane, Leukotriene Res.* **1989**, *19*, 670. (f) Thierauch, K. H.; Sturzebecher, C. S.; Schillinger, E.; Rehwinkel, H.; Raduchel, B.; Skuballa, W.; Vorbruggen, H. *Adv. Prostaglandin, Thromboxane, Leukotriene Res.* **1989**, *19*, 655. (g) Thierauch, K. H.; Sturzebecher, C. S.; Schillinger, E.; Rehwinkel, H.; Raduchel, B.; Skuballa, W.; Vorbruggen, H. *Prostaglandins* **1988**, *35*, 855. (h) Iguchi, S.; Miyata, Y.; Okuyama, S.; Miyake, H.; Okegawa, T. *Chem. Pharm. Bull.* **1988**, *36*, 1128. (i) Mori, K.; Kuwahara, S. *Liebigs Ann. Chem.* **1987**, *6*, 555. (j) Pougny, J. R.; Rollin, P. *J. Carbohydr. Chem.* **1986**, *5*, 701. (k) Falck, J. R.; Manna, S.; Capedevila, J. *Tetrahedron Lett.* **1984**, *25*, 2443. (l) Laesecke, K.; Kohn, A.; Schmidt, R. R. *Liebigs Ann. Chem.* **1983**, 1429.

(3) (a) Pianetti, P.; Rollin, P.; Pougny, J. R. *Tetrahedron Lett.* **1986**, *27*, 5853. (b) Rollin, P. *Synth. Commun.* **1986**, *16*, 611. (c) Ho, P. T.; Davies, N. *J. Org. Chem.* **1984**, *49*, 3027.

(4) For examples, see: (a) Smith, A. B., III; Hale, K. J.; Rivero, R. A. *Tetrahedron Lett.* **1986**, *27*, 5813. (b) Bowers-Nemia, M. M.; Joullié, M. M. *Heterocycles* **1983**, *20*, 817. Preparing the lactone from the carboxylic acid precursor of **1** would have added another step to the sequence.

(5) The product has also been removed by pH-controlled extraction from the Mitsunobu byproducts: King, M. L.; Forman, A. L.; Orella, C.; Pines, S. H. *Chem. Eng. Prog.* **1985**, 36.

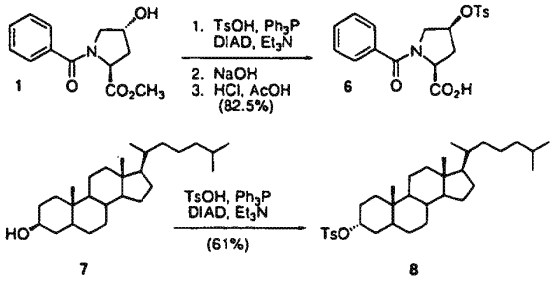
S0022-3263(96)00953-X CCC: $12.00 © 1996 American Chemical Society

UM00012869
NOVARTIS EXHIBIT 1017
Novartis v. Regents, IPR2023-01346
Page 1615 of 4460

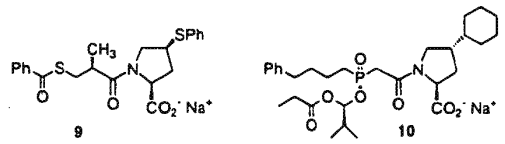
of **2** was prepared by esterification of **3**, as described in the Experimental Section.) When the Mitsunobu reaction was completed, hydrolysis was conducted by adding a small excess of aqueous sodium hydroxide and vigorously stirring the triphasic mixture at 5 °C for 1−2 h. After addition of hydrochloric acid to pH 6−7, solids were removed by filtration. These solids were found to be a 1:1 complex of triphenylphosphine oxide and diisopropyl hydrazinedicarboxylate, as shown by single-crystal X-ray analysis.[12,13] On multikilo operations, 80−85% of the triphenylphosphine oxide and diisopropyl hydrazinedicarboxylate present was routinely removed by filtration as this complex.

The aqueous phase of the biphasic filtrate was separated and acidified with hydrochloric acid to crystallize the product. A small amount of acetic acid was used to solubilize impurities during crystallization. The *cis*-mesylate acid **3** was isolated in 80−85% yield on multikilo scale. The product and the *trans*-isomer **5** are well resolved by HPLC analysis, and the stereochemistry of **3** was confirmed to be *cis* by single-crystal X-ray analysis.[13] Routinely no more than 0.1% of the *trans*-isomer **5** was detected in the isolated product. (For analytical purposes a reference sample of **5** was prepared by hydrolysis of **4** derived from L-proline, as described in the Experimental Section.) Without further purification the purity of **3** was at least 98% relative to a reference standard, with less than 0.1% each of triphenylphosphine oxide, reduced DIAD, or other impurities derived from **1**.

This procedure has been used to produce the *cis*-tosyloxy acid **6** and the tosylate **8**[1a] without chromatography. Slight modifications were undertaken: the water in *p*-toluenesulfonic acid monohydrate was removed by azeotropic distillation prior to the addition of triphenylphosphine and DIAD, as water consumes stoichiometric amounts of these reagents. The C3 methine signal in **8** was found at δ 4.74, in good agreement with that published for the α-tosylate **8**,[1a] thus indicating tosylation with inversion at this center. The protocol described should be applicable to the preparation of other sulfonates.



Conformational Preferences of 4-Substituted Prolines. The solid-state *cis*-diaxial conformation of **3** is very similar to that of zwitterionic *cis*-4-hydroxyproline.[14] Axial orientations of the 4-*cis* substituent are also favored for 4-phenoxy[15] and 4-cyano[16] derivatives. However, *cis*-4-alkyl[17,18] and *cis*-4-thio[19] substituents prefer an equatorial conformation, and we report here a similar preference for the 4-*cis*-phenylthio substituent in a crystal structure of the ACE inhibitor Zofenopril, **9**.[6,13] Although the pyrrolidine ring exhibits considerable conformational variation, 4-*trans*-monosubstituted prolines show similar preferences—aryl[6] and alkyl[18,20] groups favor an equatorial orientation—and we also report here a similar preference for the 4-*trans*-cyclohexyl substituent in a crystal structure of Fosinopril Sodium, **10**.[6,13] Axial orientations have been found for 4-*trans*-carboxylic acid[21] and hydroxylamine[22] derivatives and appear to be strongly favored by 4-*trans*-oxygen substituents in N-acylated and protonated derivatives.[23] This axial orientation in **1** may facilitate displacement of the activated phosphonium species to give the intermediate **2**.



Conclusion. We have developed improved conditions to sulfonate a secondary alcohol with inversion by using a modified Mitsunobu procedure. These conditions do not require the use or formation of zinc salts and use only a slight excesses of reagents (sulfonic acid, triphenylphosphine, and DIAD). Isolation of the product is facilitated by the prior crystallization and removal of the Mitsunobu

(6) Krapcho, J.; Turk, C.; Cushman, D. W.; Powell, J. R.; DeForrest, J. M.; Spitzmiller, E. R.; Karanewsky, D. S.; Duggan, M.; Rovnyak, G.; Schwartz, J.; Natarajan, S.; Godfrey, J. D.; Ryono, D. E.; Neubeck, R.; Atwal, K. S.; Petrillo, E. W., Jr. *J. Med. Chem.* **1988**, *31*, 1148.

(7) (a) Kronenthal, D. R.; Mueller, R. H.; Kuester, P. L.; Kissick, T. P.; Johnson, E. J. *Tetrahedron Lett.* **1990**, *31*, 1241. (b) Kronenthal, D.; Kuester, P. L.; Mueller, R. H. U.S. Pat. 4912231.

(8) Georges, M.; Mackay, D.; Fraser-Reid, B. *Can. J. Chem.* **1984**, *62*, 1539.

(9) For a discussion on safety considerations of azodicarboxylates, see: *Org. Synth.* **1995**, *73*, 278.

(10) Small amounts of the 3,4- and 4,5-dehydroproline impurities were detected, along with impurities similar to compound **4** in ref 1a.

(11) Refluxing overnight decreased the ratio to ca. 92:8, probably due to epimerization α to the methyl ester. The absolute stereochemistry of the *trans*-mesylate ester detected in this Mitsunobu reaction is not known.

(12) Conducting the Mitsunobu reaction in toluene probably promotes the crystallization of the complex, as toluene has been shown to be a suitable solvent for crystallization of weakly acidic compounds with triphenylphosphine oxide: Etter, M. C; Baures, P. W. *J. Am. Chem. Soc.* **1988**, *110*, 639.

(13) Coordinates for the X-ray determinations have been deposited in the Cambridge Crystallographic Database and can be obtained upon request from the Director, Cambridge Crystallographic Data Centre, 12 Union Road, Cambridge, CB2 1EZ, U.K.

(14) Shamala, N.; Row, T. N. G.; Venkatesan, K. *Acta Crystallogr., B* **1976**, *32*, 3267 (AHLPRO). All referenced crystal structures were retrieved from the Cambridge Structural Database, April 1996 release (CSD: Allen, F. H.; Davies, J. E.; Galloy, J. J.; Johnson, O.; Kennard, O.; Macrae, C. F.; Mitchell, E. M.; Mitchell, G.F.; Smith, J. M.; Watson, D. G. *J. Chem. Inf. Comp. Sci.* **1991**, *31*, 187−204). CSD refcodes are included at the end of each reference.

(15) Palkowitz, A. D.; Steinberg, M. I.; Thrasher, K. J.; Reel, J. K.; Hauser, K. L.; Zimmerman, K. M.; Wiest, S. A.; Whitesitt, C. A.; Simon, R. L.; Pfeifer, W.; Lifer, S. L.; Boyd, D. B.; Barnett, C. J.; Wilson, T. M.; Deeter, J. B.; Takeuchi, K.; Riley, R.E.; Miller, W. D.; Marshall, W. S. *J. Med. Chem.* **1994** *37*, 4508 (YIHJEE).

(16) Webb, T. R.; Eigenbrot, C. *J. Org. Chem.* **1991**, *56*, 3009 (TALBUD).

(17) Cerrini, S.; Lamba, D.; Scatturin, A.; Rossi, C.; Ughetto, G. *Biopolymers* **1989**, *28*, 409 (JATZIN).

(18) Flippen-Anderson, J. L.; Gilardi, R.; Karle, I. L.; Frey, M. H.; Opella, S. J.; Gierasch, L. M.; Goodman, M.; Madison, V.; Delaney, N. G. *J. Am. Chem. Soc.* **1983**, *105*, 6609 (CEDREI and CEDRAE).

(19) Yanagi, K.; Takeuchi, Y.; Sunagawa, M. *Acta Crystallogr., Sect. C* **1992**, *48*, 1737 (VUCJEI).

(20) Leban, I.; Golic, L.; Resman, A.; Zmitek, J. *Acta Chim. Slov.* **1994**, *41*, 405 (SUPBIO).

(21) Dupont, L.; Lamotte, J.; Campsteyn, H.; Vermeire, M.; Welter, A. *Acta Crystallogr., Sect. B* **1978**, *34*, 850 (CXPROL).

(22) Bernardinelli, G.; Tronchet, J. M. J.; Jorand, C. *Z. Kristallogr.* **1991**, *195*, 129 (SIYYOO).

UM00012870
NOVARTIS EXHIBIT 1017
Novartis v. Regents, IPR2023-01346
Page 1616 of 4460

redox byproducts, eliminating the need for chromatography. No more than 0.1% of the *trans*-isomer is found in the product **3**. These conditions have been extended to the preparation of two other sulfonates.

Experimental Section

General Methods. Melting points are uncorrected. All reagents and solvents were reagent grade. All reactions were conducted under nitrogen, except for hydrolyses.

Mitsunobu Sulfonation. Method A. A slurry of methanesulfonic acid (7.8 mL, 120 mmol) and triphenylphosphine (32.8 g, 125 mmol) in 250 mL of toluene was cooled to about 20 °C, and DIAD[24] (27.1 g, 140 mmol) was added, keeping the temperature below 35 °C. Then the alcohol (100 mmol) was added, followed by triethylamine (5.5 mL, 40 mmol). The slurry was heated to 60–70 °C and held at that temperature until the formation of the sulfonate was complete by HPLC, generally about 3 h. The reaction was cooled to about room temperature for workup.

Mitsunobu Sulfonation. Method B. For use with hydrated sulfonic acids. The reactor was fitted with a Dean–Stark apparatus and condenser and charged with the sulfonic acid and toluene (2.1 mL/mmol). The mixture was refluxed under nitrogen until water removal was complete and cooled to about 20 °C. Thereafter the procedure was the same as in method A.

***N*-Benzoyl-4-*cis*-(methanesulfonyloxy)-L-proline (3).** Method A was used for the Mitsunobu condensation, with alcohol **1**[25] (25.0 g, 100 mmol). The orange-brown solution was cooled to 5 °C and mixed with aqueous NaOH (150 mmol, 90 mL). The triphasic mixture was stirred vigorously at 5 °C until hydrolysis was complete by HPLC assay,[26] about 2 h, and acidified to pH 6–7 with HCl (concentrated, ca. 8 mL). The suspension was stirred at 5 °C for 1 h, and the solids of triphenylphosphine oxide–diisopropyl hydrazinedicarboxylate (see experimental below) were filtered off and washed with cold water (2 × 35 mL). The organic layer of the filtrate was extracted with distilled water (2 × 15 mL). Glacial acetic acid was added in two portions to the combined aqueous phases, first to adjust to pH 3.8–3.9 at 25 °C (*ca.* 10 mL) to initiate crystallization. The crystal slurry was stirred at room temperature for 30 min and adjusted to pH 4 (glacial acetic acid, *ca.* 6 mL). The mixture was adjusted to pH 2 by the slow addition of HCl (concentrated, *ca.* 7 mL), held at 20–25 °C for 30 min, and stirred at 0–5 °C for 1 h. The product was isolated by filtration and washed with cold water (2 × 30 mL). Drying in a vacuum oven at 50 °C/30 mmHg returned 25.8 g (84%) of **3**. By HPLC analysis the purity of this material was at least 98% relative to a standard of **3**. No more than 0.1% each of the *trans*-isomer **5**, triphenylphosphine oxide, or other individual organic impurites was detectable. The product contained about 0.1–0.2% water and acetic acid.

A reference standard was prepared by recrystallization from 10 volumes of 1:1 EtOAc:95% EtOH to provide material with mp 172–174 °C (lit.[7a] mp 173–174 °C), $[\alpha]^{20}_D$ −55.0° (*c* = 1.0, MeOH) (lit.[7a] $[\alpha]^{20}_D$ −50.6° (*c* = 1.0, MeOH)). ^{1}H NMR (300 MHz, $CDCl_3$ + drop of CD_3OD) showed a mixture of rotamers due to the tertiary amide: δ 2.51–2.76 (m, 2H), 3.07 (s, 3H), {3.89 (d, *J* = 4.4 Hz), 3.98 (br s), 4.02 (br s), 4.17 (d, *J* = 5.3 Hz), 4.22 (d, *J* = 5.3 Hz), *ca.* 2H combined}, {4.52 (d, *J* = 8.4 Hz) and 4.88 (m, *J* = 4.2, 4.9 Hz), *ca.* 1H combined}, {5.24 (t, *J* = 4.5 Hz) and 5.40 (br m), 1H combined}, 7.43–7.56 (m, 5 H). ^{13}C NMR [75 MHz, $CDCl_3$ + drop of CD_3OD]: δ 34.7, 37.4, 37.7, 37.9, 52.3, 54.2, 56.7, 59.6, 77.1, 82.5, 126.5, 128.2, 129.9, 130.3, 134.8, 135.4, 170.3, 171.2, 172.0, 172.4. IR (KBr): 1745 (br), 1595, 1570, 1335, 1165 cm^{-1}. Anal. Calcd for $C_{13}H_{15}NO_6S$: C, 49.83; H, 4.83; N, 4.47; S, 10.23. Found: C, 49.74; H, 4.73; N, 4.38; S, 10.38.

Triphenylphosphine Oxide–Diisopropyl Hydrazinedicarboxylate. This byproduct was generally not dried or characterized. A batch was found suitable for single-crystal X-ray analysis: mp 111–113 °C. ^{1}H NMR [400 MHz, $CDCl_3$]: δ 1.16 (d, 12H, *J* = 6.3 Hz), 4.88 (m, 2H, *J* = 6.3 Hz), 6.5 (brm, 2H), 7.62–7.19 (m, 15H). ^{13}C NMR [100 MHz, $CDCl_3$]: δ 21.9, 69.9, 128.4, 128.5, 131.88, 131.90, 132.1, 133.0, 156.4. IR (KBr): 3220 (br), 1710 (br), 1110 cm^{-1}. Anal. Calcd for $C_{26}H_{31}N_2O_5P$: C, 64.72; H, 6.48; N, 5.81; P, 6.42. Found: C, 64.75; H, 6.30; N, 5.78; P, 6.39.

***N*-Benzoyl-4-*cis*-(methanesulfonyloxy)-L-proline Methyl Ester (2).** The ester generated by the Mitsunobu reaction was not routinely isolated. A reference sample was prepared by adding **3** (40.0 g, 142 mmol) to a solution of thionyl chloride (11.2 mL, 154 mmol) in methanol (400 mL) that had been prepared at −15 °C and stirred 17 h at room temperature. The esterification was quenched into water (200 mL) at 10 °C and adjusted to pH 7.1 with aqueous $NaHCO_3$ (saturated, 520 mL). The slurry was cooled to 4 °C and filtered, and the product was washed with ice water (2 × 200 mL) and dried to afford 30.68 g (73.5%) of white solid: mp 90–91 °C, $[\alpha]^{20}_D$ −51.6° (*c* = 1.0, MeOH). ^{1}H NMR [400 MHz, $CDCl_3$, a mixture of rotamers due to the tertiary amide]: δ {2.59 and 2.67 (brm, 2H)}, 3.07 (s, 3H), 3.74–4.26 (brm, 2H), {3.86 (s) and 3.94 (s), 3H}, {4.57 (brm) and 5.00 (brm), 1H}, {5.26 (brm) and 5.40 (brm), 1H}, 7.48–7.59 (m, 5H). ^{13}C NMR [75 MHz, $CDCl_3$]: δ 35.0, 38.0, 38.4, 52.5, 54.3, 56.7, 59.6, 126.5, 126.9, 128.4, 130.1, 130.4, 135.2, 135.8, 169.5, 170.9, 171.2. IR (KBr): 1746, 1640, 1346, 1169 cm^{-1}. Anal. Calcd for $C_{14}H_{17}NO_6S$: C, 51.36; H, 5.23; N, 4.28; S, 9.79. Found: C 51.45; H, 5.00; N, 4.29; S, 9.49.

***N*-Benzoyl-4-*trans*-(methanesulfonyloxy)-L-proline (5) (Sodium Salt).** A suspension of **4**[7a] (200 g, 0.61 mol) in water (1 L) was treated with NaOH (10 M, 73.3 mL) at room temperature for 2.5 h and acidified to pH 1.5 with HCl (concentrated). The reaction was extracted with CH_2Cl_2 (3 × 500 mL), and the combined extracts were polish-filtered through Hyflo. The solvent was removed under reduced pressure, and the residue was taken up into absolute EtOH (1.0 L). Over 30 min sodium 2-ethylhexanoate (0.61 mol in absolute EtOH, 522 mL) was added, followed by absolute EtOH (0.50 L). The suspension was stirred at 0–4 °C for 1 h, and the product was filtered and washed with absolute EtOH (3 × 250 mL). The crystals were reslurried in absolute EtOH (1.5 L) at 4 °C for 1 h, filtered, washed with absolute EtOH (2 × 250 mL), and dried to afford 144.7 g (70.6%): mp 136 °C (endotherm, differential scanning calorimetry), $[\alpha]^{20}_D$ −79.5° (*c* = 1.0, H_2O). ^{1}H NMR [400 MHz, DMSO-d_6, a mixture of rotamers due to the tertiary amide]: δ 2.2–2.45 (brm, 2H), {3.16 (s) and 3.23 (s), (3H combined}, {3.51 (d, *J* = 12.1 Hz), 3.72 (d, *J* = 6.0 Hz), 3.76 (d, *J* = 6.0 Hz), 3.84–3.91 (m), 4.03 (dd, *J* = 4.1 and 4.2 Hz), 4.42 (t, *J* = 8.0 Hz), 5.22–5.25 (m), 4H total}, 7.34–7.50 (m, 5H). ^{13}C NMR [75 MHz, DMSO-d_6]: δ 35.8, 37.56, 37.64, 37.68, 39.7, 51.3, 55.3, 59.1, 61.8, 127.2, 127.9, 128.3, 128.5, 129.3, 129.9, 136.6, 137.0, 168.0, 169.2, 174.0, 174.3. IR (KBr): 1619, 1356, 1171 cm^{-1}. Anal. Calcd for $C_{13}H_{14}NO_6SNa\cdot0.5H_2O$: C, 45.35; H, 4.39; N, 4.07; S, 9.31; H_2O, 2.62. Found: C, 45.52; H, 4.19; N, 4.03; S, 9.46; H_2O, 2.52 (Karl Fischer titration).

***N*-Benzoyl-4-*cis*-(*p*-toluenesulfonyloxy)-L-proline (6).** Method B was used for the Mitsunobu condensation, with alcohol **1**[25] (25.0 g, 100 mmol). The reaction was stirred at 65 °C for 6 h and then without heat overnight. By HPLC[27] the ratio of intermediate tosylate ester to starting material was 40:1. The yellow solution was stirred vigorously with aqueous NaOH (0.15

(23) Seven of eight such *trans*-4-hydroxyproline structures have an axial OH (*e.g.* Koetzle, T. F.; Lehmann, M. S.; Hamilton, W. C. *Acta Crystallogr., Sect. B* **1973**, *29*, 231 (HOPROL12). Hospital, M.; Courseille, C.; Leroy, F.; Roques, B. P. *Biopolymers*, **1979**, *18*, 1141 (NAHYPL, or *N*-acetyl-*trans*-4-hydroxyproline). Garbay-Jaureguiberry, C.; Arnoux, B.; Prange, T.; Wehri-Altenburger, S.; Pascard, C.; Roques, B. P. *J. Am. Chem. Soc.* **1980**, *102*, 1827 (GLHPRC, or prolylhydroxyproline)). The last reference also contains the exception: the hydroxyl is pseudoequatorial in glycyl-L-4-hydroxyproline (GLHPRA). Intermediate conformations occur in two mono- and di-N-alkylated derivatives: Jones, G. P.; Naidu, B. P.; Paleg, L. G.; Tiekink, E. R. T. *Acta Crystallogr. Sect. C* **1988**, *44*, 2208 (GOJMAT and GOJMEX).

(24) DIAD purity may be determined by dissolving a standardized amount of triphenylphosphine in acetonitrile containing 0.2% acetic acid and titrating with DIAD until the yellow-orange color remains.

(25) Portoghese, P. S.; Turcotte, J. G. *Tetrahedron* **1971**, *27*, 951. The ester was dried to moisture levels of not more than 0.1%.

(26) Waters 30 cm μ-Bondapak C-18 column held at 31 °C, eluted at 1.0 mL/min with 28:72 methanol:(0.05 M KH_2PO_4 acidified to pH 3.0 with 3 M H_3PO_4), 215 nm. Typical retention times: **1**, 10.4 min; **2**, 16.7 min; **3**, 7.6 min; **4**, 18.0 min; **5**, 8.0 min.

(27) YMC Basic 25 cm column, eluted at 1.0 mL/min with 50:50 acetonitrile:0.01 M ammonium phosphate, acidified to pH 4 after mixing, monitored at 210 nm. Typical retention times: **1**, 3.7 min; ester intermediate, 8.5 min; **6**, 5.6 min.

UM00012871
NOVARTIS EXHIBIT 1017
Novartis v. Regents, IPR2023-01346
Page 1617 of 4460

mol, 90 mL) at room temperature for 21 h, and the solids were removed by filtration and washed with water (70 mL). The combined filtrates were acidified to pH 7.3 (concentrated HCl) and stirred at 4–5 °C for 45 min. A second crop of the TPPO–reduced DIAD complex was removed by filtration, and the filtrate was acidified to pH 5.4 with acetic acid (glacial, 2.5 mL). The suspension was stirred at room temperature for 45 min, acidified to pH 3.95 (glacial acetic acid, 7.5 mL, and concentrated HCl, 5.0 mL), and diluted with water (200 mL) and 95% EtOH (221 mL). The suspension was warmed to 50 °C, cooled to room temperature, and filtered. Product was washed with 20% EtOH in water (50 mL) and dried at ambient conditions to return 32.13 g of **6** (82.5%), mp 167–167.5 °C, 99.4% by HPLC analysis.[27] A sample was recrystallized from 95% EtOH (six volumes) to return material with mp 173–174 °C (lit.[25] mp 105–115 °C for *N*-benzoyl-*trans*-4-(*p*-toluenesulfonyloxy)-L-proline), $[\alpha]^{20}_D$ −60.6° (c = 1.0, MeOH). ^{1}H NMR [300 MHz, $CDCl_3$ + drop of CD_3OD, a mixture of rotamers due to the tertiary amide]: δ 2.31–2.58 (m, 2H), 2.45 (s, 3H), 3.73 (d, J = 4.7 Hz) and 3.77 (d, J = 3.2 Hz, 2H combined with prior peak), 4.42 (d, <1H, J = 8.3 Hz), 4.76 (m, 1H, J = 3.8, 5.2 Hz), 4.99 (t, 1H, J = 5.3 Hz), 7.33–7.48 (m, 7H), 7.75 (d, 2H, J = 8.1 Hz). ^{13}C NMR [75 MHz, $CDCl_3$ + drop of CD_3OD]: δ 21.4, 34.4, 37.6, 52.1, 53.9, 56.7, 59.7, 77.2, 78.1, 126.5, 126.8, 127.5, 128.3, 129.9, 130.1, 130.5, 132.8, 134.9, 145.3, 170.2, 171.0, 172.0. IR (KBr): 1738, 1600, 1440, 1360, 1192 cm^{-1}. Anal. Calcd for $C_{19}H_{19}NO_6S$: C, 58.60; H, 4.92; N, 3.60; S, 8.23; Found: C, 58.55; H, 4.85; N, 3.54; S, 8.30.

3α-(*p*-Toluenesulfonyloxy)cholestane (8). Method B was used, with an input of 11.30 g (59.4 mmol) of *p*-toluenesulfonic acid monohydrate in toluene (124 mL total volume). Other inputs were charged proportionally, with 19.22 g (49.5 mmol) of dihydrocholesterol ("95%"). After stirring at 65 °C for 6.5 h, the reaction was incomplete by TLC, and the suspension was cooled to room temperature and recharged with triphenylphosphine (10.39 g, 39.6 mmol) and DIAD (9.1 mL, 46.2 mmol). After 6.5 h at 65 °C, the starting material was consumed, the reaction was cooled to 4 °C, and the byproduct was filtered and washed with toluene (2 × 50 mL). The combined filtrates were concentrated under reduced pressure to a residue and dissolved at 65 °C in MeOH–EtOAc (180 mL, 150 mL). The suspension was chilled at 2–4 °C, and the product was removed by filtration and washed with chilled MeOH–EtOAc (2 × 50 mL, ratio 18:15). Vaccum drying returned 16.48 g (61.3%), mp 124.5–125 °C. ^{1}H NMR [300 MHz, $CDCl_3$]: δ 0.63–1.97 (46H), 2.44 (s, 3H), 4.74 (m, 1H), 7.32 (d, 2H, J = 8.2 Hz), 7.79 (d, 2H, J = 8.2 Hz). ^{13}C NMR [75 MHz, $CDCl_3$]: δ 11.3, 12.0, 18.6, 20.7, 21.6, 22.5, 22.8, 23.8, 24.1, 26.8, 28.0, 28.1, 28.2, 31.7, 32.2, 33.4, 35.3, 35.4, 35.8, 36.1, 39.1, 39.5, 39.9, 42.5, 53.8, 56.1, 56.4, 80.3, 127.6, 129.7, 134.7, 144.2. Anal. Calcd for $C_{34}H_{54}O_3S$: C, 75.23; H, 10.03; S, 5.91. Found: C, 75.41; H, 10.19; S, 5.86. $[\alpha]^{20}_D$ +21.8° (c = 1.0, CH_2Cl_2). IR (KBr): 2938, 1365, 1348, 1188 cm^{-1}.

The combined filtrates from the first crop were concentrated to a residue and dissolved at 65 °C in MeOH–EtOAc (100 mL, 80 mL). The suspension was cooled and the product was collected by filtration to afford after drying 4.05 g (15.1%) of white solid, impure **8**.

Acknowledgment. We thank S. Riseman for developing the DIAD titration assay, R. Deshpande for identification of impurities, and V. Palaniswamy for assistance in obtaining the NMR spectra.

Supporting Information Available: Solid-state conformational drawings of **3**, **9**, **10**, and the triphenylphosphine oxide–diisopropyl hydrazinedicarboxylate complex (4 pages). This material is contained in libraries on microfiche, immediately follows this article in the microfilm version of the journal, and can be ordered from the ACS; see any current masthead page for ordering information.

JO9609539

UM00012872
NOVARTIS EXHIBIT 1017
Novartis v. Regents, IPR2023-01346
Page 1618 of 4460

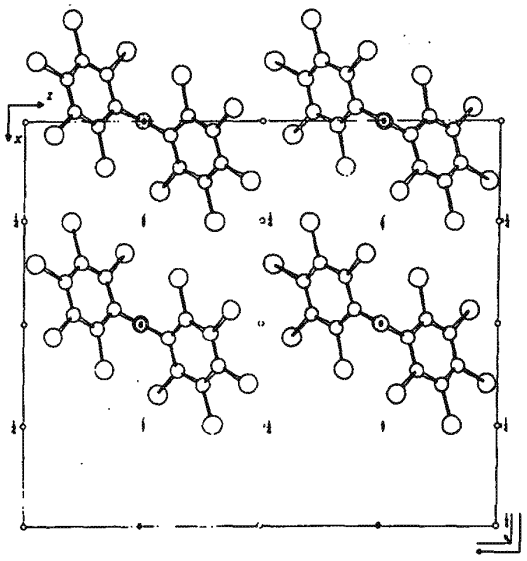


Fig. 3. A projection of the unit-cell contents down *b*.

Fig. 3 is a projection of the crystal structure down *b*. The molecules are packed in layers along the *xz* plane.

We thank the Chlorocarbon Group of the Instituto de Química Orgánica Aplicada de Catalunya (CSIC) for valuable discussions and for providing us with the samples of perchlorodiphenylnitroxide, and Enraf–Nonius, who kindly supplied us with a CAD-4 diffractometer.

References

AHMED, F. R., HALL, S. R., PIPPY, M. E. & HUBER, C. P. (1966). NRC Crystallographic Programs for the IBM/360 System. National Research Council, Ottawa.

ANDERSEN, B. & ANDERSEN, P. (1966). *Acta Chem. Scand.* **20**, 2728–2730.

BALLESTER, M., RIERA, J. & ONRUBIA, C. (1976). *Tetrahedron Lett.* **12**, 945–946.

BROWN, G. M. & STRYDOM, O. A. W. (1974). *Acta Cryst.* B**30**, 801–804.

FORRESTER, A. R., HAY, J. M. & THOMSON, R. H. (1968). *Organic Chemistry of Stable Free Radicals*, pp. 208–210. London, New York: Academic Press.

FORSYTH, J. B. & WELLS, M. (1959). *Acta Cryst.* **12**, 412–415.

GALI, S. (1975). *Crystal and Molecular Structures of Perchlorinated Organic Compounds*. Thesis. Univ. of Barcelona, Spain.

HANSON, A. W. (1953). *Acta Cryst.* **6**, 32–35.

HOWELLS, E. R., PHILLIPS, D. C. & ROGERS, D. (1950). *Acta Cryst.* **3**, 210–214.

JOHNSON, C. K. (1965). *ORTEP*. Report ORNL-3794. Oak Ridge National Laboratory, Tennessee.

KOCHI, J. K. (1972). *Free Radicals*, pp. 541–542, Vol. II. New York: Interscience.

LAJZÉROWICZ-BONNETEAU, J. (1968). *Acta Cryst.* B**24**, 196–199.

LINNETT, J. W. (1961). *J. Chem. Phys.* **29**, 2643–2654.

MAIN, P., WOOLFSON, M. M., LESSINGER, L., GERMAIN, G. & DECLERCQ, J. P. (1974). *MULTAN. A System of Computer Programs for the Automatic Solution of Crystal Structures from X-ray Diffraction Data*. Univs. York, England, and Louvain, Belgium.

PEDERSEN, B. F. (1975). *Acta Cryst.* B**31**, 2931–2933.

SILVERMAN, J., SOLTZBERG, L. J., YANNONI, N. F. & KRUKONIS, A. P. (1971). *J. Phys. Chem.* **75**, 1246–1250.

SOLANS, X. (1977). Thesis, Univ. of Barcelona, Spain.

SOLANS, X. & FONT-ALTABA, M. (1975). *Acta Geol. Hisp.* **3**, 116–117.

Acta Cryst. (1978). B**34**, 2333–2336

A 1:1 Complex of Theophylline and *p*-Nitrophenol

BY KATSUYUKI AOKI AND TADAYOSHI ICHIKAWA

The Institute of Physical and Chemical Research, Wako-shi, Saitama 351, *Japan*

AND YOKO KOINUMA AND YOICHI IITAKA*

Faculty of Pharmaceutical Sciences, University of Tokyo, Hongo, Tokyo 113, *Japan*

(*Received* 13 *January* 1978; *accepted* 6 *March* 1978)

Abstract. $(C_7H_8N_4O_2)(C_6H_5NO_3)$, triclinic, $P\bar{1}$, a = 8·29 (2), b = 11·56 (3), c = 8·95 (2) Å, α = 114·0 (2), β = 108·9 (2), γ = 75·4 (2)°, Z = 2. Block-diagonal least-squares refinement gave a final R value of 0·095. The theophylline molecules are in a dimeric arrangement by virtue of two centrosymmetrically related

* To whom correspondence should be addressed.

UM00012873
NOVARTIS EXHIBIT 1017
Novartis v. Regents, IPR2023-01346
Page 1619 of 4460

hydrogen bonds [N(7)···O(6) 2·81 Å], and are linked to *p*-nitrophenol molecules by another hydrogen bond (2·71 Å).

Introduction. Because *p*-nitrophenol activates the glycosidic bond formation reaction of purine derivatives (Sekiya, Yoshino, Tanaka & Ishido, 1973; Nakazaki, Sekiya, Yoshino & Ishido, 1973), the present study has been carried out.

White crystals were grown from a solution of chloroform. The lattice constants were obtained from precession photographs. Intensity data were collected by the use of the multiple-film equi-inclination Weissenberg technique with Cu $K\alpha$ radiation, and were measured with the aid of a microdensitometer. 1205 independent structure factors, which correspond to 36% of those theoretically possible, were obtained; these were corrected for Lorentz and polarization factors but not for the absorption effect.

The structure was solved by the symbolic addition method (Karle & Karle, 1966). Refinement of the structure by the block-diagonal least-squares method with anisotropic thermal parameters for non-hydrogen atoms and isotropic for H led to the final R value of 0·095. In this calculation, two reflexions ($\bar{1}12$ and $\bar{1}10$) having the largest calculated structure factors were excluded, since they are obviously affected by the secondary-extinction effect. The following weighting system was adopted at the final stage of the refinement: $w = 0$ when $|F_o| < 1{\cdot}5$; $w = 1$ when $1{\cdot}5 \le |F_o| \le 20{\cdot}0$; and $\sqrt{w} = 20/F_o$ when $|F_o| > 20{\cdot}0$. The final atomic coordinates are listed in Table 1.*

Discussion. Fig. 1 shows the bond lengths and angles. The standard deviations are estimated to be about 0·01 Å and 0·8°.

*Lists of structure factors and thermal parameters have been deposited with the British Library Lending Division as Supplementary Publication No. SUP 33453 (7 pp.). Copies may be obtained through The Executive Secretary, International Union of Crystallography, 5 Abbey Square, Chester CH1 2HU, England.

Table 1. *The final positional parameters* (×10⁴ *for the non-hydrogen atoms;* ×10³ *for the hydrogen atoms*)

	x	*y*	*z*
N(1)	−1144 (8)	−1637 (7)	2685 (9)
C(2)	594 (10)	−1416 (8)	3365 (12)
N(3)	1038 (8)	−444 (7)	3119 (9)
C(4)	−241 (10)	260 (8)	2214 (11)
C(5)	−1889 (9)	−18 (8)	1561 (11)
C(6)	−2474 (9)	−981 (8)	1764 (10)
N(7)	−2743 (8)	829 (7)	745 (9)
C(8)	−1563 (10)	1578 (8)	988 (11)
N(9)	12 (9)	1231 (7)	1888 (10)
C(1)	−1560 (11)	−2683 (9)	3018 (14)
O(2)	1653 (7)	−2037 (6)	4150 (8)
C(3)	2870 (10)	−228 (9)	3672 (13)
O(6)	−3943 (6)	−1268 (6)	1262 (8)
C(10)	3695 (10)	4867 (8)	1903 (11)
C(11)	2443 (10)	4177 (9)	1783 (12)
C(12)	2912 (10)	3291 (9)	2523 (12)
C(13)	4640 (10)	3055 (8)	3380 (11)
C(14)	5893 (10)	3711 (8)	3489 (12)
C(15)	5438 (10)	4638 (8)	2787 (11)
N(10)	3214 (9)	5807 (7)	1132 (10)
O(10)	1710 (8)	5985 (7)	318 (10)
O(10′)	4305 (9)	6460 (7)	1320 (10)
O(13)	4999 (8)	2155 (6)	4094 (9)
H(C1)	−268 (9)	−285 (6)	222 (9)
H′(C1)	−123 (21)	−238 (16)	450 (21)
H″(C1)	−82 (16)	−338 (12)	258 (16)
H(C3)	377 (19)	−103 (14)	320 (18)
H′(C3)	322 (12)	0 (9)	485 (12)
H″(C3)	283 (16)	47 (12)	317 (16)
H(N7)	383 (12)	85 (9)	−3 (12)
H(C8)	−179 (11)	216 (8)	22 (11)
H(C11)	122 (12)	442 (10)	107 (13)
H(C12)	210 (11)	296 (8)	268 (11)
H(C14)	698 (12)	368 (9)	428 (12)
H(C15)	620 (12)	523 (9)	281 (12)
H(O13)	579 (12)	212 (9)	478 (12)

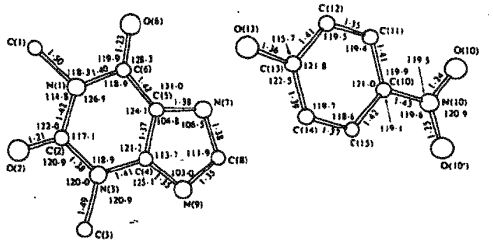


Fig. 1. Bond lengths (Å) and angles (°) (see text for standard deviations).

Table 2. *Least-squares planes and deviations* (Å) *of individual atoms from these planes*

In each of the equations of the planes, X, Y, and Z are coordinates (Å) referred to the orthogonal axes, where Z is along c, X is in the *ac* plane and Y is along b*. Atoms designated by a dagger were given zero weight in calculating the plane; other atoms were weighted equally.

(*a*) The theophylline ring

$$-0{\cdot}1410X + 0{\cdot}6521Y + 0{\cdot}7449Z = 1{\cdot}6313 \text{ Å}$$

N(1)	0·01	C(8)	0·01
C(2)	−0·01	N(9)	0·01
N(3)	−0·01	C(1)†	0·04
C(4)	0·01	O(2)†	−0·01
C(5)	−0·01	C(3)†	−0·14
C(6)	0·01	O(6)†	0·05
N(7)	−0·02		

(*b*) The benzene ring of *p*-nitrophenol

$$-0{\cdot}0953X + 0{\cdot}6950Y + 0{\cdot}7126Z = 2{\cdot}0714 \text{ Å}$$

C(10)	0·00	C(15)	0·01
C(11)	−0·01	N(10)†	−0·01
C(12)	0·01	O(10)†	−0·06
C(13)	0·00	O(10′)†	0·07
C(14)	−0·01	O(13)†	0·02

UM00012874
NOVARTIS EXHIBIT 1017
Novartis v. Regents, IPR2023-01346
Page 1620 of 4460

Table 3. *Hydrogen bonds*

D	*A*	*D*–H	*D*···*A*	H···*A*	∠H–*D*···*A*
N(7)	O(6)^a	0·94 (8) Å	2·806 (8) Å	1·88 (9) Å	9 (6)°
O(13)	O(2)^b	0·74 (9)	2·711 (8)	2·02 (9)	19 (6)

Angle subtended at each atom (°)

C(5)–N(7)···O(6)^a	136·3 (6)	C(13)–O(13)···O(2)^b	109·2 (6)
C(8)–N(7)···O(6)^a	117·2 (6)		

Symmetry code: (*a*) $-1-x, -y, -z$; (*b*) $1-x, -y, 1-z$.

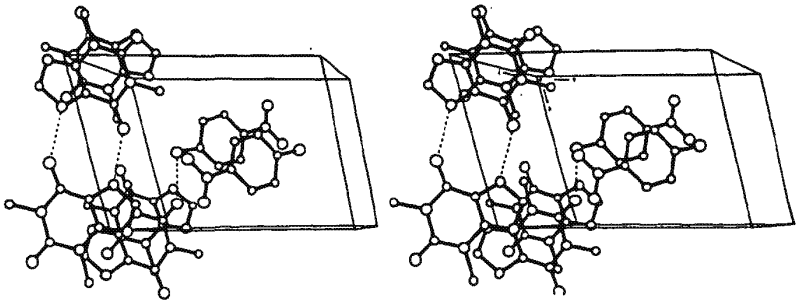


Fig. 2. Crystal packing viewed down the *c* axis. Broken lines represent hydrogen bonds.

Theophylline molecule: The bond lengths and angles are mostly as expected, except N(7)–C(8) = 1·38 Å, which is somewhat larger than values found in other purine derivatives (Voet & Rich, 1970). The purine ring is essentially planar within experimental errors (Table 2).

p-Nitrophenol molecule: The lengths of the two C–C bonds parallel to the long molecular axis, C(11)–C(12) and C(14)–C(15), are shorter than those of the other four C–C bonds. Moreover, C(10)–N(10) = 1·43 Å is significantly shorter than the usual C–N single-bond length of 1·475 Å (*International Tables for X-ray Crystallography*, 1962), and C(13)–O(13) = 1·36 Å exhibits partial double-bond character [the C–O single-bond length is 1·43 Å (*International Tables for X-ray Crystallography*, 1962)]. These shortenings show that *p*-nitrophenol takes a partial quinonoid resonance structure. As in other nitrophenols, the benzene ring is planar but the nitro group is displaced from the ring plane (Table 2); the dihedral angle between the benzene and nitro-group planes is 3·6°. The angle C–C–OH is appreciably larger on the H side, as observed in many phenols.

Crystal structure: Crystal packing is dominated by hydrogen bonds and stacking interactions. Hydrogen bonds are listed in Table 3 and are also shown in Figs. 2 and 3.

Theophylline molecules are in a dimeric arrangement by virtue of centrosymmetrically related hydrogen bonds between N(7) and O(6) (2·81 Å), and they are stacked in relation to a centre of symmetry at separations of about 3·41 Å (molecules *A* and *B* in Fig. 3) and 3·25 Å (molecules *B* and *C*). *p*-Nitrophenol molecules are also stacked at a separation of about 3·35 Å (molecules *D* and *E*), but their degree of overlap is small.

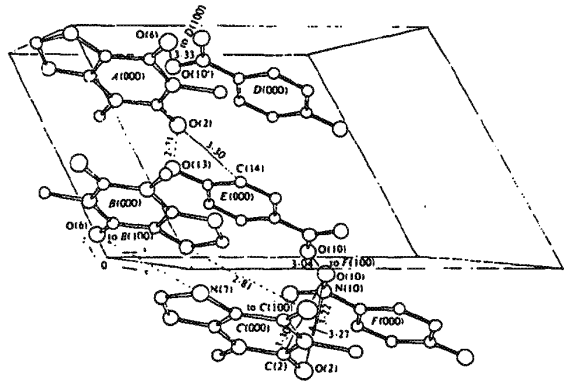


Fig. 3. Crystal packing viewed down the *a* axis. Broken lines represent hydrogen bonds. Single lines represent intermolecular contacts less than 3·35 Å. The symmetry transformations of the labelled molecules relative to Table 1 are as follows: *A*(000) $1-x, -y, 1-z$; *B*(000) $1+x, y, z$; *C*(000) $1-x, -y, -z$; *D*(000) $1-x, 1-y, 1-z$; *E*(000) x,y,z; *F*(000) $1-x, 1-y, -z$.

UM00012875
NOVARTIS EXHIBIT 1017
Novartis v. Regents, IPR2023-01346
Page 1621 of 4460

The theophylline molecule is linked to a *p*-nitrophenol molecule through a hydrogen bond between the carbonyl O(2) of theophylline and the hydroxyl O(13) of *p*-nitrophenol (2·71 Å).

The intermolecular contacts less than 3·35 Å are shown in Fig. 3. Nitro groups come into contact with a N–O···O–N distance of 3·04 Å. This short contact has also been observed in other nitro compounds (see Ichikawa, Aoki & Iitaka, 1978). There is another short contact: C(8)–H···O(10) of distance 2·40 Å [C(8)···O(10) 3·43 Å], which is less than the sum of the van der Waals radii of the H and O atoms (2·60 Å). This interaction seems to be an electrostatic one between the negative charge of the nitro group and the positive charge of H(C8). The acidic character of H(C8) may be due to the resonance contribution in the purine system (Shefter, 1968). In the crystal structures of theophylline monohydrate (Sutor, 1958*a*), theophylline–5-chlorosalicylic acid (Shefter, 1969), caffeine monohydrate (Sutor, 1958*b*), and caffeine–5-chlorosalicylic acid (Shefter, 1968), H(C8) interactions with a carbonyl O atom have also been observed.

References

ICHIKAWA, T., AOKI, K. & IITAKA, Y. (1978). *Acta Cryst.* B34, 2336–2338.

International Tables for X-ray Crystallography (1962). Vol. III, p. 276. Birmingham: Kynoch Press.

KARLE, J. & KARLE, I. L. (1966). *Acta Cryst.* 21, 849–859.

NAKAZAKI, N., SEKIYA, M., YOSHINO, T. & ISHIDO, Y. (1973). *Bull. Chem. Soc. Jpn*, 46, 3858–3863.

SEKIYA, M., YOSHINO, T., TANAKA, H. & ISHIDO, Y. (1973). *Bull. Chem. Soc. Jpn*, 46, 556–561.

SHEFTER, E. (1968). *J. Pharm. Sci.* 57, 1163–1169.

SHEFTER, E. (1969). *J. Pharm. Sci.* 58, 710–714.

SUTOR, D. J. (1958*a*). *Acta Cryst.* 11, 83–87.

SUTOR, D. J. (1958*b*). *Acta Cryst.* 11, 453–458.

VOET, D. & RICH, A. (1970). *Prog. Nucleic Acid Res. Mol. Biol.* 10, 183–265.

Acta Cryst. (1978). B34, 2336–2338

A 1:1 Complex of 2-Methylthio-6-benzamidopurine and *p*-Nitrophenol

BY TADAYOSHI ICHIKAWA AND KATSUYUKI AOKI

The Institute of Physical and Chemical Research, Wako-shi, Saitama 351, *Japan*

AND YOICHI IITAKA*

Faculty of Pharmaceutical Sciences, University of Tokyo, Hongo, Tokyo 113, *Japan*

(*Received* 13 *January* 1978; *accepted* 6 *March* 1978)

Abstract. $(C_{13}H_{11}N_5OS)(C_6H_5NO_3)$, monoclinic, $C2/c$, $a = 25{\cdot}63\ (4)$, $b = 9{\cdot}64\ (2)$, $c = 16{\cdot}90\ (3)$ Å, $\beta = 112{\cdot}9\ (2)°$, $Z = 8$. Block-diagonal least-squares refinement with anisotropic temperature factors yielded a final R value of 0·11. The complex is linked by three hydrogen bonds which form a three-dimensional network, and the benzoyl moiety is fixed by an intramolecular hydrogen bond (2·63 Å).

Introduction. Sekiya, Yoshino, Tanaka & Ishido (1973) and Nakazaki, Sekiya, Yoshino & Ishido (1973) have found that the formation of complexes of purine derivatives with *p*-nitrophenol activates the reaction of acetylated sugars with purines giving *N*-glycosides.

Pale-green single crystals were grown from a solution of chloroform. The lattice constants were measured from precession photographs taken with Cu $K\alpha$ radiation. Intensity data were collected from equi-inclination Weissenberg photographs taken with Cu $K\alpha$ radiation on multiple-film packs. Intensities were measured with the aid of a Narumi microdensitometer and were corrected for Lorentz, polarization and spot-shape (Phillips, 1954) factors, but no correction was applied for the absorption effect. 1251 independent structure factors were obtained (1657 being theoretically observable).

The structure was solved by the symbolic addition method (Karle & Karle, 1966). Refinement of the structure by the block-diagonal least-squares method with anisotropic thermal parameters for all the non-hydrogen atoms reduced the R value to 0·11. The following weighting system was adopted at the final stage of the refinement: $w = 0$ when $|F_o| \le 2{\cdot}0$; $w = 1$ when $2{\cdot}0 < |F_o| \le 8{\cdot}0$; and $\sqrt{w} = 8/|F_o|$ when $|F_o| > 8{\cdot}0$. The final atomic coordinates are listed in Table 1.†

* To whom correspondence should be addressed.

† Lists of structure factors and anisotropic thermal parameters have been deposited with the British Library Lending Division as Supplementary Publication No. SUP 33457 (7 pp.). Copies may be obtained through The Executive Secretary, International Union of Crystallography, 5 Abbey Square, Chester CH1 2HU, England.

UM00012876
NOVARTIS EXHIBIT 1017
Novartis v. Regents, IPR2023-01346
Page 1622 of 4460

Combining Different Hydrogen-Bonding Motifs To Self-Assemble Interwoven Superstructures**

Peter R. Ashton, Matthew C. T. Fyfe, Sarah K. Hickingbottom, Stephan Menzer, J. Fraser Stoddart,* Andrew J. P. White, and David J. Williams*

Abstract: A series of carboxyl-substituted dibenzylammonium salts have been cocrystallized with the macrocyclic polyethers dibenzo[24]crown-8 (DB24C8) and bis-*p*-phenylene[34]crown-10 (BPP34C10) to effect the noncovalent syntheses of a wide range of interwoven superstructures in the solid state. In all cases, the dibenzylammonium cations thread through the cavities of the macrocyclic polyethers—primarily as a result of N^+–H···O hydrogen bonds, with occasional secondary stabilization from C–H···O and aryl–aryl interactions—to form pseudorotaxane complexes possessing supplementary recognition sites (specifically, carboxyl groups) for further intercomplex association through hydrogen bonding. One unit of each of the dibenzylammonium cations threads through the DB24C8 macrocycle to make single-stranded, carboxyl-containing [2]pseudorotaxanes that interact further with one another to produce novel supramolecular architectures as a result of hydrogen bonding between their carboxyl groups (the carboxyl dimer supramolecular synthon), or between carboxyl groups and polyether oxygen atoms. Elaborate architectures, such as side-/main-chain pseudopolyrotaxanes and a daisy-chain-like supramolecular array, were thus synthesized noncovalently. BPP34C10 can accommodate two cations within its macrocyclic interior to form carboxyl-containing [3]pseudorotaxanes in which BPP34C10 acts as a girdle that helps to control the spatial orientation of the carboxylic acid-containing recognition sites for additional intersupramolecular association through the carboxyl dimer. PF_6^- anions were also found to play a role in the self-assembly processes. When the anions interact with the [3]pseudorotaxanes, these recognition sites are oriented in the same direction. This leads to the formation of doubly-encircled multicomponent supermolecules when BPP34C10 is cocrystallized with dibenzylammonium cations bearing only one carboxyl substituent. On the other hand, when BPP34C10 is cocrystallized with an isophthalic acid-substituted ammonium cation, there is no evidence of any anion assistance to self-assembly; the isophthalic acid units are aligned in opposite directions, creating an interwoven supramolecular cross-linked polymer.

Keywords: crystal engineering · hydrogen bonds · interwoven systems · self-assembly · supramolecular chemistry

Introduction

Scientists pursuing research on the chemistry of the noncovalent bond—that is, supramolecular chemistry[1]—are constantly discovering new recognition motifs that allow them to synthesize specific supramolecular architectures noncovalently with remarkable control and precision.[2] We believe that the controlled supramolecular synthesis[3] of functioning, organized nanostructures, the likes of which have been identified previously only in nature, will become possible in the near future. On account of its directionality and its ability to discriminate between various recognition motifs, the hydrogen bond has been harnessed for the noncovalent synthesis of some remarkable superstructures,[4] ranging from discrete, multicomponent supermolecules[5] to infinite, polymeric supramolecular arrays.[6] We have recently reported[7] the discovery of practicable, and remarkably simple, self-assembling supramolecular systems that utilize hydrogen bonds as their principal noncovalent adhesive. Secondary dialkylammonium cations, such as the dibenzylammonium ion ($\mathbf{1}^+$), self-assemble[8] with macrocyclic polyethers to form multicomponent pseudorotaxanes (Figure 1),[9] the stoichiometry of which may be controlled accurately. Pseudorotaxanes possessing from two to five organic compo-

[*] Prof. J. F. Stoddart,[+] Dr. M. C. T. Fyfe, P. R. Ashton
S. K. Hickingbottom
School of Chemistry, University of Birmingham
Edgbaston, Birmingham B15 2TT (UK)
Prof. D. J. Williams, Dr. S. Menzer, Dr. A. J. P. White
Department of Chemistry, Imperial College
South Kensington, London SW7 2AY (UK)
Fax: (+ 44) 171-594-5804

[+] Current address: Department of Chemistry and Biochemistry
University of California, Los Angeles
405 Hilgard Avenue, Los Angeles CA 90095-1569 (USA)
Fax: (+ 1) 310-206-1843
E-mail: stoddart@chem.ucla.edu

[**] Molecular Meccano, Part 34. For Part 33, see: P. R. Ashton, I. Baxter, M. C. T. Fyfe, F. M. Raymo, N. Spencer, J. F. Stoddart, A. J. P. White, D. J. Williams, *J. Am. Chem. Soc.* **1998**, *220*, 2297.

UM00012877
NOVARTIS EXHIBIT 1017
Novartis v. Regents, IPR2023-01346
Page 1623 of 4460

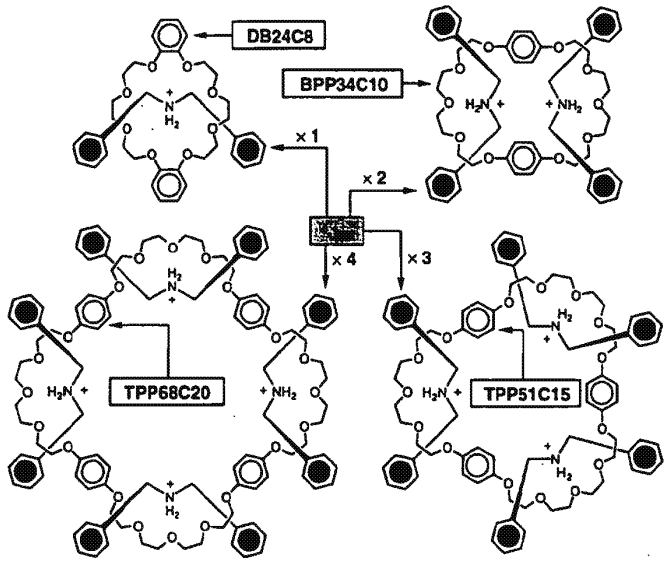


Figure 1. The wide range of multicomponent pseudorotaxane supermolecules that can be self-assembled from the dibenzylammonium cation (1^+) and various macrocyclic polyethers.

nents may be synthesized noncovalently, depending on the size of the internal cavity of the macrocyclic polyether. For instance, dibenzo[24]crown-8 (DB24C8) forms a 1:1 [2]pseudorotaxane complex with 1^+ in which the ammonium thread interpenetrates the macroring cavity by virtue of $N^+-H\cdots O$ and $C-H\cdots O$ hydrogen bonds, supplemented by $\pi-\pi$ stacking interactions.[7a, c, d] Moreover, the crown ether component can become ditopic (i.e., it can accommodate two ammonium centers within its interior) provided its two polyether loops are disassociated from one another, as in the case of bis-*p*-phenylene[34]crown-10 (BPP34C10), which forms a double-stranded [3]pseudorotaxane with 1^+.[7b-d] This paradigm can be extended even further:[7f-g] the crown ethers tris-*p*-phenylene[51]crown-15 (TPP51C15) and tetrakis-*p*-phenylene[68]-crown-20 (TPP68C20) can bind three and four 1^+ cations, respectively, within their macrocyclic cores, since they possess three and four separated polyether loops, each of which can form hydrogen bonds with the ammonium centers. Furthermore, on account of the expanded nature of their crown ether macrorings, the resultant [4]- and [5]pseudorotaxanes possess ammonium centers that are ideally predisposed to associate with anions by hydrogen bonding and anion–dipole interactions.

Another hydrogen bonding motif that has been studied extensively[10] by supramolecular chemists is the carboxyl dimer supramolecular synthon. In particular, researchers interested in crystal engineering[11] (the rational design of organized solid-state superstructures) have employed this recognition motif for the noncovalent synthesis of a wide range of supramolecular architectures. By way of illustration, crystal engineers have utilized the carboxylic dimer for the solid-state noncovalent synthesis of ribbon-like supramolecular arrays (Figure 2), such as is observed in the crystal structures of terephthalic acid[12] and isophthalic acid.[13] Moreover, the placement of bulky alkyl substituents on the isophthalic acid moiety induces[14] the production of a hexameric, hydrogen-bonded supramolecular macrocycle, thereby relieving unfavorable nonbonding interactions.

We conjectured that we could utilize the directional attributes of the hydrogen bond for the noncovalent syntheses of interwoven supramolecular architectures involving the aggregation/polymerization of pseudorotaxanes[15,16] in the solid state. It seemed to us that interwoven superstructures could be synthesized noncovalently by combining both i) the threading of secondary dialkylammonium cations through crown ethers, and ii) the supramolecular dimerization of carboxyl groups. The threading motif would allow the creation of multicomponent pseudorotaxanes that would be endowed with pendant carboxyl groups for further noncovalent association to produce novel interwoven superstructures. Here, we report that carboxyl-containing, crown ether–dialkylammonium-based pseudorotaxanes (generated when the crown ethers DB24C8 and BPP34C10 complex with the carboxyl-substituted dibenzylammonium cations 2^+-6^+, Figure 3) do indeed associate with one another to form unique interwoven supermolecules and supramolecular arrays in the solid state.[17]

Results and Discussion

Molecular synthesis: The salts $2\cdot PF_6-6\cdot PF_6$, possessing both secondary ammonium centers for the formation of pseudorotaxanes with crown ethers, and carboxyl groups for the noncovalent association of these pseudorotaxanes, were readily obtained using the protocol outlined in Scheme 1. Condensation of the appropriate aldehydes and amines furnished aldimines that were subsequently reduced to the secondary amines **13–17** possessing appended benzoate or isophthalate moieties. Ultimately, each of these esters was converted into its corresponding salt $2\cdot PF_6-6\cdot PF_6$ by boiling

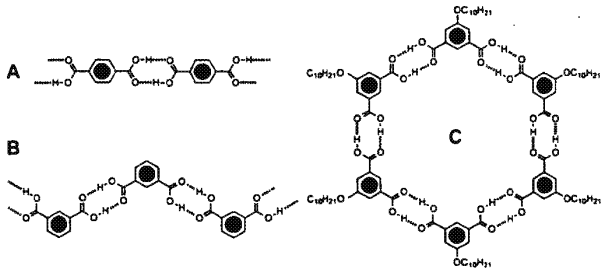


Figure 2. Examples of some of the supramolecular architectures that can be synthesized noncovalently, from various building blocks, with the carboxyl dimer supramolecular synthon. Tape-like supramolecular polymers from A) terephthalic acid and B) isophthalic acid. C) Hexameric supramolecular macrocycle from 5-decyloxyisophthalic acid.

© WILEY-VCH Verlag GmbH, D-69451 Weinheim, 1998
0947-6539/98/0404-0578 $ 17.50+.50/0 Chem. Eur. J. 1998, 4, No. 4

UM00012878
NOVARTIS EXHIBIT 1017
Novartis v. Regents, IPR2023-01346
Page 1624 of 4460

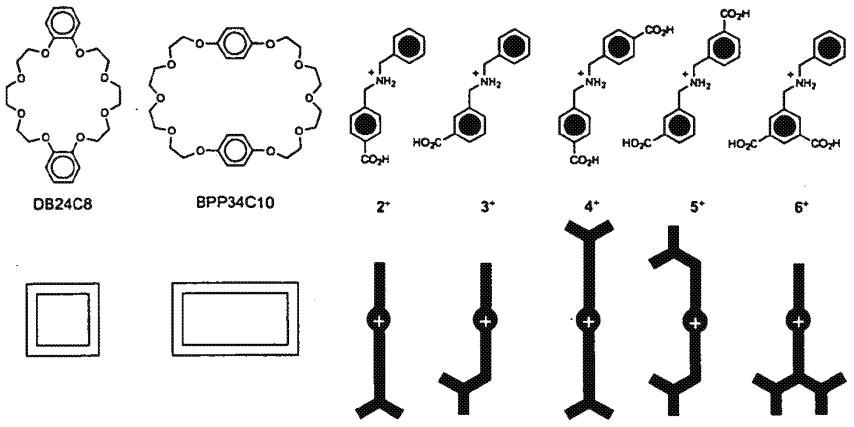
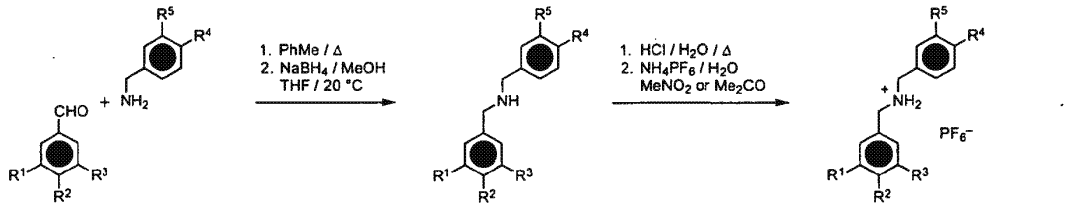


Figure 3. Chemical formulas and cartoon representations for the macrocyclic polyethers and carboxyl-substituted dibenzylammonium cations studied in this paper. Note that the aromatic rings are not represented, for the sake of clarity, in the cartoons exhibited in the ensuing figures.

with hydrochloric acid (to effect hydrolysis with concomitant protonation) followed by counterion exchange from chloride to hexafluorophosphate. With the exception of **9** and **12**, the aldehyde and amine precursors of the salts were either commercially available or were known compounds. The aldehyde **9** was prepared by oxidation of diethyl 5-bromomethylisophthalate[18] with bis(tetrabutylammonium) dichromate,[19] while the amine **12** was obtained by Fischer–Speier esterification of 3-carboxybenzylammonium chloride[20] with MeOH. The crown ethers employed in the supramolecular syntheses (specifically DB24C8 and BPP34C10) were also obtained easily: DB24C8 is commercially available, while BPP34C10 can be readily prepared[21] by a one-pot reaction of hydroquinone with tetraethylene glycol bistosylate.

Characterization of pseudorotaxanes in solution and the gas phase: In a similar manner to that of their unsubstituted congener $\mathbf{1}^+$,[7a–d] the carboxyl-substituted dibenzylammonium cations $\mathbf{2}^+$–$\mathbf{6}^+$ form pseudorotaxane complexes with DB24C8 and BPP34C10 in both solution and in the gas phase, as ascertained by ^{1}H NMR spectroscopy and liquid secondary ion mass spectrometry (LSIMS), respectively.

As anticipated from studies on the parent dibenzylammonium salt $\mathbf{1}\cdot PF_6$,[7a, c, d] solutions of DB24C8 and the salts $\mathbf{2}\cdot PF_6$–$\mathbf{6}\cdot PF_6$ exhibit somewhat slow kinetic exchange with their complexes, since it is especially difficult for the aromatic rings of the cations to pass through the relatively small cavity of the DB24C8 macrocycle. In particular, this exchange is slow enough on the NMR time scale that the ^{1}H NMR spectra of equimolar solutions of DB24C8 and the salts display three sets of resonances for i) the uncomplexed crown ether, ii) the uncomplexed carboxyl-substituted dibenzylammonium salt, and iii) the 1:1 complex formed between these two species. The chemical shift data for the compounds and complexes are listed in Table 1, which shows that the proton resonances associated with the pseudorotaxane complexes are shifted quite dramatically from those in the uncomplexed crown ether and salt. Furthermore, the observation of signals



			Compound	R1	R2	R3	R4	R5		Compound	R1	R2	R3	R4	R5
7	+	10	13	H	CO_2Me	H	H	H		$2\cdot PF_6$	H	CO_2H	H	H	H
8	+	10	14	CO_2Me	H	H	H	H		$3\cdot PF_6$	CO_2H	H	H	H	H
7	+	11	15	H	CO_2Me	H	CO_2Me	H		$4\cdot PF_6$	H	CO_2H	H	CO_2H	H
8	+	12	16	CO_2Me	H	H	H	CO_2Me		$5\cdot PF_6$	CO_2H	H	H	H	CO_2H
9	+	10	17	CO_2Et	H	CO_2Et	H	H		$6\cdot PF_6$	CO_2H	H	CO_2H	H	H

Scheme 1. Synthetic protocol employed for the preparation of the salts $\mathbf{2}\cdot PF_6$–$\mathbf{6}\cdot PF_6$. Compound **7**: methyl 4-formylbenzoate; **8**: methyl 3-formylbenzoate; **9**: diethyl 5-formylisophthalate; **10**: benzylamine; **11**: methyl 4-aminomethylbenzoate; **12**: methyl 3-aminomethylbenzoate.

UM00012879
NOVARTIS EXHIBIT 1017
Novartis v. Regents, IPR2023-01346
Page 1625 of 4460

associated with both the complex and its uncomplexed constituents permits facile single-point measurements of the [2]pseudorotaxanes' association constants (K_a),[7a, c, d] from which their related free energies of complexation ($\Delta G°$) can be derived (Table 2). The data reveal that the carboxyl-substituted ammonium cations $\mathbf{2}^+$–$\mathbf{6}^+$ form much stronger complexes with DB24C8 than does the unsubstituted cation $\mathbf{1}^+$, presumably as a direct consequence of i) resonance and inductive effects, which increase the acidity of both the benzylic methylene and NH_2^+ hydrogen atoms, and ii) the greater tendency of the π-electron-deficient $Ar(CO_2H)_n$ rings of the cation to enter into aryl–aryl stacking interactions with the π-electron-rich catechol rings of the DB24C8 macrocycle. Moreover, it can be seen that, as a result of resonance effects on the hydrogen-bonding ability of the benzylic methylene moieties, ammonium cations bearing *p*-carboxy groups form stronger complexes with DB24C8 than the *m*-substituted congeners. In addition, it is evident that ammonium cations bearing two electron-withdrawing carboxyl substituents form stronger complexes than those bearing one, but that the strength of a complex is increased more spectacularly when the two carboxyl units are situated on the *same* aromatic ring. 1:1 Mixtures of DB24C8 and the salts $\mathbf{2}\cdot PF_6$–$\mathbf{6}\cdot PF_6$ were also studied by LSIMS, where complex formation was evidenced by the discovery of strong peaks corresponding to the 1:1 complexes with the loss of their PF_6^- counterions.[22]

Table 2. Association constants (K_a) and related free energies of complexation ($-\Delta G°$) for the [2]pseudorotaxane complexes formed between DB24C8 and the dibenzylammonium salts $\mathbf{1}\cdot PF_6$–$\mathbf{6}\cdot PF_6$ in CD_3CN at 20°C.

	K_a (M^{-1})[a]	$-\Delta G°$ (kcal mol^{-1})[b]
[DB24C8·**1**][PF_6]	420	3.6
[DB24C8·**2**][PF_6]	610	3.7
[DB24C8·**3**][PF_6]	480	3.6
[DB24C8·**4**][PF_6]	950	4.0
[DB24C8·**5**][PF_6]	880	3.9
[DB24C8·**6**][PF_6]	1500	4.3

[a] Association constants (K_a) were obtained by means of single-point measurements of the concentrations of the complexed and uncomplexed species, from the relevant ^1H NMR spectra at 20°C, by the relationship $K_a = [DB24C8 \cdot salt]/[DB24C8][salt]$ (percentage error ≤15%). [b] The free energies of complexation ($-\Delta G°$) were calculated from the K_a values with the expression $-\Delta G° = RT\ln K_a$.

Complex formation was indicated (Table 3) from the ^1H NMR spectra of 1:2 mixtures of BPP34C10 with the ammonium salts $\mathbf{2}\cdot PF_6$–$\mathbf{6}\cdot PF_6$, where substantial chemical shift changes were detected for the signals[23] observed for both the host and the guest in CD_2Cl_2/CD_3CN (2:1). However, in this mixed solvent system, all of the resonances were sharp and well-defined, indicating that the medium is too polar for interpseudorotaxane association to occur through the carboxyl groups.[24] LSIMS provided proof of the existence of the 1:2

Table 1. ^1H NMR spectroscopic data[a] (δ values) for 1) DB24C8,[b] 2) the carboxyl-substituted dibenzylammonium salts $\mathbf{2}\cdot PF_6$–$\mathbf{6}\cdot PF_6$,[b] and 3) the associated [2]pseudorotaxanes in CD_3CN at 20°C.[c]

	Crown ether		Dibenzylammonium cation		
	OCH_2	$(RO)_2ArH$	$CH_2NH_2^+$	PhH	$(HO_2C)_nArH$
DB24C8	3.67 (s, 8H), 3.79 (m, 8H), 4.08 (m, 8H)	6.85–6.96 (m, 8H)	–	–	–
$\mathbf{2}\cdot PF_6$	–	–	4.25 (s, 2H), 4.29 (s, 2H)	7.46 (s, 5H)	7.57 (d, 2H), 8.06 (d, 2H)
[DB24C8·**2**][PF_6]	3.49–3.63 (m, 8H), 3.74 (m, 8H), 3.95–4.06 (m, 8H)	6.71–6.84 (m, 8H)	4.66 (m, 2H), 4.79 (m, 2H)	7.22–7.30 (m, 5H)	7.38 (d, 2H), 7.65 (d, 2H)
$\mathbf{3}\cdot PF_6$	–	–	4.25 (s, 2H), 4.31 (s, 2H)	7.46 (s, 5H)	7.58 (t, 1H), 7.71 (d, 1H), 8.07 (d, 1H), 8.16 (s, 1H)
[DB24C8·**3**][PF_6]	3.51–3.65 (m, 8H), 3.77 (m, 8H), 3.94–4.06 (m, 8H)	6.70–6.83 (m, 8H)	4.64 (m, 2H), 4.81 (m, 2H)	7.25–7.34 (m, 5H)	7.12 (t, 1H), 7.42 (d, 1H), 7.62 (d, 1H), 8.00 (s, 1H)
$\mathbf{4}\cdot PF_6$	–	–	4.31 (s, 4H)	–	7.56 (d, 4H), 8.06 (d, 4H)
[DB24C8·**4**][PF_6]	3.58 (s, 8H), 3.77 (m, 8H), 4.01 (m, 8H)	6.70–6.81 (m, 8H)	4.78 (m, 4H)	–	7.44 (d, 4H), 7.75 (d, 4H)
$\mathbf{5}\cdot PF_6$	–	–	4.31 (s, 4H)	–	7.59 (t, 2H), 7.69 (d, 2H), 8.07 (d, 2H), 8.13 (s, 2H)
[DB24C8·**5**][PF_6]	3.62 (s, 8H), 3.78 (m, 8H), 4.00 (m, 8H)	6.67–6.81 (m, 8H)	4.75 (m, 4H)	–	7.26 (t, 2H), 7.54 (d, 2H), 7.76 (d, 2H), 8.06 (s, 2H)
$\mathbf{6}\cdot PF_6$	–	–	4.25 (s, 2H), 4.38 (s, 2H)	7.46 (s, 5H)	8.35 (s, 2H), 8.58 (s, 1H)
[DB24C8·**6**][PF_6]	[d]	6.55–6.73 (m, 8H)	4.61 (m, 2H), 4.94 (m, 2H)	7.38–7.55 (m, 5H)	7.85 (s, 1H), 8.09 (s, 2H)

[a] The ^1H NMR spectra were recorded on a Bruker AC300 spectrometer (at 300.1 MHz) with CD_3CN solvent as the lock and the multiplet observed for the residual protons of this solvent (at $\delta = 1.93$) as internal reference. [b] The concentration of both components was 1.0×10^{-2} M. [c] Signals were observed simultaneously for both the uncomplexed crown ether and salt, in addition to the [2]pseudorotaxane complex. [d] A complicated band of signals was observed from $\delta = 3.55$–4.15 in the ^1H NMR spectrum of a 1:1 mixture of DB24C8 and $\mathbf{6}\cdot PF_6$, so that it was not possible to correlate signals associated with the OCH_2 protons to the uncomplexed or complexed DB24C8 macrocycle.

© WILEY-VCH Verlag GmbH, D-69451 Weinheim, 1998
0947-6539/98/0404-0580 $ 17.50+.50/0 *Chem. Eur. J.* 1998, *4*, No. 4

UM00012880
NOVARTIS EXHIBIT 1017
Novartis v. Regents, IPR2023-01346
Page 1626 of 4460

pseudorotaxane complexes in the gas phase. The LSIMS, obtained from 1:2 molar solutions of BPP34C10 with the salts $2\cdot PF_6$–$6\cdot PF_6$, displayed peaks for the 1:2 complexes (with the loss of one PF_6^- counterion) in all cases. However, these peaks were extremely small compared with the base peaks in the spectra, indicating that, as noted previously,[7c] it is extremely difficult to characterize three-component pseudorotaxane supermolecules, such as these, in the gas phase.

X-ray crystallography (supramolecular synthesis): The X-ray crystallographic analysis of the 1:1 complex formed between DB24C8 and the 2^+ cation shows (Figure 4A) the DB24C8 macrocycle to adopt a V-shaped conformation, with the cation threaded through the center of the macroring to form a [2]pseudorotaxane. Complex stabilization is achieved by means of a combination of N^+–H···O and C–H···O hydrogen bonds and a face-to-face aryl–aryl stacking interaction between the π-electron-deficient benzoic acid ring of the ammonium cation and one of the π-electron-rich catechol rings of the DB24C8 macrocycle (the mean interplanar separation is 3.71 Å, with a centroid–centroid distance of 4.12 Å, the rings being inclined by ca. 15°). Even though there is an approach of 4.18 Å between the centroids of the other catechol unit of the crown ether and the benzoic acid ring, the rings are inclined by ca. 29°, thereby precluding any significant π–π stacking interaction. Inspection of the packing of this pseudorotaxane shows glide-related complexes to be linked in a head-to-tail fashion (via bifurcated hydrogen bonds between the carboxyl hydrogen atom of one pseudorotaxane unit and the oxygen atoms of a catechol ring of the next) to generate an interwoven supramolecular architecture that is reminiscent of a *daisy chain* (Figure 4B,C).[25] This polymeric supramolecular architecture presumably originates as a result of the π–π stacking interaction, in addition to the V-shaped conformation of the polyether. The combination of these two factors means that the head-on dimerization of the $[DB24C8\cdot 2]^+$ pseudorotaxane, using the carboxyl dimer supramolecular synthon, is disfavored, since the catechol units from adjacent pseudorotaxanes would be in very close proximity to one another, resulting in detrimental nonbonding interactions.

The X-ray analysis of the 1:1 complex formed between the DB24C8 macrocycle and the cation 4^+ reveals that, in this instance, the interpenetrated DB24C8 macroring has an extended approximately C_i-symmetric conformation with its phenoxyethylene units roughly coplanar with their associated catechol rings, a conformation very similar to that adopted by the uncomplexed DB24C8 macrocycle.[26] As a result of a combination of N^+–H···O and C–H···O hydrogen-bonding interactions (Figure 5A), the cation is threaded asymmetrically through the center of the polyether macroring and has one of its benzoic acid rings oriented approximately parallel to, and overlying, one of the catechol rings of the DB24C8 macrocycle (the mean interplanar separation is 3.74 Å with a centroid–centroid distance of 3.91 Å, the rings being inclined

Table 3. ^{1}H NMR spectroscopic data[a] (δ values) for 1) BPP34C10,[b] 2) the carboxyl-substituted dibenzylammonium salts $2\cdot PF_6$–$6\cdot PF_6$,[b] and 3) 1:2 mixtures[b,c] of the two compounds in CD_2Cl_2/CD_3CN (2:1) at 20 °C.

	Crown ether		Dibenzylammonium cation		
	OCH_2	$(RO)_2ArH$	$CH_2NH_2^+$	PhH	$(HO_2C)_nArH$
BPP34C10	3.58 (m, 16H), 3.71 (m, 8H), 3.92 (m, 8H)	6.69 (s, 8H)	–	–	–
$2\cdot PF_6$	–	–	4.18 (s, 4H), 4.22 (s, 4H)	7.43 (s, 10H)	7.49 (d, 4H), 8.04 (d, 4H)
BPP34C10 + $2\cdot PF_6$	3.45–3.59 (m, 16H), 3.71 (m, 8H), 3.95 (m, 8H)	6.69 (s, 8H)	4.12 (s, 4H), 4.14 (s, 4H)	7.38–7.49 (m, 10H)	7.34 (d, 4H), 7.94 (d, 4H)
$3\cdot PF_6$	–	–	4.16 (s, 4H), 4.21 (s, 4H)	7.40 (s, 10H)	7.51 (t, 2H), 7.62 (d, 2H), 8.04 (d, 2H), 8.10 (s, 2H)
BPP34C10 + $3\cdot PF_6$	3.54 (s, 16H), 3.69 (m, 8H), 3.86 (m, 8H)	6.60 (s, 8H)	4.15 (s, 8H)	7.42 (s, 10H)	7.47 (d, 2H), 7.53 (t, 2H), 7.81 (s, 2H), 7.99 (d, 2H)
$4\cdot PF_6$	–	–	4.21 (s, 8H)	–	7.49 (d, 8H), 8.03 (d, 8H)
BPP34C10 + $4\cdot PF_6$	3.48–3.59 (m, 16H), 3.70 (m, 8H), 3.91 (m, 8H)	6.65 (s, 8H)	4.19 (br, 8H)	–	7.40 (d, 8H), 7.96 (d, 8H)
$5\cdot PF_6$	–	–	4.22 (s, 8H)	–	7.50 (t, 4H), 7.61 (d, 4H), 8.00 (d, 4H), 8.07 (s, 4H)
BPP34C10 + $5\cdot PF_6$	3.55 (s, 16H), 3.70 (m, 8H), 3.89 (m, 8H)	6.63 (s, 8H)	4.18 (s, 8H)	–	7.48–7.54 (m, 8H), 7.85 (s, 4H), 7.93 (d, 4H)
$6\cdot PF_6$	–	–	4.18 (s, 4H), 4.28 (s, 4H)	7.40 (s, 10H)	8.30 (s, 4H), 8.59 (s, 2H)
BPP34C10 + $6\cdot PF_6$	3.55 (s, 16H), 3.69 (m, 8H), 3.87 (m, 8H)	6.58 (s, 8H)	4.18 (br, 8H)	7.43 (s, 10H)	8.10 (s, 4H), 8.50 (s, 2H)

[a] The ^{1}H NMR spectra were recorded on a Bruker AC300 spectrometer (at 300.1 MHz) with CD_3CN solvent as the lock and the residual solvent peak as internal reference. [b] The concentration of BPP34C10 was 4.2×10^{-3} M, while that of the salts was 8.4×10^{-3} M. [c] In contrast to the spectra described in Table 1, time-averaged sets of signals are observed for both host and guest species in the ^{1}H NMR spectra, since fast kinetic exchange is occurring between uncomplexed and complexed states on the ^{1}H NMR time scale.

UM00012881
NOVARTIS EXHIBIT 1017
Novartis v. Regents, IPR2023-01346
Page 1627 of 4460

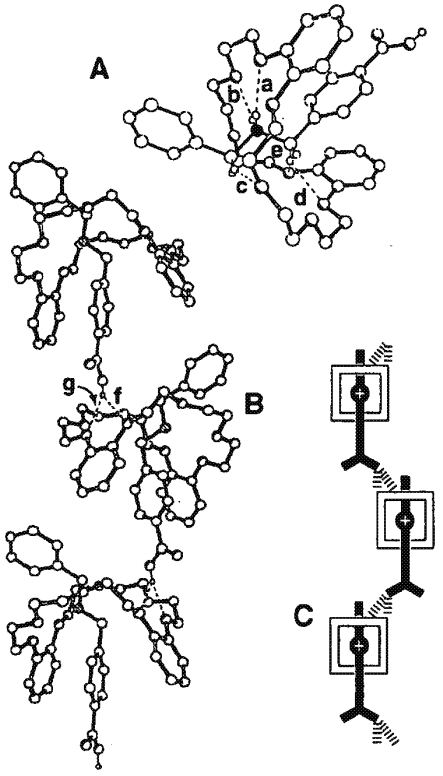


Figure 4. A: Crystal structure of the $[DB24C8 \cdot 2]^+$ pseudorotaxane. Bond lengths and angles for hydrogen bonds: a) $N^+ \cdots O$ 2.92 Å, $H \cdots O$ 2.15 Å, $N^+ - H \cdots O$ 142°; b) $N^+ \cdots O$ 2.90 Å, $H \cdots O$ 2.13 Å, $N^+ - H \cdots O$ 144°; c) $C \cdots O$ 3.18 Å, $H \cdots O$ 2.26 Å, $C - H \cdots O$ 159°; d) $C \cdots O$ 3.25 Å, $H \cdots O$ 2.46 Å, $C - H \cdots O$ 139°; e) $C \cdots O$ 3.36 Å, $H \cdots O$ 2.50 Å, $C - H \cdots O$ 148°. B: The hydrogen-bonded supramolecular array—resembling a daisy chain—produced by the noncovalent polymerization of the $[DB24C8 \cdot 2]^+$ pseudorotaxane in the solid state. Bond lengths and angles for hydrogen bonds: f) $O \cdots O$ 3.06 Å, $H \cdots O$ 2.25 Å, $O - H \cdots O$ 150°; g) $O \cdots O$ 2.92 Å, $H \cdots O$ 2.20 Å, $O - H \cdots O$ 136°. C: Cartoon representation of the daisy-chain-like supramolecular array $\{[DB24C8 \cdot 2]^+\}_n$.

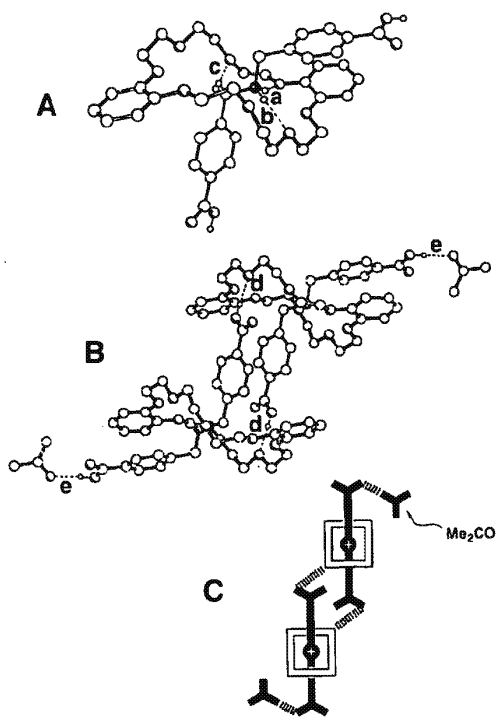


Figure 5. A: View of the structure of the $[DB24C8 \cdot 4]^+$ pseudorotaxane in the solid state. Bond lengths and angles for hydrogen bonds: a) $N^+ \cdots O$ 3.11 Å, $H \cdots O$ 2.26 Å, $N^+ - H \cdots O$ 158°; b) $N^+ \cdots O$ 3.02 Å, $H \cdots O$ 2.14 Å, $N^+ - H \cdots O$ 165°; c) $C \cdots O$ 3.21 Å, $H \cdots O$ 2.37 Å, $C - H \cdots O$ 145°. B: Association of two Me_2CO molecules with each of the pendant carboxyl groups of the $\{[DB24C8 \cdot 4]^+\}_2$ species formed by aryl–aryl stacking and hydrogen-bonding interactions. Bond lengths and angles for hydrogen bonds: d) $O \cdots O$ 2.73 Å, $H \cdots O$ 1.85 Å, $O - H \cdots O$ 165°; e) $O \cdots O$ 2.78 Å, $H \cdots O$ 1.88 Å, $O - H \cdots O$ 173°. C: Cartoon representation depicting the $\{[DB24C8 \cdot 4]^+\}_2 \cdot 2Me_2CO$ species.

by ca. 13°). The other benzoic acid ring of the cation is oriented approximately axially with respect to the DB24C8 macroring. An examination of interpseudorotaxane association (Figure 5B,C) reveals that two $[DB24C8 \cdot 4]^+$ complexes stack, via the benzoic acid ring that is excluded from intrapseudorotaxane $\pi - \pi$ stacking (the centroid–centroid and interplanar separations are 4.19 and 3.79 Å, respectively), to generate a dimer of C_i-related [2]pseudorotaxanes. This pseudorotaxane dimer is further stabilized by pairs of O–H $\cdots$ O hydrogen bonds between one of the carboxyl moieties of the 4^+ cation and an oxygen atom in one of the polyether linkages of the DB24C8 macrocycle of a symmetry-related [2]pseudorotaxane and vice versa. Further propagation of this recognition motif is halted by the intervention of an Me_2CO solvent molecule, which is hydrogen-bonded to the vacant carboxyl donor site attached to the aryl ring that is involved in intrapseudorotaxane $\pi - \pi$ stacking. This crystal structure convincingly demonstrates a fundamental difficulty associated with crystal engineering. Here, the anticipated carboxylic acid dimer pairs are not observed, presumably because interpseudorotaxane $\pi - \pi$ stacking interactions act as the dominant factor that determines the packing of the $[DB24C8 \cdot 4]^+$ species.

The coconformation[27] of the $[DB24C8 \cdot 5]^+$ [2]pseudorotaxane (Figure 6A) is remarkably similar to that of its congener $[DB24C8 \cdot 4]^+$. Nevertheless, although there are small amounts of Me_2CO solvent in the crystals of the $[DB24C8 \cdot 5]^+$ complex, it does not interfere with the expected hydrogen-bonding pattern: supramolecular polymerization, employing the carboxyl dimer supramolecular synthon, leads to the *main-chain, hydrogen-bonded pseudopolyrotaxane*[15] superstructure illustrated in Figure 6B,C.

The X-ray analysis of the 1:1 complex formed between DB24C8 and $6 \cdot PF_6$ (Figure 7A) reveals a very similar coconformation,[27] for the threading of the cation through the center of the DB24C8 crown ether macroring, to that observed for the related complex $[DB24C8 \cdot 2]^+$. The cation has a typical all-*anti* geometry for its $C - CH_2 - NH_2^+ - CH_2 - C$ backbone, but the differences in orientations of the isophthalate and benzyl rings result in a marked departure from the normal gull-wing conformation: the isophthalate ring is

© WILEY-VCH Verlag GmbH, D-69451 Weinheim, 1998
0947-6539/98/0404-0582 $ 17.50+.50/0 *Chem. Eur. J.* 1998, *4*, No. 4

UM00012882
NOVARTIS EXHIBIT 1017
Novartis v. Regents, IPR2023-01346
Page 1628 of 4460

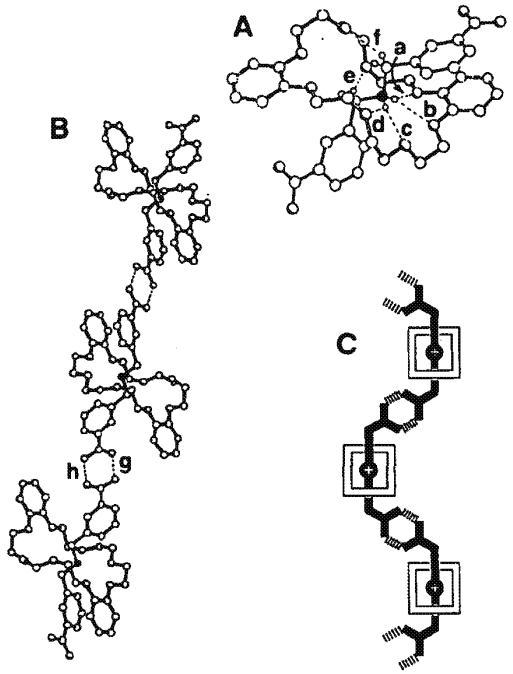


Figure 6. A: The crystal structure of the $[DB24C8 \cdot 5]^+$ pseudorotaxane. Hydrogen bonding distances and angles: a) $N^+ \cdots O$ 3.12 Å, $H \cdots O$ 2.28 Å, $N^+ - H \cdots O$ 157°; b) $N^+ \cdots O$ 3.01 Å, $H \cdots O$ 2.32 Å, $N^+ - H \cdots O$ 133°; c) $N^+ \cdots O$ 3.02 Å, $H \cdots O$ 2.20 Å, $N^+ - H \cdots O$ 151°; d) $N^+ \cdots O$ 3.05 Å, $H \cdots O$ 2.34 Å, $N^+ - H \cdots O$ 136°; e) $C \cdots O$ 3.16 Å, $H \cdots O$ 2.52 Å, $C - H \cdots O$ 157°; f) $C \cdots O$ 3.32 Å, $H \cdots O$ 2.49 Å, $C - H \cdots O$ 145°. B: The main-chain, hydrogen-bonded pseudopolyrotaxane produced by the noncovalent polymerization of the $[DB24C8 \cdot 5]^+$ pseudorotaxane by means of the carboxyl dimer supramolecular synthon. Hydrogen bond lengths: g) $O \cdots O$ 2.63 Å; h) $O \cdots O$ 2.63 Å. C: Cartoon of the $\{[DB24C8 \cdot 5]^+\}_n$ pseudopolyrotaxane.

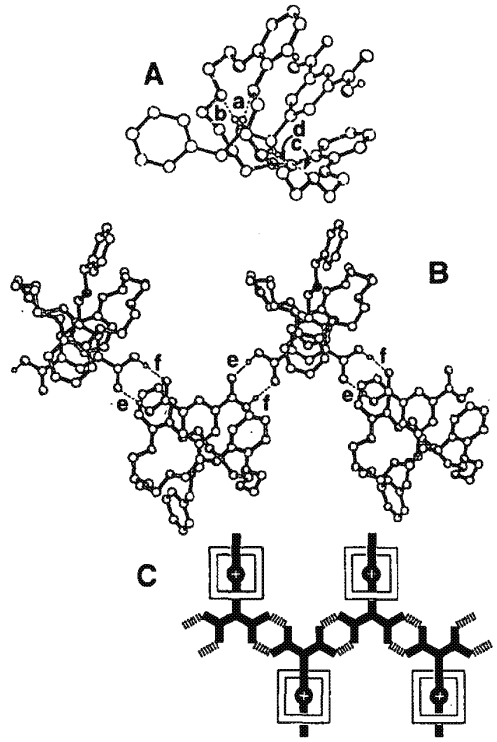


Figure 7. A: The structure of the $[DB24C8 \cdot 6]^+$ pseudorotaxane in the solid state. Bond lengths and angles for hydrogen bonds: a) $N^+ \cdots O$ 3.04 Å, $H \cdots O$ 2.15 Å, $N^+ - H \cdots O$ 170°; b) $N^+ \cdots O$ 2.88 Å, $H \cdots O$ 1.98 Å, $N^+ - H \cdots O$ 179°; c) $C \cdots O$ 3.30 Å, $H \cdots O$ 2.39 Å, $C - H \cdots O$ 156°; d) $C \cdots O$ 3.27 Å, $H \cdots O$ 2.40 Å, $C - H \cdots O$ 150°. B: The side-chain, hydrogen-bonded pseudopolyrotaxane produced by the noncovalent polymerization of the $[DB24C8 \cdot 6]^+$ pseudorotaxane by means of the carboxyl dimer supramolecular synthon. Bond lengths and angles for hydrogen bonds: e) $O \cdots O$ 2.60 Å, $H \cdots O$ 1.73 Å, $O - H \cdots O$ 163°; f) $O \cdots O$ 2.64 Å, $H \cdots O$ 1.75 Å, $O - H \cdots O$ 176°. C: Cartoon representation of the side-chain, hydrogen-bonded pseudopolyrotaxane $\{[DB24C8 \cdot 6]^+\}_n$.

inclined by 81° to the plane of the backbone, while the benzyl ring is inclined by only 23°. Complex stabilization is again achieved by a combination of $N^+ - H \cdots O$ and $C - H \cdots O$ hydrogen bonds along with a $\pi - \pi$ stacking interaction between the isophthalate ring and one of the catechol rings of the DB24C8 macrocycle (the associated centroid–centroid and mean interplanar separations are 3.79 and 3.48 Å, respectively). As observed for the $[DB24C8 \cdot 2]^+$ superstructure, there is a relatively short contact (4.12 Å) between the center of the isophthalic acid ring and the other catechol ring of the DB24C8 macrocycle. However, these rings are inclined by 26°, thus precluding any significant $\pi - \pi$ interaction. The packing of the $[DB24C8 \cdot 6]^+$ complexes (Figure 7B,C) reveals the formation of a *side-chain, hydrogen-bonded pseudopolyrotaxane*[15,28] superstructure, with one of the carboxylic acid units of one cation linking to the other of the next through the carboxyl dimer. Presumably, the formation of this supramolecular polymer is allowed, in this instance, since the catechol units of the pseudorotaxane monomers approach each other in a sterically less demanding side-on fashion as opposed to a head-on fashion (see $[DB24C8 \cdot 2]^+$). Inspection of the packing of the pseudopolyrotaxane chains does not reveal any significant interchain interactions.

The X-ray crystallographic analysis of the 1:2 complex formed between the BPP34C10 macrocycle and the cation $\mathbf{2}^+$ (Figure 8) reveals[17] that both of the cations are threaded codirectionally through the center of the macrocycle to produce a [3]pseudorotaxane that is stabilized by five $N^+ - H \cdots O$ hydrogen bonds between the NH_2^+ centers and oxygen atoms from each of the polyether loops in the macrocycle. Secondary stabilization of the [3]pseudorotaxane superarchitecture is achieved by an edge-to-face $C - H \cdots \pi$ contact between one of the methylene hydrogen atoms of the 4-carboxybenzyl group and one of the hydroquinone rings of the BPP34C10 macrocycle (the associated $H \cdots \pi$ distance and $C - H \cdots \pi$ angle are 2.88 Å and 143°, respectively). The centroid–centroid separation between the benzoic acid rings of independent $\mathbf{2}^+$ cations is ca. 4.6 Å, the rings being tilted by 28°, thereby excluding any meaningful aryl–aryl stacking interactions. An additional feature of the superstructure, which is of particular interest, is the directing of a fluorine atom from one of the PF_6^- anions into the cleft between the two dialkylammonium cations; it lies at a distance of ca. 2.5 Å

UM00012883
NOVARTIS EXHIBIT 1017
Novartis v. Regents, IPR2023-01346
Page 1629 of 4460

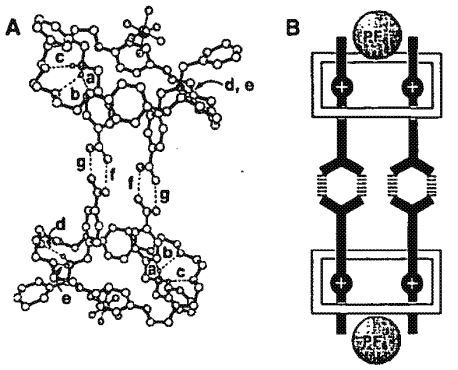


Figure 8. A: View of the $\{[BPP34C10\cdot(\mathbf{2})_2]^{2+}\}_2$ supermolecule (produced by the noncovalent dimerization of the $[BPP34C10\cdot(\mathbf{2})_2]^{2+}$ pseudorotaxane by means of the carboxyl dimer supramolecular synthon) in the solid state, showing the PF_6^- anions that may assist the self-assembly of the supermolecule. Bond lengths and angles for hydrogen bonds: a) $N^+\cdots O$ 3.18 Å, $H\cdots O$ 2.33 Å, $N^+-H\cdots O$ 157°; b) $N^+\cdots O$ 2.98 Å, $H\cdots O$ 2.32 Å, $N^+-H\cdots O$ 130°; c) $N^+\cdots O$ 2.93 Å, $H\cdots O$ 2.06 Å, $N^+-H\cdots O$ 161°; d) $N^+\cdots O$ 2.86 Å, $H\cdots O$ 2.19 Å, $N^+-H\cdots O$ 130°; e) $N^+\cdots O$ 2.93 Å, $H\cdots O$ 2.06 Å, $N^+-H\cdots O$ 163°; f) $O\cdots O$ 2.68 Å; g) $O\cdots O$ 2.61 Å. B: Cartoon portraying the $\{[BPP34C10\cdot(\mathbf{2})_2]^{2+}\}_2\cdot 2PF_6^-$ species.

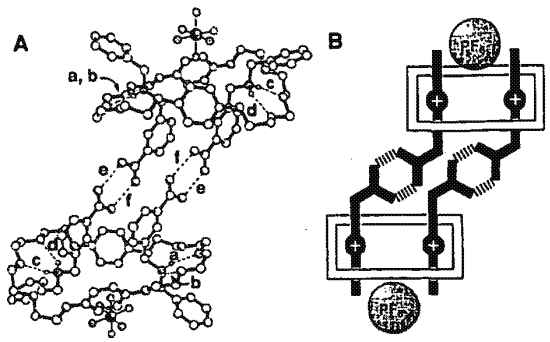


Figure 9. A: View of the crystal structure of the $\{[BPP34C10\cdot(\mathbf{3})_2]^{2+}\}_2$ supermolecule produced by the noncovalent dimerization of the $[BPP34C10\cdot(\mathbf{3})_2]^{2+}$ pseudorotaxane by means of the carboxyl dimer supramolecular synthon, showing the PF_6^- anions located in the clefts between two neighboring $\mathbf{3}^+$ cations. Bond lengths and angles for hydrogen bonds: a) $N^+\cdots O$ 2.92 Å, $H\cdots O$ 2.11 Å, $N^+-H\cdots O$ 149°; b) $N^+\cdots O$ 2.90 Å, $H\cdots O$ 2.13 Å, $N^+-H\cdots O$ 142°; c) $N^+\cdots O$ 2.90 Å, $H\cdots O$ 2.07 Å, $N^+-H\cdots O$ 153°; d) $N^+\cdots O$ 2.92 Å, $H\cdots O$ 2.18 Å, $N^+-H\cdots O$ 139°; e) $O\cdots O$ 2.57 Å; f) $O\cdots O$ 2.67 Å. B: Cartoon depicting the $\{[BPP34C10\cdot(\mathbf{3})_2]^{2+}\}_2\cdot 2PF_6^-$ supermolecule.

from the benzylic hydrogen atoms of one of the cations.[29] A similar approach of ca. 2.5 Å is also evident between one of the equatorial fluorine atoms of this anion and one of the hydrogen atoms of a hydroquinone ring. We hypothesize that this PF_6^- anion may assist[7f] the macrocyclic polyether by helping to align the two carboxyl groups of the [3]pseudorotaxane codirectionally with respect to each other, leading to the noncovalent dimerization of pairs of C_i symmetrically-related [3]pseudorotaxanes to generate doubly-encircled six-component organic supermolecules that are linked through pairs of strong $O-H\cdots O$ hydrogen bonds (Figure 8), both involving carboxyl dimers. In many respects, the structure of this six-component assemblage is similar to that of the 2:2 complex formed between α,α'-bis(benzylammonium)-*p*-xylene bis(hexafluorophosphate) and BPP34C10,[7b-c] an observation that is hardly surprising, given the fact that the carboxyl dimer may be regarded as a surrogate for a *p*-disubstituted benzene ring.[11b]

The analogous 1:2 complex formed between BPP34C10 and $\mathbf{3}^+$, in which the carboxyl substituent is located in the *meta* position, possesses a very similar supramolecular architecture to that of the $[BPP34C10\cdot(\mathbf{2})_2]^{2+}$ complex. Pairs of cations thread codirectionally through the BPP34C10 macrocycle and are hydrogen bonded, through the carboxyl groups, to their immediate neighbors in C_i-related 1:2 complexes (Figure 9). In essence, the only significant change in the overall superstructure is a shearing of one of the BPP34C10 rings in one $[BPP34C10\cdot(\mathbf{3})_2]^{2+}$ pseudorotaxane with respect to that of its hydrogen-bonded counterpart. Once again, complex stabilization is achieved by means of the same $N^+-H\cdots O$ and $O-H\cdots O$ hydrogen bonds that were observed in the $\{[BPP34C10\cdot(\mathbf{2})_2]^{2+}\}_2$ superstructure. Although there is a near-parallel alignment of the pairs of benzoic acid rings (the mean interplanar separation is ca. 3.62 Å), they are offset (the centroid–centroid separation is 4.99 Å) such as to preclude any significant $\pi-\pi$ stacking between them. A particularly interesting feature of this six-component assemblage is the positioning (Figure 9) of one of the PF_6^- anions within the cleft formed between the two $\mathbf{3}^+$ cations, an arrangement that is almost identical to that observed for the $[BPP34C10\cdot(\mathbf{2})_2]^{2+}$ complex. In the crystal lattice, this anion is notable for its order and for the proximal relationship between its fluorine atoms and pairs of hydroquinone hydrogen atoms on the BPP34C10 macroring (there are three $H\cdots F$ distances of less than 2.5 Å). We feel that this recurrence of a selective positioning of one of these anions reinforces our conclusion (vide supra) that this anion may be assisting[7f] the polyether in enforcing the codirectionality of the benzoic acid rings, thus allowing the production of the discrete multicomponent assemblage.

Contrasting with the crystal structures of the $[BPP34C10\cdot(\mathbf{2})_2]^{2+}$ and $[BPP34C10\cdot(\mathbf{3})_2]^{2+}$ pseudorotaxanes, the X-ray crystallographic analysis[17] of the 1:2 complex formed between the BPP34C10 macrocycle and the isophthalic acid-substituted cation $\mathbf{6}^+$ (Figure 10A) reveals that the secondary dialkylammonium strands are, in this instance, threaded centrosymmetrically with respect to one another—that is, in an *antiparallel* fashion—presumably since, in this case, no PF_6^- anions are involved in the self-assembly process (vide infra). Once again, stabilization of the [3]pseudorotaxane superstructure is achieved by $N^+-H\cdots O$ hydrogen bonds between the NH_2^+ centers and pairs of oxygen atoms in each of the polyether arcs of the macrocycle. The cations maintain the normal gull-wing conformation, with a planar all-*anti* $C-CH_2-NH_2^+-CH_2-C$ backbone, though with the isophthalate ring markedly skewed from an orthogonal relationship. Noncovalent association occurs between the pairs of carboxyl groups of each cation and their nonequivalent counterparts in symmetry-related complexes as a result of strong $O-H\cdots O$ hydrogen bonding between the carboxyl groups. In this case, the outcome of combining multiple carboxyl dimer and

© WILEY-VCH Verlag GmbH, D-69451 Weinheim, 1998
0947-6539/98/0404-0584 $ 17.50+.50/0 Chem. Eur. J. 1998, 4, No. 4

UM00012884
NOVARTIS EXHIBIT 1017
Novartis v. Regents, IPR2023-01346
Page 1630 of 4460

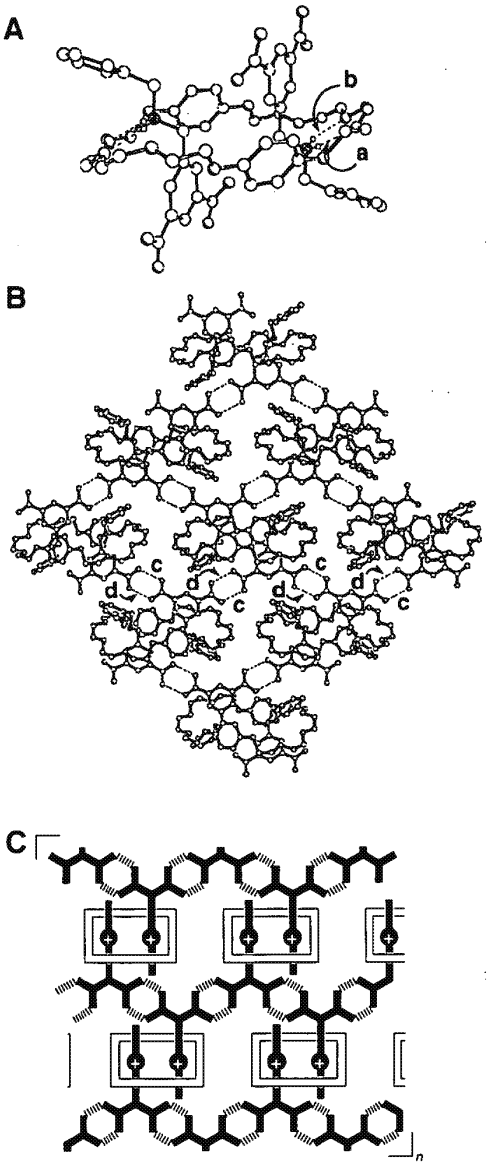


Figure 10. A: The crystal structure of the $[BPP34C10\cdot(6)_2]^{2+}$ pseudorotaxane. Bond lengths and angles for hydrogen bonds: a) $N^+\cdots O$ 2.88 Å, $H\cdots O$ 2.09 Å, $N^+-H\cdots O$ 145°; b) $N^+\cdots O$ 2.87 Å, $H\cdots O$ 2.09 Å, $N^+-H\cdots O$ 146°. B: The interwoven supramolecular cross-linked polymer formed through the noncovalent polymerization of the $[BPP34C10\cdot(6)_2]^{2+}$ pseudorotaxane by means of the carboxyl dimer supramolecular synthon. Hydrogen bond lengths: c) $O\cdots O$ 2.57 Å; d) $O\cdots O$ 2.69 Å. C: Cartoon illustrating the interwoven supramolecular cross-linked polymer $\{[BPP34C10\cdot(6)_2]^{2+}\}_n$.

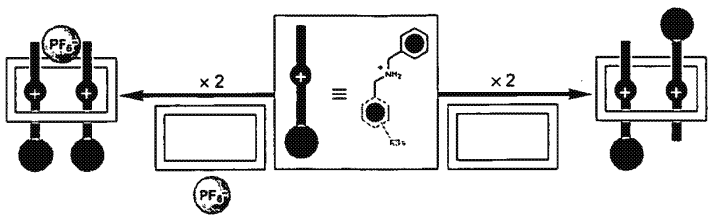
double threading motifs is the production of a novel type of supramolecular polymer (Figure 10B,C),[30] specifically, an *interwoven supramolecular cross-linked polymer*, in which cross-linking of isophthalic acid tapes[13] (cf. Figure 2B) is induced by the macrocyclic polyether, since it guides two isophthalic acid units from separate 6^+ cations in opposing directions, that is, the tapes are interlinked through the [3]pseudorotaxane unit to form two-dimensional pseudopolyrotaxane[15] sheets. The sheets are fairly thick (ca. 12.5 Å) since the planes of the $O-H\cdots O$ hydrogen bonds are approximately orthogonal to the planes of the BPP34C10 macrocycle. Included PhH solvent molecules and disordered PF_6^- counterions are located in the interstices between the polymeric layers. Neither of these species play significant roles in establishing the pseudopolyrotaxane sheet superstructure.

The crystal structures of the [3]pseudorotaxanes described above demonstrate[17] that the ditopic crown ether BPP34C10 acts as a useful unit for solid-state supramolecular synthesis in that it can, to a certain extent, direct supramolecular recognition sites in space (Scheme 2), leading to the creation of multiply encircled supermolecules and interwoven supramolecular arrays, that is, the crown ether induces *supramolecular preorganization* of the benzoic or isophthalic acid subunits for further noncovalent association using the carboxyl dimer supramolecular synthon. In fact, superstructures comparable to the $\{[BPP34C10\cdot(2)_2]^{2+}\}_2$, $\{[BPP34C10\cdot(3)_2]^{2+}\}_2$, and $\{[BPP34C10\cdot(6)_2]^{2+}\}_n$ architectures have been observed in the crystal structures of species in which *molecular preorganization*[31] dictates the spatial disposition of benzoate or isophthalate moieties by covalent frameworks. *Molecular* biscarboxylic acids that are endowed with two codirectionally-oriented carboxyl groups within the same covalent skeleton (like the *supramolecular* biscarboxylic acids $[BPP34C10\cdot(2)_2]^{2+}$ and $[BPP34C10\cdot(3)_2]^{2+}$) can combine to form dimeric supermolecules in the solid state.[5f,32] Likewise, *molecular* bisisophthalic acids, wherein two isophthalic acid moieties are located at the opposite ends of a covalent framework, exhibit (like the corresponding *supramolecular* bisisophthalic acid $[BPP34C10\cdot(6)_2]^{2+}$) the formation of supramolecular cross-linked polymers[33] in the solid state.[10c,24a] However, as we have demonstrated previously,[7f] one should not underestimate the potential role of the PF_6^- anions (and solvent molecules) in influencing these self-assembly processes.

Conclusions

The crystal structures considered in this paper illustrate a powerful synthetic supramolecular paradigm[3] that may be employed for the rational noncovalent synthesis of interwoven supramolecular architectures in the solid state. More generally, they show that complex superstructures may be generated easily by using the concomitant self-selective[7e] operation of several distinct recognition algorithms: in this instance, hydrogen-bonding motifs. In all the cases reported, the thread-like cations are inserted through the cavities of the macrocyclic polyethers with their NH_2^+ centers interacting with the polyether loops, thus leaving their pendant carboxyl groups available for additional noncovalent association. For the most part, the recognition algorithms operate independently of one another, so that crossover does not usually occur between hydrogen-bonding motifs, that is, running the crown ether–dialkylammonium cation and carboxyl dimer supramolecular synthons simultaneously allows the creation of

UM00012885
NOVARTIS EXHIBIT 1017
Novartis v. Regents, IPR2023-01346
Page 1631 of 4460



Scheme 2. Cartoon highlighting the role of BPP34C10 as a girdle for supramolecular synthesis that, possibly in conjunction with attendant anions, dictates the orientation of recognition sites in space.

elaborate supramolecular aggregates and arrays. The idea that operating concurrently at least two orthogonal recognition algorithms simplifies noncovalent syntheses dramatically is one that is rapidly gaining credence amongst those working in synthetic supramolecular chemistry. Indeed, we and others had previously used the concurrent operation of combinations of disparate recognition algorithms, such as metal–ligand/hydrogen-bonding[16] or $\pi-\pi$ stacking/hydrogen-bonding[7e, 15a,15d] algorithms, for the solid-state supramolecular synthesis of interwoven superstructures that would once have been inconceivable. The research presented here demonstrates that a combination of two different algorithms of the same type (in this case, hydrogen-bonding interactions) can also be employed for the noncovalent synthesis of interwoven superstructures in the solid state. It must be emphasized, however, that only once the factors involved in crystal packing are completely understood will synthetic supramolecular chemists be able to control inter(supra)molecular architectures with a level of precision comparable to that which has been observed hitherto in natural systems.

Experimental Section

General: Flash chromatography was carried out employing the customary procedures.[34] Melting points were determined on an Electrothermal 9200 melting point apparatus and are uncorrected. ^{1}H and ^{13}C NMR spectra were recorded at 20 °C on a Bruker AC300 spectrometer (at 300.1 and 75.5 MHz, respectively) with the deuterated solvent as the lock and the residual solvent as internal reference. Liquid secondary ion mass spectra (LSIMS) were obtained from a VG ZabSpec mass spectrometer equipped with a cesium ion source and utilizing a *m*-nitrobenzyl alcohol matrix. Electron-impact mass spectra (EIMS) were obtained from a VG ProSpec mass spectrometer. Microanalyses were performed by the University of North London Microanalytical Services.

Benzyl-4-carboxybenzylammonium hexafluorophosphate (2·PF$_6$): A solution of benzylamine (**10**, 1.50 g, 14.0 mmol) and methyl 4-formylbenzoate (**7**, 2.30 g, 14.0 mmol) in PhMe (205 mL) was heated under reflux for 15.5 h while the H_2O discharged was isolated with a Dean–Stark separator. The solution was filtered while hot and the solvent evaporated off under reduced pressure to yield 3.53 g (100%) of 4-carbomethoxybenzylidenebenzylamine as a white solid [^{1}H NMR ($CDCl_3$): $\delta = 3.95$ (s, 3H), 4.87 (s, 2H), 7.24–7.25 (m, 5H), 7.85 (d, $J = 8$ Hz, 2H), 8.09 (d, $J = 8$ Hz, 2H), 8.45 (s, 1H)], which was dissolved in a THF/MeOH solution (1:1, 110 mL). $NaBH_4$ (0.57 g, 15.0 mmol) was added with stirring at ambient temperature. A further portion of $NaBH_4$ (0.59 g, 15.5 mmol) was added to the reaction mixture after an additional 2 h. The solution was stirred subsequently for 20 h, before being treated with 1N HCl to adjust the pH to 2. After evaporation of the solvent in vacuo, the residue was partitioned between 1N NaOH (100 mL) and CH_2Cl_2 (100 mL). The aqueous phase was then further extracted with CH_2Cl_2 (2 × 100 mL). The combined organic extracts were dried ($MgSO_4$), filtered, and concentrated to afford 3.37 g (95%) of benzyl-4-carbomethoxybenzylamine **13**[7e] as a pale brown oil [^{1}H NMR ($CDCl_3$): $\delta = 3.79$ (s, 2H), 3.85 (s, 2H), 3.89 (s, 3H), 7.15–7.37 (m, 5H), 7.41 (d, $J = 8$ Hz, 2H), 7.99 (d, $J = 8$ Hz, 2H)]. A portion of this aminoester (1.03 g, 4.0 mmol) was boiled with 12N HCl (40 mL) for 19 h. On cooling, the residual white solid was collected and washed with EtOH (25 mL), $CHCl_3$ (25 mL), and Et_2O (25 mL). The solid was taken up in boiling H_2O (300 mL), then a solution of NH_4PF_6 (0.86 g, 5.3 mmol) in H_2O (8 mL) was added and the cooled solution extracted with $MeNO_2$ (3 × 200 mL). The combined $MeNO_2$ extracts were washed with H_2O (200 mL) and the solvent evaporated off under reduced pressure to provide the title compound as a white solid (0.97 g, 62%). M.p. 176–179 °C; ^{1}H NMR (CD_3CN): $\delta = 4.25$ (s, 2H), 4.29 (s, 2H), 7.46 (s, 5H), 7.57 (d, $J = 8$ Hz, 2H), 8.06 (d, $J = 8$ Hz, 2H); ^{13}C NMR (CD_3CN): $\delta = 51.9$, 52.8, 128.9, 130.2, 130.9, 131.25, 131.28, 131.32, 132.0, 136.6, 168.5; MS (LSI): *m/z* = 242 [$M - PF_6$]$^+$; $C_{15}H_{16}F_6NO_2P$ (387.3): calcd C 46.52, H 4.16, N 3.62; found C 46.41, H 4.16, N 3.53.

Benzyl-3-carboxybenzylammonium hexafluorophosphate (3·PF$_6$): Benzylamine (**10**, 1.61 g, 15.0 mmol) was condensed with methyl 3-formylbenzoate (**8**,[35] 2.46 g, 15.0 mmol) following the general procedure (vide supra) to provide 3-carbomethoxybenzylidenebenzylamine (3.80 g, 100%) as an oily white solid [^{1}H NMR ($CDCl_3$): $\delta = 3.93$ (s, 3H), 4.85 (s, 2H), 7.28–7.38 (m, 5H), 7.49 (t, $J = 8$ Hz, 1H), 8.02 (d, $J = 8$ Hz, 1H), 8.10 (d, $J = 8$ Hz, 1H), 8.39 (s, 1H), 8.43 (s, 1H)], which was reduced with $NaBH_4$ (see preparation of **13**) to furnish benzyl-3-carbomethoxybenzylamine (**14**, 3.83 g, 100%) as a yellow oil [^{1}H NMR ($CDCl_3$): $\delta = 3.81$ (s, 2H), 3.85 (s, 2H), 3.91 (s, 3H), 7.22–7.44 (m, 6H), 7.56 (d, $J = 8$ Hz, 1H), 7.93 (d, $J = 8$ Hz, 1H), 8.02 (s, 1H)]. A portion of this aminoester (1.04 g, 4.1 mmol) was converted into the title compound by a procedure similar to that described for 2·PF$_6$; a white solid (1.27 g, 80%) was obtained. M.p. 191–194 °C with decomp.; ^{1}H NMR (CD_3CN): $\delta = 4.25$ (s, 2H), 4.31 (s, 2H), 7.46 (s, 5H), 7.58 (t, $J = 8$ Hz, 1H), 7.71 (d, $J = 8$ Hz, 1H), 8.07 (d, $J = 8$ Hz, 1H), 8.16 (s, 1H); ^{13}C NMR (CD_3CN): $\delta = 52.1$, 52.7, 129.7, 130.0, 130.2, 130.6, 131.0, 131.9, 132.0, 132.4, 132.7, 136.1, 167.3; MS (LSI): *m/z* = 242 [$M - PF_6$]$^+$; $C_{15}H_{16}F_6NO_2P$ (387.3): calcd C 46.52, H 4.16, N 3.62; found C 46.68, H 4.25, N 3.68.

Bis(4-carboxybenzyl)ammonium hexafluorophosphate (4·PF$_6$): Bis(4-carbomethoxybenzyl)amine (**15**,[36] 0.52 g, 1.7 mmol) was transformed into the title compound by the general procedure given above for 2·PF$_6$. It was acquired as a white solid (0.46 g, 65%). M.p. 209–213 °C; ^{1}H NMR (CD_3CN): $\delta = 4.31$ (s, 4H), 7.56 (d, $J = 8$ Hz, 4H), 8.06 (d, $J = 8$ Hz, 4H); ^{13}C NMR (CD_3CN): $\delta = 51.9$, 131.0, 131.2, 132.1, 136.0, 167.3; MS (LSI): *m/z* = 286 [$M - PF_6$]$^+$; $C_{16}H_{16}F_6NO_4P$ (431.3): calcd C 44.56, H 3.74, N 3.25; found C 44.37, H 3.57, N 3.92.

Methyl 3-aminomethylbenzoate (12): HCl gas was bubbled through a solution of 3-carboxybenzylammonium chloride[20] (2.48 g, 13.2 mmol) in MeOH (110 mL) for 10 min. The resultant solution was heated under reflux for 14 h with protection from the atmosphere. The solution was filtered and the solvent removed in vacuo. The residual white solid was triturated with Et_2O (140 mL) before being collected and partitioned between 5% aqueous Na_2CO_3 (40 mL) and CH_2Cl_2 (60 mL). The aqueous phase was further extracted with CH_2Cl_2 (3 × 60 mL), then the combined organic extracts were dried ($MgSO_4$), filtered, and concentrated to provide the title compound as a colorless oil (0.63 g, 29%). ^{1}H NMR ($CDCl_3$): $\delta = 1.54$ (brs, 2H), 3.87 (s, 5H), 7.36 (t, $J = 8$ Hz, 1H), 7.47 (d, $J = 8$ Hz, 1H), 7.87 (d, $J = 8$ Hz, 1H), 7.95 (s, 1H); ^{13}C NMR ($CDCl_3$): $\delta = 46.1$, 52.1, 128.0, 128.1, 128.6, 130.3, 131.7, 143.6, 167.1; HRMS (EI) $C_9H_{12}NO_2$ [M+H]$^+$: calcd *m/z* = 166.0868; found *m/z* = 166.0872.

Bis(3-carboxybenzyl)ammonium hexafluorophosphate (5·PF$_6$): Methyl 3-aminomethylbenzoate (**12**, 0.62 g, 3.8 mmol) was condensed with methyl 3-formylbenzoate (**8**[35] 0.62 g, 3.8 mmol) following the general procedure (vide supra) to provide 3-carbomethoxybenzylidene-3-carbomethoxybenzylamine as a viscous yellow oil (1.13 g, 97%) [^{1}H NMR ($CDCl_3$): $\delta = 3.91$ (s, 3H), 3.93 (s, 3H), 4.88 (s, 2H), 7.41–7.61 (m, 3H), 7.93–8.14 (m, 4H), 8.40 (s, 1H), 8.46 (s, 1H)], which was reduced with $NaBH_4$ (see preparation of **13**) to provide bis(3-carbomethoxybenzyl)amine (**16**) as a thick yellow oil (1.02 g, 90%) [^{1}H NMR ($CDCl_3$): $\delta = 3.85$ (s, 4H), 3.91 (s, 6H), 7.40 (t, $J = 8$ Hz, 2H), 7.55 (d, $J = 8$ Hz, 2H), 7.93 (d, $J = 8$ Hz, 2H), 8.01 (s, 2H)], which was boiled with a stirred 12N HCl solution (28 mL) for 68 h. The

© WILEY-VCH Verlag GmbH, D-69451 Weinheim, 1998
0947-6539/98/0404-0586 $ 17.50+.50/0 *Chem. Eur. J.* 1998, *4*, No. 4

UM00012886
NOVARTIS EXHIBIT 1017
Novartis v. Regents, IPR2023-01346
Page 1632 of 4460

reaction mixture was treated with H_2O (20 mL) and the precipitated solid collected. This solid was washed with H_2O (20 mL), Me_2CO (20 mL), and Et_2O (20 mL), before being suspended in Me_2CO (300 mL). 0.2 M NH_4PF_6 was added, and the suspension stirred at room temperature for 1 h. The resulting clear solution was filtered and the Me_2CO removed under reduced pressure so that the hexafluorophosphate salt precipitated out of solution. The suspension that remained was treated with H_2O (200 mL), the solid collected and then washed with H_2O. The solid was then dissolved in Me_2CO (200 mL), 30 mg of decolorizing charcoal was added, and the solution boiled for 5 min, before being filtered while hot. This procedure was repeated and the solvent was evaporated off under reduced pressure to provide **5**·PF_6 as a white solid (1.00 g, 71%). M.p. 217 °C with decomp.; ^{1}H NMR (CD_3CN): $\delta = 4.31$ (s, 4H), 7.59 (t, $J = 8$ Hz, 2H), 7.69 (d, $J = 8$ Hz, 2H), 8.07 (d, $J = 8$ Hz, 2H), 8.13 (s, 2H); ^{13}C NMR (CD_3CN): $\delta = 51.9$, 130.3, 131.6, 131.7, 132.3, 133.6, 135.7, 166.0; MS (LSI): $m/z = 286$ $[M - PF_6]^+$; $C_{16}H_{16}F_6NO_4P$ (431.3): calcd C 44.56, H 3.74, N 3.25; found C 44.71, H 3.62, N 3.20.

Diethyl 5-formylisophthalate (9): A stirred solution of diethyl 5-bromomethylisophthalate[18] (1.26 g, 4.0 mmol) and bis(tetrabutylammonium) dichromate (5.62 g, 8.0 mmol) in $CHCl_3$ (20 mL) was heated under reflux for 2.5 h. On cooling to ambient temperature, the reaction mixture was filtered through 19.5 g of flash silica. The silica was washed with Et_2O (250 mL) and the combined $CHCl_3$ and Et_2O solutions concentrated to give a dark brown gum. Flash chromatography with CH_2Cl_2 provided the title compound as a white solid (0.76 g, 76%). M.p. 90 °C; ^{1}H NMR ($CDCl_3$): $\delta = 1.39$ (t, $J = 7$ Hz, 6H), 4.40 (q, $J = 7$ Hz, 4H), 8.65 (s, 2H), 8.85 (s, 1H), 10.09 (s, 1H); ^{13}C NMR ($CDCl_3$): $\delta = 14.3$, 61.9, 132.2, 134.2, 135.7, 136.8, 164.8, 190.6; MS (EI): $m/z = 250$ $[M]^+$; $C_{13}H_{14}O_5$ (250.3): calcd C 62.39, H 5.64; found C 62.57, H 5.54.

Benzyl-3,5-dicarboxybenzylammonium hexafluorophosphate (6·PF_6): Following the standard procedure (vide supra), benzylamine (**10**, 0.32 g, 3.0 mmol) was condensed with diethyl 5-formylisophthalate (**9**, 0.74 g, 3.0 mmol) to give 3,5-dicarboethoxybenzylidenebenzylamine as a white solid (0.98 g, 97%) [^{1}H NMR ($CDCl_3$): $\delta = 1.40$ (t, $J = 7$ Hz, 6H), 4.41 (q, $J = 7$ Hz, 4H), 4.88 (s, 2H), 7.10–7.43 (m, 5H), 8.46 (s, 2H), 8.59 (s, 1H), 8.72 (s, 1H)]. A portion of this aldimine (0.21 g, 0.6 mmol) was reduced with $NaBH_4$ (see preparation of **13**) to afford benzyl-3,5-dicarboethoxybenzylamine **17** as a yellow oil (0.20 g, 95%) [^{1}H NMR ($CDCl_3$): $\delta = 1.38$ (t, $J = 7$ Hz, 6H), 3.78 (s, 2H), 3.86 (s, 2H), 4.37 (q, $J = 7$ Hz, 4H), 7.19–7.39 (m, 5H), 8.19 (s, 2H), 8.54 (s, 1H)], that was transformed into the title compound **6**·PF_6 (employing a procedure similar to that described for **2**·PF_6), which was obtained as a white solid (0.15 g, 59%). M.p. 194–195 °C with decomp.; ^{1}H NMR (CD_3CN): $\delta = 4.25$ (s, 2H), 4.38 (s, 2H), 7.46 (s, 5H), 8.35 (s, 2H), 8.58 (s, 1H); ^{13}C NMR (CD_3CN): $\delta = 51.4$, 52.5, 130.0, 130.5, 130.7, 131.0, 131.8, 132.2, 132.4, 136.7, 166.3; MS (LSI): $m/z = 286$ $[M - PF_6]^+$; $C_{16}H_{16}F_6NO_4P$ (431.3): calcd C 44.56, H 3.74, N 3.25; found C 44.49, H 3.95, N 3.17.

Table 4. Solvents and methods employed for the crystallization of the pseudorotaxane complexes reported in this paper.

	Solvent[c]	Precipitant[d]	Method
[DB24C8·**2**][PF_6][a]	$MeNO_2$	PhH	liquid diffusion[e]
[DB24C8·**4**][PF_6][a]	Me_2CO	iPr_2O	liquid diffusion[e]
[DB24C8·**5**][PF_6][a]	Me_2CO	iPr_2O	liquid diffusion[e]
[DB24C8·**6**][PF_6][a]	Me_2CO	nC_6H_{14}	liquid diffusion[e]
[BPP34C10·$(\mathbf{2})_2$][PF_6]$_2$[b]	MeCN/$(ClCH_2)_2$	iPr_2O	liquid diffusion[e]
[BPP34C10·$(\mathbf{3})_2$][PF_6]$_2$[b]	Me_2CO	PhH	slow evaporation[f]
[BPP34C10·$(\mathbf{6})_2$][PF_6]$_2$[b]	Me_2CO	PhH	slow evaporation[f]

[a] Crystals were obtained from a solution containing equimolar amounts of the pseudorotaxane constituents. [b] Crystals were acquired from a solution containing a 1:2 molar ratio of BPP34C10 and the appropriate ammonium salt. [c] Good solvent in which the pseudorotaxane complexes are soluble. [d] Poor solvent in which the pseudorotaxane complexes are insoluble. [e] In the *liquid diffusion* method, the pseudorotaxanes' constituents were dissolved in a small amount of solvent, then the precipitant was carefully layered on top of the resulting solution. X-ray quality single crystals were obtained after several days, when the precipitant had diffused totally into the solution. [f] In the *slow evaporation* method, the pseudorotaxane components were dissolved in a small amount of solvent. The solution was mixed thoroughly with an amount of precipitant that did not induce immediate crystallization, then the solution was allowed to slowly evaporate at 20 °C over several days, resulting in the formation of single crystals that were suitable for X-ray crystallographic analysis.

Crystal growth: The crystal growing methods that were used have been described by Jones.[37] Table 4 lists the techniques employed and the solvent systems utilized for the preparation of single crystals that were suitable for X-ray crystallographic analysis.

X-ray crystallography: Table 5 provides a summary of the crystal data, data collection and refinement parameters for complexes [DB24C8·**2**][PF_6], [DB24C8·**4**][PF_6], [DB24C8·**5**][PF_6], [DB24C8·**6**][PF_6], [BPP34C10·$(\mathbf{2})_2$][PF_6]$_2$, [BPP34C10·$(\mathbf{3})_2$][PF_6]$_2$ and [BPP34C10·$(\mathbf{6})_2$][PF_6]$_2$. Although structure solution and refinement details for [BPP34C10·$(\mathbf{2})_2$][PF_6]$_2$ and [BPP34C10·$(\mathbf{6})_2$][PF_6]$_2$ have already been published,[17] the data for these compounds are included here as their structures have been refined again slightly differently. The structures were solved by direct methods and were refined by full-matrix least-squares based on F^2. In [DB24C8·**5**][PF_6] and [BPP34C10·$(\mathbf{6})_2$][PF_6]$_2$, disorder was found in part of one of the polyether linkages and, in the latter, in the benzyl ring of the cation. In each case, this disorder was resolved into two partial-occupancy orientations, the major occupancy portions of which were refined anisotropically. In [DB24C8·**2**][PF_6], [DB24C8·**4**][PF_6], [DB24C8·**6**][PF_6], and [BPP34C10·$(\mathbf{6})_2$][PF_6]$_2$, the PF_6^- anions were found to be disordered. For each structure, this disorder was resolved into two partial-occupancy orientations, the major occupancy portions of which were refined anisotropically. The PhH solvent molecules in [DB24C8·**2**][PF_6] were optimized and refined anisotropically. The included Me_2CO molecules in [DB24C8·**4**][PF_6] were ordered and refined anisotropically. The solvent molecules in [DB24C8·**5**][PF_6] were found to be disordered over two partial-occupancy sites, the atoms of both being refined isotropically. In [DB24C8·**6**][PF_6], the half-occupancy included Me_2CO molecule was refined anisotropically. The MeCN molecules in [BPP34C10·$(\mathbf{2})_2$][PF_6]$_2$ were not clearly defined, and the solvent was modeled by the assignment of various peaks of electron density to total up to two-and-a-half molecules. In [BPP34C10·$(\mathbf{3})_2$][PF_6]$_2$, the three included PhH molecules were found to be a mixture of ordered and disordered molecules (with two of the ordered ones positioned about centers of symmetry), all the non-hydrogen atoms of which were refined anisotropically. In [BPP34C10·$(\mathbf{6})_2$][PF_6]$_2$, the two PhH molecules were found to be distributed over three partial occupancy sites, all of which were refined isotropically. The remaining non-hydrogen atoms in all of the structures were refined anisotropically. In each structure, the C–H hydrogen atoms were placed in calculated positions, assigned isotropic thermal parameters, $U(H) = 1.2U_{eq}(C)$ [$U(H) = 1.5U_{eq}(C\text{–}Me)$], and allowed to ride on their parent atoms. The N–H hydrogen atoms in all the structures were optimized and refined isotropically. In [DB24C8·**2**][PF_6], [DB24C8·**4**][PF_6], and [DB24C8·**6**][PF_6] the O–H hydrogen atoms were located from ΔF maps and refined isotropically—in the other four structures, these hydrogen atoms could not be located. Computations were carried out using the SHELXTL PC program system.[38] Crystallographic data (excluding structure factors) for the structures reported in this paper have been deposited with the Cambridge Crystallographic Data Centre as supplementary publication no. CCDC-100689. Copies of the data can be obtained free of charge on application to CCDC, 12 Union Road, Cambridge CB2 1EZ, UK (Fax: (+ 44) 1223-336-033; e-mail: deposit@ccdc.cam.ac.uk).

Acknowledgments: This research was sponsored by an Engineering and Physical Sciences Research Council CASE Award (to M.C.T.F.) and the Biotechnology and by Biological Sciences Research Council.

Received: September 11, 1997 [F818]

[1] a) M. Mascal, *Contemp. Org. Synth.* **1994**, *1*, 31–46; b) J.-M. Lehn, *Supramolecular Chemistry*, VCH, Weinheim, **1995**.

[2] For some recent examples, see: a) M. Fujita, D. Oguro, M. Miyazawa, H. Oka, K. Yamaguchi, K. Ogura, *Nature (London)* **1995**, *378*, 469–471; b) J. D. Hartgerink, J. R. Granja, R. A. Milligan, M. R. Ghadiri, *J. Am. Chem. Soc.* **1996**, *118*, 43–50; c) R. W. Saalfrank, N. Low, F. Hampel, H. D. Stachel, *Angew. Chem.* **1996**, *108*, 2353–2354; *Angew. Chem. Int. Ed. Engl.* **1996**, *35*, 2209–2210; d) J. A. R. P. Sarma, F. H. Allen, V. J. Hoy, J. A. K. Howard, R. Thaimattam, K. Biradha, G. R.

UM00012887
NOVARTIS EXHIBIT 1017
Novartis v. Regents, IPR2023-01346
Page 1633 of 4460

Table 5. Crystal data, data collection, and refinement parameters.[a]

	[DB24C8·2]·[PF_6]	[DB24C8·4]·[PF_6]	[DB24C8·5]·[PF_6]	[DB24C8·6]·[PF_6]	[BPP34C10·$(2)_2$]·[PF_6]$_2$	[BPP34C10·$(3)_2$]·[PF_6]$_2$	[BPP34C10·$(6)_2$]·[PF_6]$_2$
formula	$C_{59}H_{48}NO_{10}\cdot PF_6$	$C_{40}H_{48}NO_{12}\cdot PF_6$	$C_{40}H_{48}NO_{12}\cdot PF_6$	$C_{40}H_{58}NO_{12}\cdot PF_6$	$C_{58}H_{72}N_2O_{14}\cdot 2PF_6$	$C_{58}H_{72}N_2O_{14}\cdot 2PF_6$	$C_{60}H_{72}N_2O_{18}\cdot 2PF_6$
solvent	2 PhH	Me_2CO	0.25 Me_2CO	0.5 Me_2CO	2.5 MeCN	3 PhH	2 PhH
formula weight	992.0	937.8	894.3	908.8	1413.8	1545.4	1555.4
color, habit	clear blocks	clear prisms	clear prismatic needles	clear prisms	clear plates	clear plates	clear rhombs
crystal size (mm)	0.83 × 0.83 × 0.67	0.93 × 0.83 × 0.40	0.50 × 0.30 × 0.13	0.53 × 0.50 × 0.40	0.37 × 0.33 × 0.30	0.83 × 0.63 × 0.10	0.30 × 0.28 × 0.10
lattice type	monoclinic	triclinic	triclinic	monoclinic	triclinic	triclinic	monoclinic
space group	$P2_1/c$, 14	$P\bar{1}$, 2	$P\bar{1}$, 2	$P2_1/n$, 14	$P\bar{1}$, 2	$P\bar{1}$, 2	$P2_1/c$, 14
T (K)	293	293	293	293	293	203	293
a (Å)	16.248(3)	11.908(1)	11.015(3)	16.890(1)	10.619(1)	10.154(1)	12.513(1)
b (Å)	17.194(3)	12.336(1)	11.022(1)	15.997(2)	17.292(1)	17.209(1)	16.555(1)
c (Å)	19.002(3)	16.627(2)	19.764(2)	20.949(1)	22.109(2)	24.643(5)	18.593(1)
α (°)	–	79.92(1)	78.39(1)	–	79.64(1)	105.49(1)	–
β (°)	105.99(1)	83.55(1)	77.94(2)	104.79(1)	79.54(1)	101.51(2)	96.10(1)
γ (°)	–	76.17(1)	89.81(1)	–	76.94(1)	99.27(1)	–
V (Å^3)	5103(1)	2328.8(4)	2296.6(7)	5472.7(9)	3848.2(4)	3960.1(9)	3829.7(5)
Z	4	2	2	4	2	2	2[b]
ρ_{calcd} (g cm^{-3})	1.291	1.337	1.293	1.103	1.220	1.296	1.349
$F(000)$	2088	984	936	1904	1478	1620	1624
radiation used	$Mo_{K\alpha}$	$Mo_{K\alpha}$	$Cu_{K\alpha}$	$Cu_{K\alpha}$[c]	$Cu_{K\alpha}$[c]	$Cu_{K\alpha}$[c]	$Cu_{K\alpha}$[c]
μ (mm^{-1})	0.13	0.15	1.26	1.07	1.27	1.27	1.36
θ range	1.8–22.5	2.0–25.0	2.3–63.0	3.0–57.5	2.0–55.0	1.9–55.0	3.6–60.0
no. unique reflns measured	6625	8157	7400	7421	7886	9776	5661
no. unique reflns observed, $\|F_o\| > 4\sigma(\|F_o\|)$	3994	4844	5257	3566	3167	5485	3497
no. of variables	594	622	586	614	813	933	550
R_1[d]	0.063	0.079	0.083	0.130	0.158	0.090	0.087
wR_2[e]	0.164	0.217	0.246	0.337	0.401	0.212	0.237
weighting factors a, b[f]	0.086, 4.589	0.126, 1.334	0.170, 0.713	0.249, 0.000	0.326, 5.190	0.110, 7.276	0.139, 3.740
largest difference peak, hole (e Å^{-3})	0.33, −0.25	0.50, −0.42	0.65, −0.29	0.89, −0.35	0.89, −0.49	0.53, −0.31	0.40, −0.39

[a] Details in common: graphite-monochromated radiation, ω-scans, Siemens P4 diffractometer, refinement based on F^2. [b] The supermolecule has crystallographic C_i symmetry. [c] Rotating anode source. [d] $R_1 = \Sigma\,||F_o| - |F_c||/\Sigma|F_o|$. [e] $wR_2 = \sqrt{[\Sigma[w(F_o^2 - F_c^2)^2]/\Sigma[w(F_o^2)^2]]}$. [f] $w^{-1} = \sigma^2(F_o^2) + (aP)^2 + bP$.

Desiraju, *Chem. Commun.* **1997**, 101–102; e) J. A. Whiteford, C. V. Lu, P. J. Stang, *J. Am. Chem. Soc.* **1997**, *119*, 2524–2533; f) T. L. Hennigar, D. C. MacQuarrie, P. Losier, R. D. Rogers, M. J. Zaworotko, *Angew. Chem.* **1997**, *109*, 1044–1046; *Angew. Chem. Int. Ed. Engl.* **1997**, *36*, 972–973; g) D. P. Funeriu, J.-M. Lehn, G. Baum, D. Fenske, *Chem. Eur. J.* **1997**, *3*, 99–104; h) D. L. Caulder, K. N. Raymond, *Angew. Chem.* **1997**, *109*, 1508–1510; *Angew. Chem. Int. Ed. Engl.* **1997**, *36*, 1440–1442.

[3] M. C. T. Fyfe, J. F. Stoddart, *Acc. Chem. Res.* **1997**, *30*, 393–401.

[4] J. R. Fredericks, A. D. Hamilton in *Comprehensive Supramolecular Chemistry, Vol. 9* (Eds.: J. L. Atwood, J. E. D. Davies, D. D. MacNicol, F. Vögtle), Pergamon, Oxford, **1996**, pp. 565–594.

[5] For some recent examples, see: a) J. A. Zerkowski, C. T. Seto, G. M. Whitesides, *J. Am. Chem. Soc.* **1992**, *114*, 5473–5475; b) S. C. Zimmerman, B. F. Duerr, *J. Org. Chem.* **1992**, *57*, 2215–2217; c) J. Yang, E. Fan, S. J. Geib, A. D. Hamilton, *J. Am. Chem. Soc.* **1993**, *115*, 5314–5315; d) M. Mascal, N. M. Hext, R. Warmuth, M. H. Moore, J. P. Turkenburg, *Angew. Chem.* **1996**, *108*, 2347–2350; *Angew. Chem. Int. Ed. Engl.* **1996**, *35*, 2204–2206; e) C. M. Drain, K. C. Russell, J.-M. Lehn, *Chem. Commun.* **1996**, 337–338; f) O. Struck, W. Verboom, W. J. J. Smeets, A. L. Spek, D. N. Reinhoudt, *J. Chem. Soc. Perkin Trans. 2* **1997**, 223–227; g) R. Meissner, X. Garcias, S. Mecozzi, J. Rebek, Jr., *J. Am. Chem. Soc.* **1997**, *119*, 77–85; h) R. F. M. Lange, F. H. Beijer, R. P. Sijbesma, R. W. W. Hooft, H. Kooijman, A. L. Spek, J. Kroon, E. W. Meijer, *Angew. Chem.* **1997**, *109*, 1006–1008; *Angew. Chem. Int. Ed. Engl.* **1997**, *36*, 969–971; i) E. E. Simanek, S. Qiao, I. S. Choi, G. M. Whitesides, *J. Org. Chem.* **1997**, *62*, 2619–2621; j) M. C. Feiters, M. C. T. Fyfe, M. V. Martínez-Díaz, S. Menzer, R. J. M. Nolte, J. F. Stoddart, P. J. M. van Kan, D. J. Williams, *J. Am. Chem. Soc.* **1997**, *119*, 8119–8120; k) K. D. M. Harris, B. M. Kariuki, C. Lambropoulos, D. Philp, J. M. A. Robinson, *Tetrahedron* **1997**, *53*, 8599–8612.

[6] For some recent examples, see: a) S. Hanessian, M. Simard, S. Roelens, *J. Am. Chem. Soc.* **1995**, *117*, 7630–7645; b) P. R. Ashton, G. R. Brown, W. Hayes, S. Menzer, D. Philp, J. F. Stoddart, D. J. Williams, *Adv. Mater.* **1996**, *8*, 564–567; c) K. E. Schwiebert, D. N. Chin, J. C. MacDonald, G. M. Whitesides, *J. Am. Chem. Soc.* **1996**, *118*, 4018–4029; d) R. E. Melendez, C. V. K. Sharma, M. J. Zaworotko, C. Bauer, R. D. Rogers, *Angew. Chem.* **1996**, *108*, 2357–2359; *Angew. Chem. Int. Ed. Engl.* **1996**, *35*, 2213–2215; e) C. B. Aakeröy, D. P. Hughes, M. Niewenhuyzen, *J. Am. Chem. Soc.* **1996**, *118*, 10134–10140; f) C. V. K. Sharma, M. J. Zaworotko, *Chem. Commun.* **1996**, 2655–2656; g) O. Félix, M. W. Hosseini, A. De Cian, J. Fischer, *Angew. Chem.* **1997**, *109*, 134–136; *Angew. Chem. Int. Ed. Engl.* **1997**, *36*, 102–104; h) K. Endo, T. Ezuhara, M. Koyanagi, H. Masuda, Y. Aoyama, *J. Am. Chem. Soc.* **1997**, *119*, 499–505; i) K. R. Adam, I. M. Atkinson, R. L. Davis, L. F. Lindoy, M. S. Mahinay, B. J. McCool, B. W. Skelton, A. H. White, *Chem. Commun.* **1997**, 467–468; j) P. Brunet, M. Simard, J. D. Wuest, *J. Am. Chem. Soc.* **1997**, *119*, 2737–2738; k) V. A. Russell, C. C. Evans, W. Li, M. D. Ward, *Science* **1997**, *276*, 575–579; l) I. L. Karle, D. Ranganathan, V. Haridas, *J. Am. Chem. Soc.* **1997**, *119*, 2777–2783.

[7] a) P. R. Ashton, P. J. Campbell, E. J. T. Chrystal, P. T. Glink, S. Menzer, D. Philp, N. Spencer, J. F. Stoddart, P. A. Tasker, D. J. Williams, *Angew. Chem.* **1995**, *107*, 1997–2001; *Angew. Chem. Int. Ed. Engl.* **1995**, *34*, 1865–1869; b) P. R. Ashton, E. J. T. Chrystal, P. T. Glink, S. Menzer, C. Schiavo, J. F. Stoddart, P. A. Tasker, D. J. Williams, *ibid.* **1995**, *107*, 2001–2004 and *34*, 1869–1871; c) P. R. Ashton, E. J. T. Chrystal, P. T. Glink, S. Menzer, C. Schiavo, N.

© WILEY-VCH Verlag GmbH, D-69451 Weinheim, 1998
0947-6539/98/0404-0588 $ 17.50+.50/0 *Chem. Eur. J.* **1998**, *4*, No. 4

UM00012888
NOVARTIS EXHIBIT 1017
Novartis v. Regents, IPR2023-01346
Page 1634 of 4460

Spencer, J. F. Stoddart, P. A. Tasker, A. J. P. White, D. J. Williams, *Chem. Eur. J.* **1996**, *2*, 709–728; d) P. T. Glink, C. Schiavo, J. F. Stoddart, D. J. Williams, *Chem. Commun.* **1996**, 1483–1490; e) P. R. Ashton, P. T. Glink, M.-V. Martínez-Díaz, J. F. Stoddart, A. J. P. White, D. J. Williams, *Angew. Chem.* **1996**, *108*, 2058–2061; *Angew. Chem. Int. Ed. Engl.* **1996**, *35*, 1930–1933; f) M. C. T. Fyfe, P. T. Glink, S. Menzer, J. F. Stoddart, A. J. P. White, D. J. Williams, *ibid.* **1997**, *109*, 2158–2160 and *36*, 2068–2070; g) P. R. Ashton, M. C. T. Fyfe, P. T. Glink, S. Menzer, J. F. Stoddart, A. J. P. White, D. J. Williams, *J. Am. Chem. Soc.* **1997**, *119*, 12514–12524.

[8] a) D. S. Lawrence, T. Jiang, M. Levett, *Chem. Rev.* **1995**, *95*, 2229–2260; b) D. Philp, J. F. Stoddart, *Angew. Chem.* **1996**, *108*, 1242–1286; *Angew. Chem. Int. Ed. Engl.* **1996**, *35*, 1154–1196.

[9] Pseudorotaxanes are *supramolecular* entities in which one or more thread-like species interpenetrate the cavities of one or more macrorings to generate inclusion complexes. Notably, as distinct from their mechanically-interlocked, *molecular* counterparts, the rotaxanes, pseudorotaxane supermolecules can dissociate into their individual components since they do not possess bulky stopper groups. For instance, see: a) P. R. Ashton, D. Philp, N. Spencer, J. F. Stoddart, *J. Chem. Soc. Chem. Commun.* **1991**, 1677–1679; b) P.-L. Anelli, P. R. Ashton, A. M. Z. Slawin, N. Spencer, J. F. Stoddart, D. J. Williams, *Angew. Chem.* **1991**, *103*, 1052–1054; *Angew. Chem. Int. Ed. Engl.* **1991**, *30*, 1036–1039; c) D. B. Amabilino, P.-L. Anelli, P. R. Ashton, G. R. Brown, E. Córdova, L. A. Godínez, W. Hayes, A. E. Kaifer, D. Philp, A. M. Z. Slawin, N. Spencer, J. F. Stoddart, M. S. Tolley, D. J. Williams, *J. Am. Chem. Soc.* **1995**, *117*, 11142–11170; d) P. R. Ashton, S. J. Langford, N. Spencer, J. F. Stoddart, A. J. P. White, D. J. Williams, *Chem. Commun.* **1996**, 1387–1388; e) P. N. W. Baxter, H. Sleiman, J.-M. Lehn, K. Rissanen, *Angew. Chem.* **1997**, *36*, 1350–1352; *Angew. Chem. Int. Ed. Engl.* **1997**, *36*, 1294–1296; f) A. Mirzoian, A. E. Kaifer, *Chem. Eur. J.* **1997**, *3*, 1052–1058.

[10] a) L. Leiserowitz, *Acta Crystallogr. Sect. B* **1976**, *32*, 775–802; b) Z. Berkovitch-Yellin, L. Leiserowitz, *J. Am. Chem. Soc.* **1982**, *104*, 4052–4064; c) S. V. Kolotuchin, E. E. Fenlon, S. R. Wilson, C. J. Loweth, S. C. Zimmerman, *Angew. Chem.* **1995**, *107*, 2873–2876; *Angew. Chem. Int. Ed. Engl.* **1995**, *34*, 2654–2657 and references therein.

[11] a) J. C. MacDonald, G. M. Whitesides, *Chem. Rev.* **1994**, *94*, 2383–2420; b) G. R. Desiraju, *Angew. Chem.* **1995**, *107*, 2541–2558; *Angew. Chem. Int. Ed. Engl.* **1995**, *34*, 2311–2327; c) *Comprehensive Supramolecular Chemistry, Vol. 6* (Eds.: J. L. Atwood, J. E. D. Davies, D. D. MacNicol, F. Vögtle), Pergamon, Oxford, **1996**; d) V. A. Russell, M. D. Ward, *Chem. Mater.* **1996**, *8*, 1654–1666; e) G. R. Desiraju, *Chem. Commun.* **1997**, 1475–1482.

[12] M. Bailey, C. J. Brown, *Acta Crystallogr.* **1967**, *22*, 387–391.

[13] R. Alcala, S. Martinez-Carrera, *Acta Crystallogr. Sect. B* **1972**, *28*, 1671–1677.

[14] a) J. Yang, J. L. Marendez, S. J. Geib, A. D. Hamilton, *Tetrahedron Lett.* **1994**, *35*, 3665–3668; b) S. Valiyaveettil, V. Enkelmann, G. Moessner, K. Müllen, *Macromol. Symp.* **1996**, *102*, 165–173; c) S. C. Zimmerman, F. Zeng, D. E. C. Reichert, S. V. Kolotuchin, *Science* **1996**, *271*, 1095–1098.

[15] a) M. Asakawa, P. R. Ashton, G. R. Brown, W. Hayes, S. Menzer, J. F. Stoddart, A. J. P. White, D. J. Williams, *Adv. Mater.* **1996**, *8*, 37–41; b) P. R. Ashton, R. Ballardini, V. Balzani, M. Belohradsky, M. T. Gandolfi, D. Philp, L. Prodi, F. M. Raymo, M. V. Reddington, N. Spencer, J. F. Stoddart, M. Venturi, D. J. Williams, *J. Am. Chem. Soc.* **1996**, *118*, 4931–4951; c) F. M. Raymo, J. F. Stoddart, *Trends Polym. Sci.* **1996**, *4*, 208–211; d) M. Asakawa, P. R. Ashton, C. L. Brown, M. C. T. Fyfe, S. Menzer, D. Pasini, C. Scheuer, N. Spencer, J. F. Stoddart, A. J. P. White, D. J. Williams, *Chem. Eur. J.* **1997**, *3*, 1136–1150.

[16] Kim and his associates have employed coordinate covalent bonds between ligands and metals to link pseudorotaxanes in order to form interwoven supramolecular arrays. See: a) D. Whang, Y.-M. Jeon, J. Heo, K. Kim, *J. Am. Chem. Soc.* **1996**, *118*, 11333–11334; b) D. Whang, K. Kim, *ibid.* **1997**, *119*, 451–452.

[17] A small part of this research has been reported in a communication. See: P. R. Ashton, A. N. Collins, M. C. T. Fyfe, S. Menzer, J. F. Stoddart, D. J. Williams, *Angew. Chem.* **1997**, *109*, 760–763; *Angew. Chem. Int. Ed. Engl.* **1997**, *36*, 735–739.

[18] We prepared this compound employing the synthetic procedure that was first utilized by Collman and his associates. See: J. P. Collman, X. Zhang, K. Wang, J. I. Brauman, *J. Am. Chem. Soc.* **1994**, *116*, 6245–6251. However, this compound has been prepared more recently by Fréchet's group on a much larger scale. See: J. W. Leon, M. Kawa, J. M. J. Fréchet, *J. Am. Chem. Soc.* **1996**, *118*, 8847–8859.

[19] a) D. Landini, F. Rolla, *Chem. Ind. (London)* **1979**, 213; b) G. A. Kraus, M. E. Krolski, *J. Org. Chem.* **1986**, *51*, 3347–3350; c) G. Mehta, S. R. Shah, Y. Venkateswarlu, *Tetrahedron* **1994**, *50*, 11729–11742.

[20] S. Jackson, W. DeGrado, A. Dwivedi, A. Parthasarathy, A. Higley, J. Krywko, A. Rockwell, J. Markwalder, G. Wells, R. Wexler, S. Mousa, R. Harlow, *J. Am. Chem. Soc.* **1994**, *116*, 3220–3230.

[21] a) R. C. Helgeson, T. L. Tarnowski, J. M. Timko, D. J. Cram, *J. Am. Chem. Soc.* **1977**, *99*, 6411–6418; b) H. W. Gibson, S. Liu, P. Lecavalier, C. Wu, Y. X. Shen, *ibid.* **1995**, *117*, 852–874. See also: c) Y. Delaviz, H. W. Gibson, *Polym. Commun.* **1991**, *32*, 103–105; d) Y. Delaviz, Y. X. Shen, H. W. Gibson, *Polymer* **1992**, *33*, 212–213.

[22] However, when the peaks for the [DB24C8·cation]$^+$ complexes were calibrated against peaks for the bis(4-*t*-butylbenzyl)ammonium cation (a cation that has been shown not to form complexes with DB24C8; P. R. Ashton, I. Baxter, M. C. T. Fyfe, F. M. Raymo, N. Spencer, J. F. Stoddart, A. J. P. White, D. J. Williams, *J. Am. Chem. Soc.* **1998**, *220*, 2297–2309), there appeared to be no clear relationship between the relative intensities of the peaks associated with the complexes and the K_a values obtained in solution.

[23] However, in this instance, the signals are time-averaged, since the relatively large cavity of BPP34C10 allows fast association and dissociation of the components on the ^{1}H NMR time scale at 20°C.

[24] The disruption of noncovalent association between carboxyl groups by competitive polar solvents has been noted previously by researchers from other laboratories. See: a) A. Zafar, J. Yang, S. J. Geib, A. D. Hamilton, *Tetrahedron Lett.* **1996**, *37*, 2327–2330; b) Ref. [14c]. Unfortunately, the salts were barely soluble in CD_2Cl_2 alone, even in the presence of the crown ethers, thus precluding a study of carboxyl group association and, hence, interpseudorotaxane interactions in solution.

[25] D. B. Amabilino, I. W. Parsons, J. F. Stoddart, *Trends Polym. Sci.* **1994**, *2*, 146–152.

[26] I. R. Hanson, D. L. Hughes, M. R. Truter, *J. Chem. Soc. Perkin Trans. 2* **1976**, 972–978.

[27] We have introduced the term co-conformation recently[7f] to define the three-dimensional spatial arrangement of the atoms in supramolecular systems.

[28] Swager and his associates have recently prepared side-chain pseudopolyrotaxanes possessing covalently linked polymeric backbones. See: a) M. J. Marsella, P. J. Carroll, T. M. Swager, *J. Am. Chem. Soc.* **1995**, *117*, 9832–9841; b) Q. Zhou, T. M. Swager, *ibid.* **1995**, *117*, 12593–12602.

[29] Following this discovery, we reexamined the crystal structure[7b,c] of the 2:2 [4]pseudorotaxane complex formed between α,α'-bis(benzylammonium)-*p*-xylene bis(hexafluorophosphate) and BPP34C10, where we found that one of the principal F–P–F axes of a PF_6^- anion was directed into the central cleft of the complex between two NH_2^+ cationic centers. The contact distances from the hydrogen atoms of the [4]pseudorotaxane to either of these axial fluorine atoms are all greater than 2.8 Å. Nevertheless, a contact of ca. 2.5 Å was identified between one of the benzylic hydrogen atoms of the [4]pseudorotaxane and one of the equatorial fluorine atoms of the PF_6^- anion.

[30] J.-M. Lehn, *Makromol. Chem. Macromol. Symp.* **1993**, *69*, 1–17.

[31] a) D. J. Cram, *Angew. Chem.* **1986**, *98*, 1041–1060; *Angew. Chem. Int. Ed. Engl.* **1986**, *25*, 1039–1057; b) D. J. Cram, *ibid.* **1988**, *100*, 1041–1052, and *27*, 1009–1020.

[32] For instance, see: a) F. Takusagawa, T. F. Koetzle, *Acta Crystallogr. Sect. B* **1979**, *35*, 2888–2896; b) L. J. Fitzgerald, J. C. Gallucci, R. E. Gerkin, *Acta Crystallogr. Sect. B* **1991**, *47*, 776–782; c) H. Díaz, K. Y. Tsang, D. Choo, J. W. Kelly, *Tetrahedron* **1993**, *49*, 3533–3545.

[33] Note, however, that the cross-linking component of these supramolecular polymers is entirely covalent.

[34] W. C. Still, M. Kahn, A. Mitra, *J. Org. Chem.* **1978**, *43*, 2923–2925.

[35] H. Simonis, *Chem. Ber.* **1912**, *45*, 1584–1592.

[36] P. R. Ashton, P. T. Glink, J. F. Stoddart, P. A. Tasker, A. J. P. White, D. J. Williams, *Chem. Eur. J.* **1996**, *2*, 729–736.

[37] P. G. Jones, *Chem. Br.* **1981**, *17*, 222–225.

[38] SHELXTL PC v. 5.03, Siemens Analytical X-Ray Instruments, Madison (WI), **1994**.

UM00012889
NOVARTIS EXHIBIT 1017
Novartis v. Regents, IPR2023-01346
Page 1635 of 4460

S0032-3861(96)00595-2

Polymer Vol. 38 No. 4, pp. 913–919, 1997
© 1997 Elsevier Science Ltd
Printed in Great Britain. All rights reserved
0032-3861/97/$17.00 + 0.00

Effect of crystallization temperature on the cocrystallization of hydroxybutyrate/hydroxyvalerate copolymers

P. A. Barker and P. J. Barham*
HH Wills Physics Laboratory, Royal Fort Tyndall Avenue, Bristol BS8 1TL, UK

and J. Martinez-Salazar
Institute de Estructura de la Materia, CSIC. Serrano 119, 28006 Madrid, Spain
(Received 5 February 1996; revised 10 April 1996)

Measurements on the effect of crystallization temperature on the crystallinity, long period and unit cell dimensions of P(HB/HV) copolymers with 0–27% HV crystallized isothermally at 23, 52 and 81°C are presented. The crystal composition has been estimated from the unit cell expansion and the relationship between crystallinity and density. The amount of cocrystallization of HV in the PHB crystal structure is found to decrease as the crystallization temperature is increased: the amount of HV in the crystals formed at 81°C is reduced to 2/3 of the value for crystallization at room temperature. The results are consistent with cocrystallization being an effect of the kinetics of crystallization which becomes less significant as equilibrium crystallization conditions are approached. © 1997 Elsevier Science Ltd. All rights reserved.

(Keywords: polyhydroxybutyrate; co-crystallization; isodomorphism)

INTRODUCTION

Background

P(HB/HV) copolymers are a range of biodegradable bacterial thermoplastics produced and marketed by ZENECA Bio Products under the tradename Biopol. The crystal growth, nucleation and morphology of PHB are in many ways typical for polymers[1,2], however the HB/HV copolymers have been found to have high crystallinities at all compositions[3,4], which, since the copolymers are random, implies that the two comonomers must cocrystallize. Wide angle X-ray scattering (WAXS) has been used to infer that copolymers with less than 30% HV crystallize with the PHB structure while samples with more than 49% HV have the PHV structure[4]. The existence of two crystal structures which allowed mutual cocrystallization was termed isodimorphism, in analogy to the equilibrium effects of isomorphism and dimorphism. A phase diagram with a sharply defined transition from the PHB to PHV structure at some composition (*ca.* 35% HV) was implied, however, other work[5,6] suggests that both structures are present at intermediate compositions.

The extent of cocrystallization has been measured by solid state n.m.r.[5,7,8], density[9,10], and lattice strain[8,9].

Solid state n.m.r. experiments have the potential to measure the HV content of the mobile and immobile phases, however the results published to date are inconclusive. The n.m.r. results published by Kamiya *et al.*[7] are shown in *Table 1*. The lack of HV in the crystals of the 18% HV sample is surprising given that such a sample shows a strained crystal lattice and reduced heat of fusion. Sanders *et al.*[5] have presented n.m.r. results showing lower degrees of cocrystallization, however the data were collected at temperatures where some of the samples would have partially melted, and so the results may not be typical of the structure at lower temperatures.

The lattice strain caused when the bulkier HV units crystallize into the PHB structure can be used to estimate the crystal composition (we use the term strain rather than expansion to indicate an increase in lattice dimension to avoid confusion with thermal expansion). This requires an estimate of the volume of the HV unit in the PHB crystal, for which the volume of an HV unit in the PHV structure may be used. We have published results using this method[9] on samples crystallized in a similar manner to industrial processing: holding at 55°C until the spherulites were fully grown and then storing at room temperature until crystallization was complete (which takes several weeks for high HV copolymers). The crystals were found to contain a lower fraction of HV than the sample overall: typically the HV content of the crystal was 2/3 that of the whole sample. A similar analysis by Bonthrone[8] on as supplied powders suggested that the HV composition of the crystals was the same as the sample.

Some of us have published a method for estimating the partition of HV between the crystal and amorphous phases based on sample densities[10], which was used to some success in our previous paper[9]. Furthermore we have used the same argument to show that on a strict two-phase model the densities of samples crystallized at 23 and 81°C imply that the latter have either a lower crystallinity or less HV in the crystalline phase.

*To whom correspondence should be addressed

UM00012890
NOVARTIS EXHIBIT 1017
Novartis v. Regents, IPR2023-01346
Page 1636 of 4460

Table 1 Properties of P(HB/HV) crystal from n.m.r. and d.s.c. analysis by Kamiya *et al.*[7]

HV content						
Sample v_s (mol%)	Crystal v_c (mol%)	Amorphous v_a (mol%)	% Crystal χ (mol%)	Enthalpy of fusion ΔH (kJ mol^{-1})	Corrected enthalpy $\Delta H/\chi$ (kJ mol^{-1})	Melting point T_m (°C)
0	–	–	72.3	11.2	15.5	175
18.3	0	47.8	59.4	6.2	10.4	121
31.6	10.2	64.4	60.2	3.2	6.0	81
40.7	14.2	48.6	[a]	[a]	[a]	54

[a] This sample showed crystals in the PHV structure as well as PHB

Table 2 The ICI (Zeneca) batch codes, HV content and molecular weight of samples used

Batch code	Compositon (%HV)[a]	Molecular weight[b]
PHB 300[c]	0	283 000
PV14	7	439 000
PV5	21	116 000

[a] HV content was measured by ICI using ^{1}H n.m.r.
[b] Weight average molecular weight as quoted by ICI (except PHB300 which was measured at Bristol); measured by gel permeation chromatography, polydispersities were all *ca.* 2.5. NB Degradation during melting may change the molecular weight by about 25%
[c] The original ICI code for this material is not known

In this paper we present the results of our investigations on the crystallization of random HB/HV copolymers crystallized under controlled thermodynamic conditions. In particular we investigate the effect of crystallization temperature, albeit over a limited range. The primary method of investigation is X-ray diffraction: we show how the lattice dimensions, lamellar thickness and crystallinity vary with sample composition and crystallization temperature. The samples studied all contain less than 30% HV, the crystal structures are similar to that of PHB homopolymer. This paper is in fact an extension of the work started in ref. 9 increasing the range of crystallization temperatures. Melting of similar samples is discussed in work soon to be published[11].

EXPERIMENTAL

Samples

A range of samples were supplied by ICI Biological Products Business (now ZENECA Bio Products); *Table 2* shows some of the properties of the batches used. Sequence analysis has shown that these samples have a random distribution of HV units[4,12]. These were cleaned by dissolving in chloroform, filtering, and precipitating into alcohol. For all work voidless films were required; these were best prepared by dissolving the sample in chloroform and allowing the solvent to evaporate slowly before final drying in a vacuum oven until constant mass was reached. We are confident that this preparation leaves no voids since such samples had a consistent amorphous density which agreed with the published value[10,13].

For our purposes it is essential that the thermodynamics of crystallization are well defined, therefore the samples were crystallized by remelting them at 190°C and crytallizing them in a silicone oil bath held at constant temperature until they reached constant density (which can take several weeks). (It is not necessary to measure the density at high temperature in silicone oil: after a few days crystallizing, when the spherulites have finished growing, having the samples at room temperature for the few minutes that it takes to measure density does not cause a significant increase in density.)

Ruland–Vonk measurement of crystallinity

The wide angle X-ray scatter was measured using a Rigaku vertical goniometer in symmetric reflection geometry, with collimation and sample size optimized for high intensity rather than angular resolution. Semicrystalline samples were run in step scan mode from 7 to 150° (2θ) whereas amorphous samples were run between 7 and 40° at a scan rate of 16° min^{-1}. The intensity profiles were corrected for absorption and transparency as described by Milberg[14]. The crystallinity was determined by the Ruland–Vonk method[15,16] since this corrects for the effect of diffuse scatter from crystal defects. A version of Vonk's program which had been modified to run on IBM compatible PCs was used.

Long period measurement

The scattered X-ray intensities were read off the exposed films from a Rigaku Denki camera using a Joyce–Loebel optical densitometer at ×10 magnification. The long period was estimated from the peak position by application of Bragg's law.

Lattice strain measurement

X-ray diffraction from the samples was measured using a horizontal Philips goniometer with stepper motor drive. The irradiated volume was kept small in order to minimize peak position aberrations.

Two methods of measuring the peak centroid were used: direct integration was preferred as more objective, however the (1 1 0) and (0 1 1) peaks overlap and so the peaks had to be resolved by curve fitting. In order to measure the centroid by integration it is necessary to remove the amorphous contribution to the scatter around the peak: this was achieved by subtracting a background based on the amorphous scatter which was scaled to fit the 2θ ranges which showed no Bragg scatter.

RESULTS

Crystallinity

Two factors which hindered these measurements are worth reporting: sample orientation and crystallization of material after quenching from the nominal crystallization temperature. The first of these is a result of the low nucleation density for PHB and HB/HV copolymers:

UM00012891
NOVARTIS EXHIBIT 1017
Novartis v. Regents, IPR2023-01346
Page 1637 of 4460

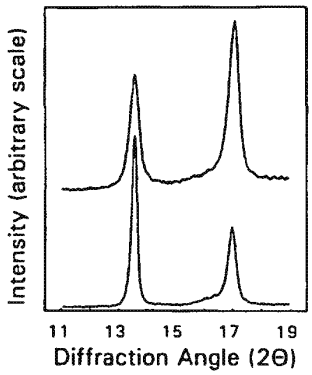


Figure 1 WAXS of PHB showing the effect on the diffraction profile of sample orientation caused by the spherulite size being similar to the sample thickness. The top curve comes from a thick sample crystallized at a low temperature to give small spherulites, the curve below comes from a thin sample crystallized at a high temperature to give large spherulites. NB samples as strongly oriented as the example shown here were not used for crystallinity determination

Table 3 The crystallinities measured by the Ruland–Vonk WAXS method, density and from the heat of fusion

Batch code	Composition (%HV)	Method	Crystallization temperature 23°C	52°C	81°C
PHB 300	0	WAXS	62%	74%	78%
		d.s.c.	60%	69%	73%
		Density	62%	n/d	77%
PV14	7	WAXS	n/d	n/d	77%
PV5	21	WAXS	67%	72%	68%

n/d, not determined

when crystallizing at high temperatures the spherulites grown can have diameters of the order of millimetres, i.e. of similar dimensions to the sample thickness. A particularly strong example of this effect is shown in *Figure 1*: this form of orientation may be the cause of the varied relative intensities of (0 2 0) and (1 1 0) reflections which can be found in the literature on PHB. The under representation of the (1 1 0) reflection causes an underestimate of crystallinity. The other phenomenon which affected the measurement, crystallization on quenching, gives rise to melting endotherms below the nominal T_c which can be seen by d.s.c.[7]. The fact that after crystallization at low supercoolings there remains some material which can only crystallize at higher supercoolings is evidence that cocrystallization is disfavoured at high crystallization temperatures.

Both of the factors described above were more pronounced for high HV crystallized at high temperatures; samples strongly affected by these errors have been discarded.

In *Table 3* we show the results of Ruland–Vonk crystallinity measurements, with comparisons to other measures of crystallinity for the same samples. From these we conclude:

(1) The Ruland–Vonk measurement of crystallinity for PHB agrees well with crystallinities measured by density and heat of fusion. For the copolymers the inclusion of HV into the crystal affects the density and heat of fusion and so we cannot make similar comparisons.

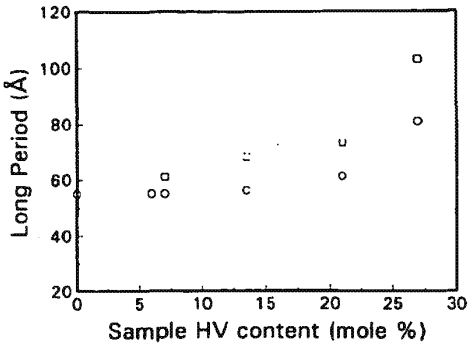


Figure 2 The long periods of various samples crystallized at 23°C (circles) and 52°C (squares). The experimental error is estimated at ±5%

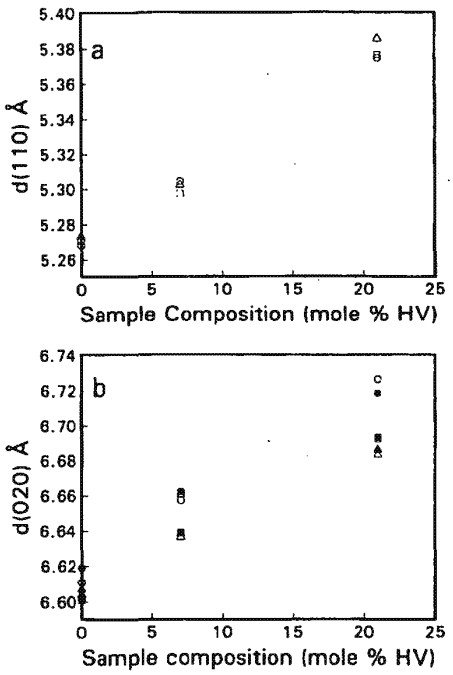


Figure 3 (a) The (1 1 0) and (b) the (0 2 0) unit cell dimensions as a function of sample HV content for after crystallization at 23°C (circles), 52°C (squares) and 81°C (triangles). In (b) the open symbols represent peak positions measured by integration and the filled symbols measurements by curve fitting

(2) For crystallization at room temperature the HV content of the sample does not significantly affect the final crystallinity (the slightly higher value for the 21% HV sample is not significant: if it is real it is quite likely to be a molecular weight effect). This confirms the previous results on samples cast from chloroform solution[3,4] with data from samples crystallized under thermodynamically controlled conditions.

(3) There is no strong evidence that crystallizing HB/HV copolymers at higher temperatures gives lower crystallinitities, contrary to our initial expectations[10].

UM00012892
NOVARTIS EXHIBIT 1017
Novartis v. Regents, IPR2023-01346
Page 1638 of 4460

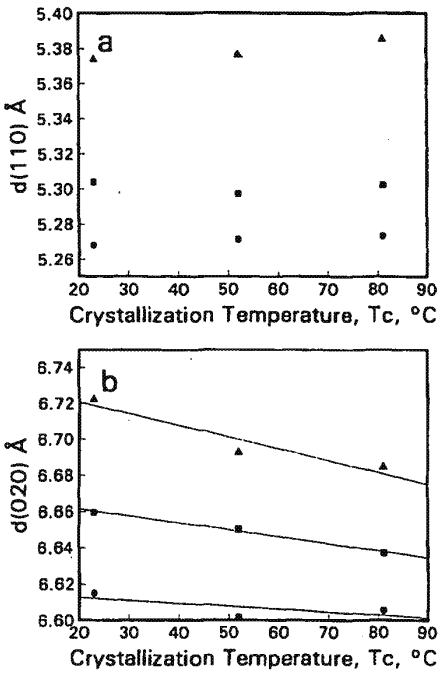


Figure 4 The same data as *Figure 3* but plotted as a function of crystallization temperature for PHB (0% HV) (circles), PV14 (7% HV) (squares) and PV5 (22% HV) (triangles). The (0 2 0) measurements are the averages of the results from integration and curve fitting

The only signs in this direction are the crystallization on quenching described above, and the fact that PHB shows a significant increase in crystallinity over the range of T_cs investigated which the higher HV samples do not. However, given the difficulties with this method for high HV samples crystallized at high temperatures, as discussed above, we do not dare draw any conclusions from this alone.

Long period measurements

The long periods of all samples measured are shown in *Figure 2*. The results are in good agreement with data from de Koning[18] who analysed the whole scattering curve and found that PHB crystallized at 60°C had a long period of 69 ± 3 Å which, modelled as two phases, consisted of 41 Å of crystal and 28 Å of amorphous material.

The increase in L with %HV agrees with Orts *et al.*[19] (who show data for samples with up to 22% HV crystallized at temperatures between 60 and 115°C). However the nonlinearity, i.e. the up turn in the graph at high HV, is present only in their $T_c = 80$°C sample. At lower temperatures our data suggests that the upturn would be insignificant over the HV range which they studied, while their data suggests that this effect reaches a maximum at $T_c \sim 80$°C, being less significant at higher temperatures.

*The values differ from those presented by some of us in ref. 20, the early results were incorrect due to misinterpretation of the (0 1 1) reflection and a systematic error in our measurements. Correction of these mistakes has not affected the conclusions of our previous paper

Lattice parameter measurements

The (1 1 0) and (0 2 0) lattice plane spacings are shown in *Figure 3* as a function of sample HV content for various crystallization temperatures*. Each point shown is the average of two or three independent measurements on different samples from the same batch crystallized under identical conditions; the typical reproducibility of these results was in the range of ±0.005 Å. A similar level of agreement was found between the measurements of the (0 2 0) peak position by direct integration and curve fitting. The (0 1 1) reflection proved to be rather difficult to fit since it is broad and tends to merge into the amorphous halo, this affects the baseline for fitting the (1 1 0) peak, the measured position of which is therefore less certain. However the fit was reproducible enough for us to discern trends in the position of that peak. The trend for the lattice to be increasingly strained as the sample HV increases shown in *Figure 3* agrees well with previous observations[4,8,9,21], and corresponds to increasing amounts of HV in the crystals.

In *Figure 4* we show the variation of the (0 2 0) and (1 1 0) plane spacings for similar samples crystallized at different temperatures. As the crystallization temperature is increased there is a significant decrease in the lattice strain in the (0 2 0) plane spacing for the copolymers. A common cause of variation in unit cell dimensions with crystallization conditions is the change in crystal thickness decreasing the effect of the fold surfaces. However since, at these supercoolings, the change in lamellar thickness with crystallization temperature is small, and does not vary greatly with HV content, and since the PHB interplane distance varies less than that of the copolymer we conclude that the greater decrease in strain for the copolymers is due to less cocrystallization of HV at lower supercoolings. The (1 1 0) lattice parameter showed no clear trend, this may be because it was more susceptible to errors caused by the curve fitting procedure used, or may be a result of the peculiar crystallography of chain folding in PHB (which is predominantly in the [1 1 0] directions[22,23]).

DISCUSSION

Effect of crystallization temperature on HV cocrystallization

The results presented above can be analysed in two independent ways to give estimates of the amount of HV in the crystalline phase: firstly the lattice strain can be assumed to be proportional to the amount of HV in the crystals; secondly the sample density, degree of crystallinity and unit cell size can be related to the partitioning of HV between amorphous and crystalline regions on a two phase model.

Since we have some doubts about the accuracy of the (1 1 0) parameter measurement perhaps the safest approach is to concentrate on the variation in the (0 2 0) lattice spacing (*Figure 4b*). Consider the strain in the b direction, i.e. difference between d(0 2 0) for PHB and for the copolymers: for samples crystallized at 81°C this is approximately 2/3 that observed when the samples are crystallized at 23°C. We therefore judge that if, for example, a copolymer crystal formed at room temperature contains as much HV as the bulk sample, the same copolymer crystallized at 81°C will have only 2/3 as much HV in the crystals. However we cannot fix the

UM00012893
NOVARTIS EXHIBIT 1017
Novartis v. Regents, IPR2023-01346
Page 1639 of 4460

Table 4 The crystal HV content (v_c) estimated from the sample density and degree of crystallinity, χ. The crystallinity value used is (A) that obtained from Ruland–Vonk measurements, (B) the values obtained from density measurements of PHB crystallized at the same temperature and (C) as B but varying with HV content in the same way as A. (Where crystallinity values for PV14 were not determined an estimate was made based on the values for PHB and PV5). The final column (lattice) shows the crystal HV content estimated from the unit cell strain

		A		B		C		Lattice
Batch	%HV	χ (%)	v_c (mol%)	χ (%)	v_c (mol%)	χ (%)	v_c (mol%)	v_c
$T_c = 23°C$								
PV14	7	62	9	62	9	62	9	9
PV5	21	62	19	62	19	62	19	26
$T_c = 52°C$								
PV14	7	74	6	69	8.5	69	8.5	8
PV5	21	73	13	69	14	68	14.5	23
$T_c = 81°C$								
PV14	7	77	3.5	73	5	68	7	7
PV5	21	68	14	73	12	63	16	(24)

absolute composition at any one temperature from this parameter alone, so it is interesting to include our estimates of the other lattice dimensions.

On purely steric grounds we can argue that the volume change in the average unit cell is a linear combination of the volume of the HB and HV units in the crystal [9], from which we derive:

$$v_c = (V - V_B)/(V_V - V_B) \quad (1)$$

where v_c is the mole fraction of HV in the crystal, V is the unit cell volume of the sample, V_B and V_V are the unit cell volumes of the PHB and PHV unit cells respectively. We have assumed that the |c| dimension of the copolymer is the same as that of PHB (5.96 Å) to produce the estimates of crystal HV content listed in the final column of *Table 4*. We estimate an accuracy of ±1% HV from consideration of experimental reproducibility, but this does not include errors due to the assumptions of our model. Although the absolute values are too high the trend of less cocrystallization for higher T_c is still present (especially considering that the (1 1 0) spacing for 22% HV, $T_c = 81°C$ sample was not particularly reliable).

Table 4 also shows the HV composition of the crystals obtained from our model of sample density[10]. The greatest uncertainty from this model comes from the necessity of using a value of crystallinity which matches the density-measured value, i.e. is based on crystal packing rather than ordering. We have therefore shown results for three likely trends in crystallinity: (A) that obtained from Ruland–Vonk measurements; (B) that obtained from density measurements on PHB, assumed to be independent of HV content; and (C) that obtained from PHB density but following the same trend observed in the WAXS measured crystallinity. Again the decrease in cocrystallization with increasing crystallization temperature is visible, and of a similar magnitude to the estimates from the (0 2 0) lattice spacing. The third assumption (C), that we should use the crystallinity of PHB measured by density but adjusted to follow the trend observed by the Ruland–Vonk measurements, shows a smaller variation in the crystal HV content than the other treatments. There is, however a reduction in the amount of cocrystallization at high crystallization temperatures since the total amount of crystalline material is less than in assumptions A and B and less than one would expect by comparison with the trend of increasing crystallinity with increasing crystallization temperature.

The observed, high, degree of cocrystallization of copolymers at all compositions is indeed unusual, for most AB copolymers the inclusion of B units into a crystal of A incurs a free energy penalty which is much greater than $K_B T_c$ (3–5 kJ mol^{-1} for T_c in the range 100–300°C). Therefore the exclusion model has been taken as typical of copolymer crystallization behaviour, e.g. Flory's analysis of copolymer melting[24]. In practice even those copolymers which give zero crystallinity at compositions with high B will crystallize if the B content is low enough. The crystals which do form in such copolymers are often observed to have some B monomers in them. For example, chlorinated polyethylene crystals are estimated to have *ca.* 1/4 the Cl content of the sample as a whole (based on measurement of small angle scattering of X-rays or neutrons and density and confirmed by measurements of lattice expansion[25,26]). The question is then whether the cocrystallization which takes place is caused by the kinetics of crystallization 'trapping' energetically unfavourable defects in the crystal, or is the energy penalty for crystallization sometimes low enough to allow some equilibrium concentration of comonomer B in the crystal. This problem has been addressed by the kinetic theories of Helfand and Lauritzen[27] and Goldbeck-Wood[28], and the equilibrium approach of Marchessault and Allegra[29].

The supercoolings used in this study are not particularly low, and the range covered is not large: taking the equilibrium melting point of PHB as our reference we have covered the range of $T_m°-T_c$ from 110–170°C. All these samples have therefore been crystallized far from equilibrium, and should not be considered as possessing equilibrium properties. It is, however, possible to use this data to show how different the equilibrium crystals would be from those observed. From the extrapolation of melting temperature as a function of crystallization temperature we have been able to estimate that the highest temperature at which HB/HV crystals can grow is *ca.* 170–195°C irrespective of HV content[17,20]. In this limit crystals would grow infinitely slowly, and so equilibrium would dominate kinetic effects. If we extrapolate the trends shown in *Figure 4* we find that there would be no significant difference in the (0 2 0) lattice spacing for different HV contents crystallized at *ca.* 190°C. While we have to be cautious about an

UM00012894
NOVARTIS EXHIBIT 1017
Novartis v. Regents, IPR2023-01346
Page 1640 of 4460

extrapolation over such a long range based on so few data, we can say that our present results are consistent with the supposition that HV would be excluded from crystals growth at equilibrium: i.e. the cocrystallization of HV is a kinetic effect.

Finally we must caution that the models used above to calculate the amount of HV in the crystals assume a homogenous crystal phase, it is possible that there may exist crystals with a range of compositions[11]. The measurements given above (and those based on other techniques) will give an average of this range, biased by the sensitivity of that technique to the difference between perfect and defective crystals.

Long periods

The tend for the higher HV samples to have larger long periods may be partly due to changes in the amount of amorphous material between the crystals. However it also agrees with the prediction of kinetic growth theories that copolymers should form thicker crystals than homopolymers if energetically unfavourable cocrystallization takes place[28,30]. The observed crystal thickness is given by

$$l = l_{min} + \delta l \quad (2)$$

where l_{min} is the minimum stable thickness for which the free energy released by crystallization, ΔG_v, is just enough to balance the free energy used at the chain folded surfaces, $2\sigma_e$.

$$l_{min} = 2.\sigma_e/\Delta G_v \quad (3)$$

and δl is a small, approximately constant, length which various kinetic growth theories seek to predict. At any temperature, T, the free energy of crystallization can be approximated by

$$\Delta G_v = \Delta H_v(T_m - T)/T_m \quad (4)$$

If cocrystallization reduces the stability of the crystals then a longer crystal stem is necessary to overcome the energy required by the surfaces. That is to say that the inclusion of defects reduces ΔH and T_m and so the minimum stable crystal thickness is increased. The consequence of this argument is that it is the observed enthalpy and melting point (corrected for surface effects) which govern the crystal thickness, not the equilibrium values normally used. Even if the equilibrium free energy of a crystal in a copolymer system is enough to overcome the surface energy, a real crystal with more defects may not be stable at that thickness, and it is the real crystal which has to exist.

These arguments may explain the upturn in plots of long period *versus* composition and its variation with crystallization temperature: the high HV copolymer crystals grown at lower temperatures contain more defects, are therefore more unstable and so a thicker crystal is necessary to balance the surface energy. However at higher temperatures there is more exclusion of HV from the crystals so that the increase of long period with temperature for the copolymer is less marked than for the homopolymer. A full analysis of the observed long periods to find the thermodynamic parameters governing the crystallization would be prohibitively complicated: equation (4) is only approximate at the high supercoolings used to crystallize PHB/HV[31], the fold surface free energy may be affected by HV content and the exclusion of HV from the crystal cores, and a rigorous treatment to find the thickness of the amorphous material between the crystalline lamellae would be required.

Isodimorphism vs kinetic cocrystallization

In comparing our results with the ideas of isodimorphism, we first note that all of our crystallizations have been carried out at high supercoolings, well away from solidus of phase diagrams predicted by Allegra[29]. Under these conditions the equilibrium concentration of HV in the crystals follows the form $\exp(-\epsilon/KT)$ where ϵ is the free energy penalty for including an HV unit in the PHB structure. We find no evidence for the increase in HV cocrystallization with increasing temperature which this predicts. Also, as we have previously noted[20], since the sample HV content, partitioning of HV between crystal and amorphous phase, and crystallinity are interrelated[10], any theory which predicts an equilibrium composition of the crystalline and amorphous phases is, in effect, predicting that the crystallinity is also at an equilibrium value. For polymers this is generally not the case.

It is easier to relate our findings to a kinetic explanation of cocrystallization where the concentration of defects decreases as the crystallization temperature increases since more rearrangement of the chain can take place during crystallization giving opportunity for more stable conditions to be found. In this case the high crystallinity of HB/HV copolymers is due in part to a moderately low defect energy for cocrystallization (we have estimated the enthalpic part to 24 kJ mol^{-1}[9]) but also due to the high undercoolings at which PHB systems can be crystallized. This explanation based on kinetic cocrystallization agrees with the conclusions of a paper by Marchessault reporting on phase separation in blends of copolymers with different HV content[32].

CONCLUSIONS

In a previous paper[10] we argued that a clear trend in sample density shows that increasing the crystallization temperature for HB/HV copolymers leads to less crystallization of HV (either by means of a reduction in crystallinity or by the crystals having less HV in them). Our present analysis shows that while there may be a reduction in crystallinity for the copolymers compared to the homopolymer, with crystallization of the latter at high temperatures excluding some material which can only crystallize on cooling, there is evidence of increasing rejection of HV from the crystal at lower supercoolings. Our best estimate, based on the (0 2 0) unit cell spacing, is that crystallization at 81°C gives crystals with 2/3 the HV:HB ratio obtained by crystallizing at 23°C. We also estimate (from the unit cell volume and relationship between density and crystallinity) that room temperature crystallization gives equal partitioning of HV between the crystal and amorphous parts. Contrary to models based on 'isodimorphism', our results suggest the amount of cocrystallization decreases as equilibrium crystallization conditions are approached.

ACKNOWLEDGEMENTS

We gratefully knowledge the help of Sally Organ and Andy Webb for sharing their expertise on PHB, Karen Bonthrone for discussions related to aspects of her PhD

UM00012895
NOVARTIS EXHIBIT 1017
Novartis v. Regents, IPR2023-01346
Page 1641 of 4460

Thesis, and Zeneca Bio Products for supplying the materials used. This work was funded by the Spanish CICYT (grant MAT94-0825), the UK SERC and a Barclays Bank personal overdraft (PAB).

REFERENCES

1 Barham, P. J., Keller, A., Otun, E. L. and Holmes, P. A. *J. Mater. Sci.* 1984, **19**, 2781
2 Barham, P. J. *J. Mater. Sci.* 1984, **19**, 3826
3 Bloembergen, S., Holden, P. A., Hamer, G. K., Bluhm, T. L. and Marchessault, R. H. *Macromolecules* 1986, **19**, 2865
4 Bluhm, T. L., Hamer, G. K., Marchessault, R. H., Fyfe, C. A. and Veregin, R. P. *Macromolecules* 1986, **19**, 2871
5 Bonthrone, K. M., Clauss, J., Horowitz, D. M., Hunter, B. K. and Sanders, J. K. M. *FEMS Microbiol. Rev.* 1992, **103**, 269
6 Mitomo, H., Morishita, N. and Doi, Y. *Macromolecules* 1993, **26**, 5809
7 Kamiya, N., Minoru, S., Inoue, Y., Chûjô, R. and Doi, Y. *Macromolecules* 1991, **24**, 2178
8 Bonthrone, K. M., *Ph.D. Thesis*, University of Cambridge, 1993
9 Sánchez-Cuesta, M., Martínez-Salazar, J., Barker, P. A. and Barham, P. J. *J. Mater. Sci.* 1992, **27**, 5335
10 Barker, P. A., Mason, F. and Barham, P. A. *J. Mater. Sci.* 1990, **25**, 1952
11 Barker, P. A. and Barham, P. J. in preparation
12 Montaudo, M. S., Ballistreri, A. and Montaudo, G. *Macromolecules* 1991, **24**, 5051
13 Holmes, P. A. in 'Developments in Crystalline Polymers—2' (Ed. D. C. Bassett), Elsevier, London, 1987, chap. 1
14 Milberg, M. E. *J. Appl. Phys.* 1958, **29**, 23
15 Ruland, W. *Acta Cryst.* 1961, **14**, 1180
16 Vonk, C. G. *J. Appl. Phys.* 1973, **6**, 148
17 Organ, S. J. and Barham, P. J. *J. Mater. Sci.* 1991, **26**, 1368
18 de Koning, G. J. M. *PhD thesis*, Technical University of Eindhoven, 1993
19 Orts, W. J., Marchessault, R. H. and Bluhm, T. L. *Macromolecules* 1991, **24**, 6435
20 Barham, P. J., Barker, P. and Organ, S. J. *FEMS Microbiol. Rev.* 1992, **103**, 289
21 Owen, A. J., Hienzel, J., Skrbic, L. and Divjakovic, V. *Polymer* 1992, **33**, 1563
22 Welland, E. L., Stejney, J., Halter, A. and Keller, A. *Polym. Commun.* 1989, **30**, 302
23 Seebach, D., Bürger, H. M., Müller, H. M., Lengweiler, U. D., Beck, A. K., Sykes, K. E., Barker, P. A. and Barham, P. J. *Helv. Chim. Acta* 1994, **77**, 1099
24 Flory, P. J. *Trans. Faraday Soc.* 1995, **51**, 848
25 Roe, R. J. and Gieniewski, C. *Macromolecules* 1973, **6**, 212
26 Kalepky, U., Fischer, E. W., Herchenröder, P., Schelten, J., Liesler, G. and Wegner, G. *J. Polym. Sci.: Polym. Phys. Ed.* 1979, **17**, 2117
27 Helfand, E. and Lauritzen, J. I. *Macromolecules* 1973, **6**, 631
28 Goldbeck-Wood, G. and Sadler, D. M. *Polym. Commun.* 1990, **31**, 143; Goldbeck-Wood, G. *Ph.D. Thesis*, University of Bristol, 1992
29 Allegra, G., Marchessault, R. H. and Bloembergen, S. *J. Polym. Sci.: Part B: Polym. Phys.* 1992, **30**, 809
30 Sanchez, I. C. and Eby, R. K. *Macromolecules* 1975, **8**, 638
31 Suzuki, T. and Kovacs, A. J. *Polymer J.* 1970, **1**, 82
32 Pearce, R. P. and Marchessault, R. H. *Macromolecules* 1994, **27**, 3869

UM00012896
NOVARTIS EXHIBIT 1017
Novartis v. Regents, IPR2023-01346
Page 1642 of 4460

Acta Cryst. (1977). B33, 3670–3677

Electron Density Distribution in Cumulenes: An X-ray Study of the Complex Allenedicarboxylic Acid–Acetamide (1:1) at −150°C

BY ZIVA BERKOVITCH-YELLIN AND LESLIE LEISEROWITZ

Department of Structural Chemistry, The Weizmann Institute of Science, Rehovot, Israel

AND FRANZ NADER

Organisch-Chemisches Institut der Universität Heidelberg, Federal Republic of Germany

(*Received* 14 *January* 1977; *accepted* 14 *May* 1977)

The crystal structure of the 1:1 complex allenedicarboxylic acid–acetamide was investigated by X-ray (λ = 0·709 Å) diffraction at −150°C. The space group is $C2/c$ with $Z = 8$ and $a = 18{\cdot}962$ (4), $b = 4{\cdot}798$ (1), $c = 21{\cdot}668$ (5) Å, $\beta = 119{\cdot}01$ (3)°. The dihedral angle between the $>C{=}C$ moieties of the allene system is 93·3°. The conformation of the $C^{\beta}{=}C^{\alpha}{-}C{=}O$ system is antiplanar. The molecular electron density distribution was determined by a least-squares procedure. The observed deformation densities in the allene, carboxyl and amide groups are discussed.

Introduction

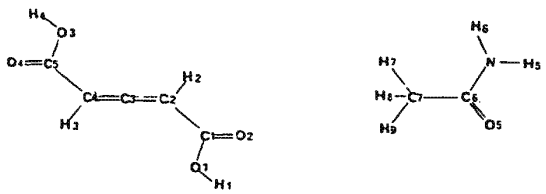
A low-temperature X-ray study of the molecular complex allenedicarboxylic acid–acetamide (1:1) was undertaken as part of a study on the electron density distribution in cumulenes, as well as in carboxyl and amide groups. The room-temperature structure of allenedicarboxylic acid–acetamide has been described (Nader, 1976). In this paper we confine ourselves to those features which were not previously discussed.

Experimental

A single crystal of the complex (1) was mounted on an Enraf–Nonius CAD-3 three-circle diffractometer linked to an IBM 1800 time-sharing computer. The crystal, which was sealed in a capillary of Lindemann glass, was cooled by a stream of cold air (van Bolhuis, 1971). The temperature of the crystal was estimated to be −150°C. The cell dimensions were derived by a least-squares procedure from high-order reflexions ($\theta > 20°$) measured with Mo $K\alpha$ radiation. The crystallographic data are given in Table 1. Details on the data collection and processing are given in Table 2. Weights were applied to the reflexion data in a similar manner to that described in the preceding paper (Berkovitch-Yellin & Leiserowitz, 1977).

Table 1. *Crystal data*

m.p.	103–105°C	β (°)	119·01 (3)
Space group	$C2/c$	V (Å^3)	1724·3
a (Å)	18·962 (4)	Z	8
b (Å)	4·798 (1)	D_c (g cm^{-3})	1·26
c (Å)	21·668 (5)	λ(Mo $K\alpha_1$) (Å)	0·70926



(1)

Table 2. *Intensity measurements and processing*

Diffractometer	Nonius CAD-3
Monochromatization	Graphite crystal
Radiation	Mo $K\alpha$
Minimum and maximum crystal dimensions (mm)	0·3, 0·4
Reciprocal lattice vector parallel to φ axis	$[\bar{1}11]$
Maximum θ angle (°)	50
Scanning mode	$\omega/2\theta$
Scan range (°) excluding the calculated α_1–α_2 separation	0·7
θ step for reflexion scan (°)	0·01
Step-scan time for intensity and background (s)	0·4, 0·2
Number of monitor reflexions	4
Monitor-reflexion interval	100
Number of unique reflexions measured in the range $\theta < 27°$	1904
Number of unique reflexions measured in the range $27 < \theta < \theta_{max}$ (percentage of the total in that range)	2490 (25%)
Number of reflexions measured	11175
Number of unique reflexions	4394
The match R'* between equivalent reflexions	5·5%
Number of reflexions with $F_o < 0$	295 (6·7%)
Number of reflexions with $F_o^2 < \sigma(F_o^2)$	1305 (29·7%)

* For definition of R', see preceding paper.

UM00012897
NOVARTIS EXHIBIT 1017
Novartis v. Regents, IPR2023-01346
Page 1643 of 4460

Refinement

The refinement was carried out in essentially three stages, details of which are presented in Table 3.

Stage a

The starting set of atomic parameters (Nader, 1976) were refined by full-matrix least-squares calculations with free-atom scattering factors. The heavy atoms were treated anisotropically, H isotropically.

Stage b

In order to reduce the number of refined parameters we treated the thermal motion of the allene skeleton (CH=C=CH) as that of a rigid body (Schomaker & Trueblood, 1968). The other heavy atoms were treated anisotropically, H isotropically.

Stage c

In this stage we introduced the deformation model (Hirshfeld, 1971; Harel & Hirshfeld, 1975) with modified scattering factors and contracted H atoms (ζ = 1·3) (Harel, 1974), and treated $F(000)$ as an observed quantity with a standard deviation of $F(000)/100$. The thermal parameters of the allene skeleton atoms were constrained by the rigid-body treatment, as in stage *b*.

In defining the deformation model, the molecule was assumed to comprise two identical HC—COOH fragments. This assumption led to sharing of identical deformation coefficients between equivalent atoms. The number of refined deformation parameters was further reduced by taking the carboxyl and amide groups to be symmetric to reflexion in the group plane. For O(2), O(4), O(5) and N a second mirror plane was assumed perpendicular to the first and intersecting in the appropriate C=O or C—N axis. The deformation density at C(3) was assumed to possess $\bar{4}$ symmetry and all the H atoms were assumed to be axially symmetric about their respective bond axes. These assumptions reduced the number of independent deformation parameters to 147. In addition to the various deformation coefficients, four Gaussian exponential parameters (Harel & Hirshfeld, 1975) were refined, one for each atomic type: C, N, O and H.

In the course of the refinement difficulties were encountered especially in the determination of the positional and thermal parameters of the H atoms. The difficulties in deriving accurate H atom parameters from X-ray intensities are well known and stem from the lack of core electrons which are especially sensitive to vibrational smearing. Following the suggestion of Hirshfeld (1976) we fixed the vibration parameters of the H atoms and the X—H lengths (X = C, N, O) on external evidence. The values of the vibration components were approximated by the stretching, bending and out-of-plane bending (torsion, rocking) frequencies obtained from spectroscopic studies of acetamide (Davies & Hallam, 1951) and *N*-methylacetamide (Szymanski, 1962). The X—H lengths of the methyl, amide and hydroxyl atoms were fixed at values obtained by neutron diffraction (Pryor & Sanger, 1970; Coppens, Sabine, Delaplane & Ibers, 1969).

Table 3. *Three-stage crystal structure refinement*

	(*a*)	(*b*)	(*c*)
Total number of parameters	154	142	265
Positional parameters	66	66	45
Thermal parameters	87	75	68
Deformation parameters	–	–	151
Number of reflexions used in the refinement	4356	4356	4393
Effective nuclear charge for H atoms	1·0	1·0	1·3
R_1 (omitting unobserved reflexions)	0·082	0·083	0·063
R_2 (all reflexions)	0·105	0·106	0·071
r*	0·148	0·149	0·118
Goodness of fit*	3·05	3·08	2·21

* For definition of r and goodness of fit see Table 3 in preceding paper.

Results

The final atomic coordinates are listed in Table 4, and observed bond lengths and angles in Table 5. Some

Table 4. *Fractional atomic coordinates and their e.s.d.'s* ($\times 10^4$ *for* C *and* $\times 10^3$ *for* H)

	x	y	z		x	y	z
C(1)	4041 (1)	1402 (3)	1227 (1)	C(2)	3974 (1)	597 (4)	1857 (1)
C(3)	3674 (1)	2232 (2)	2153 (1)	C(4)	3381 (1)	3810 (3)	2466 (1)
C(5)	3886 (1)	5853 (3)	3022 (1)	C(6)	1144 (1)	−1936 (3)	391 (1)
C(7)	1963 (1)	−3217 (4)	635 (1)	O(1)	3628 (1)	3596 (3)	888 (1)
O(2)	4461 (1)	31 (3)	1048 (0)	O(3)	4649 (1)	5878 (3)	3168 (1)
O(4)	3603 (1)	7388 (3)	3294 (1)	O(5)	918 (1)	129 (5)	11 (1)
N(1)	677 (1)	−3029 (2)	620 (1)	H(1)	380	423	49
H(2)	427 (2)	−171 (7)	212 (1)	H(3)	269 (2)	366 (3)	232 (1)
H(4)	497	757	354	H(5)	85	−464	95
H(6)	12	−230	47	H(7)	198	−530	85
H(8)	242	−187	104	H(9)	207	−339	18

UM00012898
NOVARTIS EXHIBIT 1017
Novartis v. Regents, IPR2023-01346
Page 1644 of 4460

Table 5. *Uncorrected bond lengths* (Å) *and bond angles* (°) *and their e.s.d.'s*

C(1)–C(2) 1·483 (2)	C(1)–O(1) 1·305 (2)	C(1)–O(2) 1·230 (2)
C(2)–C(3) 1·307 (2)	C(3)–C(4) 1·307 (2)	C(4)–C(5) 1·486 (2)
C(5)–O(3) 1·323 (3)	C(5)–O(4) 1·218 (2)	C(6)–N(1) 1·316 (3)
C(6)–O(5) 1·251 (2)	C(7)–C(6) 1·508 (1)	C(2)–H(2) 1·20 (2)
C(4)–H(3) 1·19 (2)	C(7)–H(7) 1·10	C(7)–H(8) 1·10
C(7)–H(9) 1·10	O(1)–H(1) 1·10	O(3)–H(4) 1·10
N(1)–H(5) 1·00	N(1)–H(6) 1·00	

C(2)–C(1)–O(1)	115·5 (2)	C(2)–C(1)–O(2)	120·5 (1)
O(1)–C(1)–O(2)	123·9 (2)	C(1)–C(2)–C(3)	123·3 (1)
C(1)–C(2)–H(2)	116·7 (10)	C(3)–C(2)–H(2)	120·0 (10)
C(2)–C(3)–C(4)	178·2 (1)	C(3)–C(4)–C(5)	122·2 (1)
C(3)–C(4)–H(3)	120·6 (8)	C(5)–C(4)–H(3)	117·2 (8)
C(4)–C(5)–O(3)	113·6 (1)	C(4)–C(5)–O(4)	121·9 (1)
O(3)–C(5)–O(4)	124·4 (1)	O(5)–C(6)–N(1)	120·8 (2)
H(7)–C(7)–H(8)	110·1 (1)	H(7)–C(7)–H(9)	110·1 (2)
H(8)–C(7)–H(9)	110·1 (2)	C(1)–O(1)–H(1)	111·7 (10)
C(5)–O(3)–H(4)	113·5 (10)	C(6)–N(1)–H(5)	122·1 (1)
C(6)–N(1)–H(6)	122·1 (1)	H(5)–N(1)–H(6)	115·7 (2)

short intermolecular contacts are given in Table 6. The deviations from the best planes of various parts of both molecules are given in Table 7.*

Discussion

Molecular shape

The carbon skeleton C–C=C=C–C adopts a conformation in keeping with allene systems; the angle between the planes of the two C–C=C moieties of the allene skeleton is 93·3°, compared with 90° in allene itself (Almenningen, Bastiansen & Trætteberg, 1959). The conformation of the two carboxyl groups with respect to their attached allene system is such that the two C=C–C=O groups are almost antiplanar. The torsion angles of C(3)=C(2)–C(1)=O(2) and C(3)=C(4)–C(5)=O(4) are 166·0 and 178·4° respectively. The significant deviation from antiplanarity of the former is probably due to H-bonding and is discussed later.

* Lists of structure factors and anisotropic thermal parameters have been deposited with the British Library Lending Division as Supplementary Publication No. SUP 32753 (14 pp.). Copies may be obtained through The Executive Secretary, International Union of Crystallography, 13 White Friars, Chester CH1 1NZ, England.

Table 6. *Intermolecular contacts* (Å)

See Table 9 in preceding paper for definition of five-digit code.

Symmetry operations

01	x,y,z	05	$\frac{1}{2}-x,\frac{1}{2}-y,-z$
02	$-x,y,\frac{1}{2}-z$	06	$x,-y,\frac{1}{2}+z$
03	$-x,-y,-z$	07	$\frac{1}{2}-x,\frac{1}{2}+y,\frac{1}{2}-z$
04	$\frac{1}{2}+x,\frac{1}{2}+y,z$	08	$\frac{1}{2}+x,\frac{1}{2}-y,\frac{1}{2}+z$

C(1)···H(4)	64502	2·58	C(1)···O(3)	65502	3·06
C(1)···O(5)	55505	3·15	C(1)···H(9)	54505	3·17
C(1)···O(3)	64502	3·43	C(2)···H(4)	65402	2·93
C(2)···O(3)	54501	3·36	C(2)···C(5)	54501	3·46
C(2)···O(3)	64502	3·48	C(2)···C(2)	65502	3·52
C(3)···C(5)	54501	3·51	C(3)···O(4)	54501	3·44
C(4)···O(4)	54507	3·36	C(4)···O(4)	54501	3·49
C(5)···O(2)	66502	3·43	C(5)···H(2)	56501	2·76
C(5)···H(5)	56507	2·96	C(5)···N(1)	55507	3·23
O(4)···N(1)	55507	3·32	C(6)···H(1)	55505	2·50
C(6)···H(6)	55503	3·01	C(6)···O(2)	54505	3·13
C(6)···O(4)	54507	3·37	C(6)···O(1)	55505	3·41
C(7)···H(1)	55505	2·96	C(7)···O(1)	54501	3·31
C(7)···O(2)	54505	3·43	O(1)···O(5)	55505	2·51
O(1)···H(4)	65502	2·94	O(1)···H(9)	56501	2·99
O(1)···O(3)	65502	3·09	O(1)···H(7)	56501	3·16
O(1)···H(9)	55505	3·19	O(1)···O(2)	56501	3·41
O(2)···H(6)	55504	2·51	O(2)···O(3)	64502	2·63
O(2)···H(5)	55504	2·75	O(2)···H(9)	54505	2·96
O(2)···N(1)	55504	3·02	O(2)···O(5)	55505	3·06
O(2)···O(3)	65502	3·29	O(2)···O(4)	64502	3·47
O(3)···H(2)	66502	2·82	O(3)···O(5)	55508	3·52
O(3)···H(6)	55507	3·13	O(3)···N(1)	55507	3·52
O(4)···H(5)	56507	2·03	O(4)···H(3)	55507	2·41
O(4)···H(7)	56507	2·90	O(4)···N(1)	56507	3·02
O(4)···N(1)	56507	3·02	O(4)···N(1)	55507	3·32
O(4)···O(5)	55507	3·55	O(5)···H(1)	55505	1·58
O(5)···H(6)	55503	2·02	O(5)···H(4)	45408	3·08
O(5)···H(7)	56501	3·10	O(5)···O(5)	55503	3·51
N(1)···N(1)	54503	3·27	N(1)···H(6)	54503	3·10
H(1)···H(6)	55504	2·75	H(1)···H(9)	55505	2·64
H(1)···H(9)	54505	3·18	H(1)···H(4)	65502	2·77
H(1)···H(8)	55505	3·18	H(2)···H(4)	64502	2·51
H(2)···H(2)	65502	2·66	H(2)···H(4)	54501	2·76
H(3)···H(3)	54507	2·89	H(3)···H(3)	55507	2·89
H(3)···H(7)	56501	2·91	H(4)···H(5)	56507	2·78

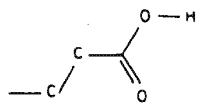
Table 7. *Deviations from best planes*

Group	Equation of the plane	$\left(\frac{\Sigma\Delta^2}{n-1}\right)^{1/2}$*
C(2)–C(1)(=O)–O	$-11{\cdot}0292x - 2{\cdot}7849y - 4{\cdot}6893z + 5{\cdot}4209 = 0$	0·002
C(5)–C(4)(=O)–O	$-2{\cdot}9531x - 3{\cdot}3026y + 15{\cdot}0634z - 1{\cdot}4610 = 0$	0·007
C(7)–C(6)(=O)–N	$-0{\cdot}2536x - 2{\cdot}9448y - 14{\cdot}8193z + 0{\cdot}0400 = 0$	0·003
Acetamide dimer	$-0{\cdot}0039x - 2{\cdot}9827y + 14{\cdot}8467z - 1{\cdot}4894 = 0$	0·018

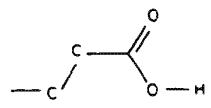
* $\Sigma\Delta^2$ is the sum of the squares of the deviations (Å) from the best plane of the n atoms forming the plane.

UM00012899
NOVARTIS EXHIBIT 1017
Novartis v. Regents, IPR2023-01346
Page 1645 of 4460

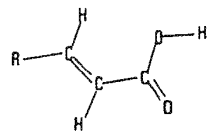
The conformational features of the carboxyl group, as well as of esters, have been analysed by a number of workers (*e.g.* Leiserowitz & Schmidt, 1965; Dunitz & Strickler, 1968; Einspahr & Donohue, 1973; Leiserowitz, 1976). In α,β-saturated carboxylic acids $R-CH_2-CH_2-CO_2H$ the synplanar $C^{\beta}-C^{\alpha}-C=O$ arrangement (2*a*) is adopted without any known exceptions. The synplanar rule does not apply to the α,β-unsaturated acids $R-CH=CH-CO_2H$; several molecules exhibit the antiplanar form (3).



(2*a*)

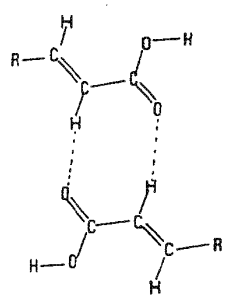


(2*b*)



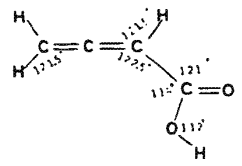
(3)

It was shown (Leiserowitz, 1976) that all those molecules which exist in the antiplanar form have similar packing environments about their carboxyl groups and that their antiplanar C=C–C=O conformations are probably induced by intermolecular forces. Specifically, these intermolecular forces comprise C–H···O(carbonyl) interactions, the motif of which is shown in (4).

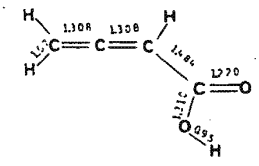


(4)

In contrast to $R-CH=CH-CO_2H$, allenedicarboxylic acid adopts the antiplanar conformation in both its own structure (Leiserowitz & Nader, 1973) and in its complex with acetamide. These results suggest that the preference for the antiplanar conformer is due to intramolecular forces. In order to corroborate this suggestion, we computed the energy difference between the two possible conformations in allenemonocarboxylic acid, $H_2-C=C=C-CO_2H$, by *ab initio* molecular orbital calculations with a STO-31G extended basis set and the *GAUSSIAN* 70 program (Hehre, Lathan, Ditchfield, Newton & Pople, 1970).

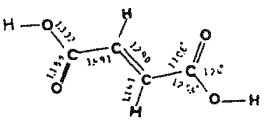


(5*a*)

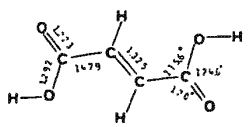


(5*b*)

The molecular geometry for the antiplanar conformation (5*a*,*b*) was taken from the crystal structure of allenedicarboxylic acid–acetamide averaging over the two independent carboxyl groups. This molecular geometry compares favourably with that observed in allenedicarboxylic acid itself (Leiserowitz & Nader, 1973). Regarding the angular geometry of the hypothetical synplanar form, the C–C–O angles do not necessarily remain constant upon change of conformation. Thus, the C–C–O angles, for the synplanar form (C–C–OH 109°, C–C=O 126·4°), were obtained from a comparison of the differences in the pertinent bond angles of fumaric acid ($HO_2C-CH=CH-CO_2H$), which is observed in the crystal phase in both synplanar (Gorres, McAfee & Jacobson, 1975) and antiplanar (Brown, 1966; Bednowitz & Post, 1966) forms with lengths and angles as shown in (6*a*) and (6*b*). Thus the C–C–OH and



(6*a*)



(6*b*)

C–C=O angles of the synplanar conformer used in the computation were 109·0 (*i.e.* 114·0 − 5·0°) and 126·4 (*i.e.* 121·0 + 5·4°) respectively. The resulting O–C=O angle is 126·6°. The antiplanar form was found to be more stable by an insignificant amount, 0·01 kcal mol^{-1}; in comparison a similar computation performed on acrylic acid, $H_2C=CHCO_2H$, incorporating bond lengths and angles as found in the syn- and antiplanar forms of fumaric acid, yielded a more stable synplanar conformer by a significant amount, 0·5 kcal mol^{-1}. The latter result is in accordance with the observation that the synplanar C=C–C=O conformer is preferred in the α,β-unsaturated carboxylic acids R–CH=CH–CO_2H (Leiserowitz, 1976). As a further test of the energy difference between the syn- and antiplanar

UM00012900
NOVARTIS EXHIBIT 1017
Novartis v. Regents, IPR2023-01346
Page 1646 of 4460

forms of allenemonocarboxylic acid, the molecular energies were computed varying the C–C–O and C–C=O angles and keeping the O–C=O angle fixed at the derived value of 124·6° for the synplanar form, and at the observed value of 125·0° for the antiplanar form. The stable conformers were obtained at C–C–OH and C–C=O angles of 110·5 and 124·9° for the synplanar form, and 113·5 and 121·5° for the antiplanar form. These angles do not differ appreciably from the observed values of the antiplanar form, and from the derived values of the synplanar form. However, a reversal in conformational stability was obtained; the synplanar form was found to be more stable by 0·1 kcal mol^{-1}. This value is appreciably less than the 0·5 kcal mol^{-1} difference computed for acrylic acid. Although this computation does not prove that the observed preference for the antiplanar conformer is due to intramolecular forces, it does demonstrate that the energy difference between the two conformers of allenemonocarboxylic acid is small.

Deviations from planes involving carboxyl groups are insignificant for the C, O and N atoms (Table 7). In carboxyl group C–C–O(1)O(2) the hydroxyl H atom lies 0·13 Å from the best plane through the carboxyl group. This O–H forms a short O–H···$OCNH_2$ contact in which the O acceptor atom lies 0·44 Å from the best plane of the carboxyl group (Table 7) to which it is H-bonded (Fig. 1). Therefore it appears that the O–H bond is turned out of the plane of its carboxyl group to form a more linear O–H···O bond. In a similar manner the hydroxyl H(4) deviates 0·08 Å from the best plane of its carboxyl group C–C–O(3)O(4) so as to make a more linear O–H···O(2) bond with the O(2) acceptor which lies 0·45 Å from the plane.

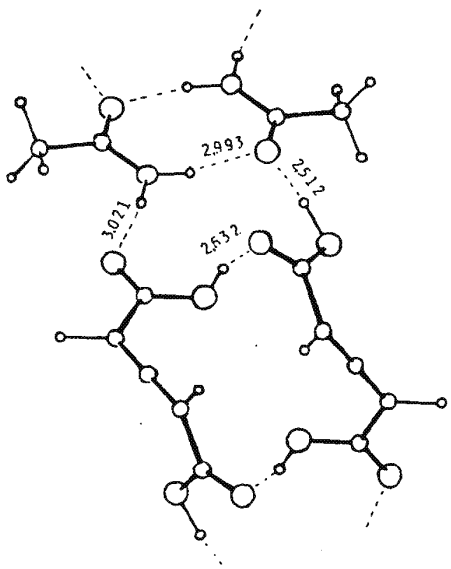


Fig. 1. The H-bonding motif in allenedicarboxylic acid–acetamide.

The heavy-atom skeleton of the amide system is planar (Table 7); the amide H atoms deviate from this plane on the average by 0·006 Å.

The methyl group adopts a conformation such that the torsion angle H(8)–C(7)–C(6)–N is 12·4°. This conformation in which H–C–C–N is almost synplanar, seems to be preferred in acetamides CH_3–C(O)–NH–*R* (Hagler, Leiserowitz & Tuval, 1976).

Packing arrangement and molecular dimensions

The packing is dictated by H bonds involving the carboxyl and amide groups (Nader, 1976). The H-bond parameters of the low-temperature structure are shown in Fig. 1.

A comparison of the two chemically equivalent moieties C=C–CO_2H leads to scatters of 0·007 Å and 0·75° in bond lengths and angles. These appear to be significantly higher than the average estimated standard deviations (0·002 Å and 0·15°) determined from the least-squares analysis. The difference in bond lengths and angles between the two 'chemically equivalent' moieties of C=C CO_2H resides mainly in the carboxyl group; comparing only the C=C–C bonds of the two moieties we obtain scatters of 0·002 Å and 0·5° which compare more favourably with the least-squares result. The question then arises whether the differences in bond lengths of the two carboxyl groups are significant and may be associated with their different H-bonding arrangements.

It is obvious from Fig. 1 that the H-bond contacts of the two carboxyl groups differ significantly. The moot point is to what extent do these differences affect the C=O and C–O(H) lengths of the two carboxyl groups. A similar H-bonding motif to Fig. 1 is found in oxalic acid–acetamide (Leiserowitz & Nader, 1972), shown in Fig. 2, which also displays bond lengths and H-bond distances. This structure, which was measured at room temperature, does not exhibit any significant differences in bond length between the two carboxyl groups which are differently H-bonded. It is also noteworthy that no significant differences were observed in the room-temperature structure of allenedicarboxylic acid–acetamide (Nader, 1976). Consequently, it remains an open question whether the differences in bond lengths between the two carboxyl groups in the low-temperature structure of allenedicarboxylic acid–acetamide are significant and are associated with differences in H-bonding. It is probable that the bond lengths obtained from the low-temperature structure are more reliable, primarily because of the far greater number of reflexions measured (4393, d^*_{max} = 2·158 *vs* 2137, d^*_{max} = 1·324). Moreover, non-spherical electron density distributions were taken into account in the low-temperature study, in contrast to the room-

UM00012901
NOVARTIS EXHIBIT 1017
Novartis v. Regents, IPR2023-01346
Page 1647 of 4460

temperature studies of both allenedicarboxylic acid–acetamide and oxalic acid–acetamide. The effect of H-bonding on the bond lengths of some carboxylic acids and acetamides was summarized by Beagley (1975); there is a pronounced shortening of 0·04 Å of the carboxyl C—OH length on formation of a H-bond. In the allenedicarboxylic acid complex the C—OH bond which participates in the very short $OH\cdots OCNH_2$ bond of 2·51 Å is 0·018 Å shorter than the C—OH bond whose O—H group participates in a relatively longer $OH\cdots OCOH$ bond of 2·63 Å.

The C=O length of the amide group (1·250 Å) is longer than that of the carboxyl groups (1·217, 1·230 Å). This is significant, for similar differences have been observed in a number of other crystal structures containing both functional groups (*e.g.* Huang, Leiserowitz & Schmidt, 1973; Benghiat, Kaufman, Leiserowitz & Schmidt, 1972).

Charge deformation maps

Electron density difference maps were obtained by plotting the sum of the deformation functions around each atom with coefficients determined by the least-squares refinement (Hirshfeld, 1971; Harel & Hirshfeld, 1975). The deformation maps show accumulation of charge between bonded atoms and distinct electron density maxima at sites predicted on the basis of sp^2 hybridization of the O atoms of allenedicarboxylic acid–acetamide, namely, at lone pairs around the O atoms. The atomic centres are in troughs of negative density indicating migration of charge from the close vicinity of the atoms to the bonds and lone pairs, owing to the formation of a molecule. The H atoms, forming one bond peak, but also contracted owing to the formation of an X—H bond, show a dipolar pattern of angular polarization superimposed on pronounced radial contraction.

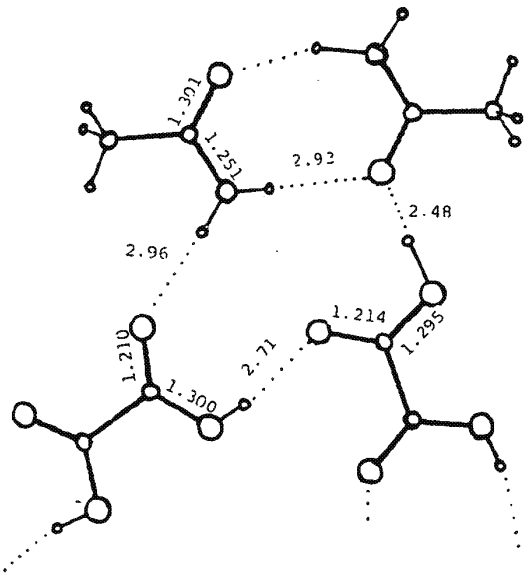


Fig. 2. The H-bonding motif in oxalic acid–acetamide (Leiserowitz & Nader, 1972).

The difference density in the plane of the allene system is shown in Fig. 3. A comparison between the electron density distributions in the two adjacent C=C bonds of the allene system indicates that the charge density in the >C=C bond extends more along the direction perpendicular to the plane of >C=C than along its in-plane direction. This electron density distribution implies that the charge densities in adjacent double bonds are mutually perpendicular, a feature displayed most convincingly in the structure of tetraphenylbutatriene (Berkovitch-Yellin & Leiserowitz, 1977).

The electron density distribution of the carboxyl group exhibits many features observed in other electron density studies, both theoretical (Hagler & Lapiccirella, 1976) and experimental (Coppens, Sabine, Delaplane & Ibers, 1969; Hecht & Hirshfeld, 1976; Griffin & Coppens, 1975). However, on close comparison there are several features which do not match well. Therefore we tend to the view that only gross features of the electron density distributions in the carboxyl and amide groups should be regarded as significant.

The section through the plane of the H-bonded acetamide dimer (Fig. 4) displays the following important features; it contains maxima (L) lying ~0·6 Å from the O atom where the angle L—O=C ≃ 100°. These maxima, commonly designated as the lone-pair electrons, lie approximately along the line of the X—H···O bonds. A section (Fig. 5) perpendicular to the plane of the amide system and passing through the two maxima of the lone-pair electrons of the amide O atom does not display two distinct lone-pair lobes. Rather, the distribution appears to be almost cylindrical in shape.

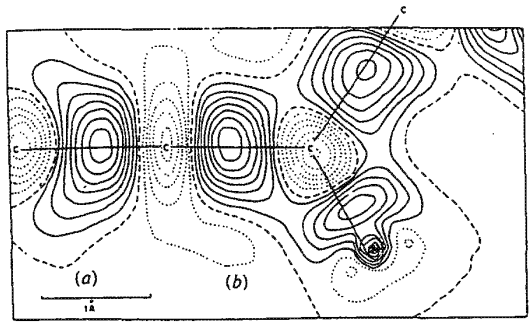


Fig. 3. Deformation density in the allene system (C=C=C<). Peaks (*a*) and (*b*) are two perpendicular sections of the deformation density in the allene C=C bond. (*a*) is perpendicular to and (*b*) is in the plane of C=C<. Contour interval 0·1 eÅ $^{-3}$. Zero contours broken, negative contours dotted.

UM00012902
NOVARTIS EXHIBIT 1017
Novartis v. Regents, IPR2023-01346
Page 1648 of 4460

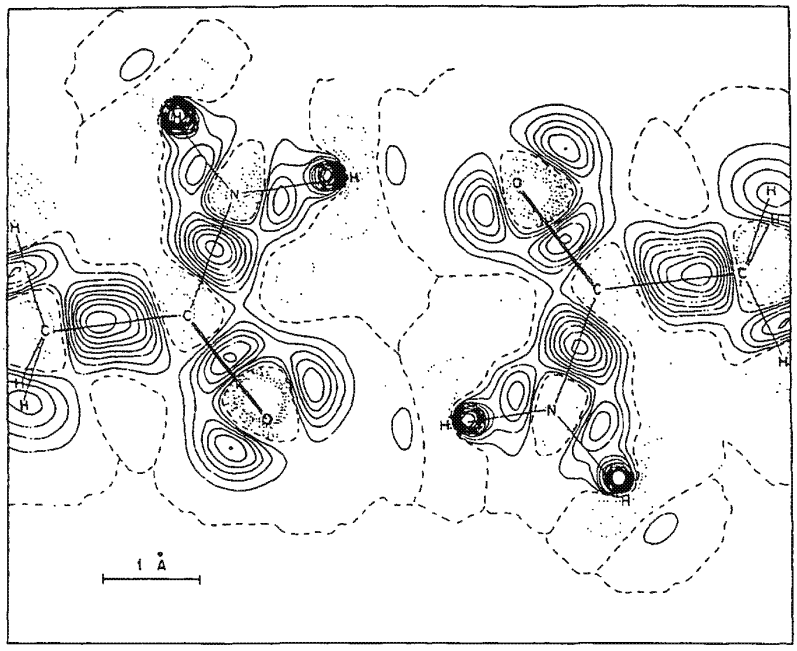
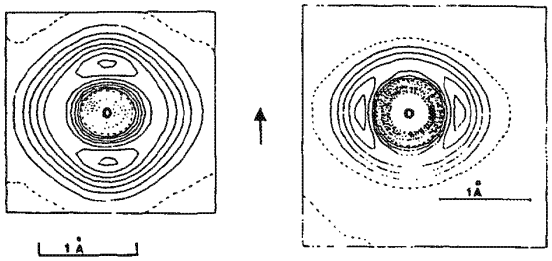


Fig. 4. Deformation density section through the plane of a H-bonded acetamide dimer. Contours as in Fig. 3.

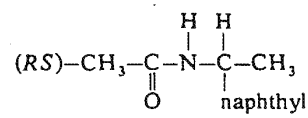


(a) (b)

Fig. 5. Deformation density sections perpendicular to (*a*) the amide group and (*b*) the carboxyl group through the lone-pair maxima. The arrow indicates the direction perpendicular to (*a*) the amide group and (*b*) the carboxyl group.

The section through the plane of the carboxyl group (Fig. 6) displays an electron density distribution about the carbonyl O atom which is similar to that of the amide O atom. The density distribution of the lone-pair lobes of the carbonyl O atom of the carboxyl group differs somewhat from that of the amide O atom. The section through the lone-pair maxima perpendicular to the plane of the carboxyl group (Fig. 5) shows that the lone-pair maxima lie in the plane of the carbonyl system. This is in contrast to what is found in the amide system. Whether this is a significant difference between the amide and the carboxyl atoms is open to question.

In this context it is noteworthy that there are other distinct differences between the amide and carboxyl C=O bonds: in bond length (amide: 1·25 Å, acid: 1·22 Å), in the average lengths of the single O–H···OCNH and O–H···OCOH bonds (amide: 2·50 Å, acid: 2·64 Å) (Leiserowitz & Nader, 1977) and in IR stretching frequencies (amide: 1650–1620 cm^{-1}, acid: 1725–1690 cm^{-1}). There also appear to be differences in the H-bonding acceptor properties of both O atoms; while the carbonyl O atom of the carboxyl group almost invariably forms H-bonds in which the *X*–H bond lies in the plane of the carbonyl system $>C=O$ to which it is H-bonded (Leiserowitz, 1976), there are several amide crystal structures in which the N–H bond is directed towards the carbonyl O atom of the molecule to which it is H-bonded from well above the plane of the carbonyl system $>C=O$. These include *N*-methyl-propiolamide, $H–C\equiv C–CONHCH_3$ (Leiserowitz & Tuval, 1977),



(Leiserowitz & Weinstein, 1976) and particularly urea (Caron & Donohue, 1969). This may imply more-localized lone-pair density peaks lying in the plane of the carbonyl system in acids, than in amides.

UM00012903
NOVARTIS EXHIBIT 1017
Novartis v. Regents, IPR2023-01346
Page 1649 of 4460

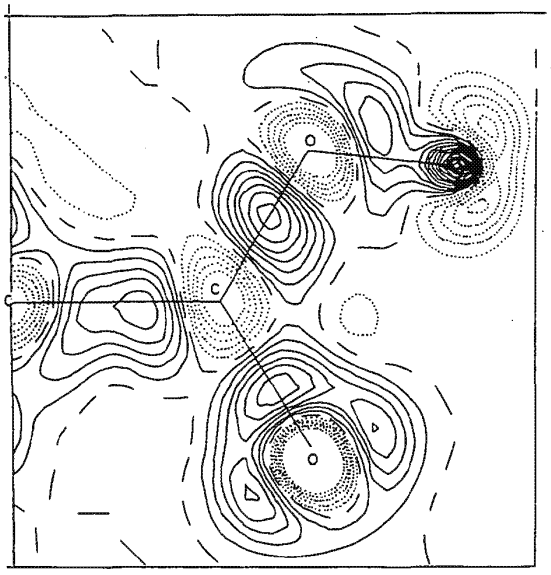


Fig. 6. Section through the plane of the carboxyl group. Contours as in Fig. 3.

The deformation density near the hydroxyl O atom (Fig. 6) seems to be at fault. In oxalic acid dihydrate (Coppens *et al.*, 1969), in a bicyclobutanedicarboxylic acid derivative (Hecht & Hirshfeld, 1976) and in a theoretical difference density map of acetic acid (Hagler & Lapiccirella, 1976) the lone-pair peak of the hydroxyl O atom is located almost on the bisector of the C–O–H bond at the back of the hydroxyl O atom and in the plane of the carboxyl group. In the carboxyl group (Fig. 6) the deformation density around the hydroxyl O atom is not resolved into a lone-pair lobe and an O–H bonding density peak but appears as one merged peak.

We thank Professor F. L. Hirshfeld for his interest and help and Mrs K. Reich for her assistance. Partial support by a MINERVA grant is acknowledged.

References

ALMENNINGEN, A., BASTIANSEN, O. & TRÆTTEBERG, M. (1959). *Acta Chem. Scand.* **13**, 1699–1702.

BEAGLEY, B. (1975). *Molecular Structure by Diffraction Methods*, Vol. 3, p. 66. Chem. Soc. Spec. Rep. London: The Chemical Society.

BEDNOWITZ, A. L. & POST, B. (1966). *Acta Cryst.* **21**, 566–571.

BENGHIAT, V., KAUFMAN, H. W., LEISEROWITZ, L. & SCHMIDT, G. M. J. (1972). *J. Chem. Soc. Perkin* II, pp. 1758–1763.

BERKOVITCH-YELLIN, Z. & LEISEROWITZ, L. (1977). *Acta Cryst.* B**33**, 3657–3669.

BOLHUIS, F. VAN (1971). *J. Appl. Cryst.* **4**, 263–264.

BROWN, C. J. (1966). *Acta Cryst.* **21**, 1–5.

CARON, A. & DONOHUE, J. (1969). *Acta Cryst.* B25, 404.

COPPENS, P., SABINE, T. M., DELAPLANE, R. G. & IBERS, J. A. (1969). *Acta Cryst.* B25, 2451–2458.

DAVIES, M. & HALLAM, H. E. (1951). *Trans. Faraday Soc.* **47**, 1170–1181.

DUNITZ, J. D. & STRICKLER, P. (1968). *Structural Chemistry and Molecular Biology*, edited by A. RICH and N. DAVIDSON, pp. 443–465. San Francisco: Freeman.

EINSPAHR, H. & DONOHUE, J. (1973). *Acta Cryst.* B29, 1875–1880.

GORRES, B., MCAFEE, E. A. & JACOBSON, R. A. (1975). *Acta Cryst.* B**31**, 158–161.

GRIFFIN, J. F. & COPPENS, P. (1975). *J. Amer. Chem. Soc.* **97**, 3496–3505.

HAGLER, A. T. & LAPICCIRELLA, A. (1976). *Biopolymers*, **15**, 1167–1200.

HAGLER, A. T., LEISEROWITZ, L. & TUVAL, M. (1976). *J. Amer. Chem. Soc.* **98**, 4600–4611.

HAREL, M. (1974). PhD Thesis, Weizmann Institute of Science, Rehovot, Israel.

HAREL, M. & HIRSHFELD, F. L. (1975). *Acta Cryst.* B**31**, 162–172.

HECHT, M. & HIRSHFELD, F. L. (1976). Private communication.

HEHRE, W. J., LATHAN, W. A., DITCHFIELD, R., NEWTON, M. W. & POPLE, J. A. (1970). Quantum Chemistry Program Exchange, Indiana Univ., Bloomington, Indiana, Program No. 236.

HIRSHFELD, F. L. (1971). *Acta Cryst.* B27, 769–781.

HIRSHFELD, F. L. (1976). *Acta Cryst.* B32, 239–244.

HUANG, C. M., LEISEROWITZ, L. & SCHMIDT, G. M. J. (1973). *J. Chem. Soc. Perkin* II, pp. 503–508.

LEISEROWITZ, L. (1976). *Acta Cryst.* B32, 775–802.

LEISEROWITZ, L. & NADER, F. (1972). *Angew. Chem. Int. Ed.* **11**, 514–515.

LEISEROWITZ, L. & NADER, F. (1973). *Angew. Chem. Int. Ed.* **12**, 158–159.

LEISEROWITZ, L. & NADER, F. (1977). *Acta Cryst.* B33, 2719–2733.

LEISEROWITZ, L. & SCHMIDT, G. M. J. (1965). *Acta Cryst.* **18**, 1058–1067.

LEISEROWITZ, L. & TUVAL, M. (1977). *Acta Cryst.* Submitted for publication.

LEISEROWITZ, L. & WEINSTEIN, S. (1976). Unpublished results.

NADER, F. W. (1976). *Liebigs Ann.* Submitted for publication.

PRYOR, A. W. & SANGER, P. L. (1970). *Acta Cryst.* A**26**, 543–558.

SCHOMAKER, V. & TRUEBLOOD, K. N. (1968). *Acta Cryst.* B**24**, 63–76.

SZYMANSKI, H. A. (1962). *Progress in IR Spectroscopy*, p. 8. New York: Plenum.

UM00012904
NOVARTIS EXHIBIT 1017
Novartis v. Regents, IPR2023-01346
Page 1650 of 4460

Acta Cryst. (1984). B40, 159–165

The Role Played by C–H···O and C–H···N Interactions in Determining Molecular Packing and Conformation

BY Z. BERKOVITCH-YELLIN AND L. LEISEROWITZ

Department of Structural Chemistry, The Weizmann Institute of Science, Rehovot 76100, Israel

(*Received* 6 *June* 1983; *accepted* 10 *October* 1983)

Abstract

The role played by C–H···O and C–H···N interactions in determining molecular packing and conformation is examined in terms of packing and atom–atom potential-energy calculations for a variety of representative molecular crystals. The Coulomb and van der Waals energy contributions of $C(sp^3)$–H···O, $C(sp^2)$–H···O and $C(sp)$–H···O interactions in various crystal structures have been analysed. C–H···O,N contacts are instrumental in fixing packing motifs in *N*-methylpropiolamide, substituted quinones, quinone–phenol complexes, α-glycine, pyrazinecarboxamide, uracil, α,β-unsaturated carboxylic acids R–CH=CH–CO_2H, barbital–acetamide complex, and ketones. The uncommon antiplanar C=C–C=O conformer in R–CH=CH–CO_2H is stabilized through C–H···O interactions.

1. Introduction

C–H···O interactions have long been a subject of controversy. Conclusive crystallographic and spectroscopic evidence for C–H···*A* interactions exist where *A* is a strong proton acceptor and the C–H forms part of a haloform molecule or hydrogen cyanide or acetylene derivatives (Sim, 1967). The existence of C–H···O hydrogen bonds had been claimed by a number of workers, notably Sutor (1963), on the basis of short C to O distances of approximately 3·2 Å. Donohue (1968) summarized the evidence in the solid state, for C–H groups which do not appear to be under the influence of activating groups which tend to promote ionization of the H atom. He challenged the existence of such C–H···O bonds, arguing that an O···H distance of 2·4 Å is not presumptive evidence of hydrogen-bond formation and doubted whether many of the short C–H···O distances (H···O 2·2 Å) can be regarded as hydrogen bonds in the same sense that the term is used for O–H···O, N–H···O and N–H···N systems. Recently crystallographic evidence for the existence of C–H···O and C–H···N hydrogen bonds was provided by Taylor & Kennard (1982). By a statistical analysis of 113 neutron diffraction crystal structures, they found that H atoms covalently bound to C have a statistically significant preference to form intermolecular contacts to O atoms rather than to C or H atoms.

We shall try to establish other criteria for the role played by the C–H···O interaction in formation of the crystal structure, such as whether the motif involving the C–H···O contact repeats itself in a number of different structures and whether the molecule in question could not have adopted a more favourable arrangement or conformation, but for the C–H···O contact. Our analysis is not a statistical overview but a focusing on a variety of representative crystal structures and motifs, incorporating the proton donors $C(sp)$–H, $C(sp^2)$–H and $C(sp^3)$–H. Our approach will be quantitative, using atom–atom potential-energy calculations. The contributions of the Coulomb (*i.e.* electrostatic) and van der Waals energies were compared for a variety of observed and hypothetical motifs. The electrostatic parameters which were used for the calculations of the Coulomb energies were derived from experimental deformation densities obtained from low-temperature X-ray diffraction data. These include atomic net charges, dipole and quadrupole moments placed at the atomic positions. Details of the method are described elsewhere (Berkovitch-Yellin & Leiserowitz, 1980, 1982).

2. Comparison of ≡C–H···O(carboxyl), ≡C–H···O(amide) and ≡C–H···C≡C interactions

The acetylenic ≡C–H···O bond has been well established from crystal structure and spectroscopic data. The crystal structure of *N*-methylpropiolamide (Leiserowitz & Tuval, 1978) is an example in which the molecules are so arranged that the O(amide) participates in both N–H···O and C–H···O hydrogen bonds (Fig. 1). In this crystal the C–H···O distance is 3·2 Å, the C–H···O system is linear, the C–O···H angle is 123° and the C–H bond is almost coplanar with the carbonyl system >C=O. In contradistinction, propiolic acid (L. Leiserowitz & I. Olovsson, unpublished results) does not incorporate an analogous motif (Fig. 2); the crystal structure shows hydrogen-bonded dimers interlinked by a C–H···C≡C(midpoint) contact of 3·8 Å (H···C≡C 2·8 Å) and a nonlinear C–H···O(carbonyl) contact of 3·3 Å (H···O 2·8 Å).

0108-7681/84/020159-07$01.50

© 1984 International Union of Crystallography

UM00012905
NOVARTIS EXHIBIT 1017
Novartis v. Regents, IPR2023-01346
Page 1651 of 4460

It appears that the carbonyl O atom and the C≡C triple bond compete for the C–H proton in the crystal structures of propiolic acid and *N*-methylpropiolamide. It is well established that the amide O atom is a far stronger proton acceptor than the corresponding O atom of the carboxyl group. This fact has been demonstrated in the solid, by packing systematics (Leiserowitz & Nader, 1977), electron density mapping (Berkovitch-Yellin, Leiserowitz & Nader, 1977), and atom–atom potential-energy calculations (Berkovitch-Yellin & Leiserowitz, 1982; Berkovitch-Yellin, Ariel & Leiserowitz, 1983). On these premises the distinct difference in C–H···O and C–H···C≡C contacts between *N*-methylpropiolamide and propiolic acid may be attributed to the relative proton-acceptor properties of the O(amide) and O(carboxyl) atoms and the C≡C bond. From a correlation curve relating the amount of bonding charge and bond length (Berkovitch-Yellin & Leiserowitz, 1977), it was deduced that the excess charge in the C≡C bond is approximately 0·4e, which is larger than the net atomic charge of −0·22e on the carbonyl O atom of the carboxyl group (Berkovitch-Yellin & Leiserowitz, 1982) but comparable to the net atomic charge of −0·38e on the amide O atom (Berkovitch-Yellin & Leiserowitz, 1980).

In order to account for the observed C–H···O and C–H···C≡C contacts in the crystal structures of propiolic acid and in *N*-methylpropiolamide, we mapped the electrostatic potential energy around these molecules by placing a positive unit charge at the locus of the points shown in Fig. 3(*a*). These points represent the nearest approach distances of the acetylenic proton donor to the reference molecule. The potential for propiolic acid (Fig. 3*b*) demonstrates comparable energies for C–H···C≡C(midpoint), and C–H···O interactions, whereas in *N*-methylpropiolamide there is a distinct preference for the C–H···O interaction. These results are completely in agreement with experiment.

3. The C(sp^2)–H···O interaction

3.1. *Quinones*

There are common geometric patterns in several quinone packing arrangements which have been interpreted in terms of C–H···O=C interactions (Bernstein, Cohen & Leiserowitz, 1974). These structures incorporate the motif shown in (1). The C–H···O

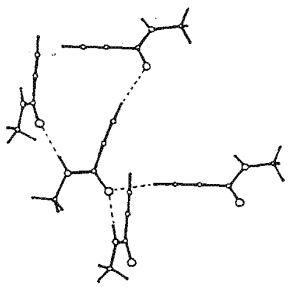


Fig. 1. Arrangement of N–H···O and C–H···O hydrogen bonds in *N*-methylpropiolamide.

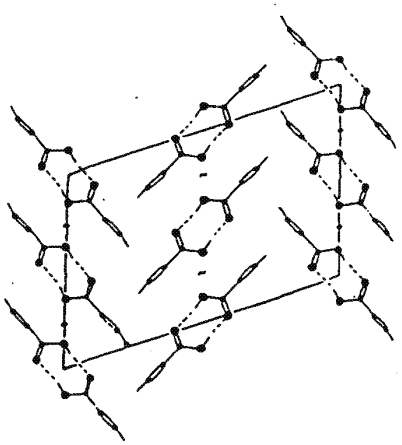
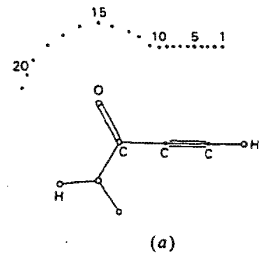
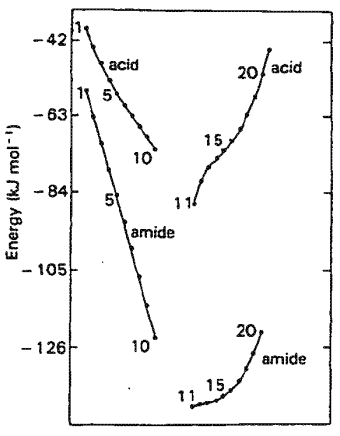


Fig. 2. Propiolic acid. Packing arrangement.



(*a*)



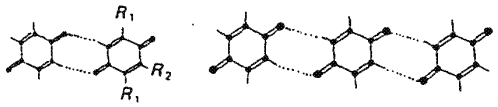
(*b*)

Fig. 3. (*a*) Discrete points of closest approach of proton donor to *N*-methylpropiolamide and propiolic acid. (*b*) Electrostatic potential energy (kJ mol^{-1}) at the discrete points of (*a*).

UM00012906
NOVARTIS EXHIBIT 1017
Novartis v. Regents, IPR2023-01346
Page 1652 of 4460

and H···O distances are about 3·5 and 2·5 Å respectively.

In 1,4-benzoquinone (Trotter, 1960) each molecule participates in several C–H···O contacts (Fig. 4), forming a layer structure. Within each layer neighbouring molecules, related by translation along the 6·7 Å axis, are connected by C–H···O contacts of 3·5 Å, as in (1), generating a coplanar ribbon (2). Adjacent ribbons, related by twofold screw axes, are interconnected by C–H···O contacts of 3·38 Å in a triangular pattern linking each molecule of one ribbon to two molecules of the adjacent ribbon.



(1) (2)

A strong argument for the role played by C–H···O interactions in determining this layer structure and other layer structures involving benzoquinone molecules is provided by the molecular arrangements in the 1:1 complex between thymine and 1,4-benzoquinone (Sakurai & Okunuki, 1971), in the quinhydrone complex (Sakurai, 1965), in the 1:1 complex of benzoquinone with chlorophenol (Shipley & Wallwork, 1967) and by the observation that tetrafluoro-*p*-benzoquinone (Meresse, Courseille & Chanh, 1974) does not form a layer structure as in 1,4-benzoquinone. The first-mentioned crystal structure contains alternating thymine and benzoquinone layers. The benzoquinone sheet structure in the thymine complex is practically identical with that in the pure benzoquinone crystal structure. Since a sheet of benzoquinone molecules has completely different environments in these two crystal structures, the layer motif must be determined by intralayer, and not interlayer, forces. The quinhydrone complex (Fig. 5) contains alternating ribbons of benzoquinone and of hydroquinone molecules stabilized by C–H···O(carbonyl) and C–H···O(hydroxyl) interactions respectively. The 1:1 complex of benzoquinone and *p*-chlorophenol (Fig. 6) displays C–H···O(carbonyl) contacts in the ribbon motif (2).

In order to verify the role played by C–H···O interactions in stabilizing motifs (1) and (2) and in determining the layer structures of the 1,4-benzoquinones cited above, we calculated the energy of the coplanar dimer (1) (with $R_1 = R_2 = H$) as a function of molecular displacement along *L* and *M* (Fig. 7*a*). The energy map (Fig. 7*b*) displays a minimum corresponding to a dimer arrangement (Fig. 7*a*) similar to that observed in the (substituted) benzoquinone crystal structures which explains the occurrence of (1) for 1,4-benzoquinone and substituted benzoquinones and of the ribbon (2) for 1,4-benzoquinone. Further, we examined the variation in energy of the 1,4-benzoquinone layer (Fig. 4) as a function of the offset along *L* between adjacent ribbons (2) related originally by twofold screw symmetry (Fig. 8). It is evident that the observed structure corresponds to the energy minimum, where electrostatic forces play the dominant role. We have also calculated the variation in energy as a function of offset between adjacent ribbons (2) related by translation (Fig. 9). The energy minimum corresponds to a layer arrangement (Fig. 9*b*) in which the interribbon offset provides for a C–H···O interaction; the major contribution to the energy is again electrostatic. The minimum in energy of this layer (Fig. 9*a*) is comparable to that of the observed layer of benzoquinone (Fig. 8), suggesting that interlayer and not intralayer forces play the deciding role in determining the observed layer structure. It is noteworthy that an arrangement similar to this hypothetical layer, in which the ribbons are related by translation, occurs in the crystal structure of the 1:1 complex of benzoquinone with *p*-chlorophenol (Fig. 6).

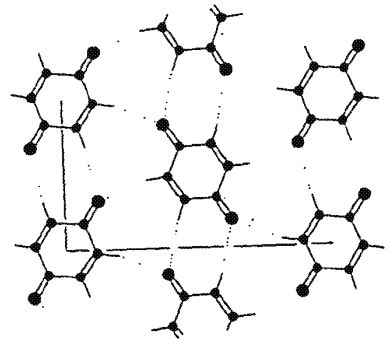


Fig. 4. Benzoquinone. Layer structure. The C–H···O contacts are marked.

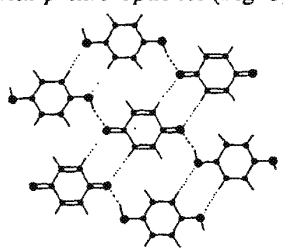


Fig. 5. Triclinic quinhydrone layer structure. C–H···O(carbonyl), C–H···O(hydroxyl) and O–H···O contacts are shown.

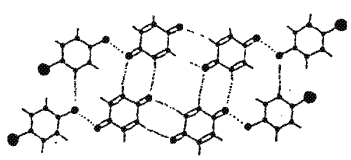


Fig. 6. The complex *p*-chlorophenol: 1,4-benzoquinone layer structure. C–H···O(carbonyl), C–H···O(hydroxyl) and O–H···O contacts are shown.

UM00012907

NOVARTIS EXHIBIT 1017
Novartis v. Regents, IPR2023-01346
Page 1653 of 4460

Acta Cryst. (1984). B40, 159–165

The Role Played by C–H···O and C–H···N Interactions in Determining Molecular Packing and Conformation

BY Z. BERKOVITCH-YELLIN AND L. LEISEROWITZ

Department of Structural Chemistry, The Weizmann Institute of Science, Rehovot 76100, Israel

(*Received* 6 *June* 1983; *accepted* 10 *October* 1983)

Abstract

The role played by C–H···O and C–H···N interactions in determining molecular packing and conformation is examined in terms of packing and atom–atom potential-energy calculations for a variety of representative molecular crystals. The Coulomb and van der Waals energy contributions of $C(sp^3)$–H···O, $C(sp^2)$–H···O and C(*sp*)–H···O interactions in various crystal structures have been analysed. C–H···O,N contacts are instrumental in fixing packing motifs in *N*-methylpropiolamide, substituted quinones, quinone–phenol complexes, α-glycine, pyrazinecarboxamide, uracil, α,β-unsaturated carboxylic acids R–CH=CH–CO_2H, barbital–acetamide complex, and ketones. The uncommon antiplanar C=C–C=O conformer in R–CH=CH–CO_2H is stabilized through C–H···O interactions.

1. Introduction

C–H···O interactions have long been a subject of controversy. Conclusive crystallographic and spectroscopic evidence for C–H···*A* interactions exist where *A* is a strong proton acceptor and the C–H forms part of a haloform molecule or hydrogen cyanide or acetylene derivatives (Sim, 1967). The existence of C–H···O hydrogen bonds had been claimed by a number of workers, notably Sutor (1963), on the basis of short C to O distances of approximately 3·2 Å. Donohue (1968) summarized the evidence in the solid state, for C–H groups which do not appear to be under the influence of activating groups which tend to promote ionization of the H atom. He challenged the existence of such C–H···O bonds, arguing that an O···H distance of 2·4 Å is not presumptive evidence of hydrogen-bond formation and doubted whether many of the short C–H···O distances (H···O 2·2 Å) can be regarded as hydrogen bonds in the same sense that the term is used for O–H···O, N–H···O and N–H···N systems. Recently crystallographic evidence for the existence of C–H···O and C–H···N hydrogen bonds was provided by Taylor & Kennard (1982). By a statistical analysis of 113 neutron diffraction crystal structures, they found that H atoms covalently bound to C have a statistically significant preference to form intermolecular contacts to O atoms rather than to C or H atoms.

We shall try to establish other criteria for the role played by the C–H···O interaction in formation of the crystal structure, such as whether the motif involving the C–H···O contact repeats itself in a number of different structures and whether the molecule in question could not have adopted a more favourable arrangement or conformation, but for the C–H···O contact. Our analysis is not a statistical overview but a focusing on a variety of representative crystal structures and motifs, incorporating the proton donors C(*sp*)–H, $C(sp^2)$–H and $C(sp^3)$–H. Our approach will be quantitative, using atom–atom potential-energy calculations. The contributions of the Coulomb (*i.e.* electrostatic) and van der Waals energies were compared for a variety of observed and hypothetical motifs. The electrostatic parameters which were used for the calculations of the Coulomb energies were derived from experimental deformation densities obtained from low-temperature X-ray diffraction data. These include atomic net charges, dipole and quadrupole moments placed at the atomic positions. Details of the method are described elsewhere (Berkovitch-Yellin & Leiserowitz, 1980, 1982).

2. Comparison of ≡C–H···O(carboxyl), ≡C–H···O(amide) and ≡C–H···C≡C interactions

The acetylenic ≡C–H···O bond has been well established from crystal structure and spectroscopic data. The crystal structure of *N*-methylpropiolamide (Leiserowitz & Tuval, 1978) is an example in which the molecules are so arranged that the O(amide) participates in both N–H···O and C–H···O hydrogen bonds (Fig. 1). In this crystal the C–H···O distance is 3·2 Å, the C–H···O system is linear, the C–O···H angle is 123° and the C–H bond is almost coplanar with the carbonyl system >C=O. In contradistinction, propiolic acid (L. Leiserowitz & I. Olovsson, unpublished results) does not incorporate an analogous motif (Fig. 2); the crystal structure shows hydrogen-bonded dimers interlinked by a C–H···C≡C(midpoint) contact of 3·8 Å (H···C≡C 2·8 Å) and a nonlinear C–H···O(carbonyl) contact of 3·3 Å (H···O 2·8 Å).

0108-7681/84/020159-07$01.50

© 1984 International Union of Crystallography

UM00012908
NOVARTIS EXHIBIT 1017
Novartis v. Regents, IPR2023-01346
Page 1654 of 4460

It appears that the carbonyl O atom and the C≡C triple bond compete for the C–H proton in the crystal structures of propiolic acid and *N*-methylpropiolamide. It is well established that the amide O atom is a far stronger proton acceptor than the corresponding O atom of the carboxyl group. This fact has been demonstrated in the solid, by packing systematics (Leiserowitz & Nader, 1977), electron density mapping (Berkovitch-Yellin, Leiserowitz & Nader, 1977), and atom–atom potential-energy calculations (Berkovitch-Yellin & Leiserowitz, 1982; Berkovitch-Yellin, Ariel & Leiserowitz, 1983). On these premises the distinct difference in C–H···O and C–H···C≡C contacts between *N*-methylpropiolamide and propiolic acid may be attributed to the relative proton-acceptor properties of the O(amide) and O(carboxyl) atoms and the C≡C bond. From a correlation curve relating the amount of bonding charge and bond length (Berkovitch-Yellin & Leiserowitz, 1977), it was deduced that the excess charge in the C≡C bond is approximately 0·4e, which is larger than the net atomic charge of −0·22e on the carbonyl O atom of the carboxyl group (Berkovitch-Yellin & Leiserowitz, 1982) but comparable to the net atomic charge of −0·38e on the amide O atom (Berkovitch-Yellin & Leiserowitz, 1980).

In order to account for the observed C–H···O and C–H···C≡C contacts in the crystal structures of propiolic acid and in *N*-methylpropiolamide, we mapped the electrostatic potential energy around these molecules by placing a positive unit charge at the locus of the points shown in Fig. 3(*a*). These points represent the nearest approach distances of the acetylenic proton donor to the reference molecule. The potential for propiolic acid (Fig. 3*b*) demonstrates comparable energies for C–H···C≡C(midpoint), and C–H···O interactions, whereas in *N*-methylpropiolamide there is a distinct preference for the C–H···O interaction. These results are completely in agreement with experiment.

3. The C(sp^2)–H···O interaction

3.1. *Quinones*

There are common geometric patterns in several quinone packing arrangements which have been interpreted in terms of C–H···O=C interactions (Bernstein, Cohen & Leiserowitz, 1974). These structures incorporate the motif shown in (1). The C–H···O

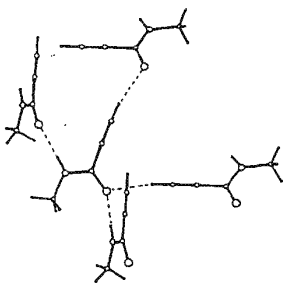


Fig. 1. Arrangement of N–H···O and C–H···O hydrogen bonds in *N*-methylpropiolamide.

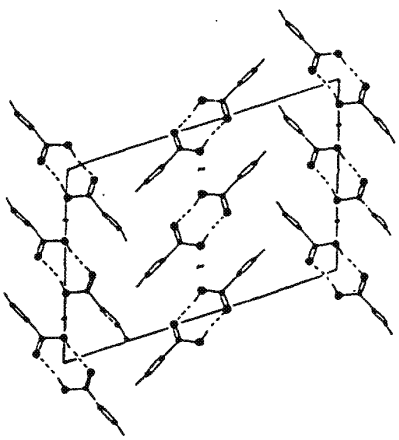
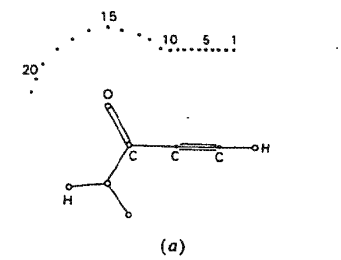
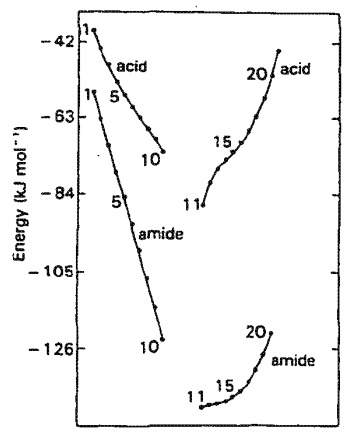


Fig. 2. Propiolic acid. Packing arrangement.



(*a*)



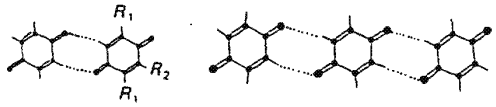
(*b*)

Fig. 3. (*a*) Discrete points of closest approach of proton donor to *N*-methylpropiolamide and propiolic acid. (*b*) Electrostatic potential energy (kJ mol^{-1}) at the discrete points of (*a*).

UM00012909
NOVARTIS EXHIBIT 1017
Novartis v. Regents, IPR2023-01346
Page 1655 of 4460

and H···O distances are about 3·5 and 2·5 Å respectively..

In 1,4-benzoquinone (Trotter, 1960) each molecule participates in several C–H···O contacts (Fig. 4), forming a layer structure. Within each layer neighbouring molecules, related by translation along the 6·7 Å axis, are connected by C–H···O contacts of 3·5 Å, as in (1), generating a coplanar ribbon (2). Adjacent ribbons, related by twofold screw axes, are interconnected by C–H···O contacts of 3·38 Å in a triangular pattern linking each molecule of one ribbon to two molecules of the adjacent ribbon.



(1) (2)

A strong argument for the role played by C–H···O interactions in determining this layer structure and other layer structures involving benzoquinone molecules is provided by the molecular arrangements in the 1:1 complex between thymine and 1,4-benzoquinone (Sakurai & Okunuki, 1971), in the quinhydrone complex (Sakurai, 1965), in the 1:1 complex of benzoquinone with chlorophenol (Shipley & Wallwork, 1967) and by the observation that tetrafluoro-*p*-benzoquinone (Meresse, Courseille & Chanh, 1974) does not form a layer structure as in 1,4-benzoquinone. The first-mentioned crystal structure contains alternating thymine and benzoquinone layers. The benzoquinone sheet structure in the thymine complex is practically identical with that in the pure benzoquinone crystal structure. Since a sheet of benzoquinone molecules has completely different environments in these two crystal structures, the layer motif must be determined by intralayer, and not interlayer, forces. The quinhydrone complex (Fig. 5) contains alternating ribbons of benzoquinone and of hydroquinone molecules stabilized by C–H···O(carbonyl) and C–H···O(hydroxyl) interactions respectively. The 1:1 complex of benzoquinone and *p*-chlorophenol (Fig. 6) displays C–H···O(carbonyl) contacts in the ribbon motif (2).

In order to verify the role played by C–H···O interactions in stabilizing motifs (1) and (2) and in determining the layer structures of the 1,4-benzoquinones cited above, we calculated the energy of the coplanar dimer (1) (with $R_1 = R_2 = H$) as a function of molecular displacement along *L* and *M* (Fig. 7*a*). The energy map (Fig. 7*b*) displays a minimum corresponding to a dimer arrangement (Fig. 7*a*) similar to that observed in the (substituted) benzoquinone crystal structures which explains the occurrence of (1) for 1,4-benzoquinone and substituted benzoquinones and of the ribbon (2) for 1,4-benzoquinone. Further, we examined the variation in energy of the 1,4-benzoquinone layer (Fig. 4) as a function of the offset along *L* between adjacent ribbons (2) related originally by twofold screw symmetry (Fig. 8). It is evident that the observed structure corresponds to the energy minimum, where electrostatic forces play the dominant role. We have also calculated the variation in energy as a function of offset between adjacent ribbons (2) related by translation (Fig. 9). The energy minimum corresponds to a layer arrangement (Fig. 9*b*) in which the interribbon offset provides for a C–H···O interaction; the major contribution to the energy is again electrostatic. The minimum in energy of this layer (Fig. 9*a*) is comparable to that of the observed layer of benzoquinone (Fig. 8), suggesting that interlayer and not intralayer forces play the deciding role in determining the observed layer structure. It is noteworthy that an arrangement similar to this hypothetical layer, in which the ribbons are related by translation, occurs in the crystal structure of the 1:1 complex of benzoquinone with *p*-chlorophenol (Fig. 6).

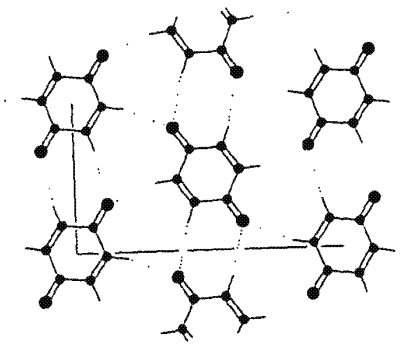


Fig. 4. Benzoquinone. Layer structure. The C–H···O contacts are marked.

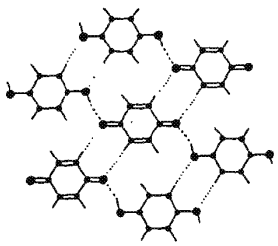


Fig. 5. Triclinic quinhydrone layer structure. C–H···O(carbonyl), C–H···O(hydroxyl) and O–H···O contacts are shown.

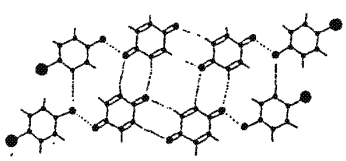


Fig. 6. The complex *p*-chlorophenol: 1,4-benzoquinone layer structure. C–H···O(carbonyl), C–H···O(hydroxyl) and O–H···O contacts are shown.

UM00012910

NOVARTIS EXHIBIT 1017
Novartis v. Regents, IPR2023-01346
Page 1656 of 4460

3.2. C(sp^2)–H···O(*carbonyl*) *interaction in carboxylic acids*

Qualitative studies of various packing arrangements in carboxylic acids had indicated that attractive C–H···O interactions play an active role in stabilizing certain packing arrangements and in fixing molecular conformation (Leiserowitz, 1976). These deductions were put on a sound footing by energy calculations (Berkovitch-Yellin & Leiserowitz, 1982); It was demonstrated that motif (3), incorporated in several crystal structures, is stabilized by C–H···O interactions. This motif is possible only if the carboxyl moiety $CH{=}CH{-}CO_2H$ exhibits the antiplanar $CH{=}CH{-}C{=}O$ conformation (4*a*), as against the synplanar conformation (4*b*) which is preferred in terms of intramolecular forces. It was found that all crystal structures which exhibit the antiplanar conformer (4*a*) incorporate the C–H···O(carbonyl) contact (3). Thus it was deduced that this conformer is stabilized by these interactions.

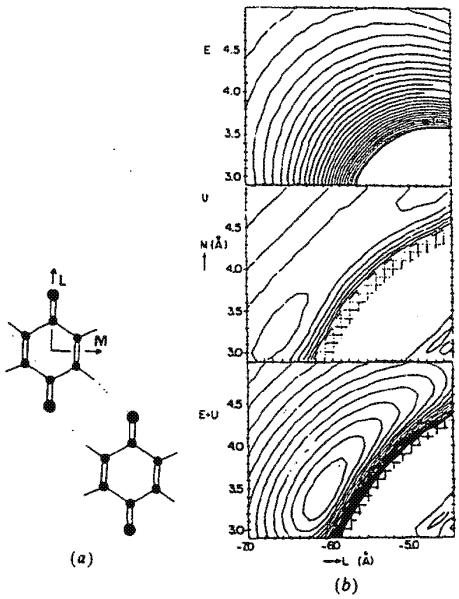


Fig. 7. (*a*) Arrangement of benzoquinone dimer. (*b*) Variation of energy of benzoquinone dimer as function of offset along *L* and *M* (*E* Coulomb energy, *U* van der Waals energy). The minimum is at $l = -6{\cdot}0$, $m = 3{\cdot}5$ Å. The observed values are $l = -5{\cdot}5$, $m = 3{\cdot}9$ Å.

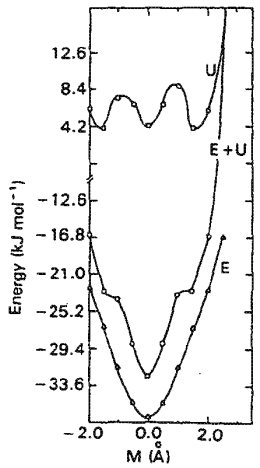
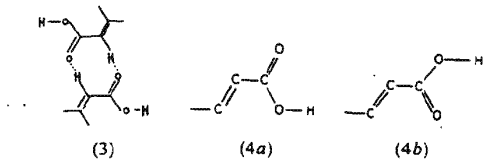


Fig. 8. Benzoquinone. Variation in energy of ribbons (2) interrelated by 'twofold screw' symmetry as a function of the offset between ribbons from the observed structure ($m = 0$). The separation of ribbons along *L* was kept at the observed distance of $l = 6{\cdot}2$ Å (see Fig. 4).



This deduction was examined in detail for fumaric acid, which exhibits an antiplanar C=C–C=O con-

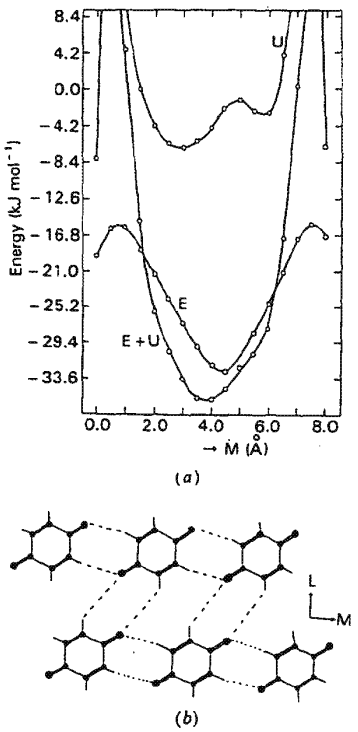
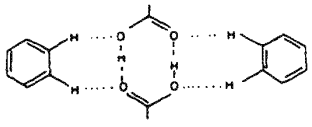


Fig. 9. Benzoquinone. (*a*) The variation in energy of ribbons (2) related by translation as a function of offset along *M*. The separation between ribbons along *L* is 6·5 Å, which was found to correspond to the minimum energy. (*b*) Arrangement which corresponds to the minimum energy ($l = 6{\cdot}5$, $m = 4$ Å).

UM00012911
NOVARTIS EXHIBIT 1017
Novartis v. Regents, IPR2023-01346
Page 1657 of 4460

formation in the layer structure shown in Fig. 10. To establish the role played by the C–H···O interactions the energy of the layer was calculated as a function of offset between adjacent hydrogen-bonded chains. The resulting energy minimum corresponds to the observed offset which is determined mainly by Coulomb forces. A similar calculation was carried out for the hypothetical synplanar conformer. Here the arrangement corresponding to the energy minimum incorporates a C–H···O(hydroxyl) contact, instead of the C–H···O(carbonyl) contact, and is 4·6 kJ mol^{-1} less stable than the observed layer structure. We concluded that in this system CH···O(carbonyl) interactions determine both the molecular conformation and the offset between the hydrogen-bonded chains.

Several substituted benzoic acids exhibit motif (5). The question as to whether this motif is stabilized by C–H···O interactions was considered by energy calculations. It was demonstrated that van der Waals forces, and not Coulomb forces, play the primary role in stabilizing motif (5) (Berkovitch-Yellin & Leiserowitz, 1982).



(5)

3.3. *Can* C(sp^2)–H···O *or* C(sp^2)–H···N *interactions induce less favourable hydrogen-bonding arrangements*?

We shall now examine the crystal structures of the β and δ forms of 2-pyrazinecarboxamide which incorporate long NH···O bonds, and that of uracil which contains an irregular N–H···O hydrogen-bond arrangement.

2-Pyrazinecarboxamide crystallizes in four modifications, α, β, γ and δ (Tamura, Kuwano & Sasada, 1961). The α form (Takaki, Sasada & Watanabe, 1960) contains two types of cyclic hydrogen-bonded pairs, N–H···O bonds of 2·90 Å and N–H···N bonds of 3·14 Å, as shown in (6).

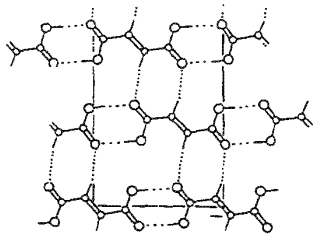
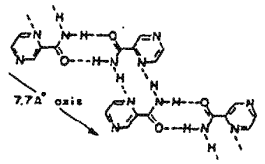
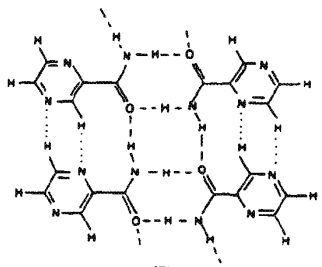


Fig. 10. Fumaric acid layer structure.



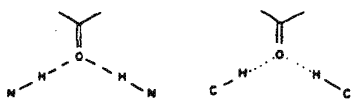
(6)

The β and δ forms exhibit hydrogen-bonding motifs which are similar to each other and exemplified in (7). In the β form (Rø & Sørum, 1972*a*) the cyclic hydrogen-bonded pairs (N–H···O 2·9 Å) are interlinked by N–H···O bonds of 3·24 Å and C–H···N contacts of 3·38 Å. In the δ form (Rø & Sørum, 1972*b*) the corresponding N–H···O and C–H···N distances are 3·48 and 3·40 Å. These results suggest that the pronounced stretchings of the N–H···O bonds in the β and δ forms are compensated by the presence of interactions involving the C–H···N contacts of 3·4 Å. Furthermore, we may, by analogy, regard a C–H···N or C–H···O interaction as not insignificant if the C···O or C···N distance is 0·2–0·3 Å longer than 3·2 Å. Such a long contact would hardly have been considered as constituting a significant C–H···N or C–H···O interaction if just distance criteria were paramount.



(7)

In the crystal structure of uracil (Stewart & Jensen, 1967) one carbonyl O atom participates in two N–H···O hydrogen bonds, (8*a*), and the other, (8*b*), makes short contacts of 3·35 Å with two C–H bonds. This arrangement is not in keeping with the observed tendency of the maximum number of potential hydrogen-bonding acceptor groups to participate in hydrogen bonds (Etter, 1982; Berkovitch-Yellin *et al.*, 1983). A more homogeneous hydrogen-bonded structure could have been formed were both carbonyl O atoms to participate in N–H···O bonds, as in 5-fluorouracil (Fallon, 1973) or 6-azauracil (Singh & Hodgson, 1974), suggesting that the observed structure of uracil is stabilized by the contributions of the two C–H···O interactions.



(8*a*) (8*b*)

UM00012912

NOVARTIS EXHIBIT 1017
Novartis v. Regents, IPR2023-01346
Page 1658 of 4460

4. The C(sp^3)–H···O contact

4.1. *Glycine*

α-Glycine (Legros & Kvick, 1980) crystallizes in the centrosymmetric monoclinic space group $P2_1/n$ ($a = 5{\cdot}18$, $b = 11{\cdot}8$, $c = 5{\cdot}45$ Å, $\beta = 112°$). As shown in Fig. 11, the molecules form hydrogen-bonded layers parallel to the *ac* plane, in which they are related to each other by translation only. Each layer is interlinked to its neighbour on one side across centres of inversion by N–H···O bonds (H···O 2·05 Å) giving a centrosymmetric bilayer, and by an *n* glide to its other neighbour, by C–H···O contacts of 3·25 Å (H···O 2·4 Å).

Given the centrosymmetric bilayer which incorporates intralayer N–H···O bonds, the question we address ourselves to is the role the C–H···O contact plays in determining the juxtaposition between bilayers. We calculated the various contributions to the energy of interaction of two glycine molecules forming the C–H···O contact. The electrostatic parameters for glycine were derived from an experimental deformation density distribution of crystalline glycine (Legros & Kvick, 1980). The total energy (electrostatic E + van der Waals U) is -14 kJ mol^{-1}.

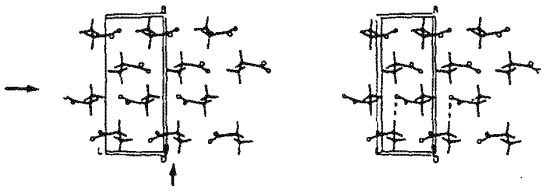


Fig. 11. The α form of glycine. Packing arrangement. The C–H···O contacts are marked. The horizontal arrow indicates the array of glide-related molecules, and the vertical arrow the donor molecule.

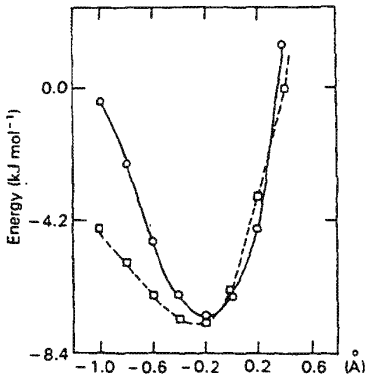


Fig. 12. The α form of glycine. The interaction energy between one glycine donor molecule and an array of glide-related molecules along the *c* axis. Open circles for the whole glycine molecule as donor, open squares for only the C–H group as donor.

Of this sum the contributions arising from interaction between only the C–H group of the proton-donor molecule and the whole acceptor molecule are $E = -13$ kJ mol^{-1} and $U = 4$ kJ mol^{-1}, yielding a total of -9 kJ mol^{-1}. Thus the contribution of the C–H···O interaction is significant. The total energy of interaction between a C–H donor glycine molecule, and an array of glide-related molecules along the *c* axis (marked in Fig. 11) was calculated as a function of offsetting this array of molecules along c, for the donor glycine molecule as a whole and for its C–H moiety only. The resulting energy curves, shown in Fig. 12, are very similar, indicating that the C–H···O interaction determines to a large extent the interbilayer arrangement. The energy of an alternative packing arrangement, in which the bilayers are related by translation, was checked as a function of the offset and separation between bilayers: it yielded a similar interbilayer arrangement incorporating approximately linear C–H···O contacts.

4.2. *Acetamide, acetic acid and the acetyl group*

The C–H groups of acetamide appear to participate in C–H···O interactions. This interaction was indirectly suggested (Berkovitch-Yellin & Leiserowitz, 1980) by a comparison of the isomorphous crystal structures of urea–barbital (Gartland & Craven, 1974) and acetamide–barbital (Hsu & Craven, 1974). Urea forms a bifurcated bond (2·95, 3·16 Å) with an O atom of barbital (Fig. 13*a*). Acetamide makes similar contacts in which an acetamide C–H···O contact of length 3·45 Å replaces a urea N–H···O bond (Fig. 13*b*). This hypothesis was substantiated by calculation which yielded a Coulomb energy of -9 kJ mol^{-1} for a C···O separation of 3·3 Å.

Acetic acid (Nahringbauer, 1970) appears in a hydrogen-bonding chain motif which incorporates the pseudo centrosymmetric dimer (9) in which the O–H···O bond, of length 2·63 Å, is complemented by a C–H···O contact of 3·43 Å. We found by calculation (Berkovitch-Yellin & Leiserowitz, 1982) that the energy of this dimer is -18 kJ mol^{-1}, almost 70% of which is due to Coulomb forces. The energy of acetic acid in a 'normal' centrosymmetric dimer (10) is -27 kJ mol^{-1}. Ascribing half of this energy to each O–H···O bond, it appears that the C–H···O interaction contributes 4 kJ mol^{-1} to the stabilization of the observed dimer (9).

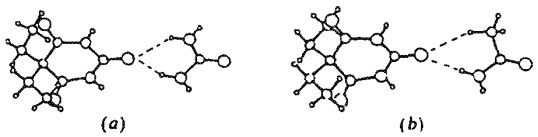
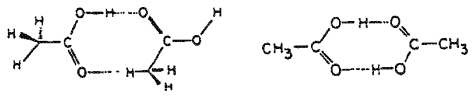


Fig. 13. Hydrogen-bonding motifs of (*a*) barbital:urea complex, and (*b*) barbital:acetamide complex.

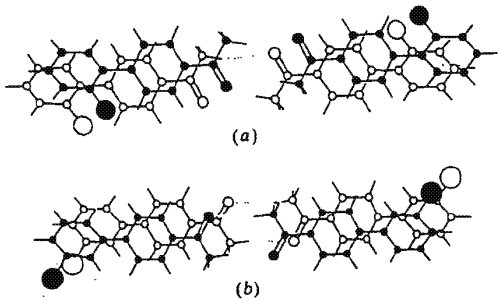
UM00012913

NOVARTIS EXHIBIT 1017
Novartis v. Regents, IPR2023-01346
Page 1659 of 4460



(9) (10)

Analogous arrangements to the dimer motif (10) have been found in two 4-acetylbiphenyl derivatives (Sutherland & Hoy, 1968, 1969) depicted in Fig. 14 and in the host–guest crystalline complexes of deoxycholic acid with methyl alkyl ketones CH_3–CO–$(CH_2)_n$–CH_3. In these complexes (Popovitz-Biro, Chang, Tang, Shochet, Lahav & Leiserowitz, 1980) the guest ketone molecules form cyclic pairs in the chiral inclusion channels, for ethyl methyl ketone and methyl pentyl ketone, with C···O distances of 3·7 Å.



(*a*)

(*b*)

Fig. 14. Part of a stack of dimers of 4-acetylbiphenyl derivatives. (*a*) 4-Acetyl-2′-chlorobiphenyl. (*b*) 4-Acetyl-3′-bromobiphenyl [H atoms of the CH_3 group of (*b*) were not reported].

References

BERKOVITCH-YELLIN, Z., ARIEL, S. & LEISEROWITZ, L. (1983). *J. Am. Chem. Soc.* **105**, 765–767.

BERKOVITCH-YELLIN, Z. & LEISEROWITZ, L. (1977). *J. Am. Chem. Soc.* **99**, 6106–6107.

BERKOVITCH-YELLIN, Z. & LEISEROWITZ, L. (1980). *J. Am. Chem. Soc.* **102**, 7677–7690.

BERKOVITCH-YELLIN, Z. & LEISEROWITZ, L. (1982). *J. Am. Chem. Soc.* **104**, 4052–4064.

BERKOVITCH-YELLIN, Z., LEISEROWITZ, L. & NADER, F. (1977). *Acta Cryst.* B**33**, 3670–3677.

BERNSTEIN, J., COHEN, M. D. & LEISEROWITZ, L. (1974). *The Chemistry of the Quinonoid Compounds.* Part 1, edited by S. PATAI, pp. 92–101. London: John Wiley.

DONOHUE, J. (1968). *Structural Chemistry and Molecular Biology*, edited by A. RICH & N. DAVIDSON, pp. 443–465. San Francisco: Freeman.

ETTER, M. C. (1982). *J. Am. Chem. Soc.* **104**, 1095–1096.

FALLON, L. (1973). *Acta Cryst.* B**29**, 2549–2556.

GARTLAND, G. L. & CRAVEN, B. M. (1974). *Acta Cryst.* B**30**, 980–987.

HSU, I. & CRAVEN, B. M. (1974). *Acta Cryst.* B**30**, 974–979.

LEGROS, J. P. & KVICK, Å. (1980). *Acta Cryst.* B**36**, 3052–3059.

LEISEROWITZ, L. (1976). *Acta Cryst.* B**32**, 775–802.

LEISEROWITZ, L. & NADER, F. (1977). *Acta Cryst.* B**33**, 2719–2733.

LEISEROWITZ, L. & TUVAL, M. (1978). *Acta Cryst.* B**34**, 1230–1247.

MERESSE, A., COURSEILLE, C. & CHANH, N. B. (1974). *Acta Cryst.* B**30**, 524–526.

NAHRINGBAUER, I. (1970). *Acta Chem. Scand.* **24**, 453–462.

PARRY, G. S. (1954). *Acta Cryst.* **7**, 313–320.

POPOVITZ-BIRO, R., CHANG, H. C., TANG, C. P., SHOCHET, N. R., LAHAV, M. & LEISEROWITZ, L. (1980). *Pure Appl. Chem.* **52**, 2693–2704.

RØ, G. & SØRUM, H. (1972*a*). *Acta Cryst.* B**28**, 991–998.

RØ, G. & SØRUM, H. (1972*b*). *Acta Cryst.* B**28**, 1677–1684.

SAKURAI, T. (1965). *Acta Cryst.* **19**, 320–330.

SAKURAI, T. & OKUNUKI, M. (1971). *Acta Cryst.* B**27**, 1445–1453.

SHIPLEY, G. G. & WALLWORK, S. C. (1967). *Acta Cryst.* **22**, 593–601.

SIM, G. A. (1967). *Annu. Rev. Phys. Chem.* **18**, 57–80.

SINGH, P. & HODGSON, D. T. (1974). *Acta Cryst.* B**30**, 1430–1435.

STEWART, R. F. & JENSEN, L. H. (1967). *Acta Cryst.* **23**, 1102–1105.

SUTHERLAND, H. H. & HOY, T. G. (1968). *Acta Cryst.* B**24**, 1207–1213.

SUTHERLAND, H. H. & HOY, T. G. (1969). *Acta Cryst.* B**25**, 2385–2391.

SUTOR, D. J. (1963). *J. Chem. Soc.* pp. 1105–1110.

TAKAKI, Y., SASADA, Y. & WATANABE, T. (1960). *Acta Cryst.* **13**, 693–702.

TAMURA, C., KUWANO, H. & SASADA, Y. (1961). *Acta Cryst.* **14**, 693.

TAYLOR, R. & KENNARD, O. (1982). *J. Am. Chem. Soc.* **104**, 5063–5070.

TROTTER, J. (1960). *Acta Cryst.* **13**, 86–95.

UM00012914
NOVARTIS EXHIBIT 1017
Novartis v. Regents, IPR2023-01346
Page 1660 of 4460

Induced Fit Selection of a Barbiturate Receptor from a Dynamic Structural and Conformational/Configurational Library

Volker Berl,[a,b] Ivan Huc,[a,c] Jean-Marie Lehn,*[a] André DeCian,[d] and Jean Fischer[d]

Keywords: Dynamic combinatorial chemistry / Molecular recognition / Hydrogen bonding / Hydrazone isomerization / Barbiturate receptor

The selection of the receptor presenting the strongest affinity for a barbiturate substrate from a dynamic combinatorial library of constituents differing in structure and conformation/configuration is described. The gradual addition of the barbiturate to an equilibrating mixture of hydrazone isomers leads to the quantitative shift towards a single species, **3**, which presents highest complementarity to the substrate and yields the supramolecular entity **3**:**4**.

Introduction

The reversible covalent or non-covalent combination of molecular components generates a potential diversity defining a dynamic combinatorial library of molecular or supramolecular constituents that may be real or virtual depending on whether or not they already exist in absence of the target or are expressed in its presence. This dynamic approach to combinatorial chemistry has recently been explored for both inorganic[1][2] and organic,[3–8] molecular or supramolecular entities.[9] It bypasses the need for synthesizing all constituents of a combinatorial library by allowing the target to select or express the most suitable component out of the equilibrating mixture.

On the other hand, structural diversity may also be generated through conformational and/or configurational exchange processes, generating a thermodynamically driven conformational/configurational dynamic library through (thermal or photo-induced) isomerization around single or double bonds, site inversion, or ring inversion. In this case, receptor–substrate interaction may be expected to be strongest for a given member of the set of conformationally or configurationally different species (conformational or configurational isomers) resulting in the displacement of the equilibrating mixture towards the preferential expression of the optimal partner. This amounts to an induced-fit process which may be of single or double (multiple) type, depending on whether only one partner, or both (several) partners are present in conformationally or configurationally different forms.

[a] Laboratoire de Chimie Supramoléculaire, ESA 7006 of the CNRS, ISIS, Université Louis Pasteur,
4 rue Blaise Pascal, F-67000 Strasbourg, France
[b] Forschungszentrum Karlsruhe GmbH, Institut für Nanotechnologie,
Postfach 3640, D-76021 Karlsruhe, Germany
[c] Present address: Institut Européen de Chimie et Biologie, ENSCPB,
Av. Pey Berland, F-33402 Talence Cedex, France
[d] Laboratoire de Cristallochimie, UMR 75 of the CNRS, Institut Le Bel, Université Louis Pasteur,
4 rue Blaise Pascal, F-67000 Strasbourg, France

Induced-fit processes, or the specific structural adaptation of a host molecule upon interaction with the guest to form a more stable complex, are widespread in nature, and are essential to the function of enzymes or biological receptors.[10] These processes have been mimicked in synthetic systems[11] in order to gain insight into the biological phenomena. In this communication, we describe an induced-fit process which leads to the substrate-driven selection of a receptor from a dynamic library of conformational and configurational isomers. Photo-isomerization around carbon–carbon double bonds has been used to induce the formation of a preferred receptor–substrate pair.[5]

Results and Discussion

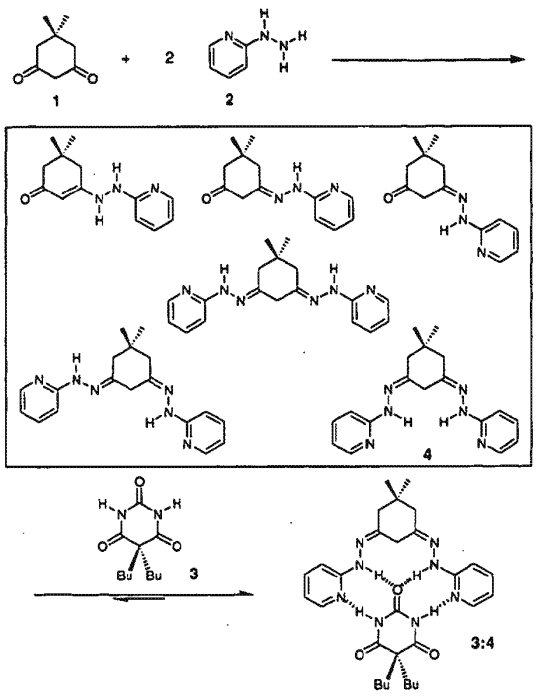
Diversity Generation

As depicted in Scheme 1, the system studied here involves the equilibration between different condensation products of 5,5-dimethyl-1,3-cyclohexanedione (**1**) and 2-hydrazinopyridine (**2**). In a 1:2 ratio in chloroform, these compounds yield the (*Z*/*Z*), (*E*/*E*), and (*E*/*Z*) dihydrazone isomers. The equilibrated mixture also contains a substantial amount of the (*E*) and (*Z*) isomers of the monohydrazone monoketone, as well as of its hydrazino–enone tautomer.[12] The conjugated tautomers of the dihydrazones were not detected. A number of equilibration processes can be envisaged: tautomerism, *cis*/*trans* isomerization about the hydrazone double bond, hydrolysis to the monohydrazone monoketone, or transamination[13] by the remaining 2-hydrazinopyridine (**2**).

The complexity of the mixture is well illustrated by its ^{1}H-NMR spectrum (Figure 1A). Slow equilibration between these compounds on the NMR time-scale results in numerous signals which could only be partially assigned to the different species.

 © WILEY-VCH Verlag GmbH, D-69451 Weinheim, 1999 1434–193X/99/1111–3089 $ 17.50+.50/0

UM00012915
NOVARTIS EXHIBIT 1017
Novartis v. Regents, IPR2023-01346
Page 1661 of 4460



Scheme 1. Equilibrating product mixture obtained from 5,5-dimethyl-1,3-cyclohexanedione (**1**) and 2-hydrazinopyridine (**2**) in a 1:2 ratio, and binding of dibutylbarbiturate to the (*Z*/*Z*) dihydrazone isomer

Induced Fit Substrate Binding

Progressive addition of dibutylbarbiturate **3**[14] to the equilibrating mixture of the various isomers and tautomers leads to a dramatic simplification of the ^{1}H-NMR spectrum, with the gradual disappearance of the different products, accompanied by the emergence of a single new species (Figure 1). At one equivalent of **3**, this species has nearly quantitatively replaced all the components initially present in the mixture. Its sharp ^{1}H-NMR spectrum (Figure 1E) is consistent with a 1:1 complex between dibutylbarbiturate **3** and a symmetrical dihydrazone. The (*Z*/*Z*) isomer (**4**) with convergent hydrazone NH groups could be unambiguously identified, and the (*E*/*E*) isomer ruled out, after NOESY experiments revealed a strong correlation between the hydrazone N*H* and the cyclohexane *H*2 protons in the complex. Accordingly, no correlation was observed with the cyclohexane *H*4 and *H*6 protons.

The amplitude of the effect of the barbiturate (**3**) on the mixture is remarkable. Not only does configurational isomerisation of the dihydrazones lead to a quantitative shift towards the (*Z*/*Z*) isomer (**4**), but the barbiturate (**3**) also promotes the reaction of the monocondensation products with the remaining hydrazino-pyridine (**1**) (Figure 1, disappearance of the alkene proton signal at 5.38 ppm). No such equilibrium shift was observed when acetic acid or 1-benzyluracil was used instead of **3**. These compounds have pK_a's similar to that of **3**, but lack some of its recognition elements and its complementarity to the target receptor. Their presence causes shifts of NMR signals due to non-specific associations, but no enrichment in a particular species.

Strong and specific hydrogen-bonding in the **3:4** supermolecule is supported by the following observations: (i) the NMR signals of the barbiturate N*H* (δ = 13.71), the hydrazone N*H* (δ = 9.95), and the pyridine *H*6 (δ = 8.34) protons are markedly deshielded; (ii) from zero to one equivalent, the barbiturate induces a stoichiometric formation of host; (iii) at more than one equivalent of barbiturate, slow exchange between bound and unbound barbiturate is observed on the NMR spectrum at 256 K or below; (iv) dilution from 10 mM to 0.156 mM causes neither shifts in the ^{1}H-NMR spectrum, nor appearance of other isomers after 6 h, which implies an association constant K_a in excess of 6400 M^{-1} for the **3:4** substrate:receptor pair.

The strength of association between **3** and **4**, as well as the reversibility of the various equilibria involved, were further established in a series of competition experiments involving the barbiturate receptor **6**[15] (Scheme 2). The association constant for the complex **3:6** was determined by analysis of the ^{1}H-NMR titration values obtained by progressive addition of **3** to **6** in $CDCl_3$. The resulting value of $5.8 \cdot 10^4$ M^{-1} is consistent with values reported in the literature for related systems.[17] When **6** (1 equiv.) is initially present in the mixture of **1** and **2**, addition of barbiturate *does not* favor the formation of the (*Z*/*Z*) isomer **4**. Instead, the barbiturate preferentially binds to **6**, and the mixture of products formed by **1** and **2** remains practically unchanged.

The same preferential binding was observed when **6** (1 equiv.) was added to a solution of a preformed complex between barbiturate **3** and induced receptor **4**. Shortly after the addition, the slowly equilibrating mixture contains free receptor **4** and free receptor **6**, as well as complexes **3:4** and **3:6**. The proportions between these species at this early stage allows us to estimate the association constant between barbiturate **3** and receptor **4** at about $1.5 \cdot 10^4$ M^{-1}. Upon standing a further 8 days, receptor **4** "diversifies back" into the original mixture of dihydrazones. A similar behavior can be observed, when [D_4]methanol (40 vol%) is added to a solution with complex **3:4** in [D]chloroform. The single species initially present is gradually replaced by the original diversity of isomers, as the association constant is decreased by interaction of the hydrogen-bonding sites with methanol.

All sets of experiments establish the strong affinity of receptor **4** for the barbiturate. The four hydrogen bonds involved in the **3:4** pair provide almost as much binding energy as the six hydrogen bonds formed by receptor **6**. When association occurs in the context of the reversible formation of **4**, it leads to its selective stabilization, and eventually its quantitative emergence from the original mixture. This phenomenon presents itself as an efficient way of recruiting and identifying a receptor from a pool of equilibrating molecules through a *molding process*.[3]

UM00012916
NOVARTIS EXHIBIT 1017
Novartis v. Regents, IPR2023-01346
Page 1662 of 4460

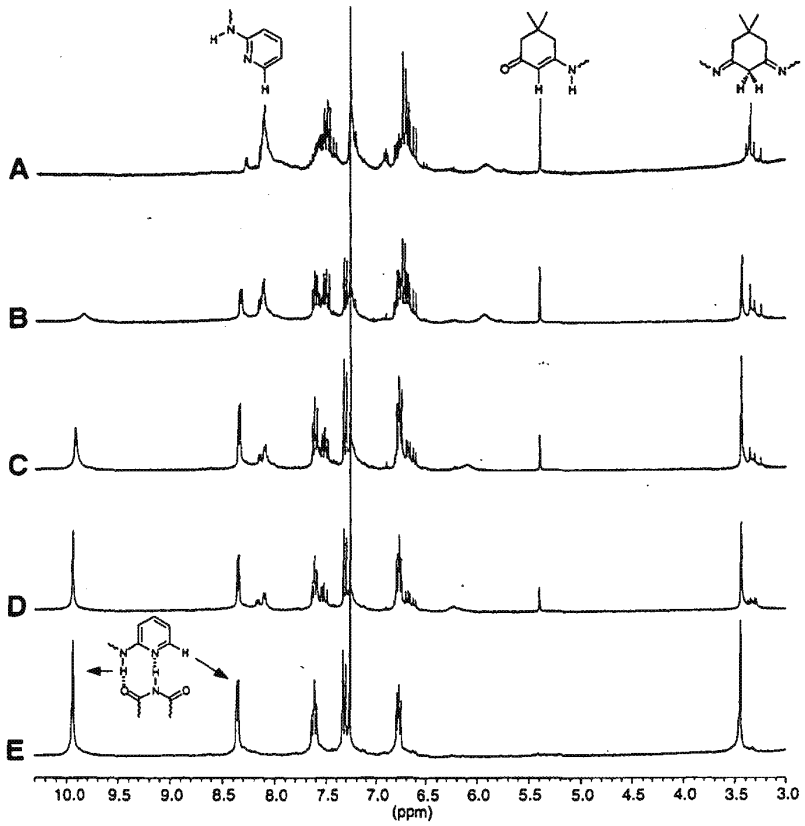
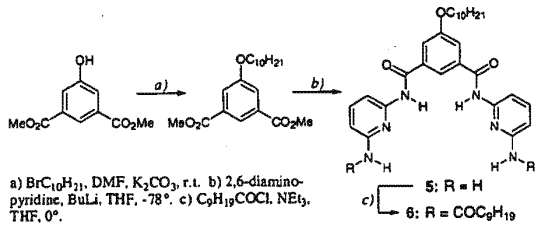
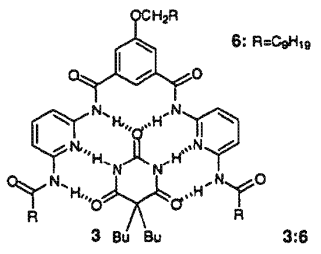


Figure 1. (A) 300 MHz ^{1}H NMR spectrum (δ = 3–10.5) of the mixture in $CDCl_3$ after two days of equilibration of 5,5-dimethyl-1,3-cyclohexanedione (**1**) (10 mM) and 2-hydrazinopyridine (**2**) (20 mM) under an oxygen free atmosphere; – (B), (C), (D), and (E) evolution of the spectrum after addition of 0.25, 0.5, 0.75, and 1.0 equivalent of dibutylbarbiturate (**3**), respectively. The structures indicate the assignment of some of the signals.



Scheme 2. Synthesis of compound **6**



Structural Data on the Substrate:Receptor Pair 3:4. Crystal Structure of 7

Attempts to crystallize the **3**:**4** substrate:receptor pair failed until now, but instead, single crystals suitable for X-ray analysis of the dimerized substrate–receptor complex 3_2:**7**[18] (Figure 2) could be obtained from a 1:1 solution of **3** and **4** in 40 mM CH_2Cl_2/hexane solution by solvent diffusion upon standing for 6 months. The crystal structure was not that of the expected monomeric **3**:**4** complex, but of a dimeric entity 3_2:**7** resulting from the formation of a C–C connection between two units of **4** to give **7**. It nevertheless confirms the solution studies on the **3**:**4** complex, as it shows the expected selection and conformational locking of the (*Z*/*Z*)-isomer by the barbiturate, also in the solid state. The hydrogen bonds in this new 2:1 three-component supermolecule (3_2:**7**) are nearly linear and of the expected length (NH–N: 2.84 Å, 169°; O–HN: 2.97 Å, 173°), which is in agreement with the relatively high binding constant displayed by the **3**:**4** complex. The formation of **7** was observed in none of the solution studies, but the oxidative carbon–carbon bond formation, previously reported only for

UM00012917
NOVARTIS EXHIBIT 1017
Novartis v. Regents, IPR2023-01346
Page 1663 of 4460

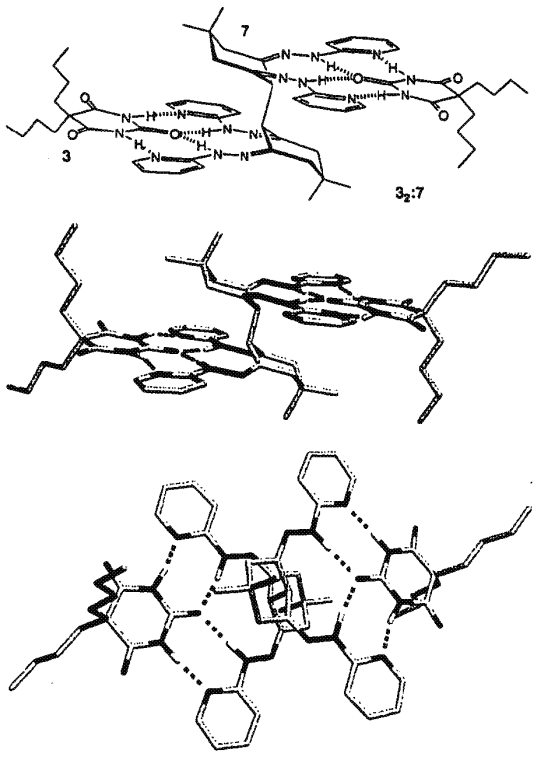
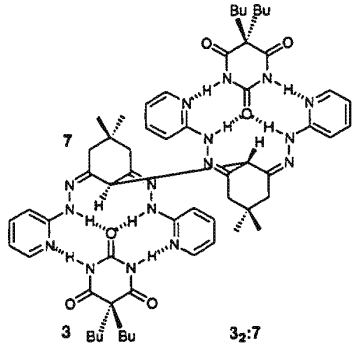


Figure 2. Schematic drawing (top) and crystal structure of the dimeric supermolecule 3_2:7 in cylindrical bond representation, side view (center) and top view (bottom).

cyclic 1,3-diones,[19] could be confirmed by letting samples of preformed 3:4 complex age in the presence of 2 equivalents of triethylamine under an oxygen atmosphere. Under these conditions, oxidative formation of dimer 7 was completed after 6 days at room temperature. Thus, the basic character of the hydrazines themselves make the slow formation of dimeric complex 3_2:7 likely, even without the presence of additional base over a longer period of time in the crystallization assays.



Conclusion

The present results demonstrate the substrate-driven selection of the optimal receptor from a *dynamic structural and conformational/configurational library*. The simultaneous operation of conformational/configurational isomerizations within a species together with the establishment of molecular or supramolecular connections between components gives more efficient access to increased diversity in dynamic combinatorial chemistry. Thus, the present system may be extended by using several different hydrazines and diones in order to evaluate the selection procedure in the context of a large structural and conformational diversity. Furthermore, it is clear that other conformational processes (such as hindered bond rotation for instance[20]) may be implemented in order to give access to a variety of shapes and spatial arrangements for an increased real/virtual dynamic diversity. From a more general point of view, developments in dynamic processes involving induced-fit events provide entries towards *adaptive chemistry*.[21]

Experimental Section

General Methods: [D]Chloroform for all NMR studies on hydrazone compounds was passed through a short column of dry aluminium oxide 90 (Merck; 70–230 mesh, standardized activity II-III) and was subsequently degassed with argon for 30 min. During the equilibration periods, NMR-tubes were carefully kept under argon. – 2-Hydrazinopyridine (2) was purchased from Aldrich (pyridine as impurity) and purified by multiple extraction with small portions of boiling hexane under argon, and subsequent solvent removal under reduced pressure. – THF was distilled over sodium/benzophenone. – Triethylamine (Lancaster, 99%) was used as received. – Flash column chromatography was performed using silica gel (Geduran, SI 60 (40–63 μm, Merck). – Infrared spectra were recorded as thin films on NaCl discs on a Perkin–Elmer 1600 Series FTIR. – 500 MHz ^{1}H NOESY spectra were recorded on a Bruker ARX 500 spectrometer, 300 MHz ^{1}H NMR spectra on a Bruker AM 300 spectrometer, and 200 MHz ^{1}H NMR and 50.3 MHz ^{13}C NMR spectra on a Bruker SY 200 spectrometer. The solvent signal was used as an internal reference for both ^{1}H- and ^{13}C-NMR spectra. The following notation is used for the ^{1}H NMR spectral splitting patterns: singlet (s), doublet (d), triplet (t), multiplet (m). – EI and FAB-mass spectrometric measurements were performed by the Service de Spectrométrie de Masse, Institut de Chimie, Université Louis Pasteur. – Melting points (m.p.) were recorded on an electrothermal Digital Melting Point Apparatus and are uncorrected. – Elemental analyses were performed by the Service de Microanalyse, Institut Charles Sadron, Strasbourg.

5,5-Dibutylpyrimidine-2,4,6-trione (3) (Dibutylbarbiturate): This known compound was prepared according to a literature procedure[14] from diethyl dibutylmalonate and urea.

Complex 3:4. – Data for 4 in Complex 3:4: ^{1}H NMR (500 MHz, $CDCl_3$, 10 mM): δ = 9.95 (s, 2 H, H–N); 8.34 (dd, $^3J_{H6-H5}$ = 5.3 Hz, $^4J_{H6-H4}$ = 1.4 Hz, 2 H, H-6); 7.62 (ddd, $^3J_{H4-H3}$ = 8.9 Hz, $^3J_{H4-H5}$ = 6.8 Hz, $^4J_{H4-H6}$ = 1.7 Hz, 2 H, H-4); 7.31 (d, $^3J_{H3-H4}$ = 8.6 Hz, 2 H, H-3); 6.77 (ddd, $^3J_{H5-H6}$ = 5.1 Hz, $^3J_{H5-H4}$ = 7.1 Hz, $^4J_{H5-H3}$ = 0.8 Hz, 2 H, H-5); 3.44, (s, 2 H, H-2'); 2.44 (s, 4 H, H-4'); 1.01 (s, 6 H, CH_3).

UM00012918
NOVARTIS EXHIBIT 1017
Novartis v. Regents, IPR2023-01346
Page 1664 of 4460

Data for 3 in Complex 3:4: ^{1}H NMR (500 MHz, $CDCl_3$, 10 mM): δ = 13.71 (s, 2 H); 2.00 (m, 4 H); 1.33–1.16 (m, 8 H); 0.85 (t, ^3J = 7.2 Hz, 6 H, CH_3).

Dimethyl 5-Decyloxyisophthalate (Scheme 2): To a flask charged with dimethyl 5-hydroxyisophthalate (8.74 g, 41.48 mmol, 115 mol-%), 1-bromodecane (7.99 g, 36.10 mmol, 100 mol-%), K_2CO_3 (7.48 g, 54.12 mmol, 150 mol-%), and DMF (36 mL, 1 M) was added, and the mixture stirred at room temperature for 48 h. Et_2O (150 mL) was added and the organic phase washed twice with sat. aq. brine. The ether layer was dried with $MgSO_4$, filtered, evaporated to dryness, and purified by chromatography (SiO_2; EtOAc/hexane, 10:90 → 15:85) to provide dimethyl 5-decyloxyisophthalate (5.90 g, 41% yield) as a white powder. – M.p. 47–48 °C. – IR (thin film): $\tilde{\nu}$ = 2953 cm^{-1}, 2920, 2841, 1715, 1583, 1454, 1423, 1334, 1302, 1237, 1216, 1112, 1099, 1048, 1037, 1005, 994, 870, 788, 757, 720. – ^{1}H NMR (200 MHz, $CDCl_3$): δ = 8.24 (t, J = 1.4 Hz, 1 H); 7.72 (d, J = 1.4 Hz, 2 H); 4.04 (t, J = 6.5 Hz, 2 H); 3.92 (s, 6 H); 1.76 (m, 2 H); 1.26 (m, 14 H); 0.87 (t, J = 6.4 Hz, 3 H). – ^{13}C NMR (50.3 MHz, $CDCl_3$): δ = 166.3; 159.3; 131.77; 122.8; 119.9; 68.7; 52.4; 32.0; 29.6; 29.4; 29.2; 26.0; 22.7; 14.2. – EI-MS: *m/z* 351.1 ([M + H]$^+$, 100%). – $C_{20}H_{30}O_5$ (350.46): calc. C 68.55, H 8.63; found C 68.52, H 8.66.

***N,N'*-Bis(6-aminopyridin-2-yl)-5-decyloxyisophthalamide (5):**[16] To a solution of 2,6-diaminopyridine (recrystallized from boiling $CHCl_3$) (5.00 g, 45.82 mmol, 800 mol-%) in dry THF (46 mL, 1 M) at −78 °C was added a 1.6 M solution of *n*BuLi (44.20 mmol, 26.3 mL) in hexane. After 20 min at −78 °C, a solution of dimethyl 5-decyloxyisophthalate (2.00 g, 5.72 mmol, 100 mol-%) in dry THF (20 mL) was added dropwise. The reaction mixture was stirred at −78 °C for 8 h and then gradually warmed to room temp. and stirred over night. The reaction was then quenched with a 1 M solution of $NaHCO_3$ (100 mL) and extracted with EtOAc. The combined organic extracts were washed with sat. aq. brine and water, dried with $MgSO_4$, filtered, evaporated to dryness, and purified using flash chromatography (SiO_2; EtOAc/hexane, 2:1) to give *N,N'*-bis(6-aminopyridin-2-yl)-5-decyloxyisophthalamide **(5)** (2.63 g, 91% yield) as a pale yellow powder. – M.p. 132–133 °C. – IR (thin film): $\tilde{\nu}$ = 3362 cm^{-1}, 3205, 2951, 2923, 2854, 1681, 1620, 1593, 1538, 1456, 1337, 1303, 1247, 1166, 1134, 1051, 989, 864, 788, 744, 722, 707. – ^{1}H NMR (200 MHz, [D_6]DMSO): δ = 10.22 (s, 2 H); 8.11 (s, 1 H); 7.60 (d, J = 0.5 Hz, 2 H); 7.41 (m, 4 H); 6.28 (dd, J = 6.5 Hz, 1.5 Hz, 2 H); 5.79 (br. s, 4 H); 4.10 (t, J = 5.3 Hz, 2 H); 1.74 (m, 2 H); 1.25 (m, 14 H); 0.84 (t, J = 6.4 Hz, 3 H). – ^{13}C NMR (50.3 MHz, [D_6]DMSO): δ = 164.5; 158.7; 158.5; 150.2; 138.9; 135.6; 118.8; 116.9; 104.1; 101.8; 67.9; 31.2; 28.9; 28.6; 28.5; 25.4; 22.0; 13.9. – FAB-MS: *m/z* 505.3 [M + H]$^+$ (100%). – $C_{28}H_{36}N_6O_3$ (504.63): calc. C 66.64, H 7.19; found C 66.48, H 7.31.

5-Decyloxy-*N,N'*-bis[6-(decanoylamino)pyridin-2-yl]-isophthalamide (6): To a solution of **5** (0.5 g, 0.99 mmol, 100 mol-%) and triethylamine (0.20 g, 1.98 mol, 200 mol-%) in dry THF (20 mL) was added dropwise a solution of decanoyl chloride (0.38 g, 1.99 mmol, 200 mol-%) in THF (5 mL) at 0°C and the reaction stirred for 1 h, before warming to room temp. The reaction mixture was filtered, evaporated to dryness, and applied to a column (SiO_2; EtOAc/hexane, 1:3) to provide **6** (0.68 g, 84% yield) as a white powder. – M.p. 158–159 °C. – IR (thin film): $\tilde{\nu}$ = 3405 cm^{-1}, 3300, 2956, 2924, 2854, 1674, 1586, 1514, 1451, 1378, 1334, 1315, 1301, 1243, 1155, 1121, 1051, 883, 801, 722. – ^{1}H NMR (200 MHz, $CDCl_3$): δ = 8.65 (br. s, 2 H); 8.44 (br. s, 2 H); 7.83 (m, 5 H); 7.55 (t, J = 8.0 Hz, 2 H); 7.44 (s, 2 H); 3.85 (t, J = 6.4 Hz, 2 H); 2.33 (t, J = 7.4 Hz, 4 H); 1.65 (m, 6 H); 1.23 (m, 38 H); 0.84 (m, 9 H). – ^{13}C NMR (50.3 MHz, $CDCl_3$): δ = 172.2; 164.6; 159.7; 149.9; 149.2; 140.5; 135.6; 117.2; 110.3; 109.6; 68.7; 37.5; 31.8; 29.5; 29.4; 29.0; 25.9; 25.3; 22.6; 14.0. – FAB-MS: *m/z* 813.6 [M + H]$^+$ (100%). – $C_{48}H_{72}N_6O_5$ (813.13): calc. C 70.9, H 8.92; found C 70.79, H 8.98.

Formation of 7 by Oxidative Coupling of 4: To a solution of preformed **3:4** (**1**: 0.05 mmol, 7.0 mg; **2**: 0.1 mmol, 10.9 mg; **3**: 0.05 mmol, 12.0 mg, aged for 2 days under argon) in [D]chloroform (5 mL, 10 mM), was added NEt_3 (10.1 mg, 0.1 mmol, 200 mol-%) and the solution allowed to age under an oxygen atmosphere. After 6 days at room temp., **3:4** was quantitatively oxidized to $\mathbf{3_2}$**:7**, as followed by ^{1}H-NMR spectroscopy.

Data for 7 in Complex $\mathbf{3_2}$:7: ^{1}H NMR (200 MHz, $CDCl_3$, 10 mM): δ = 10.50 (s, 4 H, H-N); 8.35 (dd, $^3J_{H6-H5}$ = 5.4 Hz, $^4J_{H6-H4}$ = 1.2 Hz, 4 H, H-6); 7.58 (ddd, $^3J_{H4-H3}$ = 7.8 Hz, $^3J_{H4-H5}$ = 7.2 Hz, $^4J_{H4-H6}$ = 1.7 Hz, 4 H, H-4); 7.12 (d, $^3J_{H3-H4}$ = 8.3 Hz, 4 H, H-3); 6.79 (ddd, $^3J_{H5-H6}$ = 5.5 Hz, $^3J_{H5-H4}$ = 5.9 Hz, $^4J_{H5-H3}$ = 0.8 Hz, 4 H, H-5); 5.20 (s, 2 H, H-2'); 2.95 (d, ^2J = 13.9 Hz, 4 H, CH_2); 2.19 (d, ^2J = 13.9 Hz, 4 H, CH_2); 1.02 (s, 6 H, CH_3); 0.72 (s, 6 H, CH_3).

Data for 3 in Complex $\mathbf{3_2}$:7: ^{1}H NMR (200 MHz, $CDCl_3$, 10 mM): δ = 14.42 (s, 4 H); 2.15 (m, 8 H); 1.40–1.10 (m, 16 H); 0.82 (t, ^3J = 6.6 Hz, 12 H).

Acknowledgments

This work was supported by the CNRS and by a predoctoral fellowship (V. B.) from the Forschungszentrum Karlsruhe GmbH.

[1] [1a] B. Hasenknopf, J.-M. Lehn, G. Baum, B. Kneisel, D. Fenske, *Angew. Chem. Int. Ed. Engl.* **1996**, *35*, 1838. – [1b] B. Hasenknopf, J.-M. Lehn, N. Boumediene, A. Dupont-Gervais, A. Van Dorsselaer, B. Kneisel, D. Fenske, *J. Am. Chem. Soc.* **1997**, *119*, 10956.
[2] M. Albrecht, O. Blau, R. Fröhlich, *Chem. Eur. J.* **1999**, *5*, 48.
[3] I. Huc, J.-M. Lehn, *Proc. Natl. Acad. Sci. USA* **1997**, *94*, 2106.
[4] P. A. Brady, J. K. M. Sanders, *J. Chem. Soc., Perkin Trans. 1* **1997**, 3237; *Chem. Soc. Rev.* **1997**, *26*, 327.
[5] [5a] A. V. Eliseev, M. I. Nelen, *J. Am. Chem. Soc.* **1997**, *119*, 1147. – [5b] A. V. Eliseev, M. I. Nelen, *Chem. Eur. J.* **1998**, *4*, 825.
[6] B. Klekota, M. H. Hammond, B. L. Miller, *Tetrahedron Lett.* **1997**, *38*, 8639.
[7] H. Hioki, C. Still, *J. Org. Chem.* **1998**, *63*, 904.
[8] M. Crego Calama, R. Hulst, R. Fokkens, N. M. M. Nibbering, P. Timmerman, D. N. Reinhoudt, *Chem. Commun.* **1998**, 1021.
[9] For recent reviews see: [9a] A. Ganesan, *Angew. Chem. Int. Ed.* **1998**, *37*, 2828; – [9b] A. V. Eliseev, *Current Opinion Drug. Disc. Develop.* **1998**, *1*, 106; – [9c] A. V. Eliseev, J.-M. Lehn, *Current Top. Microbiol. Immuno.*, in press.
[10] [10a] D. F. Koshland Jr., *Adv. Enzymol.* **1960**, *22*, 45; – [10b] A. Fehrst, *Enzyme structure and mechanism*, 2nd ed., W. H. Freeman & Co, New-York, **1985**.
[11] For two examples, see: [11a] J. C. Adrian, C. G. Wilcox, *J. Am. Chem. Soc.* **1992**, *114*, 1398; – [11b] T. Hayashi, T. Asai, H. Hokazono, H. Ogoshi, *J. Am. Chem. Soc.* **1993**, *115*, 12210; see also references in these papers.
[12] The identification of these compounds is based on mass spectrometry and NMR analysis of the product mixture using **1** and **2** in various proportions.
[13] S. M. Nelson, C. V. Knox, M. McCann, *J. Chem. Soc., Dalton Trans.* **1981**, 1669.
[14] E. Fischer, A. Dilthey, *Justus Liebigs Ann. Chem.* **1904**, *335*, 336.
[15] The synthesis of the barbiturate receptor **6** is achieved in 3 steps starting from dimethyl 5-hydroxyisophthalate, which is O-alkylated with decyl bromide and K_2CO_3 in DMF at room temp. The resulting dimethyl-5-decyloxy-isophthalate is then treated with an access of 2,6-diaminopyridine monolithium salt in dry

UM00012919
NOVARTIS EXHIBIT 1017
Novartis v. Regents, IPR2023-01346
Page 1665 of 4460

THF at −78 °C.[16] The resulting diamine is acylated with decanoyl chloride in THF at room temp. to give **6** (see Experimental Section).

[16] K. Motesharei, D. C. Myles, *J. Am. Chem. Soc.* **1998**, *120*, 7328.
[17] S.-K. Chang, D. Van Engen, E. Fan, A. D. Hamilton, *J. Am. Chem. Soc.* **1991**, *113*, 7640.

[18] Crystal data for $\mathbf{3}_2$:**7** complex: $C_{30}H_{41}N_8O_3$, M_r 561.71, monoclinic, space group $P2_1/n$, a = 10.1810(3), b = 16.2190(4), c = 18.4800(5) Å, β = 95.490(1)°, V = 3037.5(3) Å^3, Z = 4, μ(Mo-K_α) = 0.082 mm^{-1}, ρ_{calc} = 1.23 gcm^{-3}. Orange crystals of dimensions 0.20 × 0.20 × 0.15 mm. 46830 Reflections collected, 2.5° ≤ θ ≤ 32.49°. 4428 Independent reflections having $I > 3\,\sigma(I)$. No absorption corrections. 370 Parameters. Final results: $R(F)$ = 0.064, $Rw(F)$ = 0.072, GOF = 1.064, maximal residual electron density = 0.687 eA^{-3}. Data were recorded with a *Nonius–KappaCCD* diffractometer, using graphite monochromatized Mo-K_α radiation (λ = 0.71071 Å), phi scans, 173 K. The structures were solved using direct methods and refined against $|F|$. H-Atoms were introduced as fixed contributors. For all computations, the *Enraf–Nonius* OpenMolN Package was used (OpenMoleN, Interactive Structure Solution, Nonius B.V., Delft, The Netherlands, 1997). Crystallographic data (excluding structure factors) for the structure of complex $\mathbf{3}_2$:**7** have been deposited with the *Cambridge Crystallographic Data Centre* as supplementary publication no. CCDC-127340. Copies of the data can be obtained free of charge on application to CCDC, 12 Union Road, Cambridge CB2 1EZ, UK [fax: +44 (0)1223/ 336-033; E-mail: deposit@ccdc.cam.ac.uk].

[19] [19a] For oxidative dimerization reactions of cyclic 1,3-diones see: K. M. Johnston, J. D. Stride, *Chem. Commun.* **1966**, 325; – [19b] J.-H. Ye, J. Xue, K.-Q. Ling, J.-H. Xu, *Tetrahedron Lett.* **1999**, *40*, 1365.
[20] T. Bunyapaiboonsri, J.-M. Lehn, work in progress.
[21] J.-M. Lehn, in: *Supramolecular Science: Where It Is and Where It Is Going* (Eds.: R. Ungaro, E. Dalcanale), Kluwer, Dordrecht, **1999**, pp. 287–304.

Received April 21, 1999
[O99228]

UM00012920
NOVARTIS EXHIBIT 1017
Novartis v. Regents, IPR2023-01346
Page 1666 of 4460

Competition between hydrogen bonding and donor–acceptor interactions in co-crystals of 1,3-dimethylbarbituric acid with aromatic amines

Valerio Bertolasi,* Paola Gilli, Valeria Ferretti and Gastone Gilli*

Dipartimento di Chimica and Centro di Strutturistica Diffrattometrica, Università di Ferrara, via L. Borsari, 46, 44100 Ferrara, Italy. E-mail: m38@dns.unife.it

Received (in Montpellier, France) 12th October 2000, Accepted 23rd November 2000
First published as an Advance Article on the web 15th February 2001

In contrast to cyclohexane-1,3-diones, 1,3-dimethylbarbituric acid (DMBA) does not enolize in crystals with formation of infinite H-bonded chains. Conversely, it forms crystals that completely lack traditional H-bond donors and hence are held together by C–H···O H-bonds and $C^{\delta+}=O^{\delta-}\cdots C^{\delta+}$ interactions of a putative donor–acceptor nature. In view of these specific features, the DMBA molecule appeared to be a good candidate to study the competition of the various intermolecular forces in its co-crystals with traditional H-bond donors such as *o*-nitrophenylhydrazine, *p*-nitroaniline, 2,6-diamino-4-phenyl-1,3,5-triazine, 2,6-diaminopyridine and *p*-aminopyridine. X-Ray crystallographic results are analyzed in terms of crystal packing forces and formation of specific packing *leitmotifs* (supramolecular synthons). The conclusions indicate that, though a rational crystal engineering of co-crystals is far from being accomplished, a reasonable rationalization of the complex intermolecular forces acting in competition in the crystal packing is henceforth achievable.

Intermolecular interactions are the basis for crystal engineering, their nature and strength determining their competitive importance in forming different crystal packings.[1] Among these intermolecular forces hydrogen bonds are the most important in view of their higher energy and directionality.[2] These properties have been extensively utilized in the planning of crystal adducts of molecules or ions having complementary acceptor and donor sites.[3] It has been observed that the strength of these directional forces, and then their ability to control the formation of intermolecular aggregates, depend on the nature and polarity of the donor and acceptor groups and become very high when the hydrogen bond is assisted by resonance[4] or by charge.[5] The three dimensional network in a crystal is determined by other forces as well, such as multipolar electrostatic, donor–acceptor and van der Waals interactions.[6] Often, the weaker C–H···X (X = O, N) hydrogen bonds also act as cooperative forces in stabilizing the net formed by stronger hydrogen bonds also involving oxygen and nitrogen atoms as donors which may be competitive, with respect to traditional hydrogen bonds, aiding in the formation of the crystal adducts.[7]

1,3-Dimethylbarbituric acid (DMBA) was originally chosen as the building block or tecton[1c] of infinite chains linked by strong O–H···O resonance-assisted H-bonds (RAHB)[4a,d] on the grounds of our previous findings that practically all cyclopentane- and cyclohexane-1,3-diones, and 1,3-diethyl-2-thiobarbituric acid[8] readily enolize and give the predicted chains. DMBA, however, proved impossible to enolize in all solvents tested, even those of very low polarity. Non-enolized DMBA, however, turned out to form very interesting crystals whose packing was dominated, because of the lack of traditional H-bond donors, by perpendicular donor–acceptor C=O···C=O interactions[6b,d] and C–H···O hydrogen bonds.[7] In view of the specific features of DMBA, it was decided to attempt its co-crystallization with a number of H-bond donors, mostly amines, aimed to substitute donor–acceptor with H-bond interactions, as well as to promote the diketone enolization by increasing the crystal environment basicity. Accordingly, this paper reports the preparation and crystal structure determination of DMBA (**1**) and of its adducts DMBA · *o*-nitrophenylhydrazine (**2**), DMBA · *p*-nitroaniline (**3**), DMBA · 2,6-diamino-4-phenyl-1,3,5-triazine (**4**), DMBA · 2,6-diaminopyridine (**5**) and 5′-hydroxy-5,5′-bi(DMBA) · *p*-aminopyridine (**6**).

Description of the structures

The molecules studied are sketched in Scheme 1 and are indicated by upper case (**A** and **B**) or lower case (**a–e**) letters according to their prevalent H-bond acceptor or donor nature. Preparative and X-ray crystallographic details for the six compounds investigated are reported in the Experimental. Table 1 reports the geometrical parameters of the intra- and intermolecular contacts and Fig. 1–6 show their most characteristic packing arrangements.

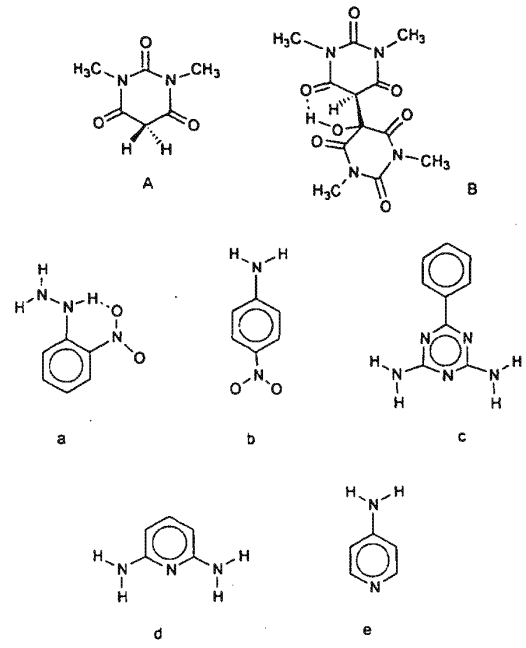
DMBA (1) A complex

Because DMBA does not have any traditional H-bond donor group, molecules interact in the crystal by means of C–H···O=C hydrogen bonds. Fig. 1(a) shows that the DMBA units are linked in chains by C2–H···O3 contacts (H···O3 = 2.38 Å) that are strictly comparable to the strongest C–H···O bonds formed with carbonyls by Cl_3C–H [average H···O of 2.31(1) Å] and –C≡C–H [average H···O of 2.40(2) Å],[7d] in agreement with the acidic nature of the $>C2H_2$ methylene group surrounded by two carbonyls. These chains are, in turn, transformed into two-dimensional arrays by weaker $C6H_3\cdots O1$ and $C5H_3\cdots O2$ interactions having an average H···O of 2.67 Å (Table 1). These C–H···O bonded planes are connected by nearly perpendicular $C^{\delta+}=O^{\delta-}\cdots C^{\delta+}=O^{\delta-}$ interactions of a plausible donor-acceptor nature [Fig. 1(b)]: C3=O2···C1 (C···O = 2.99 Å) on one side of the ring and C4=O3···C1 and C4=O3···C4 (C···O of 3.18 and 3.11 Å, respectively) on the other side. The three contacts are all well below the sum of the C and O van der Waals radii of 3.22 Å[9] and are to be compared with an

 DOI: 10.1039/b008262g

This journal is © The Royal Society of Chemistry and the Centre National de la Recherche Scientifique 2001

UM00012921
NOVARTIS EXHIBIT 1017
Novartis v. Regents, IPR2023-01346
Page 1667 of 4460



Scheme 1

average of *ca.* 3.4 Å and a minimum of some 2.8 Å found for this type of interaction.[6b] Strictly similar interaction patterns are observed in the crystal structure of 1,3-diethylbarbituric acid [Fig. 1(c)],[10] in spite of the completely different packing arrangement.

DMBA · *o*-nitrophenylhydrazine (2), A · a complex

The insertion of a molecule having three N–H H-bond donors substantially modifies the scheme of the interactions. The crystal structure consists now of rows of DMBA and 2-nitrophenylhydrazine molecules [Fig. 2(a)] held together in ribbons by means of N–H···O bonds complemented by C–H_3···O interactions. The ribbons are held in planes by C9–H···O3 hydrogen bonds and the planes are interconnected up and down through dipole–dipole interactions [Fig. 2(b)] between the C3=O2 carbonyl of DMBA and the N5–O4 moiety of the nitro group of 2-nitrophenylhydrazine (O4···C3 = 3.11, O2···N5 = 3.14 Å) and by C2–H···O1 bonds [Fig. 2(c)] linking dimers of DMBA molecules (H···O = 2.76 Å). The N3–H moiety of the hydrazinic group forms bifurcated hydrogen bonds, one intramolecular (N3···O5 = 2.61 Å) and the second intermolecular with the O1 oxygen of DMBA (N3···O1 = 2.88 Å), which is rather short in spite of the bifurcation that should weaken both H-bonds formed,[11] this strengthening can be accounted for in terms of increased N–H acidity caused by the *o*-nitro substituent. The apical NH_2 unit of the hydrazinic moiety forms two chelated and rather weak hydrogen bonds with the same O2 of DMBA (N4···O2 = 3.07 Å).

DMBA · *p*-nitroaniline (3), A · b complex

The *p*-nitroaniline adds a bifurcated N–H_2 donor and a nitro H-bond acceptor. Interestingly, it uses most of its H-bonding potentialities to form a chain of *p*-nitroanilines held together by H-bonds between its aminic and nitro functions (Fig. 3) this is a well-recognized supramolecular synthon already identified in other papers[1a,12] and appears to have a remarkable stability in spite of the rather weak H-bonds formed (average

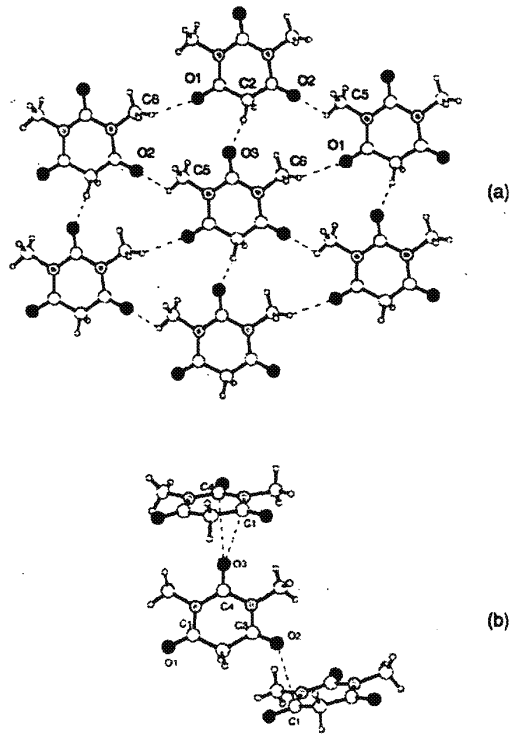


Fig. 1 (a) Layer of DMBA molecules of compound **1** linked by C–H···O interactions; (b) electrostatic donor–acceptor C=O···C=O interactions involving carbonyl groups of DBMA molecules; (c) C–H···O and C=O···C=O interactions in the crystal packing of 1,3-diethylbarbituric acid.[10]

N···O = 3.19 Å). On both sides of the chain, DMBA molecules bind by forming N3–H···O3 H-bonds by using the other N–H of the aminic function and leaving unoccupied every other position which can now accomodate a second DMBA molecule linked by chelated H-bonds: C11–H···O1 and C12–H···O2 (average H···O = 2.61 Å). The result is a planar sheet that is stacked with other similar ones through a dimeric C2–H···O1 (H···O = 2.64 Å) interaction identical to that reported in Fig. 2(c) for **2**.

DMBA · 2,6-diamino-4-phenyl-1,3,5-triazine (4), A · c complex

In this crystal structure, the asymmetric unit consists of two molecules of DMBA and two molecules of 2,6-diamino-4-phenyl-1,3,5-triazine. The asymmetric unit has now eight N–H

UM00012922
NOVARTIS EXHIBIT 1017
Novartis v. Regents, IPR2023-01346
Page 1668 of 4460

Table 1 Geometrical parameters (Å and degrees) with e.s.d.s in parentheses for hydrogen bonding and other molecular interactions with contact distances shorter than the sum of the van der Waals radii

D–H···A	D–H	H···A	D···A	D–H···A	X–D···A	D···A	X–D···A
1 = A							
C2–H21···O3^{i}	0.93(5)	2.38(5)	3.303(4)	170(4)	C4–O3···C1^{iv}	3.184(4)	118.8(3)
C5–H51···O2^{ii}	0.96	2.78	3.476(4)	130	C4–O3···C4^{iv}	3.114(4)	161.6(3)
C6–H62···O1^{iii}	0.96	2.56	3.132(4)	118	C3–O2···C1^{v}	2.986(4)	115.3(3)
Symmetry codes: *i*: $x, y, z+1$; *ii*: $x-1/2, y, z+1/2$; *iii*: $x+1/2, y, z+1/2$; *iv*: $1-x, 1/2-y, z-1/2$; *v*: $1/4+x, 1/4-y, 1/4+z$.							
2 = A · a							
N3–H30···O5^{i}	0.82(3)	2.00(3)	2.609(3)	130(3)	N5–O4···C3^{v}	3.108(3)	90.4(3)
N3–H30···O1^{i}	0.82(3)	2.22(2)	2.877(3)	138(3)	C3–O2···N5^{v}	3.136(3)	89.8(3)
N4–H410···O2^{ii}	0.82(2)	2.68(4)	3.067(3)	111(3)			
N4–H420···O2^{ii}	0.88(4)	2.71(3)	3.067(3)	106(3)			
C9–H9···O3^{iii}	0.92(2)	2.54(2)	3.305(3)	138(2)			
C2–H21···O1^{iv}	0.94(2)	2.76(2)	3.252(40)	114(2)			
C5–H53···O2^{ii}	0.92(3)	2.60(7)	3.262(40	130(5)			
Symmetry codes: *i*, x, y, z; *ii*: $x-1, y, z$; *iii*: $x, y-1, z-1$; *iv*: $1-x, 1-y, 1-z$; *v*: $1-x, 1-y, -z$.							
3 = A · b							
N3–H31···O3^{i}	0.80(3)	2.16(3)	2.949(3)	167(3)			
N3–H32···O4^{ii}	0.89(3)	2.34(3)	3.221(3)	168(3)			
N3–H32···O5^{ii}	0.89(3)	2.48(3)	3.168(3)	134(3)			
C2–H21···O2^{iii}	0.93(2)	2.64(2)	3.462(3)	149(2)			
C12–H12···O1^{iv}	0.94(2)	2.61(2)	3.216(3)	123(2)			
C11–H11···O1^{iv}	0.90(2)	2.62(2)	3.202(3)	123(2)			
Symmetry codes: *i*: x, y, z; *ii*: $1-x, 1/2+y, 1/2-z$; *iii*: $-x, 1-y, -1-z$; *iv*: $1+x, y, 1+z$.							
4 = A · c							
N61–H612···O11^{i}	1.02(5)	2.20(5)	3.192(5)	164(4)	C41–O31···C42^{vii}	3.083(5)	159.0(3)
N61–H611···O12^{i}	1.01(4)	2.12(4)	3.108(5)	162(3)	C41–O31···N22^{vii}	3.030(4)	160.2(3)
N71–H711···O22^{ii}	0.94(4)	2.05(4)	2.982(5)	170(3)			
N62–H621···O32^{iii}	0.83(4)	2.01(4)	2.958(5)	167(4)			
N71–H712···N32^{i}	0.90(3)	2.26(3)	3.132(4)	163(3)			
N62–H622···N51^{i}	0.89(4)	2.20(4)	3.049(4)	160(4)			
N72–H721···N52^{iv}	0.77(4)	2.31(4)	3.048(4)	161(4)			
N72–H722···N42^{v}	0.89(4)	2.13(4)	3.011(4)	167(4)			
C21–H212···O21^{vi}	0.92(4)	2.46(4)	3.361(5)	166(4)			
Symmetry codes: *i*: x, y, z; *ii*: $x-1, y, z$; *iii*: $x, y-1, z$; *iv*: $1-x, 1/2+y, 1/2-z$; *v*: $1-x, y-1/2, 1/2-z$; *vi*: $-x, -y, -z$; *vii*: $1-x, 1-y, -z$.							
5 = A · d							
N3–H30···O2^{i}	0.92(2)	1.87(2)	2.717(2)	153(1)			
N4–H410···O2^{i}	0.92(2)	2.02(2)	2.841(2)	147(2)			
N5–H510···O1^{ii}	0.93(2)	1.96(2)	2.883(2)	171(2)			
N5–H520···O1^{iii}	0.90(2)	1.99(2)	2.851(2)	158(2)			
N4–H420···O3^{iv}	0.89(2)	1.97(2)	2.858(2)	174(2)			
Symmetry codes: *i*: x, y, z; *ii*: $1-x, -y, -x$; *iii*: $x+1, y, z+1$; *iv*: $x, y-1, z$.							
6 = B · e							
O42–H42···O11^{i}	0.87(2)	1.76(2)	2.579(2)	156(2)	C31–O21···N22^{i}	3.008(1)	109.6(1)
N1–H1···O21^{i}	0.91(2)	1.83(2)	2.713(1)	162(2)	C31–O21···C32^{i}	2.788(1)	83.4(1)
N2–H21···O11^{ii}	0.90(3)	2.17(3)	3.054(2)	165(2)	C31–O21···C12^{i}	3.203(2)	77.2(1)
N2–H21···O12^{ii}	0.90(3)	2.71(3)	3.059(2)	104(2)	C22–O42···C42^{v}	2.812(2)	140.0(1)
N2–H22···O31^{iii}	0.92(4)	2.34(3)	3.080(3)	137(2)			
C2–H2···O31^{iii}	0.96(3)	2.55(2)	3.198(2)	125(1)			
C4–H4···O22^{iv}	0.92(3)	2.49(2)	3.262(2)	142(2)			
C4–H4···O42^{iv}	0.92(3)	2.57(2)	3.405(3)	152(2)			
C5–H5···O11^{iv}	0.94(2)	2.66(2)	3.320(2)	128(2)			
C51–H521···O32^{vi}	0.90(3)	2.77(3)	3.086(2)	102(2)			
C51–H531···O32^{vi}	1.00(4)	2.80(5)	3.086(2)	97(3)			
Symmetry codes: *i*: x, y, z; *ii*: $x, y+1, z+1$; *iii*: $x, y+1, z$; *iv*: $-x, -y, 1-z$; *v*: $-x, -y, -z$, *vi*: $x, y-1, z$.							

moieties as H-bond donors on four NH_2 groups, six N≡ aromatic acceptors, and six more DMBA carbonyls as acceptors. The resulting packing is extremely complex but can be understood, at least for our limited aims, from Fig. 4(a). One of the two triazine molecules makes an H-bonded ribbon (N72–H···N42: N···N = 3.01; N72–H···N52: N···N = 3.05 Å), again a well-known supramolecular synthon.[13] The second triazine molecule binds to both sides of the ribbon through N–H···N≡ bonds (N62–H···N51: N···N = 3.05; N71–H···N32: N···N = 3.13 Å) assuming, however, a position nearly perpendicular to the ribbon plane. In these connections four N–H groups have been engaged, leaving four others free for binding to a corresponding number of C=O DMBA oxygens [Fig. 4(b) and Table 1] (N62–H···O11: N···O = 3.19; N61–H···O12: N···O = 3.11; N62–H···O32: N···O = 2.96; N71–H···O22: N···O = 2.98 Å). This net of interconnections leaves out four acceptors [Fig. 4(a) and 4(b)], the two N31 and N41 atoms, which remain unsaturated, and the two DMBA carbonyls C31=O21 and C41=O31. The first makes the centrosymmetric C–H···O dimer already observed in structures 2 and 3 [Fig. 2(c)] while the second makes the donor–acceptor interaction [Fig. 4(c)] already observed in 1 [Fig. 1(b)].

DMBA · 2,6-diaminopyridine (5), A · d complex

In this crystal structure, enolization occurs and a hydrogen is transferred from the DMBA methylene to the pyridine nitro-

UM00012923
NOVARTIS EXHIBIT 1017
Novartis v. Regents, IPR2023-01346
Page 1669 of 4460

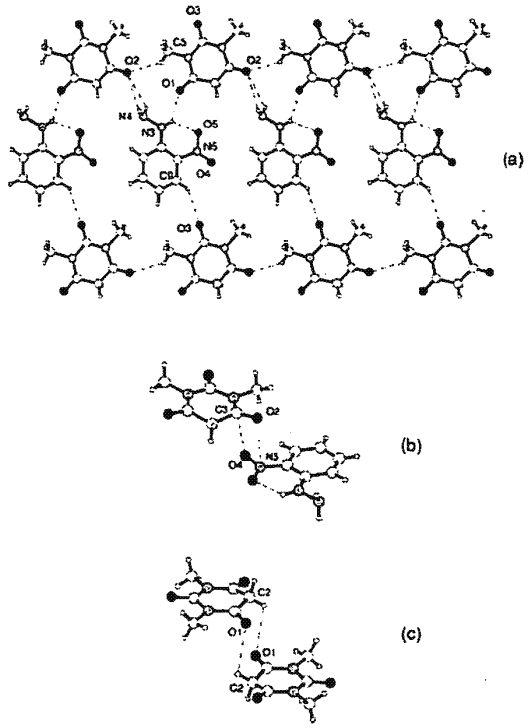


Fig. 2 (a) Layer of molecules of complex **2** (DMBA · *o*-nitrophenylhydrazine) linked by N–H···O and C–H···O hydrogen bonds; (b) dipole–dipole interactions between the carbonyl C3=O2 of DMBA and the N5–O4 moiety of the nitro group of *o*-nitrophenylhydrazine; (c) dimeric C–H···O interaction involving the acidic methylene group $C2H_2$ and the carbonyl C1=O1.

gen with formation of an ionic couple. The resulting packing is essentially ionic (CsCl type) with a coordination number of eight around both anions and cations. The donor–acceptor balance can now be summarized as follows: five N–H donors (one $\equiv NH^+$ and two $-NH_2$ groups) and three oxygens as acceptors (one C4=O3 carbonyl and the $C1–O1^{1/2-}$ and $C3–O2^{1/2-}$ groups on the β-diketoenolate moiety). Accordingly, two oxygens must become acceptors of two H-bonds each, and the third of just one, as actually found in Fig. 5.

(HBI-DMBA) · *p*-aminopyridine (6), B · e complex

The crystal structure is an aggregation of an unexpected condensation product of DMBA, that is 5′-hydroxy-5,5′-bis-DBMA (HBI-DBMA), with *p*-aminopyridine. One of the two DMBA moieties is enolized with transfer of one methylene

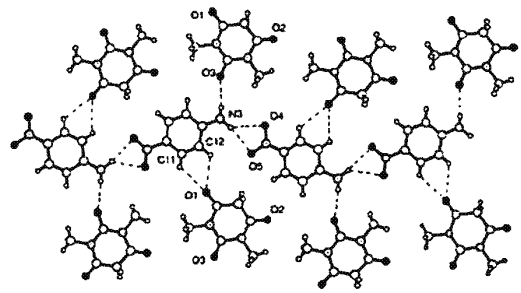


Fig. 3 Layer of molecules of complex **3** (DMBA · *p*-nitroaniline) linked by N–H···O and C–H···O hydrogen bonds.

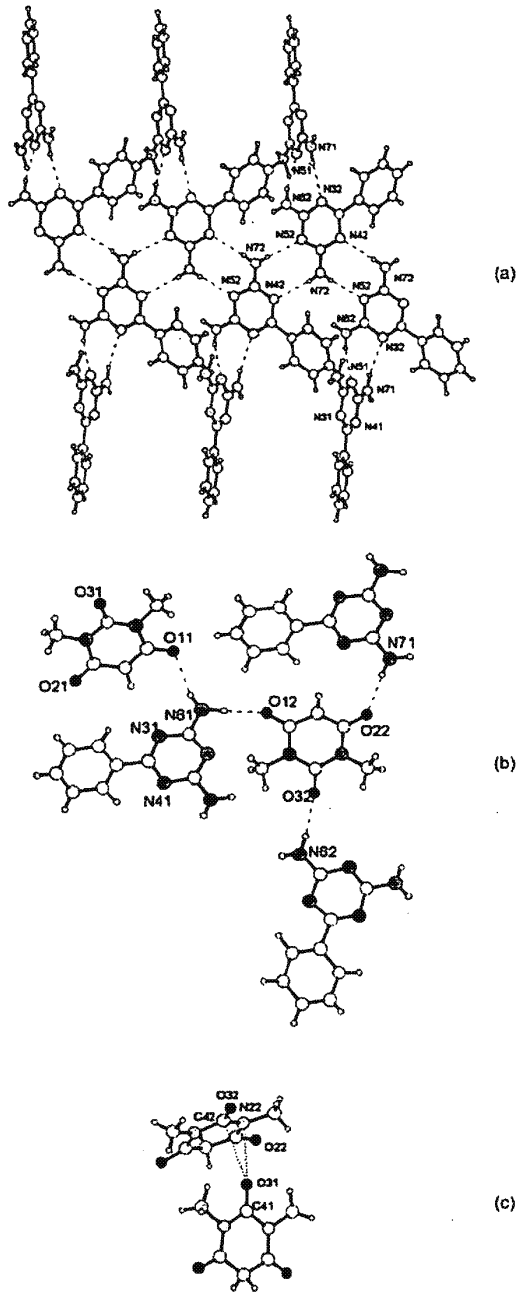


Fig. 4 (a) Molecular ribbon of complex **4** (DMBA · 2,6-diamino-4-phenyl-1,3,5-triazine) generated by molecules of 2,6-diamino-4-phenyl-1,3,5-triazine; (b) N–H···O interactions between molecules of DMBA and 2,6-diamino-4-phenyl-1,3,5-triazine; (c) donor–acceptor C=O···C/N interactions between molecules of DMBA.

proton to the pyridine nitrogen; the entire molecule is in a conformation fixed by the intramolecular O42–H···O11 bond and by the donor–acceptor interactions O21···N22 (3.01 Å), O21···C12 (3.20 Å) and O21···C32 (2.79 Å). The protonated *p*-aminopyridine is the donor of three NH···O bonds that are all formed [Fig. 6(a)] with the enolized moiety of HBI-DMBA. The $N–H^+···O^{1/2-}$ bond is stronger (N1–H···O21: N···O = 2.71 Å) than the H-bonds formed by the neutral

UM00012924
NOVARTIS EXHIBIT 1017
Novartis v. Regents, IPR2023-01346
Page 1670 of 4460

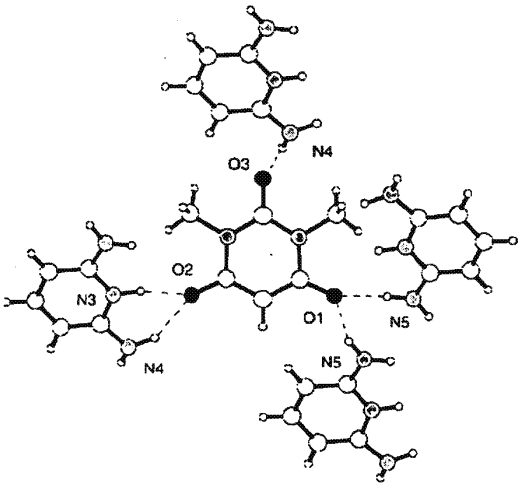


Fig. 5 The N–H···O hydrogen bond arrangements between the two ions for the complex 5 (DMBA$^-$·2,6-diaminopyridinium$^+$).

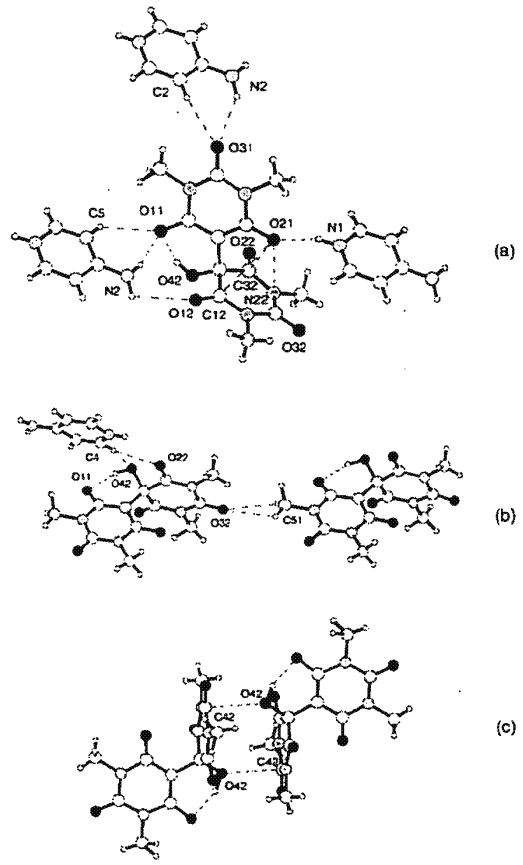


Fig. 6 (a) View of the ionic complex 6 (HBI-DMBA$^-$·*p*-aminopyridinium$^+$) showing the intramolecular electrostatic donor–acceptor interactions between the enolate O21 oxygen and the two carbonylic carbons C12 and C32, and nitrogen N22, and the N–H···O hydrogen bond arrangements between the two ions which, in two cases, are supported by C–H···O interactions; (b) simple C–H···O interactions; (c) donor–acceptor interactions between the hydroxyl O42 and C42 atoms.

amine group, which are substantially weaker (N2–H···O31, N2–H···O11 and N2–H···O12: N···O in the range 3.05–3.08 Å) despite being supported by two other weak C–H···O interactions. Having now used all the N–H donors to saturate the acceptors of the first DMBA subunit, the second one is compelled to interact in other ways through its four H-bond acceptors (the three carbonyls C12=O12, C32=O22, C42=O32 plus the O42 of the hydroxyl group). Only O12 is an acceptor of a weak N2–H···O12 H-bond, the other oxygens being involved in C–H···O bonds [Fig. 6(b)] or in a twin $>O^{\delta-}\cdots C^{\delta+}$ donor–acceptor interaction (O42···C42 = 2.81 Å), which is one of the shortest contacts of this type so far reported[6b] [Fig. 6(c)].

Discussion and conclusions

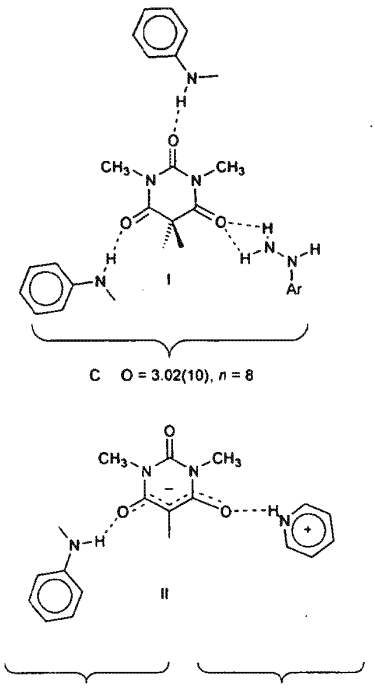
A first point to discuss is why DMBA does not enolize its β-diketone moiety to give the expected RAHB-bonded chains[4a,d] typical of all pentane- and hexane-1,3-diones and of the parent compound 1,3-diethyl-2-thiobarbituric acid, a behaviour shared by very few other β-diketones (among which the well-known case of 1,3-indandiones)[14] and most probably due to their unfavourable enolization energies. Accordingly, these have been evaluated, as energy differences between the enolized and non-enolized forms, by quantum mechanical calculations performed with GAUSSIAN98[15] at the DFT B3LYP/6-31G(d,p) level of theory for both energy and full geometry optimization. Molecules were assumed to have planar and the OH group of the enolic form to be in its *syn* conformation with respect to the C=C double bond. No zero point corrections were applied. The energies of the enols are calculated to be systematically higher than those of the diketone forms, and the corresponding enolization energies to increase in the order 1,3-cyclohexanedione, 1,3-cyclopentanedione, 1,3-dimethyl-2-thiobarbituric acid, DMBA and 1,3-indanedione, being 0.72, 0.84, 8.95, 10.96 and 11.64 kcal mol^{-1}, respectively. With respect to a β-diketone crystal, the corresponding crystal of the β-diketone enol form is then destabilized because of the loss of its enolization energy but stabilized by the formation of the infinite O–H···O RAHB-bonded chains (β-chains). The H-bond energy has been evaluated[4d] to be of the order of 7–15 kcal mol^{-1} for a series of crystals forming such O–H···O β-chains. Therefore, the order of the calculated enolization energies is consistent with the fact that only DMBA and 1,3-indandione do not undergo enolization, though the energy balance is such that it cannot exclude that the enolic forms of these molecules will be, in the end, crystallized, as actually happens for diethylthiobarbituric acid, which forms one of the strongest intermolecular O–H···O resonant H-bonds so far known (O···O = 2.455 Å; $E_{HB} \simeq 15.5$ kcal mol^{-1}).[4d,10]

Considering now the crystal packings of the compounds studied, two different factors must be accurately distinguished. The first is our putative ability to predict the actual packings by simple chemical intuition, and present findings clearly show that this aim cannot be reasonably pursued. The second concerns our degree of chemical understanding of molecular interactions, that is of the forces that determine the packing itself and the rest of this paper will show that, in this respect, the situation appears to be much more encouraging. For the sake of simplicity, the discussion is partitioned by type of molecular interaction: (i) traditional H-bonds that, in the present case, are N–H···O and, in one case, N–H···N bonds; (ii) C–H···O H-bonds, (iii) $C^{\delta+}=O^{\delta-}\cdots C^{\delta+}$ donor–acceptor interactions and (iv) the possible role played by cooperative packing *leitmotifs* (periodic supramolecular synthons)[1a].

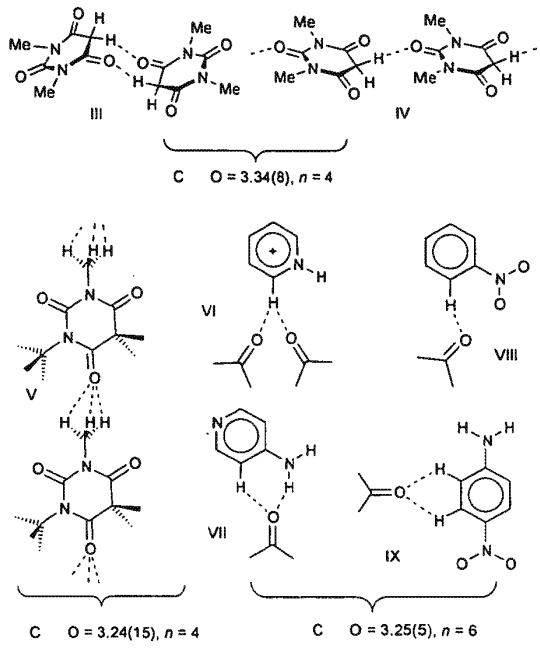
Traditional H-bonds

A summary of the N–H···O bonds formed by all the com-

UM00012925
NOVARTIS EXHIBIT 1017
Novartis v. Regents, IPR2023-01346
Page 1671 of 4460



Scheme 2



Scheme 3

pounds studied is reported in Scheme 2. They are chemically distinguishable into four different groups: (i) aromatic $\equiv N^+-H\cdots^{1/2-}O-C$ (II; structures **5** and **6**); (ii) aminic $>N-H\cdots^{1/2-}O-C$ (II; structures **5** and **6**); (iii) aminic and hydrazinic $>N-H\cdots O=C$ (I; structures **2**, **3**, **4**, **5** and **6**); and (iv) a single case of a three-centred hydrazinic interaction $ArN(H)-NH_2\cdots O=C$ (I, structure **2**). It is generally recognized that the strongest N–H···O bonds are of the type $N^+\cdots O^-$ with matching of the pK_a values of the H-bond donor and acceptor groups. These bonds are traditionally called *salt bridges*[2b] and more recently, low barrier H-bonds (LBHB)[16] or (+/−) charge-assisted H-bonds [(+/−) CAHB].[4c,17] According to expectation, the strongest H-bonds presently observed are of the (+/−) CAHB type between the protonated pyridine and the enolate of the DBMA β-diketone group [II, group (i)] with an average N···O distance of 2.715(2) Å, while those having only a charged acceptor [II, group (ii)] and the neutral ones [I, group (iii)] are progressively weaker with average N···O distances of 2.86(2) and 3.02(10) Å, respectively. However, no reason can be presently suggested for the fact that the secondary amine function, $Ar-NH-NH_2$, of the hydrazinic moiety seems able to produce shorter N–H···O=C< bonds with an N···O distance of 2.877 Å (structure **2**).

C–H···O H-bonds

Only in structure **5** are all H-bond acceptors saturated by traditional N–H donors. In the others, the donor–acceptor balance requires the formation of C–H···O and donor–acceptor interactions, the former being collected in Scheme 3. All C–H···O interactions involve a DMBA carbonyl as acceptor and, with the sole exception of VIII (where the C–H···O is in simple support of a normal N–H···O bond), the C–H groups implied are always chosen among the most acidic ones, in agreement with previous considerations on the role played by C–H acidity in determining the strength of C–H···O bonds.[7d,18] This is particularly true for the methylene of DMBA, which is so acidic as to impart the name barbituric acid, and it is the constituent of two well-defined supramolecular synthons in the form of dimers (III; structures **2**, **3** and **4**) or catemers (IV; structure **1** and 1,3-diethylbarbituric acid[10]), but it is also true for VI, VII and IX where the C–H used is *ortho* to either a N^+-H or to a NO_2 group. Finally, in V the two *ortho* carbonyls promote unusual acidic properties in the normally inert N-methyl group, and induce the formation of chains of DBMA molecules in **1**, **2** and **6** through a rather uncommon $-CH_3\cdots O=C$ interaction [average C···O = 3.24(15) Å] previously observed in the analogous compound trimethylisocyanurate.[19]

$C^{\delta+}=O^{\delta-}\cdots C^{\delta+}$ donor–acceptor interactions

Interactions between two carbonyls in molecular crystals have recently been reviewed by Allen and coworkers[6b] who have shown that they are of two different types. The first is an antiparallel matching of two C=O groups that is to be classified as a pure dipole–dipole interaction; the second is the nearly perpendicular C=O···C=O interaction displayed in Fig. 1(b), 4(c) and 6(c). In the present structures, no antiparallel C=O dipolar interactions are found, presumably because the trigonal disposition of carbonyls in DMBA wipes out the total molecular dipole moment [the only interaction of this type observed is that between a C=O and the N–O of a nitro group, shown in Fig 2(b)]. Perpendicular $N^{\delta-}\cdots C^{\delta+}=O^{\delta-}$ interactions have been extensively studied[20] in connection with the incipient nucleophilic addition of aminic nitrogen to carbonyl, which is observed in some molecular crystals. They are normally classified as charge-transfer or donor–acceptor interactions because the full range of C–N distances from van der Waals contacts to true C–N bonds is observed, together with a relevant carbonyl pyramidalization caused by the nitrogen approach. The present perpendicular C=O···C=O interactions could be, at least formally, classified as nucleophilic additions of oxygen, instead of nitrogen, to the electrophilic carbonyl carbon. They

UM00012926
NOVARTIS EXHIBIT 1017
Novartis v. Regents, IPR2023-01346
Page 1672 of 4460

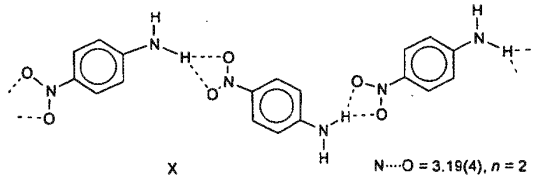
Table 2 Crystal data, data collection and refinement for 1–6

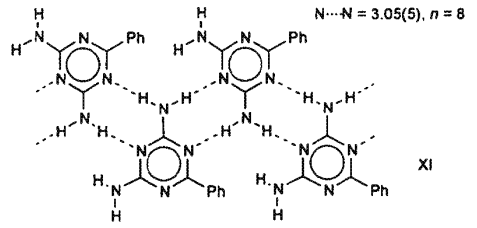
Formula	1 $C_6H_8N_2O_2$	2 $C_4H_4N_2O_2 \cdot C_6H_7N_3O_2$	3 $C_4H_4N_2O_2 \cdot C_6H_4N_2O_2$	4 $C_6H_8N_2O_2 \cdot C_6H_6N_2$	5 $C_6H_8N_2O_2 \cdot C_3H_3N_3$	6 $C_{12}H_{14}N_4O_2 \cdot C_3H_2N_2$
M	156.14	309.29	294.27	686.71	265.28	420.39
Crystal system	Orthorhombic	Triclinic	Monoclinic	Monoclinic	Triclinic	Triclinic
Space group	*Fdd2*	$P\bar{1}$	$P2_1/c$	$P2_1/c$	$P\bar{1}$	$P\bar{1}$
a/Å	15.642(3)	8.181(2)	7.586(2)	11.223(1)	7.262(1)	10.111(2)
b/Å	29.006(6)	12.891(2)	16.547(2)	7.226(2)	9.466(3)	11.747(2)
c/Å	6.556(1)	7.758(2)	10.856(2)	40.737(5)	9.839(1)	9.369(2)
α/°	90	104.73(2)	90	90	91.28(2)	107.72(1)
β/°	90	116.10(2)	97.10(2)	90.53(1)	109.46(1)	109.668(1)
γ/°	90	73.34(2)	90	90	94.01(2)	66.16(1)
U/Å^3	2974.5(9)	696.0(3)	1352.3(5)	3303.5(1)	535.4(2)	940.0(3)
Z	16	2	4	4	2	2
T/K	296	296	296	296	296	296
μ/cm^{-1}	1.13	1.17	1.15	1.01	1.04	1.18
Unique refins.	957	3026	2943	6435	2765	4524
R_{int}	0.026	0.013	0.017	0.019	0.012	0.009
Obs. refins. $[I > 2\sigma(I)]$	628	1947	1759	3539	2079	3840
R (obs. refins.)	0.046	0.048	0.053	0.066	0.041	0.040
wR (all refins.)	0.126	0.135	0.147	0.203	0.116	0.116

have, however, remarkably different features. The oxygen never approaches the carbon to less than about 2.80 Å, a distance that is shorter by only 0.40 Å than the van der Waals contact of 3.22 Å, while the accepting carbonyl is never pyramidalized in a sensible way. This may suggest that these $C^{\delta+}{=}O^{\delta-}\cdots C^{\delta+}$ interactions are at the very limit of charge transfer and, for practical purposes, preferably classifiable as closed-shell electrostatic interactions.

Cooperative packing *leitmotifs*

One of the main open questions of crystal engineering is whether there are specific packing patterns (supramolecular synthons) associated with some specific molecules or molecular fragments (tectons) that may "ensure generality and reproducibility"[1a] in our attempts at crystal design. Though this is not the kind of question that can be answered on the grounds of the few present structures, there are actually two cases (structures 3 and 4; Scheme 4) that seem to support the efficacy of supramolecular synthons in determining the overall crystal packing. In fact, *p*-nitroaniline and 2-aminotriazine (part of the 2,6-diamino-4-phenyl-1,3,5-triazine molecule in 4) are well known to form in their crystals, or in crystals of their derivatives, typical patterns in the form of chains (X)[12] and ribbons (XI)[13], respectively, and exactly these motifs are found in co-crystals 3 and 4, in spite of the presence of the co-existing DMBA molecules.





Scheme 4

Experimental

All reagents were purchased from Aldrich. Compounds 2–5 were obtained by crystallizing the two components in a 1 : 1 molar ratio from the appropriate solvent. Compound 1 was recrystallized from toluene, while co-crystals 2, 3 and 5 were crystallized from a mixture of diethyl acetate and THF, and 4 and 6 from methanol. Co-crystal 6 turned out to be an unexpected complex obtained by crystallizing DMBA with 4-aminopyridine in hot methanol in which DMBA has undergone oxidative dimerization with formation of 5'-hydroxy-5,5'-bis(DMBA).

All X-ray diffraction data were collected at room temperature, 1 on a Nonius Kappa CCD diffractometer and 2–6 on an Enraf-Nonius CAD-4 diffractometer using graphite-monochromated Mo-Kα radiation ($\lambda = 0.710\,69$ Å) with an $\omega/2\theta$ scan technique. Lattice constants were determined by least-squares fitting of the setting angles of 1708 reflections for 1 and 25 for 2–6. All intensities were corrected for Lorentz and polarization effects. The structures were solved by direct methods using the SIR92[21] system of programs and all other calculations were accomplished using SHELXL-97[22] and PARST.[23] All structures were refined on F^2 by full-matrix least-squares methods with anisotropic non-H atoms and isotropic hydrogens. Crystal data are reported in Table 2.

CCDC reference number 440/246. See http://www.rsc.org/suppdata/nj/b0/b008262g/ for crystallographic files in .cif format.

Acknowledgements

This work was supported by the Italian Ministry for University and Scientific and Technological Research (MURST, Rome).

References

1 (*a*) G. R. Desiraju, *Angew. Chem., Int. Ed. Engl.*, 1995, **34**, 2311; (*b*) G. R. Desiraju and C. V. K. Sharma, in *The Crystal as a Supramolecular Entity*, ed. G. R. Desiraju, John Wiley & Sons, Chichester, 1996, ch. 2, p. 31; (*c*) D. Simars, D. Su and J. D. Wuest, *J. Am. Chem. Soc.*, 1991, **113**, 4696.

2 (*a*) M. C. Etter, *Acc. Chem. Res.*, 1990, **23**, 120; (*b*) G. A. Jeffrey, *An Introduction to Hydrogen Bonding*, Oxford University Press, New York, 1997.

3 (*a*) M. C. Etter, Z. Urbanczyk-Lipkowska, M. Zia-Ebrahimi and T. W. Panunto, *J. Am. Chem. Soc.*, 1990, **112**, 8415; (*b*) J.-M. Lehn, M. Mascal, A. De Cian and J. Fischer, *J. Chem. Soc., Perkin Trans. 2*, 1992, 461; (*c*) J. A. Zerkowski, J. C. MacDonald, C. T. Seto, D. A. Wierda and G. M. Whitesides, *J. Am. Chem. Soc.*, 1994, **116**, 2382.

4 (*a*) G. Gilli, V. Bertolasi, V. Ferretti and P. Gilli, *Acta Crystallogr., Sect. B*, 1993, **49**, 564; (*b*) V. Bertolasi, P. Gilli, V. Ferretti and G. Gilli, *Acta Crystallogr., Sect. B*, 1995, **51**, 1004; (*c*) P. Gilli,

UM00012927
NOVARTIS EXHIBIT 1017
Novartis v. Regents, IPR2023-01346
Page 1673 of 4460

V. Ferretti, V. Bertolasi and G. Gilli, in *Advances in Molecular Structure Research*, ed. M. Hargittai and I. Hargittai, JAI Press, Greenwich, CT, 1996, vol. 2, p. 67; (*d*) V. Bertolasi, P. Gilli, V. Ferretti and G. Gilli, *Chem. Eur. J.*, 1996, **2**, 925; (*e*) V. Bertolasi, P. Gilli, V. Ferretti and G. Gilli, *Acta Crystallogr., Sect. B*, 1998, **54**, 50.

5 (*a*) V. A. Russell, M. C. Etter and M. D. Ward, *J. Am. Chem. Soc.*, 1994, **116**, 1941; (*b*) M. Mascal, P. S. Fallon, A. S. Batsanov, B. R. Heywood, S. Champ and M. Colclough, *J. Chem. Soc., Chem. Commun.*, 1995, 805.

6 (*a*) H.-B. Bürgi, J. D. Dunitz and E. Shefter, *Acta Crystallogr., Sect. B*, 1974, **30**, 1517; (*b*) F. H. Allen, C. A. Baalham, J. P. M. Lommerse and P. R. Raithby, *Acta Crystallogr., Sect B*, 1998, **54**, 320; (*c*) V. Bertolasi, P. Gilli, V. Ferretti, G. Gilli, K. Vaughan and J. V. Jollimore, *Acta Crystallogr., Sect B*, 1999, **55**, 994; (*d*) O. Ermer and J. Neudörfl, *Helv. Chim. Acta*, 2000, **83**, 300; (*e*) J. D. Dunitz, in *The Crystal as a Supramolecular Entity*, ed. G. R. Desiraju, John Wiley & Sons, Chichester, 1996, ch. 1, p. 1.

7 (*a*) R. Taylor and O. Kennard, *J. Am. Chem. Soc.*, 1982, **104**, 5063; (*b*) V. R. Pedireddi, W. Jones, A. P. Chorlton and R. Docherty, *Chem. Commun.*, 1996, 997; (*c*) G. A. Jeffrey, *J. Mol. Struct.*, 1999, **485–486**, 293; (*d*) G. R. Desiraju and T. Steiner, *The Weak Hydrogen Bond in Structural Chemistry and Biology*, Oxford University Press, Oxford, UK, 1999.

8 J.-P. Bideau, G. Bravic and A. Filhol, *Acta Crystallogr., Sect. B*, 1977, **33**, 3847.

9 A. Bondi, *J. Phys. Chem.*, 1964, **68**, 441.

10 J.-P. Bideau, P. V. Huong and S. Toure, *Acta Crystallogr., Sect. B*, 1976, **32**, 481.

11 R. Taylor, O. Kennard and W. Versichel, *J. Am. Chem. Soc.*, 1984, **106**, 244.

12 T. W. Panunto, Z. Urbanczyk-Lipkowska, R. Johnson and M. C. Etter, *J. Am. Chem. Soc.*, 1987, **109**, 7786.

13 (*a*) J. N. Varghese, A. M. O'Connell and E. N. Maslen, *Acta Crystallogr., Sect. B*, 1977, **33**, 2102; (*b*) F. H. Beijer, R. P. Sijbesma, J. A. J. M. Vekemans, E. W. Meijer, H. Kooijman and A. L. Spek, *J. Org. Chem.*, 1996, **61**, 6371; (*c*) M. Scoponi, E. Polo, F. Pradella, V. Bertolasi, V. Carassiti and P. Goberti, *J. Chem. Soc., Perkin Trans. 2*, 1992, 1127.

14 (*a*) G. Bravic, J. Gaultier and C. Hauw, *Cryst. Struct. Commun.*, 1974, **3**, 215; (*b*) G. Bravic, F. Bechtel, J. Gaultier and C. Hauw, *Cryst. Struct. Commun.*, 1976, **5**, 1; (*c*) F. Bechtel, G. Bravic, J. Gaultier and C. Hauw, *Acta Crystallogr., Sect. B*, 1974, **30**, 1499.

15 M. J. Frisch, G. W. Trucks, H. B. Schlegel, G. E. Scuseria, M. A. Robb, J. R. Cheeseman, V. G. Zakrzewski, J. A. Montgomery, Jr., R. E. Stratmann, J. C. Burant, S. Dapprich, J. M. Millam, A. D. Daniels, K. N. Kudin, M. C. Strain, O. Farkas, J. Tomasi, V. Barone, M. Cossi, R. Cammi, B. Mennucci, C. Pomelli, C. Adamo, S. Clifford, J. Ochterski, G. A. Petersson, P. Y. Ayala, Q. Cui, K. Morokuma, D. K. Malick, A. D. Rabuck, K. Raghavachari, J. B. Foresman, J. Cioslowski, J. V. Ortiz, A. G. Baboul, B. B. Stefanov, G. Liu, A. Liashenko, P. Piskorz, I. Komaromi, R. Gomperts, R. L. Martin, D. J. Fox, T. Keith, M. A. Al-Laham, C. Y. Peng, A. Nanayakkara, C. Gonzalez, M. Challacombe, P. M. W. Gill, B. Johnson, W. Chen, M. W. Wong, J. L. Andres, C. Gonzalez, M. Head-Gordon, E. S. Replogle and J. A. Pople, GAUSSIAN 98, Rev. A.7, Gaussian, Inc., Pittsburgh PA, 1998.

16 (*a*) W. W. Cleland and M. M. Kreevoy, *Science*, 1994, **264**, 1887; (*b*) S. Cassidy, L. A. Reinhardt, W. W. Cleland and P. A. Frey, *J. Chem. Soc., Perkin Trans. 2*, 1999, 635.

17 P. Gilli, V. Bertolasi, V. Ferretti and G. Gilli, *J. Am. Chem. Soc.*, 1994, **116**, 909.

18 V. R. Pedireddi and G. R. Desiraju, *J. Chem. Soc., Chem. Commun.*, 1992, 988.

19 V. R. Thalladi, K. Panneerselvam, C. J. Carrell, H. L. Carrel and G. R. Desiraju, *J. Chem. Soc., Chem. Commun.*, 1995, 341.

20 (*a*) H. B. Bürgi, J. D. Dunitz and E. Shefter, *J. Am. Chem. Soc*, 1973, **95**, 5065; (*b*) W. B. Schweizer, G. Procter, M. Kaftory and J. D. Dunitz, *Helv. Chim. Acta*, 1978, **61**, 2783.

21 A. Altomare, G. Cascarano, C. Giacovazzo, A. Guagliardi, M. C. Burla, G. Polidori and M. Camalli, *J. Appl. Crystallogr.*, 1994, **27**, 435.

22 G. M. Sheldrick, SHELXL97, Program for Crystal Structure Refinement, University of Göttingen, Göttingen, Germany, 1997.

23 M. Nardelli, *J. Appl. Crystallogr.*, 1995, **28**, 659.

UM00012928
NOVARTIS EXHIBIT 1017
Novartis v. Regents, IPR2023-01346
Page 1674 of 4460

Acta Crystallographica Section B
Structural
Science
ISSN 0108-7681

General rules for the packing of hydrogen-bonded crystals as derived from the analysis of squaric acid anions: aminoaromatic nitrogen base co-crystals

Valerio Bertolasi,* Paola Gilli, Valeria Ferretti and Gastone Gilli

Centro di Strutturistica Diffrattometrica and Dipartimento di Chimica, Università di Ferrara, Via L. Borsari 46, 44100 Ferrara, Italy

Correspondence e-mail: m38@dns.unife.it

Received 20 April 2001
Accepted 15 May 2001

Preparation and single-crystal X-ray structure determination of three co-crystals of hydrogen squarate, HSQ^-, with 2-aminopyrimidine, 3-aminopyridine and 4-aminopyridine, and one of squarate, SQ^{2-}, with 8-aminoquinoline are reported. Their crystal packings are analyzed and discussed in terms of the intermolecular O—H···O, N—H···O/N and C—H···O hydrogen bonds formed. Although the fine details of the supramolecular architecture are barely rationalizable, the comparative analysis of the data makes it possible to suggest some simple rules that may be of general application for the packing of hydrogen-bonded crystals, *i.e.* **Rule 1**: 'All hydrogen-bond acceptors available in a molecule will be engaged in hydrogen bonding as far as there are available donors'; **Rule 2**: 'The hydrogen-bond acceptors will be saturated in order of decreasing strength of the hydrogen bonds formed'.

1. Introduction

The most recent attempts at the crystal engineering of molecular crystals (Desiraju, 1989) is largely based on the arrangements of building blocks (tectons; Simars *et al.*, 1991) consisting of molecules or ions which present complementary molecular interactions (supramolecular synthons; Desiraju, 1995). In order to produce stable co-crystals it is therefore indispensable to have a detailed knowledge of the forces that may determine the structural motifs of the crystalline materials. Hydrogen bonds, in view of their energy and directionality, are among the most important forces utilized by the molecules to interact (Etter, 1990; Bertolasi *et al.*, 1995; Jeffrey, 1997) and the formation of co-crystals is often directed by heteromolecular hydrogen bonds which turn out to be stronger than the homomolecular ones (Desiraju & Sharma, 1995). In particular, the mixing of couples of molecules with acid/base properties may make a crucial improvement in the predictability of the recognition processes owing to the dominating contribution of charge-assisted hydrogen bonds (Russell *et al.*, 1994; Aakeröy *et al.*, 1996; Burchell *et al.*, 2001).

Squaric acid, H_2SQ, is a molecule frequently used to build up co-crystals with organic bases to give specific two- or three-dimensional aggregates (Reetz *et al.*, 1994; Karle *et al.*, 1996; Angelova *et al.*, 1996; Bouma *et al.*, 1999; McLean, Wheatley, Ferguson & Glidewell, 1999; McLean, Wheatley, Ferguson, Glidewell & Lough, 1999). Being a strong diprotic acid (pK_1 = 1.2–1.7; pK_2 = 3.2–3.5; Ireland & Walton, 1967; MacDonald, 1968) it can crystallize as H_2SQ (Semmingsen *et al.*, 1977; Gilli & Bertolasi, 1990) as well as HSQ^- or SQ^{2-} anions, the last

© 2001 International Union of Crystallography
Printed in Great Britain – all rights reserved

UM00012929
NOVARTIS EXHIBIT 1017
Novartis v. Regents, IPR2023-01346
Page 1675 of 4460

Table 1
Experimental details.

	(1)	(2)	(3)	(4)
Crystal data				
Chemical formula	$C_7H_5N_3\cdot C_4HO_4$	$C_7H_7N_2\cdot C_4HO_4$	$C_7H_7N_2\cdot C_4HO_4$	$C_6H_9N_2\cdot 1/2(C_4O_4)$
Chemical formula weight	209.17	208.18	208.17	201.2
Cell setting, space group	Triclinic, $P\overline{1}$	Triclinic, $P\overline{1}$	Monoclinic, $P2_1/c$	Triclinic, $P\overline{1}$
a, b, c (Å)	8.279 (1), 10.184 (1), 5.353 (2)	3.812 (1), 11.012 (2), 21.942 (5)	10.283 (3), 7.068 (1), 12.642 (2)	7.209 (1), 7.861 (1), 18.443 (1)
α, β, γ (°)	99.72 (2), 104.05 (2), 87.73 (1)	100.78 (2), 91.66 (2), 88.26 (2)	90, 97.95 (2), 90	108.07 (1), 91.62 (1), 89.83 (1)
V (Å^3)	431.5 (2)	904.1 (4)	910.0 (3)	454.7 (1)
Z	2	4	4	2
D_x (Mg m^{-3})	1.610	1.529	1.519	1.470
Radiation type	Mo $K\alpha$	Mo $K\alpha$	Mo $K\alpha$	Mo $K\alpha$
No. of reflections for cell parameters	25	25	25	25
θ range (°)	8–14	8–13	9–13	7–13
μ (mm^{-1})	0.132	0.123	0.122	0.104
Temperature (K)	296 (2)	296 (2)	296 (2)	296 (2)
Crystal form, colour	Plate, colourless	Prism, pale yellow	Irregular, colourless	Irregular, brown
Crystal size (mm)	0.52 × 0.36 × 0.10	0.52 × 0.30 × 0.14	0.60 × 0.36 × 0.28	0.50 × 0.40 × 0.38
Data collection				
Diffractometer	Enraf–Nonius CAD-4	Enraf–Nonius CAD-4	Enraf–Nonius CAD-4	Enraf–Nonius CAD-4
Data collection method	$\omega/2\theta$ scans	$\omega/2\theta$ scans	$\omega/2\theta$ scans	$\omega/2\theta$ scans
No. of measured, independent and observed parameters	2769, 2078, 1596	4454, 3913, 2471	2995, 2647, 2216	2828, 2628, 2310
Criterion for observed reflections	$I > 2\sigma(I)$	$I > 2\sigma(I)$	$I > 2\sigma(I)$	$I > 2\sigma(I)$
R_{int}	0.013	0.022	0.030	0.010
θ_{max} (°)	28.00	27.00	30	29.97
Range of h, k, l	$0 \rightarrow h \rightarrow 10$ $-13 \rightarrow k \rightarrow 13$ $-7 \rightarrow l \rightarrow 6$	$0 \rightarrow h \rightarrow 4$ $-13 \rightarrow k \rightarrow 14$ $-28 \rightarrow l \rightarrow 27$	$0 \rightarrow h \rightarrow 14$ $0 \rightarrow k \rightarrow 9$ $-17 \rightarrow l \rightarrow 17$	$0 \rightarrow h \rightarrow 10$ $-10 \rightarrow k \rightarrow 11$ $-11 \rightarrow l \rightarrow 11$
No. and frequency of standard reflections	3 every 120 min	3 every 120 min	3 every 120 min	3 every 120 min
Refinement				
Refinement on	F^2	F^2	F^2	F^2
$R[F^2>2\sigma(F^2)]$, $wR(F^2)$, S	0.0498, 0.1496, 1.016	0.064, 0.2029, 1.056	0.0379, 0.1186, 1.072	0.043, 0.1295, 1.056
No. of reflections and parameters used in refinement	2078, 164	3913, 336	2647, 169	2628, 172
H-atom treatment	All H-atom parameters refined	All H-atom parameters refined	All H-atom parameters refined	All H-atom parameters refined
Weighting scheme	$w = 1/[\sigma^2(F_o^2) + (0.1114P)^2 + 0.0000P]$, where $P = (F_o^2 + 2F_c^2)/3$	$w = 1/[\sigma^2(F_o^2) + (0.1236P)^2 + 0.1121P]$, where $P = (F_o^2 + 2F_c^2)/3$	$w = 1/[\sigma^2(F_o^2) + (0.0708P)^2 + 0.1027P]$, where $P = (F_o^2 + 2F_c^2)/3$	$w = 1/[\sigma^2(F_o^2) + (0.0847P)^2 + 0.0419P]$, where $P = (F_o^2 + 2F_c^2)/3$
$(\Delta/\sigma)_{max}$	0.003	0.018	0.006	0.012
$\Delta\rho_{max}, \Delta\rho_{min}$ (e Å^{-3})	0.341, −0.33	0.347, −0.388	0.367, −0.175	0.269, −0.271
Extinction method	None	*SHELXL97* (Sheldrick, 1997)	*SHELXL97* (Sheldrick, 1997)	None
Extinction coefficient	–	0.011 (4)	0.036 (5)	–

Computer programs used: *CAD-4* (Enraf–Nonius, 1984), *MolEN* (Fair, 1990), *SIR92* (Altomare *et al.*, 1994), *SHELXL97* (Sheldrick, 1997).

two being particularly suited to interact with molecules rich in hydrogen-bond donors such as the aminoaromatic bases presently investigated, which can be hydrogen-bond donors both by the aminic group and the aromatic $\equiv N^+H$ function obtained by proton transfer from the squaric acid itself. In general, squaric acid and its anions are of potential interest in crystal engineering because of their nature of small, flat and rigid molecules which can self-assemble by strong $-O=C-C=C-OH\cdots$ resonance-assisted hydrogen bonds (RAHBs; Gilli *et al.*, 1989; Gilli *et al.*, 1993; Bertolasi *et al.*, 1996) in H_2SQ and HSQ^-, or even stronger $-O-H\cdots O^-$ [negative charge-assisted hydrogen bonds (–)CAHB] (Gilli *et al.*, 1994, 1996) in HSQ^- and moreover may be acceptors of further hydrogen bonds donated by aminic, iminic and hydroxilic functions. Finally, squaric acid may donate one or two protons to planar aromatic nitrogen bases forming $\equiv N^+H\cdots O^-$ bonds which potentially belong to the class of $\equiv N^+H\cdots O^- \leftrightarrow \equiv N\cdots HO$ bonds which are often called LBHBs (low-barrier hydrogen bonds, Cleland & Kreevoy, 1994; Cassidy *et al.*, 1999) or (+/–)CAHB (positive/negative charge-assisted hydrogen

UM00012930
NOVARTIS EXHIBIT 1017
Novartis v. Regents, IPR2023-01346
Page 1676 of 4460

Table 2
Selected bond distances (Å).

(1)			
O1—C1	1.304 (2)	N1—C5	1.351 (2)
O2—C2	1.259 (2)	N1—C6	1.346 (2)
O3—C3	1.223 (2)	N2—C5	1.347 (2)
O4—C4	1.220 (2)	N2—C8	1.316 (2)
C1—C2	1.405 (2)	N3—C5	1.312 (2)
C1—C4	1.445 (2)	C6—C7	1.351 (3)
C2—C3	1.470 (2)	C7—C8	1.392 (2)
C3—C4	1.516 (2)		
(2)			
O11—C11	1.307 (3)	O12—C12	1.307 (4)
O21—C21	1.240 (3)	O22—C22	1.239 (3)
O31—C31	1.215 (3)	O32—C32	1.198 (4)
O41—C41	1.242 (3)	O42—C42	1.239 (3)
C11—C21	1.434 (3)	C12—C22	1.431 (4)
C11—C41	1.412 (4)	C12—C42	1.425 (4)
C21—C31	1.480 (4)	C22—C32	1.496 (4)
C31—C41	1.485 (3)	C32—C42	1.490 (4)
N11—C81	1.329 (4)	N12—C82	1.307 (4)
N11—C91	1.322 (4)	N11—C92	1.353 (4)
N21—C51	1.344 (4)	N22—C52	1.348 (4)
C51—C61	1.404 (4)	C52—C62	1.392 (4)
C51—C91	1.398 (3)	C52—C92	1.400 (4)
C61—C71	1.346 (4)	C62—C72	1.378 (4)
C71—C81	1.386 (4)	C72—C82	1.379 (4)
(3)			
O1—C1	1.309 (1)	N1—C7	1.338 (2)
O2—C2	1.249 (1)	N1—C8	1.343 (2)
O3—C3	1.225 (1)	N2—C5	1.336 (1)
O4—C4	1.232 (1)	C5—C6	1.411 (2)
C1—C2	1.423 (1)	C5—C9	1.410 (1)
C1—C4	1.441 (1)	C6—C7	1.363 (2)
C2—C3	1.482 (1)	C8—C9	1.360 (2)
C3—C4	1.503 (1)		
(4)			
O1—C1	1.256 (1)	C4—C5	1.358 (2)
O2—C2	1.243 (1)	C5—C6	1.417 (2)
C1—C2	1.465 (2)	C6—C7	1.420 (1)
C1—C7	1.459 (2)	C6—C8	1.407 (2)
N1—C3	1.328 (2)	C7—C11	1.429 (2)
N1—C7	1.369 (1)	C8—C9	1.364 (2)
N2—C11	1.367 (1)	C9—C10	1.402 (2)
C3—C4	1.392 (2)	C10—C11	1.387 (1)

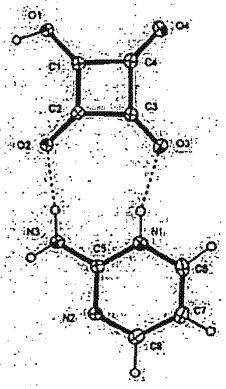


Figure 1
The molecular components of (1), showing the atom-labelling scheme. Displacement ellipsoids are drawn at the 30% probability level.

bonds; Gilli *et al.*, 1994, 1996), and whose strength is determined by the matching of the pK_a values of the squaric acid and of the base involved.

The present paper reports the crystal structures of four adducts between squaric acid and aminoaromatic bases, *i.e.* 2-amino-1,3-pyrimidine, 3-amino- and 4-aminopyridine and 8-aminoquinoline, which are found to form either $(HSQ^-)_2$ dimers or SQ^{2-} isolated anions. It is shown that the crystal packing analysis of these co-crystals seems able to suggest some rules of general validity for all crystals whose supramolecular architecture is dominated by hydrogen-bond formation.

2. Experimental

Squaric acid and aminoaromatic nitrogen bases were dissolved in water/ethanol mixture in the molar ratio 1:1 for (1)–(3) and 1:2 for (4), and allowed to crystallize slowly at room temperature. Crystal data, data collection and refinement details are given in Table 1.[1] X-ray diffraction data were collected at room temperature on an Enraf–Nonius CAD-4 diffractometer using graphite-monochromated Mo $K\alpha$ radiation (λ = 0.71069 Å) with $\omega/2\theta$ scans. Lattice constants were determined by least-squares fitting of the setting angles of 25 reflections in the range $9 \leq \theta \leq 14°$. The intensities of three

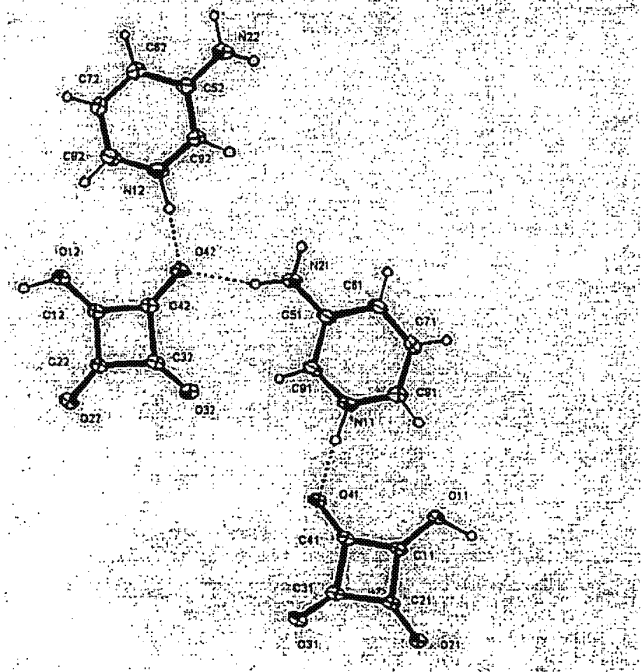


Figure 2
The molecular components of (2), showing the atom-labelling scheme. Displacement ellipsoids are drawn at the 30% probability level.

UM00012931
NOVARTIS EXHIBIT 1017
Novartis v. Regents, IPR2023-01346
Page 1677 of 4460

Table 3
Hydrogen-bonding parameters (Å, °).

	D—H	H···A	D···A	D—H···A
(1)				
O1—H1···O2^{i}	0.94 (2)	1.58 (2)	2.498 (2)	163 (2)
N3—H32···O2	0.92 (2)	1.83 (2)	2.745 (2)	177 (2)
N1—H10···O3	0.94 (2)	1.88 (2)	2.796 (2)	165 (2)
N3—H31···N2^{ii}	0.92 (2)	2.13 (2)	3.044 (2)	176 (2)
C7—H7···O4^{iii}	0.92 (2)	2.33 (2)	3.215 (2)	159 (2)
C8—H8···O1^{iv}	1.04 (2)	2.29 (2)	3.263 (2)	156 (2)
C6—H6···O3^{iii}	1.00 (2)	2.38 (2)	3.311 (2)	154 (2)
(2)				
O12—H12···O22^{v}	1.11 (4)	1.41 (4)	2.507 (3)	169 (4)
O11—H11···O21^{vi}	0.90 (4)	1.63 (4)	2.514 (3)	166 (3)
N12—H120···O42	1.14 (7)	1.54 (7)	2.669 (3)	170 (6)
N11—H110···O41	1.11 (4)	1.60 (4)	2.682 (3)	165 (4)
N21—H212···O31^{vii}	0.91 (4)	1.99 (4)	2.896 (4)	172 (4)
N22—H222···O32^{vii}	0.88 (6)	2.06 (6)	2.932 (4)	175 (5)
N22—H222···O41^{viii}	0.78 (4)	2.24 (4)	2.948 (4)	153 (4)
N21—H211···O42	0.93 (3)	2.05 (4)	2.929 (4)	157 (3)
C91—H91···O32	0.95 (3)	2.34 (3)	3.284 (4)	169 (3)
C92—H92···O31^{vii}	0.89 (4)	2.42 (3)	3.290 (4)	165 (3)
C62—H62···O22^{vii}	0.94 (4)	2.45 (4)	3.346 (4)	158 (3)
C61—H61···O21^{vi}	0.97 (3)	2.42 (3)	3.359 (3)	164 (3)
C81—H81···O11	1.02 (4)	2.51 (4)	3.409 (4)	146 (3)
C82—H82···O12	1.03 (4)	2.65 (4)	3.441 (4)	133 (3)
(3)				
O1—H1···O2^{iii}	0.93 (2)	1.59 (2)	2.504 (2)	164 (2)
N1—H10···O4	0.92 (2)	1.97 (2)	2.784 (2)	146 (2)
N2—H22···O3^{ix}	0.92 (2)	1.95 (2)	2.871 (2)	175 (2)
N2—H21···O2^{x}	0.85 (2)	2.11 (2)	2.918 (1)	161 (2)
C7—H7···O4^{xi}	0.98 (2)	2.47 (2)	3.186 (2)	130 (1)
C7—H7···O1^{xi}	0.98 (2)	2.50 (2)	3.301 (2)	139 (2)
C9—H9···O3^{x}	0.95 (1)	2.48 (1)	3.400 (2)	161 (2)
(4)				
N1—H1···O1	0.97 (2)	1.66 (2)	2.627 (1)	174 (2)
N2—H21···O2^{iii}	0.89 (2)	2.00 (2)	2.883 (1)	172 (1)
N2—H22···O1	0.91 (2)	2.04 (2)	2.917 (1)	161 (1)
C3—H3···O2	1.02 (1)	2.22 (1)	3.171 (1)	156 (1)

Symmetry codes: (i) $1-x,-y,-z$; (ii) $2-x,-y,2-z$; (iii) $1-x,1-y,2-z$; (iv) $1+x,y,2+z$; (v) $-x,-y,-z$; (vi) $2-x,-1-y,1-z$; (vii) $1+x,1+y,z$; (viii) $1-x,-y,1-z$; (ix) $-x,-y,2-z$; (x) $-x,y-\frac{1}{2},\frac{1}{2}-z$; (xi) $1-x,-y,2-z$; (xii) $x,y,z+1$.

standard reflections were measured every 2 h and did not show significant variations for all the compounds investigated. Intensities were corrected for Lorentz and polarization effects. Scattering factors were taken from *International Tables for X-ray Crystallography* (Cromer & Waber, 1974). The structures were solved by direct methods using the *SIR*92 (Altomare *et al.*, 1994) system of programs and refined by full-matrix least-squares with anisotropic non-H and isotropic H atoms using *SHELXL*97 (Sheldrick, 1997); all other calculations were accomplished using *PARST* (Nardelli, 1983, 1995) and *PLATON* (Spek, 1998). Selected bond distances are reported in Table 2 and hydrogen-bonding parameters in Table 3. *ORTEPII* (Johnson, 1976) views are shown in Figs. 1–4.

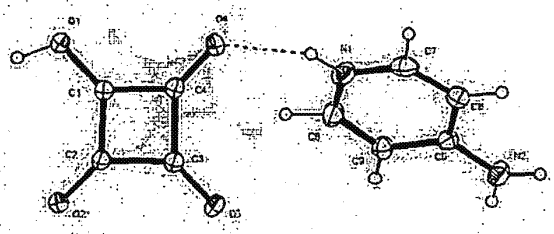


Figure 3
The molecular components of (3), showing the atom-labelling scheme. Displacement ellipsoids are drawn at the 30% probability level.

3. Description of crystal packings

3.1. Structure (1): 2-aminopyrimidinium (2APMH$^+$) hydrogen squarate (HSQ^-)

The crystal consists of a three-dimensional van der Waals packing of two-dimensional planes which, in turn, are parallel associations of hydrogen-bonded ribbons held together by weak C—H···O interactions (Fig. 5). The ribbons are ladders whose rungs are alternated centrosymmetric dimers of HSQ^-

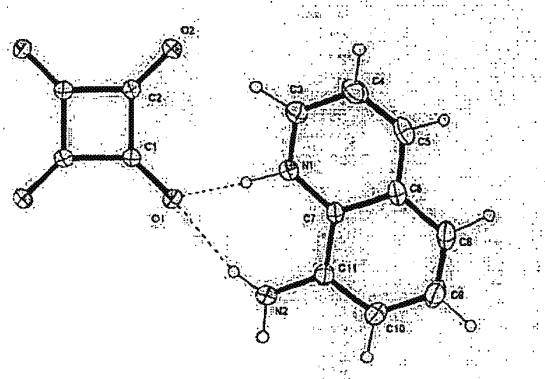


Figure 4
The molecular components of (4), showing the atom-labelling scheme. Displacement ellipsoids are drawn at the 30% probability level.

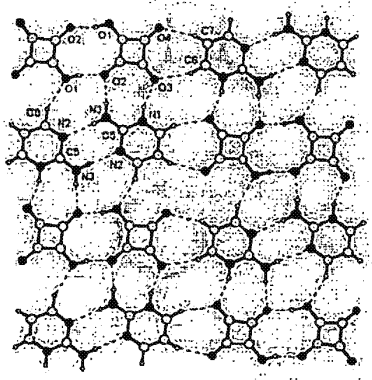
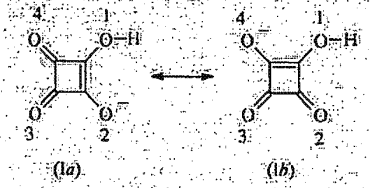


Figure 5
Layer of molecules of co-crystal (1)-linked by hydrogen bonds.

UM00012932
NOVARTIS EXHIBIT 1017
Novartis v. Regents, IPR2023-01346
Page 1678 of 4460

and 2APMH$^+$ ions. The $(HSQ^-)_2$ dimer is linked by two strong negative-charge-assisted O1—H···O2$^{1/2-}$ bonds having a O···O distance of 2.498 (2) Å, which is at the upper limit of the range of 2.44–2.49 Å (Gilli *et al.*, 1994) observed in carboxylic acid–carboxylate complexes, most probably because of the weakening effects produced by the further hydrogen bonds accepted by O atoms. The 2APMH$^+$ dimer is held by two neutral N—H···N bonds [N2···N3 3.044 (2) Å] according to a motif which is a very well known supramolecular synthon (Etter & Desmond, 1990; Aakeröy *et al.*, 1998). The two different dimers are interconnected by two N1—H···O3 and N3—H···O2 bonds and one C—H···O interaction [C8···O1 3.263 (2) Å, H···O1 2.29 (2) Å], which is strictly comparable with the strongest C—H···O bonds found in Cl_3C—H···O [average H···O of 2.31 (1) Å] and —C≡C—H···O [average H···O of 2.40 (2) Å] interactions (Desiraju & Steiner, 1999). The N3—H···O2 bond is shorter [2.745 (2) Å] than N1—H···O3 [2.796 (2) Å], in spite of the fact that the formal positive charge is residing on the N1$^+$—H group and that positively charged hydrogen bonds are normally stronger. A reason for that is illustrated by the resonance (I*a*) ↔ (I*b*), for which the oxygen negative charge can never be on O3, being potentially shared only by the O2 and O4 atoms. The most energetically favoured N3$^+$—H···O2$^{1/2-}$ interaction is then achieved by moving the positive charge from N1 to N3, as clearly shown by the N3—C5 distance which is 1.312 (2) Å against the normal value of 1.34–1.35 Å in neutral 2APM (Furberg *et al.*, 1979; Scheinbeim & Schempp, 1976), and in touch with the same distance of 1.322 Å observed in the hydrochloride salt where the same transfer of charge to the —NH_2^+ group occurs (Furberg & Grogaard, 1980).



3.2. Structure (2): 3-aminopyridinium (3APH$^+$) hydrogen squarate (HSQ^-)

Also the crystal of (2) is a three-dimensional van der Waals packing of hydrogen-bonded planes (Fig. 6) and one of its structural motifs is the $(HSQ^-)_2$ dimer connected by O—H···O$^{1/2-}$ bonds of remarkable strength [2.510 Å as an average over two molecules of the asymmetric unit]. The interplane packing can be described in terms of ribbons of centrosymmetric $(HSQ^-)_2$ dimers interconnected with centrosymmetric 3APH$^+$ pairs through two N$^+$—H···O$^{1/2-}$ [N12···O42 2.669 (3) and N11···O41 2.682 (3) Å], two N—H···O= [N21···O31 2.896 (4) and N22···O32 2.932 (4) Å] and six C—H···O [on average, C···O 3.39 (4) and H···O 2.51 (9) Å] hydrogen bonds. Both sides of the ribbon contain only hydrophilic groups, *i.e.* hydrogen-bond donor and acceptor atoms which become complementary when the adjacent ribbon is shifted upwards by one half of the distance between two $(HSQ^-)_2$ dimers. The resulting supramolecular architecture thus has two non-crystallographic glides perpendicular to its mean plane and approximately belongs to the plane group *pgg*. This symmetry is not retained by the three-dimensional crystal (space group *P*1), which allocates the supramolecular symmetry in the form of a double asymmetric unit. The inter-ribbon connections are given by N—H···O bonds [N12···O42 2.669 (4) and N22···O41 2.948 (4) Å] and by C—H···O [C91···O32 3.284 (4), C92···O31 3.290 (4) Å], which are to be classified as relatively strong C—H···O bonds, in agreement with the acidic nature of the C atoms surrounded by two electronegative groups.

3.3. Structure (3): 4-aminopyridinium (4APH$^+$) hydrogen squarate (HSQ^-)

Crystals of (3) are not built up of van der Waals planes, but consist of a three-dimensional hydrogen-bonded structure.

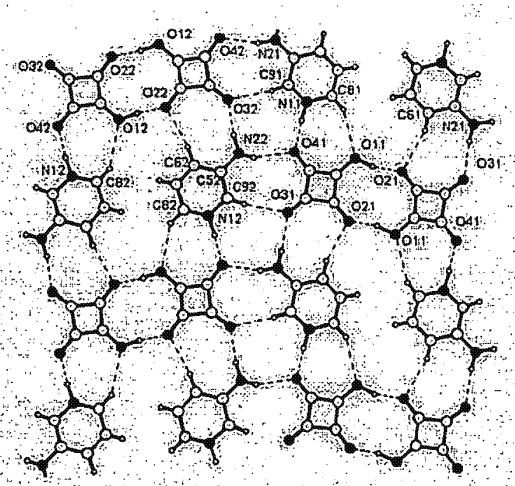


Figure 6
Layer of molecules of co-crystal (2) linked by hydrogen bonds.

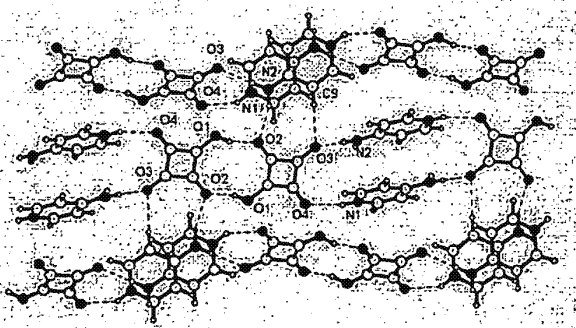


Figure 7
Three-dimensional arrangement of molecules of co-crystal (3) linked by hydrogen bonds.

UM00012933
NOVARTIS EXHIBIT 1017
Novartis v. Regents, IPR2023-01346
Page 1679 of 4460

Table 4
Saturation of potential hydrogen-bond donor and acceptor groups in the structures considered.

Hydrogen-bond donors (base pair or dimer)			Hydrogen-bond acceptors [$(HSQ^-)_2$ dimer or SQ^{2-} ion]		
Type	Potential	Used	Type	Potential	Used
(1)					
N—H$^+$	2	2	$O^{1/2-}$	12	10
N—H	2	2			
C—H	6	6			
(2)					
N—H$^+$	2	2	$O^{1/2-}$	12	12
N—H	4	4			
C—H	8	6			
(3)					
N—H$^+$	2	2	$O^{1/2-}$	12	12
N—H	4	4			
C—H	8	4†			
(4)					
N—H$^+$	2	2	$O^{1/2-}$	8	8
N—H	4	4			
C—H	12	2			

† Two bifurcated C—H···O bonds.

which can be described according to Fig. 7. Centrosymmetric $(HSQ^-)_2$ dimers linked by O—H···$O^{1/2-}$ bonds having O1···O2 2.504 (2) Å make horizontal chains with a non-bonded centrosymmetric pair of 4APH$^+$ ions through N—H···O [N2···O3 2.871 (2) Å] and N$^+$—H···$O^{1/2-}$ [N1···O4 2.784 (2) Å] bonds. The chains are connected in a three-dimensional structure by N—H···O bonds between the second hydrogen of the aminic function and the O2 atom of the HSQ^- unit [N2···O2 2.918 (1) Å]. The N—H functions link the chains in planes nearly parallel to the plane of the drawing, while the 4APAH$^+$ moieties nearly perpendicular to it connect the plane with other similar and parallel planes. The structure is complemented by rather short bifurcated C7—H···O1 and O4 [on average, C···O 3.24 and H···O 2.48 Å] and by C9—H···O3 [C···O 3.400 (2), H···O 2.48 (1) Å] interactions.

3.4. Structure (4): 8-aminoquinolinium (8AQH$^+$) hemisquarate (1/2 SQ^{2-})

The SQ^{2-} anions lie on centres of symmetry and the supramolecular architecture of this crystal is particularly simple. Each SQ^{2-} anion is surrounded by two centrosymmetric 8AQH$^+$ cations, each one connected by two chelated N$^+$—H···$O^{1/2-}$ [N1···O1$_a$ 2.627 (1) Å] and N—H···$O^{1/2-}$ [N2···O1 2.917 (1) Å] bonds and, by one short C—H···O [C3···O2$_b$ 3.171 (1) Å] interaction (Fig. 8). These three molecular units are linked in chains by N2—H···$O^{1/2-}$ bonds having a N···O distance of 2.833 (1) Å. The resulting ribbons are completely hydrophobic and pack together in a staggered pattern by van der Waals forces.

4. Discussion

In a previous paper (Bertolasi *et al.*, 2001) we have stressed the great difficulties that any prediction of co-crystal packing schemes may encounter even when the dominating molecular interactions are essentially known. The present structures make no exception to what was previously observed. Apart from the problem of *ab initio* prediction of the crystal packing by lattice energy calculations or molecular dynamics methods (which is far beyond the scope of the present paper), the simple understanding of the crystal supramolecular architectures appears to be out of the question for all structures except (4) and, perhaps, some aspects of (1). In (4) it could have been predicted that the presence of strong hydrogen-bond donors only on one side of the 8-aminoquinolinium (8AQH$^+$) cation would have produced the specular aggregation of two rows of 8AQH$^+$ molecules around the same spine of squarate anions with the final formation of hydrophobic ribbons (Fig. 8). In (1) the previous knowledge that 2-aminopyrimidinium is liable to form a typical dimeric synthon could have induced us to forsee, as a plausible structural motif, the ribbon of alternating $(HSQ^-)_2$ and $(2APMH^+)_2$ dimers displayed in Fig. 5. Much more encouraging appear to be the degree of chemical understanding of the molecular interactions (Bertolasi *et al.*, 2001) determining the packing itself. Table 3 reports all the *D*—H···*A* interactions (where *D* and *A* are the hydrogen-bond donor and acceptor atoms, respectively) found in co-crystals (1)–(4). These data can be rearranged in order of increasing *D*···*A* distances, according to the following classes:

(*a*) —O—H···$O^{1/2-}$ in (1), (2) and (3) with 2.498 (2) ≤ *d*(O···O) ≤ 2.514 (5) Å;

(*b*1) ≡N$^+$—H···$O^{1/2-}$ in (2), (3) and (4) with 2.627 (1) ≤ *d*(N···O) ≤ 2.784 (2) Å;

(*b*2) ≡N$^+$(H)—H···$O^{1/2-}$ in (1) with *d*(N···O) 2.745 (2) Å;

(*b*3) —N(H)—H···O═ in (2) and (3) with 2.871 (1) ≤ *d*(N···O) ≤ 2.932 (4) Å;

(*b*4) —N(H)—H···$O^{1/2-}$ in (2), (3) and (4) with 2.883 (1) ≤ *d*(N···O) ≤ 2.929 (4) Å;

(*c*) ═N$^+$(H)—H···N≡ in (1) with *d*(N···N) = 3.044 (2) Å;

(*d*1) ≡C—H···$O^{1/2-}$ in (1), (2), (3) and (4) with 3.171 (1) ≤ *d*(C···O) ≤ 3.359 (2) Å.

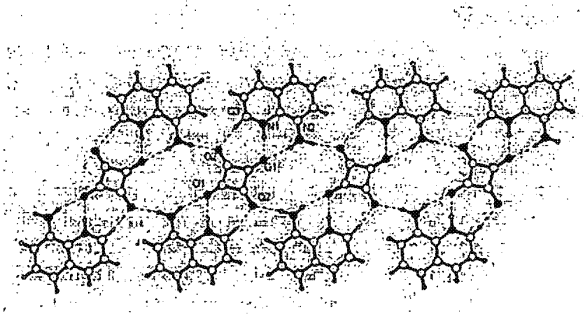


Figure 8
Ribbon of molecules of co-crystal (4) linked by hydrogen bonds.

UM00012934
NOVARTIS EXHIBIT 1017
Novartis v. Regents, IPR2023-01346
Page 1680 of 4460

(*d*2) ≡C—H···O in (1), (2) and (3) with 3.263 (1) ≤ *d*(C···O) ≤ 3.441 (2) Å,

where the positive and negative charges reported are to be taken as purely formal. The shortest *D*···*A* distances belong to the negative-charge-assisted (–)CAHB class of [O—H···O]$^-$ bonds, for which *d*(O···O) values of 2.39–2.49 Å have already been reported (Gilli *et al.*, 1994; Bertolasi *et al.*, 1996). Values presently observed are on the longer-distance side of the distribution; this is to be imputed to the fact that the formal charge here is 1/2− or better, to an indirect weakening produced by further hydrogen bonds accepted by the two O atoms from the crystalline environment. Some interesting regularities are also observed for the N—H···O bonds [classes (*b*1)–(*b*4)]. Bonds where the nitrogen and the oxygen bear opposite charges [classes (*b*1) and (*b*2)] are remarkably stronger than those where the N—H group is uncharged, in agreement with anything previously found for a much larger series of N—H···O bonds (Gilli & Gilli, 2000). N—H···N [class (*c*)] and C—H···O [class (*d*)] are, as expected in view of the lower electronegativities of the atoms involved, increasingly weaker although, as remarked above, all C—H···O presently observed are actually to be considered strong within their class of bonds, in view of the higher acidities of the C—H groups in nitrogen bases.

Table 4 summarizes the donor–acceptor properties of the hydrogen bonds observed in (1)–(4), taking as constitutive units of the crystal the centrosymmetric $(HSQ^-)_2$ dimer or the SQ^{2-} ion [for structures (1)–(3) and (4), respectively] and the adjacent centrosymmetric pair of nitrogen bases, irrespective of whether or not they are linked in hydrogen-bond dimers [which actually happens only for (1); see Fig. 5]. Since H_2SQ is a flat and π-delocalized molecule, the four O atoms of its anions can be considered sp^2 electron donors. In this hypothesis the $(HSQ^-)_2$ dimer and SQ^{2-} ion are possible acceptors of 1/2 and eight hydrogen bonds, respectively. The data of Table 4 indicate that all these acceptor positions are systematically matched by hydrogen-bond donors following a rather precise energy rule, in the sense that the packing is chosen in such a way to realise firstly the strongest possible bonds, *i.e.* O—H···O$^{1/2-}$, N—H···O$^{1/2-}$ and N—H···O for which all possible donor groups turns out to be fully utilized. The remaining acceptors are then totally saturated through weaker C—H···O interactions.

The observed behaviour suggests some considerations of quite general character on the process of crystal packing of hydrogen-bonded molecular crystals. It has been sometimes stated (Donohue, 1952; Etter, 1991) that the main rule for hydrogen-bonded crystals is that *'all acidic H atoms available in a molecule will be used in hydrogen bonding in the crystal structure of that compound'* (of course, if there are acceptors). This rule also holds for the present set of data (Table 4) provided that C—H···O interactions are not considered to be hydrogen bonds. If these are considered, it seems more reasonable to rewrite the rule as **Rule 1**: 'All the hydrogen-bond acceptors available in a molecule will be engaged in hydrogen bonding as far as there are available donors' and to complement it by the useful auxiliary rule that is **Rule 2**: 'The hydrogen-bond acceptors will be saturated in order of decreasing strength of the hydrogen bond formed'. This second rule tells us that since C—H···O and C—H···N are usually the weakest bonds, the crystal hydrogen-bond pattern will normally be completed by the maximum number of these weaker interactions. Notice that Rule 1 is in agreement with previous remarks by Taylor & Kennard (1984) that one of the factors determining the hydrogen-bond arrangements is 'a preference for including as many acceptors as possible in the hydrogen-bonding scheme'.

Much could be said on the validity of Rules 1 and 2 and on their transferability from the limited dataset of Table 4 to the crystal packings of all molecular crystals consisting of potentially hydrogen-bonding molecules. The two rules can be considered to hold in general on condition that the hydrogen bonds formed do not become too weak, and the present data seem to indicate that C—H···O bonds can easily satisfy this condition when, as in the present case, all C—H groups involved in hydrogen-bond formation have some extra acidic character due to both the aromatic nature of the ring and the presence of electronegative adjacent N atoms. It may be of interest to remark that the principle of saturation of all acceptors by hydrogen-bond donors down to acidic C—H groups has previously called upon to explain the higher bioactivity of drugs endowed with a number of functional groups able to enhance C—H acidity (Bertolasi *et al.*, 1990; Saenger, 1973; Jeffrey & Maluszynska, 1982).

References

Aakeröy, C. B., Hughes, D. P. & Nieuwenhuyzen, M. (1996). *J. Am. Chem. Soc.* **118**, 10134–10140.

Aakeröy, C. B., Nieuwenhuyzen, M. & Price, S. L. (1998). *J. Am. Chem. Soc.* **120**, 8986–8993.

Altomare, A., Cascarano, G., Giacovazzo, C., Guagliardi, A., Burla, M.C., Polidori, G. & Camalli, M. (1994). *J. Appl. Cryst.* **27**, 435.

Angelova, O., Velikova, V., Kolev, T. & Rodomirska, V. (1996). *Acta Cryst.* C**52**, 3252–3256.

Bertolasi, V., Ferretti, V., Gilli, G. & Borea, P. A. (1990). *J. Chem. Soc. Perkin Trans. 2*, pp. 283–289.

Bertolasi, V., Gilli, P., Ferretti, V. & Gilli, G. (1995). *Acta Cryst.* B**51**, 1004–1015.

Bertolasi, V., Gilli, P., Ferretti, V. & Gilli, G. (1996). *Chem. Eur. J.* **2**, 924–934.

Bertolasi, V., Gilli, P., Ferretti, V. & Gilli, G. (2001). *New J. Chem.* **25**, 408–415.

Bouma, B., Kodijman, H., Kroon, J., Grech, E. & Brzeziński, B. (1999). *Acta Cryst.* C**55**, 1824–1826.

Burchell, C. J., Glidewell, C., Lough, A. J. & Ferguson, G. (2001). *Acta Cryst.* B**57**, 201–212.

Cassidy, S., Reinhardt, L. A., Clelend, W. W. & Frey, P. A. (1999). *J. Chem. Soc. Perkin Trans. 2*, pp. 635–641.

Cleland, W. W. & Kreevoy, M. M. (1994). *Science*, **264**, 1887–1890.

Cromer, D. T. & Waber, J. T. (1974). *International Tables for X-ray Crystallography*, Vol. IV, Table 2.2A, pp. 149–150. Birmingham: Kynoch Press. (Present distributor Kluwer Academic Press Publishers, Dordrecht.)

Desiraju, G. R. (1989). *Crystal Engineering: The Design of Organic Solids*. Amsterdam: Elsevier.

Desiraju, G. R. (1995). *Angew. Chem. Int. Ed. Engl.* **34**, 2311–2325.

UM00012935
NOVARTIS EXHIBIT 1017
Novartis v. Regents, IPR2023-01346
Page 1681 of 4460

Desiraju, G. R. & Sharma, C. V. K. (1995). *The Crystal as a Supramolecular Entity*, edited by G. R. Desiraju, ch. 2, pp. 31–61. Chichester: J. Wiley and Sons.
Desiraju, G. R. & Steiner, T. (1999). *The Weak Hydrogen Bond in Structural Chemistry and Biology*. Oxford University Press.
Donohue, J. (1952). *J. Phys. Chem.* 56, 502–510.
Enraf–Nonius (1984). *CAD-4 Software*. Enraf–Nonius, Delft, The Netherlands.
Etter, M. C. (1990). *Acc. Chem. Res.* 23, 120–126.
Etter, M. C. (1991). *J. Phys. Chem.* 95, 4601–4610.
Etter, M. C. & Desmond, D. A. J. (1990). *J. Chem. Soc., Chem. Commun.* pp. 589–591.
Fair, C. K. (1990). *MolEN*. Enraf–Nonius, Delft, The Netherlands.
Furberg, S. & Grogaard, J. (1980). *Acta Chem. Scand. A*, 34, 695–698.
Furberg, S., Grogaard, J. & Smedsrud, B. (1979). *Acta Chem. Scand. B*, 33, 715–724.
Gilli, G., Bellucci, F., Ferretti, V. & Bertolasi, V. (1989). *J. Am. Chem. Soc.* 111, 1023–1028.
Gilli, G. & Bertolasi, V. (1990). *The Chemistry of Enols*, edited by Z. Rappoport, ch. 13, pp. 713–764. Chichester: Wiley and Sons.
Gilli, G., Bertolasi, V., Ferretti, V. & Gilli, P. (1993). *Acta Cryst.* B49, 564–576.
Gilli, P., Bertolasi, V., Ferretti, V. & Gilli, G. (1994). *J. Am. Chem. Soc.* 116, 909–915.
Gilli, P., Ferretti, V., Bertolasi, V. & Gilli, G. (1996). *Advances in Molecular Structure Research*, edited by M. Hargittai and I. Hargittai, Vol. 2, pp. 67–102. Greenwich, CT: JAI.
Gilli, G. & Gilli, P. (2000). *J. Mol. Struct.* 552, 1–15.
Ireland, D. T. & Walton, H. F. (1967). *J. Phys. Chem.* 71, 751–754.
Jeffrey, G. A. (1997). *An Introduction to Hydrogen Bonding*. New York: Oxford University Press.
Jeffrey, G. A. & Maluszynska, H. (1982). *Int. J. Biol. Macromol.* 4, 173–180.
Johnson, C. K. (1976). *ORTEPII*. Report 5138. Oak Ridge National Laboratory, Oak Ridge, Tennessee, USA.
Karle, I. L., Ranganathan, D. & Haridas, V. (1996). *J. Am. Chem. Soc.* 118, 7128–7133.
MacDonald, D. J. (1968). *J. Org. Chem.* 33, 4559–4560.
McLean, E. J., Wheatley, P. S., Ferguson, G. & Glidewell, C. (1999). *Acta Cryst.* C55, 1892–1896.
McLean, E. J., Wheatley, P. S., Ferguson, G., Glidewell, C. & Lough, A. J. (1999). *Acta Cryst.* C55, 1896–1899.
Nardelli, M. (1983). *Comput. Chem.* 7, 95–98.
Nardelli, M. (1995). *J. Appl. Cryst.* 28, 659.
Reetz, M. T., Höger, S. & Harms, K. (1994). *Angew. Chem. Int. Ed. Engl.* 33, 181–183.
Russell, V. A., Etter, M. C. & Ward, M. D. (1994). *J. Am. Chem. Soc.* 116, 1941–1952.
Saenger, W. (1973). *Angew. Chem.* 86, 690–693.
Scheinbeim, J. & Schempp, E. (1976). *Acta Cryst.* B32, 607–609.
Semmingsen, D., Hollander, F. J. & Koetzle, T. F. (1977). *J. Chem. Phys.* 66, 4405–4412.
Sheldrick, G. M. (1997). *SHELXL97*. University of Göttingen, Germany.
Simars, D., Su, D. & Wuest, J. D. (1991). *J. Am. Chem. Soc.* 113, 4696–4698.
Spek, A. L. (1998). *PLATON*. University of Utrecht, The Netherlands.
Taylor, R. & Kennard, O. (1984). *Acc. Chem. Res.* 17, 320–326.

UM00012936
NOVARTIS EXHIBIT 1017
Novartis v. Regents, IPR2023-01346
Page 1682 of 4460

This Page is Inserted by IFW Indexing and Scanning Operations and is not part of the Official Record

BEST AVAILABLE IMAGES

Defective images within this document are accurate representations of the original documents submitted by the applicant.

Defects in the images include but are not limited to the items checked:

- ☐ BLACK BORDERS
- ☐ IMAGE CUT OFF AT TOP, BOTTOM OR SIDES
- ☐ FADED TEXT OR DRAWING
- ☐ BLURRED OR ILLEGIBLE TEXT OR DRAWING
- ☐ SKEWED/SLANTED IMAGES
- ☐ COLOR OR BLACK AND WHITE PHOTOGRAPHS
- ☐ GRAY SCALE DOCUMENTS
- ☐ LINES OR MARKS ON ORIGINAL DOCUMENT
- ☐ REFERENCE(S) OR EXHIBIT(S) SUBMITTED ARE POOR QUALITY
- ☐ OTHER: _____

IMAGES ARE BEST AVAILABLE COPY.
As rescanning these documents will not correct the image problems checked, please do not report these problems to the IFW Image Problem Mailbox.

Structure and Solid-State Chemistry of Anhydrous and Hydrated Crystal Forms of the Trimethoprim-Sulfamethoxypyridazine 1:1 Molecular Complex

GIAMPIERO BETTINETTI,[1] MINO R. CAIRA,[2] ATHOS CALLEGARI,[3] MARCELLO MERLI,[3] MILENA SORRENTI,[1] CARLA TADINI[3]

[1] Dipartimento di Chimica Farmaceutica, Università di Pavia, Viale Taramelli 12, I-27100 Pavia, Italy

[2] Department of Chemistry, University of Cape Town, Rondebosch 7701, South Africa

[3] CNR Centro di Studio per la Cristallografia Strutturale, c/o Dipartimento di Scienze della Terra, Università di Pavia, Via Ferrata 1, I-27100 PV

Received 28 July 1999; accepted 28 December 1999

ABSTRACT: The crystal structure of the equimolar trimethoprim (TMP) and sulfamethoxypyridazine (SMPD) complex in the anhydrous form (TMP.SMPD) and that of the species with 1.5 molecules of water of crystallization (TMP.SMPD.W) are reported in this article. X-ray powder diffraction patterns (both computer generated and experimental) and thermal analytical data from differential scanning calorimetry (DSC) and thermogravimetry useful for the characterization of TMP.SMPD and TMP.SMPD.W are provided. The stability of TMP.SMPD.W, which retains its crystallographic order under 0% relative humidity (RH) conditions at room temperature (22°C) and 20 mmHg, is accounted for in terms of crystal structure and hydrogen bonding. Transformation of TMP.SMPD to the hydrate complex by exposure to ≈100% RH, suspension in water, and wet granulation, and dehydration of TMP.SMPD.W by thermal treatment and by desiccation with methanol were investigated and tentatively interpreted in terms of crystal properties. Interactions in the physical mixture of TMP and SMPD by grinding, compression, heating, and contact with water were also studied. Water-mediated formation of TMP.SMPD.W by wetting and metastable eutectic melting-mediated formation of TMP.SMPD by heating was demonstrated. Mechanical activation by milling makes the physical mixture prone to solid-state transformation into dimorphic anhydrous cocrystals by supply of thermal energy during a DSC scan. © 2000 Wiley-Liss, Inc. and the American Pharmaceutical Association J Pharm Sci 89: 478–489, 2000

Keywords: trimethoprim-sulfamethoxypyridazine molecular complex; anhydrous and hydrated crystal forms; crystal structure; computer generated x-ray powder patterns; thermal anlysis; anhydrous-hydrate interconversion; metastable eutectic; mechanical activation

INTRODUCTION

The antifolate drug trimethoprim (5-[(3,4,5-trimethoxyphenyl)methyl]pyrimidine-2,4-diamine; TMP) shows a high activity at the target enzyme dihydrofolate reductase (DHFR), coupled with the ability to discriminate between DHFR of bacterial and mammalian origin.[1] Crystallographic studies have been carried out on TMP and TMP analogues in the free[2,3] and bound[4,5] states, with the aim of shedding light on the drug-receptor binding mode and the parameters involved in the interaction. Our investigations of the benzoate salts of TMP showed that the N-1 protonated 2-aminopyrimidine portion of the

Correspondence to: G. Bettinetti. (E-mail: betti@chifar.unipv.it)

Journal of Pharmaceutical Sciences, Vol. 89, 478–489 (2000)
© 2000 Wiley-Liss, Inc. and the American Pharmaceutical Association

UM00012938
NOVARTIS EXHIBIT 1017
Novartis v. Regents, IPR2023-01346
Page 1684 of 4460

TMP cation is hydrogen bonded to the carboxylate anion.[6–8] Parallel studies on the molecular complexes between TMP and sulfa drugs present in pharmaceutical associations showed that the 2-aminopyrimidine portion of TMP is hydrogen bonded to the N(heteroatom)-C-NH(sulfonamide) moiety of sulfamethoxazole (SMZ)[9] and sulfadimidine (SDMD),[10,11] and to the O(sulfonamide)-C-NH(sulfonamide) portion of sulfametrole (SMTR).[12] Proton transfer from the sulfonamide N atom to the pyrimidine basic N1 atom of TMP occurs in the equimolar complexes with SMZ[13] (pKa 5.7) and SMTR (pKa 4.8), whereas no deprotonation of the sulfonamide N atom was observed for the complexes with SDMD (pKa 7.4). Sulfamethoxypyridazine (4-amino-*N*-(6-methoxy-3-pyridazinyl)benzenesulfanilamide, SMPD), for which pKa values of 7.2[14] and 6.7[15] are reported, is used in combination with TMP in Velaten® (Hoechst Pharma, Milano, Italy) capsules and suppositories.[16] SMPD and TMP crystallize from methanol as the anhydrous equimolar complex (TMP.SMPD) and from water as the equimolar complex 1.5 H_2O hydrate (TMP.SMPD.W).[14] The hydrated complex can also be formed rapidly by water-mediated interaction in a physical mixture of the components at room temperature.[16] This crystallographic study was undertaken to explain the way in which SMPD and TMP are linked in TMP.SMPD and to compare the molecular structures with those of analogous TMP-sulfa drug complexes. The structure of TMP.SMPD.W was also analyzed with the aim of demonstrating how the incorporation of water molecules into TMP.SMPD influences the intermolecular interactions and the crystalline disorder, as well as crystal packing. Possible relationships between structural data (hydrogen bonding, intermolecular contacts, bonding and structure of water molecules), thermal parameters (temperature and enthalpy of desolvation/melting[14,15]), and solid-state chemistry (i.e., phase transitions between the hydrate and anhydrate complexes) were also examined. In addition, the possible formation of cocrystals of TMP and SMPD in the solid state[17] by mechanical treatment (e.g., grinding or compression), heating, exposure to various humidity conditions, suspension in water and wet granulation was investigated. The single crystal X-ray data were used to compute the powder diffraction patterns of both complexes that were used for unambiguous identification of the solid phases produced in anhydrous-hydrate complex interconversion and cocrystal formation experiments.

EXPERIMENTAL SECTION

Materials

TMP (a gift from Pharmacia Upjohn, Milano, Italy) was recrystallized from ethanol-water 7:3 (v/v) (form I^{14}, mp 199.7 ± 0.2°C, fusion enthalpy 164 ± 1 J g^{-1}; n = 4). SMPD (Sigma-Aldrich, Milano, Italy) was recrystallized from ethanol-water 7:3 (v/v) (form I^{14}, mp 180.9 ± 0.2°C, fusion enthalpy 116.5 ± 0.8 J g^{-1}; n = 4). TMP, 14.5 g (0.05 mol), and SMPD, 14.0 g (0.05 mol), separately passed through a 250-μm sieve were mixed in a turbula apparatus for 15 min, and the equimolar physical mixture was used in the following experiments.

Crystal Preparation and Preliminary Characterization

Prismatic crystals of TMP.SMPD were obtained in a 90% yield by crystallization of 2.85 g of the equimolar mixture from 45 mL of methanol. The solution at the boiling point was filtered and allowed to recrystallize by spontaneous cooling to room temperature. *Anal.* Calc. $C_{25}H_{30}N_8O_6S$: C, 52.62; H, 5.30; N, 19.64. Found: C, 52.75; H, 5.35; N, 19.84. Elongated needlelike crystals of TMP.SMPD.W were obtained in quantitative yields by crystallization of 2.85 g of the equimolar mixture from 250 mL of distilled water under the same experimental conditions as the crystallization from methanol. *Anal.* Calc. $C_{25}H_{30}N_8O_6S.1.5H_2O$: C, 50.25; H, 5.56; N, 18.75. Found: C, 50.30; H, 5.58; N, 18.98.

Water contents of the TMP.SMPD.W samples were determined by Karl Fischer titrimetry (Mettler DL40GP Memo titrator apparatus) using Hydranal® Composite 5 (Riedel-de Haen®, Milano, Italy). The results (expressed as the mean of three measurements) showed that there was 4.54% w/w water in the samples, which corresponds to a water-complex molar ratio of 1.51 ± 0.12.

The anhydrous and hydrate complex were characterized by differential scanning calorimetry (DSC) and thermogravimetry (TG). DSC was carried out with a METTLER STAR^e system equipped with a DSC821^e Module on 3 to 5-mg (Mettler M3 Microbalance) samples in uncovered aluminium pans over the 30 to 250°C temperature range at the heating rate of 10 K min^{-1} under static air. TG was carried out with a Mettler TA 4000 apparatus equipped with a TG 50 cell on 7 to 10-mg samples in open alumina crucibles over the

UM00012939

NOVARTIS EXHIBIT 1017
Novartis v. Regents, IPR2023-01346
Page 1685 of 4460

30 to 250°C temperature range at the heating rate of 10 K min^{-1} under static air.

X-Ray Diffraction Studies

X-ray precession photography showed 2/m Laue symmetry for both TMP.SMPD and TMP.SMPD.W. For the former, the space group $P2_1/c$ was uniquely indicated. Reflection conditions for the hydrate were consistent with space groups Cc and C2/c, the latter being chosen on the basis of intensity statistics ($|E^2 - 1| = 0.970$). Colorless prismatic specimens of the compounds were mounted on glass fibers, and intensity data were collected on a Nonius Kappa CCD diffractometer at 293(1) K with graphite-monochromated MoK_α-radiation ($\lambda = 0.71069$ Å) using strategies based on the Collect Software.[18] For TMP.SMPD data were collected in one set using 1° φ-scans (360 frames, 35 s per frame), whereas for TMP.SMPD.W, 1° φ- and ω-scans were used to collect data in three sets (651 frames, 20 s/frame). Data were processed using programs Denzo and Scalepack.[19] Corrections for Lorentz-polarization effects were applied. Absorption was negligible for the sizes of specimens used ($\mu R \approx 0.04$ in both cases). Both structures were solved by direct methods[20] that yielded the positions of the non-H atoms. The basic unit in both species was revealed as a 1:1 hydrogen bonded associate of TMP and SMPD with atoms N20, N27 of TMP and atoms N11, N19 of SMPD engaging in hydrogen bonding in chemically and geometrically different modes in the two cases. For TMP.SMPD, all H atoms were located in difference electron density (ΔF) maps. The SMPD molecule was found to exist as the imido-tautomer with the pyridazine atom N19 bearing the H atom and N11 devoid of H. All non-H atoms refined anisotropically. H atoms attached to carbons were included in idealized positions in a riding model, whereas those on N atoms were constrained by distance only (N-H 1.00 Å). Separate common variable U_{iso} values for H on TMP and SMPD were used. All H atoms in TMP.SMPD.W except those of the water oxygens O42 and O43 were located in ΔF maps. In particular, atom N27 of the pyrimidine ring of TMP was found to be protonated, whereas atom N11 of SMPD was deprotonated. Of the three sites identified as those of O(water) atoms, two (O41, O43) were located in general positions, and the third (O42) lay on a diad (Wyckoff (e)). An unacceptably short O42 ····· O43 distance (≈ 1.69 Å) indicated that these atoms were disordered. In the final model the assigned site-occupancy factors were 1.0 for O41, 0.25 for O42, and 0.25 for O43 (based on ΔF peak height). These assignments also ensured that for the two mutually exclusive combinations (O41, O42 and O41, O43), the model accounted for 12 water molecules per unit cell (and hence $1.5H_2O$ per TMP.SMPD unit) in accordance with the analytical data. All non-H atoms were modeled anisotropically. Treatment of H atoms was as for TMP.SMPD. Crystal data and structure refinement details are presented in Table 1. Refinement for both complexes used full-matrix least-squares[21,22] based on F^2 with weights $w = 1/[\sigma^2(F_o)^2 + (aP)^2 + bP]$, $P = [\max(F_o^2, 0) + 2F_c^2]/3$. Molecular parameters were calculated using PARST95[23] and programs ZORTEP[24] and PLUTO[25] were used for illustrations.

The unit cell data for both complexes were used as input to the program LAZY PULVERIX[26] to generate the idealized X-ray powder diffraction (XRD) patterns for these species. Experimental XRD patterns were recorded on a Philips PW 1800/10 apparatus equipped with specific PC-APD software with powdered samples placed in Al holders (wavelengths, $CuK_{\alpha,1} = 1.54060$ Å, $CuK_{\alpha,2} = 1.54439$ Å; scan range, 2–50° 2θ; scan speed, 0.02° 2θ s^{-1}; monochromator, graphite crystal).

Interconversion Between TMP.SMPD and TMP.SMPD.W

Hydration of TMP.SMPD was studied under the following conditions: (i) by exposure to humidity of 2-g samples spread on Petri dishes in a desiccator at room temperature (22°C) (rt), which was kept at a relative humidity (RH) of 45% or ≈100% by equilibrating over a saturated solution of KNO_2 or pure water, respectively; (ii) by suspension of 2-g samples in 100 mL of distilled water at rt; (iii) by wetting 2-g samples with 5 mL of distilled water or ethanol-water 7:3 (v/v) solution in a simulated granulation process. Samples (5–25 mg) were taken out at appropriate intervals and checked for the solid phase composition by DSC and XRD. Dehydration of TMP.SMPD.W was studied under the following conditions: (i) by convective heating of 2-g samples spread on Petri dishes in a hot air oven; (ii) under vacuum desiccation (20 mmHg in a drying pistol over P_2O_5) on 1-g samples in a small test tube at a series of temperatures (from rt to 100°C at 20°C intervals) and times (15, 30, 60, 90, 120 min); (iii) by disper-

UM00012940
NOVARTIS EXHIBIT 1017
Novartis v. Regents, IPR2023-01346
Page 1686 of 4460

Table 1. Crystal Data and Refinement Details for TMP.SMPD and TMP.SMPD.W

	TMP.SMPD	TMP.SMPD.W
Molecular formula	$C_{25}H_{30}N_8O_6S$	$C_{25}H_{30}N_8O_6S \cdot 1.5H_2O$
M_r	570.64	597.65
Crystal system	Monoclinic	Monoclinic
Space group	$P2_1/c$	C2/c
a, Å	12.499(1)	42.4543(8)
b, Å	24.993(1)	6.5404(1)
c, Å	9.393(1)	20.9017(4)
β, deg	93.163(1)	100.292(1)
V, Å^3	2929.8(4)	5710.4(2)
Z	4	8
D_c/g cm^{-3}	1.294	1.390
F(000)	1200	2520
μ (Mo K_α)/cm^{-1}	1.63	1.72
Crystal size/mm	0.40 × 0.33 × 0.15	0.37 × 0.34 × 0.20
Range of indices	−17, 17; −30, 0; 0, 13	0, 58; 0, 8; −28, 27
No. reflections collected	26 789	32 572
Unique reflections	8120	7712
R_{int}	0.043	0.029
Reflections with I > 2σ (I)	5325	5690
No. parameters	388	417
R (F), F > 4σ (F)	0.0573	0.0479
wR (F^2), F > 4σ (F)	0.1549	0.1376
wR (F^2), all data	0.2210	0.1513
a, b in weighting scheme	0.1111, 0.93	0.0812, 3.62
Δρ (max., min.) e Å^{-3}	0.47, −0.47	0.39, −0.49

sion desiccation of 2-g samples suspended in 50 mL of methanol.

Interaction in the Physical Mixture

The equimolar mixture of TMP and SMPD was treated mechanically by manual grinding in an agate mortar with a pestle, by milling (10-g sample in a laboratory mortar grinder RM 0 Retsch equipped with a mortar and pestle of sintered alumina), and by compression (300 mg of unmilled sample compressed using a Perkin-Elmer hydraulic press for KBr discs for IR spectroscopy, at a force of 1.5 t cm^{-2} for 10 min). Untreated powder samples of the mixture (2 g) were also exposed to ≈100% RH, suspended in water, and wetted with an appropriate amount (20–25% w/w) of distilled water or ethanol-water 7:3 (v/v) solution under the same experimental conditions as the complexes (see preceding). The effect of convective heating on 2-g samples of treated and untreated mixture spread on Petri dishes in a hot air oven was also tested.

RESULTS AND DISCUSSION

Molecular Structures

The molecular structures of the complex units are shown in Figures 1 and 2, whereas selected bond lengths and bond angles are listed in Table 2. Selected torsion angles are listed in Table 3. A pair of N-H · · · N hydrogen bonds effects molecular association in TMP.SMPD with no proton transfer from SMPD to TMP (Table 4). SMPD is present in the imido-tautomeric form, whereas the amide form was found in the free molecule[27] and in its complex with the acridinium cation.[28] The imido-tautomer is characterized by a nearly trigonal angle S8-N11-C12 and double bond character for N11-C12 (Table 2), whereas in the amido-form (two independent molecules),[27] the corresponding parameters are 125.6(2)°, 1.408(4) Å (molecule A), and 124.4(2)°, 1.416(5) Å (molecule B). Various sulfonamide structures are capable of attaining the imido-tautomeric form, for example sulfapyridine in all three polymorphic structures[29] and sulfathiazole both as free molecule[30]

UM00012941
NOVARTIS EXHIBIT 1017
Novartis v. Regents, IPR2023-01346
Page 1687 of 4460

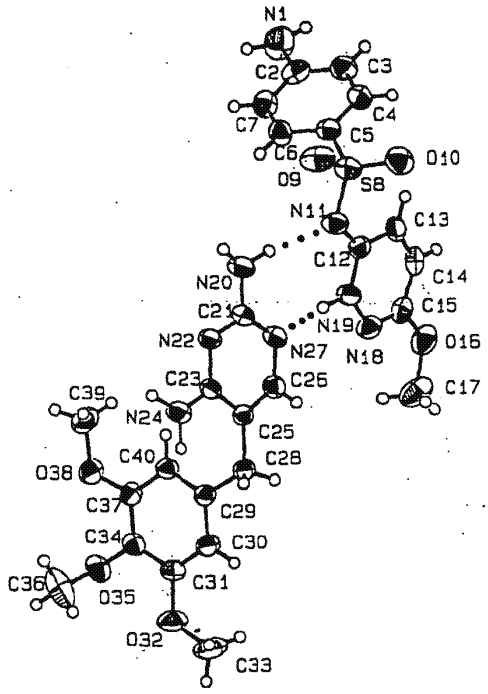


Figure 1. Perspective view of the complex unit in TMP.SMPD showing atom numbering, 50% thermal probability ellipsoids, and hydrogen bonds.

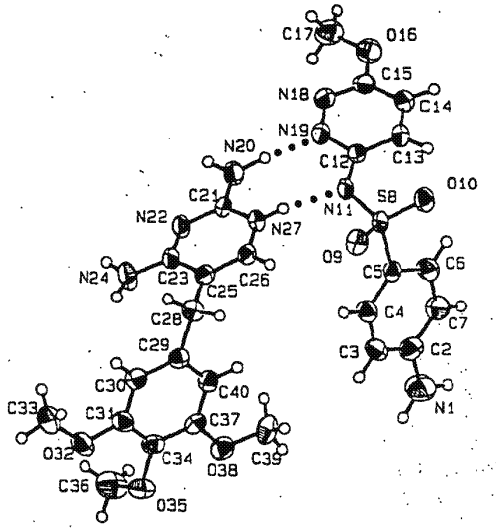


Figure 2. Perspective view of the complex unit in TMP.SMPD.W showing atom numbering, 50% thermal probability ellipsoids, and hydrogen bonds.

and molecular complex.[31] As a consequence, in the anhydrous complex the counterpart of the N11 sulfonimide atom is the N20 amino group of TMP, whereas the N27 basic nitrogen atom of TMP is hydrogen bonded to the N19 pyridazine nitrogen atom of SMPD. The hydrogen-bonding motif has the graph set $R_2^2(8)$ in the notation of Etter,[32] indicating that the hydrogen bonds result in the formation of an eight-membered ring and that two donors and two acceptors are used in assembling the motif. The acceptor and donor pairs are shared between the aminopyrimidine portion of TMP and imidopyridazine portion of SMPD. The solid-state conformation adopted by SMPD is similar to that found in the complex with 9-aminoacridine[28] (Table 3). The conformation of TMP, which may assume a variety of conformations in the free state[2] and quite different conformations of comparable energy in the bound state,[33] is instead different from those found in other structures (Table 3). This is due to the conformational flexibility about the methylene bridge in TMP. Crystal packing for TMP.SMPD is shown in the stereoview of Figure 3. Cohesion between the complex units is maintained by several N-H · · · O and N-H · · · N hydrogen bonds (Table 4) involving the amino groups of both TMP and SMPD, a pyrimidine N atom and a methoxyl O atom of TMP, as well as a sulfonyl O atom of SMPD. Molecular association in TMP.SMPD.W (Fig. 2) is also effected by a pair of N-H · · · N hydrogen bonds (Table 4), one of which involves

Table 2. Selected Bond Distances (Å) and Bond Angles (deg) in TMP.SMPD and TMP.SMPD.W

Parameter	TMP.SMPD	TMP.SMPD.W
C21-N20	1.352(3)	1.323(2)
C21-N27	1.335(3)	1.353(2)
N27-C26	1.349(3)	1.361(2)
S8-N11	1.598(2)	1.571(2)
N11-C12	1.340(3)	1.385(2)
C12-N19	1.335(3)	1.330(2)
N18-N19	1.355(2)	1.363(2)
C12-C13	1.436(3)	1.421(3)
C13-C14	1.347(3)	1.354(3)
C14-C15	1.410(3)	1.403(3)
C15-N18	1.301(3)	1.309(3)
C21-N27-C26	116.0(2)	119.5(1)
S8-N11-C12	121.7(1)	125.2(1)
C12-N19-N18	127.3(2)	121.6(2)

UM00012942
NOVARTIS EXHIBIT 1017
Novartis v. Regents, IPR2023-01346
Page 1688 of 4460

Table 3. Selected Torsion Angles (deg) in Species Containing the TMP and SMPD Molecules (All e.s.d.'s are in the range 0.1–0.4°)

τ, TMP	TMP.SMPD	TMP.SMPD.W	TMP.SMTR[12]	TMP.SMZ[13]	TMP.2SDMD.H_2O[11]
C23-C25-C28-C29	75.4	61.6	62.1	−172.9	166.7
C25-C28-C29-C40	−5.1	54.8	42.2	90.6	−76.1
τ, SMPD	**TMP.SMPD**	**TMP.SMPD.W**	**SMPD (A)[27]**	**SMPD (B)[27]**	**SMPD.ACR[28]**
N19-C12-N11-S8	171.6	172.3	−7.9	140.3	−157.2
C12-N11-S8-C5	73.0	−86.0	66.5	−57.7	60.1
N11-S8-C5-C4	−124.6	−91.5	49.9	−68.9	−114.2

N11, the deprotonated sulfonamide N atom and the protonated atom N27 of the TMP cation. The complex that crystallizes from water is therefore characterized by an ionic structure because in an aqueous environment the pyrimidine ring is protonated at N27 by SMPD. As noted previously,[12] a significant increase in the pyrimidine bond angle C21-N27-C26 accompanies protonation of TMP relative to the neutral molecule (Table 2). SMPD is present in the amide tautomeric form, and of the two possible resonating forms of the pyridazine ring, that with a single bond (1.363(2) Å) between the endocyclic nitrogen atoms is dominant, as in other structures.[27,28] The hydrogen bonding pattern is similar to that found in the complex of TMP with SMZ[13] and shows the same graph set $R_2^2(8)$ as that in TMP.SMPD (see preceding). The acceptor and donor pairs are, however, not shared as in the anhydrous complex but located on the imidopyridazine portion of SMPD and the aminopyrimidine portion of TMP, respectively. Also the solid-state conformations adopted by SMPD and

Table 4. Hydrogen Bond Data for TMP.SMPD and TMP.SMPD.W

D-H···A	D···A/Å	H···A/Å	D-H···A/deg
TMP.SMPD:			
N19-H19···N27	2.732(2)	1.74(2)	170(2)
N20-H20A···N11	3.074(3)	2.08(2)	172(2)
N1-H1A···O9[a]	3.017(3)	2.29(2)	129(2)
N1-H1B···N22[b]	3.206(3)	2.26(2)	158(2)
N20-H20B···N22[c]	3.115(2)	2.12(2)	176(1)
N24-H24A···O9[c]	3.050(3)	2.12(2)	154(1)
N24-H24B···O38[d]	2.969(2)	2.10(2)	145(2)
TMP.SMPD.W			
N20-H20A···N19	2.793(2)	1.80(2)	173(1)
N27-H27···N11	2.816(2)	1.84(2)	165(2)
O41-H41A···O9[e]	2.925(2)	1.94(1)	172(1)
O41-H41B···N22	2.977(2)	2.01(2)	163(2)
N24-H24B···O41[f]	2.945(3)	2.30(2)	121(1)
N24-H24A···O10[e]	2.863(2)	1.88(2)	169(2)
N20-H20B···O42	2.967(3)	2.37(2)	118(2)
O42···N18[g]	3.167(2)		
O43···N18[g]	2.84(1)		
N20-H20B···O43	2.90(1)	1.99(3)	151(2)
N1-H1A···O35[h]	3.088(3)	2.20(2)	147(1)
N1-H1B···O38[i]	3.105(3)	2.13(2)	166(2)

Symmetry code: [a] x, y, z − 1; [b] −x, −y + 1, −z + 1; [c] −x, −y + 1, −z + 2; [d] x, −y + 1/2, z + 1/2; [e] x, −y + 1, z + 1/2; [f] x, y + 1, z; [g] −x, y, −z + 1/2; [h] −x + 1/2, y −3/2, −z + 1/2; [i] −x + 1/2, y − 1/2, −z + 1/2.

UM00012943
NOVARTIS EXHIBIT 1017
Novartis v. Regents, IPR2023-01346
Page 1689 of 4460

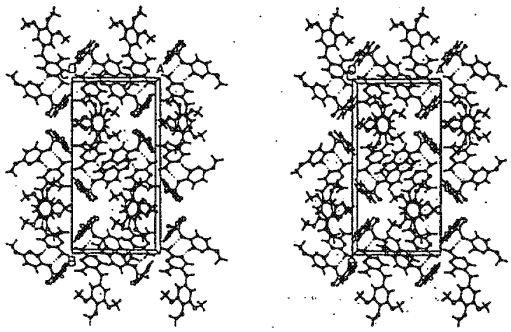


Figure 3. Stereoview of the crystal packing in TMP.SMPD viewed down the *c*-axis.

TMP in TMP.SMPD.W are different from those found in TMP.SMPD (Table 3).

The general crystal packing arrangement in the TMP.SMPD.W structure is shown in Figure 4 from which it is evident that the water molecules are concentrated in regions near to the (200) crystal planes. A detailed view of the environment of the water molecules is shown as a stereoview in Figure 5. All possible hydrogen bonding interactions involving water O atoms are indicated, including those generated by the diad on which O42 is located. Table 4 lists all geometric data. The sites occupied by water oxygen atoms O42 and O43 are mutually exclusive as a result of disorder. Therefore, two separate hydrogen-bonding schemes obtain in Figure 5, depending on which water molecule is considered. When O42 is present, it engages in two pairs of diad-related hydrogen bonds, one pair involving the amino H atom of a TMP molecule as donor and the other a pyridazine N atom of the SMPD molecule as acceptor. Atom O42 thus bridges two complex units across the diad by way of four hydrogen bonds. On the other hand, when O43 is present, it acts as a bridge between the $-NH_2$ group of a TMP molecule of one complex unit and the pyridazine N atom of an SMPD molecule of the diad-related complex unit. The role of the third water molecule (O41) is also evident in Figure 5. It bridges two *c*-glide–related complex units by donating one H atom to the unprotonated pyrimidine N atom of a TMP molecule and the other to a sulfonyl O atom of an SMPD molecule. A third hydrogen bond N24-H24B · · · O41^{f} (not shown in Fig. 5) is directed along the *y*-axis, linking this water molecule to a translated TMP molecule. With the exception of the interaction O42 · · · N18^{g} (3.167(2)

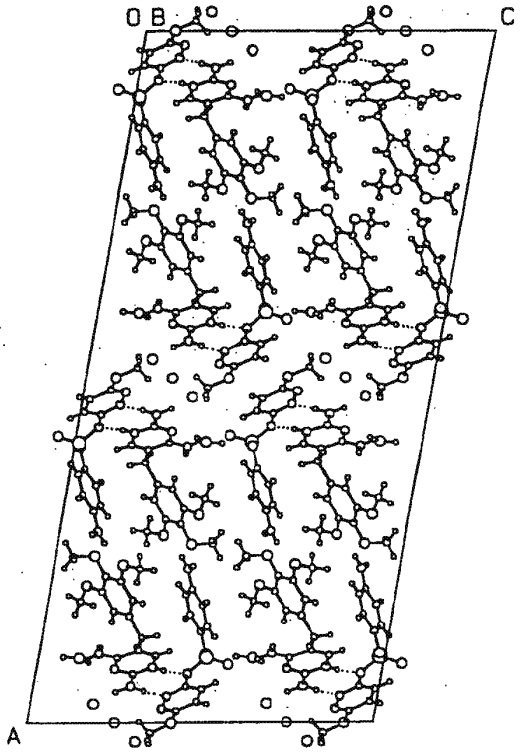


Figure 4. Crystal packing in TMP.SMPD.W viewed along the *b*-axis. The disordered water oxygen atoms are shown as single open circles.

Å), all O · · · O and O · · · N hydrogen bonding distances involving water molecules are relatively short and lie in the narrow range of 2.84(1) to 2.977(2) Å, indicating that the water molecules are very firmly bound to the complex units. Furthermore, each water molecule engages in multiple hydrogen bonds. A detailed study of the topology of water inclusion revealed further that all water sites correspond with closed cavities rather than channels in the crystal structure. These findings are consistent with the high thermal stability of the phase TMP.SMPD.W (see later) and indicate that complete disruption of the hydrogen-bonding network involving the water molecules accompanies the dehydration process. A further noteworthy point is that because the complexed TMP and SMPD molecules in TMP.SMPD and TMP.SMPD.W are in "antiparallel" alignment owing to interchange of hydrogen bonding partners (Figs. 1 and 2), transition from the TMP.SMPD.W phase to TMP.SMPD must also be

UM00012944
NOVARTIS EXHIBIT 1017
Novartis v. Regents, IPR2023-01346
Page 1690 of 4460

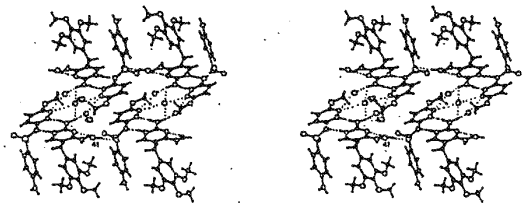


Figure 5. Stereoview showing hydrogen bonds involving the water molecules in TMP.SMPD.W. The orientation is the same as that in Figure 4.

accompanied by complete disruption of the hydrogen bonds N20-H · · · N19, $N27^{+}$-H · · · $N11^{-}$ and formation of new intermolecular hydrogen bonds N19-H · · · N27, N20-H · · · N11. We include in Figure 6 the XRD patterns of TMP.SMPD and TMP.SMPD.W computed from the single crystal data as the best representation of the pure materials,[29] together with the experimental traces.

Characterization of TMP.SMPD and TMP.SMPD.W by Thermal Analysis

Figure 7 shows the DSC and TG traces for TMP.SMPD and TMP.SMPD.W. TMP.SMPD shows a sharp endothermal effect (T_{onset} = 169.6 ± 0.6°C, T_{peak} = 171.3 ± 0.4°C, $\Delta_f H$ = 123.9 ± 0.8 J g^{-1}; n = 6) with no associated TG mass loss, which is attributable to melting of the anhydrous complex. TMP.SMPD.W has a broad DSC endotherm (T_{onset} = 96 ± 2°C, T_{peak} = 107 ± 2°C, $\Delta_{deh}H$ = 181 ± 17 J g^{-1}; n = 6) over the 80–120°C temperature range, which is accompanied by a one-step weight loss of (4.7 ± 0.5)% in TG. This weight change indicates that TMP.SMPD.W is a hydrate of TMP.SMPD with a molar stoichiometry of 1: (1.56 ± 0.16), in agreement with elemental analysis and KFT data. Dehydration is followed by a sharp exothermal effect peaking at 140 ± 3°C attributable to crystallization of TMP.SMPD, which then melts at 169.9 ± 0.5°C. Thermal behavior shows that, in accordance with crystal data, the hydrate structure contains solvent as an integral part of its lattice and collapses to an intermediate (amorphous) phase that rearranges rapidly to a stable anhydrous structure.

Interconversion between TMP.SMPD and TMP.SMPD.W

Because XRD patterns can differentiate TMP.SMPD and TMP.SMPD.W, the experimental XRD traces, which matched the computed ones (see Fig. 6), were used to follow the solid-state transformation between the complexes. TMP.SMPD remains in the anhydrous state at 45% RH and rt for 2 months, whereas it takes up about 6% w/w (by TG) of water by exposure to ≈100% RH under the same experimental condi-

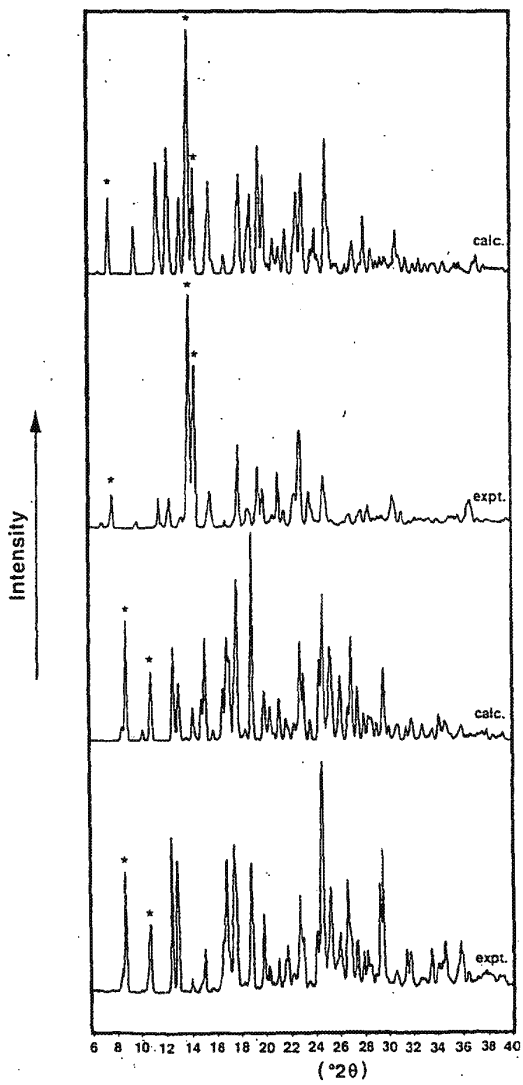


Figure 6. Calculated (calc) and experimental (expt) XRD patterns for TMP.SMPD (top) and TMP.SMPD.W (bottom). The diffraction peaks useful for TMP.SMPD (8.1, 14.2, and 14.6 °2θ) and TMP.SMPD.W (9.0 and 11.1 °2θ) characterization are marked with asterisks.

UM00012945
NOVARTIS EXHIBIT 1017
Novartis v. Regents, IPR2023-01346
Page 1691 of 4460

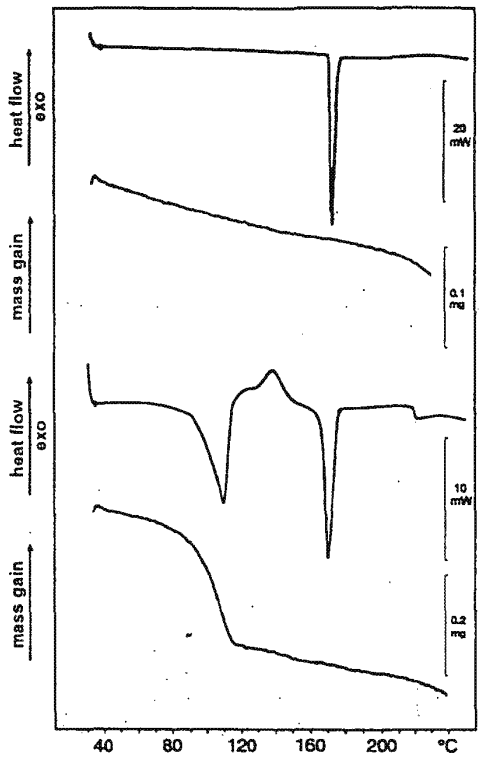


Figure 7. DSC and TG traces of TMP.SMPD (top) and TMP.SMPD.W (bottom).

tions. Regardless of the source of TMP.SMPD used (recrystallization from methanol, thermal dehydration, or desiccation by methanol of TMP.SMPD.W), the XRD pattern (not shown) of the hydration product matched perfectly that of TMP.SMPD.W and revealed an apparent crystallinity even higher (see later) than that of the sample recrystallized from water. Excess water with respect to the 1.5 hydrate stoichiometry was therefore adsorbed water. Immediate conversion of TMP.SMPD to TMP.SMPD.W was brought about by suspension in water or by wetting with 20 to 25% (w/w) of water [or ethanol-water 7:3 (v/v)] in a simulated granulation process with a mortar and pestle. The experimental results strongly suggest that hydration of TMP.SMPD to TMP.SMPD.W is achieved by means of a solvent-mediated process. The higher crystallinity of the hydrate prepared by exposing to ≈100% RH may be explained by the rate of crystallization. When hydration was carried out by exposure to ≈100% RH, crystallization occurs in the film of condensed water (i.e., under conditions of low supersaturation). Therefore crystallization proceeds with low rate at rt and yields products with high crystallinity. Under the conditions of recrystallization from water, instead, the supersaturation is higher and crystallization is much faster and yields products with lower crystallinity. When stored in a vacuum desiccator over P_2O_5 (0% RH) even after a relatively long period, the physical structure of TMP.SMPD.W did not change. Storing in a drying pistol (20 mmHg, 0% RH) at 80°C for 2 h or 100°C for 1 h was necessary for total loss of water from TMP.SMPD.W and transformation into TMP.SMPD crystals. Despite the high thermal stability of the hydrated phase, which was accounted for also by the topology of water in the crystal (see Results and Discussion of Molecular Structures), water of crystallization can be easily removed by desiccation with methanol (i.e., solvent-mediated dehydration). Profound changes in H-bonding arrangements are necessary for the TMP.SMPD.W to TMP.SMPD transformation, which is quite easy when solvent (e.g., methanol) is present but difficult in the dry state. Probably the attainment of the anhydrous structure after water removal is energetically favored by the N19-H19 · · · N27 hydrogen bond, which is established between TMP and the imido-tautomeric form of SMPD. This bond represents the strongest interaction between the molecular units in the complex (see Table 4).

Interaction in the Equimolar Physical Mixture

XRD patterns and DSC traces were run on the untreated physical mixture and after it was subjected to various treatments (Fig. 8). Characteristic diffraction peaks of pure TMP and SMPD in the XRD pattern of the untreated physical mixture [Fig. 8(a)] complied with the standard data files of both materials.[34] Diffraction peaks at 8.1, 14.2–14.3, and 14.6–14.8° (2θ) for TMP.SMPD and at 4.4 and 11.1° (2θ) for TMP.SMPD.W (see Fig. 6), which did not overlap those of TMP and SMPD, were chosen to follow interactions between TMP and SMPD. XRD patterns did not reveal cocrystal formation by grinding, compression, or milling [Fig. 8(b to e)], as well as by exposure of untreated or milled powder samples to ≈100% RH at rt or by heating in a hot air oven at 100°C for 3 h. Rapid formation of the hydrated complex by suspension of the mixture in water at rt or by wetting with 20 to 25% (w/w) of water [or ethanol-water 7:3 (v/v)] in a simulated granula-

UM00012946
NOVARTIS EXHIBIT 1017
Novartis v. Regents, IPR2023-01346
Page 1692 of 4460

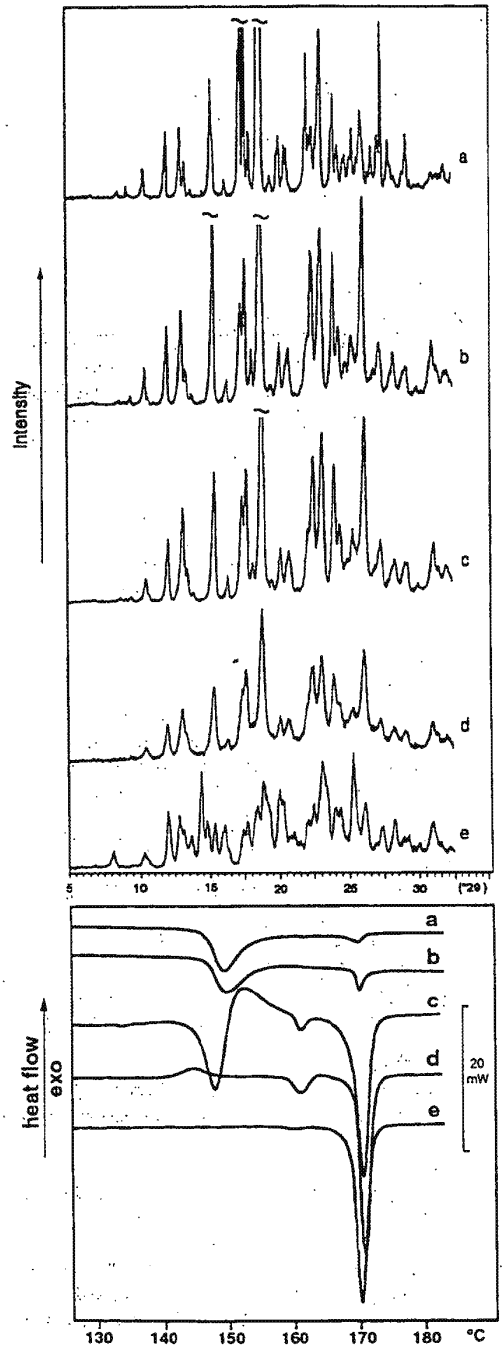


Figure 8. XRD patterns and DSC traces of the equimolar physical mixture of TMP and SMPD untreated (a), manually ground for 10 min (b), and milled for 10 min (c), 40 min (d), and 60 min (e). The compressed sample shows the same behavior as sample (b).

tion process was instead demonstrated by the XRD pattern (not shown) corresponding to that of TMP.SMPD.W (see Fig. 6).

DSC curves of untreated [Fig. 8(a)] or gently treated [Fig. 8(b)] mixtures show melting of a metastable eutectic [composed of 60% SMPD and 40% TMP (w/w)] at 148.4 ± 0.4°C. Melting was followed by a very small endothermal effect at about 161°C (see later) and an endothermal peak at about 170°C attributable to the fusion of TMP.SMPD formed in the eutectic melt.[14] In the DSC curve of the mixture milled for 10 min [Fig. 8(c)], eutectic melting was followed by crystallization and fusion at 161.0 ± 0.2°C of a solid phase, which can be considered to be a polymorphic modification of the anhydrous complex which then melts at 169.8 ± 0.1°C. Eutectic melting disappeared in the DSC trace of the mixture milled for 40 min [Fig. 8(d)], where the exotherm of crystallization and the endotherms of fusion of the assumed polymorphic modifications of the anhydrous complex were observed. Neither eutectic melting nor exothermal crystallization was present any longer, and fusion at 161°C tended to disappear after 60 min of mechanical treatment [Fig. 8(e)]. This thermal behavior can be interpreted assuming a milling-induced mechanical activation[35] disturbing the crystal structure at the surface of the particles in the mixture (decrease in degree of crystallinity, particularly evident by the broadening of diffraction peaks in the sample milled for 60 min [Fig. 8(e)]. The activated mixture was prone to be transformed into anhydrous cocrystals in the solid state by thermal energy supplied in a DSC scan, without the eutectic melting-mediated interaction characteristic of the nonactivated mixture.

CONCLUSIONS

TMP and SMPD crystallize from methanol as anhydrous complex (hydrogen bonded cocrystals of TMP and SMPD in the imido-tautomeric form) and from water or aqueous ethanol as hydrated complex, which is characterized by an ionic structure. Dimorphic anhydrous cocrystals grow during a DSC scan of the equimolar mixture of TMP and SMPD by means of a metastable eutectic at 148.4°C. Anhydrous cocrystals may form without the eutectic melting-mediated interaction as a consequence of the milling-induced mechanical activation of the system. Nucleation of the hydrated complex rapidly occurs by suspension in

UM00012947
NOVARTIS EXHIBIT 1017
Novartis v. Regents, IPR2023-01346
Page 1693 of 4460

water or by wet granulation of the equimolar mixture. The analysis and comparison of the hydrogen-bonding networks of the anhydrous and hydrated complexes are consistent with their solid-state chemistry. Even though the water molecules are held in the crystal by defined hydrogen bonds, a stable anhydrous structure can be easily accessed after their elimination. Thermal behavior of TMP.SMPD and TMP.SMPD.W is consistent with their crystal structures. Generally, anhydrate-hydrate interconversion is of biopharmaceutical and technologic relevance because water loss in processing operations involving thermal energy and water uptake by contact with water or exposure to humidity might cause compatibility problems. The formation of elongated needlelike crystals of TMP.SMPD.W caused by a small amount of water (as low as 0.8% w/w) in a suppository formula mass of Velaten®, which makes the mass clotted and not pourable, represents a relevant example.[16]

Supporting Information

The following tables of data for TMP.SMPD and TMP.SMPD.W are available from the authors: fractional atomic coordinates, fractional coordinates for hydrogen atoms, bond lengths and angles, thermal parameters for nonhydrogen atoms, least-squares plane data, and structure factors. The structures are deposited at the Cambridge Crystallographic Data Centre (CCDC 137664/CCDC 137665).

ACKNOWLEDGMENTS

This work was supported by a grant from Istituto Superiore di Sanità-Roma (Progetto proprietà chimico-fisiche dei medicamenti e loro sicurezza d'uso) to GB. MRC thanks the NRF (Pretoria) and the University of Cape Town for financial assistance. The authors thank Dr. A. Negri for her skillful technical assistance.

REFERENCES

1. Roth B, Cheng CC. 1982. Recent progress in the medicinal chemistry of 2,4-diaminopyrimidines. In: Ellis GP, West GB, editors. Progress in medicinal chemistry. Vol. 19. Amsterdam: Elsevier Biomedical Press. p 269.
2. Koetzle TF, Williams GJB. 1976. The crystal and molecular structure of the antifolate drug trimethoprim (2,4-diamino-5-(3,4,5-trimethoxybenzyl) pyrimidine). A neutron diffraction study. J Am Chem Soc 98:2074–2078.
3. Cody V. 1984. Structures of two active trimethoprim analogues: 2,4-diamino-5-(4-isopropenyl-3,5-dimethoxybenzyl)pyrimidinium ethanesulfonate, $C_{16}H_{21}NO_2^+ \cdot C_2H_5O_3S^-$ (I), and 2,4-diamino-5-(3,5-dimethoxy-4-methoxycarbonylbenzyl)pyrimidine, $C_{15}H_{18}N_4O_4$ (II). Acta Crystallogr C40:1000–1004.
4. Baker DJ, Beddell CR, Champness JN, Goodford PJ, Norrington FEA, Smith DR, Stammers DK. 1981. FEBS Letters 126:49–52.
5. Baker DJ, Beddell CR, Champness JN, Goodford PJ, Norrington FEA, Roth BR, Stammers DK. 1983. X-ray studies of the binding of trimethoprim, methotrexate, pyrimethamine and two trimethoprim analogues to bacterial dihydrofolate reductase. In: Blair JA, editor. Chemistry and biology of pteridines. Berlin: Walter de Gruyter & Co. p 545.
6. Giuseppetti G, Tadini C, Bettinetti GP, Giordano F, La Manna A. 1984. Structure of 2,4-diamino-5-(3,4,5-trimethoxybenzyl)pyrimidinium benzoate (trimethoprim monobenzoate), $C_{14}H_{19}N_4O_3^+ \cdot C_7H_5O_2^-$. Acta Crystallogr C40: 650–653.
7. Bettinetti GP, Giordano F, La Manna A, Giuseppetti G, Tadini C. 1985. Structure of a polymorph of the 1/1 addition compound between benzoic acid and 2,4-diamino-5-(3,4,5-trimethoxybenzyl)pyrimidinium benzoate (trimethoprim monobenzoate-benzoic acid 1/1 complex, form II), $C_{14}H_{19}N_4O_3^+ \cdot C_7H_5O_2^- \cdot C_7H_6O_2$. Acta Crystallogr C41:1249–1253.
8. Giuseppetti G, Tadini C, Bettinetti GP, Giordano F, La Manna A. 1988. Structure of the high-melting polymorph of the 1/1 addition compound between benzoic acid and 2,4-diamino-5-(3,4,5-trimethoxybenzyl)pyrimidinium benzoate (trimethoprim monobenzoate-benzoic acid 1/1 complex, form I), $C_{14}H_{19}N_4O_3^+ \cdot C_7H_5O_2^- \cdot C_7H_6O_2$. Acta Crystallogr C44:856–860.
9. Giuseppetti G, Tadini C, Bettinetti GP, Giordano F, La Manna A. 1980. The crystal structure of a sulfamethoxazole-trimethoprim 1:1 molecular compound. Il Farmaco, Ed Sci, 35:138–151.
10. Bettinetti GP, Sardone N. 1997. Methanol solvate of the 1:1 molecular complex of trimethoprim and sulfadimidine. Acta Crystallogr C53:594–597.
11. Sardone N, Bettinetti GP, Sorrenti M. 1997. Trimethoprim and sulfadimidine 1:2 molecular complex monohydrate. Acta Crystallogr C53: 1295–1299.
12. Giuseppetti G, Tadini C, Bettinetti GP. 1994. 1:1 Molecular complex of trimethoprim and sulfametrole. Acta Crystallogr C50:1289–1291.
13. Nakai H, Takasuka M, Shiro M. 1984. X-ray and infrared spectral studies of the ionic structure of

UM00012948
NOVARTIS EXHIBIT 1017
Novartis v. Regents, IPR2023-01346
Page 1694 of 4460

trimethoprim-sulfamethoxazole 1:1 molecular complex. J Chem Soc Perkin Trans II:1459–1464.
14. Bettinetti GP, Giordano F. 1988. Interaction between trimethoprim and some sulfa drugs. Drug Dev Ind Pharm 14:431–449.
15. Bustamante P, Escalera B. 1995. Enthalpy and entropy contributions to the solubility of sulphamethoxypyridazine in solvent mixtures showing two solubility maxima. J Pharm Pharmacol 47: 550–555.
16. Giordano F, La Manna A, Bettinetti GP, Zamparutti M. 1990. Preformulation studies on suppositories by thermal methods. Boll Chim Farm 129: 160–165.
17. Caira MR, Nassimbeni LR, Wildervanck AF. 1995. Selective formation of hydrogen bonded cocrystals between a sulfonamide and aromatic carboxylic acids in the solid state. J Chem Soc Perkin Trans 2:2213–2216.
18. "Collect" data collection software, Nonius B.V., 1998.
19. Otwinowski Z, Minor W. 1996. Processing of x-ray diffraction data in oscillation mode. In: Carter CW, Sweet RM, editors. Methods in enzymology. Vol. 276. New York: Academic Press. p 307–326.
20. Sheldrick GM, SHELXS-86. 1985. In: Sheldrick GM, Kruger C, Goddard R, editors. Crystallographic computing 3. Oxford: Oxford University Press. p 175–178.
21. Sheldrick GM. 1993. SHELXL-93, Program for the refinement of crystal structures. Germany: University of Gottingen.
22. Sheldrick GM. 1997. SHELXL-97, Program for crystal structure refinement. Gottingen, Germany: Institut für Anorganische Chemie der Universität, Tammanstraße 4, D-3400.
23. Nardelli M. 1995. A system of computer routines for calculating molecular parameters from results of crystal structure analyses. J Appl Crystallogr 28:659.
24. Zsolnai L, Pritzkow H. 1994. ZORTEP: Ortep program for personal computer. Germany: University of Heidelberg.
25. Motherwell WDS. 1978. PLUTO, A program for plotting molecular and crystal structures. Cambridge: University of Cambridge.
26. Yvon K, Jeitschko W, Parthe EJ. 1977. LAZY PULVERIX, a computer program for calculating x-ray and neutron diffraction powder patterns. J Appl Crystallogr 10:73–74.
27. Basak AK, Mazumdar SK, Chaudhuri S. 1987. Structure of *N'*-(6-methoxy-3-pyridazinyl)sulfanilamide (sulfamethoxypyridazine). Acta Crystallogr C43:735–738.
28. Ghose S, Chakrabarti C, Dattagupta JK. 1987. Structural studies on molecular complexes, I: crystal and molecular structure of 9-aminoacridine-sulfamethoxypyridazine (1:1), $C_{13}H_{10}N_2 \cdot C_{11}H_{12}N_4O_3S$. J Cryst Spectr Res 17: 197–206.
29. Bar I, Bernstein J. 1985. Conformational polymorphism VI: the crystal and molecular structures of form II, form III, and form V of 4-amino-N-2-pyridinylbenzenesulfonamide (sulfapyridine). J Pharm Sci 74:255–263.
30. Anwar J, Tarling SE, Barnes P. 1989. Polymorphism of sulfathiazole. J Pharm Sci 78:337–342.
31. Shefter E, Sackman P. 1971. Structural studies on molecular complexes V: crystal structures of sulphathiazole-sulfanilamide and sulphathiazole-theophylline complexes. J Pharm Sci 60:282–286.
32. Etter MC, MacDonald JC, Bernstein J. 1990. Graph-set analysis of hydrogen-bond patterns in organic crystals. Acta Crystallogr B46:256–262.
33. Bryan RF, Haltiwanger RC, Woode MK. 1987. Trimethoprim acetate. Acta Crystallogr C43: 2412–2415.
34. Powder diffraction files, PDF files 40-1707 (1989) and 38-1716 (1987). Newton Square, PA: International Center for Diffraction Data; 1993.
35. Hersey JA, Krycer I. 1980. Biopharmaceutical implications of technological change. Int J Pharm Tech Prod Mfr 1:18–21.

UM00012949
NOVARTIS EXHIBIT 1017
Novartis v. Regents, IPR2023-01346
Page 1695 of 4460

This Page is Inserted by IFW Indexing and Scanning Operations and is not part of the Official Record

BEST AVAILABLE IMAGES

Defective images within this document are accurate representations of the original documents submitted by the applicant.

Defects in the images include but are not limited to the items checked:

- ☐ BLACK BORDERS
- ☐ IMAGE CUT OFF AT TOP, BOTTOM OR SIDES
- ☐ FADED TEXT OR DRAWING
- ☐ BLURRED OR ILLEGIBLE TEXT OR DRAWING
- ☐ SKEWED/SLANTED IMAGES
- ☐ COLOR OR BLACK AND WHITE PHOTOGRAPHS
- ☐ GRAY SCALE DOCUMENTS
- ☐ LINES OR MARKS ON ORIGINAL DOCUMENT
- ☐ REFERENCE(S) OR EXHIBIT(S) SUBMITTED ARE POOR QUALITY
- ☐ OTHER: _____

IMAGES ARE BEST AVAILABLE COPY.
As rescanning these documents will not correct the image problems checked, please do not report these problems to the IFW Image Problem Mailbox.

Journal of Thermal Analysis, Vol. 28 (1983) 285–294

THERMAL ANALYSIS OF BINARY SYSTEMS OF THE PHARMACEUTICALS TRIMETHOPRIM AND BENZOIC ACID

G. P. Bettinetti, C. Caramella, F. Giordano, A. La Manna, C. Margheritis and C. Sinistri**

DEPARTMENT OF PHARMACEUTICAL CHEMISTRY, UNIVERSITY OF PAVIA,
*DEPARTMENT OF PHYSICAL CHEMISTRY, UNIVERSITY OF PAVIA, ITALY

Thermal analysis of the binary system benzoic acid (BA) and trimethoprim (TMP) provided evidence of the formation of two molecular compounds. BA—TMP and two crystalline forms of $(BA)_2$—TMP were characterized on the basis of their thermodynamic parameters as well as of crystallographic and spectroscopic properties. The availability of these compounds (by recrystallization) allowed interpretation of thermal effects in the DSC curves of the mixtures and the theoretical phase diagrams could be drawn. The results are consistent with the model of a very slight dissociation of the molecular compounds in the melt.

Thermal analysis and particularly microcalorimetric differential techniques are widely employed in pharmaceutical technology when interactions between active or inert ingredients of solid (tablets, capsules, powders) or semisolid (suspensions) pharmaceutical forms are concerned. This field of investigation is of practical relevance owing to possible changes in the physical properties and bioavailability of drugs. Microcalorimetric differential techniques allow investigation of the existence and nature of molecular compounds. In addition, on-line control of possible interactions at every stage of the production process (grinding, mixing, sieving, granulation, compression) or after various storage times can be achieved.

In previous papers from our group, investigations on interactions between trimethoprim (TMP) and some organic acids (formic, acetic, propanoic) [1] and between TMP and sulfamethoxazole [2–5] were reported. Investigations were successively extended to binary systems including TMP and some aromatic acids of pharmaceutical interest, such as benzoic, salicylic, acetylsalicylic and nicotinic acids. This paper is concerned with the TMP and benzoic acid (BA) binary system. Different interaction products from TMP and BA were prepared following various procedures, and a comprehensive picture of the thermal properties of this system is reported. IR and X-ray diffraction data were also taken into account when further analytical parameters were required.

Experimental

Apparatus

Thermal analysis was performed with a DSC Mettler TA 3000. Samples (1–4 mg) sealed in Al pans were scanned between 35° and the melt region at heating rates of

UM00012951
NOVARTIS EXHIBIT 1017
Novartis v. Regents, IPR2023-01346
Page 1697 of 4460

5 and 10 degree min^{-1}. Additional information on the thermal behaviour of samples was obtained by visual observation with a heating stage microscope (Kofler).

X-ray diffraction patterns (powder method) were obtained with a Philips PW 1050/25 diffractometer, with CuK_α radiation. X-ray diffraction on a single crystal was performed with a Philips four-circle computer-controlled diffractometer PW 1100, by using CuK_α radiation monochromatized with a graphite crystal.

Samples for IR analysis were prepared as Nujol mulls and examined by means of a Perkin–Elmer 421 dual grating IR spectrophotometer, previously checked with a polystyrene film.

Materials

Commercial trimethoprim (TMP) was purified by recrystallization from water–ethanol mixtures (10/90 v/v) (form I, mp. 199.3°). Benzoic acid (BA) complying with F.U.I. VIII Ed. requirements, mp. 122.0° after recrystallization from water, was used.

Preparation of the molecular compounds

BA–TMP (1:1 complex, $C_{21}H_{24}N_4O_5$)

A mixture containing equimolecular amounts (0.05 mole) of BA and TMP was crystallized from 100 ml of distilled water. The solid was filtered by suction and dried in a drying pistol charged with P_2O_5 (0.1 mm Hg, 90°) to give 0.0475 mole of the title compound, mp. 145.9°.

This compound was also isolated by evaporation in solutions of equimolecular amounts of BA and TMP in methanol or in ethyl acetate.

$(BA)_2$–TMP (2:1 complex, $C_{28}H_{30}N_4O_7$)

A mixture of 0.1 mole of BA and 0.05 mole of TMP was crystallized from 200 ml of distilled water. The solid was filtered by suction, washed with water, and dried under vacuum (P_2O_5) at 0.1 mm Hg and 90° to give 0.048 mole of a 2:1 complex melting at 126.5° (form II). A complex of the same molecular formula, melting at 134.2° (form I), crystallized from the melt on cooling. This latter form of $(BA)_2$–TMP was also isolated by evaporation of a solution containing BA and TMP in 2:1 molar ratio in diethylene glycol.

Preparation of physical mixtures for thermal analysis

Physical mixtures were prepared in a Turbula apparatus by dry-mixing the components, previously powdered by thorough grinding in a china mortar. Table 1 summarizes the mixtures tested in the DSC runs. In particular, BA and TMP mixtures, and mixtures with the same BA content (mole %) containing molecular compound(s), are reported.

Table 1 Physical mi

BA content, mole %	BA/ n
95	
90	
85	
80	
75	
70	
67.5	
66.7	
65	
62.5	
60	
57.5	
57	
55	
52.5	
50	
47.5	
45	
43	
40	
37.5	
35	
30	
27.5	
25	
22.5	
20	
15	
10	
5	

* Both as-form

Results and dis

The 1:1 cc
(trihydrate) wl
On heating, th
form of BA–T

UM00012952
NOVARTIS EXHIBIT 1017
Novartis v. Regents, IPR2023-01346
Page 1698 of 4460

Table 1 Physical mixtures scanned in DSC runs

BA content, mole %	BA/TMP mixtures, mole/mole	Equivalent mixtures (mole/mole) or compounds				
		BA/(2:1)*	BA/(1:1)	(2:1)*/(1:1)	(2:1)*/TMP	(1:1)/TMP
95	19/1	17/1	18/1			
90	9/1	7/1	8/1			
85	5.67/1	3.67/1	4.67/1			
80	4/1	2/1	3/1			
75	3/1	1/1	2/1			
70	2.34/1	0.34/1	1.34/1			
67.5	2.08/1	0.08/1	1/08/1			
66.7	2/1	$(BA)_2$–TMP*	1/1			
65	1.86/1		0.86/1	6/1	13/1	
62.5	1.67/1		0.67/1	2/1	5/1	
60	1.5/1		0.5/1	1/1	3/1	
57.5	1.35/1		0.355/1	0.55/1	2.1/1	
57	1.33/1		0.33/1	0.5/1	2/1	
55	1.22/1		0.22/1	0.3/1	1.57/1	
52.5	1.11/1		0.125/1	0.12/1	1/24/1	
50	1/1		BA–TMP		1/1	
47.5	0.91/1				0.826/1	9.7/1
45	0.82/1				0.7/1	4.5/1
43	0.76/1				0.61/1	3.1/1
40	0.67/1				0.5/1	2/1
37.5	0.6/1				0.43/1	1.5/1
35	0.54/1				0.37/1	1.16/1
30	0.43/1				0.275/1	0.75/1
27.5	0.38/1				0.234/1	0.61/1
25	0.33/1				0.2/1	0.5/1
22.5	0.29/1				0.17/1	0.41/1
20	0.25/1				0.144/1	0.335/1
15	0.18/1				0.098/1	0.215/1
10	0.11/1				0.06/1	0.125/1
5	0.053/1				0.027/1	0.056/1

*Both as-form I and form II

Results and discussion

The 1:1 complex can be obtained by recrystallization from water as a solvate (trihydrate) which, by loss of water in a desiccator over P_2O_5, becomes amorphous. On heating, the amorphous material is transformed, at about 90°, into a crystalline form of BA–TMP which then melts at 145.9° (Fig. 1a).

UM00012953
NOVARTIS EXHIBIT 1017
Novartis v. Regents, IPR2023-01346
Page 1699 of 4460

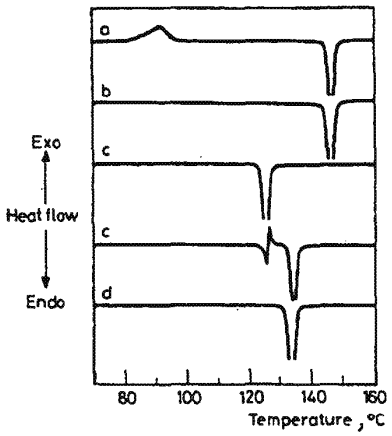


Fig. 1 DSC curves (scan speed 5 degree min^{-1}) of the molecular compounds. a) amorphous BA–TMP; b) crystalline BA–TMP; c) $(BA)_2$–TMP recrystallized from water (form II): non-ground sample (upper curve), ground sample (lower curve); d) $(BA)_2$–TMP obtained by evaporation (solution in diethylene glycol) (form I)

The same crystalline form can be obtained by evaporation of a methanolic solution of stoichiometric amounts of BA and TMP, or obviously by heating the trihydrate in a drying pistol (see Fig. 1b for DSC trace).

The thermal behaviour of the 2:1 complex depends mainly on the sample preparation procedures. Samples not previously ground, isolated by recrystallization from water, melt at 125.6° (Fig. 1c, upper curve). Ground samples, in contrast, show an endothermic effect at the same temperature, immediately followed by an exothermic one, with final fusion at 134.2° (Fig. 1c, lower curve). This exo effect can be ascribed to the formation of the higher-melting $(BA)_2$–TMP modification (form I) within the melt of the lower-melting modification ($(BA)_2$–TMP form II).

Rescanning of samples previously heated up to 125.6° did not show the endo and exo effects described here. The trace thus obtained is of type 1d. The crystal growth of form I can easily be observed with the heating stage microscope. The effect of grinding on the thermal behaviour of polymorphs was earlier reported for sulfamethoxydiazine crystal forms [6]. The slow evaporation of a BA/TMP (2:1 molar ratio) solution in diethylene glycol leaves crystals of a 2:1 complex giving the DSC trace in Fig. 1d, i.e. of the form I of the 2:1 complex.

In Table 2 the fusion temperatures (T_f) and enthalpies (ΔH_f) of the molecular compounds and their constituents are reported.

X-ray diffraction patterns taken on the molecular compounds proved the arrangements of the BA and TMP molecules in new crystal structures, whereas diffractograms of physical mixtures of BA and TMP corresponded (as expected) to the averages of those taken on pure BA and TMP.

The main bands in the IR spectra of the molecular compounds are reported in Fig. 3.

Fig. 2 X-ray di
clinic cr
$P2_1/N$,
analysis
$a = 14.5$
or $P\bar{1}$, U

Fig. 3 The ma
c) (BA)

UM00012954
NOVARTIS EXHIBIT 1017
Novartis v. Regents, IPR2023-01346
Page 1700 of 4460

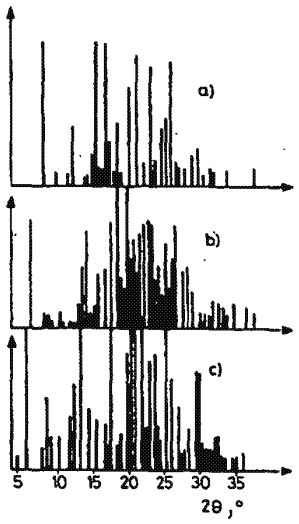


Fig. 2 X-ray diffraction patterns. Unit cell data on the molecular compounds: a) BA—TMP, monoclinic crystalline form: $a = 11.295$, $b = 28.266$, $c = 6.543$ Å, $\beta = 100.97°$, space group $P2_1/N$, $U = 2050.78$ Å^3, $Z = 4$, $M = 412.43$; b) $(BA)_2$—TMP form I: X-ray diffraction analysis on a single crystal is in progress; c) $(BA)_2$—TMP form II, triclinic crystalline form: $a = 14.595$, $b = 10.195$, $c = 9.455$ Å, $\alpha = 89.67°$, $\beta = 97.37°$, $\gamma = 104.6°$, space group P_1 or $P\bar{1}$, $U = 1349.95$ Å^3, $Z = 2$, $M = 543.56$

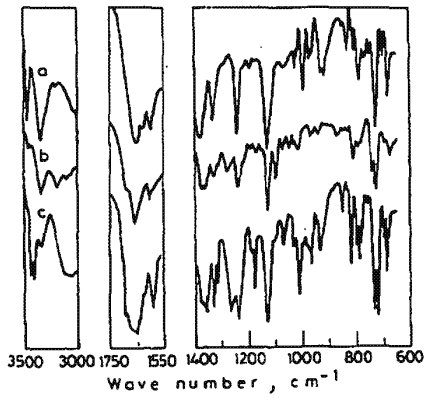


Fig. 3 The main bands in the IR spectra (Nujol mull) of a) BA—TMP; b) $(BA)_2$—TMP form I; c) $(BA)_2$—TMP form II

UM00012955
NOVARTIS EXHIBIT 1017
Novartis v. Regents, IPR2023-01346
Page 1701 of 4460

The IR absorption bands in the 3500–3000 cm^{-1} N–H stretching region, when compared with those of TMP alone and those of the TMP–SMZ molecular compound [2], show that in the solid state the BA molecule(s) is linked to the aminopyrimidine portion(s) of TMP.

The phase diagram of the binary system BA–TMP was studied both by experimental thermal analysis of the mixtures reported in Table 1 and by theoretical calculations on the solid–liquid equilibria using appropriate models of the melt, as in previous work [3]. The overall, and most significant experimental results are reported in Fig. 4: the system presents two intermediate compounds (2:1, 1:1) with congruent melting points, and three simple eutectics: E_1 (at 106.8° and $x_{BA} = 0.86$), E_2 (at 132.5° and $x_{BA} = 0.63$), and E_3 (at 145.0° and $x_{BA} = 0.48$). Moreover, the diagram shows, by a dashed line, the composition range where, at 125.6°, the endo–exothermal effects described in Fig. 1c for the pure form II of the 2:1 compound can be observed for the mixtures containing this crystalline form (Table 1). A dotted line shows the composition range where, at 120.2°, the mixtures of the 2:1 compound and TMP in Table 1 exhibit a thermal effect which could be indicative of the existence of a metastable eutectic between the 2:1 compound and TMP.

In order to study the molecular arrangement of the melt, three different structural models were first developed.

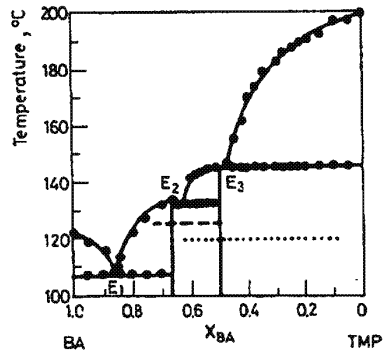


Fig. 4 Experimental phase diagram of the binary system BA/TMP *vs.* mole fraction of BA. The dashed line represents the endo and exo effects of the 2:1 compound (see text), while the dotted line can be ascribed to a metastable eutectic between TMP and the 2:1 compound

1) *A model which assumes total dissociation of the* 2:1 *and* 1:1 *compounds in the melt.*

Curve *a* of Fig. 5 is the geometrical expression of the function $T(x_{BA})$ that can be obtained by using this model along with the methods previously described [3] and the thermal data reported in Table 2.

Fig. 5 Phase dia
a) total d
compoun

A compari
experimental
pounds: their

2) *A model w*
ular compo

Curve *b* of
pounds are c
librium points

3) *A model w*
ular compo

Curve *c* o
liquidus curv
compound.

UM00012956
NOVARTIS EXHIBIT 1017
Novartis v. Regents, IPR2023-01346
Page 1702 of 4460

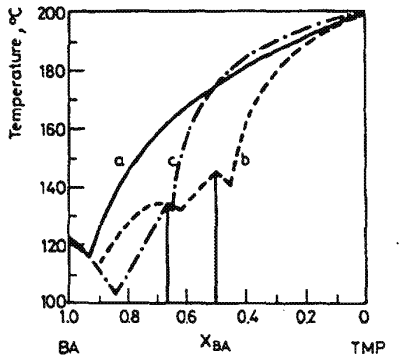


Fig. 5 Phase diagrams calculated by means of the following molecular models of the melt: a) total dissociation of the 2:1 and 1:1 compounds; b) total non-dissociation of the 1:1 compound; c) total non-dissociation of the 2:1 compound

Table 2

Compound		T_f, °C	ΔH_f, kJ mol^{-1}
TMP		199.3	49.4±1.2
BA		122.0	17.2±0.2
BA–TMP		145.9	52.3±0.8
$(BA)_2$–TMP	form I	134.2	56.1±1.2
	form II	126.5	59.0±1.2

A comparison with Fig. 4 shows that this model is totally inconsistent with the experimental results, and particularly with the features of the intermediate compounds: their melting points lie beneath the liquidus curve.

2) *A model which assumes total non-dissociation in the melt only for the* 1:1 *molecular compound.*

Curve *b* of Fig. 5 was obtained with this model. In this case two intermediate compounds are correctly predicted, but the agreement between the experimental equilibrium points and the calculated ones is poor.

3) *A model which assumes total non-dissociation in the melt only for the* 2:1 *molecular compound.*

Curve *c* of Fig. 5 shows the results obtained with this model. The calculated liquidus curve is inconsistent with the experimental thermal parameters of the 1:1 compound.

UM00012957
NOVARTIS EXHIBIT 1017
Novartis v. Regents, IPR2023-01346
Page 1703 of 4460

Following these results, a new and more complex model was developed, which assumes partial dissociation in the melt of the 1:1 and 2:1 molecular compounds. In particular, the equilibrium constant ($k_{1:1}$) of the dissociation:

$$BA{-}TMP \rightleftharpoons BA + TMP$$

and that ($k_{2:1}$) of the dissociation:

$$(BA)_2{-}TMP \rightleftharpoons 2\,BA + TMP$$

were taken into account. Their values were chosen by minimizing the difference between the calculated equilibrium curves and the experimental ones.

Figure 6 shows the phase diagram calculated by using $k_{1:1} = 5 \cdot 10^{-3}$ and $k_{2:1} = 5 \cdot 10^{-4}$.

Although these values should be taken as merely indicative, owing to the uncertainties inherent in the experimental solid–liquid equilibrium points, the calculated phase diagram nevertheless now shows a noteworthy agreement with the experimental one. For example, the calculated eutectics E_1 (at 107.0° and $x_{BA} = 0.86$), E_2 (at 131.5° and $x_{BA} = 0.625$) and E_3 (at 145.5° and $x_{BA} = 0.48$) compare very well with the experimental ones.

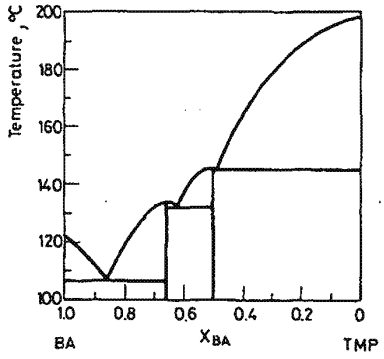


Fig. 6 Phase diagram calculated with a structural model which assumes partial dissociation of the two compounds in the melt ($k_{1:1} = 5 \cdot 10^{-3}$ and $k_{2:1} = 5 \cdot 10^{-4}$)

Conclusions

The availability of pure molecular compounds between BA and TMP allowed interpretation of the thermal effects in the DSC curves of various mixtures (e.g. metastable eutectics, polymorphic transitions, crystallization from the melt) and the construction of theoretical phase diagrams.

In this way it
binary system T
the solid phase
equilibrium diag
tion in the mel
bonds (and not
pound [4]), wit
nitrogen atom(s)

The authors g
Giuseppetti in the
The work was
and in part by a C

References

1 G. P. Bettin
Ferloni, Il Fa
706.
2 F. Giordano,
and P. Ferlo
(1977) 889.
3 C. Margheriti
Ed. Sci., 33 (1

Zusammenfassun
prim (TMP) erbr
zwei kristalline F
als auch durch kr
barkeit dieser V
mischen Effekte
diagramme. Die
Molekularverbinc

Резюме — Тер
(TMP) показал
и две кристал
намическими
ристиками. До
лила интерпрет
кений, и уста
суются с модел

UM00012958
NOVARTIS EXHIBIT 1017
Novartis v. Regents, IPR2023-01346
Page 1704 of 4460

In this way it was possible to prove that no total dissociation, as in the case of the binary system TMP/SMZ [3], occurs on melting. The molecular compounds present in the solid phase are also present in the melt. The correlation between the experimental equilibrium diagram and the theoretical diagram, consistent with a very slight dissociation in the melt, confirms the high stability of these molecular compounds. Ion-pair bonds (and not merely hydrogen-bonds as for the TMP–SMZ 1:1 molecular compound [4]), with proton transfer from benzoic acid to the molecular pyrimidinic nitrogen atom(s) of TMP, seem to be the main reason for this behavior.

* * *

The authors gratefully acknowledge the skilful assistance of Prof. C. Tadini and Prof. G. Giuseppetti in the X-ray analyses.

The work was supported in part by a grant from the Ministero Pubblica Istruzione to A. L. M. and in part by a CNR grant to C. M. and C. S.

References

1 G. P. Bettinetti, F. Giordano and P. Ferloni, Il Farmaco, Ed. Sci., 35 (1980) 706.
2 F. Giordano, G. P. Bettinetti, A. La Manna and P. Ferloni, Il Farmaco, Ed. Sci., 32 (1977) 889.
3 C. Margheritis and C. Sinistri, Il Farmaco, Ed. Sci., 33 (1978) 788.
4 G. Giuseppetti, C. Tadini, G. P. Bettinetti, F. Giordano and A. La Manna, Il Farmaco, Ed. Sci., 35 (1980) 138.
5 G. P. Bettinetti, F. Giordano, C. Caramella, P. Colombo, U. Conte and A. La Manna, Il Farmaco, Ed. Pr., 38 (1983) 259.
6 F. Giordano, G. P. Bettinetti, C. Caramella and U. Conte, Boll. Chim. Farm., 116 (1977) 433.

Zusammenfassung — Die thermische Analyse des binären Systems Benzoesäure (BA) – Trimethoprim (TMP) erbrachte Hinweise auf die Bildung von zwei Molekülverbindungen. BA–TMP und zwei kristalline Formen von $(BA)_2$–TMP wurden sowohl durch ihre thermodynamischen Parameter als auch durch kristallographische und spektroskopische Eigenschaften charakterisiert. Die Darstellbarkeit dieser Verbindungen (durch Rekristallisation) ermöglichte die Interpretation der thermischen Effekte in den DSC-Kurven der Gemische und die Aufstellung der theoretischen Phasendiagramme. Die Ergebnisse sind vereinbar mit dem Modell einer sehr schwachen Dissoziation der Molekülarverbindungen in der Schmelze.

Резюме — Термический анализ двойной системы бензойная кислота (БК)—триметоприм (TMP) показал обращование двух молекулярных соединений. Бинарная система БК–ТМП и две кристаллические формы системы $(БК)_2$–ТМП были охарактеризованы терм одинамическими параметрами, кристаллографическими и спектроскопическими характеристиками. Доступность этих соединений, получаемых путем перекристаллизации, позволила интерпретировать термические эффекты, наблюдаемые на ДСК-кривых смесей соединений, и установить теоретические фазовые диаграммы. Полученные результаты согласуются с моделью очень малой диссоциации молекулярных соединений в расплаве.

UM00012959
NOVARTIS EXHIBIT 1017
Novartis v. Regents, IPR2023-01346
Page 1705 of 4460

This Page is Inserted by IFW Indexing and Scanning Operations and is not part of the Official Record

BEST AVAILABLE IMAGES

Defective images within this document are accurate representations of the original documents submitted by the applicant.

Defects in the images include but are not limited to the items checked:

- ☐ BLACK BORDERS
- ☐ IMAGE CUT OFF AT TOP, BOTTOM OR SIDES
- ☐ FADED TEXT OR DRAWING
- ☐ BLURRED OR ILLEGIBLE TEXT OR DRAWING
- ☐ SKEWED/SLANTED IMAGES
- ☐ COLOR OR BLACK AND WHITE PHOTOGRAPHS
- ☐ GRAY SCALE DOCUMENTS
- ☐ LINES OR MARKS ON ORIGINAL DOCUMENT
- ☐ REFERENCE(S) OR EXHIBIT(S) SUBMITTED ARE POOR QUALITY
- ☐ OTHER: _____

IMAGES ARE BEST AVAILABLE COPY.
As rescanning these documents will not correct the image problems checked, please do not report these problems to the IFW Image Problem Mailbox.

Amer. J. Hosp. Pharm. 30: 240–243 (Mar.) 1973

Biopharmaceutics and dosage form design

edited by Gerald E. Schumacher, Pharm.D., Ph.D.

Effect of Complexation with Phenobarbital on the Biologic Availability of Theophylline from Three Tablet Formulations

John W. Bettis, John L. Lach and James Hood

A study was conducted to test the hypothesis that clinical differences occurring after the administration of theophylline, phenobarbital and ephedrine tablets of different manufacturers were due not only to formulation factors but also to complexation between theophylline and phenobarbital.

A complex of phenobarbital with theophylline had a slower dissolution in three dissolution media than theophylline. The significance of this dissolution behavior was demonstrated in humans as higher serum levels of theophylline were measured after the oral administration of theophylline than upon the administration of the complex. Three tablet formulations containing theophylline, ephedrine and phenobarbital possessed different dissolution profiles in simulated gastric fluid. For the three tablet formulations tested in nine humans, the relationship of serum level of theophylline and time correlated with the dissolution profiles.

This study indicates that bioavailability may be influenced by complexation or interaction between two drugs in a tablet.

Key words: Complexes; Drugs; Equivalency; Formulations; Incompatibilities; Phenobarbital; Tablets; Theophylline

It is generally recognized that variables in the formulation of pharmaceutical dosage forms may significantly alter the clinical effectiveness of drugs.[1–3] Most of the examples studied have involved sparingly soluble single-entity drug products, where drug particle size or polymorphism have been implicated as the factors affecting dissolution rate and, hence, biologic availability. However, the biologic availability of relatively water soluble drugs from their dosage forms has been shown to be influenced by drug-excipient interactions, as in the complexation of tetracycline with calcium phosphate. The possibilities for drug complexation with other dosage form components are exacerbated in multicomponent or combination drug products since $drug_1$-$drug_2$ complexation as well as drug-excipient interactions reactions may occur.

This report examines the hypothesis that clinical differences occurring after the administration of theophylline, phenobarbital and ephedrine tablets of different manufacturers were due, not only to formulation factors, but also to the long-known phenomenon of complexation between theophylline and phenobarbital.[4,5] The dissolution profiles of powdered theophylline and theophylline-phenobarbital complex were compared, and in a similar manner the dissolution profiles of theophylline from three tablet formulations were compared. The serum levels of theophylline in humans were compared after the oral administration of theophylline and theophylline-phenobarbital complex and after the administration of three tablet formulations.

Experimental

Theophylline Preparation. Theophylline, anhydrous, USP, m.p. 270–274 C, which passed a 100-mesh standard sieve, and preformed theophylline-phenobarbital (2:1), prepared as follows, were studied.

Anhydrous theophylline, 3.1 g (17.2 mmol), and 2.0 g (8.6 mmol) of phenobarbital were intimately mixed in a mortar and made to a paste with a small amount of water. The mixture was transferred to a bottle with a total of about 90 ml of water, and the slurry was tumbled for 24 hours to insure complete interaction. Water was removed under reduced pressure at 40 C, and the dried powder was mixed and passed through a 100-mesh sieve. The material exhibited an endotherm in differential thermal analysis at 252 C.[5] Higgins and Dunker[4] report 250.7–251.7 C as the melting range for the 2:1 theophylline-phenobarbital complex. This stoichiometry was further confirmed by X-ray powder diffractometry.[5]

The following tablet formulations were used:

—Tedral Tablets, lot 35806, Warner-Chilcott Laboratories brand of Theophylline, Ephedrine Hydrochloride and Phenobarbital Tablets, NF,[a] declaring 130 mg of hydrous theophylline (118.2 mg anhydrous), 25 mg of ephedrine hydrochloride, and 8 mg of phenobarbital per tablet,
—Lot 08864 of American Pharmaceutical Company tablets with the same label declaration as the above, and
—"Theophedrine" tablets, University of Iowa Pharmaceutical Services Lot 58-053, declaring 80 mg of hydrous theophylline, 25 mg of racephedrine hydrochloride, and 8 mg of phenobarbital per tablet.

Dissolution Studies. (1) Dissolution of Powders. A modification of the beaker method[6] was used in studies of the dissolution of theophylline and theophylline-phenobarbital complex powders. The apparatus consisted of a T-shaped glass stirrer, 5.5 cm by 0.5 cm, attached to a

John W. Bettis, Ph.D., is with Pfizer, Inc., Medical Research Laboratories, Groton, Connecticut 06340. John L. Lach, Ph.D. is Professor of Pharmacy, The University of Iowa, Iowa City, Iowa 52240. James Hood, M.B., Ch.B., was Instructor, College of Medicine, The University of Iowa, when this study was performed, and is now with Medical Associates, 1328 Second Avenue, S. E., Cedar Rapids, Iowa 52403.

[a] NF status for this formulation was attained after this study was completed.

UM00012961
NOVARTIS EXHIBIT 1017
Novartis v. Regents, IPR2023-01346
Page 1707 of 4460

60 RPM electric motor, centered and immersed to within 1 cm of the bottom of a 1000-ml beaker. Dissolution media were 500-ml volumes of distilled water, 0.02% (w/v) polysorbate 80, and USP simulated gastric fluid T.S. The beaker was immersed in a constant temperature water bath maintained at 37 ± 0.1 C. Test quantities were 50 mg of theophylline or the equivalent amount of theophylline-phenobarbital complex (82 mg). Aliquots of the dissolution medium were analyzed for theophylline at intervals by UV spectrophotometry at 274 nm after dilution with *p*H 9.5 borate buffer. Solutions from the theophylline-phenobarbital tests were measured at 240 nm and 274 nm, and the concentrations of each component determined by solutions of simultaneous equations.

(2) Dissolution of Theophylline from Tablets. The USP basket rack assembly tablet disintegration apparatus, without disks, was used with 750 ml of simulated gastric fluid T.S. as the dissolution medium, maintained at 37 C in a constant temperature bath. Six tablets were used per test. Aliquots of the dissolution medium were filtered through sintered glass and analyzed spectrophotometrically for theophylline at 271 nm.

Theophylline Blood Levels. (1) Protocol. Nine normal healthy subjects, six men and three women, ranging in age from 23 to 39 years, were used. The subjects took no other medication during the study and abstained from xanthine-containing beverages, such as coffee, tea, cola and cocoa, for 18 hours before test; then each was given a single dose of theophylline, theophylline-phenobarbital complex, or a tablet. A minimum of one week was allowed between tests on any one subject. Breakfast, one-half to one hour before test, consisted of cereal and milk. After breakfast, the subjects fasted until the final blood sample was collected. Blood samples, 20 ml, were withdrawn from an antecubital vein just before dosage (for the blank value) and at 30±2 minutes, 60±2 minutes, 120 minutes and 240 minutes after dosage. The blood specimens were allowed to clot at room temperature, the serum separated by centrifugation, and refrigerated in tightly stoppered sterile tubes for no longer than one week before analysis.

(2) Analytical Method for Serum Theophylline. A slight modification of the well-established Schack and Waxler method[7] was used; the modification consisting of saving all of the solvent extract of serum instead of 70% of it. Analyses were performed in duplicate on 3 ml of serum, and each data point presented is an average.

Results and Discussion

Dissolution Tests. A comparison of the dissolution profiles of theophylline and theophylline-phenobarbital complex is given in Table 1. It is evident that complexation retards the dissolution rate of theophylline in all three media (polysorbate 80 was selected in an attempt to overcome the hydrophobic character of the complex). The dissolution behavior of the three tablet formulations in simulated gastric fluid T.S. is represented in Figure 1. It is evident that the alternates for Tedral tablets pro-

Table 1. Dissolution Profiles of the Powdered Theophylline Preparations Used in the Clinical Study

DISSOLUTION MEDIA (37 C)	MINUTES	% DISSOLVED			
		THEOPHYLLINE	THEOPHYLLINE FROM COMPLEX	FREE PHENOBARBITAL	PHENOBARBITAL FROM COMPLEX
Distilled water	5	90.2	22.9	39.8	24.2
	10	94.8	41.1	64.6	40.7
	15	97.7	55.2	83.5	55.9
	20	98.6	63.8	93.1	65.7
	30	99.0	75.0	98.4	74.9
	40	99.3	82.9	101.7	84.0
Polysorbate 80, 0.02% v/v	5	87.0	44.9	81.1	46.1
	10	95.8	54.0	82.7	52.9
	15	100.0	62.4	86.7	61.7
	20	100.0	68.0	90.6	67.5
	30	100.0	75.4	91.2	72.6
	40	100.0	82.2	94.5	80.0
Simulated gastric fluid, T.S.	5	95.3	65.6	44.0	60.2
	10	95.5	72.7	63.6	65.6
	15	97.2	78.0	74.5	71.8
	20	96.8	80.4	80.3	73.2
	30	96.9	82.9	83.8	76.5
	40	96.5	85.3	84.1	77.9

UM00012962
NOVARTIS EXHIBIT 1017
Novartis v. Regents, IPR2023-01346
Page 1708 of 4460

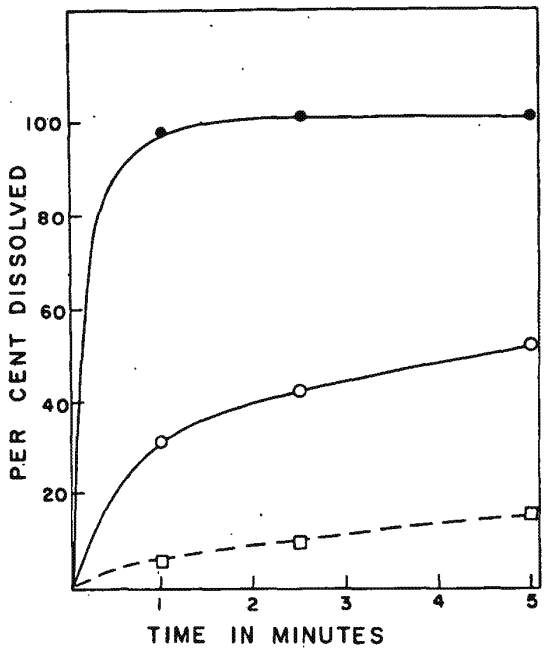


Figure 1. Dissolution profiles of theophylline in simulated gastric fluid at 37 C, from theophylline, ephedrine hydrochloride, and phenobarbital tablets; key: ●——●, brand name; ○——○, generic-B; □——□, generic-A

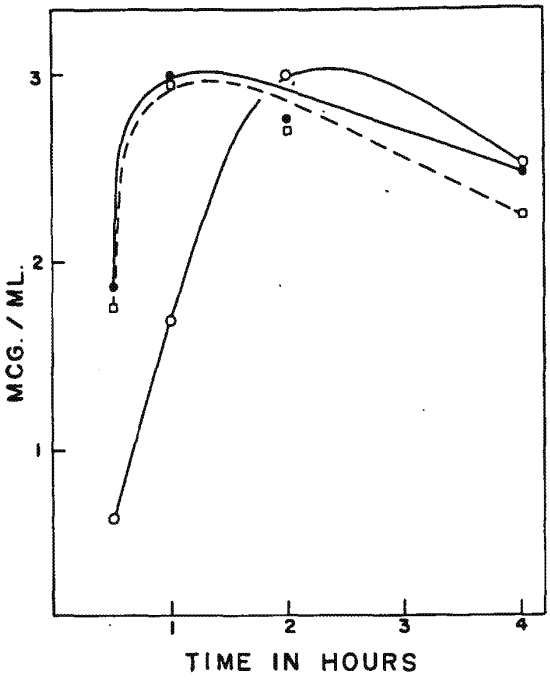


Figure 3. Theophylline serum levels, subject JWB, following a single 100-mg oral dose of theophylline (a) physically mixed with phenobarbital and (b) complexed with phenobarbital; key: ●——●, free; ○——○, complex; □——□, physical mixture

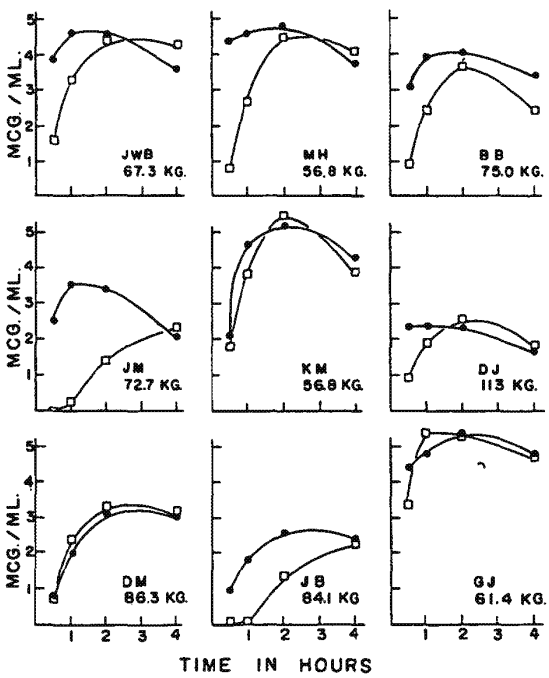


Figure 2. Comparative theophylline serum concentrations following oral ingestion of the powder preparations (equivalent to 130 mg); key: ●——●, free theophylline; □——□, theophylline-phenobarbital complex

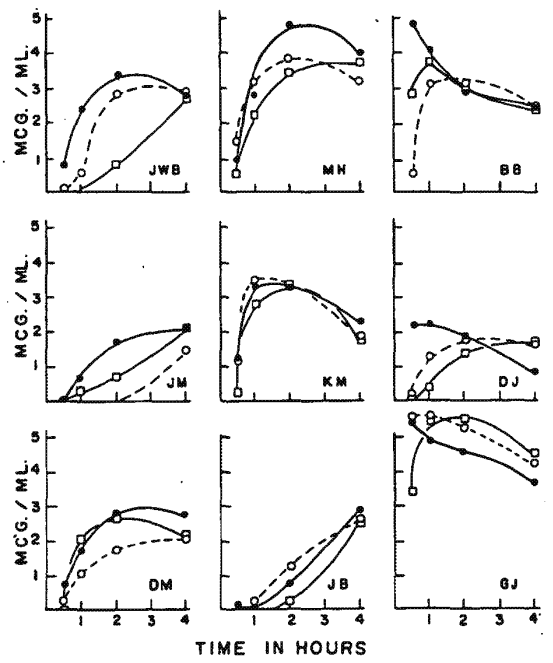


Figure 4. Comparative theophylline serum concentrations following oral ingestion of the tablet formulations (equivalent to 130 mg theophylline); key: ●——●, brand name; ○——○, generic-A; □——□, generic-B

UM00012963
NOVARTIS EXHIBIT 1017
Novartis v. Regents, IPR2023-01346
Page 1709 of 4460

vide a much slower dissolution rate of theophylline than the reference product.[b]

Serum Theophylline Levels. Figure 2 shows the serum levels of theophylline attained after the oral administration of theophylline and theophylline-phenobarbital complex. In seven of the nine subjects, dosage with theophylline produced high serum levels more rapidly than dosage with the complex. A physical mixture of theophylline and phenobarbital was given to one of the subjects (Figure 3), and the serum theophylline curve obtained was very nearly congruent with that obtained with theophylline alone. This observation tends to exclude the hypothesis that the difference observed could be due to a pharmacodynamic effect of phenobarbital on theophylline absorption rate.

Serum level is considered an important parameter in the evaluation of a formulation for clinical use. Figure 4 illustrates theophylline serum levels attained after the oral administration of Tedral and the two other tablet formulations. (Data for the tablets declaring 80 mg theophylline, where a two-tablet dose was given, are adjusted to 130 mg to allow comparison). In six of nine subjects the serum theophylline levels were highest in the 1/2- to 4-hour period after administration of the trade-named product.

There appears to be good correlation between the in vitro dissolution rate experiments and the blood level findings both in the comparisons of theophylline and theophylline-phenobarbital complex and in comparisons of the tablet formulations. The hypothesis that the difference in clinical response among the tablet formulations may relate in part to different degrees of complexation between theophylline and phenobarbital is supported by the data. These differences may relate to differences in manufacturing methods.

This study documents one of the few examples of a $drug_1$-$drug_2$ interaction reported in practical therapy.

Summary and Conclusions

In vitro dissolution rate studies and human blood level studies on theophylline were performed comparing Tedral tablets, a brand of Theophylline, Ephedrine Hydrochloride, and Phenobarbital Tablets, NF, with two chemically equivalent tablets. Dissolution rate of theophylline from the trade-named product was much faster than from the two tablets, and the difference was reflected in blood level comparisons of the three products in six of nine subjects. Comparison of dissolution rates of theophylline and as the preformed 2:1 theophylline-phenobarbital showed clearly that theophylline dissolves much faster than from the complex. In seven of nine subjects, the faster dissolution rate was attended by higher blood levels which were more rapidly attained. The data support the hypothesis that the differences in clinical performance observed between the trade-named product and two other tablet formulations may be due to differences in the extent of theophylline-phenobarbital complexation achieved during manufacture. Such a $drug_1$-$drug_2$ interaction, although previously shown to occur in vitro, has not been clearly demonstrated by in vivo studies in humans.

[b]As noted previously, the NF XIII monograph for Theophylline, Ephedrine Hydrochloride, and Phenobarbital Tablets became official after completion of this work. Nevertheless, it is interesting to observe that the monograph requires that not less than 66% of the labeled amount of theophylline in tablets be dissolved within 2.0 minutes (using the same dissolution test method described here). It is obvious from Figure 1 that neither of the alternates meet this requirement. In practice, however, one has no assurance that all commercially available drug dosage forms covered by an official monograph will meet official requirements. Moreover, a formulary alternate, such as the product with the lesser amount of theophylline and substitution of ephedrine with racephedrine, is not covered by monograph requirements.

References

1. Wagner, J. G.: Biopharmaceutics and Relevant Pharmacokinetics, Drug Intelligence Publications, Hamilton, Illinois, 1971, p. 169–173.

2. Poole, J. W.: Drug Formulation and Biologic Availability, *Seminar in Drug Treatment 1*:148–176 (Sept.) 1971.

3. Monkhouse, D. C. and Lach, J. L.: Drug-Excipient Interactions, *Can. J. Pharm. Sci.* 7:29–46 (Nov.) 1972.

4. Higgins, W. and Dunker, M.: A Study of the Reaction of Theophylline with Barbiturates, *J. Amer. Pharm. Ass., Sci. Ed. 33*:310–314 (Sept.) 1944

5. Guillory, J. K., Hwang, S. C. and Lach, J. L.: Interactions Between Pharmaceuticals Compounds by Thermol Methods, *J. Pharm. Sci. 58*:301–308 (Mar.) 1969.

6. Levy, G. and Hayes, B. A.: Physicochemical Basis of the Buffered Acetylsalicylic Acid Controversy, *N. Engl. J. Med. 262*:1053–1058 (May 26) 1960.

7. Schack, J. A. and Waxler, J. A.: An Ultraviolet Spectrophotometric Method for the Determination of Theophyllic and Theobromine in Blood and Tissues, *J. Amer. Med. Ass. 143*:736–789 (June) 1950.

This column covers a broad range of topics pertinent to dosage form and biopharmaceutical design. It emphasizes (1) the pharmaceutic and biopharmaceutic principles required for dosage form design in hospital pharmacy, (2) topics in these areas which are of general interest to the clinical pharmacist in his interpretation of dosage form effects and (3) brief research projects in these areas.

Formulations published in this column are intended only as guides to preliminary evaluation in individual laboratories. Since no program of bulk compounding should be conducted without the provision for quality control, all formulations are considered incomplete until individual laboratories judge their merit on the basis of appropriate analytical procedures.

Contributions of 500-2,000 words are invited if they demonstrate the practical application of sound dosage form and biopharmaceutical design theory. The theoretical justification for all procedures, formulations and interpretations is required. Address all correspondence to:

Gerald E. Schumacher, Pharm.D., Ph.D.
Associate Professor of Pharmaceutics
College of Pharmacy
Wayne State University
Detroit, Michigan 48202

UM00012964
NOVARTIS EXHIBIT 1017
Novartis v. Regents, IPR2023-01346
Page 1710 of 4460

This Page is Inserted by IFW Indexing and Scanning Operations and is not part of the Official Record

BEST AVAILABLE IMAGES

Defective images within this document are accurate representations of the original documents submitted by the applicant.

Defects in the images include but are not limited to the items checked:

- ☐ BLACK BORDERS
- ☐ IMAGE CUT OFF AT TOP, BOTTOM OR SIDES
- ☐ FADED TEXT OR DRAWING
- ☐ BLURRED OR ILLEGIBLE TEXT OR DRAWING
- ☐ SKEWED/SLANTED IMAGES
- ☐ COLOR OR BLACK AND WHITE PHOTOGRAPHS
- ☐ GRAY SCALE DOCUMENTS
- ☐ LINES OR MARKS ON ORIGINAL DOCUMENT
- ☐ REFERENCE(S) OR EXHIBIT(S) SUBMITTED ARE POOR QUALITY
- ☐ OTHER: _____

IMAGES ARE BEST AVAILABLE COPY.
As rescanning these documents will not correct the image problems checked, please do not report these problems to the IFW Image Problem Mailbox.

This study indicates that caffeine is not unique in its ability to stabilize an ester through complex formation. It would seem that other complexing agents of similar structure are also effective in stabilizing through this mechanism.

EXPERIMENTAL

Reagents.—Caffeine, U. S. P., recrystallized from water, m. p. 235–237°; 1-Ethyltheobromine, synthesized according to the method of Blitz (5); Benzocaine, U. S. P., recrystallized from ethyl alcohol and water, m. p. 92–93°; Silicic Acid, Mallinckrodt Chromatography Grade, was used to prepare the columns; and Diisopropyl Ether was purified as described in a previous report (1).

Apparatus.—Pyrex glass chromatographic columns 45 cm. long and 2 cm. in diameter; a tight fitting glass plunger to pack the columns; Beckman Model D U spectrophotometer; and a constant temperature bath set at 30° ± 0.05°.

Chromatographic Columns.—The columns were packed according to the procedure of Higuchi and Patel (1). In preparing the slurry, distilled water was used as the internal phase and Skellysolve-C as the external phase.

Complexing Behavior of Benzocaine-1-Ethyltheobromine System.—Benzocaine in excess of its solubility (0.3 Gm.) was weighed and placed into 125-ml. glass-stoppered bottles. Then varying volumes of stock solution containing 1-ethyltheobromine were added from a buret. Each bottle was brought up to a volume of 50 ml. with distilled water. The bottles were stoppered and agitated in a constant temperature bath at 30° for 12 hours. Five-milliliter aliquots of the clear supernatant liquid were then withdrawn and diluted to 25 ml. with distilled water. Five ml. of the resulting dilution was analyzed for benzocaine by a partition chromatographic method similar to that used by Higuchi and Lachman (1).

Chemical Kinetic Study.—The progress of the degradation of benzocaine was followed by the method utilized in the study of the benzocaine-caffeine system (1). In this study, however, the $Ba(OH)_2$ remaining unreacted in the samples taken for assay was neutralized by the addition of 10% excess 0.5 *N* HCl.

REFERENCES

(1) Higuchi, T., and Lachman, L., THIS JOURNAL, 44, 521(1955).
(2) Lachman, L., Ravin, L. J., and Higuchi, T., *ibid.*, 45, 290(1956).
(3) Lachman, L., and Higuchi, T., *ibid.*, 46, 32(1957).
(4) Higuchi, T., and Lach, J. L., *ibid.*, 43, 465(1954).
(5) Biltz, M., *Ann.*, 414, 69(1917).

Complexes Formed in Solution by Homologs of Caffeine.*

Interactions Between *p*-Hydroxybenzoic Acid and Ethyl, Propyl, and Butyl Derivatives of Theobromine, and Theophylline

By SANFORD BOLTON, DAVID GUTTMAN, and TAKERU HIGUCHI

The results show that the compounds investigated behave similarly in their interaction with *p*-hydroxybenzoic acid despite their differences in structure. The solubilities of the complexes formed, however, appear to be markedly dependent on the structure of the parent xanthines. Only one to one species are precipitated in the systems under the conditions employed. The suggestion is made, however, that soluble forms of higher order may be present in solution.

PREVIOUS INVESTIGATIONS (1–5) have shown that caffeine and other naturally occurring xanthines form stable complexes with a variety of organic compounds. Since this type of interaction has possible useful applications in pharmaceutical formulations (6), it seemed desirable to extend the study to higher molecular weight synthetic xanthine derivatives. Such studies, it was thought, might help uncover a better complexing agent and give further insights into the mechanism of these interactions.

EXPERIMENTAL PROCEDURE

Reagents—Recrystallized ethyl theophylline, m. p. 156–157°; butyl theophylline, m. p. 108–109°; propyl theophylline, m. p. 99–100°; ethyl theobromine, m. p. 167–168°; propyl theobromine, m. p. 138–139°; butyl theobromine, m. p. 122–123°; *p*-hydroxybenzoic acid, m. p. 214–216°; 0.05 *N* alcoholic KOH solution; alphanaphthol benzein as indicator.

Procedure.—The experimental procedure and the method of analysis were the same as those used for the caffeine study (3). A 0.005 *N* sulfuric acid solution was used as the solvent to suppress any

* Received March, 1956, from the School of Pharmacy, University of Wisconsin, Madison.
Presented to the Scientific Section, A. PH. A., Detroit meeting, April, 1956.
Supported in part by the Research Committee of the Graduate School from funds supplied by the Wisconsin Alumni Research Foundation.

TABLE I.—PHYSIC
TH

Xanthine
Theophylline
Theobromine
Caffeine
7-Ethyl theophy
7-Propyl theoph
7-Butyl theophy
1-Ethyl theobro
1-Propyl theobr
1-Butyl theobro

[a] Uncorrected.

dissociation of *p*-l
tems were equilib
temperature water
amount of *p*-hydrc
of solvent was 0.5 C
The theophyllin
were prepared acc
(8) and Biltz (9), r
A number of xa
their physical prop
It is seen that r
ture result in marl
and melting point
be expected that t
xanthine derivativ
forces responsible
to be similar to th
This study is c
p-hydroxybenzoic
butyl derivatives c
The experimental
scribed in previo
consists of noting t
consideration on t
benzoic acid.

RESULTS

The results obta
trated by means of
It is seen that the
the system initiall
apparent solubility
linear relationship
first order with res
librium can be repr

$n[p\text{-hydroxybenzoi}$
$[p\text{-hyd}$

The equilibrium

$K = [p\text{-hydroxybe}$
$[p\text{-hydr}$

Since the concen
constant in this re
possible to determi
rium on the acid
ever, from Figs. 1
mole of xanthine
mately one mole of
In all cases, as s

UM00012966
NOVARTIS EXHIBIT 1017
Novartis v. Regents, IPR2023-01346
Page 1712 of 4460

TABLE I.—PHYSICAL CONSTANTS OF SOME XANTHINE DERIVATIVES

Xanthine	M. P., °C.	Solubility at 30°, Moles/Liter × 10^3
Theophylline	270	4.5
Theobromine	357	0.3
Caffeine	238	13.3
7-Ethyl theophylline	156[a]	17.6
7-Propyl theophylline	99[a]	104.4
7-Butyl theophylline	108[a]	1.56
1-Ethyl theobromine	167[a]	19.1
1-Propyl theobromine	138[a]	6.19
1-Butyl theobromine	122[a]	2.37

[a] Uncorrected.

dissociation of *p*-hydroxybenzoic acid. The systems were equilibrated by shaking in a constant temperature water bath for 16 hours at 30°. The amount of *p*-hydroxybenzoic acid added per 25 ml. of solvent was 0.5 Gm.

The theophylline and theobromine derivatives were prepared according to the methods of Schwab (8) and Biltz (9), respectively.

A number of xanthine derivatives and some of their physical properties are listed in Table I.

It is seen that relatively minor changes in structure result in marked variations in the solubilities and melting points of these compounds. It might be expected that the complexing tendencies of these xanthine derivatives would also differ, since the forces responsible for such phenomena are thought to be similar to those causing complex formation.

This study is concerned with the interaction of *p*-hydroxybenzoic acid with the ethyl, propyl, and butyl derivatives of theobromine and theophylline. The experimental procedure is essentially that described in previous papers (1–2). The method consists of noting the effect of the compounds under consideration on the water solubility of *p*-hydroxybenzoic acid.

RESULTS AND OBSERVATIONS

The results obtained are most conveniently illustrated by means of the accompanying Figs. 1 and 2. It is seen that the addition of xanthine derivative to the system initially results in an increase in the apparent solubility of *p*-hydroxybenzoic acid. The linear relationship indicates that the interaction is first order with respect to the xanthine. The equilibrium can be represented by the equation:

$$n[p\text{-hydroxybenzoic acid}] + [\text{xanthine}] \rightleftarrows [p\text{-hydroxybenzoic acid}_n\text{-xanthine}] \quad (1)$$

The equilibrium quotient may be written as:

$$K = [p\text{-hydroxybenzoic acid}_n\text{-xanthine}] / [p\text{-hydroxybenzoic acid}]^n[\text{xanthine}] \quad (2)$$

Since the concentration of free acid in solution is constant in this region of the curve (3), it is impossible to determine the dependency of the equilibrium on the acid concentration. It is seen, however, from Figs. 1 and 2 that the addition of one mole of xanthine derivative solubilizes approximately one mole of *p*-hydroxybenzoic acid.

In all cases, as seen from Figs. 1 and 2, the solubility of acid is increased with addition of xanthine derivative until a plateau region is reached, where the concentration of *p*-hydroxybenzoic acid in solution remains constant. This indicates the appearance of an insoluble species. This point of maximum solubility varies among the different compounds and is seemingly dependent on the length of the alkyl substituent. This maximum solubility decreases as the length of the substituent alkyl group is increased. The fact that in the caffeine-*p*-hydroxybenzoic acid system (3) no insoluble species appeared up to approximately 0.09 *M* caffeine concentrations is in agreement with the above observation.

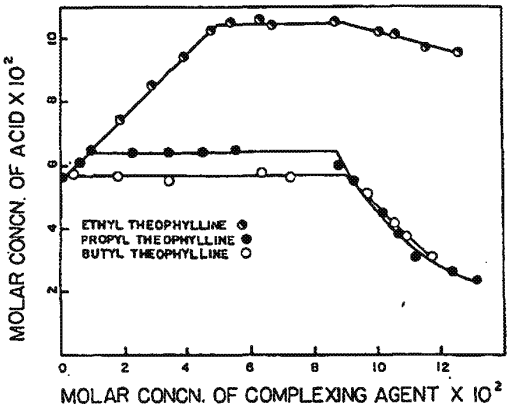


Fig. 1.—Phase diagram showing the effect of several theophylline derivatives on the apparent solubility of *p*-hydroxybenzoic acid in water at 30°.

The stoichiometry of an insoluble complex can be calculated from these phase diagrams according to the method used by Higuchi and Lach (4). In the case of ethyl theobromine, for example, it can be seen from Fig. 2 that the concentration of acid in solution remains invariant along the line AB. At point B all the excess solid acid has been precipitated as complex, and after this point *p*-hydroxybenzoic acid is being precipitated from solution. The amount of ethyl theobromine represented by the length of the plateau is equal to that entering

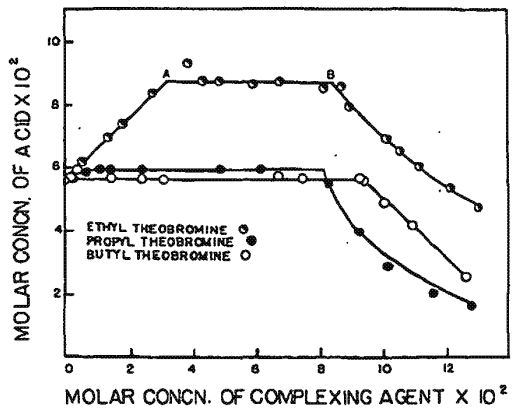


Fig. 2.—Phase diagram showing the effect of several theobromine derivatives on the apparent solubility of *p*-hydroxybenzoic acid in water at 30°.

UM00012967
NOVARTIS EXHIBIT 1017
Novartis v. Regents, IPR2023-01346
Page 1713 of 4460

into the insoluble complex during that interval. The corresponding amount of acid converted to the insoluble complex is equal to the difference between the total amount of *p*-hydroxybenzoic acid added to the system and that found in solution at point A. Table II lists the stoichiometry of these various insoluble complexes calculated in this manner. The values obtained by this method were verified by isolation and chemical analysis of the insoluble reaction product. It is seen that the ratio of acid to xanthine derivative is close to one-to-one in all cases considered in this study.

TABLE II.—STOICHIOMETRIC RATIO OF THE INSOLUBLE COMPLEXES

Xanthine Derivative Entering into Insol. Complex	Molar Ratio of Acid to Xanthine Derivative
Ethyl theophylline	1.04
Propyl theophylline	1.02
Butyl theophylline	0.99
Ethyl theobromine	1.09
Propyl theobromine	1.12
Butyl theobromine	0.97

Although the above results suggest that the prominent reaction in these systems is of a one-to-one nature, there is suggestive evidence that this is not the only equilibrium existing in solution. The equilibrium constants calculated solely on a one-to-one basis are abnormally large. In the ethyl theobromine-*p*-hydroxybenzoic acid system, for example, the constant calculated on the above basis is of the order of 2,000 (moles/liter)$^{-1}$.

The descending portion of the curve can also give valuable information on the nature of these reactions. Equation 4 describes the experimental behavior of the systems in question if the interaction is exclusively one to one.

$$[\text{Total acid in sol.}] = [\text{Free acid in sol.}] + [\text{complex in sol.}] \quad (3)$$

From Equation 2 and 3,

$$[\text{Total acid in sol.}] = [\text{Complex in sol.}]\,[1 + (1)/(K \times \text{free xanthine in sol.})] \quad (4)$$

The values of the total acid in solution on the down curve can be calculated in the following manner: Let X = total acid in solution at the plateau; Y = amount of complex precipitated as indicated by the length of the plateau; and Z = total acid in solution. Then, [Complex in solution] = $[X - 5.54 \times 10^{-2}]$ moles/liter where 5.54×10^{-2} moles/liter = solubility of *p*-hydroxybenzoic acid at 30°. [Free xanthine in sol.] = [Total xanthine added]-[complex in sol.] − $[Y]$ − $[X - Z]$.

By substituting these values into Eq. 4, the theoretical concentration of acid in solution based on a one-to-one complex formation can be estimated. The concentrations of total acid in solution calculated on this basis differed from the concentrations obtained experimentally. Some representative values for the ethyl theobromine-*p*-hydroxybenzoic acid interaction are listed in Table III. The appreciable discrepancy between the observed and calculated values plus the fact that these xanthine derivatives associate to considerable extents in solution (7) seem to indicate that a one-to-one interaction is not the sole equilibrium existing in solution.

TABLE III.—COMPARISON OF SOME CALCULATED AND OBSERVED VALUES OF *p*-HYDROXYBENZOIC ACID IN SOLUTION

Total Ethyl theobromine added, Moles/Liter × 10^2	Total Acid in Sol. Calcd. from Equation 4, Moles/Liter × 10^2	Total Acid in Sol. Obs., Moles/Liter × 10^2
14	3.63	4.50
13	4.32	4.80
12	5.24	5.42

If there are a number of simultaneous equilibria in solution an exact statement describing the nature of the interaction cannot be derived by this method of investigation. The initial slope of the solubility curve, however, does reflect the complexing tendency and, therefore, can be used to characterize, qualitatively, the relative reactivity of these compounds. The slopes for all the xanthine derivatives studied appear to be the same and parallel that of caffeine (5). This seems to indicate that in this series of xanthines the degree of interaction with *p*-hydroxybenzoic acid either is not significantly affected by the substituted alkyl group or, if of a one-to-one type, is very high.

The results of the simultaneous effect, on equimolar mixture, of two xanthine derivatives on the solubility of *p*-hydroxybenzoic acid are illustrated in Fig. 3. It appears that the solubilizing action on *p*-hydroxybenzoic acid is dependent on the combined total moles of complexing agent present.

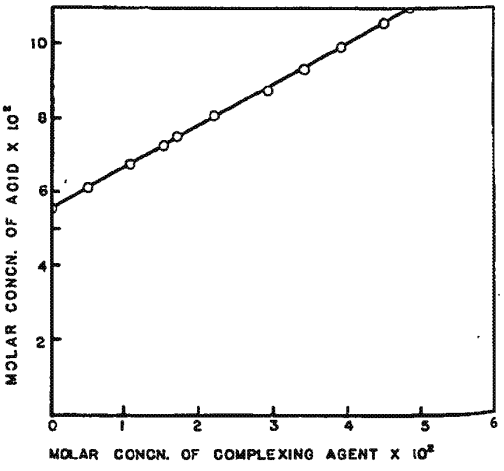


Fig. 3.—Phase diagram showing the solubility behavior of *p*-hydroxybenzoic acid in the presence of equimolor mixture of ethyl theobromine and ethyl theophylline in water at 30°. The molar concentration of complexing agent is equal to the combined total moles of xanthine derivative present.

1. The xant
strong complexi
benzoic acid as
solubility curves
libria in solution
2. These de
plexes of a on
depending on th
theobromine or
feine-*p*-hydroxyl

Effect

A study
Newtor
it was fc
concent
Yield v
(5% w/
additio
The am

THE LITERATU
importance c
producing thixo
clays (1–3). Th
the addition or r
ions from the cl
havior. Howeve
edge as to the
flow behavior i
official pharmac
trolytes are adde
With these th
were carried out
electrolytes on
thixotropic beha
cal bentonite in a

* Received April 1
macy, Philadelphia C
delphia 4, Pa.
Abstracted in par
Graduate School, P
Science, by Harris B
requirements for the
Presented to the
meeting, April, 1956.
[1] Volclay Bentonit
meets the requireme

UM00012968
NOVARTIS EXHIBIT 1017
Novartis v. Regents, IPR2023-01346
Page 1714 of 4460

CONCLUSIONS

1. The xanthine derivatives studied show strong complexing tendencies with *p*-hydroxybenzoic acid as indicated by the slopes of their solubility curves. The exact nature of the equilibria in solution, however, is in doubt.

2. These derivatives form insoluble complexes of a one-to-one nature, the solubility depending on the alkyl group substituted in the theobromine or theophylline nucleus. The caffeine-*p*-hydroxybenzoic acid system produces the most soluble complex in the homologous series of xanthine derivatives investigated thus far.

REFERENCES

(1) Higuchi, T., and Zuck, D. A., THIS JOURNAL, 41, 10 (1952).
(2) *Ibid.*, 42, 132(1953).
(3) *Ibid.*, 42, 138(1953).
(4) Higuchi, T., and Lach, J. L., THIS JOURNAL, 43, 349 (1954).
(5) *Ibid.*, 43, 524(1954).
(6) Higuchi, T., and Lachman, L., THIS JOURNAL, 44, 521 (1955).
(7) Guttman, D., and Higuchi, T., *ibid.*, in press.
(8) Schwab, W., *Arch. Pharm.*, 245, 323(1908).
(9) Biltz, M., *Ann.*, 414, 69(1917).

Effect of Electrolytes on Bentonite Suspensions*

By HARRIS B. BERNSTEIN and MARTIN BARR

A study of the effect of electrolytes on the degree of unipolar coacervation and non-Newtonian behavior of bentonite in aqueous suspension has been made. Although it was found that thixotropic behavior was not induced in the clay at a nonthixotropic concentration (3% w/v), yield values were affected by the addition of electrolytes. Yield values were also affected by ions in a thixotropic concentration of the clay (5% w/v). Thixotropic behavior of 5% w/v suspensions was not increased by the addition of electrolytes although two electrolytes caused a decrease in behavior. The amount of water which separated from the suspensions at different electrolyte concentrations was also studied.

THE LITERATURE contains many works on the importance of the presence of electrolytes in producing thixotropic systems with earths or clays (1–3). These experiments were based on the addition or removal of electrolytes or certain ions from the clay and observing the flow behavior. However, there exists little or no knowledge as to the degree of water separation and flow behavior in aqueous suspensions of the official pharmaceutical bentonite[1] when electrolytes are added to them.

With these thoughts in mind, investigations were carried out to observe the effect of different electrolytes on the unipolar coacervation and thixotropic behavior of the official pharmaceutical bentonite in aqueous suspensions.

* Received April 13, 1956, from the Department of Pharmacy, Philadelphia College of Pharmacy and Science, Philadelphia 4, Pa.
Abstracted in part from a dissertation submitted to the Graduate School, Philadelphia College of Pharmacy and Science, by Harris B. Bernstein in partial fulfillment of the requirements for the degree of Doctor of Science.
Presented to the Scientific Section, A. PH. A., Detroit meeting, April, 1956.

[1] Volclay Bentonite, American Colloid Company, which meets the requirements of Bentonite, U. S. P. XV.

EXPERIMENTAL

The electrolytes used in this study fall into two classes: (*a*) those that have ions included in the lyotropic series of ions (citrate, tartrate, acetate, chloride, sulfate, nitrate, chlorate, iodide, thiocyanate, lithium, sodium, potassium, ammonium and magnesium; (*b*) and those electrolytes that would show the effect of different valent ions which are not included in the lyotropic series (bromide, sulfate, carbonate, phosphate, aluminum, calcium, magnesium) (4, 5).

The effects of electrolytes or ions were studied in nonthixotropic 3% w/v bentonite suspensions and thixotropic 5% w/v bentonite suspensons (6). Electrolyte concentrations, chosen from preliminary experiments, were the following:

(*a*) 2×10^{-3} *M*. This concentration was the most suitable for observing the degree of coacervation in bentonite suspensions since lower concentrations caused little water separation from the suspensions.

(*b*) 2×10^{-2} *M*. This was the highest concentration which could be added to bentonite suspensions and permit thixotropic measurement with the MacMichael viscometer.

(*c*) 2×10^{-5} *M*. This concentration was used

UM00012969
NOVARTIS EXHIBIT 1017
Novartis v. Regents, IPR2023-01346
Page 1715 of 4460

This Page is Inserted by IFW Indexing and Scanning Operations and is not part of the Official Record

BEST AVAILABLE IMAGES

Defective images within this document are accurate representations of the original documents submitted by the applicant.

Defects in the images include but are not limited to the items checked:

- ☐ BLACK BORDERS
- ☐ IMAGE CUT OFF AT TOP, BOTTOM OR SIDES
- ☐ FADED TEXT OR DRAWING
- ☐ BLURRED OR ILLEGIBLE TEXT OR DRAWING
- ☐ SKEWED/SLANTED IMAGES
- ☐ COLOR OR BLACK AND WHITE PHOTOGRAPHS
- ☐ GRAY SCALE DOCUMENTS
- ☐ LINES OR MARKS ON ORIGINAL DOCUMENT
- ☐ REFERENCE(S) OR EXHIBIT(S) SUBMITTED ARE POOR QUALITY
- ☐ OTHER: _____

IMAGES ARE BEST AVAILABLE COPY.
As rescanning these documents will not correct the image problems checked, please do not report these problems to the IFW Image Problem Mailbox.

Chem. Commun., 2003, (2), 250 - 251
DOI: 10.1039/b208904a



In situ co-crystallisation as a tool for low-temperature crystal engineering†

Communication

Andrew D. Bond
University of Cambridge, Department of Chemistry, Lensfield Road, Cambridge, UK.
mailto:adb29@cam.ac.uk

Received (in Cambridge, UK) 12th September 2002, Accepted 4th December 2002

First published on the web 17th December 2002

Synthesis and single-crystal X-ray diffraction of a series of low-melting co-crystals of pyrazine and *n*-alkyl carboxylic acids demonstrates *in situ* co-crystallisation as a versatile tool for low-temperature crystal engineering.

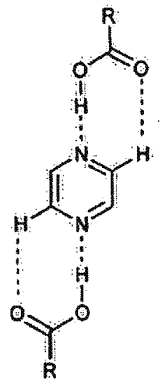
Research in the diverse field of crystal engineering continues to expand at a dramatic rate, with the scope for production of new crystalline and co-crystalline molecular materials seemingly unbounded.[1] Preparation of multi-component molecular crystals represents genuine synthesis on a supramolecular scale, forming non-covalent rather than covalent bonds between molecular components during co-crystallisation. Since the resulting materials exist only in the solid state however, there arises a practical difficulty when studying co-crystals that melt below room temperature. This complicates the synthesis and solid-state characterisation of multi-component crystals of many of the simplest molecules. As a consequence, studies of co-crystalline molecular materials have to date generally been restricted to those that are solid under ambient conditions.

Single-crystal X-ray diffraction analysis of low-melting materials has recently undergone something of a resurgence,[2–5] principally as a result of improvements in equipment and techniques for *in situ* crystal growth.[6,7] While these techniques have become well established for single-component systems, their extension to multi-component systems has not been reported. Successful application of *in situ* techniques to multi-component mixtures should expand dramatically the range of co-crystals that may be prepared and studied by single-crystal X-ray diffraction, presenting new opportunities for study of multi-component crystals that do not exist under ambient conditions. Reported here is the *in situ* synthesis and single-crystal X-ray diffraction analysis of a series of co-crystals containing pyrazine and *n*-alkyl carboxylic acids, all of which melt around or below room temperature. The study demonstrates that *in situ* co-crystallisation may indeed be employed successfully for the synthesis and characterisation of low-melting multi-component crystals, and the technique should prove to be a versatile tool for low-temperature crystal engineering.

f e c e e g c e ec e

UM00012971
NOVARTIS EXHIBIT 1017
Novartis v. Regents, IPR2023-01346
Page 1717 of 4460

Co-crystals **1–10** were prepared from 1 : 2 stoichiometric mixtures of pyrazine and the appropriate *n*-alkyl carboxylic acid, the stoichiometry being selected by consideration of the trimeric supramolecular motif shown in Scheme 1, predicted on the basis of the supramolecular synthon approach.[8,9] In the 1 : 2 stoichiometry, the mixtures may be considered to be pure molten co-crystals rather than simply solutions of pyrazine in the respective carboxylic acids. Mixtures **1–8**, containing methanoic to octanoic acid respectively, are liquid under ambient conditions (295 K, 1 atm), while mixture **9**, containing nonanoic acid, solidifies slowly at room temperature. A solution of pyrazine in decanoic acid (which is just solid under ambient conditions) was effected by gentle heating, and mixture **10** solidifies on returning to room temperature. Crystals of **1–8** were grown in 0.2 mm diameter glass capillaries at a temperature just below the melting point of the solid, using a simple zone-refinement technique.[4,7] Crystals of **9** and **10** were grown using a slight variation of the technique: the mixture was melted and loaded into a capillary, and the crystal was obtained by temperature cycling of ±1 K around the melting point. It is considerably more difficult to obtain a satisfactory single crystal using this technique. Once grown, all crystals were cooled to 180 K prior to data collection.‡ A certain degree of flexibility is possible in the stoichiometry of the mixture since the zone-refinement technique effectively purifies the co-crystalline product, but the process of obtaining a single crystal becomes considerably more difficult as the stoichiometry deviates from ideal. The melting points of the crystals (Scheme 1) were also determined *in situ* by warming the crystal in the N_2 gas stream after data collection — melting is readily detectable by the abrupt loss of the diffraction pattern.[10]



	R	m.p. / K
1	H	285
2	CH_3	268
3	CH_2CH_3	252
4	$(CH_2)_2CH_3$	260
5	$(CH_2)_3CH_3$	260
6	$(CH_2)_4CH_3$	272
7	$(CH_2)_5CH_3$	282
8	$(CH_2)_6CH_3$	283
9	$(CH_2)_7CH_3$	295
10	$(CH_2)_8CH_3$	300

Scheme 1

Table 1 Crystal system, space group, unit-cell parameters and crystal density at 180 K for **1–10**

			Z[a]	a/Å	b/Å	c/Å	α/°	β/°	γ/°	U/Å^3	D_c/g cm^{-3}
1	Monoclinic	$P2_1/c$	2	3.6994(1)	7.0340 (3)	16.1607 (9)	90	96.068(2)	90	418.17(3)	1.367
2	Triclinic	$P\bar{1}$	2	5.4869(2)	8.1885 (2)	11.9960 (4)	70.076 (1)	86.667(1)	89.925 (2)	505.76(3)	1.315
3	Monoclinic	$P2_1/n$	2	4.8735(2)	5.4384 (2)	23.2428 (10)	90	93.197(1)	90	615.07(4)	1.232
4	Monoclinic	$P2_1/n$	2	9.8544(7)	5.7127 (4)	13.5338 (13)	90	109.736 (3)	90	717.13 (10)	1.187
5	Monoclinic		2	13.2449	5.4022	11.9960	90	105.716	90	826.24(7)	1.143

f e c e e g c e ec e

UM00012972
NOVARTIS EXHIBIT 1017
Novartis v. Regents, IPR2023-01346
Page 1718 of 4460

		$P2_1/c$		(1)	(3)	(8)		(3)		
6	Monoclinic	$C2/c$	4	27.6365 (7)	5.4294 (1)	12.2322 (4)	90	94.639(1)	90	1829.42 (8) 1.134
7	Triclinic	$P\bar{1}$	1	5.5106(3)	6.8970 (3)	13.7860 (8)	76.816 (2)	85.697(2)	76.802 (2)	496.53(5) 1.139
8	Triclinic	$P\bar{1}$	1	5.4774(2)	6.9086 (3)	15.2102 (8)	81.541 (2)	84.977(2)	76.158 (4)	551.95(4) 1.109
9	Triclinic	$P\bar{1}$	1	5.4731(2)	6.8775 (2)	16.3824 (6)	89.776 (1)	82.992(1)	76.091 (1)	593.89(4) 1.109
10	Triclinic	$P\bar{1}$	1	5.4573(2)	6.8970 (2)	18.0387 (6)	80.575 (1)	81.940(1)	75.554 (2)	645.10(4) 1.093

[a] Z is the number of trimeric supermolecules in the unit cell.

Although the pyrazine–carboxylic acid system was studied primarily as a test for the *in situ* co-crystallisation technique, the resulting materials are of interest in themselves since they form a complete homologous series of co-crystal structures studied at a common temperature. Similar studies of single-component molecular materials have yielded notable insight into the correlation between crystal structures and physical properties, in particular melting points.[2,3] In each co-crystal **1**–**10**, the expected trimeric supramolecular motif is formed *via* an $R_2^2(7)$ hydrogen-bond pattern (Fig. 1), the C–H···O interaction providing the driving force for adoption of co-planarity between the carboxyl group and pyrazine ring.[9] In common with the early members of homologous single-component series, the structures of **1**–**6** exhibit considerable variation (Table 1) as a result of the complex balance between competing intermolecular forces. The structures of **7**–**10**, however, exhibit regularity, with the trimeric moieties arranged in layers similar to those in the *n*-alkanes and *n*-alkyl carboxylic acids (Fig. 2). Both of the latter molecular series display an alternation in their melting points, those members of each series with an odd number of carbon atoms having a relatively lower melting point than those with an even number of carbon atoms. In both cases, this is correlated with alternating crystal density.[2,11] In this respect, it is interesting to note that the densities and melting points of **7**–**10** appear also to signify the onset of an alternating trend, suggesting that melting point alternation may be a property of this two-component system, as well as of the carboxylic acids themselves.[1] Studies of the co-crystals of pyrazine with the higher acids, all of which are solid under ambient conditions, are underway in an effort to confirm this observation.

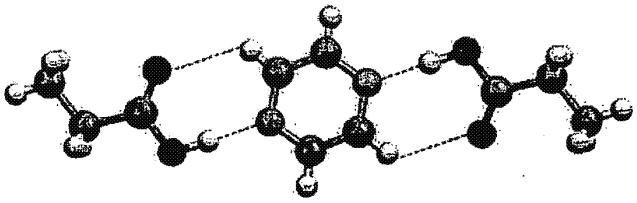


Fig. 1 Trimeric supramolecular moiety in **3** with hydrogen bonds shown as dotted lines. Comparable motifs are observed in the other co-crystals.

f e c e e g c e ec e

UM00012973
NOVARTIS EXHIBIT 1017
Novartis v. Regents, IPR2023-01346
Page 1719 of 4460

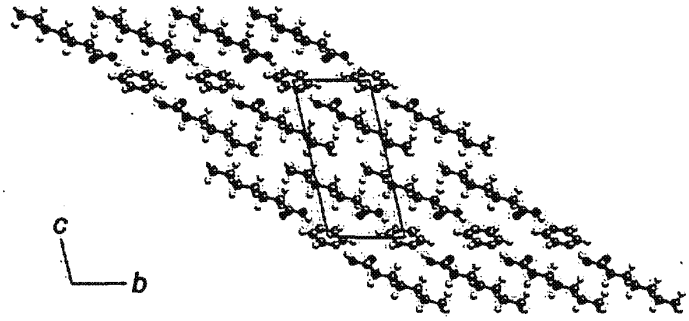


Fig. 2 Projection of **7** along the *a* direction showing the layered arrangement of the supramolecular moieties. Similar layered structures are adopted by **8–10**.

I am grateful to EPSRC for funding, to Professors Jeremy K. M. Sanders and Andrew B. Holmes (University of Cambridge) for facilitating this research, and to Dr John E. Davies (University of Cambridge) for his continued support and encouragement.

Notes and references

1 From the vast crystal engineering literature, two of the most relevant, relatively recent reviews are: C. B. Aakeröy, *Acta Crystallogr.*, 1997, **B53**, 569 [Links]; A. Nangia and G. R. Desiraju, *Acta Crystallogr.*, 1998, **A54**, 934 [Links].

2 R. Boese, H.-C. Weiss and D. Bläser, *Angew Chem., Int. Ed.*, 1999, **38**, 988 [Links].

3 V. R. Thalladi, R. Boese and H.-C. Weiss, *J. Am. Chem. Soc.*, 2000, **122**, 1186 [Links].

4 A. D. Bond and J. E. Davies, *Aust. J. Chem.*, 2001, **54**, 683 [Links].

5 A. D. Bond, *J. Chem. Soc., Chem. Commun.*, 2002, 1664 [Links].

6 R. Boese and M. Nussbaumer in *Correlations, Transformations and Interactions in Organic Crystal Chemistry, IUCR Crystallogrpahic Symposia*, ed. D. W. Jones and A. Katrusiak, Oxford University Press, Oxford, 1994.

7 J. E. Davies and A. D. Bond, *Acta Crystallogr.*, 2001, **E57**, o947 [Links].

8 G. R. Desiraju, *Angew. Chem., Int. Ed.*, 1995, **34**, 2311–2327 [Links].

9 E. Batchelor, J. Klinowski and W. Jones, *J. Mater. Chem.*, 2000, **10**, 839 [Links].

10 The temperature at the sample was calibrated by measuring the melting points of the series of pure *n*-alkyl carboxylic acids from heptanoic to decanoic acid, comparing these with literature values (see ESI).

11 A. D. Bond, manuscript submitted.

Footnotes

† Electronic supplementary information (ESI) available: details of the *in situ* melting point determinations and a plot of the variation in crystal density and melting point for **1–10**. See http://80-www.rsc.org.ezp1.harvard.edu/suppdata/cc/b2/b208904a/

‡ Crystal systems, space groups, unit-cell parameters and crystal densities for **1–10** are listed in Table 1. All data were collected at 180 K. *Crystal data for* **1**: $C_6H_8N_2O_4$, $M = 172.14$, μ(Mo-Kα) = 0.116 mm^{-1}. Of 2895 reflections measured, 760 were unique ($R_{int} = 0.1556$) and were used in all calculations. The final $wR2 = 0.1925$ (all data), $R1$ [$F^2 > 2\sigma(F^2)$] = 0.0723, and goodness-of-fit on F^2, $S = 1.11$ (CCDC 192849). *Crystal data for* **2**: $C_8H_{12}N_2O_4$, $M = 200.20$, μ(Mo-Kα) = 0.106 mm^{-1}.

f e c e e g c e ec e

UM00012974
NOVARTIS EXHIBIT 1017
Novartis v. Regents, IPR2023-01346
Page 1720 of 4460

Of 5274 reflections measured, 2287 were unique (R_{int} = 0.0719) and were used in all calculations. The final $wR2$ = 0.1499 (all data), $R1$ [$F^2 > 2\sigma(F^2)$] = 0.0518, and goodness-of-fit on F^2, S = 1.06 (CCDC 192850). *Crystal data for* **3**: $C_{10}H_{16}N_2O_4$, M = 228.25, μ(Mo-Kα) = 0.096 mm^{-1}. Of 1845 reflections measured, 891 were unique (R_{int} = 0.1186) and were used in all calculations. The final $wR2$ = 0.2189 (all data), $R1$ [$F^2 > 2\sigma(F^2)$] = 0.0749, and goodness-of-fit on F^2, S = 1.25 (CCDC 192851). *Crystal data for* **4**: $C_{12}H_{20}N_2O_4$, M = 256.30, μ(Mo-Kα) = 0.089 mm^{-1}. Of 3855 reflections measured, 1245 were unique (R_{int} = 0.0363) and were used in all calculations. The final $wR2$ = 0.1154 (all data), $R1$ [$F^2 > 2\sigma(F^2)$] = 0.0448, and goodness-of-fit on F^2, S = 1.04 (CCDC-192852). *Crystal data for* **5**: $C_{14}H_{24}N_2O_4$, M = 284.35, μ(Mo-Kα) = 0.084 mm^{-1}. Of 4881 reflections measured, 1374 were unique (R_{int} = 0.1216) and were used in all calculations. The final $wR2$ = 0.1962 (all data), $R1$ [$F^2 > 2\sigma(F^2)$] = 0.0726, and goodness-of-fit on F^2, S = 1.09 (CCDC 192853). *Crystal data for* **6**: $C_{16}H_{28}N_2O_4$, M = 312.40, μ(Mo-Kα) = 0.081 mm^{-1}. Of 8015 reflections measured, 2092 were unique (R_{int} = 0.0443) and were used in all calculations. The final $wR2$ = 0.1318 (all data), $R1$ [$F^2 > 2\sigma(F^2)$] = 0.0475, and goodness-of-fit on F^2, S = 1.06 (CCDC 192854). *Crystal data for* **7**: $C_{18}H_{32}N_2O_4$, M = 340.46, μ(Mo-Kα) = 0.080 mm^{-1}. Of 5160 reflections measured, 2210 were unique (R_{int} = 0.0383) and were used in all calculations. The final $wR2$ = 0.1192 (all data), $R1$ [$F^2 > 2\sigma(F^2)$] = 0.0436, and goodness-of-fit on F^2, S = 1.07 (CCDC 192855). *Crystal data for* **8**: $C_{20}H_{36}N_2O_4$, M = 368.51, μ(Mo-Kα) = 0.076 mm^{-1}. Of 4435 reflections measured, 2441 were unique (R_{int} = 0.0786) and were used in all calculations. The final $wR2$ = 0.2571 (all data), $R1$ [$F^2 > 2\sigma(F^2)$] = 0.0882, and goodness-of-fit on F^2, S = 1.10 (CCDC-192856). *Crystal data for* **9**: $C_{22}H_{40}N_2O_4$, M = 396.56, μ(Mo-Kα) = 0.075 mm^{-1}. Of 6194 reflections measured, 2652 were unique (R_{int} = 0.0648) and were used in all calculations. The final $wR2$ = 0.1489 (all data), $R1$ [$F^2 > 2\sigma(F^2)$] = 0.0533, and goodness-of-fit on F^2, S = 1.05 (CCDC 192857). *Crystal data for* **10**: $C_{24}H_{44}N_2O_4$, M = 424.61, μ(Mo-Kα) = 0.073 mm^{-1}. Of 4697 reflections measured, 2235 were unique (R_{int} = 0.0417) and were used in all calculations. The final $wR2$ = 0.1324 (all data), $R1$ [$F^2 > 2\sigma(F^2)$] = 0.0470, and goodness-of-fit on F^2, S = 1.10 (CCDC 192858). See http://80-www.rsc.org.ezp1.harvard.edu/suppdata/cc/b2/b208904a for crystallographic data in CIF format.

This journal is © The Royal Society of Chemistry 2002

UM00012975
NOVARTIS EXHIBIT 1017
Novartis v. Regents, IPR2023-01346
Page 1721 of 4460

Acta Crystallographica Section B
Structural
Science
ISSN 0108-7681

Urotropin azelate: a rather unwilling co-crystal

Michel Bonin,[a] T. Richard Welberry,[b] Marc Hostettler,[a] Manuel Gardon,[a] Henrik Birkedal,[a] Gervais Chapuis,[a] Pedro Möckli,[c] Craig A. Ogle[d] and Kurt J. Schenk[a]*

[a]Institut de Cristallographie, Université de Lausanne, BSP Dorigny, CH-1015 Lausanne, Switzerland, [b]Research School of Chemistry, Australian National University, Canberra, ACT 0200, Australia, [c]Department for Ceramics, Swiss Federal Technology Institute, CH-1015 Lausanne, Switzerland, and [d]Chemistry Department, University of North Carolina Charlotte, 9210 University City Blvd, Charlotte, NC 28223-0001, USA

Correspondence e-mail: kurt.schenk@ic.unil.ch

Received 16 July 2002
Accepted 26 November 2002

Dieter Schwarzenbach zu seinem Ruhestand gewidmet. 'Deine umfassende kristallographische Kultur wird uns immer Vorbild sein.'

Urotropin (U) and azelaic acid (AA) form 1:1 co-crystals (UA) that give rise to a rather complex diffraction pattern, the main features of which are diffuse rods and bands in addition to the Bragg reflections. UA is characterized by solvent inclusions, parasite phases, and high vacancy and dislocation densities. These defects compounded with the pronounced tendency of U to escape from the crystal edifice lead to at least seven exotic phase transitions (many of which barely manifest themselves in a differential scanning calorimetry trace). These involve different incommensurate phases and a peritectoid reaction in the recrystallization regime ($T_h > 0.6$). The system may be understood as an OD (order–disorder) structure based on a layer with layer group $P(c)c2$ and cell $a_o \simeq 4.7$, $b \simeq 26.1$ and $c \simeq 14.4$ Å. At 338 K the layer stacking is random, but with decreasing temperature the build-up of an orthorhombic MDO (maximal degree of order) structure with cell $\mathbf{a}_1 = 2\mathbf{a}_o$, $\mathbf{b}_1 = \mathbf{b}$, $\mathbf{c}_1 = \mathbf{c}$ and space group $Pcc2$ is begun (at ~301 K). The superposition structure of the OD system at $T = 286$ (1) K with space group $Bmmb$ and cell $\widehat{\mathbf{a}} = 2\mathbf{a}_o$, $\widehat{\mathbf{b}} = \mathbf{b}$ and $\widehat{\mathbf{c}} = \mathbf{c}/2$ owes its cohesion to van der Waals interactions between the AA chains and to three types of hydrogen bonds of varied strength between U—U and U—AA. Before reaching completion, this MDO structure is transformed, at 282 K, into a monoclinic one with cell $\mathbf{a}_m = -\mathbf{a}_o + \mathbf{c}/4$, $\mathbf{b}_m = \mathbf{b}$, $\mathbf{c}_m = -2(\mathbf{a}_o + c/2)$, space group $P2_1/c$, spontaneous deformation ~2°, and ferroelastic domains. This transformation is achieved in two steps: first a furtive triggering transition, which is not yet fully understood, and second an improper ferroelastic transition. At ~233 K, the system reaches its ground state (cell $\mathbf{a}_M = \mathbf{a}_m$, $\mathbf{b}_M = \mathbf{b}$, $\mathbf{c}_M = \mathbf{c}_m$ and space group $P2_1/c$) *via* an irreversible transition. The phase transitions below 338 K are described by a model based on the interaction of two thermally activated slip systems. The OD structure is described in terms of a three-dimensional Monte Carlo model that involves first- and second-neighbour interactions along the a axis and first-neighbour interactions along the b and c axes. This model includes random shifts of the chains along their axes and satisfactorily accounts for most features that are seen in the observed diffraction pattern.

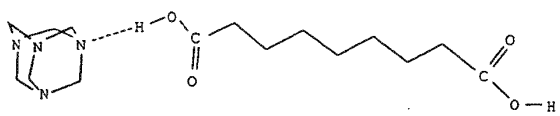
1. Introduction

Urotropin (U), besides its obvious medical importance (*ουρον - τρεπειν*), distinguishes itself by forming almost perfect single crystals with very low dislocation density (< 1 mm^{-2}; DiPersio & Escaig, 1972) and a mosaic spread half-width of 7″ (Kampermann *et al.*, 1995). It is a much studied classic capable of the most surprising applications. On the one hand the quasi-spherical molecule does not have a plastic phase but forms a

© 2003 International Union of Crystallography
Printed in Great Britain – all rights reserved

UM00012976
NOVARTIS EXHIBIT 1017
Novartis v. Regents, IPR2023-01346
Page 1722 of 4460

very compact structure (packing coefficient 0.74) that persists from 15 to 548 K, at which temperature sublimation occurs (Klipping & Stranski, 1958). U owes this behaviour to the rather weak (2.866 Å) C—H···N hydrogen bonds that hold the molecules together. The molecules themselves may be treated to a very good approximation as rigid bodies (libration is 5° at 200 K and 2° at 5 K), especially below 200 K (there is only some CH_2 vibration present). The intermolecular correlations (Canut & Amorós, 1958) between these rigid bodies lead to rather strong TDS in inter-Bragg space. On the other hand the situation is compounded by the tendency of U to start subliming at as low as 330 K (Birkedal, 1996) and, above 468 K, to chemically (Blažević *et al.*, 1979) and thermally



(Klipping & Stranski, 1958) decompose.

Azelaic acid (AA) crystallizes with packing that owes its cohesion within a layer to van der Waals forces and between layers to O—H ···O hydrogen bonds. The stable RT β form transforms into the α form at 346 K, but the reverse transition takes place under particular circumstances only (after a long time or under pressure). This mysterious behaviour is especially surprising in view of the similarity in magnitude (to 0.01 Å) of the hydrogen bonds mentioned above. The reason for the hysteresis must be sought in the chain packing. Here there are several differences. First the packing coefficient for the β form is 0.71 while for the α form it is 0.67. An approximate p-cell may be defined for the α form [p-cell is a term used in structures of close-packed long-chain alkanes that relates to the $-CH_2-$ molecular repeat (Abrahamsson *et al.*, 1978)] but not for the β form. Finally there are differences in conformation around the α-C atoms so that in the β form the chains are extended (all *trans* conformation) while in the α form there is one *gauche* conformation. Note that both forms develop a different habitus and, even more baffling, that under certain conditions both forms crystallize from the same solvent at the same temperature (Caspari, 1929). In regard to this last point AA must be considered to be one of the earliest reported examples of dimorphism (Dupré La Tour, 1935). It is also interesting to note that AA plays a (not yet understood) role in the inhibition of the activity of 5-α-reductase, which converts testosterone into the fatal dihydrotestosterone (Stamatiadis *et al.*, 1988). Finally, mention should be made of the antibacterial, antimycotic and antitumoral properties of AA.

In view of all the fundamental differences between the two molecules it seemed tempting to combine them in a co-crystal and study the manner in which their often contradictory properties expressed themselves in such a new compound. It was considered that the most exotic behaviour might be expected with regard to the structural packing, molecular motion, static disorder, defects, solvent inclusions, and stability and phase transitions. In this contribution, we present results for the room-temperature phase (II) of urotropin azelate (UA) and an overview of its rather complex phase diagram below 338 K (phases α, II, f, III and IV), which was studied by means of calorimetry, orthoscopy, X-ray diffraction and Monte Carlo simulations. This investigation highlights the earlier structural study of phase III (Hostettler *et al.*, 1999) as one of many pieces in the complex puzzle of OD phenomena and phase transitions in this system. Throughout the present report a subscript m will stand for phase III, a subscript M will stand for phase IV and quantities without subscript are with respect to phase II.

2. Experimental

2.1. Synthesis

FLUKA reagent-grade chemicals were used without further purification. Equimolar quantities of the reagents were dissolved in ethanol (U) and water (AA) and made to react by mixing the two solutions. The resulting white precipitate was recrystallized twice from ethanol. Finally the crystals used in this investigation were grown from a solution in acetonitrile. It was found that these crystals contained some of the solvent. When crystallized in this way UA grows as (010) platelets of varying thickness. As a result of the growth conditions a {100} pinacoid was occasionally developed, but {101} and {10$\bar{1}$} pinacoids were found to be always present.

2.2. Gas chromatography

Experiments were performed on an HP 5890 gas chromatograph (GC) equipped with a 5% diphenyl–95% dimethylpolysiloxane capillary column and an FID detector. The UA crystals for this study were grown at ambient temperature from reagent-grade acetonitrile (FLUKA) and were then air-dried. A solution of acetonitrile, 5 µl in 10 ml of distilled water (9.29 mM), was found to give a signal of 71.7 at a retention time t_R of 0.57 min, while a solution of 40 mg of UA in 2 ml of distilled water (60.24 mM) gave a signal of 4.64 at the same t_R. Distilled water alone gave no signal whatsoever. Taking into account the different molarities, we find that the UA · $x(H_3CCN)$ solution is roughly a hundred times poorer in acetonitrile than the reference sample. The formula for UA must therefore be written as UA · $0.01(H_3CCN)$. From the crystal and unit-cell dimensions, we estimate that the crystal contains about 10^{16} unit cells of which 10^{11} lie at the surface. We know that 1% of the cells contain one acetonitrile, and thus the crystal contains 10^{14} molecules of acetonitrile. It is therefore impossible that the whole of the solvent is at the surface only.

2.3. Differential scanning calorimetry

At ambient pressure, the thermotropic phase sequence was investigated by differential scanning calorimetry (DSC) using a Mettler DSC30 system. This was calibrated with In, Zn and

UM00012977
NOVARTIS EXHIBIT 1017
Novartis v. Regents, IPR2023-01346
Page 1723 of 4460

Table 1
Summary of DSC results for UA.

Values given are averages over several measurements.

Transition	T (K)	ΔH (J g^{-1})
I → Decomposition	401	
I → II	371	−2.3
II → I	375	1.57
II → III	282	1.65
III → II	283	−1.74 *not passing* through III → IV
II → III → IV	282, 236	1.65, 0.50
IV → II	283	−2.1

Pb at a rate of 1 K min^{-1}, and all measurements were performed at this rate. They were made in cycles in order to investigate hysteresis and reversibility of the phase transitions. Four phases, of which the transition temperatures and corresponding enthalpies are given in Table 1, have been identified. The transition at 371 K is reversible, but the melting transition at 401 K is often indicative of decomposition. This is due to a peritectoid reaction that sets in above ~363 K. The reaction is accompanied by an ever increasing weight loss above ~363 K. This loss is detected by thermogravimetry and is shown by GC and NMR to be due to a massive exodus of U from the co-crystal. The I ↔ II and II ↔ III transitions are thermodynamically reversible but subject to slight hystereses of 4 and 1.5 K, respectively. On lowering the temperature (Fig. 1) from ambient temperature, two phase transitions are observed: II → III at 282 K and III → IV at 236 K. However, on raising the temperature from phase IV, the IV → III transition is not observed and the crystal transforms directly to phase II at 283 K (roughly at the same temperature as the II → III transition in a cooling run). The enthalpy of the IV → II transition corresponds to the sum of the enthalpies of the II → III and III → IV transitions. The III → II transition occurs at the same temperature as the IV→II transition, provided that phase IV has not been reached. This temperature differs only slightly from the temperature of the II → III transition (ΔT_{trans} ~ 1.5 K).

2.4. Optical studies

Orthoscopic studies under crossed Nicols were performed with a WILD M8 Heerbrugg binocular and a LEITZ SM-POL polarizing microscope. Crystals were immersed in perfluoropolyether oil (*RS* 3000, Riedel-de Haën). The observations indicate that crystals grown at room temperature (phase II) are single-domain states. The habitus of the crystals is tabular and these {010} platelets are bounded by {100} pinacoids and {101} prisms. The ratio of the lengths of the edges [010] and [101] depends on the growth conditions of the specific crystal and varies within a batch. This phase is birefringent. We used λ and λ/4 plates in order to determine the principal axes of Fletcher's indicatrix in the (010) plane and the fast and slow propagation directions of light. We found these parameters by comparing the birefringence patterns, with and without plates, using Bloss' table of the different orders of interference colour (Bloss, 1990). The main axes of the indicatrix are along the orthorhombic axes and the fast propagation direction of light lies along **a** (Fig. 2).

On cooling UA crystals in a stream of nitrogen gas, a two-step phenomenon can be observed at the II → III transition:

(i) Formation of (401) domain walls. These are associated with orientational domains and propagate through the entire sample.

(ii) Appearance of a fuzzy phase front associated with a transformation of the (401) domains into ferroelastic (100) domains.

This transformation sets in a few seconds after the creation of the (401) domains, but for some crystals the transition

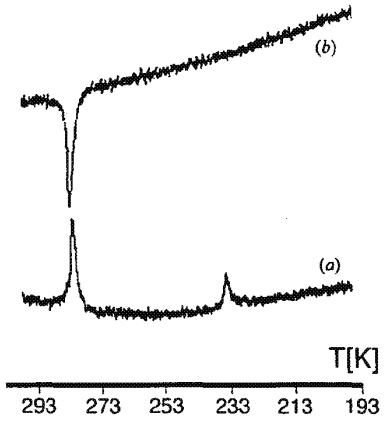


Figure 1
(*a*) Cooling and (*b*) heating (in that order) DSC traces at 1 K min^{-1}. Note the absence of the IV → III transition upon heating.

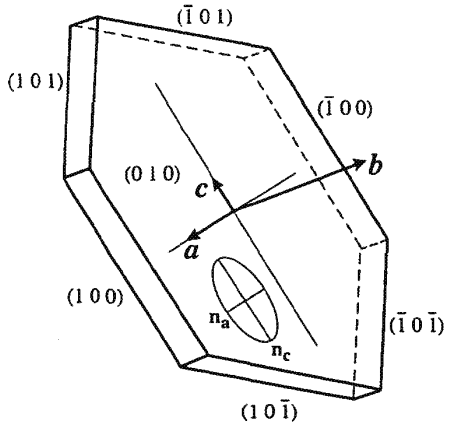


Figure 2
Typical habitus and Fletcher's indicatrix of a UA crystal with respect to the cell of Table 4.

UM00012978
NOVARTIS EXHIBIT 1017
Novartis v. Regents, IPR2023-01346
Page 1724 of 4460

Table 2
Crystal data of the known solid phases of UA.

	Phase II	Phase III	Phase IV
Temperature (K)	286 (1)	258 (1)	200 (1)
Lattice constants (Å, °)	$\hat{a}$ = 9.416 (2), $\hat{b}$ = 26.124 (5), $\hat{c}$ = 7.203 (1)	a_m = 5.911 (1), b_m = 26.103 (5), c_m = 11.874 (2), β_m = 106.11 (3)	a_M = 5.951 (1), b_M = 25.223 (5), c_M = 23.593 (4), β_M = 103.60 (2)
Crystal system	Orthorhombic	Monoclinic	Monoclinic
Space group	*Bmmb*	$P2_1/c$	$P2_1/c$
Multiplicity	4	4	8
R_1 [$F_o > 4\sigma(F_o)$]	0.0405	0.0363	0.0459
Comments	Two chains superimposed Disordered acid group	Two orientational domains One chain conformation Disordered acid group volume ratios: $\alpha = 0.88/\beta = 0.12$	Two orientational domains One chain conformation Ordered acid group volume ratios: $\alpha = 0.67/\beta = 0.33$

process was so fast that we could not observe the (401) domains. The presence of both (401) and (40$\bar{1}$) domains in Fig. 3(*a*) proves the ferroelastic nature of the transition process. Figs. 3(*b*), 3(*c*) and 3(*d*) allow a better visualization of the propagation of the phase front. The II → III transition begins with the formation of lancet-shaped (40$\bar{1}$) domains at the [101] edge of the crystal (Fig. 3*b*). These gradually pierce the whole crystal towards the (10$\bar{1}$) edge. A few moments later these (40$\bar{1}$) needles are transformed into the already mentioned (100) domains. The phase front (black line) associated with this process is rather fuzzy and may be approximated by (001); the front's advancement is indicated by the black arrow (Figs. 3*b* and 3*c*). Fig. 3(*d*) illustrates the III → II transition. This figure shows the total reversibility of the process: the (100) domains give way to the (40$\bar{1}$) domains and finally phase II is reestablished. The III → II transition is again initiated by a (001) phase front that transforms into a hybrid type of phase front (white line). The domain sizes and their dynamics vary from crystal to crystal, as expected. This behaviour certainly depends on experimental conditions such as temperature gradient, sample quality and thickness. These observations lead us to postulate that the II → III transition is actually a two-step process, which, henceforth, we shall denote II → *f* → III. The fact that this fascinating result was not revealed by either diffraction or calorimetry demonstrates the value of orthoscopy. The angle between the extinction directions in the two domains in phase III was estimated to lie between 2 and 4°. In view of the experimental uncertainties (domains measure ~1 μm) this result represents a satisfactory agreement with the spontaneous deformation, which is computed as twice the angle between $[201]_m$ and [001] of 2°.

On cooling further, at $T_{III \rightarrow IV}$ another phase front crosses the crystal from one [101] edge to the corresponding edge on the other side of the platelet (Fig. 4). This front can also emerge at the [10$\bar{1}$] edge but not always on the same edge in subsequent cycles. The orientational (100) domains are no longer seen, but some rather large and deep cracks and furrows appear on the (010) face, their direction being [001]. In some crystals the transition is particularly violent and whole chips are torn out of the core. No further major changes occur down to ~183 K. When reheating, no visual phenomena are detected up to ~282 K, at which temperature some, but not all, of the fissures seem to heal. Further cooling and heating cycles confirm this sequence of events, except that the III → IV phase front starts sometimes at the [101] edge and sometimes at the [10$\bar{1}$] edge.

Table 3
Some characteristics of the two simplest MDOs.

	Nickname	Maxima	Cell		Space group
MDO_1	Screwed	$\xi = \frac{1}{2}, 1, \frac{3}{2}$	$\mathbf{a}_1 = 2\mathbf{a}_o$ $\mathbf{b}_1 = \mathbf{b}$ $\mathbf{c}_1 = \mathbf{c}$		*Pcc*2
MDO_2	Slated	$\xi - \frac{\xi}{4} \in Z$	$\mathbf{a}_2 = -\mathbf{a}_o + \mathbf{c}/4$ $\mathbf{b}_2 = \mathbf{b}$ $\mathbf{c}_2 = -(2\mathbf{a}_o + \mathbf{c}/2)$	$\beta \simeq 106°$	$P2_1/c$

2.5. X-ray diffraction

2.5.1. Bragg reflection data and reciprocal space survey. A shiny, translucent, colourless, rhomb-shaped crystal was glued onto a thin glass fibre and kept at 286 (1) K in a stream of nitrogen gas during data collection, which took place on a Stoe IPDS system using Mo $K\alpha$ radiation. (Note that, once out of the stream, the crystal surfaces became infested with whitish-opaque stains in a matter of hours; we presumed that these stains were due to solvent loss.) The image-plate-to-crystal distance was set to 60 mm and a φ interval of 1° was chosen. Two hundred images were then exposed for 5 min each. The integration was carried out using profiles of between 15 and 11 pixels and an effective mosaic spread of 0.013. (The unusual profile function stems from the diffuse scattering; see below). The intensities were corrected for Lorentz and polarization effects, but no absorption correction was deemed necessary. An inspection of reciprocal space revealed that most of the maxima found in the images could be indexed in the cell given in Table 2; the remaining maxima lay on lines $(\xi, k, l + \frac{1}{2})$, $\xi \in R$ and $k, l \in Z$. These rods and other more complex regions of diffuse scattering have also been observed on precession photographs recorded using Cu $K\alpha$ radiation. In lieu of such a photograph we display a reconstruction of the

UM00012979
NOVARTIS EXHIBIT 1017
Novartis v. Regents, IPR2023-01346
Page 1725 of 4460

(ξ,4,l) layer (Fig. 5a) from the oscillation diffractograms of the image-plate data collection. This figure shows clearly the rods of diffuse scattering along $\mathbf{a}^*$. A closer inspection of this diffraction pattern immediately reveals that it may be interpreted to a good approximation as stemming from an OD structure as defined by Dornberger-Schiff (1966). The whole diffraction pattern is found to be indexable based on a layer group $P(c)c2$ and a cell $a_o = 4.708$ (1), $b = 26.124$ (5) and $c = 14.406$ (2) Å. Further inspection of the diffuse lines reveals two classes of weak maxima within the lines, namely $(h+\frac{1}{2}, k, l+\frac{1}{2})$ and $(h, k, l+\frac{1}{2})$, $h, k, l \in Z$. These two classes of reflections correspond to the simplest maximal degree of order (MDO) structures in this OD structure (Table 3). The latter $(h, k, l+\frac{1}{2})$ corresponds to MDO_1, which is realized in phase II of UA but is completely crystallized in urotropin pimalate (Gardon, Pinheiro & Chapuis, 2003), whereas MDO_2 corresponds exactly to phase III (Hostettler *et al.*, 1999) of UA. Phase II of UA is thus found to be a mixture of the two simplest MDOs at 286 K. The $(\xi, 4, l)$ layer of phase III is displayed in Fig. 5(b). A detailed analysis reveals that this layer can be understood as arising from a stacking fault created by the C_{2x} partial operation that leads to twin domains described in the monoclinic cell $\mathbf{a}_m = -\mathbf{a}_o + \mathbf{c}/4$, $\mathbf{b}_m = \mathbf{b}$, $\mathbf{c}_m = -2(\mathbf{a}_o + \mathbf{c}/2)$ and in the cell equiva-

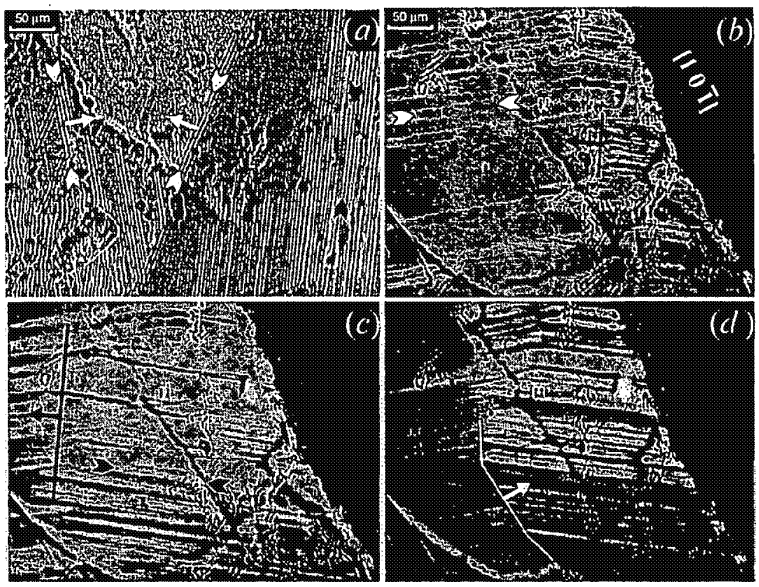


Figure 3
Two typical (010) platelets of UA, (a) and (b, c, d), as seen under crossed Nicols. White double-arrows indicate (401) and (40$\bar{1}$) domains, black double-arrows (100) domains, while white and black lines emphasize the phase fronts.

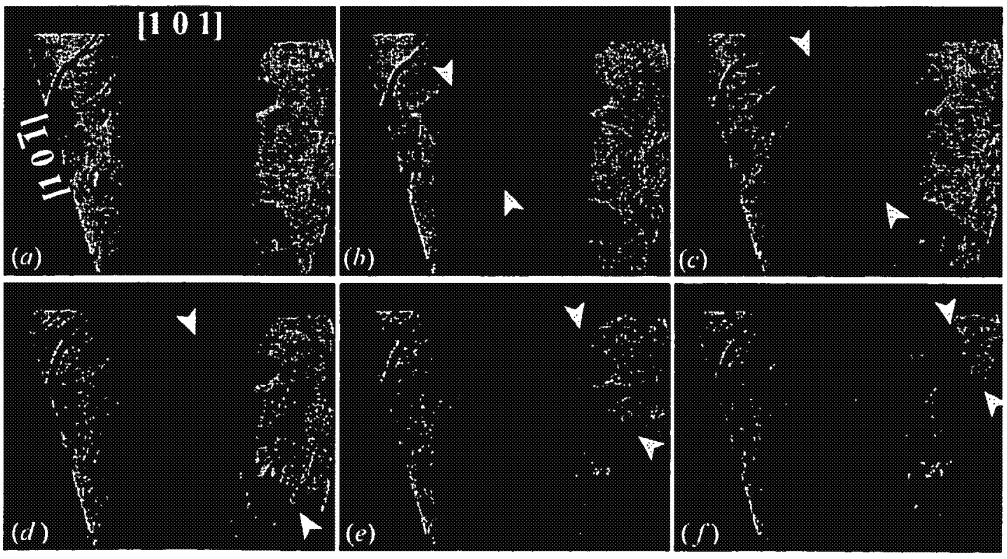


Figure 4
(010) platelet of UA as seen under crossed Nicols. (a) Displays the platelet shortly before the II → IV transition, (b)–(f) show the progress of the (101) phase front (best recognized between the white arrows) during the transition and the ensuing damage to the crystal.

UM00012980
NOVARTIS EXHIBIT 1017
Novartis v. Regents, IPR2023-01346
Page 1726 of 4460

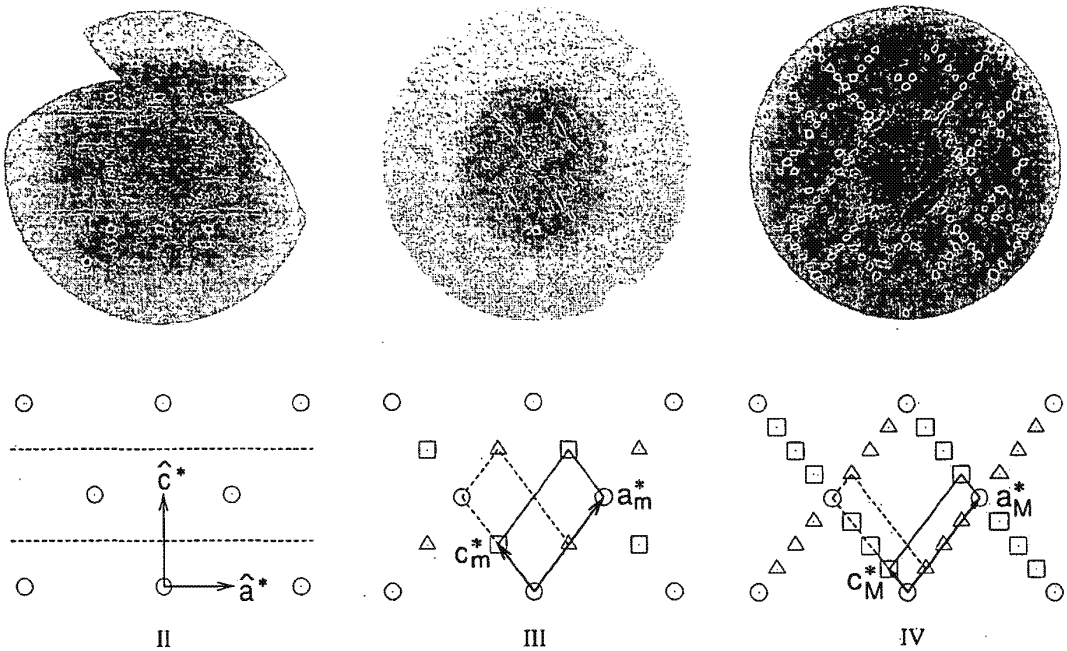


Figure 5
($\xi 4\ell$) layers of phase II, phase III and phase IV reconstructed from 200 images with the program *SPACE* (Stoe & CIE GmbH, 1997).

lent to it by the action of σ_x.

Fig. 5(*c*) shows the ($\xi 4l$) diffraction pattern of phase IV (at 200 K). This phase, which is the ground state of the system, is completely ordered (Birkedal *et al.*, 2003) and is clearly most interesting. Not only is this phase none of the simplest MDO structures, but the transition towards it is associated with a point in the interior of the Brillouin zone of phase II.

The structure of phase II was solved by direct methods (Sheldrick, 1997*b*) and refined using *SHELXL* (Sheldrick, 1997*a*). The U molecules lie on the C_{2v} site, which is a subgroup of the full T_d symmetry of U: no problems there. The AA chains, however, turn out to lie perpendicular to the (100) plane. Since their long axes make an angle of 54° with the *b* axis, they do not occupy the only site compatible with their natural C_{2v} symmetry: there are two disordered half-chains related by σ_x. This result is not at all surprising since we are considering the superposition structure. This structure contains unrealistic atomic positions, which must then be 'distributed' in order to obtain the true OD structure. Each disordered chain contains two disordered carboxyl groups, because there are two hydrogen-bond donor atoms available. The methylene H atoms were inserted at appropriate positions relative to their associated C atoms, upon which the H atoms were made to ride. However, the acid proton was found in a difference map and naively refined with *x*, *y*, *z* and U. It reached a position about halfway between O_{1b} and N_2.

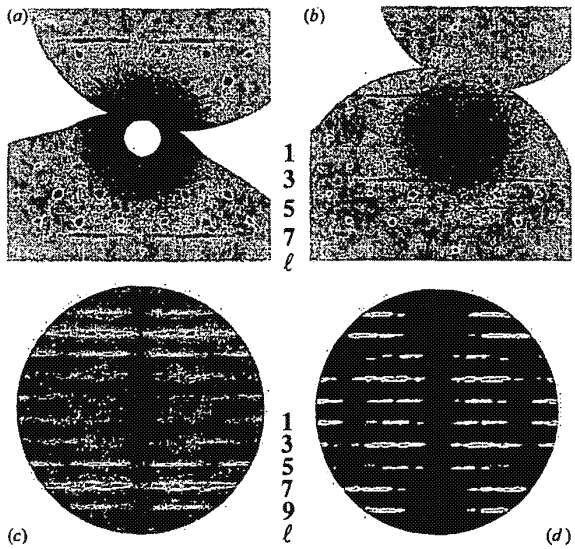


Figure 6
(*a*) ($\xi 1\ell$) and (*b*) ($\xi 4\ell$) layers reconstructed from 200 images with the program *SPACE* (Stoe & CIE GmbH, 1997). (*c*) ($\xi 1\ell$) and (*d*) ($\xi 4\ell$) layers simulated using correlations $C_1^{\bullet} \simeq 0.6$ and $C_2^{\bullet} \simeq 0.2$. The temperature factor fall-off is not taken into account and Bragg spots have been eliminated in the calculations for the sake of clarity.

UM00012981
NOVARTIS EXHIBIT 1017
Novartis v. Regents, IPR2023-01346
Page 1727 of 4460

Table 4
Experimental details for phase II of UA.

Chemical formula	$C_6H_{12}N_4{\cdot}C_9H_{16}O_4$
Chemical formula weight	328.41
Cell setting, space group	Orthorhombic, *Bmmb*
a, b, c (Å)	9.4157 (19), 26.124 (5), 7.2034 (14)
V (Å^3)	1771.9 (6)
Z	4
D_x (Mg m^{-3})	1.231
Radiation type	Mo $K\alpha$
No. of reflections for cell parameters	721
θ range (°)	14.5–24.1
μ (mm^{-1})	0.09
Temperature (K)	286 (1)
Crystal form, colour	Platelet, colourless
Crystal habitus	{101}, {10$\bar{1}$} and {010} pinacoids
Crystal size (mm)	0.72 × 0.56 × 0.04
Diffractometer	Stoe IPDS
Data collection method	φ scans
Absorption correction	None
T_{min}	–
T_{max}	–
No. of measured, independent and observed parameters	6062, 818, 539
Criterion for observed reflections	$I > 2\sigma(I)$
R_{int}	0.053
θ_{max}	25
$F(000)$	712
Range of h, k, l	$-10 > h > 10$ $-31 > k > 31$ $-8 > l > 8$
Refinement on	F^2
$R[F^2 > 2\sigma(F^2)]$, $wR(F^2)$, S	0.041, 0.126, 0.91
No. of reflections and parameters used in refinement	818, 110
H-atom treatment	Mixed
Weighting scheme	$w = 1/[\sigma^2(F_o^2) + (0.0754P)^2 + 0.4007P]$ where $P = (F_o^2 + 2F_c^2)/3$
$(\Delta/\sigma)_{max}$	< 0.001
$\Delta\rho_{max}$, $\Delta\rho_{min}$ (e Å^{-3})	0.15, −0.13

Computer programs: *Stoe IPDS* (Stoe & CIE GmbH, 1997); *SHELXS97* (Sheldrick, 1997*b*); *SHELXL97* (Sheldrick, 1997*a*).

Table 5
Normalized hydrogen-bonding geometry (Å, °).

D—H···A	$d(D$—H)	d(H···A)	$d(D$···$A)$	<(D—H···A)
O1—H1···N1	1.34 (5)	1.56 (7)	2.732 (4)	140.2 (19)
C7—H7a···O2b^{i}	1.092	2.53	3.240 (12)	121.6
C7—H7b···O2a^{i}	1.092	2.69	3.186 (14)	107.1
C8—H8a···O2b^{ii}	1.092	2.30	3.349 (11)	160.3
C9—H9a···N2^{iii}	1.092	2.65	3.654 (2)	153.0
C2—H2b···O1	1.092	2.66	3.730 (5)	165.1

Symmetry codes: (i) $\frac{1}{2}+x, y, \frac{1}{2}+z$; (ii) $x, \frac{1}{2}-y, 1+z$; (iii) $-\frac{1}{2}+x, y, -\frac{1}{2}+z$; (iv) $\frac{1}{2}-x, y, -\frac{1}{2}+z$.

The final refinement results are given in Table 4, together with additional information on the diffraction experiment. Releasing the C—H distance in the CH_2 groups did not improve the residuals. Fractional coordinates of the final model are given in the supplementary material.[1]

2.5.2. PSD diffuse-scattering data. Although the reciprocal space images shown in Fig. 6 were obtained with the image-plate system that was used for measuring the Bragg reflection data, we also carried out diffraction experiments on the dedicated Weißenberg position-sensitive detector (PSD) diffractometer (Osborn & Welberry, 1990), which was designed especially for recording diffuse-scattering data. This system is capable of recording complete reciprocal lattice sections with a high resolution and low noise. Two examples of the data recorded in the present study are shown in Fig. 7. The quality of the patterns obtained in the present experiment is much poorer than would normally be expected from this instrument, although the patterns do show more detail than the images of Fig. 6. The main reasons for this poor quality are the presence of the powder rings, streaking emanating from the strong Bragg peaks and the generally high levels of parasitic scattering that may be seen. Despite repeated attempts to obtain *clean* high-quality samples it was invariably found that during the course of the ~3 d required to record each section the quality of the crystal deteriorated and the powder rings and other parasitic scattering effects could not be avoided. Further experiments are in progress to try to improve on the quality of these data.

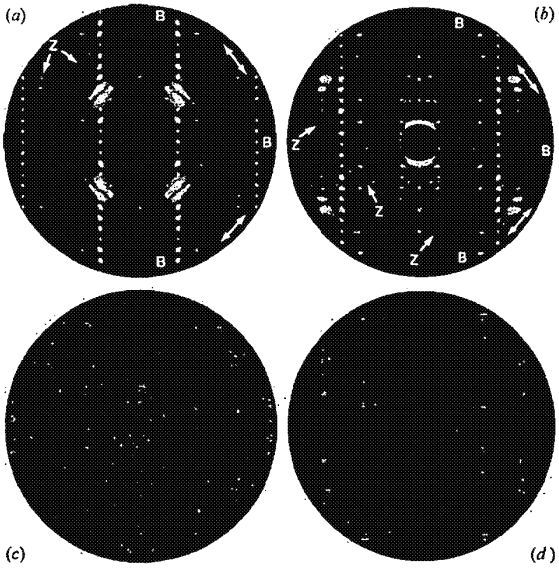


Figure 7
(*a*) (1$k\ell$) and (*b*) (2$k\ell$) layers recorded on the Weiβenberg PSD diffractometer system (Osborn & Welberry, 1990). (*c*) (1$k\ell$) and (*d*) (2$k\ell$) layers simulated with the help of the program *DIFFUSE* using correlations $C_1^a \simeq 0.6$, $C_2^a \simeq 0.2$, $C_1^b \simeq -0.7$ and $C_1^c \simeq -0.7$. Bragg spots have been omitted in the calculations for the sake of clarity and temperature factor fall-off has been neglected.

[1] Supplementary data for this paper are available from the IUCr electronic archives (Reference: LC0055). Services for accessing these data are described at the back of the journal.

UM00012982
NOVARTIS EXHIBIT 1017
Novartis v. Regents, IPR2023-01346
Page 1728 of 4460

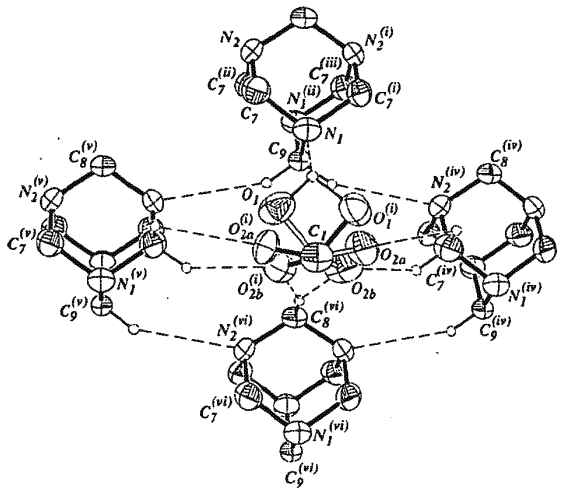


Figure 8
The hydrogen bonds involved in the packing of UA in Phase II. (i) stands for $\sigma_x|100$, (ii) for $\sigma_y|0\frac{1}{2}0$, (iii) for $C_2z|1\frac{1}{2}0$, (iv) for $E|\frac{1}{2}0\frac{1}{2}$, (v) for $E|\frac{1}{2}01\frac{1}{2}$ and (vi) for $E|00\bar{1}$. Atoms are drawn at the 30% probability level and only pertinent H atoms are plotted for the sake of clarity.

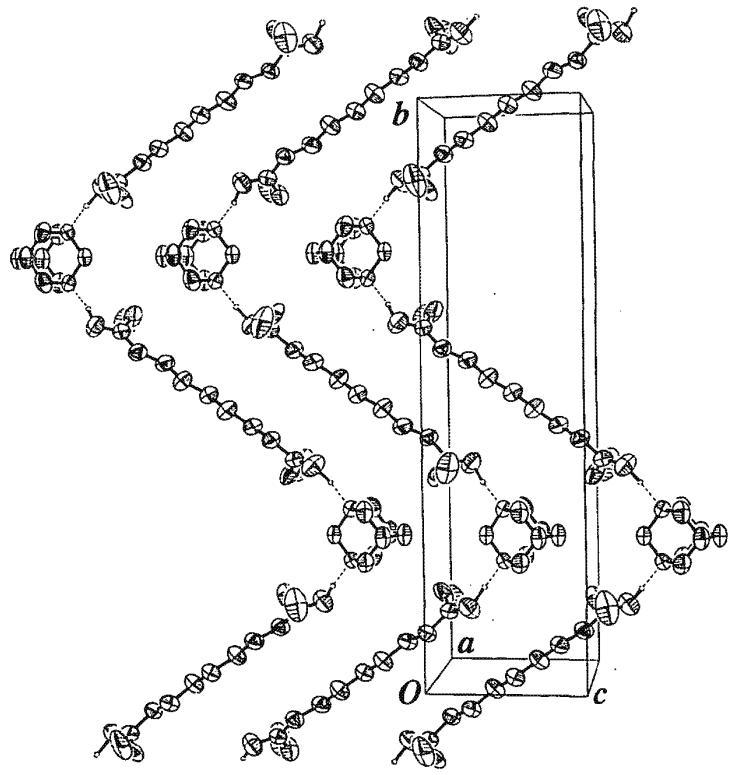


Figure 9
(100) layer of phase II of UA. Only one of the two disordered chains is shown, so the view represents the layer group $P(c)c2$ as well. The next layer (before or behind) would be shifted by $\vec{c}/2$.

3. Discussion

3.1. The superposition structure

UA is a co-crystal of U balls and AA sticks. In view of the alternating (010) sheets of balls and sticks, it might be classified as a layer structure for the sake of chemical homogeneity. However, the weakness of the bonding between successive (100) sheets suggests that it is the latter that will turn out to be the important layers for most if not all of the extraordinary phenomena observed in UA. Five different hydrogen bonds play a role in UA (Table 5, Fig. 8). Their normalized distances and angles all lie within the accepted ranges (Jeffrey & Sänger, 1991; Steiner & Desiraju, 1998). One bond even qualifies as strong, since the refined H atom lies about halfway between N_2 and O_{1b}. The pertinent N_2-H-O_{1b} angle is a little on the small side, but it appears nevertheless to play a crucial role in the phase transitions and other phenomena that occur in UA. The (100) layers are connected by one weak C—H···O=C bond, one esoteric C—H···N hydrogen bond and van der Waals forces, whereas the (010) layers are held together by one strong N···H···O and three weak C—H···O=C hydrogen bonds. The sometimes discredited C—H···O=C hydrogen bond is indisputably effective in determining the packing of UA. Its approximate energy of 2 kcal mol^{-1} (Jeffrey & Sänger, 1991) is certainly comparable with the sum of van der Waals energies of the various methylene groups [the typical energy of which is roughly 0.3 kcal mol^{-1} for methylene groups 4 Å apart (Salem, 1962)].

The AA chains all lie with their long axes perpendicular to [100] such that the axes make an angle of 54° with the *b* axis. Within any one (010) layer the molecular planes defined by their zig-zag backbone are all parallel to each other and perpendicular to the (100) plane. The $\{C_{2y}|0\frac{1}{2}0\}$ axis causes successive layers of chains to turn by 180° such that the chains are arranged in a herringbone-like pattern when viewed along the *a* axis (Fig. 9). The packing of the AA chains may best be approximated by Abrahamson's *p*-cell $O_{\parallel}$ (Abrahamsson *et al.*, 1978), although this is actually a gross idealization. In UA we find for this *p*-cell $a = 9.42$, $b = 4.12$, $c = 2.50$ Å, but the angles clearly differ from 90°, especially β. The typical chain–chain distances in UA start at ~4.10 Å and the area per methylene group is 19.1 Å^2. [Below we compare some values with those of a typical long-chain structure, *n*-tetradecylammoniumchloride (*C*14*Cl*), at room temperature (Schenk, 1984).] In this almost ideal structure the area per methylene group is 18.3 Å^2 and the chain–chain distances are about 0.1 Å

UM00012983
NOVARTIS EXHIBIT 1017
Novartis v. Regents, IPR2023-01346
Page 1729 of 4460

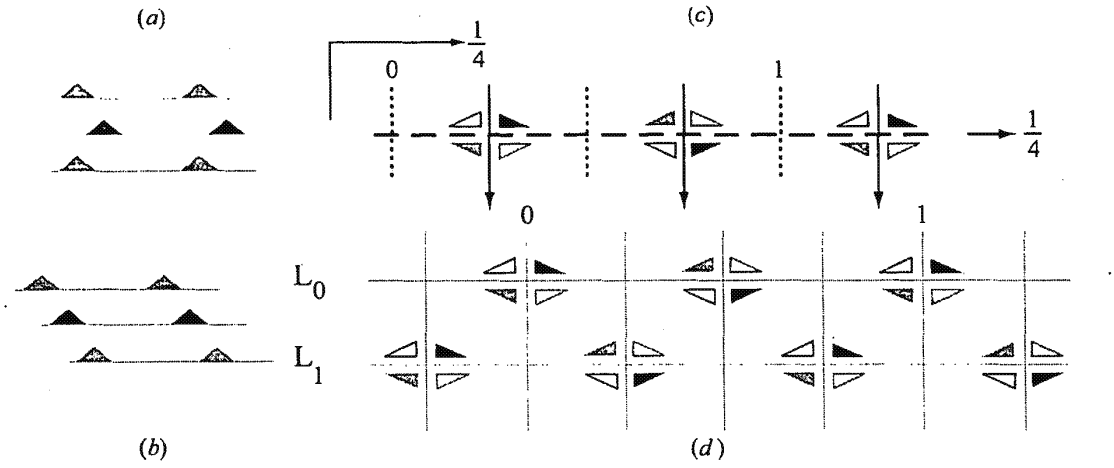


Figure 10
(*a*) The 'screwed' triple (think of the profile of a screw). (*b*) The 'slated' triple (reminiscent of the steps in a slab of the mineral slate). (*c*) The layer group *P*(*c*)*cb*. (*d*) The gruppoid family No. 27 of Dornberger-Schiff (1966).

shorter than in UA. These facts indicate that the chains are not as densely packed in UA as in a comparable alkane or alkanedioic acid structure. It appears that U is the determining factor for the crystal packing.

The geometry of the AA chains is rather far from normal. In UA the C—C distances, C—C—C angles and C—C—C—C torsion angles are 1.516 (8) Å, 114 (2) and 175 (1)°, respectively. For *C*14*Cl* the corresponding values are 1.512 (6) Å, 114.4 (6) and 179.4 (4)°, respectively, and the angles of the *p*-cell are within 0.3° of the expected 90°. With the information that the chain–chain distances in UA are rather long along the *a* axis, a picture of not very rigid chains emerges, where these chains are possibly subject to kink diffusion or torsional vibrations. This latter subject will be taken up in a forthcoming communication and has been described by other authors (Thalladi *et al.*, 2000). The loose-chain packing is also suitable for solvent inclusions. Indeed, we have shown by means of GC that the UA crystals contain traces of acetonitrile (about one molecule per one hundred cells of UA).

Of the two refined O-atom positions one corresponds to a carboxyl group that lies very roughly in the zig-zag plane of AA ($O_{1b}-C_1-O_{1a2}$ dihedral angle is ~11°) and the other corresponds to a COOH group with a dihedral angle of ~40° ($O_{1b}-C_1-O_{1a1}$). These values are surprisingly close to those found in the α form of AA. In this phase, which is stable above 75°, one finds angles of 6 and 37°. The geometry of the disordered carboxyl group is not altogether unsatisfactory: the double bond measures 1.10 (1) Å for O_{1a1} and 1.13 (1) Å for O_{1a2}, whereas the single bond is 1.372 (4) Å. The corresponding values in the β form of AA (Housty & Hospital, 1967; Bond *et al.*, 2001) are 1.23 and 1.30 Å. The $O-C-O_{1b}$ angles are 123.0 (7)° for O_{1a1} and 115.8 (8)° for O_{1a2}; these values are not too different from the angle in AA(β), namely 123.5°. Although our refinement is not completely satisfactory it still reproduces, at least qualitatively, the geometrical characteristics of the pure AA chains. A comprehensive search (Birkedal *et al.*, 2003) of the CSD database has shown that $C_\beta-C_\alpha-O_1-O_2$ is essentially planar and that the sum of the angles is 360 (0.5)°. In phase II of UA these values are 0.031 Å and 358.7° for the $C_2-C_1-O_1-O_{2a}$ group and 0.083 Å and

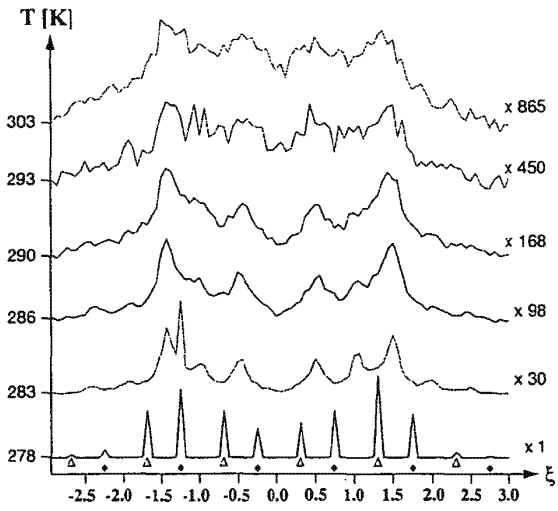


Figure 11
Scan along the diffuse rod (ξ, 1, 7). The ξ index is with respect to the layer separation a_o. The topmost scan is an average of five scans on and ±0.02 off the line. The intensities are normalized with respect to the scan at T = 278 K (normalization factors are given at the right end of each scan). The second scan from the bottom sits right on the transition as can be learned from the breakthrough of the line of phase III. Besides the obvious II → III transition there is another subtle, but irrefutable, transition within phase II that appears between 293 and 290 K.

UM00012984
NOVARTIS EXHIBIT 1017
Novartis v. Regents, IPR2023-01346
Page 1730 of 4460

Table 6
Systematic absences in the diffraction pattern.

	In	There are	If
i	$(\hat{h}, k, \hat{l})$	Sharp reflections	$\hat{h}+\hat{l}$ even
ii	$(\hat{h}, k, 0)$	Sharp reflections	k even
iii	(ξ, k, ℓ)	Sharp reflections	$\ell = 2\hat{l}$
iv	(ξ, k, ℓ)	Diffuse rods	ℓ odd
v	$(\xi, 0, \ell)$	No diffuse rods	
vi	(ξ, k, ℓ)	Vanishing intensities of diffuse rods	$\xi \to 0$

351.2° for the $C_2-C_1-O_1-O_{2b}$ group. We have tried to split the α carbon, but the ideal geometry cannot be obtained without restraints. However, in view of the OD character of UA and the quite large anisotropic displacement parameters, these values seem to warrant reasonable chains even at the chain ends. It might, however, be interesting to check with spectroscopic methods whether this non-ideal behaviour is the expression of the fact that the two chains ends might have different degrees of deprotonation (Housty & Hospital, 1967).

We have said that the packing of the co-crystal seems to be governed by the packing of the U balls. Indeed, the (101) planes of U alone (Kampermann *et al.*, 1995) closely resemble the (010) planes of UA. The translations in the (101) plane are 7.02 and 9.93 Å at 298 K and the distances between the U molecules are 6.08 Å. The same translations in UA are 7.2034 and 9.416 Å at 286 K and the distance between U molecules is 5.9 Å. U is not a plastic crystal and therefore the C—H···N subunits (1.098 Å, 2.785 Å, 151.4°) may be assessed as hydrogen bonds. In UA we have the same situation (1.092 Å, 2.65 Å, 153°; Table 5). On formation of the co-crystal the U molecules seem, compared with pure U, to have approached each other a little more closely and to have formed slightly stronger hydrogen bonds.

3.2. The OD structure

We have already mentioned (see §2.2) the rods of diffuse scattering that are the most salient features of the diffraction pattern of phase II. Following Guinier's elegant derivation (Guinier, 1964), we conclude that we are dealing with a planar disorder in this phase, *i.e.* a more or less random sequence of (**b**, **c**) layers along $\mathbf{a}_o$. Making use of Käte Dornberger-Schiff's formalism (Dornberger-Schiff, 1966), we shall now give a more complete description of phase II that will account for more of the diffraction pattern than the mere superposition structure.

A more detailed analysis of the said diffraction pattern results in the systematic absences of Table 6 (these are given with respect to a cell $\mathbf{a}_o$, **b**, **c**, where $\mathbf{a}_o$ is the layer separation). Condition (iii) tells us that the **c** base vector of the superposition structure is $\widehat{\mathbf{c}} = \mathbf{c}/2$ and (i) that the structure is *B* centred. Absence (ii) reveals that there is a *b*-glide plane perpendicular to **c**. The global law (i) furthermore includes an *n*-glide plane perpendicular to **b** and a *c*-glide plane perpendicular to **c**. These results amount to the space group *Bmmb* for the superposition structure and the base vectors $\widehat{\mathbf{a}} = 2\mathbf{a}_o$, $\widehat{\mathbf{b}} = \mathbf{b}$ and $\widehat{\mathbf{c}} = \mathbf{c}/2$. According to (v) there are no diffuse rods in $(\xi, 0, \ell)$; the absence $\ell = 2$ corresponds to a *c*-glide plane perpendicular to **b** in the OD structure. The condition $k = 2n$ in $(\xi, k, 0)$ indicates a *b*-glide plane perpendicular to **c**. The absence $\ell = 2n$ in $(0, k, \ell)$ results from a *c*-glide plane perpendicular to **a**. Combining all these λ POs (partial operations) leads to the layer group $P(c)cb$, as shown in Fig. 10(*c*).

The $\widehat{\mathbf{c}}$ base vector of $\mathbf{c}/2$ reveals that the layer L_1 is shifted by $\mathbf{c}/4$ with respect to the layer L_o. The combination of this displacement, namely $\mathbf{t} = \mathbf{a}_o + \mathbf{c}/4$, with the λ POs leads to the following OD gruppoid family:

$$\begin{matrix} P & (c) & c & b \\ & \{(c_{1/2}) & n_{1/2,2} & n_{2,1}\} \end{matrix}.$$

This OD gruppoid is represented in Fig. 10(*c*) and corresponds, in a different setting, to the OD gruppoid family No. 27 of Dornberger-Schiff (1966). The figure also demonstrates that there is only one type of layer in this OD structure. (It does not appear necessary in the context of diffuse scattering to be overly concerned with the presence or absence of an inversion centre in the layer.)

If we write the equipoints of this OD structure

$$[L_0] = [\pm(x, y, z), \pm(x, \bar{y}, \tfrac{1}{2} - z), \pm(\bar{x}, \tfrac{1}{2} + y, \tfrac{1}{2} - z), \pm(\bar{x}, \tfrac{1}{2} - y, z)], \quad (1)$$

$$[L_p] = (p, 0, \gamma_p) + [L_0],\ \alpha_j = \pm 1,\ \gamma_p = \sum_{j=1}^{p} \alpha_j \quad (2),$$

and define $\gamma_p := p + 2m_p$, we obtain

$$|S(\xi, \ell)|^2 = P^{-2}\Big\{P + \sum_{p=1}^{P-2} \sum_{p'=p+1}^{P-1} \cos 2\pi\big[\ell(m_p - m_{p'})/2 + (\xi + \ell/4)(p - p')\big]\Big\} \quad (3)$$

for the square of the stacking factor. The difference between the various members of the OD gruppoid family lies in the various values of the parameters m_p and $m_{p'}$. While, obviously, we cannot know these in any direct way, we can at least derive them for some special OD structures, the so-called MDO structures. In this OD gruppoid family there exist two simplest MDO structures. One is based on 'screwed' layer triples (Fig. 10*a*), the other on 'slated' layer triples (Fig. 10*b*). By either simple geometrical considerations (which sine wave has maximal overlap with the MDO structure) or substitution for the m_p values in the expression for $|S(\xi, \ell)|^2$, we can derive conditions on ξ for the MDO structures. Therefore, if we have sizeable regions in the OD structure that have crystallized according to one MDO structure or the other, we shall find pronounced and broad maxima in the diffuse rods at the positions indicated in Table 3. In order to study this point further we undertook to record so-called Q-scans for phase II. They were performed on a SYNTEX P3 diffractometer equipped with Cu $K\alpha$ radiation. The temperature was controlled by means of a stream of nitrogen gas. In Fig. 11 we recognize three types of Q-scans:

UM00012985
NOVARTIS EXHIBIT 1017
Novartis v. Regents, IPR2023-01346
Page 1731 of 4460

(i) The scans at $T = 303$ and 293 K correspond to an OD structure with a rather random layer sequence. Both triples are present in almost equal percentages and no large region of either MDO structure is present.

(ii) The scans at $T = 290, 286$ and 283 K present maxima for $\xi = \frac{1}{2}, 1, \frac{3}{2}, 2, \ldots$, those at $\xi = \pm\frac{3}{2}$ being the highest. From the analysis above we know that these maxima stem from the 'screwed' MDO structure.

(iii) The scan at $T = 278$ K displays maxima at $\xi - \ell/4 \in Z$. These maxima are due to the 'slated' MDO structure (phase III). This qualitative assessment is fully corroborated by a structural study (Hostettler *et al.*, 1999). The two ferroelastic domains of this phase are indicated by open triangles and diamonds.

At 303 K the stacking sequence seems to be fairly arbitrary, although some very broad maxima at $\xi = \pm\frac{1}{2}$ and $\xi = \pm\frac{3}{2}$ may be perceived. There are 'screwed' and 'slated' MDO structures in almost equal proportion, but there is no larger region of either of them. At 293 K, the situation is pretty much the same, but we may already detect some narrowing of the maxima mentioned above. However, between 293 and 290 K, a fundamental change occurs in the OD structure: the peaks have very clearly narrowed to about one third of their FWHM at 293 K and the maxima at $\xi = \pm\frac{3}{2}$ have doubled in intensity with respect to those at $\xi = \pm\frac{1}{2}$. We shall henceforth refer to the phase above $T_\alpha = 292$ K as α and to that below T_α as II. This tendency continues down to 283 K, the temperature of the II $\rightarrow$ III transition. During this transition all the maxima at $\xi = \pm\frac{1}{2}, \pm 1$ and $\pm\frac{3}{2}$ disappear and new maxima at $-\frac{9}{4}, -\frac{5}{4}, -\frac{1}{4}, \frac{3}{4}, \frac{7}{4}$ and $\frac{11}{4}$ begin to bulge. These results yield the following picture: At 303 K, both types of triples are present. The regions of the MDO structures are not very large at all. At 292 K, a very diffuse, but irrefutable, phase transition takes place during which the regions of the MDO_1 structure suddenly increase in dimension. Obviously, although the maxima that correspond to the screwed MDO are more conspicuous, there are also portions of the slated type in the OD structure. Down to the II $\rightarrow$ III transition, the MDO_1 regions become larger until at $T_{II\rightarrow III}$ the MDO_1 surprisingly switches over to the 'slated' type. It is as if the OD structure had planned to adopt a fully screwed MDO (like it does in UP; Gardon, Pinheiro & Chapuis, 2003), but suddenly a different thermodynamic path imposed itself towards the slated MDO.

The II $\rightarrow$ III transition is weakly of first order and most puzzling, not only because the system suddenly changes its mind, but also because the transition takes place in two steps. (We will refer to the furtive phase between phases II and III as phase *f*). This two-step nature of the transition is reminiscent of the triggered variant of phase transition pioneered by Holakovský (1973), a very interesting example of which has been observed (Bonin *et al.*, 1999). Note that there is no trace at all of this phase transition in the DSC curve. Incidentally, this feature is one of the more salient features of phase II (which according to calorimetry is stable between 283 and ~363 K), namely that it undergoes subtle changes again and again. So far we have counted four clearly distinguished subphases within the original phase II. These and the associated phenomena will be described in a forthcoming paper (Gardon, Schenk *et al.*, 2003). Recently a refined optical experiment conceived by Glazer (Wood & Glazer, 1980; Geday & Glazer, 2002) provided some independent evidence of the $\alpha \rightarrow$ II transition. Indeed, $|\sin\delta|$ and φ images display $(101)/(10\bar{1})$ phase fronts at roughly 293 K. Even more intriguingly, the same phase fronts also appear shortly before the II $\rightarrow$ III transition and may therefore be associated with the creation and annihilation of the screwed MDO structure.

3.3. Beyond the OD structure

We have mentioned before that the diffraction pattern of UA is more complex than that of a mere OD structure. Indeed, Figs. 7(*a*) and 7(*b*) reveal a few special features: rhomb-shaped (*B*) and cross-shaped [*e.g.* in $(3k\ell)$; not shown] bands of diffuse intensities and deviations from half-integer values of the index ℓ of the diffuse rods (*Z*). A comparison of this figure with Plate 24 of the *Atlas of Optical Transforms* (Harburn *et al.*, 1975) suggested that these crosses and bands might be related to an occupational disorder of the AA chains. Such a disorder can easily be imagined as growth disorder, since black and white chains occupy strictly the same volume and since the adhesion energies along the **c** direction are only very weak van der Waals energies.

Therefore, we began by studying a model in which the rigorous λ POs of the layer group $P(c)c2$ were represented by binary random variables that stand in, respectively, for the black or white chains in Fig. 12. Each chain is associated with such a variable, σ, which can take a value of either 0 for a black chain or 1 for a white chain. Different degrees of short-range order can be introduced into this system of random variables (and hence the corresponding molecules) with a Monte Carlo simulation using an energy of the form:

$$E = \sum_{i=1}^{64}\sum_{j=1}^{64}\sum_{k=1}^{64}(J_1^a\sigma_{ijk}\sigma_{i\pm 1jk} + J_2^a\sigma_{ijk}\sigma_{i\pm 2jk} + J_1^b\sigma_{ijk}\sigma_{ij\pm 1k} + J_1^c\sigma_{ijk}\sigma_{ijk\pm 1}). \quad (4)$$

Here J_1^a, J_2^a *etc.* are effective interactions that may be adjusted in order to obtain desired values of the correlations, C_i, between neighbouring molecules in different crystal directions. We used the interactions between first-nearest-neighbour chains along the *c* and *b* axes and first- and second-nearest-neighbour chains along the *a* direction. The MC calculation used an array of $64 \times 64 \times 64$ σ_{ijk} variables, which correspond to $32 \times 32 \times 64$ unit cells of the structure, and each unit cell contains four independent chains. Overall the simulation involved 262144 chains and 6029312 atoms. Diffraction patterns were computed using the program *DIFFUSE* (Butler & Welberry, 1992). This obtains the calculated diffuse diffraction pattern by averaging the diffraction patterns obtained from a large number of subregions (lots) taken at random from the total simulation array. In the present case, 50 individual lots of $4 \times 4 \times 15$ unit cells were used. Calculations were made on the 200×200 grid used for the observed patterns. The total CPU time for a single calculated pattern with these specifications was ~15 min on a DEC DS20

UM00012986
NOVARTIS EXHIBIT 1017
Novartis v. Regents, IPR2023-01346
Page 1732 of 4460

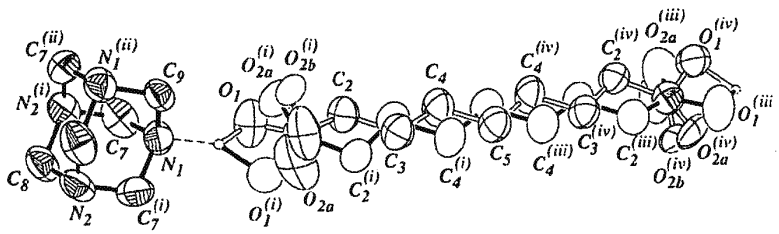


Figure 12
The two disordered chains in UA. The chain with the full bonds will be referred to as the *black* chain, the chain with the open bonds as the *white* chain. $^{(i)}$ stands for $\sigma_x|100$, $^{(ii)}$ for $\sigma_y|0\frac{1}{2}0$, $^{(iii)}$ for $C_i|11\bar{1}$, $^{(iv)}$ for $C_2x|01\bar{1}$. Atoms are drawn at the 50% probability level and methylene H atoms are omitted for the sake of clarity.

processor. Using correlations $C_1^a \simeq 0.6$, $C_2^a \simeq 0.2$, $C_1^b \simeq -0.7$ and $C_1^c \simeq -0.7$ we obtain a satisfactory correspondence for the $(\xi k\ell)$ layers with k odd (Figs. 6*a* and 6*c*) but disappointingly disparate relative intensities for the diffuse rods in the layers with k even (not shown). The relative intensities for the $(\xi 2\ell)$ rods were very-weak–strong–strong–weak–strong for $\ell = 1, 3, 5, 7, 9$, whereas the observed values (Fig. 6*b*) were medium–strong–weak–very-weak for $\ell = 1, 3, 5, 7$. Since the correlations only affect the shape of the diffuse peaks and their intensity is related to the difference of the structure factors of the two types of molecule, it was clear that we needed to modify the structure of the layers in order to obtain a better fit. Consequently we tried modifying the molecules in various ways: for example, rotating the carboxyl groups at one chain end in every second layer, shifting the whole or parts of every second layer in all reasonable directions, and rotating the whole chains. None of these modifications resulted in any significant improvement. At this point, however, we obtained results for phase II of urotropin pimalate (UP) (Gardon, Pinheiro & Chapuis, 2003) and this suggested a possible solution. In Fig. 13 we show the *bc* projections of UA and UP. The structure of UA certainly justifies our first decision to include only the chains in our MC model. Although *a posteriori* one might suspect some degree of rotational disorder around the C_{2z} axis, we had decided that the U molecules did not contribute to the diffuse scattering. However, in UP the same U molecules are clearly turned around the c axis by ~10°, and every second layer is different too. Consequently we decided to include the U molecules of UP in our MC model for UA and obtained the $(\xi 4\ell)$ layer shown in Fig. 6(*d*). The agreement with the experimental pattern is now qualitatively much more satisfactory: *i.e.* the profiles along the rods, *e.g.* $(\xi 17)$, display a qualitative (number and positions of maxima) correspondence with the profiles observed in the Q-scans. By varying the C_1^c and C_2^a correlations it was even possible to toggle between the two MDO structures and their intermediate OD states, but it was considered too time-consuming to adjust these correlations by trial and error in order to obtain a quantitative fit of intensities. Also note that the image reconstructions (Figs. 6*a* and 6*b*) were of relatively poor quality compared with the data obtainable from the Weißenberg PSD diffractometer system (Figs. 7*a* and 7*b*) and were far too noisy to allow more than a qualitative fit. A more detailed analysis is underway, which uses a more sophisticated MC automatic refinement technique (Welberry *et al.*, 1998) that uses Z-matrices. A preliminary report of this analysis has been presented elsewhere (Goossens & Welberry, 2001).

The $(1k\ell)$ and $(2k\ell)$ sections of data shown in Figs. 7(*a*) and 7(*b*) contain diffuse peaks that correspond to the cross-section of the diffuse rods that are seen in Figs. 6(*a*) and 6(*b*). In addition these layers show rather broad rhomb-shaped diffuse bands. In order to reproduce these bands in the simulated patterns each chain in our $32 \times 32 \times 64$ unit cells was shifted by a random displacement of between −0.5 and +0.5 Å along its chain axis. With this simple addition to the model described above the simulated layers shown in Figs. 7(*c*) and 7(*d*) were obtained. The $(0k\ell)$ layer (not shown) does not contain any SRO peaks but the rhomb-shaped diffuse bands were reproduced here too.

The observed and calculated $(1k\ell)$ and $(2k\ell)$ reciprocal layers displayed in Fig. 7 show generally broad agreement. The SRO peaks are seen to occur in the ℓ = odd reciprocal rows (vertical) and the distributions of peak intensities along these rows show qualitative similarity. Note that the strongest peaks occur in regions where the broad diffuse bands, which result from the chain displacements, are also strong. This simple relationship reflects the fact that for both the short-range order and the displacements the scattering comes predominantly from the azelaic acid molecules. In view of the simplistic nature of the present model this level of agreement can be considered satisfactory. Clearly the detailed distribu-

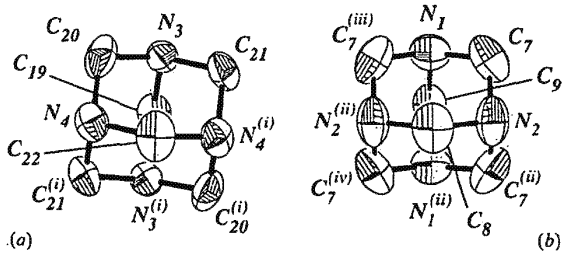


Figure 13
(*a*) The U molecule in a layer of UP has C_2 site symmetry. $^{(i)}$ stands for $C_2z|000$, $^{(ii)}$ for $\sigma_y|0\frac{1}{2}0$, $^{(iii)}$ for $\sigma_x|100$ and $^{(iv)}$ for $C_2z|1\frac{1}{2}0$. This structure corresponds to the pure 'screwed' MDO. (*b*) The U molecule in a layer of UA has site symmetry C_{2v}. The symmetry codes are the those used in Fig. 12. Atoms are drawn at the 50% level and H atoms are omitted for the sake of clarity.

UM00012987
NOVARTIS EXHIBIT 1017
Novartis v. Regents, IPR2023-01346
Page 1733 of 4460

tion of intensity is very sensitive to the exact detail of the two molecular form factors F_{black}, F_{white}.

It is also noticeable that the peak maxima do not occur precisely on the ℓ integral positions but are shifted sideways to varying degrees. Again the overall pattern of these shifts is qualitatively reasonably well reproduced in the simulated patterns. In many systems such peak shifts occur as a result of size-effect distortions (Welberry & Mayo, 1996), but in this case the shifts are found to occur when no such effects have been included in the model. The shifts occur because of the steep gradients in the overall diffuse intensity distribution, which is proportional to the difference in the two molecular form factors $|F_{\text{black}} - F_{\text{white}}|^2$.

Clearly the present model in which the molecules are shifted at random along the length of the chain is a very crude approximation. In practice we would expect such shifts to be correlated from molecule to molecule and to be cross-correlated with the occupational disorder (*i.e.* with σ). The observed patterns provide clear evidence of the former effect, which generally tends to produce diffuse scattering in the neighbourhood of strong Bragg peaks. In particular the strong elongated diffuse peaks that occur close to the (124) and (125) reflections can be attributed to such correlation of the molecular displacements.

It is also worth mentioning that if the displacement shifts along the chain axes are considered to be coupled to the occupational disorder then the effects that are seen in phase II may be considered as precursors of the modulations that are formed in UA at higher temperatures. For example, modulation vectors of the type $\alpha \mathbf{a}_o + \gamma \mathbf{c}_o$ with $\alpha \simeq -0.02$ and $\gamma \simeq 0.24$ have been found between ~351 and ~363 K (Gardon, 2001).

4. Conclusions

The tale of U and AA is the story of a shaky marriage. The two components are able to form a co-crystal, but this is far from being a unified and homogeneous object. Each partner appears to take every opportunity to impose itself on the other or, failing this, to break apart from it. Our study has shown that it is possible to design a clearly novel system that exhibits unusual, even exotic, properties by mixing the appropriate components. The co-crystals are stable only under rather precise values of chemical potential, temperature or pressure and dissociate under even a slight deviation from these equilibrium conditions. Note, though, that if the co-crystals are kept under even a modest pressure, say $\sim 6 \times 10^5$ Pa, they display a completely different behaviour with more classical, but less interesting, phase transitions and are stable up to the melting point (Bonin *et al.*, 2003).

The association of AA and U in their mother liquor is very tenuous. It is probably easier to form aggregates of U alone (for geometric reasons) or of AA alone (because of existing micelles) than aggregates of UA. For this reason we believe that the nucleation of UA initiates from existing seeds of the α form of AA and that these will partly survive in the UA co-crystal. The role of the small percentage of included acetonitrile might be to stabilize the grain boundaries between the AA and UA domains since these do not exhibit a very favourable epitaxic ratio. We also believe that there is always a certain amount of U alone at the (010) surfaces of a UA co-crystal.

The UA co-crystals are thus considered to be quite inhomogenous objects that contain a wide variety of defects including solvent inclusions, parasite phases, dislocations, point defects and surface rearrangements. It is difficult to conceive experiments that could yield precise information on all these defects since their total concentration must be less than a few percent. Nevertheless, the various experimental techniques described in this paper have provided evidence for the existence of these defects, and some of them clearly play a crucial role in the phase transitions at higher temperatures (Gardon, Schenk *et al.*, 2003).

The percentage of the AA domains [their existence is proven by the powder rings in Figs. 7(*a*) and 7(*b*)] will vary from crystal to crystal, as will the concentration of acetonitrile (shown by GC) and the precise stacking sequence of the (100) layers (echoed in the rods of diffuse scattering), but all of these effects are necessary to account for the often surprising phenomena in UA. For example, the exotic phase front phenomena described earlier seem to depend on the size of the crystal studied; this behaviour now becomes understandable in the light of our picture of the inhomogenous nature of the crystals.

The acetonitrile inclusions play a crucial role in the surface cleansing at ~338 K and in the recrystallization of U on the (010) surface (Gardon, Schenk *et al.*, 2003). The AA regions within the co-crystal might furnish an even better model for the $\beta \rightarrow \gamma$ transition that is accompanied by the spectacular phase fronts at ~351 K. (The similarity of this temperature to that of the $\beta \rightarrow \alpha$ transition in pure AA may be significant.) The acetonitriles and U are again very probably essential for the diffusion-controlled mechanisms at low temperature.

The packing of UA is less compact than that of either single component. Consequently, UA is characterized by a greater amount and a more diverse range of molecular motions and more defects than either AA or especially U. In that sense it may be said that UA is different from, rather than similar to, either AA or U. While it is true that certain properties of the original components persist in the co-crystal, they are amalgamated to lend UA a much richer spectrum of features. For example, the $(110)_c$ layer of U is preserved in the co-crystal with only very minor changes and similarly the instabilities due to the tendency of U to sublime are also preserved. AA provides, *via* the carboxyl group, the major and some of the minor hydrogen bonds in UA. The inclination of AA to form polymorphs probably contributes to the wealth of phase transitions of UA and its deprotonation ambiguity is preserved as well [phases II and III (Hostettler *et al.*, 1999)]. However, some features such as the number and variety of phase transitions are clearly specific to UA and are due to the exceptional inhomogeneity and the very complex real structure. For example, the profusion of hydrogen bonding and the rather uncommon dynamics (*e.g.* non-localized vibrations) of the AA

UM00012988
NOVARTIS EXHIBIT 1017
Novartis v. Regents, IPR2023-01346
Page 1734 of 4460

chains that are strung between pairs of U molecular layers are not present in crystals of the individual components.

In order to explain the spectacular phase fronts that have been seen in the study of the $\beta \rightarrow \gamma$ transition (Gardon, Schenk *et al.*, 2003) in UA, a novel diffusion-controlled competition between two slightly different incommensurate phases is postulated.

In phase α at, say, $T \simeq 303$ K, the homologous temperature, $T_h \simeq 0.75$, is indicative of a 'recrystallization' regime. Indeed, this regime extends over the whole temperature range within which the phase transitions occur. The system is therefore characterized by high diffusion (of vacancies, U molecules and acetonitriles) and important thermal fluctuations. These entail movement of dislocations, domain walls and grain boundaries. Nevertheless, the average structure is well defined. The stacking of the (100) layers is quasi-random (Fig. 11). The weak interlayer forces together with the internal stress at the various boundaries ($UA \leftrightarrow AA$, $UA \leftrightarrow U$) and at the diverse point defects create the prerequisites for the thermal activation of edge dislocations with a Burgers vector $\mathbf{c}/4$. With changing temperature the stacking sequence can therefore change as well.

At $T_{\alpha\rightarrow II}$ the building-up of the screwed MDO sets in. We believe (although this hypothesis will have to be subjected to the experimental test of vibrational and NMR spectroscopies) that this build-up is triggered by the locking-in of the four-site hopping of the U molecules. Once they are locked, they can establish C—H $\cdots$N hydrogen bonds with neighbouring U molecules. This interaction, though weak, is structurally important. (We note that in U this interaction prevents the crystal from being a plastic crystal like adamantane.) These bonds are along [101]/[10$\bar{1}$] and the progression of their establishment provides a mechanistic explanation for the (101)/(10$\bar{1}$) phase fronts. The formation of these bonds results in the creation of a two-dimensional network. Concomitantly, this advancement provides the internal stress necessary for dislocation movement favourable to the creation of the screwed MDO. Note that this latter is compatible with the orthorhombic metric of the OD structure and does not require a spontaneous macroscopic deformation.

Between 293 K and $T_{II\rightarrow III}$ the domains of the screwed MDO grow thicker. It appears that the MDO would eventually be converted to a pure three-dimensional structure with space group *Pcc*2 (like UP; Gardon, Pinheiro & Chapuis, 2003), although at a lower temperature. At ~283K similar transitions occur in UP and UA: in the former from a three-dimensional 'screwed' MDO to a three-dimensional 'slated' MDO, and in the latter from a mixture of 'screwed' and 'slated' MDOs to a three-dimensional 'slated' MDO. Since such similar phenomena appear at such similar temperatures in the two materials, the initiator of the transition ought to be a common factor present in both compounds. This hypothesis is certainly true for the U (010) layer, and therefore we conjecture that a soft mode that involves the U molecules of such a layer starts the II $\rightarrow$ III transition. However, the transition does not proceed in the same manner in the two compounds. Phase II of UP may be understood as a regular stacking of microscopic (*i.e.* just two layers thick) ferroelastic (100) domains of phase III (Fig. 14*a*). All UP would have to do during the transition is to increase the size of these domains (in UA they consist of ~200 layers), and indeed this layer rearrangement can be achieved by means of an enthalpy of ~1 J g^{-1}. In UA the layer stacking is less regular and some regions are already in the 'right' sequence, but strangely enough the presence of the 'slated' regions does not seem to help the transition. Possibly, this behaviour occurs because the process of growing larger domains from the 'slated' nuclei that are already present might be costly in terms of elastic energy. In any case the direct II $\rightarrow$ III transition is not possible and the system first grows a furtive triggering phase from which it can then build up the 'slated' stacking more easily ($\Delta H \simeq 2$ J g^{-1}). The intermediate phase, f, is likely to be triclinic since the 40$\bar{1}$ domains do not correspond to any symmetry direction of the orthorhombic parent phase. After the condensation of the soft mode, the hydrogen bonds on one side of the σ_x mirror plane become stronger (shorter by roughly 0.1 Å). This preference leads then to the growth of phase III. On a microscopic level the transition involves the propagation (much like falling dominos) of these shorter hydrogen bonds along [101]/[10$\bar{1}$]. As a consequence of this bias and of the symmetry compatibility (monoclinic metric) the slated MDO (space group $P2_1/c$) then becomes the more stable and the (100) layers are shifted by dislocation movement to build up the structure. Again, the decisive reconstruction takes place along the diagonals of the orthorhombic cell and this explains the (101)/(10$\bar{1}$) phase fronts.

It is thus seen that the phase sequences in UA and UP are really quite similar; the major difference lies in the conversion of the screwed MDO to a fully fledged three-dimensional structure in UP, whereas in UA this conversion is by-passed by the condensation of the soft mode, which leads to the nucleation and growth of phase III. In the α phase the screwed MDO is being formed. When this is converted to the perfect

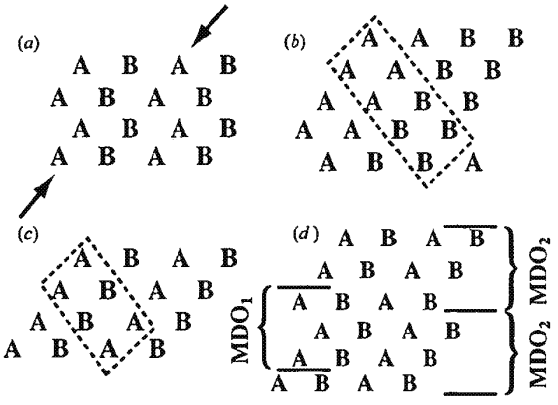


Figure 14
Chain and layer sequence in (*a*) MDO_1, (*b*) phase IV, (*c*) phase III, MDO_2. (*d*) Stacking fault leading to an MDO_1 domain wall.

UM00012989
NOVARTIS EXHIBIT 1017
Novartis v. Regents, IPR2023-01346
Page 1735 of 4460

three-dimensional structure, considerable energy is released [in the case of UP (Gardon, Pinheiro & Chapuis, 2003) $\Delta H \sim 17.3\ J\ g^{-1}$]. In the case of UA the condensation of the soft mode occurs before this conversion and the energy is kept within the system. Phase II is therefore a more energetic state. This excess energy can then be used to activate the $\{(\bar{1}51)|\mathbf{t} = \mathbf{a}_m\}$ slip system during the III $\rightarrow$ IV transition.

In the screwed MDO there exists an *AABB* sequence (Fig. 14*a*) of chains along [101]/[10$\bar{1}$]. The sequence in the neighbouring row is the same, but shifted by $\mathbf{a}_m$. The same chain sequence also exists in phase IV, and the system is thus very close to its ground state. (Incidentally, this similarity to the ground state also means that phase IV cannot be described as emerging from the OD structure.) All the system had to do was to shift alternate rows by opposite displacements. Obviously, this process is energetically too expensive in UP and UA, but such shifts do occur in urotropin undecanoate [UU] (Pinheiro *et al.*, 2003). There is no intermediate phase and the system goes directly from the screwed MDO to phase IV (Fig. 14*b*).

In UA the activation of this slip system has to wait until $T \simeq 233$ K, at which temperature the transition takes place. This transformation is achieved by a combination of two slip systems: the $\{(100)|\mathbf{t} = \mathbf{c}/4\}$ already used above and the more energetic $\{(\bar{1}51)|\mathbf{t} = \mathbf{a}_m/4\}$. The latter and its equivalents produce displacements of [101]/[10$\bar{1}$] rows of chains accompanied by displacements along (100). Nucleation of phase IV may involve an occasional residual domain of screwed MDO (Fig. 14*d*). Again, the reconstruction proceeds along the (101)/(10$\bar{1}$) phase fronts. For the $\{(\bar{1}51)|\mathbf{t} = \mathbf{a}_m\}$ slip system to cross the ubiquitous $\{(100)|\mathbf{t} = \mathbf{c}/4\}$ system is difficult and can lead to climb, cross slip and sessile dislocations. As a result the crystal may be torn apart; its fate depends on its precise microstructure. In this context we should mention that a synchrotron powder diffraction experiment has shown that the already thin (100) domains in phase III are reduced to really tiny regions (along **a** and **c**). These lead to considerable line broadening in phase IV.

Let us finally mention (Mucciolò, 1999) that these ubiquitous (101)/(10$\bar{1}$) phase fronts have also been observed in UP.

We sincerely thank Dr Monique Vogel for elucidating discussions on the biological aspects of AA. We express our heartfelt gratitude towards Antonio Mucciolò for his competent and generous help with the orthoscopic experiments. HB gratefully acknowledges the Danish Research Training Council for financial support.

References

Abrahamsson, S., Dahlén, B., Löfgren, H. & Pascher, I. (1978). *Prog. Chem. Fats Other Lipids*, **16**, 125–143.
Birkedal, H. (1996). Diploma Thesis, Copenhagen University.
Birkedal, H., Gardon, M., Hostettler, M., Duc, F., Schwarzenbach, D., Chapuis, G. & Bonin, M. (2003). In preparation.
Blažević, N., Kolbah, D., Belin, B., Šunjić, V. & Kajfež, F. (1979). *Synthesis*, pp. 161–176.
Bloss, F. D. (1990). *An Introduction to the Methods of Optical Crystallography*, ch. VIII. Marietta, OH 454750, USA: RAN Publishers. [Interference colour chart.]
Bond, A. D., Edwards, M. R. & Jones, W. (2001). *Acta Cryst.* E**57**, o143–o144.
Bonin, M., Bonin, L. G., Černy, R. & Schenk, K. J. (2003). In preparation.
Bonin, M., Fuith, A., Schenk, K. J. & Tolédano, P. (1999). *Phys. Rev.* **59**, 14246–14252.
Butler, B. D. & Welberry, T. R. (1992). *J. Appl. Cryst.*, **25**, 391–399.
Canut, M. L. & Amorós, J. L. (1958). *Bol. Real Soc. Espan. Hist. Nat.* G**56**, 323–338.
Caspari, W. A. (1929). *J. Chem. Soc.* pp. 2709–2712.
DiPersio, J. & Escaig, B. (1972). *Crystal Lattice Defects*, **3**, 55–58.
Dornberger-Schiff, K. (1966). *Lehrgang über OD-Strukturen.* Akademie Verlag Berlin.
Dupré La Tour, F. (1935). *C. R. Acad. Sci.* **201**, 479–481.
Gardon, M. (2001). PhD thesis, University of Lausanne, Switzerland.
Gardon, M., Pinheiro, C. B. & Chapuis, G. (2003). In preparation.
Gardon, M., Schenk, K. J., Bonin, M. & Tolédano, P. (2003). In preparation.
Geday, M. A. & Glazer, A. M. (2002). *J. Appl. Cryst.* **35**, 185–190.
Goossens, D. J. & Welberry, T. R. (2001). *Comput. Phys. Commun.* **142**, 387–390.
Guinier, A. (1964). *Théorie et technique de la radiocristallographie*, ch. XIII, 3rd ed. Paris: Dunod.
Harburn, G., Taylor, C. A. & Welberry, T. R. (1975). *Atlas of Optical Transforms*, Plate 24. London: G. Bell and Sons.
Holakovský, J. (1973). *Phys. Status Solidi B*, **56**, 615–619.
Hostettler, M. Birkedal, H., Gardon, M., Chapuis, G., Schwarzenbach, D. & Bonin, M. (1999). *Acta Cryst.* B**55**, 448–458.
Housty, J. & Hospital, M. (1967). *Acta Cryst.* **22**, 288–295.
Jeffrey, G. A. & Sänger, W. (1991). *Hydrogen Bonding in Biological Structures.* Berlin: Springer Verlag.
Kampermann, S. P., Sabine, T. M., Craven, B. M. & McMullan, R. K. (1995). *Acta Cryst.* A**51**, 489–497.
Klipping, G. & Stranski, I. N. (1958). *Z. Anorg. Allg. Chem.* **297**, 23–31.
Mucciolò, A. (1999). Private communication.
Osborn, J. C. & Welberry, T. R. (1990). *J. Appl. Cryst.* **23**, 476–484.
Pinheiro, C. B., Gardon, M. & Chapuis, G. (2003). In preparation.
Salem, L. (1962). *J. Chem. Phys.* **37**, 2100–2113.
Schenk, K. J. (1984). PhD thesis, University of Lausanne, Switzerland.
Sheldrick, G. M. (1997*a*). *SHELXL*97. *Program for the Refinement of Crystal Structures.* University of Göttingen, Germany.
Sheldrick, G. M. (1997*b*). *SHELXS*97. *Program for the Solution of Crystal Structures.* University of Göttingen, Germany.
Stamatiadis, D., Bulteau-Portois, M. C. & Mowszowicz, I. (1988). *Br. J. Dermatol.* **119**, 627–632.
Steiner, T. & Desiraju, G. R. (1998). *Chem. Commun.* pp. 891–892.
Stoe & CIE GmbH (1997). *IPDS* 2.89 *Software Manual.* Stoe and CIE, Darmstadt, Germany.
Thalladi, V. R., Nüsse, M. & Boese, R. (2000). *J. Am. Chem. Soc.* **122**, 9227–9236.
Welberry, T. R. & Mayo, S. C. (1996). *J. Appl. Cryst.* **29**, 353–364.
Welberry, T. R., Proffen, Th. & Bown, M. (1998). *Acta Cryst.* A**54**, 661–674.

UM00012990
NOVARTIS EXHIBIT 1017
Novartis v. Regents, IPR2023-01346
Page 1736 of 4460

This Page is Inserted by IFW Indexing and Scanning Operations and is not part of the Official Record

BEST AVAILABLE IMAGES

Defective images within this document are accurate representations of the original documents submitted by the applicant.

Defects in the images include but are not limited to the items checked:

- ☐ BLACK BORDERS
- ☐ IMAGE CUT OFF AT TOP, BOTTOM OR SIDES
- ☐ FADED TEXT OR DRAWING
- ☐ BLURRED OR ILLEGIBLE TEXT OR DRAWING
- ☐ SKEWED/SLANTED IMAGES
- ☐ COLOR OR BLACK AND WHITE PHOTOGRAPHS
- ☐ GRAY SCALE DOCUMENTS
- ☐ LINES OR MARKS ON ORIGINAL DOCUMENT
- ☐ REFERENCE(S) OR EXHIBIT(S) SUBMITTED ARE POOR QUALITY
- ☐ OTHER: _____

IMAGES ARE BEST AVAILABLE COPY.
As rescanning these documents will not correct the image problems checked, please do not report these problems to the IFW Image Problem Mailbox.

Microscopic nonlinearities of two-component organic crystals

Christian Bosshard,* Rolf Spreiter, and Peter Günter

Nonlinear Optics Laboratory, Institute of Quantum Electronics, ETH Hönggerberg, CH-8093 Zürich, Switzerland

Received November 7, 2000; revised manuscript received May 30, 2001

We determine the molecular first-order hyperpolarizability β of the highly nonlinear organic salt 4-N,N-dimethylamino-4′-N′-methyl stilbazolium tosylate (DAST, $\beta_{zzz} = (1540 \pm 250) \times 10^{-40}$ m⁴/V at λ=1542 nm) and the cocrystal 4-{2-[1−(2-hydroxyethyl)-4-pyridylidene]-ethylidene}-cyclo-hexa-2,5-dien-1-one)–(methyl 2,4-dihydroxybenzoate) (M2-MDB, $\beta_{zzz} = (1510 \pm 250) \times 10^{-40}$ m⁴/V at λ=1907 nm) in solution. These values are compared with the molecular first-order hyperpolarizabilities in the solid state, calculated with the measured nonlinear optical coefficient of the crystals. For both materials we show that the molecular nonlinearity in the solid state is considerably smaller than in solution. This lowering of the nonlinearity is attributed to the relatively strong Coulomb interactions in DAST and to the very strong hydrogen bonding in M2-MDB. © 2001 Optical Society of America

OCIS codes: 160.4330, 160.4890, 190.4400, 190.4710.

1. INTRODUCTION

Since the electro-optic effect in organic single crystals is mainly of electronic origin, these materials are very attractive for fast modulation of light. They offer almost unlimited design possibilities to fine tune the optical properties leading to large electro-optic effects with short response times. In this paper we investigate the microscopic nonlinear optical properties of two organic crystals that are optimized for electro-optics, namely, the organic salt 4-N,N-dimethylamino-4′-N′-methyl stilbazolium tosylate (DAST),[1,2] and the cocrystal 4-{2-[1-(2-hydroxyethyl)4-pyridylidene]-ethylidene}-cyclo-hexa-2,5-dien-1-one)–(methyl 2,4-dihydroxybenzoate) (M2-MDB).[3] We demonstrate through a comparison of microscopic and macroscopic properties that intermolecular interactions strongly influence the nonlinear optical response in the solid state.

A light beam, polarized along the charge-transfer axis of the molecule, can induce an asymmetric response of the molecular dipole (nonlinear response). On a microscopic scale, for a nonabsorbing molecule with an instantaneous response, the dipole moment $\mathbf{p}(t)$ of a molecule under a local electric field $\tilde{\mathbf{E}}(t)$ is expanded in a power series,

$$p_i(t) = \mu_i + \epsilon_0[\alpha_{ij}\tilde{E}_j(t) + \beta_{ijk}\tilde{E}_j(t)\tilde{E}_k(t) + \gamma_{ijkl}\tilde{E}_j(t)\tilde{E}_k(t)\tilde{E}_l(t) + \ldots], \quad (1)$$

where μ_i is the ground-state dipole moment, α_{ij} is the (linear) polarizability tensor, β_{ijk} is the first-order hyperpolarizability tensor, γ_{ijkl} is the second-order hyperpolarizability tensor, and ϵ_0 is the vacuum permittivity. For second-order nonlinear optical effects such as linear electro-optics, the first-order hyperpolarizability β_{ijk} has to be optimized.

For molecules with a single charge-transfer axis the first-order hyperpolarizability is dominated by a single tensor element β_{zzz}. Using the simple two-level model[4] with one ground state g and one excited state e, β_{zzz} can be written as[5]

$$\beta_{zzz}^{(-2\omega,\,\omega,\,\omega)} = \frac{\omega_{eg}^4}{(\omega_{eg}^2 - \omega^2)(\omega_{eg}^2 - 4\omega^2)}\beta_0 \quad (2)$$

for the case of second-harmonic generation. ω_{eg} is the resonance frequency of the transition and β_0 is the static first-order hyperpolarizability reached when all three frequencies approach zero.

Based on the assumption of weak interactions between the molecules in condensed matter, we relate the microscopic first-order hyperpolarizability to the macroscopic second-order nonlinear-optical susceptibility $\chi_{ijk}^{(-2\omega,\,\omega,\,\omega)}$ (defined analogously to Eq. (1))[6] and the nonlinear-optical coefficient for frequency doubling $d_{ijk}^{(-2\omega,\,\omega,\,\omega)}$,

$$d_{ijk}^{(-2\omega,\,\omega\,\omega)} = \frac{1}{2}\chi_{ijk}^{(-2\omega,\,\omega\,\omega)} = \frac{1}{2}\frac{N}{n(g)}f_i^{2\omega}f_j^{\omega}f_k^{\omega}\sum_s^{n(g)}\sum_{lmn}^{3}\cos\theta_{il}^s\cos\theta_{jm}^s \times \cos\theta_{kn}^s\beta_{lmn}^{(-2\omega,\,\omega,\,\omega)}. \quad (3)$$

N is the number density of molecules, $n(g)$ is the number of molecules in the unit cell, and θ_{il}^s is the angle between the dielectric axis i and the molecular axis l of molecule s in the unit cell. The local-field correction factors relate the macroscopic field to the local field at the place of the molecules and take to some extent intermolecular effects into account. Usually only the simplest Lorentz approximation[7] $f_i^{\omega} = [(n_i^{\omega})^2 + 2]/3$ is used.

0740-3224/2001/111620-07$15.00 © 2001 Optical Society of America

UM00012992
NOVARTIS EXHIBIT 1017
Novartis v. Regents, IPR2023-01346
Page 1738 of 4460

2. MATERIALS

Depending on the crystal-growth conditions, DAST can crystallize in either of two phases, in a centrosymmetric phase (space group $P\bar{1}$, point group $\bar{1}$, $z = 2$) containing water (orange color), or in the monoclinic space group Cc (point group m, $z = 4$) in red color (Fig. 1). There is a slight difference between the crystallographic and the dielectric axes of the latter, noncentrosymmetric structure. The dielectric axes x_1, x_2, and x_3 are defined as the principal axes of the crystal's refractive-index ellipsoid. The angles between the dielectric axes x_1 and x_3 and the crystallographic axes a and c are 5.4° and 3.2°, respectively, whereas the x_2 axis coincides with the b axis.

The crystal DAST is composed of consecutive layers of stilbazolium and tosylate molecules. The charge-transfer axis of the stilbazolium chromophore deviates by only 20° from the polar a axis of the crystal, which is a very well optimized arrangement for linear electro-optics. The reduction factor of the linear electro-optic coefficient compared with the optimum parallel alignment is only $\cos^3(20°) = 0.83$.

The classical merocyanine dye M1 (Fig. 2) has been studied already in 1951 by L. Brooker *et al.*[8] because of the exceptionally large shift of the wavelength of maximum absorption when the polarity of the solvent is changed. This shift can have several origins, such as a geometrical change of the molecule or a redistribution of charge density. They observed a shift of the absorption peak of 161 nm when changing the solvent mixture from pure pyridine to pure water and proposed to use this compound for the colorimetric determination of the water concentration in pyridine.

M1 has been reported to show very large first-order hyperpolarizabilities and good photostability.[9,10] To develop the merocyanine dye into a useful crystalline structure is therefore of great interest. Unfortunately the merocyanine dye M1 does not crystallize noncentrosymmetrically.

Using a modified merocyanine M2 and a properly designed phenolic derivative MDB as a guest molecule (Fig. 2), we could achieve cocrystallization with an almost perfect parallel alignment of the chromophores (angle of 2.8° between the charge-transfer axis of two symmetry related chromophores in the crystal lattice).[3] This favorable orientation makes this crystal very interesting for linear electro-optics.[11] Cocrystallization is induced due to the short and very strong hydrogen bond ($R_{O\text{-}O} = 2.5$ Å) between the two phenolic oxygen atoms of M2 and MDB, respectively.

Depending on the growth conditions, three different phases (phase I, phase II, and phase III) of M2-MDB were

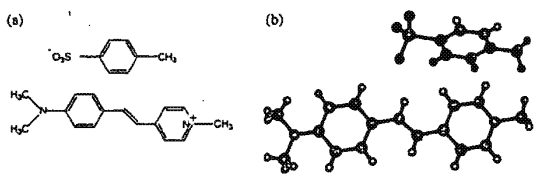


Fig. 1. (a) Molecular units of the ionic DAST crystal. The negatively charged tosylate and the positively charged, nonlinear optical chromophore stilbazolium. (b) The molecules are shown as they are embedded in the crystal lattice.

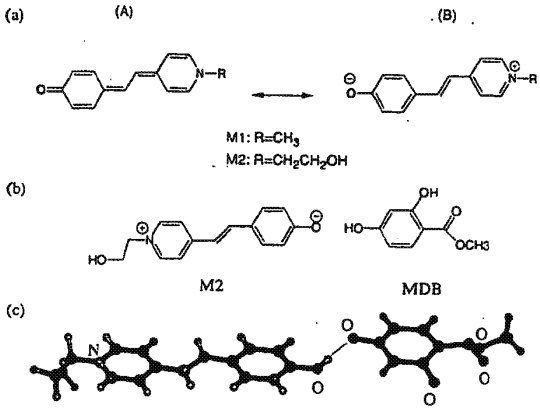


Fig. 2. (a) Resonance structures of the merocyanine dyes M1 and M2. (A) is the quinoid form and (B) is the zwitterionic form. (b) Molecular units of M2-MDB. The MDB guest molecule (right) and the nonlinear optical modified merocyanine chromophore (left) form a molecular aggregate by building a very short hydrogen bond. (c) The molecules as they are arranged in the crystal lattice.

obtained by the solution growth method in methanol.[11] Interestingly, phase I and phase II have the same structure (monoclinic, space group Cc, point group m) within the measurement error of x-ray structure determination but strongly differing linear and nonlinear optical and linear electro-optical properties.[3]

In the following we present results of the molecular properties of the above compounds and demonstrate that the strong intermolecular interactions (Coulomb forces for DAST and hydrogen bonds for M2-MDB) considerably modify the optical properties in the crystalline state.

3. MOLECULAR NONLINEARITIES

There exist several methods for determining the molecular first-order hyperpolarizability β. We used hyper-Rayleigh scattering (HRS)[12,13] for DAST and electric-field-induced second-harmonic generation (EFISH)[14,4] for M2-MDB. Finally, we used the semiempirical quantum-mechanical program package MOPAC (version 6.2)[15] to theoretically evaluate the molecular properties of DAST and the merocyanine dyes.

A. EFISH Experiments of M2-MDB

EFISH is the standard method for measuring the first-order hyperpolarizability of organic molecules in solution. By applying a strong pulsed electric field to the solution, the nonlinear optical molecules are partially oriented, and the second-harmonic signal is measured as a function of the light path of the fundamental beam. The EFISH method therefore works only for polar and nonionic molecules. Another drawback of this method is that always a combination of first- and second-order hyperpolarizabilities is determined.[4]

In the EFISH experiment a combination of tensor elements of β_{ijk} is measured. Under the assumption of a single charge-transfer axis along the ground-state dipole moment this combination reduces to $\beta_{zzz} = \beta$.

UM00012993
NOVARTIS EXHIBIT 1017
Novartis v. Regents, IPR2023-01346
Page 1739 of 4460

The sample solution is placed in a wedged cell, which is moved perpendicularly to the fundamental laser beam. The polarization of the incident beam is parallel to the direction of the applied electric field. The change in the path length leads to a second-harmonic signal that varies with the period of the coherence length and is detected with a photomultiplier. These data are then analyzed relative to a reference solution leading to a third-order susceptibility Γ_L that is proportional to β (see, e.g., Ref. 16). By measuring a series of different concentrations, the first-order hyperpolarizability is obtained.

The measurements were carried out at λ=1907 nm. The β values were calibrated against a reference solution of 2-methyl-4-nitroaniline (MNA) with $\beta = (44 \pm 4) \times 10^{-40}$ m^4/V^6 at λ=1907 nm, as determined by an EFISH experiment relative to crystalline quartz with the most recently proposed nonlinear optical susceptibility $d_{111} = (0.277 \pm 0.01)$ pm/V at λ=1907 nm[17,18]. For a reliable comparison between the hyperpolarizability determined by EFISH and HRS (see below), we also measured Disperse Red 1 (DR1), a chromophore often used in guest–host polymers, in dioxane. For each compound we measured three to four different concentrations as well as the pure solvent. A detailed description of our setup and the analysis can be found in Ref. 16.

At a fundamental wavelength of λ=1907 nm we obtained $\beta = (570 \pm 60) \times 10^{-40}$ m^4/V for DR 1 dissolved in dioxane. In the same solvent but at λ=1542 nm a value of $\beta = (1145 \pm 100) \times 10^{-40}$ m^4/V was measured.[19] For the evaluation of both measurements the calculated ground-state dipole moment of $\mu = 3.2 \times 10^{29}$ Cm (Ref. 19) was used. Note that the large difference of the first-order hyperpolarizabilities between these two wavelengths cannot be described by the two-level model with the measured wavelength of maximum absorption of λ_{eg} = 473 nm. This fact suggests that the two-level model is too simple a description for these kinds of molecules when any of the interacting frequencies approaches the absorption region of the material.

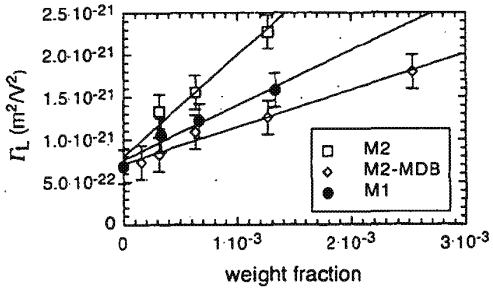


Fig. 3. Measured dependence of the third-order susceptibility Γ_L of M2, M2-MDB, and M1 on the chromophore weight fraction in methanol.

The merocyanine compounds show low solubility in most solvents. Even in methanol, which is the best solvent for these kinds of compounds, the solubilities were <0.3 wt. %. Moreover, when using methanol, one observes electrical breakdown in the EFISH cell, already at moderate applied fields. Therefore we used high-voltage pulses of 4.5 kV with suitable rise and fall times of 50 ns and a duration of 250 ns, short enough to prevent any breakdown and long enough to allow the orientation of the chromophores.

The first-order hyperpolarizabilities β of M2, M2-MDB, and M1 for comparison were then measured in methanol at a fundamental wavelength of λ=1907 nm. The concentration dependence of the third-order susceptibility Γ_L is shown in Fig. 3. From this dependence a negative sign of β can be deduced as is shown below. This sign is normally defined relative to the positive direction of the ground-state dipole moment. A positive slope in Fig. 3 implies that the chromophores have the same sign of the first-order hyperpolarizability as the solvent, whereas opposite signs would correspond to a negative slope. By EFISH measurements in the gas phase it was shown that β of methanol is negative and large enough to allow the assumption that β in the liquid has the same sign.[20] Therefore all the values of β for the merocyanine compounds in methanol are negative (Table 1). Moreover, all measured values are larger than for DR1.

The fact that the value of β for M2 is considerably larger than for M1 might be due to a different equilibrium of the molecules [unprotonated versus protonated (i.e., when a hydrogen is attached at the basic donor of the M2 chromophore)] in solution when modifying R (see Fig. 2), which would result in a difference of the values of β. The same behavior was already observed for the second-order hyperpolarizability γ of the same compounds.[21] Our experimental findings of reduced nonlinearities of M2-MDB with respect to M2 can be explained by looking at the to-

Table 1. Measured First-Order Hyperpolarizabilities of the Merocyanine Dyes at λ=1907 nm and DAST at λ=1542 nm[a]

Material	λ_{eg} [nm]	$\mu\beta$ [10^{-69} Cm^5/V]	μ [10^{-30} Cm]	$\beta = \beta_{zzz}$ [10^{-40} m^4/V]	β/β_{DR1} at λ_{meas}	β/β_{DR1} at $\lambda=\infty$
M1 (methanol)	480	−510 ± 70	3.8	−1340 ± 250	−2.4	−2.3
M2 (methanol)	485	−1080 ± 140	3.6	−3000 ± 450	−5.3	−5.2
M2-MDB (methanol)	490	−670 ± 60	6.3	−1060 ± 120	−1.9	−1.8
M2-MDB (DMSO)	576	950 ± 150	6.3	1510 ± 250	2.6	2.2
DAST (DMSO)	471	–	–	1540 ± 250	1.3	2.2

[a] The values for the dipole moments are calculated values based on the finite-field method with the AM1 parametrization. β/β_{DR1} is given for the experimental wavelength and calculated for infinite wavelengths with the two-level model ($\beta_{DR1} = (1145 \pm 100) \times 10^{-40}$ m^4/V at λ=1542 nm based on $\beta_{DR1} = (570 \pm 60) \times 10^{-40}$ m^4/V at λ=1907 nm measured in dioxane) λ_{eg} is the wavelength corresponding to the main electronic transition. It should be noted that we assumed in first approximation that $\beta = \beta_{zzz}$.

UM00012994
NOVARTIS EXHIBIT 1017
Novartis v. Regents, IPR2023-01346
Page 1740 of 4460

Table 2. Calculated First-Order Hyperpolarizabilities β^{MOPAC} and Absolute Values of the Experimental First-Order Hyperpolarizabilities Extrapolated to Infinite Wavelengths and Multiplied by 6/5 to Convert to the Calculated Values [see Eq. (8)]

Material	β^{MOPAC} [10^{-40} m^4/V]	(6/5)$\lvert\beta_0^{exp}\rvert$ [10^{-40} m^4/V]
M2	201	2500
M2, protonated	151	-
MDB	1.4	-
M2-MDB	293	870 (methanol)
Stilbazolium	201	880
Tosylate	8.4	-

tal absorption spectrum. We find that the solution contains not only M2-MDB but also M2 and MDB alone (with a very small value of β; see Table 2) as well as the protonated form of M2 (with a smaller value of β than M2; see Table 2). Therefore we have to consider a mixture of molecules in solution that leads to a reduction of the total value of β.

To obtain information about the influence of the molecular environment on the nonlinearity, we also performed EFISH measurements in the solvent dimethyl sulfoxide (DMSO), which is much more polar than methanol. In this case, only M2-MDB showed enough solubility to obtain a reliable result. Due to the very low concentration and the relatively high nonlinearity of the pure solvent DMSO, the error in the final molecular hyperpolarizability is rather large. Since β of DMSO is known to be positive, the positive slope we obtained corresponds to a positive first-order hyperpolarizability of M2-MDB in DMSO.

We thus see that changing the solvent not only modifies the value but also the sign of β. This result is in agreement with the strong solvatochromic behavior discussed above and can also be explained in terms of bond-length alternation.[22]

B. Hyper-Rayleigh Scattering Experiments of DAST

HRS uses the effect of thermal fluctuation. Due to the orientational fluctuations of the molecules, the centrosymmetry of a certain scattering volume element of the solution is broken and a weak second-harmonic signal is generated. Since no electric field has to be applied also conducting (ionic) solutions (such as DAST) can be measured. Due to electrical discharge through the solution when a high voltage is applied, the electric field cannot build up, and the standard EFISH experiment does not work with DAST.

For typical nonlinear optical molecules with a single charge-transfer axis, one tensor element β_{zzz} of the first-order hyperpolarizability dominates. The relevant quantity that is determined for this case is the rotational average $\langle\beta_{ZZZ}^2\rangle$, where Z denotes the polarizer/analyzer axis in the experiment. For the above condition of a dominant single tensor element of β we obtain the relation $\langle\beta_{ZZZ}^2\rangle = \beta_{zzz}^2/7$. Since some of the experimental constants cannot easily be determined, a reference solution of molecules with known first-order hyperpolarizability is used. The second-harmonic intensity ratio between sample and reference solution $I_{2\omega}/I_{2\omega}^{ref}$ is then measured, and for HRS, β_{zzz} of the molecule under consideration is then given by

$$\beta_{zzz} = \beta_{zzz}^{ref}\frac{(f^{\omega}{}_{ref})^2(f^{2\omega}{}_{ref})}{(f^{\omega})^2(f^{2\omega})}\sqrt{\frac{I_{2\omega}N_{ref}}{I_{2\omega}^{ref}N}}, \tag{4}$$

where N is the number of molecules per volume and $f^{\omega} = [(n^{\omega})^2 + 2]/3$ is the local field correction in the simple Lorentz–Lorentz approximation (see, e.g., Ref. 16 for more details on our theoretical evaluation). Note that Eq. (4) is only valid for one dominant tensor element of β.

In the following we describe our experiment in more detail since special procedures had to be applied for successful results. In our HRS experiment (Fig. 4) the fundamental laser beam with adjustable power is focused with a lens (f = 200 mm) into the center of the liquid cell containing the sample. As a light source we used a Nd:YAG laser with a pulse width of τ=7 ns and a repetition rate of 5 Hz. The laser output of λ=1064 nm was Raman shifted in a methane gas cell to λ=1542 nm. Filter 1 blocks all but the fundamental, whereas filter 2 blocks all but the second-harmonic signal. In order to determine the dependence of the second-harmonic intensity on the fundamental beam intensity, a motor-controlled polarization rotator together with a polarizer was used to continuously adjust the fundamental intensity. The scattered second-harmonic light was measured perpendicularly to the fundamental beam. Different aperture diameters allowed us to vary the solid angle of the collected light. Beside the signal at 2ω generated by second-harmonic generation, also a signal at the same frequency resulting from three-photon induced luminescence can be expected. Since the spectral distribution is quite different for light generated by the two mentioned processes, we measured the spectral distribution by using interference filters with several different bandwidths (see below).

Although the solubility of DAST is better in methanol, we dissolved it in DMSO, since methanol strongly absorbs at the fundamental wavelength λ=1542 nm. The absorption for both the fundamental and the second harmonic could be neglected for DAST in DMSO. The well

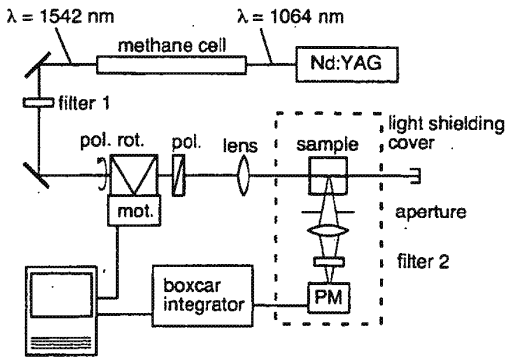


Fig. 4. Experimental setup for the HRS experiment. The scattered second-harmonic power is measured as a function of the fundamental power.

UM00012995
NOVARTIS EXHIBIT 1017
Novartis v. Regents, IPR2023-01346
Page 1741 of 4460

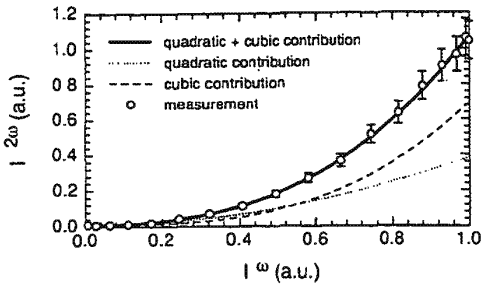


Fig. 5. Typical measurement of a solution of 0.8 wt. % DAST in the solvent DMSO heated to 50 °C. Shown are the calculated contributions from second-harmonic generation and three-photon-induced luminescence.

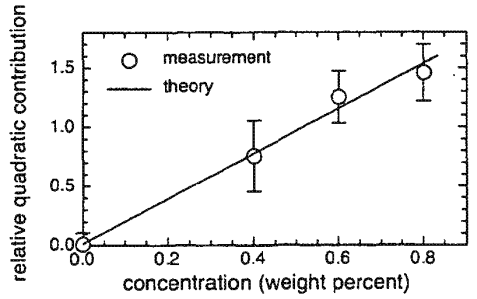


Fig. 6. Second-harmonic signal of DAST in DMSO versus concentration. The second-harmonic intensity is relative to that of DR1 in a 1.0 wt % solution in dioxane.

known reference compound MNA produced too little signal to be used as a reference at this wavelength. Instead, we used a solution of DR1 in dioxane. DR1 [β = (1145 ± 100) × 10^{-40} m^4/V at λ=1542 nm[19]] was measured with an EFISH experiment against MNA by use of the new value of quartz (d_{11} = 0.28 pm/V at λ=1542 nm).[17,18]

We measured the dependence of the second-harmonic signal on the fundamental intensity. From a pure second-order effect a quadratic dependence on the fundamental intensity is expected. It turned out that the fundamental intensity dependence was a mixture of a quadratic and cubic contribution (Fig. 5).

The second-harmonic intensity dependence was therefore modeled with a third-order polynomial,

$$I_{2\omega}(I_\omega) = a_2 I_\omega^2 + a_3 I_\omega^3. \quad (5)$$

Using interference filters with the same peak wavelength of λ=772 nm (at 2ω) but different 50% transmission bandwidths of 1.5 nm, 3 nm, and 10 nm, we could show the quadratic contribution being independent and the cubic contribution being linearly dependent on the filter bandwidth. This is the behavior we expect for a narrow-band second-harmonic signal, mixed with a broadband three-photon-induced luminescent signal.

Concentrations of 0.4%, 0.6%, and 0.8% of DAST dissolved in DMSO were characterized. At room temperature we could dissolve only 0.004 weight fraction of DAST in DMSO. Heating the cell to 50 °C allowed us to dissolve up to 0.008 weight fraction. This heating was essential since otherwise the signal-to-noise ratio was too low for a precise measurement. From theory we do not expect a dependence of the scattered second-harmonic signal on temperature. However, we used a concentration of 0.004 weight fraction to compare the measurement at room temperature and at the elevated temperature of 50 °C. We did not detect any difference larger than the statistical fluctuations from measurement to measurement. All concentrations had to be measured between 4 and 12 times in order to reduce the relatively large errors. In Fig. 6 the average for each concentration is shown.

The linear behavior in Fig. 6 results in a first-order hyperpolarizability of DAST relative to Disperse Red 1 (DR1) of

$$\langle\beta_{zzz}^2\rangle^{1/2}_{\mathrm{DAST}} = (1.34 \pm 0.2) \times \langle\beta_{zzz}^2\rangle^{1/2}_{\mathrm{DR1}}. \quad (6)$$

Inserting the first-order hyperpolarizability of DR1 [β = (1145 ± 100) × 10^{-40} m^4/V] at a fundamental wavelength of λ=1542 nm, we obtain a value of

$$\beta_{zzz} = (1540 \pm 250) \times 10^{-40}\ m^4/V. \quad (7)$$

C. Calculation of the Molecular Hyperpolarizabilities of DAST and M2-MDB

Absolute and accurate calculations of molecular hyperpolarizabilities are difficult. Usually the results differ considerably from the experimental measurements, mainly because of three reasons. First, a complete quantum-mechanical calculation is only possible for small molecules on supercomputers. Therefore strong simplifications have to be assumed, and the parametrization is usually optimized for one certain class of molecules. Second, because of limited calculation power, only a single molecule in the gas phase neglecting interactions with the environment is considered. In practice, the molecules are either in solution or in the solid state, and the used conjugated donor acceptor substituted compounds are known to react very sensitively to their environment. Third, the calculated hyperpolarizabilities are often static values, whereas in the experiment the applied fields are rapidly oscillating fields. Therefore to compare the experimental values with the calculated ones, a model to take into account the dispersion (usually the two-level model (see Eq. (2)) has to be applied. Nevertheless, calculations can be very useful to compare a series of similar molecules, such as the influence of different donor–acceptor substitutions.[23]

We used the finite-field method[24] with the Austin Model 1 parametrization, as implemented in the semiempirical structure-optimization program MOPAC[15] to optimize a given structure and to calculate physical properties such as the first-order hyperpolarizabilities and the ground-state dipole moments.

The method is based on the expansion of the electronic energy of the molecule on the magnitude of an applied electric field. The energy is calculated for five different applied electric fields (including zero field). The dipole moment, linear polarizability, and first-order hyperpolarizability correspond to the first, second, and third derivative of the energy with respect to the applied fields, which can be easily calculated.[15]

An alternate method is the expansion of the induced dipole moment with respect to the applied field. In MOPAC

UM00012996
NOVARTIS EXHIBIT 1017
Novartis v. Regents, IPR2023-01346
Page 1742 of 4460

this second method is always applied at the same time for calculating the same properties. The comparison of the results obtained by the two methods gives a valuable indication on the reliability of the calculation.

Since different definitions are used for the experimental and calculated hyperpolarizabilities, the following equation has to be used[21]:

$$\beta^{\mathrm{MOPAC}} = \frac{6}{5}\beta_0^{\mathrm{Exp}}. \tag{8}$$

In Table 2 the calculated dipole moments and static first-order hyperpolarizabilities along the dipole moment are shown. The calculated hyperpolarizabilities are generally smaller than the ones measured in solution. Although it is well known that the absolute values, calculated by this method, cannot be compared with the experimental ones, we can compare the calculated values relative to each other. The values of M2 and DAST are of similar magnitude both theoretically and experimentally. Our results show that the calculated hyperpolarizability of M2 is reduced when the molecule is protonated. This behavior is exactly what we also observe in the solid state for phase I where the photon is closer to the donor of M2 compared with phase II.[11] Theoretically M2-MDB has larger values of β than M2. This fact could not be observed experimentally since, as discussed above, we have a mixture of M2, MDB, and M2-MDB in the solution.

However, one has to be careful with the interpretation of the calculated hyperpolarizabilities, especially of the merocyanine compounds, since we have static values, and it is known that their electronic properties are extremely sensitive to changes of their environment, as can be seen by solvatochromic methods and the strongly solvent-dependent values of β.

4. DISCUSSION AND CONCLUSIONS

In the following we compare the molecular first-order hyperpolarizabilities measured in the solid state to the ones measured in solution. The nonlinear optical coefficients of DAST and M2-MDB were previously measured by use of the Maker–Fringe technique[25,3] and are summarized in Table 3.

Using the orientation and density of the chromophores in the crystal lattice, we can calculate the first-order hyperpolarizability $\beta_{zzz}^{(-2\omega,\,\omega,\,\omega)}$ of the chromophores in the solid state based on Eq. (3). These values together with the first-order hyperpolarizability in solution are summarized in Table 4.

Besides the molecular nonlinearity the required quantities for this evaluation are $N = 1.906 \times 10^{27}$ m^{-3}, $n_g = 4$, $\theta = 20°$, $n_1^{\omega} = 2.132$, and $n_1^{2\omega} = 2.417$ for DAST; $N = 1.974 \times 10^{27}$ m^{-3}, $n_g = 4$, $\theta = 2.8°$, $n_1^{\omega} = 2.008$, and $n_1^{2\omega} = 2.153$ for phase II of M2-MDB; and $n_1^{\omega} = 1.935$, $n_1^{2\omega} = 2.030$ for phase I of M2-MDB, with all optical values at $\lambda = 1542$ nm.

For DAST and M2-MDB (phase I and phase II) the first-order hyperpolarizability $\beta_{zzz}^{(-2\omega,\omega,\omega)}$ in the solid state is significantly lower than it is in solution. β is reduced by a factor of 5.3 in the case of DAST and by a factor of 12–20 for M2-MDB (Table 4). These results show that the molecular environment has a great influence on the nonlinearity of the molecule. The usually made assumption of independent molecules in the crystal lattice (oriented gas model) for calculating the molecular properties is not justified for DAST and M2-MDB. For the oriented gas model to be valid it is assumed that the chromophores are bound only by weak intermolecular forces. This is justified for materials where Van der Waals interactions are the dominant binding force but not for the cases discussed here.

Table 3. Measured Nonlinear Optical Coefficients d_{111} (at $\lambda = 1542$ nm) and Wavelength of Maximum Absorption of DAST and M2-MDB (Phases I and II) in the Solid State Derived from the Dispersion of the Refractive Indices[a]

Material	λ_{max} [nm]	d_{111} [pm/V]	d_{111}^{theor} [pm/V]
DAST	535	290 ± 15	1530 ± 100
M2-MDB phase I	474	78 ± 10	980 ± 130
M2-MDB phase II	540	107 ± 10	2140 ± 200

[a] Also given are the nonlinear optical coefficients d_{111}^{theor} estimated from measured first-order hyperpolarizability β_{zzz} by use of the diluted gas model

Table 4. Comparison of the First-Order Hyperpolarizabilities of DAST and M2-MDB in Solution and in the Solid State[a]

Material	$\lvert\beta_{zzz}\rvert$ [10^{-40} m^4/V] (solution)	β_{zzz} [10^{-40} m^4/V] (solid state)	$\beta_{zzz}^{\mathrm{solid}}/\lvert\beta_{zzz}^{\mathrm{solution}}\rvert$
DAST	1540 ± 250, λ = 1542 nm(*),	290 ± 15, λ = 1542 nm(*)	0.19
	880 ± 130, λ = ∞	165 ± 10, λ = ∞	
	(solvent: DMSO)		
M2-MDB	−1060 ± 120, λ = 1970 nm(*)	106 ± 15, λ = 1542 nm(*)	0.08
phase I	−730 ± 90, λ = ∞	83 ± 13, λ = 1907 nm	
(light)	(solvent: methanol)	57 ± 9, λ = ∞	
M2-MDB	1510 ± 250, λ = 1907 nm(*)	122 ± 20, λ = 1542 nm(*)	0.05
phase II	870 ± 100, λ = ∞	80 ± 13, λ = 1907 nm	
(dark)	(solvent: DMSO)	46 ± 9, λ = ∞	

[a] The measured values are indicated by (*), the values at other wavelengths are calculated from the measured ones by use of the two-level model to take into account dispersion. The value at $\lambda = \infty$ was extrapolated to infinite wavelengths (= static value), also by use of the two-level model. It should be noted that we assumed in first approximation that $\beta = \beta_{zzz}$, which, however, does not influence the main conclusion drawn from this study.

UM00012997
NOVARTIS EXHIBIT 1017
Novartis v. Regents, IPR2023-01346
Page 1743 of 4460

In DAST, due to the ionic character of the molecules, there also exist strong Coulomb interactions between the molecules, and in M2-MDB the very strong hydrogen bonds possess binding energies in the range of covalent bonds. In phase I and phase II of M2-MDB, quite different nonlinear optical coefficients were measured (Table 3). This behavior has its origin mainly in the different electronic resonance frequencies ω_{eg} of the two phases, as can be concluded from the essentially identical static values of the first-order hyperpolarizability β_0. Such drastic modifications of the molecular nonlinearities due to the transition from solution to the solid state have also been observed in organominerals.[26] Since the exact strength and influence on the nonlinearities in the solid state are difficult to assess, we cannot discuss the relevant interactions in more detail at the moment.

In conclusion, we have used combined nonlinear optical experiments on molecules and single crystals of DAST and M2-MDB to demonstrate the importance of intermolecular interactions in two-component organic crystals based on highly polarizable molecules. The molecular nonlinearities of DAST and M2-MDB in solution are large with respect to the standard dye DR1 and by a factor of 5–20 larger than the corresponding ones in the solid state if intermolecular interactions are neglected (Table 3). These findings suggest new routes for the design of highly nonlinear optical organic crystals where a decoupling of the molecules in terms of intermolecular interactions has to be considered. If we look at the already extremely large nonlinearities of DAST and M2-MDB, nonlinear optical coefficients of the order of several 1000 pm/V and electro-optic coefficients of a few 100 pm/V might be feasible that way.

ACKNOWLEDGMENT

We gratefully acknowledge financial support from the Swiss National Science Foundation.

*E-mail: christian.bosshard@csem.ch.

REFERENCES

1. F. Pan, G. Knöpfle, Ch. Bosshard, S. Follonier, R. Spreiter, M. S. Wong, and P. Günter, "Electro-optic properties of the organic salt 4-N,N-dimethylamino-4′-N′-methyl-stilbazolium tosylate," Appl. Phys. Lett. **69**, 13–15 (1996).
2. R. Spreiter, Ch. Bosshard, and P. Günter, "High frequency response and acoustic phonon contribution of the linear electro-optic effect in DAST," Opt. Lett. **22**, 564–566 (1997).
3. M. S. Wong, F. Pan, M. Bösch, R. Spreiter, Ch. Bosshard, and P. Günter, "Novel electro-optic molecular co-crystals with ideal chromophoric orientation and large second-order nonlinearities," J. Opt. Soc. Am. B **15**, 426–431 (1998).
4. J. L. Oudar and D. S. Chemla, "Hyperpolarizabilities of the nitroanilines and their relations to the excited state dipole moment," J. Chem. Phys. **66**, 2664–2668 (1977).
5. C. C. Teng and A. F. Garito, "Dispersion of the nonlinear second-order optical susceptibility of organic systems," Phys. Rev. B **28**, 6766–6773 (1983).
6. J. Zyss and J. L. Oudar, "Relation between microscopic and macroscopic low-order optical nonlinearities of molecular crystals with one- or two-dimensional units," Phys. Rev. A **26**, 2028–2048 (1982).
7. C. J. Boettcher, *Theory of Electric Polarization* (Elsevier, Amsterdam, 1952).
8. L. G. S. Brooker, G. H. Keyes, and D. W. Heseltine, "Color and constitution. XI. Anhydronium bases of *p*-hydroxystyryl dyes as solvent polarity indicators," J. Am. Chem. Soc. **73**, 5330 (1951).
9. B. F. Levine, C. G. Bethea, E. Wasserman, and L. Leenders, "Solvent dependent hyperpolarizability of a merocyanine dye," J. Chem. Phys. **68**, 5042–5045 (1978).
10. A. Dulic and C. Flytzanis, "A new class of conjugated molecules with large second order polarizability," Opt. Commun. **25**, 402–406 (1978).
11. Ch. Bosshard, F. Pan, M. S. Wong, S. Manetta, R. Spreiter, C. Cai, P. Günter, and V. Gramlich, "Nonlinear optical organic co-crystals of merocyanine dyes and phenolic derivatives with short hydrogen bonds," Chem. Phys. **245**, 377–394 (1999).
12. R. W. Terhune, P. D. Maker, and C. M. Savage, "Measurement of nonlinear light scattering," Phys. Rev. Lett. **14**, 681–684 (1965).
13. K. Clays and A. Persoons, "Hyper-Rayleigh scattering in solution," Phys. Rev. Lett. **66**, 2980–2983 (1991).
14. S. Kielich, "Optical second-harmonic generation by electrically polarized isotropic media," IEEE J. Quantum Electron. **5**, 562–568 (1969).
15. H. A. Kurtz, "Calculation of the nonlinear optical properties of molecules," J. Comput. Chem. **11**, 82 (1989).
16. Ch. Bosshard, M. Bösch, I. Liakatas, M. Jäger, and P. Günter, "Second-order nonlinear optical organic materials: recent developments," in *Nonlinear Optical Effects and Materials*, P. Günter, eds., Vol. 72 of Springer Series in Optical Sciences (Springer Verlag, New York, 2000), pp. 163–299.
17. Ch. Bosshard, U. Gubler, P. Kaatz, W. Mazerant, and U. Meier, "Non-phase-matched optical third-harmonic generation in noncentrosymmetric media: cascaded second-order contributions for the calibration of third-order nonlinearities," Phys. Rev. B **61**, 10688–10701 (2000).
18. U. Gubler and Ch. Bosshard, "Optical third-harmonic generation of fused silica in gas atmosphere: absolute value of the third-order susceptibility $\chi^{(3)}$," Phys. Rev. B **61**, 10702–10710 (2000).
19. I. Liakatas, M. S. Wong, V. Gramlich, Ch. Bosshard, and P. Günter, "Novel, highly nonlinear optical molecular crystals based on multidonor-substituted 4-nitrophenylhydrazones," Adv. Mater. **10**, 777–782 (1998).
20. Ph. Kaatz, E. A. Donley, and D. Shelton, "A comparison of molecular hyperpolarizabilities from gas and liquid phase measurements," J. Chem. Phys. **108**, 849–856 (1998).
21. Ch. Bosshard, "Third-order nonlinear optics in polar materials," in *Nonlinear Optical Effects and Materials*, P. Günter, ed., Vol. 72 of Springer Series in Optical Sciences (Springer Verlag, New York, 2000), pp. 7–161.
22. S. Marker, L.-T. Cheng, B. G. Tiemann, A. C. Friedli, M. Blanchard-Desce, J. W. Perry, and J. Sindhoj, "Large first hyperpolarizability in push-pull polyenes by tuning of the bond length alternation and aromaticity," Science **263**, 511–514 (1994).
23. Ch. Bosshard, R. Spreiter, P. Günter, R. R. Tykwinski, M. Schreiber, and F. Diederich, "Structure–property relationships in nonlinear optical tetrathynylethenes," Adv. Mater. **8**, 231–234 (1996).
24. J. Zyss, "Hyperpolarizabilities of substituted conjugated molecules. I. Perturbated INDO approach to monosubstituted benzene," J. Chem. Phys. **70**, 3333–3340 (1979).
25. U. Meier, M. Bösch, Ch. Bosshard, F. Pan, and P. Günter, "Parametric interactions in the organic salt 4-N,N-dimethylamino-4′-N′-methyl-stilbazolium tosylate at telecommunication wavelengths," J. Appl. Phys. **83**, 3486–3489 (1998).
26. Z. Kotler, R. Hierle, D. Josse, J. Zyss, and R. Masse, "Quadratic nonlinear optical properties of a transparent and highly efficient organic-inorganic crystal: 2-amino-5-nitropyridinium dihydrogen phosphate (2A5NPDP)," J. Opt. Soc. Am. B **9**, 534–547 (1992).

UM00012998
NOVARTIS EXHIBIT 1017
Novartis v. Regents, IPR2023-01346
Page 1744 of 4460

This Page is Inserted by IFW Indexing and Scanning Operations and is not part of the Official Record

BEST AVAILABLE IMAGES

Defective images within this document are accurate representations of the original documents submitted by the applicant.

Defects in the images include but are not limited to the items checked:

- ☐ BLACK BORDERS
- ☐ IMAGE CUT OFF AT TOP, BOTTOM OR SIDES
- ☐ FADED TEXT OR DRAWING
- ☐ BLURRED OR ILLEGIBLE TEXT OR DRAWING
- ☐ SKEWED/SLANTED IMAGES
- ☐ COLOR OR BLACK AND WHITE PHOTOGRAPHS
- ☐ GRAY SCALE DOCUMENTS
- ☐ LINES OR MARKS ON ORIGINAL DOCUMENT
- ☐ REFERENCE(S) OR EXHIBIT(S) SUBMITTED ARE POOR QUALITY
- ☐ OTHER: _____

IMAGES ARE BEST AVAILABLE COPY.
As rescanning these documents will not correct the image problems checked, please do not report these problems to the IFW Image Problem Mailbox.

Structure and Bonding, Vol. 111 (2004): 1–32
DOI 10.1007/b14139

Hydrogen Bonding Interactions Between Ions: A Powerful Tool in Molecular Crystal Engineering

Dario Braga[1] · Lucia Maini[1] · Marco Polito[1] · Fabrizia Grepioni[2]

[1] Dipartimento di Chimica G. Ciamician, Università degli Studi di Bologna, Via F. Selmi 2, 40126 Bologna, Italy
E-mail: dario.braga@unibo.it
[2] Dipartimento di Chimica, Università degli Studi di Sassari, Via Vienna 2, 07100 Sassari, Italy
E-mail: grepioni@ssmain.uniss.it

Abstract Hydrogen bonding interactions are the strongest of the non-covalent interactions and are highly directional (hence transportable and reproducible). With respect to hydrogen bonds between neutral molecules the hydrogen bonding interactions between ions (inter-ionic hydrogen bonds) respond to additional energetic and topological constrains that depend on the convolution of the proton donor- proton acceptor interactions with the Coulombic field generated by the presence of ions. Directionality and strength are exploited in the design of molecular crystals, hence in molecular crystal engineering strategies. Molecular crystal engineering is the planning and utilisation of crystal-oriented syntheses for the bottom-up construction of functional molecular solids from molecules and ions. The success of crystal engineering strategies depends on the availability of robust and transferable interactions to *glue* together construction materials. This chapter is devoted to an important subset of non-covalent interactions, namely those involving hydrogen bonding and π-stacking interactions between ions. Some relevant analogies and differences between organic-type intermolecular interactions and those in which metal atoms are involved will be outlined. Selected examples of the utilization of inter-ionic hydrogen bonding interactions in crystal reactivity will also be described.

Keywords Hydrogen bond · Ions · Molecular crystal engineering · Crystal synthesis · Gas-solid reactions

1 Introduction 2
2 Charge-Assistance: Internal vs External 3
3 Data-Mining 5
4 How to Make Weak Hydrogen Bonds Less Weak 7
5 O-H···O Interactions Between Polycarboxylic Acid Anions and Zwitterions 11
6 External Charge-Assistance to C-H···O Interactions and to π-Stacking 15
7 How to Use Non-Covalent Interactions Between Ions 19
8 Hydrogen Bonded Networks Can React or Transform 22
9 Conclusions 28
10 References 29

© Springer-Verlag Berlin Heidelberg 2004

UM00013000
NOVARTIS EXHIBIT 1017
Novartis v. Regents, IPR2023-01346
Page 1746 of 4460

1 Introduction

The investigation of the *bonds between molecules* is one of the topical issues of our time [1]. It involves all areas of chemistry, in particular the thriving areas of supramolecular [2] and materials chemistry [3]. The motivation behind this broad interest is both scientific and utilitarian. Studies of intermolecular (or inter-ionic) bonds have great relevance for the fundamental sciences, but are also promising in terms of practical applications. It is recognized that an intelligent control of the recognition and assembly processes that lead from components to superstructures via tailoring of intermolecular interactions will allow us to obtain desired collective chemical and physical properties [4]. All these ideas also apply to crystal engineering [5], the area of supramolecular chemistry is devoted to the controlled design of molecular crystalline materials. The *paradigm* of molecular crystal engineering can be thus phrased: as non-covalent interactions are responsible for the existence and functioning of supermolecules, it is the convolution of crystal periodicity with intermolecular and/or interionic interactions that determines topology, energetics and properties of solid supermolecules.

On this premise, those interactions that *combine* strength and directionality allow a better control of the aggregation process. Strength is synonym of cohesion and stability, while directionality implies topological control and selectivity. Directionality combined with strength are essential requisites to assemble building blocks in a desired and stable way. Directionality also implies reproducibility: only if the topological properties of a given interaction persist in different structural environments, i.e. on passing from one solid supermolecule to another, is the interaction useful in the construction of new solids [6]. The topological control can be reinforced by the use of multiple directional interactions within the same molecule [7].

The intermolecular interaction that best combines strength and directionality is the hydrogen bond (HB). The number of papers, reviews and books dealing with hydrogen bonds is countless. A recent ISI [8] search of the keywords "hydrogen bond" in abstracts and titles yielded a count of 15356 and 2794 occurrences in abstracts and titles, respectively, in the years 2000–2002. Some recent review articles or relevant books are listed in [9] but the reader is warned that new papers and new interesting findings are likely to appear in the literature by the time this contribution in *Structure and Bonding* is published.

Because of the vastness of the subject matter, we shall focus our attention on *hydrogen bonding interactions between ions* and on the possibilities and limitations of their use in the design and construction of molecular materials of desired architectures and/or destined to predetermined functions. Obviously, the crystal engineer (or supramolecular chemist) needs to know the nature of the forces s/he is planning to master, since molecular and ionic crystals, even if constructed with similar building blocks, differ substantially in chemical and physical properties (solubility, melting points, conductivity, mechanical robustness, etc.).

Since the identification of bona-fide hydrogen bonds in solid state studies is often a controversial issue, in particular in the cases involving weak donors [10]

UM00013001
NOVARTIS EXHIBIT 1017
Novartis v. Regents, IPR2023-01346
Page 1747 of 4460

or ions [11], we will remain in the following with Linus Pauling's definition: "*There is a chemical bond between two atoms or groups of atoms in case that the forces acting between them are such as to lead to the formation of an aggregate with sufficient stability to make it convenient for the chemist to consider it as an independent molecular species*" [12]. In Pauling's approach the existence of a bond is linked to the energetic stability of the aggregate formed as consequence of the bond. This definition was adapted to intermolecular bonding by M. Etter [13]: "*A hydrogen bond is an interaction that directs the association of a covalently bound hydrogen atom with one or more other atoms, groups of atoms, or molecules into an aggregate structure that is sufficiently stable to make it convenient for the chemist to consider it as an independent chemical species*". The focus is on the concept of "directed" association and of stability, and the existence of an intermolecular bond is conceptually associated to the energetic stability of the aggregate. In terms of energy, hydrogen bonding interactions span a large interval, ranging from tiny energies (few kJ/mol in the case of C-H···O or comparably weak interactions, see below) [10] to large values when the acceptor is an anion (more than a hundred kJ/mol in the case of O-H···$O^{(-)}$ or F-H···$F^{(-)}$ and similar interactions) [14]. Generally speaking, however, the HB interaction is generally stronger (when not much stronger) than the strongest van der Waals interaction. For this reason, within X-H···Y HB systems, H···Y and X···Y separations shorter than van der Waals contact distances and X-H···Y angles that tend to linearity are considered diagnostic of the presence of strong HB [9]. The X···Y distance criterion is, however, not sufficient when dealing with weak and very weak HB interactions [10]. It has been pointed out by Jeffrey and Saenger [9a] that "*The use of a van der Waals distance cut-off criterion carries the wrong implication that hydrogen bonds become van der Waals interactions at longer distances*" and overlooks the essentially electrostatic nature of the interaction. While van der Waals interactions fall off very rapidly (r^{-6}), electrostatic interactions follow an r^{-1}dependence (assuming primarily monopole-monopole and monopole-dipole interactions); thus HB can be stabilising at distances much greater than the sum of van der Waals radii. Furthermore, the distinction between strong and weak hydrogen bonds is, often, only conventional, and there is a difference between hydrogen bonding interactions involving ions and those involving neutral molecules in crystals because of the fundamentally different nature of the dominant forces, the differences in physical properties (solubility, melting point, behaviour under mechanical stress, etc.) arising from the presence of ions or neutral molecules.

2 Charge-Assistance: Internal vs External

In this chapter, we shall focus on cases where the combination of ionic charges and non-covalent interactions, especially of the hydrogen bonding type, provides not only a simple means to devise stable architectures but also affords properties that are a convolution of those of molecular crystals and of molecular salts. In the case of hydrogen bonding it is, however, useful to recall in a schematic way how charges and location of donor-acceptor hydrogen bonding systems can be "com-

UM00013002
NOVARTIS EXHIBIT 1017
Novartis v. Regents, IPR2023-01346
Page 1748 of 4460

Table 1 The possible combinations of neutral and ionic proton donor/proton acceptor systems and the relationship between internal and external charge assistance

Neutral HB	Internal charge assistance	Requires external charge assistance
X-H···Y	X-H···$Y^{(-)}$ $^{(+)}$X-H···Y $^{(+)}$X-H···$Y^{(-)}$ $^{(-)}$X-H···$Y^{(+)}$ X-H···$Y^{(+)}$	$^{(-)}$X-H···$Y^{(-)}$ $^{(+)}$X-H···$Y^{(+)}$

bined". This is summarised in Table 1 [15]. The ionic charge in brackets indicates the charge carried by the *whole* fragment carrying the HB donor or acceptor group.

Leaving aside the "null option", i.e. when both fragments are neutral, we distinguish between "internal" and "external" charge assistance to the hydrogen bonding interactions. This discrimination depends on whether the proton acceptor/proton donor systems carry charges of opposite sign, e.g. $^{(+)}$X-H···$Y^{(-)}$, or one of them is neutral (middle column), or charges of the same sign, e.g. $^{(-)}$X H···$Y^{(-)}$ and $^{(+)}$X-H···$Y^{(+)}$ (right column). In the case of "external" charge assistance the stability of the hydrogen bonding aggregate towards dissociation will depend upon the presence of counterions. This is the case, for instance, of chains of cations or of chains of anions, which would be unstable towards dissociation in the absence of counterions [16] that are need to (over)compensate for the electrostatic repulsions. The implications are quite relevant: (i) even though the *stabilising* contribution of the HB interaction is small, the directionality is fully

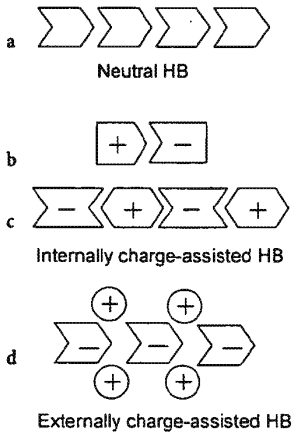


Fig. 1a–d Schematic representation of the relationship between neutral, internally charge-assisted and externally charge-assisted hydrogen bonds

UM00013003
NOVARTIS EXHIBIT 1017
Novartis v. Regents, IPR2023-01346
Page 1749 of 4460

operative and (ii) the common assumption that the intermolecular separation between atoms or groups of atoms reflect the strength of the *local* interaction is not directly transferable from neutral to ionic environments [16]. The comparison between neutral HB and inter-ionic HB interactions is schematically represented in Fig. 1.

"Internal" or "external" charge assistance can be successfully used to build periodical supermolecules based on HB. The utilization of ionic building blocks is, however, more common in inorganic crystal engineering, where metal atoms give easy access to charged species. Moreover, the variability of oxidation states makes possible the utilization of the same building block in both neutral and ionic environments.

3 Data-Mining

The Cambridge structural database (CSD) [17] is a primary source of structural information validated statistically via the observation of recurring behaviours in large numerical sets of data. For this reason *data-mining* is yet another powerful tool available to the crystal engineer, mainly in the initial steps of project analysis and architecture design. The identification in a large number of different structural environments of *the same* interaction, or of the same packing motif associated with several interactions, guarantees that, when this motif is purposely encoded into a molecular or ionic building block, the chances that it will lead to the desired supramolecular arrangement are proportional to its frequency of occurrence in different crystal packings. This approach has led to the extension to the area of molecular crystal engineering of the concepts of *retrosynthesis* and supramolecular *synthons* [18] originally developed in the field of organic chemistry. Hydrogen bonding functional molecules are the *synthons* of choice in many crystal construction strategies [19]. By comparing organic and inorganic supramolecular synthons it has been shown that strong hydrogen bonding donor/acceptor groups, such as -COOH and -OH systems, as well as primary $-CONH_2$ and secondary -CONHR amido groups, form essentially the same type of hydrogen bonding interactions whether as part of organic molecules or as metal co-ordinated ligands. This is not surprising, since hydrogen bonds formed by these groups are at least one order of magnitude stronger than most non-covalent interactions, and are most often already present in solution. In addition to these strong bonds and to the plethora of weaker (e.g. C-H···O, C-H···N, C-H···π etc.) 'organic'-type hydrogen bonding interactions, the presence of metal atoms in molecular building blocks generates *new* types of interactions, which are characteristic of inorganic and organometallic systems. Several research groups are exploiting hydrogen bonded synthons to *combine* co-ordination chemistry and hydrogen bonding functionalities. Some examples of the utilization of the CSD in the evaluation of some cases of neutral vs ionic HB interactions will be discussed in the following section.

The power of the CSD [17] and, of course, of the ICSD (although this latter database has yet to develop a *user friendly* interface for data mining) [20] – in the context of crystal engineering – lies in the statistical approach it permits in the

UM00013004
NOVARTIS EXHIBIT 1017
Novartis v. Regents, IPR2023-01346
Page 1750 of 4460

analysis of crystal structures, which, in turns, allows the identification of recurring synthons. As the number of crystal structures in the databases have increased enormously in the recent past, intermolecular interactions have begun to be reliably examined. Quite apart from the fact that it is impossible today to exhaustively peruse the crystallographic literature manually, the sort of *chemical* conclusions that a CSD/ICSD analysis permits cannot be obtained from *reading* of the journals. Indeed, it is (conservatively) estimated that the number of entries in the CSD will increase to not less than 500,000 within the first decade of this century. Moreover, both CSD and ICSD can nowadays be utilized on conventional personal computers or on the web, with no need for expensive mainframe computers.

Thanks to these factors *new* interactions are being discovered, or re-discovered, almost daily and *data-mining* is still one of the preliminary steps of any crystal engineering project [21]. For this reason some cautionary words may be in order. Very weak interactions, falling in the fluctuations of the crystal structure energetics – those due, for instance, to motions of atoms or atomic groups – may be useless in design strategies, because they are too feeble to control crystal construction. It is dangerous to focus exclusively on pairwise interactions, as one may forget that it is the overall balance of interactions, some acting at short range only, some acting at very long range, that accounts for cohesion in molecular crystals [22]. Only strong pairwise interactions (e.g. O-H···O, but also Cl···Cl, or Au···Au) may stand out above the noise level and act as true packing directors [23]. Preservation or preformation of robust intermolecular bonds often leads to molecular packings that do not correspond to the best van der Waals energy. This is, for instance, the case of water and accounts for the absorption of ca. 6 kJ mol^{-1} upon melting [24a]. This energy is required to break about 10% of the O-H···O bonds from the HB scaffolding of ice, hence determining the lower density of ice with respect to liquid water.

One further point of concern arises from the customary 'frozen' picture of molecules in crystals, and from the consequent 'frozen' perception of the network of intermolecular interactions. When a non-rigid molecule or ion is taken from solution or gas phase into the solid state its geometry is distorted along soft deformational paths, and its rotations and vibrations, though restricted, often persist to a very large extent. Large amplitude oscillations and full-scale reorientational motions are often observed in crystals. The deformation on passing from vacuum to solid state is particularly dramatic in the case of supermolecules held together by intermolecular interactions; simple examples are the NH_3:BH_3 Lewis acid/base system or the acetic acid dimer $CH_3COOH\cdots CH_3COOH$ [24b], where the distinction between inter- and intramolecular structures is not so straightforward. In these cases the solid state structure of the molecular aggregate does not correspond to the vacuum or solution structure, because the supramolecular bonding energies are low enough to be significantly perturbed by intermolecular interactions. Distortions and dynamics are obviously significant in the case of flexible compounds: structural non-rigidity of the building blocks needs to be taken into account in evaluating the factors responsible for crystal stability, since molecular and crystal structure may affect each other in an often unpredictable manner.

UM00013005
NOVARTIS EXHIBIT 1017
Novartis v. Regents, IPR2023-01346
Page 1751 of 4460

4 How to Make Weak Hydrogen Bonds Less Weak

For the reasons given in the previous section, one can anticipate that database searches of intermolecular interactions that do no discriminate between ionic and neutral fragments may end up with unreliable (or only partially reliable) results.

The situation of the prototype of strong hydrogen bonds, namely that between an O-H donor and an O acceptor in solid protonated or partially deprotonated polycarboxylic acids, provides an educative example. Figure 2 shows the result of an "acritical" CSD search of the O(H)···O distance distribution for all intermolecular interactions satisfying the criterion of O···O separations shorter than 2.80 Å. In order to avoid low quality X-ray structures, the R-factor was required to be <10%. One can see that the mean value for such an interaction (Fig. 2, top histogram) is at 2.632_1 Å and that the lowest 10% percentile distances being shorter that 2.551 Å. When the presence of an ionic charge is taken into account and the distribution is split in COOH···COOH (Fig. 2, middle histogram), and-$COOH\cdots COO^{(-)}$ (Fig. 2, bottom histogram) one can see that inter-neutral and inter-ionic distances follow different distributions, with shorter separations usually associated with the latter cases (mean O···O values 2.650_1, 2.533_3 Å and lowest 10% percentile 2.614, 2.462 Å, respectively). Clearly, neglect of the effect of charges can lead to untrustworthy conclusions. However, even this analysis is not entirely correct, as it does not take into account the possibility that the ionic charge could be localized on a given fragment and not on the entire ion. This is the case, for instance, of amino acid molecules in zwitterionic form and will be discussed later on within this chapter.

The distinction between inter-neutral and inter-ionic interactions is not only important when dealing with strong interactions, those with a high directionality feature, but also when the interactions are weak or very weak. As an example, the role of ionic charges on C-H···O interactions between anions and cations has been investigated [25] by searching the CSD for inter-molecular and inter-ionic (C)H···O distances (H···O in the range 2.0–3.0 Å, C-H···O angles larger than 110°) for metal bound C-H systems, i.e. neutral systems containing (M)C-H···O interactions, and charged systems containing $[(M)C\text{-}H]^+\cdots[O]^-$, respectively, where M=first row transition metal.

The analysis is statistically sound because C-H···O hydrogen bonds, though weak, are very numerous in organometallic crystals as a consequence of the popularity of ligands such as arenes and cylopentadienyl ligands which carry a plethora of C-H units [26]. The analysis shows that interionic C-H···O hydrogen bond distances follow the order $[(M)C\text{-}H]^+\cdots[O]^-$<(M)C-H···O (M=first row transition metal), which is the order of decreasing *charge assistance* to the weak hydrogen bonds (mean H···O values 2.629_{15}, 2.741_{12} Å, and lowest deciles 2.347, 2.491 Å, respectively, see Fig. 3).

Further insight on the effect of charges on weak bonds has been obtained by analysing C-H···O interactions involving the cations $[PPh_4]^+$and $[PPN]^+$and the anion$[BPh_4]^-$ and O-acceptors in anionic and cationic transition metal complexes $[O_M]$ (see Fig. 4).$[PPh_4]^+$,$[PPN]^+$and $[BPh_4]^-$ are amongst the most commonly used counterions for the crystallization of charged species and are very com-

UM00013006
NOVARTIS EXHIBIT 1017
Novartis v. Regents, IPR2023-01346
Page 1752 of 4460

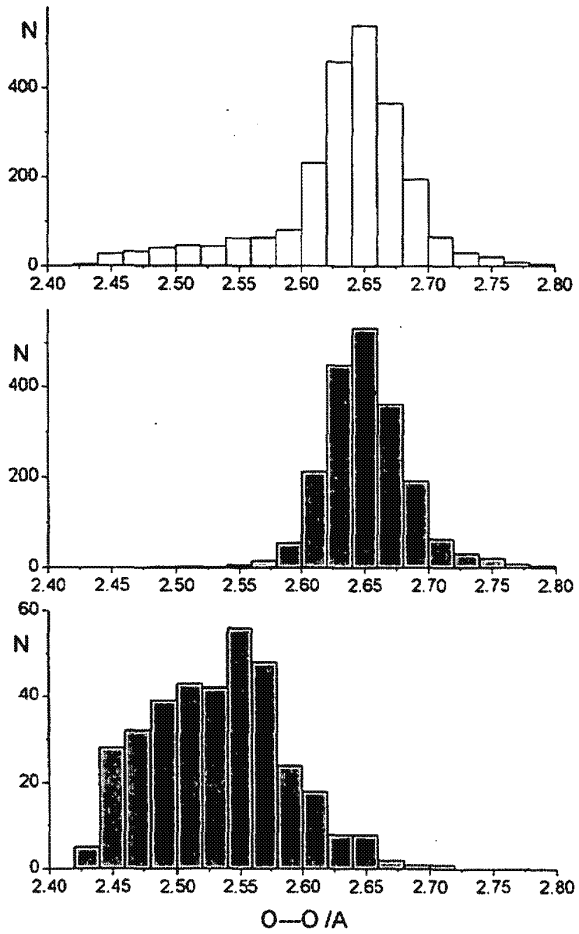


Fig. 2 O···O intermolecular/interionic interactions between COOH and $COOH/COO^{(-)}$ groups in protonated or partially deprotonated polycarboxylic acids. *Top histogram*: the distribution of O···O interactions obtained without neutral/charge discrimination (mean value 2.632_1 Å). When the presence of an ionic charge is taken into account the distributions of O···O distances are those in the *middle* $[^{(n)}O(H)\cdots O_{COOH}{}^{(n)}$ and $^{(n)}O(H)\cdots O_{COOH}{}^{(-)}$, mean value 2.650_1 Å] and in the *bottom* $[^{(-)}O(H)\cdots O_{COO}{}^{(-)}$, mean value 2.533_3 Å] histograms

monly used when X-ray suitable crystals of large coordination compounds are sought. The results are shown in Fig. 4. As in the previous case the analysis affords a rather consistent picture: the H···O distances, in both average and percentile values, follow the order $[(PPh_4)C\text{-}H]^+\cdots[O_M]^-<[(PPN)C\text{-}H]^+\cdots[O_M]^-<[(BPh_4)C\text{-}H]^-\cdots[O_M]^+$ (mean H···O distance 2.700_4, 2.723_3 and 2.756_9 Å, lowest deciles 2.428, 2.475 and 2.551 Å, respectively) which is the order of decreasing electro-

UM00013007
NOVARTIS EXHIBIT 1017
Novartis v. Regents, IPR2023-01346
Page 1753 of 4460

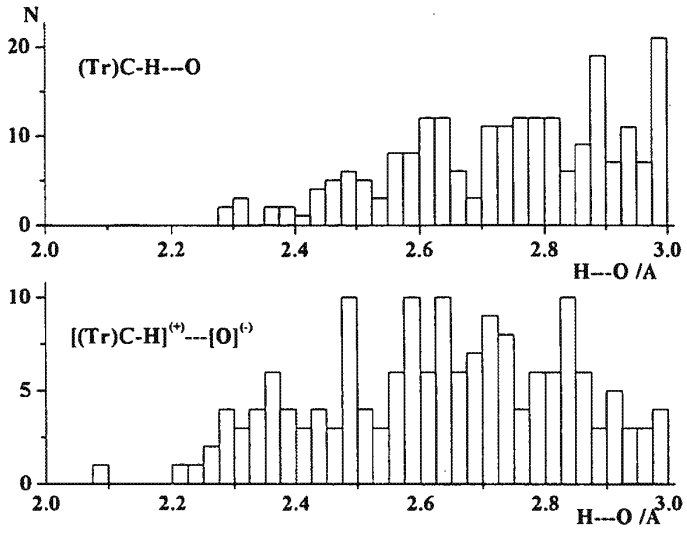


Fig. 3 CSD intermolecular searches on H···O interactions in (M)C-H···O; and [(M)C-H]$^+$···[O]$^-$ systems [metal bound C-atoms with M=first row transition metal)

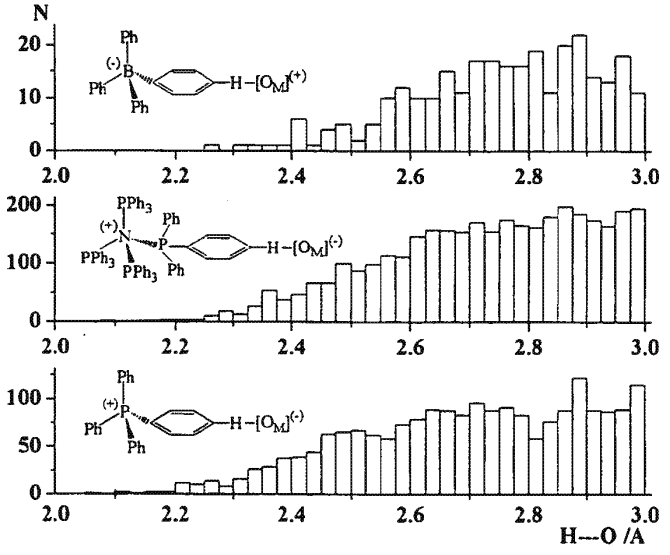


Fig. 4 CSD intermolecular searches on H···O interactions in [(PPh_4)C-H]$^+$···[OM]$^-$, [(PPN)C-H]$^+$···[OM]$^-$, [(BPh_4)C-H]$^-$···[OM]$^+$ systems (OM indicates that the oxygen atom belongs to an organometallic or coordination complex)

UM00013008
NOVARTIS EXHIBIT 1017
Novartis v. Regents, IPR2023-01346
Page 1754 of 4460

static reinforcement of the C-H···O interaction. The comparison between BPh_4^- and PPh_4^+ is particularly educative, since the $[(BPh_4)C\text{-}H]^-\cdots[O_M]^+$ represents a situation of *charge opposition* to the C-H···O bonds and, in fact, this group of data is characterized by average distance values longer also with respect to the neutral sample. In terms of angularity, all these interactions follow the trend expected for hydrogen bonds, namely the C-H···O angle opens up as the distance between donor and acceptor increases.

Another case which has given rise to controversial interpretations is that of the C-H···F interactions. The analysis of statistical data has led authors to conclude that, at least in the case of C-H···F contacts between neutral organic molecules, when fluorine is covalently bound to carbon it does not form hydrogen bonds with conventional hydrogen bond donors, including O-H, N-H and C-H groups [27]. The situation is different in crystals of coordination and organometallic cationic complexes crystallized with the "very popular" $[PF_6]^-$ and $[BF_4]^-$ anions. The CSD has been searched for intermolecular H-bonds of the $^{(+)}C\text{-}H\cdots F^{(-)}$ type involving the $[PF_6]^-$ and the $[BF_4]^-$ anions [28] (data have been updated for this work on the basis of the April 2002 version of the CSD). Since the number of compounds containing C-H groups is very large, two separate searches were carried out. In the first only C-H fragments for which the C atom is directly bound to the metal atom were considered (561 and 452 hits, for a total of 3972 and 2925 observations, for $[PF_6]^-$ and $[BF_4]^-$ compounds, respectively). In the second one no restrictions were applied to the C atom (1354 and 930 hits, for a total of 31,639 and 17,057 observations, for $[PF_6]^-$ and $[BF_4]^-$ compounds, respectively). Scattergrams of $(Tr)C\text{-}H\cdots F_{[PF6]-}$ angles vs $(Tr\text{-}C)H\cdots F_{[PF6]-}$ distances and of $(Tr)C\text{-}H\cdots F_{[BF4]-}$ angles vs $(Tr\text{-}C)H\cdots F_{[BF4]-}$ distances, respectively, are shown in Fig. 5. Although the number of hits is different in the two cases, the two types of interactions follow the normal trend observed for hydrogen bonds, i.e. as the distance between hydrogen and acceptor atoms decreases, the C-H···F vectors becomes straighter and the bond approaches linearity. Beside this general behaviour, there are a large number of bonds that fall below the van der Waals cut-off distances and are clearly indicative of specific and directional interactions involving donors and acceptors. Comparison of the two types of search also show that there is no appreciable effect of the direct bonding to transition metal atoms on the geometry of the interaction, as the two populations have the same distributions. Interestingly, while 10% of the contacts fall in the range 2.000–2.391 Å in the case of $(Tr\text{-}C)H\cdots F_{[PF6]-}$ interactions, the same percentage of contacts falls in the narrower range 2.000–2.322 on passing to $(Tr\text{-}C)H\cdots F_{[BF4]-}$ interactions. This difference may be equally well explained with two hypotheses: (i) the presence of a large number of short contacts in the case of phosphorus bound to boron than in the case of phosphorus may reflect the higher polarity of the F-atom in the formed anion than in the latter (the anion charge is shared by four vs six fluorine atoms), and (ii) the smaller $[BF_4]^-$ anion can approach the C-H donors more effectively than the bulkier $[PF_6]^-$.

All examples discussed above, whether concerning very strong O-H···O hydrogen bonds or weak C-H···O and C-H···F interactions, clearly show that a donor-acceptor distance criterion is an unsafe instrument to check the relevance of hydrogen bonding interactions if the effect of ionic charges is neglected.

UM00013009
NOVARTIS EXHIBIT 1017
Novartis v. Regents, IPR2023-01346
Page 1755 of 4460

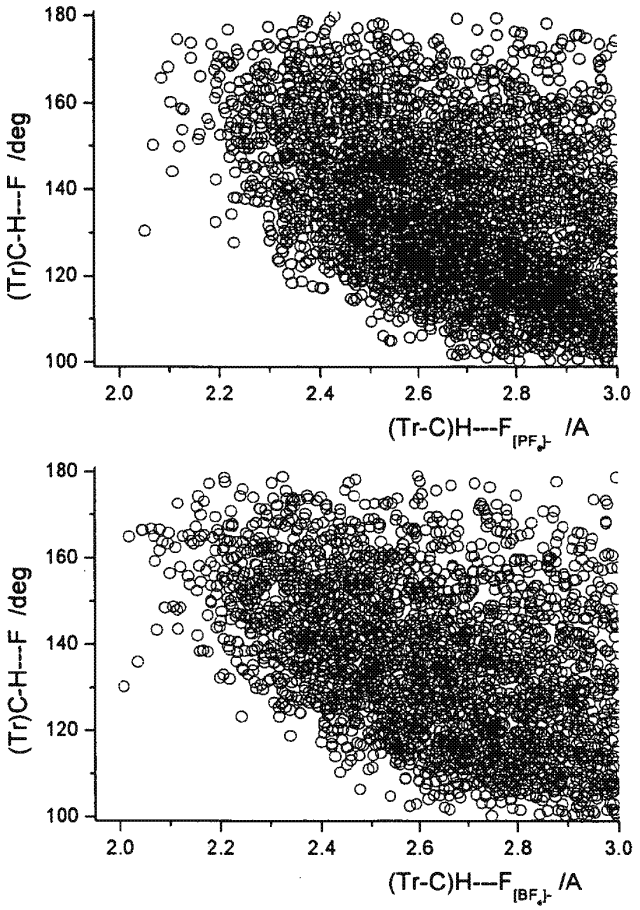


Fig. 5 CSD (April 2002 version) intermolecular searches for intermolecular H···F of the $^{(+)}$C-H···F$^{(-)}$ type involving the $[PF_6]^-$ and the $[BF_4]^-$ anions: Scattergrams of (Tr)C-H···$F_{[PF6]-}$ angles vs (Tr-C)H···$F_{[PF6]-}$ distances (*top*) and of (Tr)C-H···$F_{[BF4]-}$ angles vs (Tr-C)H···$F_{[BF4]-}$ distances (*bottom*)

5
O-H···O Interactions Between Polycarboxylic Acid Anions and Zwitterions

We mentioned above that the interaction between carboxylic and carboxylate groups constitutes a benchmark system for the investigation of the relationship between topology and charge carried by the components. In the case of inter-anion $^{(-)}$O-H···O$^{(-)}$ hydrogen bonding interactions on mono-deprotonated polycarboxylic acids it has been shown [29] that deprotonated [COO^-] groups are strongly polarised in the solid state and always behaving as -$COO^{(-)}$ groups,

UM00013010
NOVARTIS EXHIBIT 1017
Novartis v. Regents, IPR2023-01346
Page 1756 of 4460

Table 2 Comparison of average C-O structural parameters (Å) for neutral and partially deprotonated polycarboxylic acids as extracted from the Cambridge Structural Database (CSD)

Interaction	I $[COOH]_N$ $\cdots[COOH]_N$ N=Neutral system	II $[COOH]_A$ $\cdots[COOH]_A$ A=Anionic system	III $[COOH]_A$ $\cdots[COO^-]_A$ A=Anionic system	IV $[COOH]_A$ $\cdots[COO^-]_A$ A=$[HC_2O_4]^-$
O1···O3	2.665_3	2.644_8	2.532_3	2.545_6
C1O1	1.298_1	1.308_5	1.301_1	1.299_1
C1O2	1.224_1	1.215_4	1.211_1	1.208_1
C2O3	1.225_1	1.224_3	1.261_1	1.256_2
C2O4	1.297_1	1.300_5	1.238_1	1.234_2

irrespective of the ionic or neutral nature of the components. In contrast, protonated [COOH] groups, even when belonging to anions, behave exactly as in neutral molecules. The same behaviour is shown by the smallest dicarboxylic acid anion, the hydrogen oxalate anion $[HC_2O_4]^-$. The study of zwitterionic amino acid molecules carrying more than one [COOH] group (e.g. aspartic and glutamic acids and derivatives) has been particularly informative, since these molecules carry both a protonated [COOH] and a deprotonated $[COO^-]$ group. The results of a CSD investigation are summarized in Table 2.

Table 2 summarizes the numerical results on average intermolecular/interionic O···O and intramolecular/intra-ionic C-O structural parameters for the $[COOH]_N\cdots[COOH]_N$, $[COOH]_A\cdots[COOH]_A$ and $[COOH]_A\cdots[COO^-]_A$ intermolecular interactions, together with those obtained for the $[COOH]_A\cdots[COO^-]_A$ sample in the case of the hydrogen oxalate anion. Data were retrieved from the CSD with a cut-off distance on O···O separations of 3.0 Å. A visual prospect of the data listed in column III is provided in Fig. 6, where histograms of intramolecular C-O distances within the protonated and deprotonated COOH/COO groups are presented.

Though not very large, the samples represent the behaviour of a well defined class of interactions. One can see that O···O distances between protonated groups belonging to anions compare strictly with those between neutral molecules, whilst O···O distances between protonated and deprotonated groups are shorter than those between protonated groups belonging to anions or neutral molecules. Furthermore, in both neutral molecules and ions the C-O and C-O(H) distances within the COOH groups form two distinct sets of long and short ones (C1-O1>C1-O2), while C-O distances within the COO^- groups show a much smaller difference in length (C2-O3≅C2-O4). Hence, the metric analysis shows that (i) there is no appreciable structural consequence of the fact that the protonated COOH group belongs to an anion or to a neutral molecule, and (ii) proton removal from the COOH group leaves the extra electron essentially localised on the deprotonated $[COO^-]$ system. It has also been noted that the distribution of distances does not depend on the size of the fragment: with the small $HC_2O_4^-$ anion the protonated $[COOH]_A$ groups are geometrically similar to neutral $[COOH]_N$ groups and the extra electron remains 'confined' onto the deprotonated $[COO^-]_A$ groups.

UM00013011
NOVARTIS EXHIBIT 1017
Novartis v. Regents, IPR2023-01346
Page 1757 of 4460

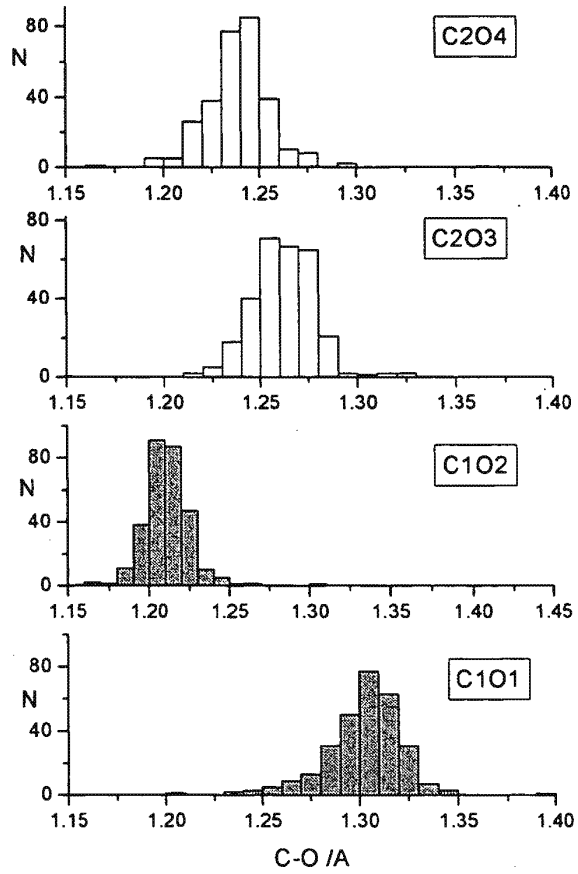


Fig. 6 Histograms of C-O distances in the -$COO^{(-)}$ and -COOH groups belonging to hydrogen bonded systems of the type $[COOH]_A\cdots[COO^-]_A$ (A=anionic system) [column III in Table 2]

Carboxylic zwitterions, i.e. those containing the deprotonated -$COO^{(-)}$ group, are useful for the present discussion because the molecules are formally neutral. Crystals of zwitterionic molecules are particularly relevant for the present discussion, because they are *formally molecular* in nature, i.e. they do not contain ions carrying charges of opposite sign. The number of zwitterionic molecules is quite large, but only 49 compounds, extracted from the CSD, show the simultaneous presence of a protonated -COOH and a deprotonated -$COO^{(-)}$ groups. Though small, the sample is amenable to some statistical considerations, mainly in the light of the observations made above. In terms of average values and lowest decile (10%) the distances are C1-O1 1.307_2, 1.282; C1-O2 1.211_2, 1.119; C2-O3 1.260_2, 1.245; C2-O4 1.242_2, 1.220 Å. From these figures it is easy to appreciate that, *although formally neutral*, the zwitterionic molecule behave, in HB formation, *ex-*

UM00013012
NOVARTIS EXHIBIT 1017
Novartis v. Regents, IPR2023-01346
Page 1758 of 4460

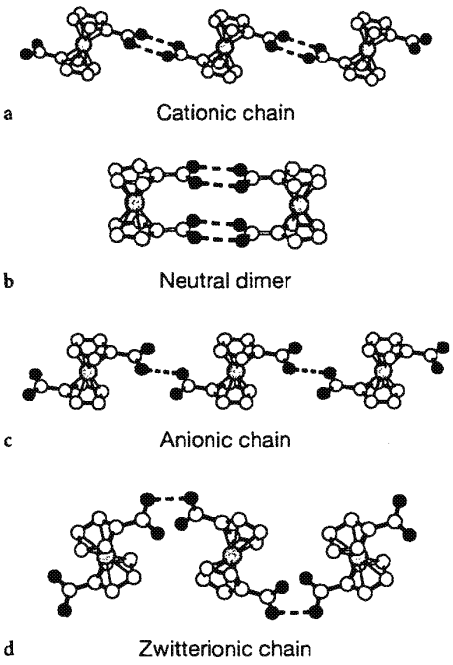


Fig. 7a–d A comparison of the geometries and O···O separations (in brackets) in a selection of neutral, charged and zwitterionic metallocene diacids: a the *cationic chain* in crystalline $[(\eta^5\text{-}C_5H_4COOH)_2Co^{III}]^+[PF_6^-]$; b the *neutral dimer* in $[(\eta^5\text{-}C_5H_4COOH)_2Fe^{II}]$, [O···O 2.600(2), and 2.606(2) Å, respectively]; c the *anionic chain* in $[(\eta^5\text{-}C_5H_4COO)(\eta^5\text{-}C_5H_4COOH)Fe^{II}]^-[(\eta^5\text{-}C_5H_5)_2Co^{III}]^+$; d the *neutral chain* formed by the zwitterion in $[(\eta^5\text{-}C_5H_4COO)(\eta^5\text{-}C_5H_4COOH)Co^{III}]$ [O···O 2.453(3), and 2.456(2) Å, respectively]

actly as their anionic partners. This is also true when the average O···O separations, i.e. $[COOH]_{ZW}\cdots[COO^-]_{ZW}$ are considered (the value of 2.568_8 Å is comparable with the values of 2.532_3 and 2.545_6 reported in Table 2). This is a further indication that proton removal (or proton transfer) "leaves" the extra-charge essentially localized onto the -COO group.

A small selection of specific cases can be used to illustrate the intriguing relationship between metrics and nature of the interactions. Figure 7 shows hydrogen bonding interaction geometries in a selection of neutral, cationic, anionic and zwitterionic chains of cobalt and iron dicarboxylic acid complexes. A comparison between (a) the *cationic chain* formed by $[(\eta^5\text{-}C_5H_4COOH)_2Co^{III}]^+$ and (b) the *neutral dimer* present in crystalline $[(\eta^5\text{-}C_5H_4COOH)_2Fe^{II}]$, and between the chains formed by (c) the *anionic* species $[(\eta^5\text{-}C_5H_4COO)(\eta^5\text{-}C_5H_4COOH)Fe^{II}]^-$ and (d) the neutral *zwitterion* $[(\eta^5\text{-}C_5H_4COO)(\eta^5\text{-}C_5H_4COOH)Co^{III}]$, confirms that the difference in O···O separations (reported in the figure caption) between COOH···OC(OH) and COOH···$^{(-)}$OOC interactions does not depend on the neutral or ionic nature of the complex. The presence of shorter O···O separations in

UM00013013
NOVARTIS EXHIBIT 1017
Novartis v. Regents, IPR2023-01346
Page 1759 of 4460

cases (a) and (b) with respect to (c) and (d) suggests that, at least in the solid state, proton removal from COOH groups, whether belonging to a neutral or cationic acid, 'leaves' the extra-electron localized on the deprotonated group. The electron localization on the acceptor group allows it to take full advantage of the stabilizing contribution arising from the electrostatic (δ+)-(δ–) component of the interaction even in the case of building blocks carrying the same charge. It may be argued that the stabilization cannot offset the dominating repulsive forces between like charges and is not sufficient per se to keep the anions together in the absence of counterions.

In summary, COOH groups possess the same average metrics irrespective of the neutral or ionic nature of the system they belong to, and irrespective of the protonated or deprotonated nature of the acceptor site. On the other hand the deprotonated [COO^-] groups appear to *keep* the negative charge after proton removal, irrespective of the size of the acid anion. At this stage, one may wonder if the same 'conservative' behaviour is shown, *on passing from ionic to neutral crystals*, by protonated and deprotonated groups.

However, though interesting (perhaps) to theoreticians and crystallographers, the problem discussed in this section could be found of little relevance to the crystal engineers seeking reproducible and useful synthetic strategies. And yet it will be shown that the knowledge of the way zwitterions may react with acids and bases in proton transfer processes can be useful in devising gas-solid and solid-solid reactions [30, 31]. Furthermore, it should be recalled that superprotonic conductivity, an important process investigated for the development of fuel cells, is dependent on the possibility of proton jumps in chains of hydrogen phosphates and sulfates [32] associated with the onset of reorientational motions in the solid state. Some examples will be provided in the last section of this contribution.

6
External Charge-Assistance to C-H···O Interactions and to π-Stacking

We have shown in the previous sections that the distance criterion is not always trustworthy when dealing with intermolecular interactions. There are several examples of close contacts that do not correspond to stable interactions or of *cation* assisted chemical bonds between ions [33a,b], as well as examples of short contacts that are not hydrogen bonds [33c].

For instance, in the cases of crystalline salts containing π-[TCNE] dimers (TCNE=tetracyanoethylene) the existence of exceptionally long (>2.9 Å) C-C bonding interactions involving π-electrons has been explained on the basis of the existence in the crystals of dimer dianions stabilized by cation···$[TCNE]^{(-)}$ interactions, which provide the electrostatic stabilization necessary to overcome the intradimer electrostatic repulsion [33a].

The reasoning applied above to O···O interactions can be extended to weak C-H···O bonds. The presence of a short C-H···O distance is not necessarily indicative of an overall attractive interaction, if the C-H donor and the O acceptor groups belong to anions, as illustrated in the following example. The structure of the mixed-valent species $[(\eta^6\text{-}C_6H_6)_2Cr]^+[CrO_3(OCH_3)]^-$ [34] is based on columns of methoxychromate anions and of columns of bis-benzene chromium

UM00013014
NOVARTIS EXHIBIT 1017
Novartis v. Regents, IPR2023-01346
Page 1760 of 4460

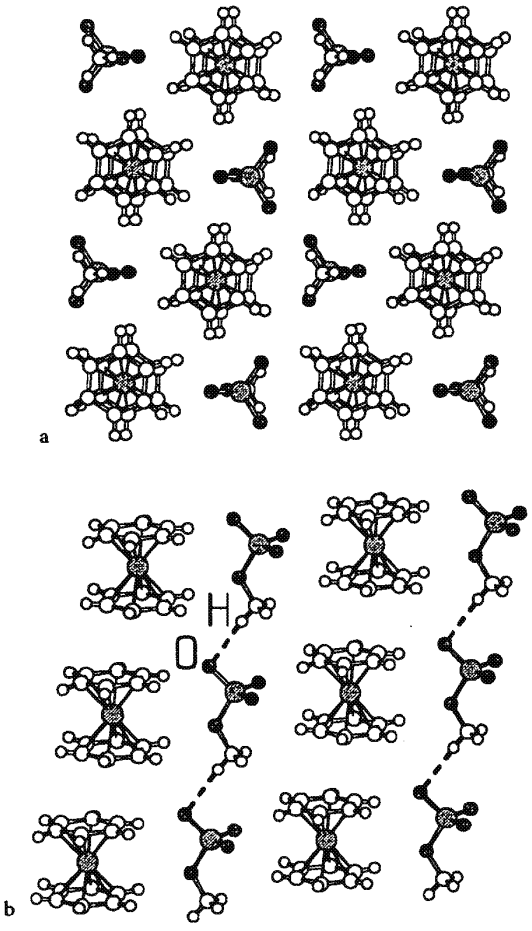


Fig. 8 a The crystal is formed of columns of methoxychromate anions and of columns of bis-benzene chromium cations extending parallel to the *c*-axis. b The anions are apparently "linked" along the column via a short C-H···O interaction (H···O 2.381 Å, C-H···O 173°) between a methyl hydrogen and a chromate oxygen

cations (see Fig. 8a). The cations stack in piles (see Fig. 8b) with benzene-benzene distances of ca. 3.50 Å. While the interaction between cations and anions is based on "charge-assisted" $C\text{-}H^{(+)}\cdots O^{(-)}$ hydrogen bonds, the anions are apparently "linked" along the column via a short C-H···O interaction [H···C 2.381 Å, C-H···O angle 173°] between a methyl hydrogen and a chromate oxygen (see Fig. 8b).

This $[(Cr)C\text{-}H]^{(-)}\cdots[O]^{(-)}$ interaction between anions along the chain has been investigated by means of theoretical ab initio calculations [34]. It has been shown

UM00013015
NOVARTIS EXHIBIT 1017
Novartis v. Regents, IPR2023-01346
Page 1761 of 4460

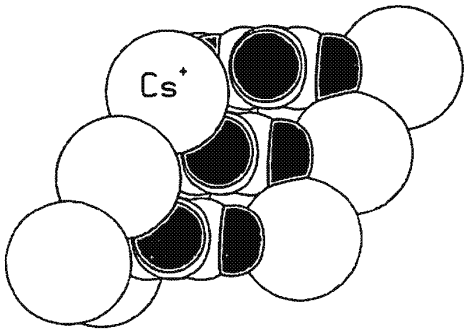


Fig. 9 The ion organization in crystalline $CsHC_4O_4$ (stacking separation 3.32 Å]

that, in the absence of cations, the C-H···O interaction would be unable to hold together the anions in the chain because of the strong Coulombic repulsion between consecutive anions along the chain. The overall crystal stability is guaranteed by the balance between (–)···(+) attractive interactions and those of repulsive nature [(–)···(–) and (+)···(+)]. The $[(Cr)C\text{-}H]^{(-)}\cdots[O]^{(-)}$ interaction is stabilizing only on a relative scale; it contributes to crystal cohesion by decreasing the inter-anion repulsion and by conferring directionality to the linear arrangement, while the major cohesive contribution results from Coulombic interactions between the methoxychromate anions and the bis-benzene cations. Hence, the reasoning developed for negatively charged hydrogen bonding $O\text{-}H^{(-)}\cdots O^{(-)}$ interactions in chains formed by monodeprotonated dicarboxylic acids holds also in the case of weak C-H···O interactions.

Another situation of *external charge assistance* to weak interactions has been observed when considering the occurrence of short interplanar stacking separations between flat systems containing π-electrons [35]. In the family of alkali hydrogen squarate salts MHC_4O_4 (M=Li, Na, K, Cs) the hydrogen squarate anions $[HC_4O_4]^-$ are connected via $O\text{-}H^{(-)}\cdots O^{(-)}$ interactions [O···O separations in the range 2.417–2.503 Å] [35], and the hydrogen squarates overlap to a various extent (see Fig. 9 for the packing in $CsHC_4O_4$); the stacking separation between squarate planes is considerably shorter than in neutral systems (range 3.13–3.32 vs 3.43–3.46 Å in organic crystals) and increases slightly on increasing the cation size, being apparently unrelated to the type of alkali cation (although the shortest value is with Li^+).

A theoretical approach analogous to that employed in the cases discussed above has demonstrated that the electrostatic component of the anion···anion interaction is repulsive in all regions relevant for intermolecular interactions [29]. Thus the short interplanar separation appears to originate from the electrostatic "compression" that brings the squarate planes at a distance shorter than between neutral systems. It is worth stressing that, even though the stabilizing contribution of inter-anionic π-interactions may be overridden by the presence of a strong electrostatic field, the directionality of the interactions is retained. Thus, while crystal cohesion is determined by the balance of attractive and repulsive

UM00013016
NOVARTIS EXHIBIT 1017
Novartis v. Regents, IPR2023-01346
Page 1762 of 4460

ionic interactions (as in NaCl, for instance) the actual structure is controlled by the optimisation of inter-anionic π-stacking.

The same reasoning applies to the family of the alkaline and ammonium croconate salts, i.e. containing the croconate dianion, $C_5O_5^{2-}$ [36]. The dianions $C_5O_5^{2-}$organize themselves in columns, with interplanar separations falling in the narrow range 3.12–3.42 Å, i.e. comparable to that observed in the squarate family discussed above. As in these latter cases, the short interplanar separation does not necessarily reflect the presence of a π-stacking interaction. It has been argued that the close interplanar separation is the result of a compromise between packing of flat croconate units and the spherical cations together with the water molecules that fill the alkali metal coordination spheres. The croconate dianion, $C_5O_5^{2-}$, belongs, together with the rhodizonate $C_6O_6^{2-}$, the squarate $C_4O_4^{2-}$ and the deltate $C_3O_3^{2-}$ dianions to the family of oxocarbon dianions. The prototype of

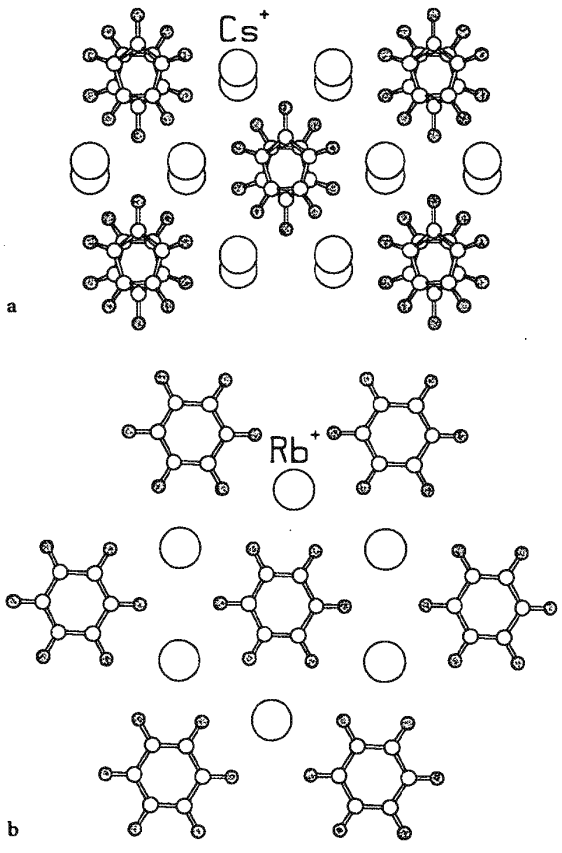


Fig. 10a,b The ion organization in: a crystalline $Cs_2C_5O_5$ (the Rb^+ salt is isomorphous); b crystalline $Rb_2C_6O_6$

UM00013017
NOVARTIS EXHIBIT 1017
Novartis v. Regents, IPR2023-01346
Page 1763 of 4460

these dianions is represented by the rhodizonate dianion $C_6O_6^{2-}$, which has attracted the interest of many researchers in view of the structural analogy with benzene, C_6H_6. The structure of rubidium rhodizonate has also been reported showing that similar charge-assisted π-stacking interactions are established [37].

The study of the salts of cyclic oxocarbon anions demonstrates that the packing problem is that of accommodating together spherical objects (the alkali cations) and flat discoidal units (the croconate and rhodizonate dianions, but also the squarates, the hydrogen croconates, etc.). The best compromise is often attained by placing the disks "flat-on-flat" in a stack and by placing the spherical cations around the stack, as shown in Fig. 10 for crystalline $Cs_2C_5O_5$ (the Rb^+ salt is isomorphous) and $Rb_2C_6O_6$. If this is not sufficient to complete the coordination sphere of the smaller alkali cations, water molecules are brought in the crystal to take the place of the large dianions as coordination and space *fillers*. The fact that the discoidal dianions do not show a preferential relative orientation, and can slide on each other, indicates that the electronic gain from this type of weak non-covalent interaction is either null or too small to be of any relevance in the presence of the much stronger electrostatic interactions. Altogether, the short interatomic/interplanar separations in the oxocarbon salts appear to be the result of the "electrostatic compression" arising from the attractive $M^+\cdots C_5O_5^{2-}$ interactions, that largely overcompensate for the repulsive $M^+\cdots M^+$ and $C_5O_5^{2-}\cdots C_5O_5^{2-}$ interactions.

7
How to Use Non-Covalent Interactions Between Ions

Several crystal engineering groups are exploiting the possibility of sustaining hydrogen bonding networks with ionic charges on the building blocks. The utilization of coordination complexes [38] allows the incorporation of transition metals into the design of hydrogen bonded crystalline solids. The metal centres are either used to provide a directing influence upon the hydrogen bonded links between neighbouring building blocks, e.g. perhalometallate systems and combined coordination chemistry-hydrogen bonded systems, or are appended as potentially functional groups to the parent hydrogen-bonded organic network, e.g. π-bonded organometallic systems. For instance, coordination of halide ligands to transition metals leads to good hydrogen bond acceptor capability. Methods have been developed to prepare salts of perhalometallate complexes ($[MX_n]^{m-}$, X=Cl, Br etc.; M=Pt, Zn, Mn, Pb etc.) with organic cations with N-H hydrogen bond donor functionality [39]. These systems are modular and robust and offer the opportunity to exploit shape, charge and functional groups of the ions in order to control the crystal structures and the hydrogen bond networks they form [40].

An alternative, widely used, approach to charge assisted networks is based on the exploitation of direct acid-base reactions. There are, broadly speaking, essentially two different means to obtain charge-assisted interactions, which depend on whether the network is constructed of ions of the same charge (*homo-ionic* hydrogen bonded networks) or of ions of opposite charge (*hetero-ionic* networks). These two limiting situations are shown in Fig. 1c,d. The utilization of

UM00013018
NOVARTIS EXHIBIT 1017
Novartis v. Regents, IPR2023-01346
Page 1764 of 4460

multiple hydrogen bonding systems allows also intermediate situations, whereby homo-ionic chains are interlinked by hetero-ionic interactions. The most common situation is encountered when the proton acceptor is chosen such as to interact directly with the proton donor, e.g. assisted hydrogen bonding interactions of the $^{(-)}X\cdots H\text{-}Y^{(+)}$ types are formed. This is the case, for instance, of nitrogen containing bases, which are protonated upon reaction with polycarboxylic acid molecules, e.g. $RCOOH^{-}+NR_3 \rightarrow RCOO^{(-)}\cdots{}^{(+)}HNR_3$, leading to formation of strong $^{(-)}O\cdots H\text{-}N^{(+)}$ interactions, hence an anion-cation pairing in the solid state.

The assembly can result in *homo-ionic* chains when the base *cannot form* competing hydrogen bonding interactions with the acid moiety. This is the case of the reaction between polycarboxylic acids with bases that do not carry strong acceptor/donor hydrogen bond groups. Partial deprotonation of the -COOH groups leads to self-assembly of acid anions via $O\text{-}H\cdots O^{(-)}$ and $^{(-)}O\text{-}H\cdots O^{(-)}$ interactions [41]. By choosing the number of carboxylic groups (hence the number of potential donor/acceptor systems) and the stoichiometric ratios in the acid-base reactions, one can control the formation of $O\text{-}H\cdots O^{(-)}$ and/or $^{(-)}O\text{-}H\cdots O^{(-)}$ interactions, hence homo-ionic self-assembly.

There is a vast literature on the utilization of crystal engineering based on of inter-ionic hydrogen bonding interactions [42]; because of space limitations we shall be able to discuss only very few representative examples. The neutral dicarboxylic acid $[Cr^0(\eta^6\text{-}C_6H_5COOH)_2]$ and its oxidation product $[Cr^I(\eta^6\text{-}C_6H_5COOH)_2]^+$ are isostructural, but not isoelectronic [43]. The two systems can be regarded as composed of a fundamental building block unit, "$Cr(\eta^6\text{-}C_6H_5COO)_2$", which can participate in hydrogen bonding interactions as a mono-cation, a neutral species, a mono-anion or a di-anion, depending on the extent of protonation and on the metal atom oxidation state. Figure 11 shows a comparison of the neutral dimer formed by $Cr^0(\eta^6\text{-}C_6H_5COO)_2$ molecules and the *cationic* chain formed by $[Cr^I(\eta^6\text{-}C_6H_5COOH)_2]^+$ units in the $[PF_6]^-$ salt.

Soft molecular host networks based on layers of guanidinium cations spaced by pillars of sulfonate anions have been developed by Ward et al. (see Fig. 12) [44]. The $^{(+)}N\text{-}H\cdots O^{(-)}$ interactions between guanidinium cations and sulfonate anions render the superstructures at the same time robust and adaptable to the guest requirements, while the porosity can be tuned by changing the length of the pillars. These properties have been exploited in several applications, such as shape-selective separation of molecular isomers. Chiral crystals based on hydrogen L-malate anions have been assembled by Aakeröy et al. via $^{(-)}O\text{-}H\cdots O^{(-)}$ bridges in anionic layers. Since the two-dimensional network is highly reproducible, it can be transferred from crystal to crystal inducing non-centrosymmetry, a target on the route to materials for second harmonic generation. Analogous strategy has been used by us to self-assemble chiral frameworks around organometallic cations [45].

Lehn et al. have used inter-ionic hydrogen bridges to direct the recognition and self aggregation of metal complexes carrying terpyridine derived ligands joined by inter-cation $^{(+)}N\text{-}H\cdots N^{(+)}$ bridges [46]. The solid state arrangement of the $Co(terpy)_2^{2+}$complex is highly dependent on the choice of counterion: in the $[PF_6]^-$ salt a two-dimensional infinite network is formed via pairs of $N\text{-}H\cdots N$ in-

UM00013019
NOVARTIS EXHIBIT 1017
Novartis v. Regents, IPR2023-01346
Page 1765 of 4460

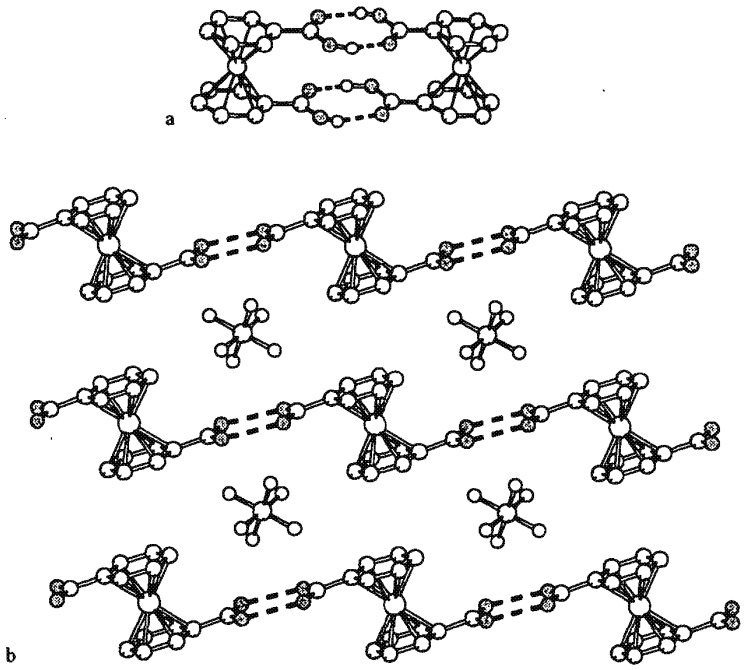


Fig. 11a,b The neutral dimer formed by: a two $Cr(\eta^6\text{-}C_6H_5COO)_2$ molecules is compared with; b the cationic chains formed by $[Cr^I(\eta^6\text{-}C_6H_5COOH)_2]^+$ units in the $[PF_6]^{(-)}$ salt

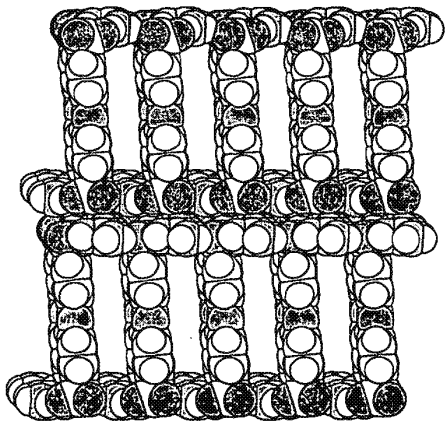


Fig. 12 An example of guanidinium-sulfonate superstructures. The fundamental interaction responsible for both robustness and flexibility is the charge-assisted $^{(+)}N\text{-}H\cdots O^{(-)}$ hydrogen bonding between the guanidinium cations and the sulfonate anions, which can be varied in shape and length [44]

UM00013020
NOVARTIS EXHIBIT 1017
Novartis v. Regents, IPR2023-01346
Page 1766 of 4460

THIS PAGE BLANK (USPTO)

NOVARTIS EXHIBIT 1017
Novartis v. Regents, IPR2023-01346
Page 1767 of 4460

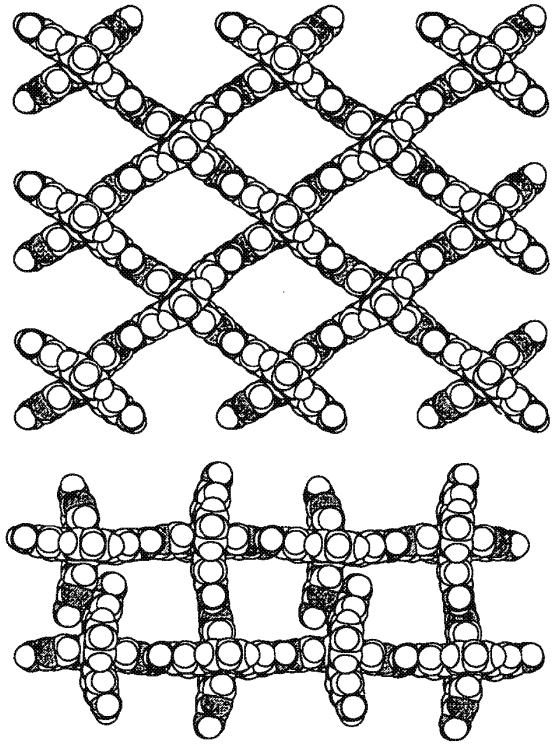


Fig. 13 A two-dimensional infinite network is formed via pairs of $^{(+)}$N-H···N$^{(+)}$ interactions in the $[PF_6]^-$ salt of the cobalt complex $Co(terpy)_2^{2+}$ (*top*), while a quarter of the potential HB interactions are not formed leading to a broken network in the case of the $[BF_4]^-$ salt (*bottom*) [46]

teractions, while in the BF_4^- salt a broken network is observed (Fig. 13). This provides an example of competition between formation of N-H···N interactions and optimisation of the Coulombic interactions that, in turns, depends on the size of the ions.

8
Hydrogen Bonded Networks Can React or Transform

The exploitation of the reactivity of molecular crystals lies close to the origins of crystal engineering and is at the heart of the pioneering work of Schmidt [47a]. The idea is that of organizing molecules in the solid state using the principles of molecular recognition and self-assembly. Successful results have been obtained with bimolecular reactions, particularly [2+2] photoreactivity and cyclisation [47b,c]. Another important area is that of host-guest chemistry.

UM00013022
NOVARTIS EXHIBIT 1017
Novartis v. Regents, IPR2023-01346
Page 1768 of 4460

Diverse applications of inclusion compounds have been described by Toda, Kaupp and Nassimbeni [48] and others. Many reactions involve breaking and formation of hydrogen bonded networks.

Another important application of *hydrogen bond reactivity* is in the investigation of reactions between engineered molecular solids and molecules in the vapour phase. Heterogeneous gas-solid reactions are well known in chemistry thanks to the pioneering work of Curtin and Paul [49]. A case study is the reaction of crystalline benzoic acid, which forms cyclic hydrogen bonded carboxylic rings in the solid state, with ammonia vapours. The reaction leads to quantitative formation of a 1:1 ammonium salt. Curtin and Paul were able to demonstrate that certain crystal faces are attacked preferentially by the ammonia vapour, and the resulting reaction front travels more rapidly through the crystals along directions corresponding to specific molecular arrangements [50, 51]. Crystalline *p*-chlorobenzoic anhydride reacts with gaseous ammonia to give the corresponding amide and ammonium salt [52]; similar reactions have been investigated in the case of optically active cyclopropane carboxylic acid crystals [53]. All these reactions imply rupture of O-H···O hydrogen bonds between neutral molecules, and replacement with N-H···O bonds between cations and anions.

One particularly useful combination is that between ionic charge and number of hydrogen bonding donor groups, when the ionic or neutral nature of the molecule can be *tuned* by means of acid-base reactions. An example is provided by the dicarboxylic acid $[Co^{II}(\eta^5\text{-}C_5H_4COOH)_2]$, which is readily oxidised in air to the cation $[Co^{III}(\eta^5\text{-}C_5H_4COOH)_2]^+$ [54]. The zwitterion $[Co^{III}(\eta^5\text{-}C_5H_4COOH)(\eta^5\text{-}C_5H_4COO)]$ can be quantitatively prepared from the corresponding dicarboxylic cationic acid $[Co^{III}(\eta^5\text{-}C_5H_4COOH)_2]^+$. The "cobaltocene diacid" family provides a grand total of six building blocks potentially useful in crystal engineering (see Fig. 14). By controlling the oxidation state and/or the pH, this relatively simple chemical system can afford complexes that can be diamagnetic or paramagnetic [Co(III), and Co(II)], neutral, cationic or anionic [from +1 to −2], hydrogen bonding donor or acceptor [-COOH, and $-COO^{(-)}$], or a combination of these charac-

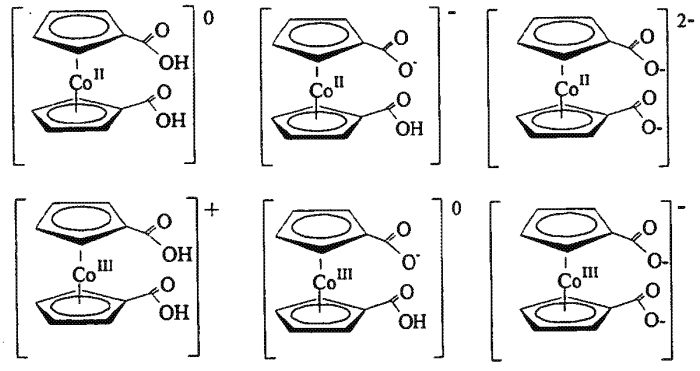


Fig. 14 *Top*: $[(C_5H_4COOH)_2Co^{II}]$ and deprotonation derivatives. *Bottom*: $[(C_5H_4COOH)_2Co^{III}]^+$ and deprotonation derivatives

UM00013023
NOVARTIS EXHIBIT 1017
Novartis v. Regents, IPR2023-01346
Page 1769 of 4460

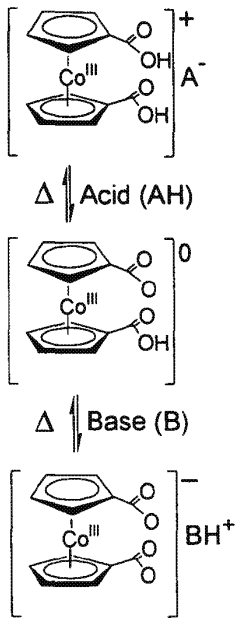


Fig. 15 The solid zwitterion $[Co^{III}(\eta^5\text{-}C_5H_4COOH)(\eta^5\text{-}C_5H_4COO)]$ reacts reversibly with acid and base vapours

teristics. The zwitterion $[Co^{III}(\eta^5\text{-}C_5H_4COOH)(\eta^5\text{-}C_5H_4COO)]$ possesses amphoteric behaviour because of the presence of one -COOH group, which can react with bases, and one $-COO^{(-)}$ group, which can react with acids. The zwitterion undergoes fully reversible heterogeneous reactions, exploiting the possibility of *switching* between neutral and charged hydrogen bonding interactions. These features can be exploited to prepare a *reversible gas-trap system* by reacting the zwitterionic species with hydrated vapours of a variety of acids (e.g. HCl, CF_3COOH, HBF_4, and HCOOH) and bases (e.g. NH_3, NMe_3, NH_2Me) with formation of the corresponding salts [54]. The salts resulting from the heterogeneous reaction contain the organometallic moiety either in its fully protonated form $[Co^{III}(\eta^5\text{-}C_5H_4COOH)_2]^+$ (in the reaction with acids) or in its fully deprotonated form $[Co^{III}(\eta^5\text{-}C_5H_4COO)_2]^-$ (in the reaction with bases), as shown in Fig. 15. The two types of reactions imply the interconversion between neutral O-H···O hydrogen bonding interactions and $^{(+)}O\text{-}H\cdots X^{(-)}$ and $^{(-)}O\cdots H\text{-}N^{(+)}$ interactions, respectively.

Contrary to all other reactions with acids the behaviour of the zwitterion towards vapours of formic acid is intriguing, since no proton transfer is observed. The formic acid vapour uptake generates a material composed of pairs of zwitterion molecules, linked by O-H···O bonds between the protonated -COOH and the deprotonated $-COO^{(-)}$ groups [O···O separation 2.526(4) Å] residing on the organometallic moiety. The zwitterion dimers interact with two formic acid molecules via O-H···O and C-H···O hydrogen bonds [O···O distance 2.541(4),

UM00013024
NOVARTIS EXHIBIT 1017
Novartis v. Regents, IPR2023-01346
Page 1770 of 4460

(C)H···O distance 2.43(5) Å]. The intramolecular parameters are indicative of the presence of distinct -COOH and -COO^- groups over the zwitterionic complex [C-O1 1.209(4), C-O2 1.306(4); C-O3 1.243(4), C-O4 1.247(4) Å]. On the other hand, the C-O distances within the HCOOH moiety [C-O5 1.305(5), C-O6 1.199(5) Å] indicate that the formic acid molecule retains its acidic hydrogen. This has also been confirmed by ^{13}C CPMAS NMR spectroscopy [54c]. Since HCOOH is a weaker Brønsted acid than HCl, HBF_4 and CF_3COOH, the different behaviour has been attributed to the difference in relative acidity of the absorbed acid with respect to the zwitterion. Even though the weaker HCOOH acid does not protonate the zwitterion, it is still capable of association with the zwitterion via strong O-H···O hydrogen bonding interactions. On this premise, the reaction between the solid zwitterion and HCOOH(vapour) could be regarded as a special kind of solvation rather than as a heterogeneous acid-base reaction. In a sense, gas-solid reactions and gas-solid solvation differ only in the energetic ranking of the interactions (whether covalent or non-covalent) that are broken or formed through the processes. In the reversible *supramolecular reaction* of solid [$Co^{III}(\eta^5\text{-}C_5H_4COOH)(\eta^5\text{-}C_5H_4COO)$] with gaseous HCOOH, O-H···O and C-H···O bonds are disrupted and/or rearranged, while covalent bonds are not affected.

The location of the hydrogen atoms in hydrogen bonded systems is often difficult to ascertain. When X-ray diffraction is used there is an experimental limitation to face, as it is usually difficult to locate the very light H-atom in Fourier maps and, even when this is possible, the technique can provide information on electron density centroids rather than on the position of the light nucleus. Neutron diffraction is required for an unambiguous location of the H-atom. In ionic hydrogen bonds the situation may occur where a knowledge of the proton position in a donor-acceptor system is necessary to know whether proton transfer, i.e. protonation of a suitable base, has occurred or not.

The proton transfer process along an X-H···Y interaction, whether associated with a phase transition or not, may imply the transformation of a molecular crystal into a molecular salt. Wilson [55] has discussed, on the basis of an elegant neutron diffraction study, the migration of the proton along an O-H···O bond in a co-crystal urea-phosphoric acid (1:1), whereby the proton migrates towards the mid-point of the hydrogen bond as the temperature is increased, becoming essentially centred at T=335 K (see Fig. 16). Mootz and Wiechert [56], on the other hand, have isolated two crystalline materials composed of pyridine and formic acid of different composition. In the 1:1 co-crystal the formic acid molecule retains its proton and transfer to the basic N-atom on the pyridine does not take place (hence molecules are linked by neutral O-H···N interactions). In the 1:4 co-crystal, on the contrary, one formic acid molecules releases its proton to the pyridine molecule establishing $N\text{-}H^{(+)}\cdots O$ interactions. In a sense this latter case could be regarded as an unusual case of solvate crystal (see Fig. 17).

It is a useful notion to consider that the *reaction* of a molecular solid, whether formed of organic, organometallic molecules or coordination compounds, with a vapour is conceptually related to the *supramolecular reaction* of a crystalline material with a volatile solvent to form a new crystalline solid (Fig. 18). Indeed, the two processes, solid-gas reaction and solid-gas solvation, differ only in the

UM00013025
NOVARTIS EXHIBIT 1017
Novartis v. Regents, IPR2023-01346
Page 1771 of 4460

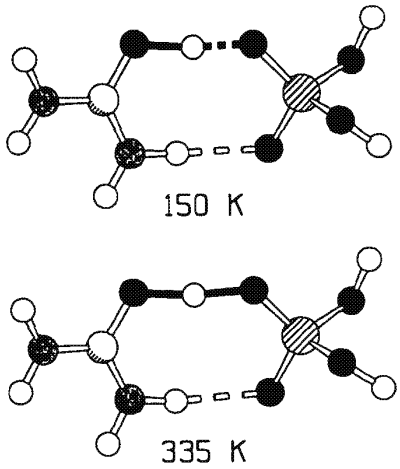


Fig. 16 The migration of the proton along an O-H···O bond in a co-crystal urea-phosphoric acid (1:1), as the temperature is increased from 150 K (*top*) to 335 K (*bottom*), becoming essentially centred (neutron study) [55]

energetic ranking of the interactions that are broken or formed through the processes. In solvation-desolvation processes one is dealing mainly with non-covalent van der Waals or hydrogen bonding interactions, whilst in chemical reactions covalent bonds are broken or formed. This awareness is useful to the *engineering* of molecular materials whereby gas uptake is exploited not only to produce new crystalline forms of a given substance but also as a means to produce new materials in crystalline form. Clearly, the conceptual borderline between the two types of processes is very thin. One may purposefully plan to assemble molecules that are capable of absorbing molecules from the gas phase and, possibly, to react with them.

The existence of different configurations of the proton atom location within O-H···O systems is at the basis of the possibility of constructing proton conducting materials. These materials, in particular those based on solid acids such as $CsHSO_4$ [57a] (see Fig. 19), $Rb_3H(SeO_4)_2$ etc., have applications in a number of devices such as H_2 and H_2O sensors, fuel and steam cells and high energy density batteries. The solid acids derived from polyprotic acids such as H_3PO_4 and $H_2SO_4$by partial deprotonation all show the presence of strong inter-anionic hydrogen bonding association in the solid state. These systems often undergo an order-disorder phase transition at high temperature, which is associated with a dramatic increase of the conductivity [57b,c]. Such behaviour is called *superprotonic* transition and has been recently begun to be exploited as solid fuel cell electrolytes because they have the advantage of anhydrous proton transport and are thermally stable (up to 500–550 K). Hybrid anionic systems, such as $Cs_2(HSeO_4)(H_2PO_4)$, have also begun to be investigated [58]. The salt undergoes a gradual super-protonic transition over the temperature range 334–378 K, with

UM00013026
NOVARTIS EXHIBIT 1017
Novartis v. Regents, IPR2023-01346
Page 1772 of 4460

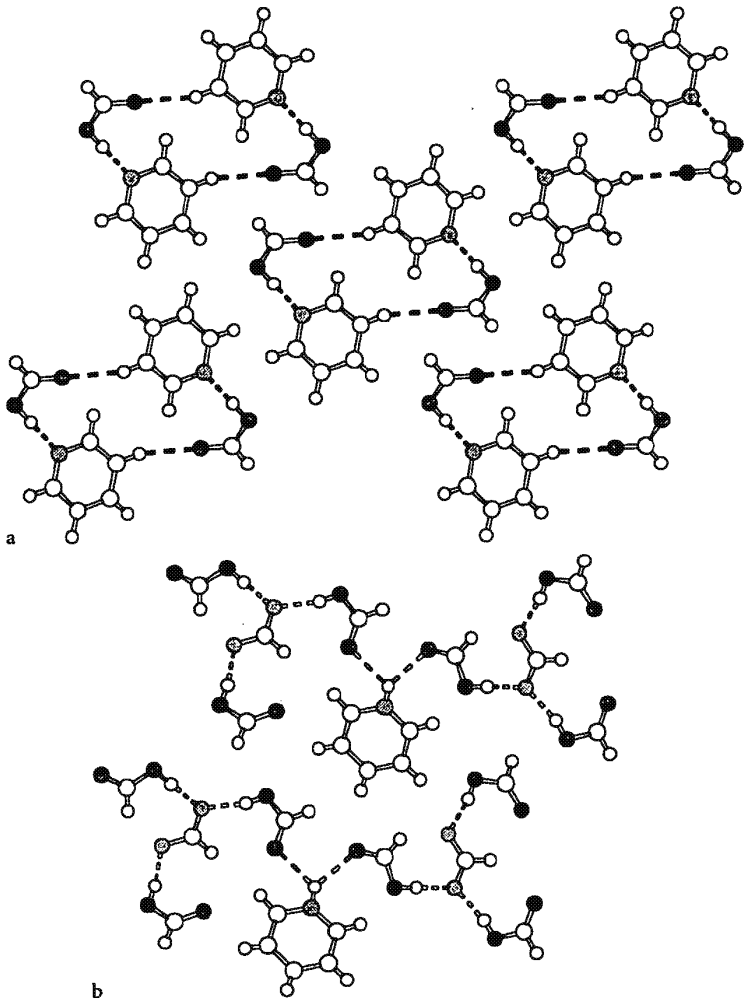


Fig. 17a,b The two forms of the adduct between pyridine and formic acid of different composition: **a** in the 1:1 co-crystal **a** the formic acid molecules retains its proton and transfer to the basic N-atom on the pyridine does not take place (hence molecules are linked by neutral O-H···N interactions); **b** in the 1:4 co-crystal, in contrast, one formic acid molecules releases its proton to the pyridine molecule establishing $N\text{-}H^{(+)}\cdots O$ interactions [56]

UM00013027
NOVARTIS EXHIBIT 1017
Novartis v. Regents, IPR2023-01346
Page 1773 of 4460

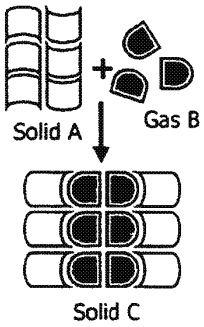


Fig. 18 The *reaction* of a molecular solid, whether formed of organic, organometallic molecules or coordination compounds, with a vapour is conceptually related to the *supramolecular reaction* of a crystalline material with a volatile solvent to form a new crystalline solid

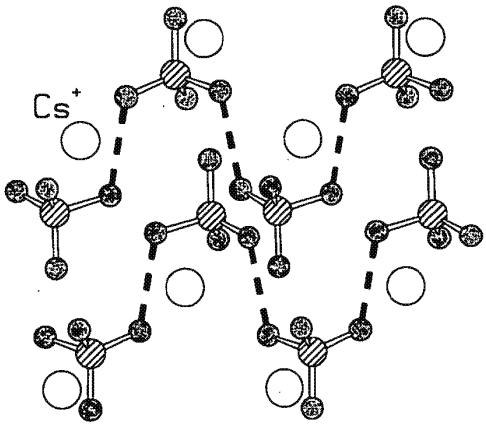


Fig. 19 The structure of crystalline $CsHSO_4$ at 150 K (hydrogen atoms were not located) [57a]

an activation energy for proton conduction of 149.37 kJ mol^{-1}. The phenomenon of superprotonic conductivity is explained with the possibility of proton jumps from one anion to the nearby one associated with the onset of the reorientational motion of the oxoacid anions.

9 Conclusions

The principal non-covalent interaction in molecule-based crystal engineering is the hydrogen bond. The reason for this preference is simple, the hydrogen bond is the strongest of the non-covalent interactions and possesses a high degree of directionality. Strength and directionality (namely transferability and repro-

UM00013028
NOVARTIS EXHIBIT 1017
Novartis v. Regents, IPR2023-01346
Page 1774 of 4460

ducibility) are conditional for an interaction to be useful in the *making* and *holding together* superstructures, whether supermolecules or crystals. In this respect the combination of weak non-covalent interactions (hydrogen bonding and π-stacking) with the Coulombic field generated by ions poses an intriguing problem: the architectural features are largely determined by the steric and energetic demand of the directional interactions, whilst much of the cohesion is provided – just as in any ionic crystal – by the balance of Coulombic attractions and repulsions.

Hydrogen bonding interactions between ions need to occupy a special place in the library of non-covalent interactions of interest to supramolecular chemists and crystal engineers. We have argued in this chapter that the utilization of hydrogen bonding and π-stacking interactions between ions is a useful instrument to confer directionality to the Coulombic field generated by the ions. The (few) examples provided in the latter section demonstrate that the issue stated in the title is not academic only, but carries practical implications. As with the hydrogen bonds between molecules, the hydrogen bonding interactions between ions can be used to make aggregates, because they are directional, hence reproducible and transferable. The cohesion of the aggregate does of course depend on the Coulombic field generated by the ions. Consequently that the physical and chemical properties of the crystalline solid (solubility, melting, conductivity, etc.) will be those of ionic salts and not those of molecular crystals. An awareness of the importance of these factors is necessary when planning the construction or the exploitation of the resulting materials.

When discussing the relative weights of the various types of interactions, simultaneously and not independently at work in a stable solid, it should be kept in mind that stabilizing interactions can be effective even in the presence of repulsive forces, as well as the opposite, namely destabilizing interactions may be observed in the presence of attractive forces. An appreciation of this conceptual distinction is crucial to the understanding of the effect of ionic charges on the nature of pair-wise non-covalent interactions. Particularly when the ions carry the same charge.

We have shown that crystals held together by hydrogen bonding interactions between ions or molecular ions can be devised, designed and constructed by using the principles of molecular crystal engineering. These materials can then be reacted and/or transformed, for instance, by *manipulating* the hydrogen bond network. This is particularly relevant in the case of superprotonic conductivity and or gas-solid reactions discussed above.

10 References

1. (a) Lehn JM (1990) Angew Chem Int Ed Engl 29:1304; (b) Whitesides GM, Simanek EE, Mathias JP, Seto CT, Chin DN, Mammen M, Gordon DM (1995) Acc Chem Res 28:37; (c) Gans W, Boyens JCA (1997) Intermolecular interactions. Plenum, New York. (d) Braga D, Grepioni F (2000) Acc Chem Res 33:601
2. (a) Lehn, JM (1995) Supramolecular chemistry: concepts and perspectives. VCH, Weinheim; (b) Philp D, Stoddard JF (1996) Angew Chem Int Ed Engl 35:1154; (c) Steed JW, Atwood JL (2000) (eds) Supramolecular chemistry. Wiley, Chichester, UK; (d) Haiduc I, Edelmann FT

UM00013029
NOVARTIS EXHIBIT 1017
Novartis v. Regents, IPR2023-01346
Page 1775 of 4460

19. (a) Braga D, Grepioni F (1996) J Chem Soc Chem Commun 571
20. Inorganic Crystal Structure Database (ICSD), Fachinformationszentrum (FIZ) Karlsruhe and Gmelin Institut
21. (a) Nangia A (2002) Cryst Eng Comm 4:93; (b) Steiner T (2001) Acta Cryst B57:103; (c) Ziao N, Laurence C, Le Questel JY (2002) Cryst Eng Comm 326; (d) Allen FH, Motherwell WDS (2002) Acta Cryst B58:407; (e) Steiner T, Schreurs AMM, Lutz M, Kroon J (2001) New J Chem 25:174; (f) Nangia A, Biradha K, Desiraju GR (1996) J Chem Soc Perkin Trans 2:943; (g) Takahashi O, Kohno Y, Iwasaki S, Saito K, Iwaoka M, Tomoda S, Umezawa Y, Tsuboyama S, Nishio M (2001) Bull Chem Soc Jpn 74:2421; (h) Suezawa H, Yoshida T, Umezawa Y, Tsuboyama S, Nishio M (2002) Eur J Inorg Chem 3148; (i) Ziao N, Graton J, Laurence C, Le Questel JY (2001) Acta Cryst B57:850; (i) Aakeroy CB, Evans TA, Seddon KR, Palinko I (1999) New J Chem 23:145
22. Dunitz JD, Gavezzotti A (1999) Acc Chem Res 32:677
23. (a) Pyykkö P (1997) Chem Rev 97:597; (b) Mathieson T, Schier A, Schmidbaur H (2000) J Chem Soc Dalton Trans 21:3881
24. (a) Ohmine I, Saito S (1999) Acc Chem Res 32:741; (b) Leopold KB, Canagartna M, Phillips JA (1997) Acc Chem Res 30:57
25. Braga D, Grepioni F (1998) New J Chem 1159
26. Braga D, Grepioni F (1997) Acc Chem Res 30:81
27. Dunitz JD, Taylor R (1997) Chem Eur J 3:89
28. Braga D, Scaccianoce L, Grepioni F, Draper SM (1996) Organometallics 15:4675
29. Braga D, Novoa JJ, Grepioni F (2001) New J Chem 25:226
30. (a) Toda F, Takumi H, Akehi M (1990) J Chem Soc Chem Commun 1270; (b) Toda F, Okuda K (1991) J Chem Soc Chem Commun 1212; (c) Tanaka K, Fujimoto D, Oeser T, Irngartinger H, Toda F (2000) Chem Commun 413
31. (a) Etter MC, Reutzel SM, Choo CG (1993) J Am Chem Soc 115:4411; (b) Rastogi R, Singh NB (1968) J Phys Chem 72:4446; (c) Caira MR, Nassimbeni LR, Wildervanck AF (1995) J Chem Soc Perkin Trans 2213; (d) Pedireddi VR, Jones W, Chorlton AP, Docherty R (1996) Chem Commun 987; (e) Nichols PJ, Raston CL, Steed JW (2001) Chem Commun 1062; (f) Fernandez-Bertran JF (1999) Pure Appl Chem 71:581; (g) Boldyrev VV (1993) Solid State Ionics 63/65:537; (h) Toda F, Miyamoto H (1995) Chem Letters 861; (i) Makhaev VD, Borisov AP, Petrova LA (1999) J Organomet Chem 590:222; (l) Cave GWV, Raston CL, Scott JL (2001) Chem Commun 2159
32. Norby T (2001) Nature 400:877
33. (a) Del Sesto RE, Miller JS, Lafuente P, Novoa JJ (2002) Chem Eur J 8:4894; (b) Novoa JJ, Lafuente P, Del Sesto RE, Miller JS (2002) Cryst Eng Comm 373; (c) Steiner T (1999) Chem Commun 313
34. Braga D, Grepioni F, Tagliavini E, Novoa JJ, Mota F (1998) New J Chem 755
35. Braga D, Bazzi C, Grepioni F, Novoa JJ (1999) New J Chem 23:577
36. Braga D, Maini L, Grepioni F (2002) Chem Eur J 8:1804
37. Dunitz JD, Seiler P, Czchtizky W (2001) Angew Chem Int Ed 40:1779
38. Braga D, Grepioni F, Desiraju GR (1998) Chem Rev 98:1375
39. (a) Aullon G, Bellamy D, Brammer L, Bruton EA, Orpen AG (1998) Chem Commun 653; (b) Gillon AL, Lewis GR, Orpen AG, Rotter S, Starbuck J, Wang XM, Rodriguez-Martin Y, Ruiz-Perez C (2000) J Chem Soc Dalton Trans 3897
40. Brammer L, Swearingen JK, Bruton EA, Sherwood P (2002) Proc Nat Acad Sci USA 99:4956
41. Braga D, Grepioni F (1999) J Chem Soc Dalton Trans 1
42. See for example: (a) Beatty AM (2001) Cryst Eng Comm 51; (b) Aakeroy CB, Beatty AM, Leinen DS (2002) Cryst Eng Comm 310; (c) Brammer L, Burgard MD, Eddleston MD, Rodger CS, Rath NP, Adams H (2002) Cryst Eng Comm 239; (d) Beauchamp DA, Loeb SJ (2002) Chem Eur J 8:5084; (e) Uemura K, Kitagawa S, Kondo M, Fukui K, Kitaura R, Chang HC, Mizutani T (2002) Chem Eur J 8:3586
43. Braga D, Maini L, Grepioni F, Elschenbroich C, Paganelli F, Schiemann O (2001) Organometallics 20:1875
44. Holman KT, Pivovar AM, Swift JA, Ward MD (2001) Acc Chem Res 34:107

UM00013030
NOVARTIS EXHIBIT 1017
Novartis v. Regents, IPR2023-01346
Page 1776 of 4460

45. Aakeröy CB, Nieuwenbuyzen M (1994) J Am Chem Soc 116:10983
46. Ziener U, Breuning E, Lehn J-M, Wegelius E, Rissanen K, Baum G, Fenske D, Vaughan G (2000) Chem Eur J 6:4132
47. (a) Schmidt GMJ (1971) Pure Appl Chem 27:647; (b) MacGillivray LR, Reid JL, Ripmeester JA (2000) J Am Chem Soc 122:7817; (c) McGillivray LR (2002) Cryst Eng Comm 4:37
48. (a) Tanaka K, Toda F, Mochizuki E, Yasui N, Kai Y, Miyahara I, Hirotsu K (1999) Angew Chem Int Ed 38:3523; (b) Toda F (1995) Acc Chem Res 28:480; (c) Toda F (2002) Cryst Eng Comm 4:215; (d) Kaupp G (1996) In: Davies JED (ed) Comprehensive supramolecular chemistry. Elsevier, Oxford 8:381; (e) Nassimbeni LR, Su H (2002) New J Chem 26:989; (f) Caira MR, Nassimbeni LR, Toda F, Vujovic D (2000) J Am Chem Soc 122:9367; (g) Apel S, Lennartz M, Nassimbeni LR, Weber E (2002) Chem Eur J 8:3678
49. Paul IC, Curtin DY (1975) Science 187:19
50. (a) Miller RS, Curtin DY, Paul IC (1974) J Am Chem Soc 96:6329; (b) Chiang CC, Lin C-T, Wang AH-J, Curtin DY, Paul IC (1977) J Am Chem Soc 99:6303
51. Miller RS, Paul IC, Curtin DY (1974) J Am Chem Soc 96:6334
52. Lin CT, Paul IC, Curtin DY (1974) J Am Chem Soc 96:3699
53. Miller RS, Curtin DY, Paul IC (1974) J Am Chem Soc 96:6340
54. (a) Braga D, Cojazzi G, Emiliani D, Maini L, Grepioni F (2001) Chem Commun 2272; (b) Braga D, Cojazzi G, Emiliani D, Maini L, Grepioni F (2002) Organometallics 21:1315; (c) Braga D, Maini L, Mazzotti M, Rubini K, Masic A, Gobetto R, Grepioni F (2002) Chem Commun 2296
55. (a) Wilson CC (2001) Acta Cryst B57:435; (b) Steiner T, Majerz I, Wilson CC (2001) Angew Chem Int Ed 40:2651
56. Wiechert D, Mootz D (1999) Angew Chem Int Ed 38:1974
57. (a) Lipkowski J, Baranowski B, Lunden A (1993) Pol J Chem 67:1867; (b) Haile SM (1999) In: Solid state chemistry of inorganic materials II. Mat Res Soc Symp Proc 547:315; (c) Haile SM, Boyens DA, Chisholm CRI, Merie RB (2001) Nature 400:910
58. Chisholm CRI, Haile SM (2000) Solid State Ionics 136/137:229

UM00013031
NOVARTIS EXHIBIT 1017
Novartis v. Regents, IPR2023-01346
Page 1777 of 4460

This Page is Inserted by IFW Indexing and Scanning Operations and is not part of the Official Record

BEST AVAILABLE IMAGES

Defective images within this document are accurate representations of the original documents submitted by the applicant.

Defects in the images include but are not limited to the items checked:

- ☐ BLACK BORDERS
- ☐ IMAGE CUT OFF AT TOP, BOTTOM OR SIDES
- ☐ FADED TEXT OR DRAWING
- ☐ BLURRED OR ILLEGIBLE TEXT OR DRAWING
- ☐ SKEWED/SLANTED IMAGES
- ☐ COLOR OR BLACK AND WHITE PHOTOGRAPHS
- ☐ GRAY SCALE DOCUMENTS
- ☐ LINES OR MARKS ON ORIGINAL DOCUMENT
- ☐ REFERENCE(S) OR EXHIBIT(S) SUBMITTED ARE POOR QUALITY
- ☐ OTHER: _____

IMAGES ARE BEST AVAILABLE COPY.

As rescanning these documents will not correct the image problems checked, please do not report these problems to the IFW Image Problem Mailbox.

Preparation and structure of the 1:2 π-molecular complex of phenothiazine with pyromellitic dianhydride

C. Brierley, R. Barton, and B. Robertson
Faculty of Science, University of Regina, Regina, Saskatchewan, Canada S4S 0A2

R. Anthonj and N. Karl
Physikalisches Institut, Teilinstitut 3, Universität Stuttgart, Pfaffenwaldring 57, D 7000 Stuttgart 80, Federal Republic of Germany

(Received 30 July 1984; accepted 23 October 1984)

Single crystals of the black 1:2 donor–acceptor complex of phenothiazine with pyromellitic dianhydride, PTZ:$(PMDA)_2$, were grown by plate sublimation at $\sim$163 °C from the zone-refined components. The 1:1 complex is produced at lower temperatures. Crystals of the 1:2 complex are monoclinic, $P2_1/c$, $Z = 4$, $a = 7.689(3)$, $b = 12.953(5)$, $c = 28.14(2)$ Å, $\beta = 104.30(2)°$ at $T = 19$ °C. The structure was refined from 2863 x-ray diffraction reflection intensities for which $I > 2.0\sigma(I)$ to $R = 0.064$ and $R_w = 0.057$. The structure consists of continuous ... DADA ... polar stacks as does the 1:1 complex, but the stacks, which are parallel to the a axis, are separated in the c direction by the extra PMDA molecule. The overlap of adjacent molecules in the stack in the 1:2 complex is more closely related to the overlap of adjacent molecules in the π-molecular complex of PMDA with anthracene. The resultant angle between the stack axis and the normal to the planar molecules is 27.1°. The geometry of the individual molecules in the 1:2 complex is not significantly different from those in the 1:1 complex.

INTRODUCTION

Donor–acceptor (D:A) complexes of aromatic π-electron systems with nominally neutral ground states usually crystallize in the form of infinite $\cdots$DADA$\cdots$ stacks with perpendicular distances between the planes of the molecules near 3.4 Å. The associated physical properties of the complex depend upon the electronic states of the constituent molecules (especially on the ionization energy of the donor and on the electron affinity of the acceptor), on their geometry and on the precise nature of the interactions of the atoms (and hence the sign and overlap of the electronic wave functions) in the donor and acceptor molecules. Variations in the nature of the interaction of adjacent molecules (and the tendency to maximize the overall molecular interactions) lead to variations in the angle between the stack axis and the normal to the planes of the molecules within the stacks; i.e., the stack angle.

In order to correlate the structural features of D:A complexes with their electrical and optical properties, it is essential that very pure material be used because the influence of impurities on these properties may be substantial. We report here on studies of the binary system composed of phenothiazine (PTZ) and pyromellitic dianhydride (PMDA) where both components were first purified separately by multipass zone refining. We have described previously the details of the purification procedure;[1] further, we have reported on the growth of single crystals by plate sublimation,[2] and on structure, optical and electrical properties of the *1:1 complex* ($C_{12}H_9SN$:$C_{10}H_2O_6$).[1] In addition, UV-photoelectron spectra have been measured[3] and compared with those obtained with the neat donor crystal. There is also a *1:2 complex* [$C_{12}H_9SN$:2($C_{10}H_2O_6$)] formed in the binary PTZ/PMDA system which we discuss in this publication.

The structures of several other D:A π-molecular complexes containing PMDA as acceptor have been reported. In these cases the donor molecules have been acridine,[4] anthracene,[5,6] carbazole,[7] fluorene,[8] naphthalene,[9,10] phenanthrene,[11] phenazine,[12,13] pyrene,[14] perylene,[5] and thianthrene.[15] Whereas the individual components absorb in the near UV and are therefore colorless or weakly yellow, the complex crystals are brightly colored or in some cases, black, because of light absorption in a broad more or less unstructured band in the visible part of the spectrum. This is due to an optical transition with charge transfer from the donor to the acceptor. Both the 1:1 and 1:2 complexes between PTZ and PMDA are black.

The black appearance of the 1:1 and 1:2 complexes is related to the low ionization potential of PTZ, leading to a small energy requirement for the transfer of an electronic charge from the highest occupied molecular orbital of PTZ to the lowest unoccupied orbital of PMDA. The charge transfer energy and hence the energy of the excited charge transfer state is low enough to overlap with high lying combinations and overtones of molecular vibrations, thus explaining the absence of any emission between 4.2 and 300 K[1] of the 1:1 complex. The energy of the excited state may preferentially be dissipated though strong coupling with "butterfly" molecular motions of PTZ along its N$\cdots$S fold axis. In the 1:1 complex the fold angle of planes through the atoms of the two moieties

 0021-9606/85/031522-07$02.10 © 1985 American Institute of Physics

UM00013033
NOVARTIS EXHIBIT 1017
Novartis v. Regents, IPR2023-01346
Page 1779 of 4460

of the central ring was found to be 173.8°[1] which is taken as an indication that the (ground state) molecule, which is much more flat here than in the neat PTZ crystal (153.3°),[16] has gained binding energy by increasing its aromaticity and concomitantly decreasing its ionization threshold upon flattening. Hence the butterfly flapping motion would be expected to be strongly coupled to the charge transfer transition.

In the structure of PTZ:$SbCl_6$[17] the ground state of PTZ is a free radical with approximately unit positive charge as it would be in the excited state of a PTZ donor–acceptor complex with PMDA. Here the fold angle at the N–S vector is 177.1°. In conjunction with the near 180° fold angle, the S–C and N–C bonds strengths are enhanced to bond lengths of 1.71(2) and 1.38(2) Å from 1.758(1) and 1.403(2) Å in PTZ:PMDA[1] suggesting enhanced delocalization through the center of the molecule. Therefore, it is reasonable to also expect further flattening of the PTZ molecule in the CT-excited state of complexes with a near neutral ground state, such as PTZ:PMDA. The further flattening of the CT-excited PTZ molecule, should also be connected with increased aromaticity and S–C and N–C bond length contraction. This consideration further contributes toward concluding that a strong coupling of the PTZ CT transition to phonons should exist.

π-Molecular complexes with D:A ratios other than 1:1 usually consist of "sandwiches" formed by two molecules of one species and by one of the other, such as in the 2:1 complex of acridine with PMDA[18] or in the complex [(perylene)$_2$–perylene]:TCNQ.[19] The unit of three sandwich molecules may pack in linear stacks as in the latter case, or the units may pack in a herringbone zigzag pattern (commonly encountered with simple aromatic compounds such as napthalene, anthracene) without a common axis, as in the former case. In the latter, the third perylene molecule lies approximately orthogonal to the molecules in the stack and separates neighboring stacks of DAD units.

The DAD units allow CT transitions within themselves and the appearance of crystals containing such units is not significantly different from those with infinite · · ·DADA· · · stacks.

In consideration of the foregoing discussion, crystals of PTZ:$(PMDA)_2$ might reasonably be expected to contain sandwiched ADA units; infinite · · ·DADA· · · stacks, however, with the extra PMDA acceptor molecules excluded from the stacks, might also form the basis of the structure of the 1:2 complex phase, but this seemed less likely. In either case, a comparison of the optical and electrical properties of the two PTZ/PMDA phases and their correlation with structural geometry of the two phases should promise closer insight into the physics of π-molecular interactions.

EXPERIMENTAL

From an equimolar (1:1) starting mixture of zone-refined phenothiazine and pyromellitic–dianhydride and with the growth temperature kept at ~163 °C, black crystals were obtained by plate sublimation[2] which were different from the 1:1 complex[1] which grows at ~150 °C and below. The lattice parameters of the new phase in conjunction with the chemical composition determined by elemental analysis suggested that the crystals contained units of PTZ:$(PMDA)_2$ in the unit cell. Whereas the 1:1 phase is triclinic, the 1:2 phase is monoclinic, space group $P2_1/c$ from systematic extinctions [$(0k0)$, $k = 2n$; $(h0l)$, $l = 2n$]. Mass spectrometry yielded PTZ and PMDA entities, proving that no chemical reaction had taken place between the components. Very thin cleaved crystals (or solution-grown platelets) of the 1:1 complex are green in transmission and exhibit strongly different absorption for the two principal polarizations (in conjunction with directional pleochroism). In contrast, thin fragments of the other complex appear brownish and exhibit only weak dichroism as a function of the E and k vector.

A crystal with dimensions 0.4 × 0.4 × 1.0 mm^3 was used for x-ray diffraction on a modified Picker diffractometer. Lattice constants (a = 7.689(3), b = 12.953(5), c = 28.14(2) Å, β = 104.30(2)°, V = 2716.0 Å^3) were determined from the centered positions of 70 reflections in the range 46° ≤ 2θ ≤ 55° (Mo$K\alpha_1$) λ = 0.709 26 Å, T = 19 °C). The long axis of the crystal corresponded to the c axis of the unit cell and to the axis of the fiber with which the crystal was mounted on the goniometer. The large relative error in the value of c arises from imprecision in the crystal height adjustment and in the radius of the goniostat. For Z = 4, ρ_{cal} = 1.554 g cm^{-3}; 1.55 < ρ_{obs} < 1.59 g cm^{-3}.

The integrated intensities of 6258 reflections with 3° ≤ 2θ ≤ 55° were measured in the θ–2θ scan mode with Mo$K\alpha$ radiation, using a highly oriented graphite monochromator, a scan width of (1.60 + 0.692 tan θ)°, and minimum background times of 0.40 peak time. Data for which 3° ≤ 2θ ≤ 45° were collected with a scan speed of 2° min^{-1}. Data for which 45° < 2θ ≤ 55° were collected with a scan speed of 1° min^{-1}.

The intensities of three standard reflections decreased by 4% during the period of the data collection. The data were corrected for this decrease in intensity and the individual intensities were reduced to structure factors using standard procedures. Corrections for the effects of absorption (μ = 2.00 cm^{-1}) were not made. The standard deviations of the individual structure factors were calculated from the counting statistics associated with their measurement, with an additional contribution (approximately proportional to the square of the intensity) derived from the extent to which the scatter of the intensities of the standard reflections exceeded those expected from the statistics of their measurement.

The structure was solved by direct methods using the NRCC program package.[20] Further calculations used the X-RAY 76 system of programs.[21] Only 2863 reflections showed $I < 2.0\ \sigma(I)$ and were used in the blocked full-matrix least-squares calculations. Of these, three strong reflections were believed to be affected by secondary extinction and were excluded from the refinement. An analysis of the weighting scheme based on $\sigma^{-2}(F)$ showed a strong bias toward the stronger reflections. Therefore final cycles of least squares used constant weights. Refine-

UM00013034
NOVARTIS EXHIBIT 1017
Novartis v. Regents, IPR2023-01346
Page 1780 of 4460

ment converged with anisotropic temperature factors applied to all atoms, except hydrogen atoms, to $R = (\Sigma||Fo| - |Fc||)/\Sigma|Fo| = 0.064$ and $R_w = \{\Sigma(|Fo| - |Fc|)^2/\Sigma Fo^2\}^{1/2} = 0.057$ with an average shift to error ratio of 0.04. The fractional atomic coordinates, anisotropic temperature factors for nonhydrogen atoms, and isotropic temperature factors for hydrogen atoms are listed in Tables I, II, and III. Figure 1 shows the atom labeling, the bond lengths, and bond angles in the three molecules of the asymmetric unit. The equations of relevant molecular planes and lines are given in Table IV.[22]

TABLE I. Positional parameters with estimated standard deviations ($\times 10^4$) for carbon, oxygen, nitrogen, and sulfur atoms.

PMDA 1	x/a	y/b	z/c
C (1)	1641 (4)	6112 (2)	348 (1)
C (2)	2386 (3)	6382 (2)	828 (1)
C (3)	2112 (3)	7336 (2)	1020 (1)
C (4)	1021 (4)	8097 (2)	746 (1)
C (5)	273 (3)	7808 (2)	265 (1)
C (6)	553 (3)	6859 (2)	73 (1)
C (7)	−926 (4)	8423 (2)	−130 (1)
C (8)	−409 (4)	6853 (2)	−452 (1)
C (9)	3590 (4)	5778 (2)	1226 (1)
C (10)	3181 (4)	7379 (3)	1536 (1)
O (1)	−1559 (3)	9248 (2)	−140 (1)
O (2)	−1267 (2)	7802 (1)	−560 (1)
O (3)	−509 (3)	6199 (2)	−756 (1)
O (4)	3398 (3)	8048 (2)	1829 (1)
O (5)	4029 (3)	6423 (2)	1639 (1)
O (6)	4167 (3)	4928 (1)	1234 (1)
PMDA 2			
C (11)	−3997 (3)	8248 (2)	2874 (1)
C (12)	−5584 (3)	8075 (2)	2956 (1)
C (13)	−5716 (4)	7131 (2)	3180 (1)
C (14)	−4121 (4)	6591 (2)	3310 (1)
C (15)	−2537 (3)	6942 (4)	3225 (1)
C (16)	−2416 (3)	7884 (2)	2998 (1)
C (17)	−1135 (5)	6162 (2)	3405 (1)
C (18)	−3737 (5)	5578 (2)	3563 (1)
C (19)	−6973 (4)	8866 (2)	2772 (1)
C (20)	−4387 (4)	9443 (2)	2618 (1)
O (7)	405 (3)	6130 (2)	3403 (1)
O (8)	−1927 (3)	5359 (1)	3614 (1)
O (9)	−4672 (3)	5022 (2)	3725 (1)
O (10)	−8522 (3)	8879 (2)	2772 (1)
O (11)	−6178 (3)	9669 (1)	2573 (1)
O (12)	−3443 (3)	9998 (2)	2458 (1)
PTZ			
C (21)	7565 (3)	6474 (2)	973 (1)
C (22)	7236 (4)	7460 (2)	1123 (1)
C (23)	5209 (4)	7975 (2)	327 (1)
C (24)	5357 (3)	7062 (2)	86 (1)
C (25)	4494 (5)	6956 (2)	−405 (1)
C (26)	3433 (5)	7737 (3)	−654 (1)
C (27)	3276 (5)	8646 (3)	−413 (2)
C (28)	4134 (4)	8768 (2)	76 (1)
C (29)	8120 (4)	7776 (3)	1601 (1)
C (30)	9257 (4)	7105 (3)	1907 (1)
C (31)	9542 (5)	6122 (3)	1765 (1)
C (32)	8717 (5)	5817 (3)	1294 (2)
N	6030 (4)	8115 (2)	824 (1)
S	6553 (1)	5983 (1)	381 (1)

TABLE II. Anisotropic thermal parameters with estimated standard deviations ($\times 10^3$) for carbon, oxygen, nitrogen, and sulfur atoms.

PMDA 1	U_{11}	U_{22}	U_{33}	U_{12}	U_{13}	U_{23}
C (1)	66 (2)	47 (2)	55 (2)	−0 (1)	16 (1)	−2 (1)
C (2)	63 (2)	59 (2)	48 (2)	−5 (1)	17 (1)	8 (1)
C (3)	56 (2)	72 (2)	40 (2)	−14 (2)	15 (1)	−3 (1)
C (4)	67 (2)	54 (2)	56 (2)	−7 (1)	24 (2)	−14 (1)
C (5)	55 (2)	52 (2)	54 (2)	−4 (1)	16 (1)	2 (1)
C (6)	56 (2)	52 (2)	45 (2)	−8 (1)	11 (1)	−6 (1)
C (7)	59 (2)	70 (2)	66 (2)	−5 (2)	11 (2)	9 (2)
C (8)	65 (2)	60 (2)	58 (2)	−3 (2)	10 (2)	−1 (2)
C (9)	65 (2)	74 (2)	65 (2)	−8 (2)	14 (2)	17 (2)
C (10)	68 (2)	84 (2)	47 (2)	−14 (2)	16 (2)	−1 (2)
O (1)	85 (2)	67 (1)	106 (2)	20 (1)	15 (1)	10 (1)
O (2)	73 (1)	74 (1)	59 (1)	2 (1)	0 (1)	4 (1)
O (3)	115 (2)	86 (2)	56 (1)	−6 (1)	4 (1)	−19 (1)
O (4)	114 (2)	107 (2)	51 (1)	−14 (1)	11 (1)	−24 (1)
O (5)	78 (1)	95 (2)	50 (1)	−5 (1)	4 (1)	11 (1)
O (6)	92 (1)	77 (1)	83 (1)	14 (1)	12 (1)	21 (1)
PMDA 2						
C (11)	61 (2)	49 (2)	41 (2)	−6 (1)	5 (1)	1 (1)
C (12)	55 (2)	53 (2)	47 (2)	−1 (1)	9 (1)	−16 (1)
C (13)	66 (2)	66 (2)	49 (2)	−23 (2)	17 (1)	−12 (1)
C (14)	63 (2)	49 (2)	42 (2)	−9 (1)	12 (1)	−4 (1)
C (15)	59 (2)	50 (1)	46 (2)	−3 (1)	5 (1)	−5 (1)
C (16)	55 (2)	61 (2)	43 (2)	−12 (1)	9 (1)	15 (1)
C (17)	75 (2)	66 (2)	59 (2)	−7 (2)	3 (2)	1 (2)
C (18)	93 (2)	58 (2)	41 (2)	−18 (2)	8 (2)	4 (1)
C (19)	65 (2)	68 (2)	64 (2)	−6 (2)	8 (2)	−21 (2)
C (20)	74 (2)	53 (2)	45 (2)	−8 (2)	2 (2)	−1 (1)
O (7)	64 (1)	88 (2)	121 (2)	4 (1)	9 (1)	17 (1)
O (8)	86 (2)	62 (1)	72 (1)	−3 (1)	−1 (1)	11 (1)
O (9)	122 (2)	65 (1)	75 (2)	−28 (1)	32 (1)	11 (1)
O (10)	63 (1)	82 (2)	128 (2)	5 (1)	19 (1)	−15 (1)
O (11)	72 (1)	58 (1)	68 (1)	2 (1)	0 (1)	−3 (1)
O (12)	100 (2)	66 (1)	76 (2)	−7 (1)	15 (1)	15 (1)
PTZ						
C (21)	51 (2)	66 (2)	75 (2)	−5 (1)	19 (1)	−15 (2)
C (22)	49 (2)	71 (2)	86 (2)	−4 (2)	20 (2)	−24 (2)
C (23)	57 (2)	57 (2)	89 (2)	−6 (1)	28 (2)	−12 (2)
C (24)	60 (2)	58 (2)	68 (2)	−3 (1)	24 (2)	−3 (2)
C (25)	101 (3)	68 (2)	77 (2)	−4 (2)	48 (2)	−3 (2)
C (26)	107 (3)	106 (3)	67 (2)	−6 (2)	34 (2)	12 (2)
C (27)	92 (3)	86 (3)	103 (3)	6 (2)	42 (2)	29 (2)
C (28)	76 (2)	58 (2)	106 (3)	1 (2)	36 (2)	4 (2)
C (29)	71 (2)	95 (2)	88 (3)	−11 (2)	25 (2)	−41 (2)
C (30)	80 (2)	120 (3)	72 (2)	−20 (2)	17 (2)	−13 (2)
C (31)	91 (3)	101 (3)	77 (3)	−7 (2)	19 (2)	−1 (2)
C (32)	87 (2)	67 (2)	99 (3)	−11 (2)	22 (2)	−10 (2)
N	89 (2)	68 (2)	113 (2)	14 (2)	4 (2)	−44 (2)
S	76.4 (5)	59.0 (5)	87.9 (6)	7.1 (4)	5.6 (5)	−27.7 (5)

DISCUSSION

Contrary to expections, the structure of PTZ:$(PMDA)_2$ contains infinite DADA stacks as does the 1:1 complex. The *a* axis is the stack axis. The extra acceptor PMDA molecule (PMDA II) sits outside the stack with its length and the normal to the plane of the molecule approximately perpendicular to the stack axis (67.9° and 89.5°, respectively). The packing is represented in Fig. 2. The sides of the stacks are in van der Waals contact along the *b* direction, but the extra acceptor molecules completely separate the stacks in the *c* direction.

UM00013035
NOVARTIS EXHIBIT 1017
Novartis v. Regents, IPR2023-01346
Page 1781 of 4460

TABLE III. Positional and isotropic thermal parameters ($\times 10^3$) for hydrogen atoms.

PMDA 1	x/a	y/b	z/c	U
H (1)	178 (2)	545 (2)	23 (1)	55 (6)
H (4)	83 (2)	879 (1)	85 (1)	56 (6)
PMDA 2				
H (13)	−691 (3)	688 (2)	322 (1)	71 (2)
H (16)	−127 (2)	815 (1)	296 (1)	56 (6)
PTZ				
H (25)	463 (3)	633 (1)	−57 (1)	47 (6)
H (26)	271 (3)	753 (2)	−101 (1)	98 (9)
H (27)	253 (3)	915 (2)	−58 (1)	73 (7)
H (28)	405 (3)	944 (2)	26 (1)	80 (8)
H (29)	793 (3)	851 (2)	166 (1)	99 (9)
H (30)	990 (3)	734 (2)	226 (1)	86 (8)
H (31)	1032 (4)	557 (2)	203 (1)	130 (10)
H (32)	871 (3)	519 (2)	118 (1)	49 (8)
H (N)	595 (3)	869 (1)	93 (1)	62 (7)

In the 1:1 complex the stacks are in good contact both on their broad and on their narrow side.

The nature of the overlap of adjacent molecules in the stack is shown in side view in Fig. 3 and as viewed along the stack axis in Fig. 4. The increased stack angle causes a greater repeat distance [a = 7.689(3) Å] along the stack in the 1:2 complex than in the 1:1 complex [c = 6.886(1) Å]. However, the interplanar spacing between molecules (half the separation between two consecutive PMDA molecules in the stack along the normals to the planes of the molecules) are identically 3.425 Å. Also the folding of the PTZ molecules is similar in the two structures. The angle between the two planes of the two phenyl rings of PTZ are 175.7° and 176.4°. As in the 1:1 complex all PTZ molecules in one stack are folded in the same direction, thus giving rise to noncentrosymmetric, polar ("pyroelectric") stacks. Point group symmetry, 2/m, is fullfilled by pairs of stacks with mutually opposite polarity, related by interstack inversion centers.

Among the factors that influence the overlap of adjacent aromatic molecules in π-molecular complexes, the tendency for bonds common to two rings to lie over or under the centers of the rings of neighboring molecules is important. Such a tendency seems to play a role in the overlap of adjacent molecules in both stacking modes observed for PTZ and PMDA. However, the steric requirements of the sulfur atom are also important. In the stack found in the 1:1 complex the sulfur atom fits into one of the four clefts of the PMDA molecule above and below formed by a carbonyl group and a central CH group. (H–C–C–C=O). In the 1:1 complex the two clefts are equivalent, related by a cell translation along the stack axis. As a result the line of centers of the PTZ molecules is offset from the line of centers of the PMDA molecules, and the longer PTZ molecules protrude from the stack at one end. Also, the angle between the stack axis and the normal to the plane of the PMDA molecule is small at 5.9°.

In the 1:2 complex the sulfur atom of the PTZ molecule is similarly oriented with respect to the PMDA molecule on the "outside" of the slight fold of the PTZ molecule. The distances from the sulfur atom to the atoms forming the cleft, H(1), C(1), C(2), C(9), O(6) are 3.65(2), 3.758(3), 3.756(3), 3.688(4), and 3.630(3) Å, respectively. However, the cleft of the PMDA molecule on the "inside" of the fold of the PTZ molecule which is

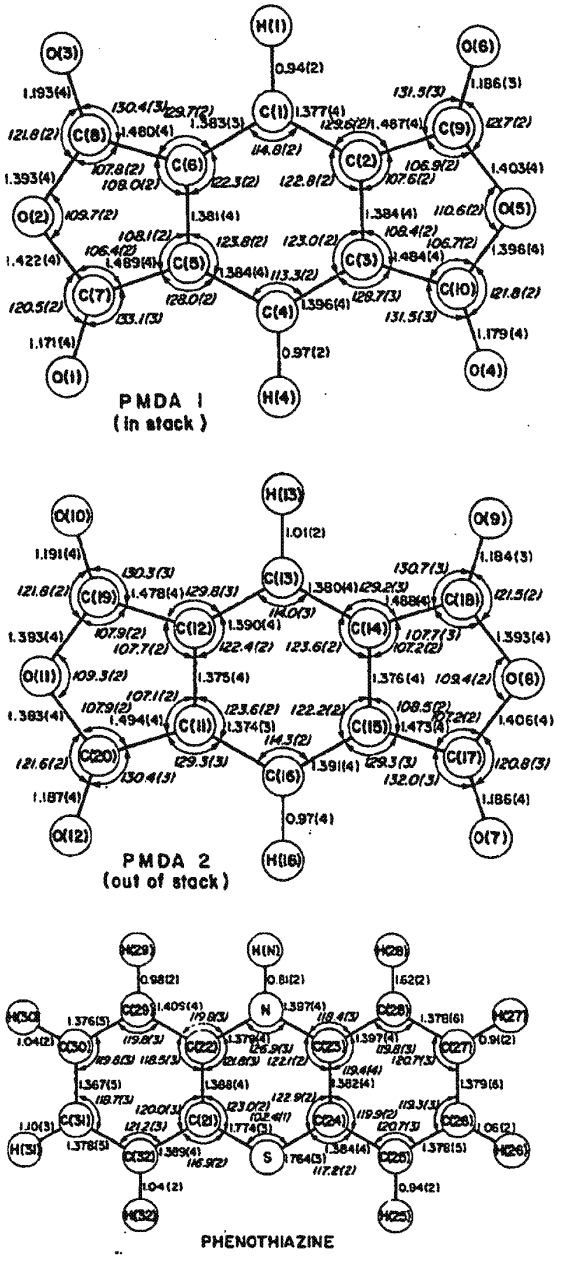


FIG. 1. Atom labeling, bond lengths (Å), and bond angles (°) for PTZ:2PMDA, with estimated standard deviations in parentheses. (a) PMDA(I) (in stack), (b) PMDA(II) (out of stack), (c) PTZ.

UM00013036
NOVARTIS EXHIBIT 1017
Novartis v. Regents, IPR2023-01346
Page 1782 of 4460

TABLE IV. Equations of the least-squares planes and lines.

The x, y, and z axes of the orthogonal coordinate system are in the directions a, b, and c^*, respectively. In that coordinate system:

The plane of the nonhydrogen atoms of the PMDA molecule in the stack (PMDA I) is given by

$$-0.8901x - 0.3673y + 0.2699z = -3.5650.$$

The plane of the nonhydrogen atoms of the PMDA molecule not in the stack (PMDA II) is given by

$$0.0080x + 0.4544y + 0.8908z = 11.8861.$$

The line of the long axis of the PMDA molecule in the stack is given by

$$x = 0.6865 + 0.3764t,$$

$$y = 9.2130 - 0.2645t,$$

$$z = 1.4719 + 0.8879t.$$

The line of the long axis of the molecule PMDA not in the stack is given by

$$x = -5.2667 - 0.3764t,$$

$$y = 9.7329 + 0.8259t,$$

$$z = 8.4357 - 0.4198t.$$

The plane of the phenyl ring of PTZ formed by atoms C (23) to C (28) is given by

$$-0.8888x - 0.3737y + 0.2653z = -6.9736.$$

The plane of the phenyl ring of PTZ formed by atoms C (21), C (22), C (29)–C (32) is given by

$$-0.8796x - 0.3404y + 0.3324z = -6.4880.$$

The plane of PTZ formed by atom C (23), C (24), N, and S is given by

$$-0.9123x - 0.3376y + 0.2317z = -6.7328.$$

The plane of PTZ formed by atoms C (21), C (22), N, and S is given by

$$-0.8600x - 0.3706y + 0.3507z = -6.6080.$$

In terms of a, b, and c and in terms of the unit vectors along x, y, and z (i.e. $\hat{i}$, $\hat{j}$, and $\hat{k}$) the unit normal to the central ring of the PMDA molecule in the stack may be expressed as

$$N = -0.1068a - 0.0284b + 0.0099c,$$

$$N = -0.8901\hat{i} - 0.3673\hat{j} + 0.2699\hat{k}.$$

The angle between this normal and the c axis is 27.1°.

associated with the sulfur atom is that on the opposite side of C(1). This is essentially the stacking mode of PMDA and anthracene in the 1:1 π-molecular complex formed by them.[6] In anthracene:PMDA the stack angle

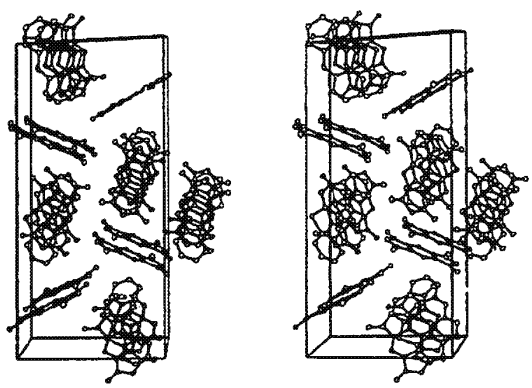


FIG. 2. Stereoscopic drawings of the molecular packing. The c axis points up, the b axis is to the right of the a axis is the stack axis and points out of the page.

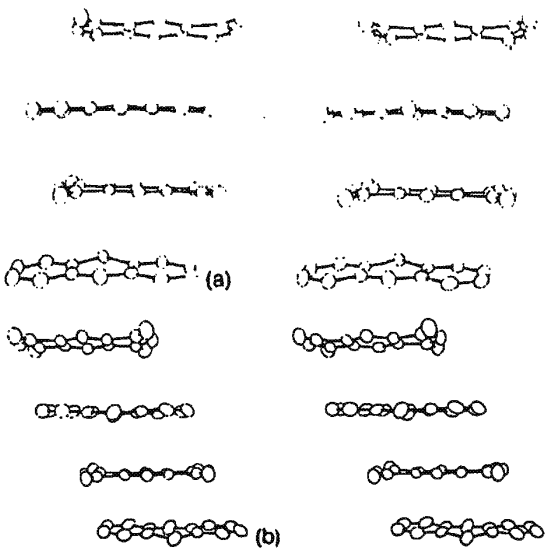


FIG. 3. Side view of the molecular packing and overlap within the stacks (a) 1:1 complex, (b) 1:2 complex.

UM00013037
NOVARTIS EXHIBIT 1017
Novartis v. Regents, IPR2023-01346
Page 1783 of 4460

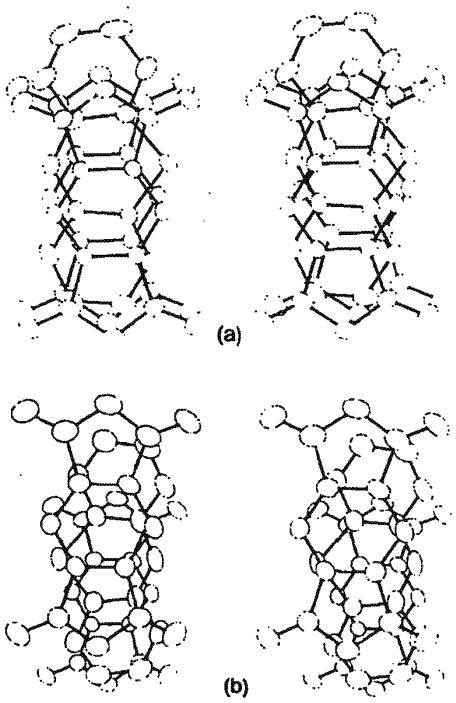


FIG. 4. Stereoscopic drawings of the molecular overlap looking normal to the PMDA molecular plane. (a) 1:1 complex, (b) 1:2 complex.

is 20.7° and the tilt of the molecules is nearly entirely along their long axis. In the 1:2 complex of PTZ with PMDA, the stack angle (between the normal to the PMDA molecule and the stack axis) is greater at 27.1°. However, this tilt contains a significant component of 15.8° along the breadth of the PMDA molecule. The component of the tilt along the long axis of the molecule is 22.1°, similar to the value in the 1:1 complex. The component along the breadth is evident in Figs. 3(b) and 4(b). As a result of the latter component, the sulfur atom of PTZ is brought near the apex of the cleft of the PMDA molecule on the inside of the fold and [S–C(6)] = 3.580(3) Å.

The N atom of PTZ forms close contacts [N–C(3)] = 3.349(4) Å, [N–C(10)] = 3.448(5) Å to the PMDA molecule on the outside of the fold. The closest C–C contacts in the stack are [C(26)–C(8)] = 3.345(5) Å, [C(24)–C(1)] = 3.356(4) Å, and [C(28)–C(5)] = 3.380(4) Å, all between PTZ and the PMDA molecule on the outside of the fold. The close S–C(6) contact seems to prevent a close approach of other atoms to the PMDA molecule on the inside of the fold.

The shortest contact between the atoms in the stack and those in the extrastack PMDA II molecule is [O(4)–O(11)] = 2.926(3) Å. All of the oxygen atoms in PMDA I enter into close contacts with oxygen and carbon atoms of PMDA II, but O(4) forms the shortest contacts. Others are to C(19) [2.937(4)], to C(20) [3.037(4)], to C(12) [3.074(4)], and to C(11) [3.160(4) Å]. Other important intrastack contacts are [S–S] = 3.775(2) Å, [S–H(1)] = 3.02(2) Å, [O(1)–O(1)] = 3.093(3) Å, and [O(6)–O(3)] = 3.159(3) Å. The shortest intramolecular PMDA II to PMDA II contacts are [O(9)–O(12)] = 3.285(4) Å, [O(12)–C(14)] = 3.231(3) Å, and [O(12)–C(18)] = 3.232(3) Å.

The bond lengths and angles within the donor and acceptor molecules are similar in both stacks. The S–C bonds are slightly larger in the 1:2 complex and the N–C bonds are slightly shorter, but the differences are only marginally significant. In both structures the nitrogen atom is hydrogen bonded to an oxygen atom on a PMDA molecule. In the present case the oxygen atom involved is O(9) on the extrastack PMDA molecule. The relevant parameters are [N–O(9)] = 3.077(4) Å, [H(N)–O(9)] = 2.31(2) Å, and [N–H(N)···O(9)] = 158(1)°. The equivalent N–O distance in the 1:1 complex is 3.189(2) Å. The electron density in the 1:2 complex shows no evidence of limited disorder (by N ↔ S interchange) as in the 1:1 complex. Within the available resolution the extrastack PMDA molecule also exhibits no significant geometric difference from the intrastack one.

The presence of the near orthogonal extra acceptor molecule between the ···DADA··· stacks raises several interesting questions with respect to molecular interactions, energy and charge transfer, and charge carrier mobility. It will be important to find out if the extra acceptor molecule, though nearly orthogonal, tends to decrease the energy of the charge transfer transition. Indications that charge transfer interaction is not necessarily dependent upon parallel arrangement of planes containing conjugated π electrons has been obtained recently by a crystal structure analysis of the black–red 1:2 complex between PTZ and phenazine[23] (both forming light yellow crystals in their one-component phases).

Further, since the [1 0 0]-oriented ···DADA··· stacks are "isolated" from one another by the extra PMDA molecules in one dimension ([0 0 1]) in the 1:2 complex it is possible to study how the interstack interactions differ in the close contact [0 1 0] and the isolated [0 0 1] directions; e.g., by measuring the interstack hopping rates of charge transfer excitons. Another interesting but conceptually different problem concerns the anisotropy of the electron and hole mobility tensors. The significance of this question lies in the fact that it has been argued[24] that in D:A complexes the hole band might essentially originate from the highest occupied molecular orbital (HOMO) of the donor molecule, whereas the electron band should be formed by the lowest unoccupied orbitals (LUMO) of the acceptor. Hence in the D:A complexes with extra acceptor (or extra donor)[19] molecules the electron and hole mobility tensors may differ much more in their anisotropy than generally encountered with one-component organic molecular crystals; cf. Ref. 25. UV-photoelectron spectroscopy of PTZ:PMDA and other PMDA complexes has recently established[3] that, besides a small acceptor-induced shift of ~0.25 eV, the hole band is in fact due to the donor HOMOs.

Finally, the apparent absence of disorder in this complex, in contrast to the situation in the 1:1 complex will afford the opportunity to draw conclusions from experimental results on the effect of intrastack disorder

UM00013038
NOVARTIS EXHIBIT 1017
Novartis v. Regents, IPR2023-01346
Page 1784 of 4460

on the intrastack motion of elementary excitations such as excitons or charge carriers.

ACKNOWLEDGMENTS

The authors acknowledge the support of the Natural Sciences and Engineering Research Council of Canada. We are indebted to Professor H. Schulz and K. H. Thiemann at the Max-Planck-Institut für Festkörperforschung Stuttgart for their help with the initial characterization of the crystals and to Professor P. Fischer, Institut für Organische Chemie, Biochemie und Isotopenforschung der Univesität Stuttgart, for chemical elemental analysis. We also thank K. Wolbaum for assistance with the data collection in Regina.

[1] R. Anthonj, N. Karl, B. E. Robertson, and J. J. Stezowski, J. Chem. Phys. 72, 1244 (1980).
[2] N. Karl, *Crystals*, edited by H. C. Freyhardt (Springer, Berlin, 1980), Vol. 4, pp. 59–66.
[3] N. Karl, N. Sato, K. Seki, and H. Inokuchi, J. Chem. Phys. 77, 4870 (1982).
[4] W. Binder, N. Karl, and J. J. Stezowski, Acta Crystallogr. Sect. B 38, 2915 (1982).
[5] J. C. A. Boeyens and F. H. Herbstein, J. Phys. Chem. 69, 2160 (1965).
[6] B. E. Robertson and J. J. Stezowski, Mol. Cryst. Liq. Cryst. 52, 319 (1979); Acta Crystallogr. Sect. B 34, 3005 (1978).
[7] J. J. Stezowski, W. Binder, and N. Karl, Acta Crystallogr. Sect. B 38, 2912 (1982).
[8] D. L. Evans and W. T. Robinson, (unpublished results).
[9] J. C. A. Boeyens and F. H. Herbstein, J. Phys. Chem. 69, 2153 (1965).
[10] M. LeBars-Combe, B. Chion, and J. Lajzérowicz-Bonneteau, Acta Crystallogr. Sect. B 35, 913 (1979); M. LeBars-Combe and J. Lajzérowicz-Bonneteau, *ibid.* 37, 1707 (1981); 38, 162 (1982).
[11] D. L. Evans and W. T. Robinson, Acta Crystallogr. Sect. B 33, 2891 (1977).
[12] N. Karl, W. Ketterer, and J. J. Stezowski, Acta Crystallogr. Sect. B 38, 2917 (1982).
[13] I. V. Bugarovskaya, V. M. Vozzhennikov, V. P. Krasavin, B. V. Kotov, and L. Ya. Karpov, Cryst. Struct. Commun. 11, 501 (1982) (a different choice of the axes than in Ref. 12 has been used by these authors).
[14] F. H. Herbstein and J. A. Snyman, Philos. Trans. R. Soc. London Ser. A 264, 635 (1969).
[15] D. L. Evans and W. T. Robinson (unpublished results).
[16] J. D. Bell, J. F. Blount, O. V. Briscoe, and H. C. Freeman, Chem. Commun. 1968, 1656.
[17] T. Uchida, M. Ito, and K. Kozawa, Bull. Chem. Soc. Jpn. 56, 577 (1983).
[18] N. Karl, W. Binder, P. Kollat, and J. J. Stezowski, Acta Crystallogr. Sect. B 38, 2919 (1982).
[19] A. W. Hanson, Acta Crystallogr. Sect. B 34, 2339 (1978).
[20] A. C. Larson and E. J. Gabe, *Computing in Crystallography*, edited by H. Shenk, R. Olthof-Hazekamp, H. van Koningsveld, and G. C. Bassi (Delft University, The Netherlands, 1978), pp. 81–89.
[21] J. M. Stewart, P. A. Machin, C. W. Dickinson, H. L. Ammon, H. Heck, and H. Flack, Technical Report TR-446, University of Maryland, Computer Science Center, College Park, MD, (1976).
[22] See AIP document No. PAPS JCPSA-81-1522-26 for 26 pages of supplementary material containing observed and calculated structure factors. Order by PAPS number and journal reference from American Institute of Physics, Physics Auxiliary Publication Service, 335 East 45th Street, New York, NY 10017. The price is $1.50 for each microfiche (98 pages) or $5.00 for photocopies of up to 30 pages, and $0.15 for each additional page over 30 pages. Airmail additional. Make checks payable to the American Institute of Physics.
[23] J. J. Stezowski, R. D. Stigler, N. Karl, and K. Schuller, Mol. Cryst. Liq. Cryst. 94, 243 (1983).
[24] N. Karl and J. Ziegler, Chem. Phys. Let. 32, 438 (1975).
[25] N. Karl, in *Properties of Organic Semiconductors*, edited by O. Madelung, M. Schulz, and H. Weiss (Springer, Berlin, 1985), Vol. III/17i.

UM00013039
NOVARTIS EXHIBIT 1017
Novartis v. Regents, IPR2023-01346
Page 1785 of 4460

This Page is Inserted by IFW Indexing and Scanning Operations and is not part of the Official Record

BEST AVAILABLE IMAGES

Defective images within this document are accurate representations of the original documents submitted by the applicant.

Defects in the images include but are not limited to the items checked:

- ☐ BLACK BORDERS
- ☐ IMAGE CUT OFF AT TOP, BOTTOM OR SIDES
- ☐ FADED TEXT OR DRAWING
- ☐ BLURRED OR ILLEGIBLE TEXT OR DRAWING
- ☐ SKEWED/SLANTED IMAGES
- ☐ COLOR OR BLACK AND WHITE PHOTOGRAPHS
- ☐ GRAY SCALE DOCUMENTS
- ☐ LINES OR MARKS ON ORIGINAL DOCUMENT
- ☐ REFERENCE(S) OR EXHIBIT(S) SUBMITTED ARE POOR QUALITY
- ☐ OTHER: _____

IMAGES ARE BEST AVAILABLE COPY.
As rescanning these documents will not correct the image problems checked, please do not report these problems to the IFW Image Problem Mailbox.

Crystallisation of supramolecular materials

Hans-Beat Bürgi*, Jürg Hulliger†‡, Philip J Langley†§

The design and synthesis of crystalline materials with tailor-made properties is one of the more difficult and therefore challenging tasks in supramolecular chemistry. Increasingly, both the properties and the structures of the molecular building blocks are being optimised prior to crystallisation, with special emphasis being given to the design of directional intermolecular interaction sites. Multicomponent systems such as co-crystals are gaining in attractiveness because they allow greater synthetic flexibility and thus enhance diversity in the structures and properties of the final crystals. Several new techniques for monitoring growth behaviour (often *in situ*) at the crystal surface have been reported. There is a clear need to understand in more detail the fundamental processes taking place in the early stages of the supramolecular synthesis.

Addresses
*Laboratory for Chemical and Mineralogical Crystallography, University of Berne, Freiestrasse 3, CH-3012 Berne, Switzerland;
e-mail: hans-beat.buergi@krist.unibe.ch
†Department of Chemistry and Biochemistry, University of Berne, Freiestrasse 3, CH-3012 Berne, Switzerland
‡e-mail: juerg.hulliger@iac.unibe.ch
§e-mail: philip.langley@iac.unibe.ch

Correspondence: Bürgi and Hulliger

Current Opinion in Solid State & Materials Science 1998, 3:425–430

Electronic identifier: 1359-0286-003-00425

© Current Chemistry ISSN 1359-0286

Abbreviations

A	acceptor
D	donor
NLO	nonlinear optical

Introduction

The contemporary chemical literature tends to give the impression that any crystal built from discernible molecular entities and held together by noncovalent interactions, is a representative supramolecular material. For the present opinion, we adopt a somewhat more restricted view and consider primarily stable molecular crystals displaying specific physical and chemical properties which are intimately related to the supramolecular organisation, or have their origin in the crystal growth process.

Dunitz [1] has described molecular crystals as 'supermolecules par excellence'. By analogy, crystallisation is the ultimate challenge in supramolecular synthesis, an assertion which is easily justified when considering the multitude of design strategies employed by Nature in the assembly of (mineralised) biological materials [2]. Crystallisation of supramolecular materials, like any synthetic procedure, involves a number of conceptual steps: firstly, the search for molecules with optimised molecular properties, for example, polarity, large molecular hyperpolarisabilities, extended π-orbital delocalisation, chirality, unpaired spins, and so on; secondly, analysis of noncovalent interactions, their strength and directionality [3]; thirdly, the search for molecules or combinations of molecules which produce stable and robust structural motifs in one, two and three dimensions [3]; fourthly, the study of the mechanisms of the crystallisation process; and fifthly, characterisation of possible intermediates and of the final products with respect to their structural, physical and chemical properties. In practice, the evolution of molecular crystals from their precursor molecules is one of the more complicated chemical processes, and it can be divided into several steps: from molecules to aggregates to nanocrystals, and finally, to macroscopic crystals (Figure 1). With each step can be associated a number of characteristic synthesis conditions such as the purity and physical state of the reactants (e.g. gas, solution, or melt), temperature, pressure, concentration, and their gradients in space and time. A utopian approach to engineering crystalline materials with tailor-made properties would be to understand comprehensively each of the conceptual and practical aspects mentioned above. This would permit us to influence and control the supramolecular synthesis at each point along its reaction coordinate. In any practical problem, however, there is only limited information or experience available on each of these points, and intuition, probability and even serendipity, have their roles to play.

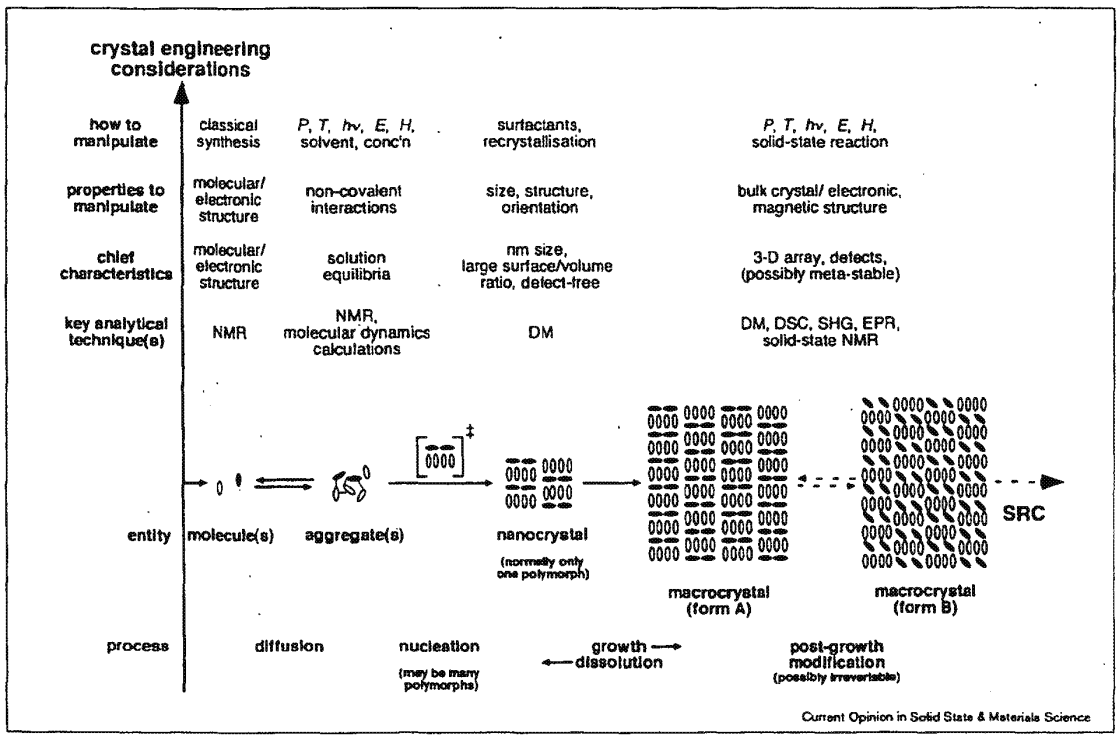
Commenting in detail on all aspects of Figure 1 would not only exceed the space allowed but also stretch our combined expertise! We have therefore chosen to present some recent (1997–1998) achievements in two areas which, in our opinion, have advanced at all stages the science and art of engineering the physical and chemical properties of solid state supramolecular materials: first, characterisation of specific aspects of the reaction coordinate in Figure 1; and second, ways in which to control the course and outcome of a crystallisation.

Choice of molecular building blocks

The molecular properties of the starting materials for crystallisation must be optimised in two respects: they must be conducive to the desired crystal properties and they should ensure aggregation into a suitable crystal structure. The two conditions are not always compatible; for example, whilst dipolar molecules with extended π-systems are the staple source of materials for nonlinear optical (NLO) applications [4], they often crystallise into centrosymmetric space groups. An alternative is to use octupolar molecules (i.e. those with zero net dipoles), for example, branched cyanine or *tris*acceptor-substituted benzene and triazine molecules which possess three-fold symmetry and

UM00013041
NOVARTIS EXHIBIT 1017
Novartis v. Regents, IPR2023-01346
Page 1787 of 4460

Figure 1



Crystallisation viewed as a supramolecular synthesis. The nature of the entities employed or produced, and the processes involved, as the synthesis proceeds along its supramolecular reaction coordinate (SRC) are illustrated. Considerations to be made when attempting to control such a synthesis are presented on the ordinate. Note that the macroscopic crystal obtained (form A) may not be the final product: external interference may change (reversibly or irreversibly) the packing, conformation and electronic structure of the molecular building blocks, giving rise to different bulk crystal properties (form B). DM, diffraction methods; DSC, differential scanning calorimetry; EPR, electron paramagnetic resonance; SHG, second harmonic generation.

significant off-diagonal elements of the molecular hyperpolarisability tensor, β [5•,6].

Hydrogen–bonding interactions continue to be exploited to control order and dimensionality in molecular organic magnets based on substituted α-nitronyl nitroxide radicals [7–9]. In a magneto-structural study on such materials, one group [7] was able to correlate the observed magnetic properties with the molecular packing. Weak C-H···O(-N) interactions seem to play a significant orienting role. Whilst in most examples coupling is anti-ferromagnetic, the interactions differ markedly in dimensionality and strength. The dithiadiazolyl radical, *p*-NC-C_6F_4-CNSSN•, is remarkable because the unpaired electron density associated with the heterocyclic ring has been proposed (after extensive characterisation) to couple throughout the whole 3D lattice *via* strong, directional, intermolecular S···N contacts [10]. The ordering temperature in the β-form is the highest to date for a purely organic free radical (36K).

The introduction into crystal synthesis of additional molecular entities, for example, a counter-ion or a hydrogen-bonding partner molecule, opens up the possibility of co-crystal formation. Such additions (which can be individually tailor-made) give enhanced synthetic flexibility; however, their use has to be weighed against the increased complexity inherent to multicomponent systems. Strategies for generating NLO co-crystals have been illustrated with merocyanine-type dye molecules combined with *para*-acceptor-substituted phenolic compounds [4,11••]. Highly polar co-crystals were obtained from solution, and were found to be composed of two-component polar strings with an almost perfect alignment for the electro-optic effect. The relative orientation of the molecules in the crystal structure could be altered through careful structural modifications of the molecular aggregates, permitting tuning of the NLO properties. Complete transfer of acidic protons (from, for example, *p*-A-substituted phenols to *p*-D-substituted pyridines) is another way to enhance NLO responses in organic acid/base co-crystals [12].

UM00013042
NOVARTIS EXHIBIT 1017
Novartis v. Regents, IPR2023-01346
Page 1788 of 4460

The role of the second molecular component as a structure-directing template is cleverly illustrated by a series of metal-oxalate framework structures. Crystallisation of $[M^{z+}(oxalate)_3]^{(6-z)-}$ building blocks and additional metal ions in the presence of templating *tris*-bipyridine metal complexes, leads to chiral 3D metal-oxalate networks which encapsulate the chiral templates [13]. The same units, together with tetra-substituted ammonium or phosphonium cations produce 2D honeycomb sheet structures. Here, control of dimensionality helps to govern the interactions of the spins of neighbouring metal ions, and eventually, the magnetic properties of the solid.

Auxiliary molecular components may direct crystallisation without necessarily being incorporated into the final solid. A recent example is the cocrystallisation of benzene-1,3,5-tricarboxylic acid ($BTCH_3$) with transition-metal salts in the presence of various bases [14]. The latter control the deprotonation of $BTCH_3$, the coordination environment of the metal ion, and affect the dimensionality of the porous network structure. When a strong, non-coordinating base is used, cubic channel structures are formed whose calculated pore volume is ~44%. Flushing with N_2 removes a substantial amount of solvent but does not destroy the porous network.

An illustration of the enhanced synthetic flexibility derived from multicomponent systems comes again from the field of porous molecular solids (organic zeolites). Guanidinium cations and alkyl- or arylsulphonate anions form two-dimensional, hydrogen-bonded sheets, in which every cation is bonded *via* three pairs of hydrogen bonds to three anions and *vice versa* [15]. These supramolecular 'modules' are robust in the sense that their general structural features are maintained when changes in ancillary functional groups are made. Replacing the monosulphonate by disulphonate ions leads to pillared, porous bilayer motifs whose height can be varied by varying the length of the disulphonate anions; increasing their widths leads to continuous layer stacking. This structure can adapt somewhat to the shape of included guest molecules and happens to be quite selective for 1-alkanenitrile guests.

Aggregation and nucleation

Aggregation of molecular building blocks in solution may be considered as a kind of pre-equilibrium process, which in all probability influences the subsequent nucleation step [16••]. The pre-equilibria depend on the competition between solute–solute and solute–solvent interactions, and thus on the solvent. Aggregation constants are often small, making it difficult to obtain even qualitative information on aggregate structures and their frequency of occurrence. NMR experiments as a function of concentration or temperature are used in the related field of supramolecular solution chemistry to provide information of this type [17]. Molecular dynamics calculations are a powerful theoretical alternative [16••].

The bottleneck in characterising crystallisation processes is probably nucleation. As there are many different types of molecular aggregates, it is likely that several polymorphic nuclei are formed initially; moreover, crystal structure predictions usually suggest the formation of several polymorphs in a narrow energy range [16••]. In general, however, only one crystal form survives the growth process. Methods of probing the nucleation phase are mostly indirect, for example, crystallising in the presence of additives (often the solvent itself) which suppress the growth of the 'naturally' dominant phase [18]. In one recent example, careful selection of the solvent and the crystallisation method permitted the selective growth of all three known crystal polymorphs of an organic hydrazone-based NLO molecule [19•].

Nanocrystals

Nanocrystals are the stable product of the kinetically controlled nucleation process, and can be characterised using methods that are also employed for their macroscopic descendants [20]. Nanocrystalline structures resemble those of the corresponding bulk solid, but are essentially free of defects. Their physical and chemical properties, for example, phase behaviour, density of electronic states and remanent magnetisations, scale smoothly with their size. In contrast to extended solids, they convert from one structure to another by single nucleation events; the transformation obeys simple kinetics and the barrier heights increase with nanocrystal size, at least up to the point where multiple nucleation events set in. The properties of nanocrystals are also sensitive to the surrounding medium, as they are characterised by a large surface:volume ratio [20]. Although these observations have been made for the binary phase CdSe, scaling phenomena may also be relevant to the behaviour of molecular nanocrystals. The size, structure and orientation of nanocrystals in a matrix can be controlled using novel techniques such as metastable phase recrystallisation [21].

Monitoring crystal growth

There are many open questions concerning the crystal growth process and its influence on the properties of the finished product. Grazing incidence X-ray diffraction (GID) complements atomic force microscopy as a method of characterising surfaces of molecular crystals at atomic resolution and under conditions of crystal growth or dissolution. The technique has the potential for investigating the nature of the entities which are added to the crystal surface during growth [22]. Second-harmonic microscopy (SHM) is a sensitive technique used to probe symmetries and local order of NLO-active molecules on surfaces [23]. While their arrangement may be centrosymmetric in the bulk, it lacks this symmetry at the surface. This makes SHM a fascinating new method of sensing *in situ* a large variety of interfaces.

Molecular factors governing crystal growth

The general hypothesis in crystal growth is that the crystal surface directs the attachment of incoming molecules

UM00013043
NOVARTIS EXHIBIT 1017
Novartis v. Regents, IPR2023-01346
Page 1789 of 4460

according to the rules prescribed by the space group of the macroscopic crystal structure. Although this assumption is a reasonable one, given the high degree of order in most crystal structures, it does not always hold. The polycyclic hydrocarbon perhydrotriphenylene forms a host lattice with apolar centrosymmetric channels (at least on average), and includes polar donor-acceptor (D-A) guest molecules in a macroscopically polar fashion [24–26]. This phenomenon has been studied using several experimental methods, including the fairly novel technique of scanning pyroelectric microscopy [27]. Somewhat surprisingly, polarity is not due to the structure of the crystal nuclei (which may be apolar), but to the nature and frequency of the defects introduced into the growing crystal. Although the formation of (bulk)DA···DA(surface) interactions predominates, there are also two types of defects: (bulk)AD···DA(surface) and (bulk)DA···AD(surface). If the former are formed preferentially, the D-groups on the growing crystal surface eventually die out and large domains of uniform polarity develop. A Markov model of crystal growth shows how defect generation and discrimination can be harnessed to control in a logical fashion the properties of the macroscopic crystal [24,25,28].

Other factors governing crystal growth

The final properties of the crystal can be influenced advantageously by crystallising from the melt. The orientation of an azo-dye crystal prepared in this manner between two conducting (indium-tin-oxide coated) glass slides could be manipulated during growth by an applied electric field [29]. The procedure did not change the crystal structure of the azo-dye but improved considerably its photoconducting properties. For multicomponent supramolecular crystals, incongruent melting behaviour may pose a serious problem. Therefore, the characterisation of such systems using often-overlooked thermodynamic techniques is vital [30].

Crystallisation from the vapour phase is important when dealing with insoluble or solvent-labile materials [10]. For example, highly oriented, single crystalline thin films of the high-melting compound α-octithiophene have been prepared, simply by controlling the sublimation deposition rate [31]. These single crystal films fulfil many of the conditions required for a molecular laser crystal (molecular orientation, high structural anisotropy and chemical purity, luminescence), and have provided the first evidence of stimulated emission from a single-component organic crystal [32•].

Although there is still no general or reliable scheme to predict molecular packing (not even if the conditions of crystallisation are specified), there are still a number of empirical and probabilistic rules to fall back on. For example, 15–20% of molecular compounds crystallise in the chiral space groups $P2_1$ and $P2_12_12_1$, both of which provide the chiral molecular environment necessary to effect solid state asymmetric synthesis from achiral precursor molecules. Such statistics, together with the widespread occurrence of polymorphs, have undoubtedly been an important factor in the discovery of many useful enantioselective topochemical photoreactions [33]. Statistics limited to specific families of molecules also improve the odds of probabilistic approaches [34].

Manipulation of crystal properties after growth

The properties of the final macroscopic crystal can be further manipulated *via* the external parameters given in Figure 1. Temperature-induced changes in the crystal structure and its properties are well-known (e.g. the pyroelectric effect [27]). A recent paper has described for the first time total reversibility in the photoswitching of the NLO response of photochromic crystals of *N*-salicylidene-4-bromoaniline [35]. Perhaps the most striking, recent example of post-growth modification concerns elemental sulphur. Application of high pressure (93 GPa) converts this insulating molecular solid into a superconductor with a transition temperature of 10.1K, increasing linearly to 17K near 160 GPa [36•]. Pressure, temperature and light, are all powerful means to elicit structure and property changes in the solid state.

Conclusion

In this comment we have tried to illustrate that crystallisation of molecular materials has several aspects. On the one hand, it is a matter of choosing molecular building blocks with optimised physical and chemical properties and with properly positioned intermolecular interaction sites. On the other hand, it also requires careful consideration of numerable other factors because they can be equally decisive in affecting the outcome of the supramolecular synthesis as it proceeds along its reaction coordinate. The understanding of many of these factors is still quite limited. Interesting challenges lie ahead.

Note added in proof

A more comprehensive paper by Thalladi *et al.* [37] on a related family of molecules as that described in [5•] has come to light during proof reading, and is recommended to the reader.

Acknowledgements

We would like to thank L Leiserowitz and JF Stoddart for giving us the opportunity to present our views on this stimulating and rapidly flourishing area of supramolecular chemistry.

References and recommended reading

Papers of particular interest, published within the annual period of review, have been highlighted as:

- • of special interest
- •• of outstanding interest

1. Dunitz JD: **Thoughts on crystals as supermolecules.** In *The Crystal as a Supramolecular Entity – Perspectives in Supramolecular Chemistry Volume 2.* Edited by Desiraju GR. Chichester: John Wiley & Sons; 1996:1-30.
2. Weiner S, Addadi L: **Design strategies in mineralized biological materials.** *J Mater Chem* 1997, 7:689-702.
3. Desiraju GR: **Crystal engineering: solid state supramolecular synthesis.** *Curr Opin Solid State Mater Sci* 1997, 2:451-454.
4. Wong MS, Bosshard C, Günter P: **Crystal engineering of molecular NLO materials.** *Adv Mater* 1997, 9:837-842.

UM00013044
NOVARTIS EXHIBIT 1017
Novartis v. Regents, IPR2023-01346
Page 1790 of 4460

5. Thalladi VR, Brasselet S, Bläser D, Boese R, Zyss J, Nangia A, • Desiraju GR: **Engineering of an octupolar non-linear optical crystal: tribenzyl isocyanurate.** *Chem Commun* 1997:1841-1842.
In dipolar NLO-active molecules, the β_{zzz} component of the molecular hyperpolarisability tensor (along the charge-transfer axis) is the most important optimisation parameter, whereas in trigonal octupolar molecules, off-diagonal elements are significant too. An advantage of octupolar systems is the fact that the crucial efficiency-transparency trade-off is optimised: the absorption wavelengths of such molecules are not as long as those normally found for their highly conjugated dipolar analogues, and therefore the frequency-doubled radiation is not re-absorbed by the crystal. A clever marriage of advanced theoretical thinking with conceptual crystal engineering strategies has led, in the case of the title molecule, to a non-centrosymmetric network structure held together by weak C-H···O interactions, and showing many of the desired properties.

6. Wortmann R, Glania C, Krämer P, Matschiner R, Wolff JJ, Kraft S, Treptow B, Barbu E, Längle D, Görlitz G: **Nondipolar structures with threefold symmetry for nonlinear optics.** *Chem Eur J* 1997, 3:1765-1773.

7. Jürgens O, Cirujeda J, Mas M, Mata I, Cabrero A, Vidal-Gancedo J, Rovira C, Molins E, Veciana J: **Magnetostructural study of substituted α-nitronyl aminoxyl radicals with chlorine and hydroxy groups as crystalline design elements.** *J Mater Chem* 1997, 7:1723-1730.

8. Akita T, Kobayashi K: **Magnetic properties of nitronyl nitroxide radicals substituted in phenylboronic acid: the BOH···O hydrogen bond as a constituent unit of a one-dimensional suprastructure exhibiting a ferromagnetic spin interaction.** *Adv Mater* 1997, 9:346-348.

9. Matsushita MM, Izuoka A, Sugawara T, Kobayashi T, Wada N, Takeda N, Ishikawa M: **Hydrogen-bonded organic ferromagnet.** *J Am Chem Soc* 1997, 119:4369-4379.

10. Palacio F, Antorrena G, Castro M, Burriel R, Rawson JM, Smith JNB, Bricklebank N, Novoa J, Ritter C: **High-temperature magnetic ordering in a new organic magnet.** *Phys Rev Lett* 1997, 79:2336-2339.

11. Wong MS, Pan F, Bösch M, Spreiter R, Bosshard C, Günter P, •• Gramlich V: **Novel electro-optic molecular cocrystals with ideal chromophoric orientation and large second-order optical nonlinearities.** *J Opt Soc Am B* 1998, 15:426-431.
Parallel alignment of dipolar NLO-active molecules is a prerequisite to maximising the electro-optic coefficient, r of the bulk material (in this case, a crystal). Many methods of achieving this suffer from their tendency to dilute the NLO-active component. It seems that a two-component approach, with carefully selected molecular units, can realise the former requirement without falling foul of the latter. The present authors, building upon extensive experience in this particular field, have been rewarded with one of the first examples of a geometrically and electronically optimised electro-optic crystal. The r values obtained are similar to those found for $LiNbO_3$, a commercially exploited material.

12. Evans CC, Bagieu-Beucher M, Masse R, Nicoud J-F: **Nonlinearity enhancement by solid-state proton transfer: a new strategy for the design of nonlinear optical materials.** *Chem Mater* 1998, 10:847-854.

13. Decurtins S, Schmalle H, Pellaux R: **Polymeric two- and three-dimensional transition-metal complexes comprising supramolecular host-guest systems.** *New J Chem* 1998:117-121.

14. Yaghi OM, Davis CE, Li G, Li H: **Selective guest binding by tailored channels in a 3-D porous zinc(II)-benzenetricarboxylate network.** *J Am Chem Soc* 1997, 119:2861-2868.

15. Russell VA, Evans CC, Li W, Ward MD: **Nanoporous molecular sandwiches: pillared two-dimensional hydrogen-bonded networks with adjustable porosity.** *Science* 1997, 276:575-579.

16. Gavezzotti A, Filippini G: **Self-organization of small organic •• molecules in liquids, solutions and crystals: static and dynamic calculations.** *Chem Commun* 1998:287-294.
This feature article is a candid and clear exposition of the computational methods available at present which complement experimental methods for studying all stages of crystallisation. The methods of calculation available (quantum mechanical, Monte Carlo, molecular dynamics) to model various aspects of the crystallisation procedure (see Figure 1 in the main text of our review) are discussed in terms of their scope and limitations. Given the shortage of other methods to monitor the crucial early stages of crystallisation, such calculations add significantly to our understanding of the kinetic and thermodynamic processes taking place between the molecular engineering and crystal growth steps of the supramolecular reaction coordinate.

17. Ashton PR, Boyd SE, Claessens CG, Gillard RE, Menzer S, Stoddart JF, Tolley MS, White AJP, Williams DJ: **A novel type of isomerism in [3]catenanes.** *Chem Eur J* 1997, 3:788-798.

18. Weissbuch I, Leiserowitz L, Lahav M: **"Tailor-made" and charge-transfer auxiliaries for the control of the crystal polymorphism of glycine.** *Adv Mater* 1994, 6:952-956.

19. Pan F, Bosshard C, Wong MS, Serbutoviez C, Schenk K, Gramlich V, • Günter P: **Selective growth of polymorphs: an investigation of the organic nonlinear optical crystal 5-nitro-2-thiophenecarboxaldehyde-4-methylphenylhydrazone.** *Chem Mater* 1997, 9:1328-1334.
Polymorphism is often regarded as an irritating problem by the various disciplines of materials synthesis. Yet, by taking the time to examine the phenomenon, it is often possible to control it in a useful way. Here, the authors developed methods to obtain selectively all three of the polymorphs known for the title compound. By analysing the different intermolecular forces present in the respective crystal structures, they were able to rationalise whether a particular polymorph was formed either under kinetic or thermodynamic control, and to adjust the growth conditions accordingly. Only one of the polymorphs is non-centrosymmetric (a prerequisite for second harmonic generation), thus highlighting the utility of selective polymorph growth.

20. Alivisatos AP: **Nanocrystals: building blocks for modern materials design.** *Endeavour* 1997, 21:56-60.

21. Budai JD, White CW, Withrow SP, Chisholm MF, Zhu J, Zuhr RA: **Controlling the size, structure and orientation of semiconductor nanocrystals using metastable phase recrystallization.** *Nature* 1997, 390:384-386.

22. Gidalevitz D, Feidenhans'l R, Matlis S, Smilgies D-M, Christensen MJ, Leiserowitz L: **Monitoring in situ growth and dissolution of molecular crystals: towards determination of the growth units.** *Angew Chem Int Ed Engl* 1997, 36:955-959.

23. Försheimer M, Bösch M, Brillert C, Wierschem M, Fuchs H: **Second-harmonic microscopy – a quantitative probe for molecular surface order.** *Adv Mater* 1997, 9:1061-1065.

24. Hulliger J, Rogin P, Quintel A, Rechsteiner P, König O, Wübbenhorst M: **The crystallization of polar, channel-type inclusion compounds: property-directed supramolecular synthesis.** *Adv Mater* 1997, 9:677-680.

25. König O, Bürgi H-B, Armbruster T, Hulliger J, Weber T: **A study in crystal engineering: structure, crystal growth, and physical properties of a polar perhydrotriphenylene inclusion compound.** *J Am Chem Soc* 1997, 119:10632-10640.

26. Hulliger J, Langley PJ, König O, Roth SW, Quintel A, Rechsteiner P: **A supramolecular approach to the parallel alignment of nonlinear optical molecules.** *Pure Appl Opt* 1998, 7:221-227.

27. Hulliger J, Quintel A, Wübbenhorst M, Langley PJ, Roth SW, Rechsteiner P: **Theory and pyroelectric characterization of polar inclusion compounds of perhydrotriphenylene.** *Opt Mater* 1998, 9:259-264.

28. Harris KDM, Jupp PE: **Mathematical analysis of the alignment of guest molecules in solid one-dimensional inclusion compounds: the design of materials for applications in non-linear optics.** *Chem Phys Lett* 1997, 274:525-534.

29. Liu C-Y, Lynch V, Bard AJ: **Effect of an electric field on the growth and optoelectronic properties of quasi-one-dimensional organic single crystals of 1-(phenylazo)-2-naphthol.** *Chem Mater* 1997, 9:943-949.

30. White MA, Hamish RS: **Thermodynamic studies of two different inclusion compounds with the same guest: toward a general understanding of melting behavior in binary compounds.** *Chem Mater* 1998, 10:833-839.

31. Fichou D, Teulade-Fichou M-P, Horowitz G, Demanze F: **Thermal and optical characterization of high purity α-octithiophene.** *Adv Mater* 1997, 9:75-80.

32. Fichou D, Delysse S, Nunzi J-M: **First evidence of stimulated • emission from a monolithic organic single crystal: α-octithiophene.** *Adv Mater* 1997, 9:1178-1181.
Single crystal organic lasers are a very rare breed of molecular-based devices. As the authors point out, previous examples were normally two-

UM00013045
NOVARTIS EXHIBIT 1017
Novartis v. Regents, IPR2023-01346
Page 1791 of 4460

component materials: one main component acting as the laser host and the other component (typically 0.2% w/w) acting as the fluorescent emitter. Whilst the present use of a single-component, monocrystalline system does not yet produce laser action, the authors have some interesting ideas as to how this could eventually be realised. The results reported here are a commendable step forward and should 'stimulate' further work in this field.

33. Sakamoto M: **Absolute asymmetric synthesis from achiral molecules in the chiral crystalline environment.** *Chem Eur J* 1997, 3:684-689.

34. Wu L-C, Cheer CJ, Olovsson G, Scheffer JR, Trotter J, Wang S-L, Liao F-L: **Crystal engineering for absolute asymmetric synthesis through the use of *meta*-substituted aryl groups.** *Tet Lett* 1997, 38:3135-3138.

35. Nakatani K, Delaire JA: **Reversible photoswitching of second-order nonlinear optical properties in an organic photochromic crystal.** *Chem Mater* 1997, 9:2682-2684.

36. Struzhkin VV, Hemley RJ, Mao H-K, Timofeev YA: **Superconductivity at 10–17K in compressed sulphur.** *Nature* 1997, 390:382-384.

The results reported here are quite exciting and refreshing. Research into molecular-based superconductors has tended to stagnate around the preparation and characterisation of multitudes of derivatives of just a few special families (e.g. the BEDT-TTF system). These new results were obtained using a fairly new, highly sensitive and noninvasive magnetic susceptibility technique, combined with diamond-anvil cell methods in the megabar range. The authors point out that the relative simplicity of elemental sulphur should facilitate electronic structure calculations, and knowledge of its various polymorphs at high pressure should allow the testing of new proposed mechanisms of superconduction.

37 Thalladi VR, Brasselet S, Weiss H-C, Bläser D, Carrell HL, Boese R, Zyss J, Nangia A, Desiraju GR: **Crystal engineering of some 2,4,6-triaryloxy-1,3,5-triazines: octupolar nonlinear materials.** *J Am Chem Soc* 1998, 120:2563-2577.

UM00013046
NOVARTIS EXHIBIT 1017
Novartis v. Regents, IPR2023-01346
Page 1792 of 4460

Solid-State Pharmaceutical Chemistry

S. R. Byrn,*,† R. R. Pfeiffer,† G. Stephenson,† D. J. W. Grant,‡ and W. B. Gleason§

Department of Medicinal Chemistry and Pharmacognosy, Purdue University, West Lafayette, Indiana, 47907 and Department of Pharmaceutics and Department of Laboratory Medicine and Pathology, Biomedical Engineering Center, University of Minnesota, Minneapolis, Minnesota 55455

Received February 8, 1994. Revised Manuscript Received June 24, 1994•

Solid-state pharmaceutical chemistry encompasses a wide range of studies on pharmaceutical solids including (1) determination of the physical properties of polymorphs and solvates, (2) physical transformations between polymorphs and solvates, (3) chemical reactions in the solid state, and (4) solid–solid reactions which occur in pharmaceutical preparations. Recent advances in this field include improved understanding of crystallization processes, improved understanding of the need for characterization of polymorphs and solvates for both control and regulatory purposes, and a better understanding of the mechanisms of solid-state degradations and solid–solid reactions. This review will briefly describe recent advances in the following areas: (1) crystallization and the properties of crystals of pharmaceutical solids; (2) characterizations of crystal forms of drugs using solid-state NMR spectroscopy.

The study of the solid-state chemistry of drugs not only encompasses many scientific disciplines but also impinges on virtually all phases of the pharmaceutical industry, from discovery to successful marketing. It is clear that an understanding of the molecular structure of the solid state can lead to better design and control of drug performance.

The mission of those working in the field of solid-state pharmaceutical chemistry is to provide each drug in a solid form that has optimum performance in a given application. Pursuit of this mission requires recognition of several general, interrelated points: (1) Drugs can exist in a number of solid forms, each having different properties of pharmaceutical importance, including stability and bioavailability; the number and properties of these forms are largely unpredictable and vary considerably from case to case. (2) The forms of a drug may interconvert under various conditions. (3) Once a solid form is chosen for a product, methods for analysis and control of the form must be devised.

Let us briefly review each of these points with regard to their status in current practice and to some associated scientific challenges that remain.

(1) The most common solid forms that may be found for a given drug substance are as follows: **crystalline polymorphs**, forms having the same chemical composition but different crystal structures and therefore different densities, melting points, solubilities, and many other important properties; **solvates**, forms containing solvent molecules within the crystal structure, giving rise to unique differences in solubility, response to atmospheric moisture, loss of solvent, etc. Sometimes a drug product may be a **desolvated solvate**, formed when solvent is removed from a specific solvate while the crystal structure is essentially retained—again, many important properties are unique to such a form; finally, **amorphous** solid forms that have no long-range molecular order (i.e., no crystallinity) and which tend to be more soluble, more prone to moisture uptake, and less chemically stable than their crystalline counterparts (pharmaceutical processing operations may produce solids of low crystallinity intermediate between that of a crystalline solid and an amorphous solid).

To be sure, differentiating among the various solid forms of a substance is generally a routine matter. A number of analytical methods, used together, make this possible. Various familiar methods reveal the chemical composition of the solid and reveal the presence of solvent. The physical form is further characterized by X-ray powder diffraction, infrared and solid-state NMR spectroscopy, differential scanning calorimetry, and microscopy. The single most valuable piece of information about a crystalline solid, although not always available, is the molecular structure, determined by single-crystal X-ray diffraction.

Perhaps the chief challenge in managing the phenomenon of multiple solid forms of drugs is our inability to predict how many forms can be expected in a given case: too often costly delays are encountered when a less soluble solid form suddenly appears late in a development program. Progress along these lines awaits analysis and quantification of the myriad intermolecular forces within any proposed crystal structure as well as the ability to postulate the likely packing modes for a given molecule in all its configurations. Further research similar to that of Margaret Etter and co-workers, reviewed in section A, will doubtless lead to better success in predicting alternative solid forms of new drugs.

A second challenge relates to the strikingly different reactivity of different solid forms of many substances, whether it be oxidation, dehydration, decarboxylation, or other chemical reactions. Kinetics involving the solid state, in which specific contacts (or noncontacts) between reactive groups are dictated by the structure of a given solid form, are apt to be more complex than kinetics in solution, where the corresponding molecular encounters are much more random. Much the same can be said about the relative difficulty of elucidating mechanisms in these two states. Moreover, reactions in the solid state may be further complicated by other, often unknown factors such

† Purdue University.
‡ Department of Pharmaceutics, University of Minnesota.
§ Department of Laboratory Medicine and Pathology, University of Minnesota.
• Abstract published in *Advance ACS Abstracts*, August 15, 1994.

0897-4756/94/2806-1148$04.50/0 © 1994 American Chemical Society

UM00013047
NOVARTIS EXHIBIT 1017
Novartis v. Regents, IPR2023-01346
Page 1793 of 4460

as nucleation of a reaction product phase, presence of various amounts of amorphous component, strain or disorder in the crystal structure, and multiplicity of reaction products. As a result, there is very little information available to guide in any general way the prediction of the stability of compounds in the solid state, let alone in their different solid forms or different formulations. Thus, the stability of all but the most rugged products is generally characterized empirically at actual storage temperatures, and the value of studies at elevated temperatures must be assessed case by case. Elucidation of the kinetics and mechanisms of solid-state reactions is pursued in only the most pressing cases.

(2) A dictate of formulation technology is that the physical form of the drug substance, after being defined and verified, should not change once the product has been manufactured. Therefore, in addition to identifying various solid forms of a drug, an understanding of the specific factors that may bring about *transformations* between the forms is also essential.

Rates of solid-to-solid transformations in drugs are affected by one or more of the following variables: temperature, solubility in a given liquid phase, and vapor pressure of solvent. At a minimum, the investigator must therefore first identify and obtain certain physicochemical data on each relevant solid form:

- transition temperature(s) between polymorphs
- solubility of the drug in all solvents and solvent mixtures used in preparation of the final drug substance and throughout the formulation process
- equilibrium water vapor pressure *vs* composition isotherm

This information reveals which solid form is the most physically stable (least soluble) under specific conditions of temperature and composition; thus, if that form is already the one present, no transformation will occur. If, however, a less physically stable (more soluble) form is present, the *direction* of any transformation can now be predicted for given conditions. One might well ask why the most stable form is not always selected and, indeed, that is usually the case. There are however, situations where the peculiar properties of a less stable solid form are required for a product's performance—achieving higher solubility, for example. In such cases, the manufacturer has the added burden of demonstrating the *lack* of transformation to a more stable solid form throughout the life of the product. As discussed in the previous section, this task requires dealing with the problems of solid-state kinetics and must usually be approached empirically.

(3) Two main challenges to the analysis of pharmaceutical solids are dealing quantitatively with mixtures of forms in the drug substance and identifying the solid form of the active ingredient in the formulated product, particularly when the drug is a minor component in the presence of numerous other materials (excipients).

With this background on the current status of solid-state pharmaceutical chemistry, we can now turn to a number of recent advances in this field.

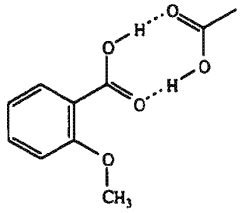
The work of Margaret Etter and co-workers, treated in section A, is an example of how present research addresses some of the issues of structure prediction raised above.

The topics discussed in sections B–D have significant bearing on many of the issues discussed in all three of the introductory subsections.

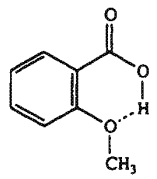
A. Forces Holding Crystals Together

Two main types of forces are responsible for holding drug crystals together: nonbonded interactions and hydrogen bonding. Nonbonded interactions occur in all crystals while hydrogen bonding is important in many compounds, especially pharmaceuticals. Etter has reviewed the extent and types of hydrogen bonding which can exist in organic solids.[1,2]

Carboxylic acids have been a particularly useful class of compounds for investigating alternative hydrogen bonding possibilities. For example, in *o*-alkoxybenzoic acids both dimerization and formation of intramolecular hydrogen bonding are observed.[3] In *o*-anisic acid, dimers are observed in the solid state while intramolecular hydrogen bonds are observed in dilute solution. However,

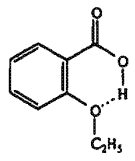


Solid State



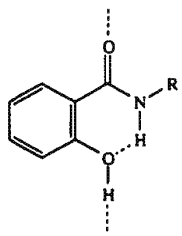
Solution

in *o*-ethoxybenzoic acid, only intramolecular hydrogen bonds are observed in the solid state and in solution.

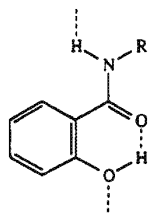


Solution and Solid State

The Etter group studied the hydrogen bonding in salicylamide derivatives and pointed out that two types of hydrogen bonding are possible in these compounds.[4] One type involves an intramolecular NH···O hydrogen bond and an intermolecular C═O···HO— hydrogen bond and the other an intramolecular C═O···HO— hydrogen bond and an intermolecular NH···O hydrogen bond.



Intra: HN··· O
Inter: C═O··· HO



Intra: C═O··· HO
Inter: HN··· O

(1) Goerbitz, C. H.; Etter, M. C. *Int. J. Pept. Protein Res.* **1992**, *39*, 93–110.
(2) Etter, M. C. *Acc. Chem. Res.* **1990**, *23*, 120–6.
(3) Etter, M. C.; Urbanczyk-Lipkowska, Z.; Fiah, P. A.; Panunto, T. W.; Baures, P. W.; Frye, J. S. *J. Crystallogr. Spectrosc. Res.* **1988**, *18*, 311–25.

UM00013048
NOVARTIS EXHIBIT 1017
Novartis v. Regents, IPR2023-01346
Page 1794 of 4460

Table 1. Reliable and Occasional Hydrogen-Bond Donors and Acceptors

type	functional group involved
reliable donor	–OH,[a] –NH_2, –NHR, –$CONH_2$, –CONHR, –COOH
occasional donor	–COH, –XH, –SH, –CH
reliable acceptors	–COOH, –CONHCO–, –NHCONH–, –CON< (1–3°), >P=O, >S=O, –OH
occasional acceptors	>O, –NO_2, –CN, –CO, –COOR, –N<, –Cl

[a] Not COH.

Etter, MacDonald, and Bernstein developed a graph-theory-based approach to classifying and symbolically representing the different types of hydrogen bonds that can be formed.[5]

Etter also developed rules governing hydrogen bonding in solids. These rules require a classification of hydrogen bond donors and acceptors into "reliable" hydrogen-bond donors and acceptors and "occasional" donors and acceptors (Table 1). Using these classifications, three rules were devised: (1) All (or as many as possible) good proton donors and acceptors are used in hydrogen bonding. (2) Six-membered ring intramolecular hydrogen bonds form in preference to intermolecular hydrogen bonds. (3) The best proton donors and acceptors remaining after intramolecular hydrogen bond formation will form intermolecular hydrogen bonds. These rules apply quite well to hydrogen bonding of small molecules. However, in some larger molecules, e.g., erythromycins, steric factors make it impossible to satisfy all of the possible hydrogen bonded interactions, and some donors and acceptors are not involved in any hydrogen bonds.

Cocrystals. An important aspect of research into hydrogen bonding involves the realization that cocrystals can be obtained from certain solutions containing more than one molecular species. Cocrystals can also be formed by mixing or grinding two solids together. Cocrystals are usually formed between a hydrogen-bond donor molecule and a hydrogen-bond acceptor molecule. The nature of hydrogen bonding in cocrystals can also be described using the above rules. The cocrystals observed by Etter's group include numerous ureas with ketones, carboxylic acids with 2-aminopyridine, and also adenine or cytosine combined with many acidic organic compounds[6] such as carboxylic acids and *N*-acylamino acids. Other classes of cocrystals investigated by Etter's group are

pyrimidine, pyridines: carboxylic acids

pyridine-N-oxides: acids, alcohols, amines

phosphine oxides: acids, amides, alcohols, ureas sulfonamides, amines, water

carboxylic acids: other carboxylic acide, amides

m-dinitroureas: acids, ethers, phosphine oxides, sulfoxides, nitroanilines

imides: other imides, amides

The formation of cocrystals may be quite important in explaining solid–solid interactions in many fields including those of pharmaceuticals.

(4) Etter, M. C.; Reutzel, S. M. *J. Am. Chem. Soc.* 1991, *113*, 2586–98.
(5) Etter, M. C.; MacDonald, J. C.; Bernstein, J. *Acta Crystallogr., Sect. B* 1990, *B46*, 256–62.
(6) Etter, M. C.; Reutzel, S. M. *J. Am. Chem. Soc.* 1991, *113*, 2586–98.

This elegant work of Etter and co-workers has greatly increased our understanding of the hydrogen-bonding interactions of molecules in both the solid state and in solution.

B. How Crystals Form

Crystallization and the factors controlling the formation of crystals is an extremely important area in solid-state pharmaceutical chemistry. Dr. Margaret Etter made an extremely important observation when she pointed out that molecules in solution often tend to form different types of hydrogen-bonded aggregates and hypothesized that these aggregate precursors are related to the crystal structures that form from the supersaturated solution.[2] This concept helps to explain the many different hydrogen-bonding motifs seen in different solids.

A number of factors can affect the crystal formed either by influencing the hydrogen-bonded aggregate precursors in solution or influencing one of the many other factors involved in crystallization. These include (1) solvent composition or polarity, (2) concentration or degree of supersaturation, (3) temperature including cooling rate and the cooling profile, (4) additives, (5) seeds and the presence of seeds, (6) pH (pH is important for crystallization of salts), and (7) agitation.

The composition of the solvent used is known to influence crystallizations either directly or by influencing the temperature at which the crystallization is initiated. For example, in the mannitol system, the α-polymorph is formed by evaporation of 100% ethanol while the β-polymorph is formed by crystallization from aqueous ethanol.[7] In a study of inosine, Suzuki showed that crystallization from water gave the α-form whereas crystallization from 70% DMSO gave the β-form.[8]

A second important factor influencing crystallization is the degree of supersaturation—the ratio of the concentration of the solution to that of a saturated solution. In his study of the polymorphism of cimetidine, Sudo showed[9,10] that in isopropyl alcohol at high supersaturation ratios (greater than 3.6) form A crystallized spontaneously or in the presence of seeds of either form A or form B, whereas in lower supersaturation ratios (less than 2) form A crystallized if there were A seeds and B crystallized if there were B seeds.

Temperature can have a very significant effect on the polymorph produced. Studies by Kitamura[11] on the crystallization of L-glutamic acid showed that at 45° the α-form nucleates slowly resulting in β-form growth, whereas at 25 °C the α-form nucleates rapidly causing α-form growth.

The effect of additives on crystallization has been of interest for many years. Early work by Simonelli indicated that polymeric additives could prevent the crystallization of certain phases.[12] Significantly, studies in recent years by Lahav and co-workers[13] have shown that additives (as

(7) Berman, H. M.; Jeffrey, G. A.; Rosenstein, R. D. *Acta Crystallogr.* 1968, *B24*, 442–449.
(8) Suzuki, Y. *Bull. Chem. Soc. Jpn.* 1974, *47*, 2551–2552.
(9) Sudo, S.; Sato, K.; Harano, Y. *J. Chem. Eng. Jpn.* 1991, *24*, 237–242.
(10) Sudo, S.; Sato, K.; Harano, Y. *J. Chem. Eng. Jpn.* 1991, *24*, 628–632.
(11) Kitamura, M. *J. Cryst. Growth* 1989, *96*, 541–546.
(12) Simonelli, A. P.; Mehta, S. C.; Higuchi, W. I. *J. Pharm. Sci.* 1970, *59*, 633.
(13) Weissbuch, I.; Addadi, L.; Lahav, M.; Leiserowitz, L. *Science* 1991, *253*, 637–646.

UM00013049
NOVARTIS EXHIBIT 1017
Novartis v. Regents, IPR2023-01346
Page 1795 of 4460

little as 0.03%) can inhibit nucleation and crystal growth of a stable polymorph, thus favoring the growth of a metastable polymorph. They also showed that it is possible to design crystal nucleation inhibitors to control polymorphism.

In addition, Grant et al. have shown the effects of additives on the properties of adipic acid, acetaminophen (paracetamol), and (*R,S*)-(−)-ephedrinium-2-naphthalenesulfonate, a chiral drug. The effects on each of these crystalline solids will now be considered in turn.

When adipic acid is crystallized from water containing traces of *n*-alkanoic acids[14] or oleic acid,[15] the additive is taken up by the crystals, while the very small water content is not significantly affected. Changes in crystal habit and in the crystal growth kinetics are consistent with a structural model in which the added *n*-alkanoic acid molecules occupy lattice sites at the crystal surfaces.[16] The incorporated additive also changes the thermodynamic properties of the crystal. Notably, the crystal energy and entropy are increased, as measured by reductions in the enthalpies of fusion and solution, while the melting point is little affected.[14,15] In addition, the Gibbs free energy of the crystal increases, as measured by the dissolution rate and the specific surface area, and the density of the crystals is changed. Furthermore, the compaction properties, as measured by Hiestand's indices of tableting performance of the crystals are also modified.[17] Low levels of incorporated *n*-octanoic acid produce an increase in lattice strain, reducing the energy required for plastic deformation leading to improved tableting performance. At higher levels of incorporated *n*-octanoic acid, the tableting performance again approaches that of the pure crystal, indicating a reduction in plasticity. The above results with adipic acid may be explained by the impurity defects and attendant dislocations introduced by incorporated additive, resulting in increased lattice strain at low concentrations of additive and in reversal of the effects at higher concentrations. These proposed changes in lattice strain have recently been confirmed by corresponding increases and decreases in the mosaic spread of the Laue diffraction pattern when single crystals are irradiated by white X-radiation from a synchrotron source.[18]

When acetaminophen is crystallized from water containing the structurally related synthetic impurity, *p*-acetoxyacetanilide (PAA), the additive is incorporated and the crystals become acicular (needle-shaped). Increasing concentrations of PAA lead to increasing uptake of PAA to a maximum constant value (suggesting a saturated solid solution), to a decrease in water content, and to an increase in the length/width ratio.[15] Higher concentrations of PAA cause the length/width ratio and the water content to return to nearly the initial values. The maximum length/width ratio and the minimum in water content correspond approximately to maxima in the enthalpy and entropy of fusion and in the intrinsic dissolution rate of the crystals, the melting point being little affected. The physical properties of the acetaminophen crystals mentioned above were measured under 29 different crystallization conditions, defined by the initial concentration of PAA, the initial supersaturation of acetaminophen, and the rate of stirring of the crystallization solution.[19] Statistical analysis of the properties of these crystals, crystallized and analyzed in triplicate, showed strong correlations between the length/width ratio and the concentration of PAA taken up by the crystal and between the intrinsic dissolution rate and the length/width ratio, the thermodynamic quantities playing a minor role.[20] These results demonstrate the significance of additive-induced changes in crystal habit in influencing the intrinsic dissolution rate of acetaminophen crystals. Thus, whereas the behavior of doped crystals of adipic acid may be attributed to differences in lattice strain, the behavior of doped acetaminophen crystals may be attributed to differences in crystal habit.

In the above examples, adipic acid and acetaminophen exist as achiral molecules and crystallize in achiral space groups. The question arises as to the effect of traces of the opposite enantiomer on the crystal properties of a chiral drug. To help answer this question, the chiral drug (*R,S*)-(−)-ephedrinium 2-naphthalenesulfonate [(−)-EN] was crystallized from aqueous solutions containing traces of the opposite enantiomer (*S,R*)-(+)-ephedrinium 2-naphthalenesulfonate [(+)-EN].[21] Crystals of (−)-EN took up the opposite enantiomer with an appreciable segregation coefficient (0.153), while the water content and melting point of the crystals remained constant. Uptake of the opposite enantiomer led to changes in the thermodynamic properties and intrinsic dissolution rate. These changes are similar to those observed when adipic acid incorporated *n*-alkanoic acid from the crystallization solution. The similar behavior suggests an analogous molecular mechanism in the solid state, implying that doping with the opposite enantiomer produces changes in crystal properties that are analogous to doping of a foreign molecule of different, but related structure. Interestingly, (−)-EN and (+)-EN when heated together give a phase equilibrium diagram with a eutectic (together with limited solid solution formation) between each enantiomer and the racemic compound. This observation suggests that the observed changes in the thermodynamic properties and intrinsic dissolution rate of (−)-EN may be attributed to doping of the crystals with [(+)-EN/(−)-EN] molecular pairs or clusters rather than simply with the added (+)-EN molecules.

Seeding is used extensively to control crystal form and also to control the extent of nucleation (i.e., final particle size). In almost all cases, seeding can be used to control the desired crystal form. For example, Suzuki et al.[8] showed that the α-form of inosine could be obtained by crystallization from water whereas to obtain the β-form, seeds of the β-form must be used. An interesting study of the effect of seeding was reported by Konapudi, and the mechanism of crystallization was elucidated by McBride and Carter.[22] Sodium chlorate crystallizes in both a chiral and a racemic form. Since sodium chlorate is not chiral in solution, crystallization from aqueous solution produces equal numbers of L and D crystals.

(14) Chow, K. Y.; Go, J.; Mehdiadeh, M.; Grant, D. J. W. *Int. J. Pharm.* **1984**, *20*, 3–24.
(15) Chow, A. H. L.; Chow, P. K. K.; Wang, Z.; Grant, D. J. W. *Int. J. Pharm.* **1985**, *25*, 41–55.
(16) Davey, R. J.; Black, S. N.; Logan, D.; Maginn, S. J.; Fairbrother, J. E.; Grant, D. J. W. *J. Chem. Soc., Faraday Trans.* **1992**, *88*, 3461–3466.
(17) Law, D.; Grant, D. J. W. *Pharm. Res.* **1993**, *10*, S-152, PT-6102.
(18) Grant, D. J. W.; Law, D.; Ristic, R.; Shekunov, B.; Sherwood, J. N. *24th Annual Meeting of the Fine Particle Society, August 24–28, Chicago, IL*, 1993.
(19) Chow, A. H. L.; Grant, D. J. W. *Int. J. Pharm.* **1988**, *42*, 123–133.
(20) Chow, A. H. L.; Grant, D. J. W. *Int. J. Pharm.* **1989**, *51*, 129–135.
(21) Duddu, S. P.; Fung, F. K. Y.; Grant, D. J. W. *Int. J. Pharm.* **1993**, *94*, 171–179.
(22) McBride, J. M.; Carter, R. L. *Angew. Chem., Int. Ed. Engl.* **1991**, *30*, 293–295.

UM00013050
NOVARTIS EXHIBIT 1017
Novartis v. Regents, IPR2023-01346
Page 1796 of 4460

Surprisingly, crystallization of an aqueous solution with stirring gives mostly crystals of one chirality, either L or D. Investigation showed that this effect was due to the fact that once a particular crystal (either L or D) has formed, when that initial crystal collides with the stirrer and is broken into many small seeds which then nucleate further crystallization of that hand crystal (either L or D). This observation supports the idea that one nucleating seed can produce a single crystalline form. It also suggests that in this particular crystallization, if one added a seed of either L or D crystals then one would obtain entirely that crystal form. This is one of the best examples of the concept: one seed, one crystal.

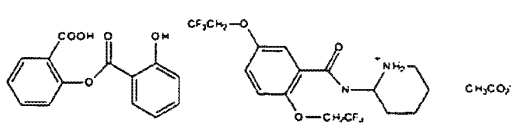
McCrone, in a letter to the editor of the *Journal of Applied Crystallography*, suggested that nucleation by seeding was the best explanation for the situation in which one unexpectedly obtains a new, more stable crystal form and then finds it is difficult or impossible to obtain the older less stable crystal form.[23] In response to this letter Jacewicz et al.[24] suggested that it is not impossible to produce the earlier form. They stated that the original crystal form should be capable of being produced but that the selection of the right conditions may require some time and trouble.

C. Disorder in Crystals of Pharmaceutical Solids

Another solid-state phenomenon which has important implications for pharmaceutical solids is disorder. Just as crystals of chiral and racemic drugs may have different physical properties, the presence of disorder in a crystal may also affect the physical properties of a crystal. One method of classifying disorder is to distinguish between cases involving static and dynamic disorder. Because single-crystal X-ray techniques give results which are averages over a long time period relative to molecular motion, X-ray crystallography at one temperature is usually unable to distinguish between static and dynamic disorder. Static and dynamic disorder can often be distinguished by comparing X-ray thermal parameters (ADPs) for two different temperatures. If the disorder results in observable resonance peaks in solid-state NMR spectra, then clearly this technique can be used to study this disorder.

In the crystallographic literature there are numerous examples of disorder which are caused by a molecule crystallizing in a single conformation but in a different orientation relative to other molecules in the crystal. There are also examples where the disorder is due to molecules crystallizing in different conformations.

Two such examples of conformational disorder are the crystal structures of nonsteroidal antiinflammatory (NSAID) drug salicylsalicylic acid (SALSALATE)[25,26] and the antiarrhythmic compound flecainide (TAMBOCOR).[27]



SALSALATE TAMBOCOR

(23) McCrone, W. C. *J. Appl. Crystallogr.* 1975, *8*, 342.
(24) Jacewicz, V. W.; Nayler, J. H. C. *J. Appl. Crystallogr.* 1979, *12*, 396–397.

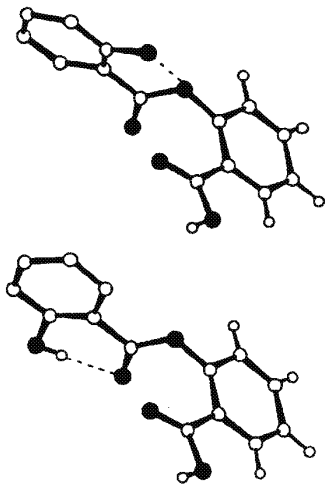


Figure 1. The two geometries of the SALSALATE molecule which are incorporated into the disordered crystal.

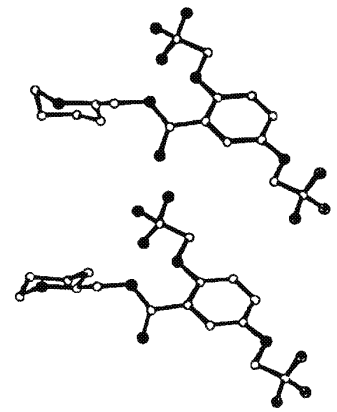


Figure 2. The two geometries of the TAMBOCOR which are incorporated into the disordered crystal.

The salsalate molecule can crystallize in two different conformations, each of which is intramolecularly hydrogen-bonded. Presumably, these two different intramolecular modes of hydrogen bonding are roughly equivalent energetically and the gross shape of the molecule in both conformations is similar so that both conformations can be incorporated into a single crystal as shown in Figure 1.

The other interesting example is the antiarrhythmic compound flecainide which is disordered in the solid state. The form of the compound which exhibits this disorder is actually the acetate salt, which was originally used for therapeutic purposes. Here the piperidinium ring takes on two alternate chair conformations as shown in Figure 2.

What are the consequences of such disorder? At the level of processing, the difficulty in reproducing material with the same properties may be responsible for different

(25) Frink, N.; Gleason, W. B.; Sweeting, L. M. In *IVth Midwest Organic Solid-State Chemistry Symposium*; Lincoln, NE, 1992.
(26) Frink, N.; Beaurline, J.; Gleason, W. B. In *Am. Cryst. Assoc. Annual Meeting*; Pittsburgh, PA, 1992.
(27) Gleason, W. B.; Bannit, E. H. In *Am. Cryst. Assoc., Annual Meeting*, 1987; p PE18.

UM00013051
NOVARTIS EXHIBIT 1017
Novartis v. Regents, IPR2023-01346
Page 1797 of 4460

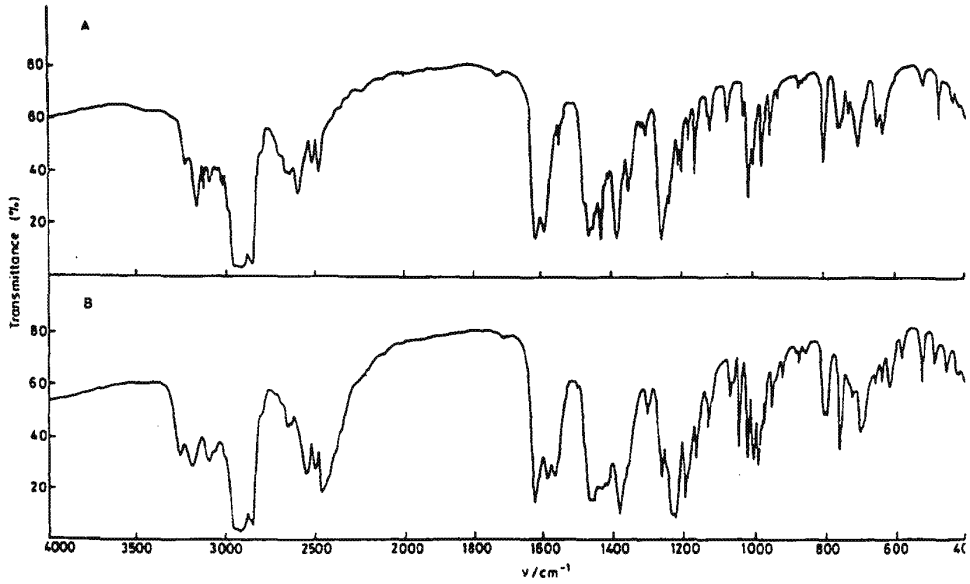


Figure 3. IR spectra of Nujol mulls of the two polymorphs of ranitidine hydrochloride: A, form 1; B, form 2.[29]

batches having dissimilar behavior. Batch-to-batch variability may be caused by differences in the ratio of the different conformations of molecule in the bulk sample.

Although disorder is a well-known phenomenon in the crystallography of small organics, the consequences of disorder in drug molecules appears not to have been widely considered. Just as crystals of chiral and racemic drugs may have different physical properties, the presence of disorder in a crystal may also affect the physical properties of the crystal. The amount of disorder (overall ratio of high occupancy to low occupancy conformations in the batch sample) found in a material may be highly dependent on the exact crystallization conditions. In turn the physical properties of individual batches may range from free-flowing powders to flocculent precipitates suffering badly from the effects of static electricity.

In addition, dynamic disorder reflects enhanced molecular mobility in the solid state. This enhanced molecular mobility may lead to enhanced chemical reactivity as suggested by the four-step mechanism of solid-state reactions first advanced by Paul and Curtin.[28] In this mechanism the first step is molecular loosening. Obviously, crystals possessing dynamic disorder are relatively loosely packed (at least near the site of disorder) and thus may be expected to be more reactive. At Purdue University, we are presently investigating cases in which the disorder of the system may relate to enhanced reactivity.

Are disordered samples with different amounts of disorder distinguishable? One method to distinguish this is discussed later in this review, solid-state NMR spectroscopy. Another approach is powder diffraction. Whether a particular sample will give a powder diffraction line which will change as a function of the disorder is a function of the scattering power of atoms in the alternate conformations and their contribution to scattering for a particular scattering plane. Computer programs are available for the calculation of powder diffraction patterns from single-crystal X-ray diffraction data. In one case we have examined, that of salicylsalicylic acid, our calculations indicate that certain diffraction lines are sensitive to the ratio of high occupancy to low occupancy conformations present in the salicylsalicylate sample. Thus the ratio of the intensities calculated for the two strongest lines in the powder pattern (311/202) varies from 0.80 to 1.75 as the amount of the "major conformer" is varied from 30% to 95%. Even though one must always be concerned with the effect of preferred orientation upon intensities for a powder sample, this calculation is encouraging for the possibility of using powder diffraction as a monitor for disorder in a material intended for pharmaceutical, or other use.

Salicylsalicylic acid crystallizes in Fdd2, an acentric space group, even though the molecule itself is not chiral.[25,26] This compound, as other salicyl esters, also exhibits strong triboluminescence. It is also disordered in the solid. The exact crystallization conditions for this compound can lead to solid material with a broad range of physical behavior. The variability in physical properties of this material may be tied to disorder in the crystalline material and may be a function of the amount of disorder found in the bulk sample.

D. Characterization of Pharmaceutical Solids

In this section the characterization of pharmaceutical solids will be briefly reviewed. This section is intended to provide the reader with a picture of the structure and properties of the various solid forms of pharmaceuticals.

The clearest indication of the existence of polymorphs and solvates comes from X-ray crystallographic examination of single crystals of various samples that are known to have the same composition but which may be suspected of being polymorphic. If single crystals of these materials have different unit-cell parameters then they may be polymorphs. Often, however, X-ray powder diffraction is sufficient to establish the existence of polymorphs. Thus polymorphs can be uniquely identified by their X-ray powder diffraction pattern and their structure completely elucidated by single-crystal X-ray diffraction.

(28) Paul, I. C.; Curtin, D. Y. *Acc. Chem. Res.* **1973**, *7*, 223.

UM00013052
NOVARTIS EXHIBIT 1017
Novartis v. Regents, IPR2023-01346
Page 1798 of 4460

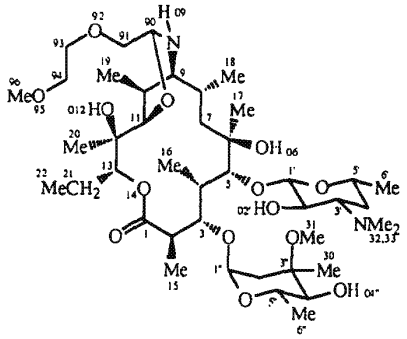
Knowledge of the polymorphs, solvates, and habits in which a drug crystallizes can lead to a dramatic improvement in understanding the stability, bioavailability, and ease of processing of pharmaceutical solids.

1. **Infrared Spectroscopy of Solids.** Infrared spectroscopy is quite useful for the analysis of solids, because it can be performed on small amounts of the solid substance. The method involves grinding the sample and measuring its infrared spectrum in one of several types of cells available. Infrared spectra of solids can also be obtained after suspending the sample in Nujol or grinding the sample with KBr and compressing this mixture into a disc. FT-IR microscopy can be used to measure the infrared spectrum of a single crystal or group of crystals. If care is taken to study only crystals of the same morphology, this method minimizes the possibility of obtaining infrared spectra of mixtures of crystal forms which is a distinct advantage over approaches that use powdered samples.

The infrared spectrum is extremely sensitive to the structure and conformation of a compound and, thus, can be used to compare the structure and conformation of the compound in different solids or in solid and solution. Infrared spectroscopy is thus a powerful method for the determination of polymorphs.

Cholerton et al.[29] reported the use of infrared spectroscopy to differentiate form 1 and form 2 of ranitidine hydrochloride (Figure 3). This is a classic example of the power of infrared analysis in polymorph studies.

Infrared spectroscopy is also useful for the investigation of solvates, as demonstrated by a study of erythromycin derivative (I).[30] Figure 4 shows the spectra of forms I and



II and the amorphous form of this compound. Clearly these three forms have different spectra especially in the carbonyl region. Note that form I shows two carbonyl absorptions, whereas the amorphous form and form II show only a single carbonyl absorption. Figure 5 shows the infrared spectra of three of the many solvates of this erythromycin derivative. These spectra are fairly similar except for the obvious C≡N stretching absorption in the acetonitrile·$3H_2O$ solvate. There are also slight differences among these three solvates in the fingerprint region. Figure 6 shows the infrared spectra of six solvates which are isomorphous (have the same crystallographic unit cell). These spectra are fairly similar as might be expected since they crystallize in the same unit cell. In cases where the solvents contain keto groups (e and f) the ketone absorption is obvious as a second carbonyl absorption in the spectrum.

(29) Cholerton, T. *J. Chem. Soc., Perkin Trans 2* 1984, 1761.
(30) Stephenson, G. Unpublished observations, 1993.

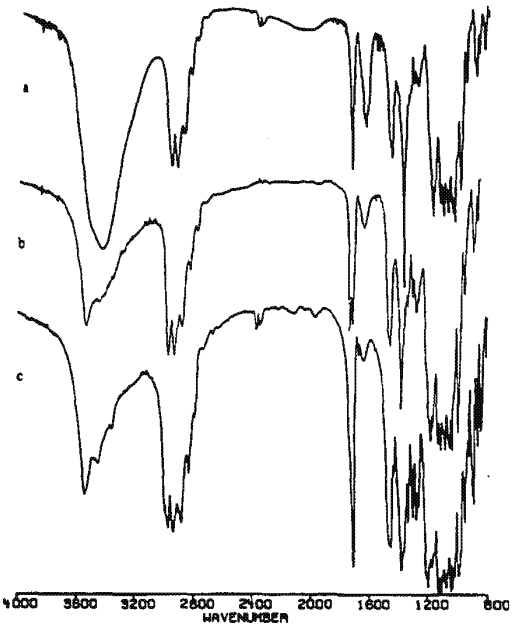


Figure 4. Infrared spectra of the amorphous form (a) and two anhydrous forms, I and II, (b and c) of an erythromycin derivative.[30]

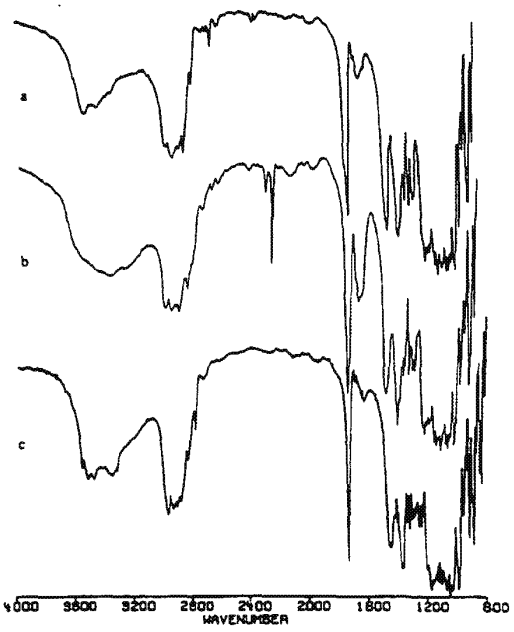


Figure 5. Infrared spectra of three nonisomorphic solvates of an erythromycin derivative: (a) tricyclohexane, (b) acetonitrile·$3H_2O$, and (c) *tert*-butyl alcohol solvate.[30]

Figure 7 shows an enlarged view of the ester carbonyl region of the spectrum in three of the crystal forms of the erythromycin derivative. These spectra suggest that the *n*-propanol solvate contains non-hydrogen-bonded carbonyl groups, that form II contains hydrogen-bonded carbonyl groups, and that form I contains both hydrogen-bonded and non-hydrogen-bonded carbonyl groups. These suggestions have been confirmed by the crystal structures

UM00013053
NOVARTIS EXHIBIT 1017
Novartis v. Regents, IPR2023-01346
Page 1799 of 4460

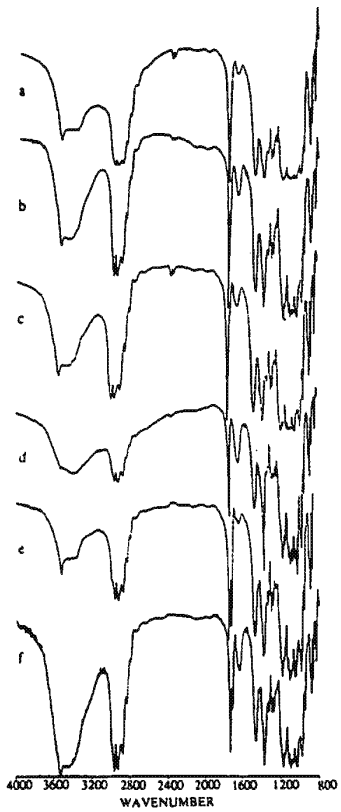


Figure 6. Infrared spectra of the isomorphic solvates of an erythromycin derivative: (a) ethanol, (b) *n*-propanol, (c) isopropyl alcohol, (d) *n*-butanol, (e) acetone, (f) methyl ethyl ketone.[30]

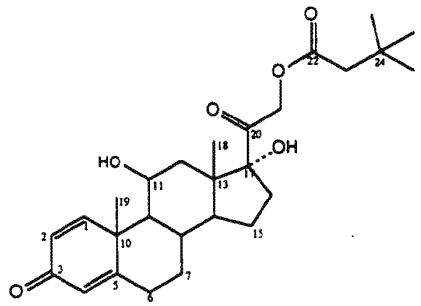
of the *n*-propanol solvate and hydrogen-bonded form II. Unfortunately, the crystal structure of form I could not be determined. Solid-state NMR confirms these suggestions as shown in Figure 8. Again, form I, which shows two carbonyl stretching vibrations in the IR also shows two carbonyl resonances in the solid-state NMR spectrum and the hydrogen bonded form shows a shift to lower field as expected based on model studies (see below).

2. Solid-State NMR Spectroscopy of Pharmaceutical Solids. Solid-state ^{13}C CP/MAS NMR offers significant advantages for the study of solid drugs.[31,32] Figure 9 shows the solid-state ^{13}C NMR spectra of two crystal forms of prednisolone and shows that they can be differentiated on the basis of differences in these spectra. Apparently changing the crystal packing results in significantly different magnetic environments for some of the carbon nuclei. This observation has considerable practical value: Figure 10 shows the ^{13}C CP/MAS NMR spectra of three prednisolone tablets from different vendors. It is clear that one can still observe resonances due to prednisolone, although these tablets contain only 5 mg of prednisolone in 95 mg of excipients. Comparison of Figures 9 and 10 shows that in tablets A and B form I exists, whereas in tablet C form II exists.

(31) Saindon, P. A.; Cauchon, N. S.; Sutton, P. A.; Chang, C. J.; Peck, G.; Byrn, S. R. *Pharm. Res.* **1993**, *10*, 197.
(32) Byrn, S. R.; Sutton, P. A.; Tobias, B. *J. Am. Chem. Soc.* **1988**, *110*, 1609–14.

Other reports show that different polymorphs of cellulose show different ^{13}C CP/MAS NMR spectra.[33] Moreover, solid-state ^{13}C CP/MAS NMR spectroscopy also offers the possibility of the analysis and characterization of amorphous forms. A particularly important question in this area is, What is the mobility of the molecule in amorphous forms? This question can be addressed by comparing the T_1 relaxation times of carbon atoms in the crystalline and amorphous state. In addition, the technique can be used to examine conformational and dynamic changes which occur in solid drugs by determining the coalescence temperature and associated rate constants for the process. In addition, because the time-scale of solid-state NMR spectroscopy is much shorter than X-ray crystallography, it offers the potential for analysis of a range of dynamic processes which cannot be studied by X-ray crystallography. These facts could lead to the widespread use of solid-state NMR spectroscopy in the pharmaceutical industry.

In our laboratory, we have used solid-state NMR to study the different crystal forms of prednisolone *tert*-butylacetate.[32] These studies show that the different crystal forms of prednisolone *tert*-butylacetate have different



Prednisolone 21-*tert*-butylacetate

solid-state NMR spectra. This is no doubt due to different crystal packing. Even forms I and II which have very similar unit cells have slightly different chemical shifts. However, the biggest difference between forms I and II is the position of the solvent peaks. In form I the ethanol solvent shows resonances at 18.1 and 58.2 ppm; in form II the propanol solvent shows resonances at 26.3 and 64.3 ppm. The solid-state NMR spectra of forms III, IV, and V are much different from those of form I and II and from each other. The biggest difference involves carbon 1 which shows chemical shifts which differ by up to 8 ppm from each other in the different crystal forms. Several of the other carbon atoms also show fairly large chemical shift differences. Figure 11 shows a plot of the difference between the solid state and solution chemical shift of carbon 1 vs the hydrogen-bond distance to the O3 carbonyl oxygen which is part of the α,β-unsaturated ketone system which contains carbon 1. It is important to note that this hydrogen bond to O3 is intermolecular and one of the forces responsible for holding the crystals of this steroid together. As can be seen from this plot (Figure 11), there is a more or less gradual shift to larger changes in ppm as the hydrogen-bond distance gets shorter and shorter. This observation is consistent with other studies of hydrogen bonding and also with solution studies

(33) Atalla, R. H.; Gast, J. C.; Sindorf, D. W.; Bartuska, V. J.; Maciel, G. E. *J. Am. Chem. Soc.* **1980**, *102*, 3249.

UM00013054
NOVARTIS EXHIBIT 1017
Novartis v. Regents, IPR2023-01346
Page 1800 of 4460

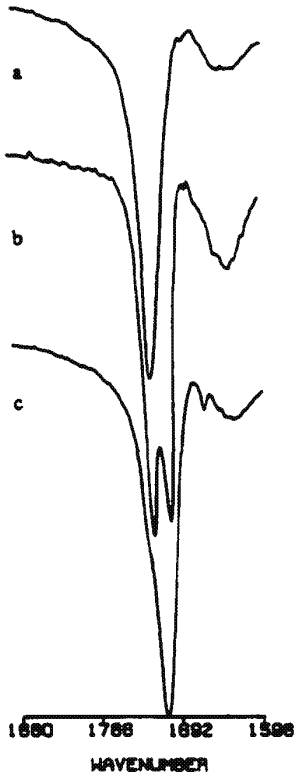
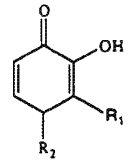


Figure 7. Ester carbonyl region of the *n*-propanol solvate (a), form I (b), and form II (c).[30]

where the stronger the hydrogen bonding the greater the chemical shift changes in ppm.

This type of correlation for different polymorphs and solvates shown in Figure 11 may also apply to members of a series of closely related compounds. Figure 12 shows that the $^{13}C(4)$ chemical shift difference between solid state and solution is a negative linear function of the crystallographic O(4)···O hydrogen bond distance in the crystal structures of a series of 1,2-dialkyl-3-hydroxy-4-pyridones (DAHPs) whose molecular structures are shown below:[34]



EMHP	$R_1 = CH_3$	$R_2 = C_2H_5$
PMHP	$R_1 = CH_3$	$R_2 = C_3H_7$
BMHP	$R_1 = CH_3$	$R_2 = C_4H_9$
MEHP	$R_1 = C_2H_5$	$R_2 = CH_3$
DEHP	$R_1 = C_2H_5$	$R_2 = C_2H_5$
EMHP	$R_1 = C_2H_5$	$R_2 = C_3H_7$

The DHAPs are iron chelators some of which may be promising drugs for oral administration in the treatment of diseases associated with iron overload. Although the crystal structure of the compound BMHP could not be determined, this compound provided an excellent ^{13}C NMR spectrum. The measured $^{13}C(4)$ chemical shift of BMHP might enable the O(4)···O hydrogen bond distance to be predicted using Figure 12, if this correlation is generally applicable.

(34) Ghosh, S. Ph.D. Thesis, University of Minnesota, 1993.

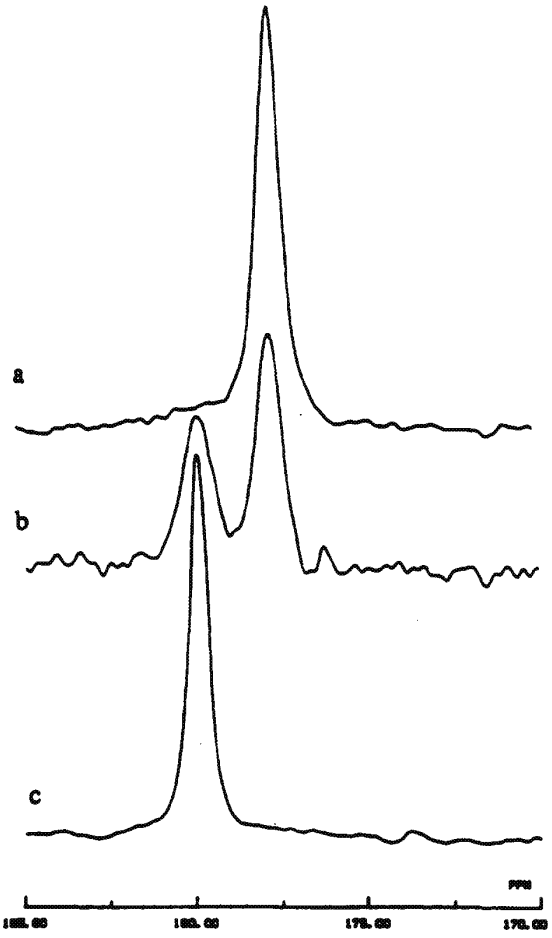


Figure 8. Solid-state NMR spectra of the ester carbonyl carbon: (a) *n*-propanol solvate, (b) form I, and (c) hydrogen-bonded form II.[30]

Solid-state NMR is also useful for the study of mobility in solids. The rate of relaxation of the carbon spins toward equilibrium is characterized by the spin lattice relaxation time, T_1.[35] In this process the excess energy from the spin system is transferred to "the lattice". Interactions of randomly fluctuating magnetic fields at the Larmor frequency of the nucleus stimulate these transitions. Such fields arise from motions of other nuclear magnetic moments such as protons. Spin–lattice relaxation is thus most efficient when these motions are near the Larmor frequency of the nucleus being observed. Studies of relaxation times can give valuable information about fast motions in the megahertz range such as methyl group rotations. Numerous studies of molecular motion using

(35) Fukushima, E.; Roeder, S. B. W. *Experimental Pulse NMR*; AddisonWesley: Reading, MA, 1988.

UM00013055
NOVARTIS EXHIBIT 1017
Novartis v. Regents, IPR2023-01346
Page 1801 of 4460

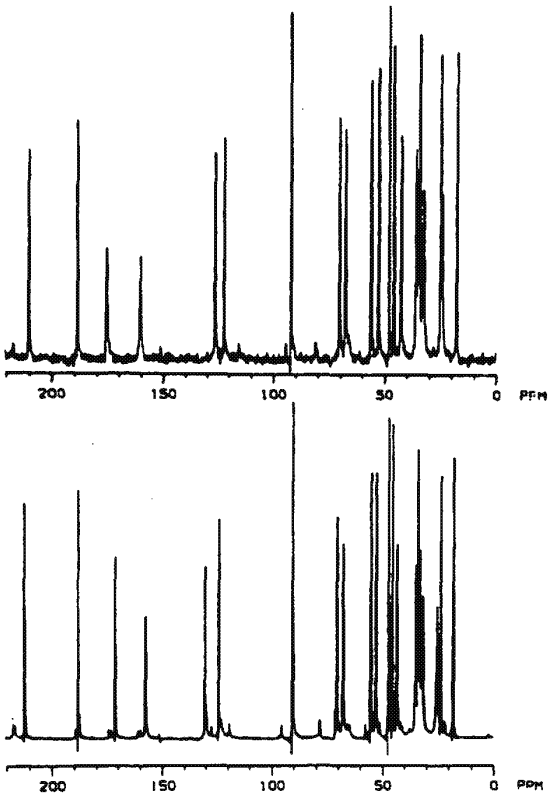


Figure 9. Solid-state ^{13}C CP/MAS NMR spectra of two polymorphs of prednisolone.[31] The top spectrum is form 1 and the bottom spectrum is form 2.

relaxation times have been published.[36] In particular, applications in the field of polymer science have been widespread. For example, solid-state NMR has been used to study both main chain and side group motion in polymers.[37-40] In addition, studies have been made of the relationship between polymer crystallinity and relaxation parameters including T_1, $T_{1\rho}$, and T_2.[41-43]

The mobility of functional groups in solids has been of interest for many years. An understanding of this mobility can lead to insight into the mobility of molecules, the forces responsible for conformational interconversions, and the factors responsible for solid-state reactions. In 1973, Paul and Curtin[28] suggested that molecular loosening or molecular mobility is the first step in a solid-state reaction, and, in our laboratory, we have suggested that solid-state

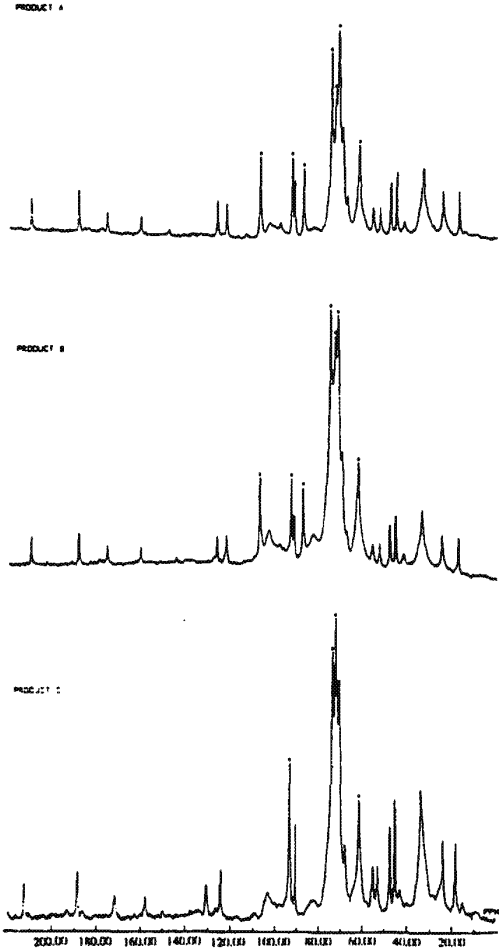


Figure 10. Solid-state ^{13}C CP/MAS NMR spectra of prednisolone tablets from three different vendors.[31]

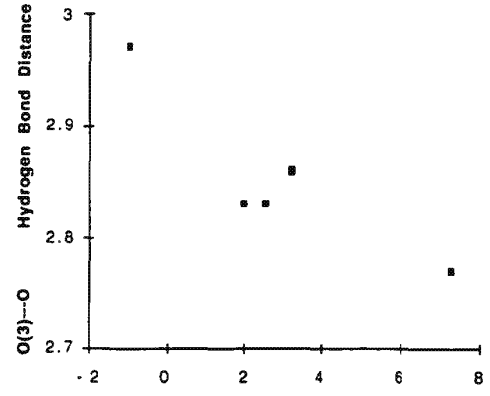


Figure 11. Plot of the difference in chemical shift for carbon 1 between the solid state and solution and the O(3)---O hydrogen bond distance.[32]

degradations of pharmaceuticals are related to molecular mobility.[32,44,45] In addition, Zografi has suggested that water absorption enhances the molecular mobility of amorphous pharmaceutical solids, perhaps explaining the

(36) Fyfe, C. A. *Solid-state NMR for chemists*; CFC Press: Toronto, Ontario, 1983.
(37) Lyerla, J. R. *Contemporary Topics in Polymer Science*; Shen, M., Ed.; Plenum Press: New York, 1979; Vol. 3, pp 143–213.
(38) Garroway, A. N.; Moniz, W. B.; Resing, H. A. In *Carbon-13 NMR in Polymer Science*; Pasika, W. M., Ed.; American Chemical Society: Washington, DC, 1979; pp 67–86.
(39) Tonelli, A. E.; G., M. A.; Tanaka, H.; Schilling, F. C.; Cozine, M. H.; Lovinger, A. J.; Bovey, F. A. *ACS Adv. Chem. Ser.*; Craver, C. D., Provder, T., Eds.; American Chemical Society: Washington, DC, 1990; Vol. 227, pp 409–451.
(40) Axelson, D. E. *Carbon-13 NMR in Polymer Science*; Pasika, W. M., Ed.; American Chemical Society: Washington, DC, 1979; pp 181–214.
(41) Menger, E. M.; Veeman, W. S.; de Boer, E. *Macromolecules* **1982**, *15*, 1406.
(42) Kitamara, R.; Horii, F.; Murayama, K. *Macromolecules* **1986**, *19*, 636–643.
(43) Earl, W. L.; VanderHart, D. L. *Macromolecules* **1979**, *12*, 762.

UM00013056
NOVARTIS EXHIBIT 1017
Novartis v. Regents, IPR2023-01346
Page 1802 of 4460

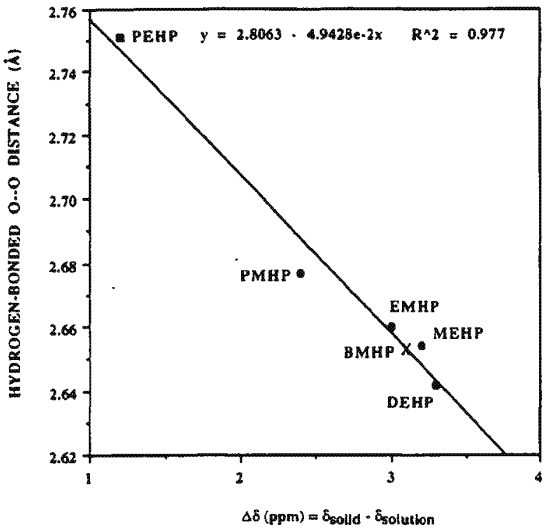


Figure 12. Plot of the hydrogen bonded O···O distances against the differences ($\Delta\delta$) between the ^{13}C chemical shifts of the pyridone carbonyl (O4) and the solid state (δ_{solid}) and the solution state ($\delta_{solution}$) of DAHPs. Although the crystal structure of BMHP is unknown, its hydrogen-bonded O···O distance can be estimated from the plot using the NMR chemical shift data (point X).[34]

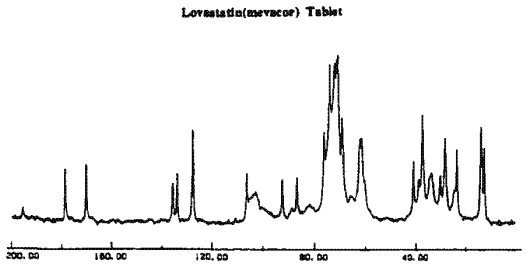
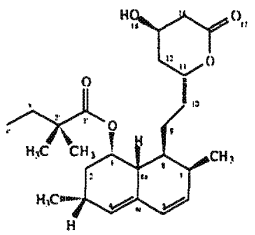


Figure 13. Solid-state CP/MAS NMR spectrum of a lovastatin tablet.

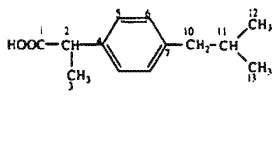
enhanced chemical reactivity of these materials in the presence of water.[46] Further study of the relationship between molecular mobility and solid-state reactivity requires the development of new approaches to determine molecular mobility especially in mixtures such as pharmaceutical dosage forms where single-crystal X-ray methods cannot be used.

Solid-state NMR offers several approaches to studying the molecular mobility of solids. These include (1) determination of the activation energies for T_1 relaxation of individual carbon atoms using variable-temperature solid-state NMR, (2) study of processes which result in peak coalescence of solid-state NMR resonances using variable-temperature solid-state NMR, (3) use of interrupted decoupling to detect methylene and possible methine groups with unusual mobility, and (4) comparison of solid-state MAS spectra measured with and without cross polarization.

Recent research at Purdue University is using all of these approaches but especially the first one to study the relative mobility of methyl groups in a number of drugs which contain multiple methyl groups including simvastatin, lovastatin, ibuprofen, and phenacetin.[47-49] The results of these studies will be published shortly.



Simvastatin



Ibuprofen

In addition, Maverick and Dunitz[50] have suggested that solid-state NMR activation energies and X-ray thermal parameters are related. Therefore, solid-state NMR appears to be a good method for study of the mobility of methyl groups in solids. Because solid-state NMR can be used to study pharmaceutical dosage forms and other mixtures,[31] this powerful method will find increased application in the determination of the molecular mobility of drugs in mixtures and dosage forms.

Surprisingly little research has been done on the solid-state NMR spectra of pharmaceutical dosage forms. To our knowledge, prior to the paper by Saindon et al.,[31] solid-state NMR has been used to study only two tablets both consisting almost entirely of pure drug: aspirin[51,52] and acetaminophen.[53] This paper shows that solid-state NMR is useful for the study of more complex pharmaceutical products.[31]

For example, Figure 13 shows the solid-state NMR spectrum of lovastatin tablets, which contain a rather large excess of excipients. The excipients, which have resonances in the 50–100 ppm range obscure resonances of lovastatin which appear at the same chemical shift but have little effect on resonances at other chemical shifts. Similar results were obtained for tablets of another closely related HMG-CoA reductase inhibitor, simvastatin.

E. Summary

In this review, areas of particular interest to Peggy Etter and her group were discussed including crystallization, hydrogen bonding, solvates and solid-state NMR. It is clear that her pioneering work has tremendously important implications for solid-state pharmaceutical chemistry.

(44) Byrn, S. R.; Lin, C. T. *J. Am. Chem. Soc.* **1976**, *98*, 4004.
(45) Byrn, S. R.; Kessler, D. W. *Tetrahedron* **1987**, *43*, 1335–43.
(46) Zografi, G. Z.; Ahlneck, K. V. *Int. J. Pharm.* **1990**, *62*, 87.
(47) Cauchon, N. Ph.D. Thesis, Purdue University, 1992.
(48) Saindon, P. Ph.D. Thesis, Purdue University, 1992.
(49) Toma, P. Ph.D. Thesis, Purdue University, 1993.
(50) Maverick, E.; Dunitz, J. *Mol. Phys.* **1987**, *62*, 451.
(51) Chang, C. J.; Diaz, L. E.; Morin, F.; Grant, D. *Magn. Reson. Chem.* **1986**, *1986*, 768.
(52) Diaz, L. E.; Frydman, L.; Olivieri, A.; Frydman, B. *Anal. Lett.* **1987**, *20*, 1657.
(53) Jagannathan, N. R. *Curr. Sci.* **1988**, *56*, 827.

UM00013057
NOVARTIS EXHIBIT 1017
Novartis v. Regents, IPR2023-01346
Page 1803 of 4460

Journal of Crystallographic and Spectroscopic Research, Vol. 21, No. 5, 1991

Molecular complexes of sulfonamides. Part 1. 1:1 complexes between sulfadimidine [4-amino-N-(4,6-dimethyl-2-pyrimidinyl)benzenesulfonamide] and 2- and 4-aminobenzoic acids

Mino R. Caira[1]

Received January 31, 1991

The crystal and molecular structures of the 1 : 1 complexes sulfadimidine·2-aminobenzoic acid (**I**) and sulfadimidine · 4-aminobenzoic acid (**II**) are described and compared with known structures containing sulfadimidine. In each complex, molecular association is maintained by one N—H · · · O hydrogen bond, and one O—H · · · N hydrogen bond involving the imino N and one pyrimidinyl N atom of sulfadimidine and the two carboxyl O atoms of the aromatic acid. The conformation of the sulfadimidine molecule in **II** is unusual for an N^1-substituted arylsulfonamide. Molecular dimensions for the complexed aminobenzoic acids are virtually the same as those reported for the free acids. Partial correlation between carboxylic acid strengths and the hydrogen bonded N · · · O distances is observed in sulfadimidine complexes of this type.

Introduction

Structural studies of molecular complexes of sulfonamides provide useful data relating to the binding capabilities and preferred conformations of these antimicrobial agents (Ghose *et al.*, 1987; Shefter and Sackman, 1971; Simonov *et al.*, 1990). Such complexes may also display differences in dissolution behavior relative to the parent sulfonamides or exhibit synergistic antimicrobial activity, and thus have potential for clinical use (Ghose *et al.*, 1988; Nagai *et al.*, 1979).

Sulfadimidine, [4-amino-*N*-(4,6-dimethyl-2-pyrimidinyl) benzenesulfonamide], also known as sulfamethazine, is used widely to treat urinary tract infections (Grahame-Smith and Aronson, 1985). It is rapidly absorbed from the gastrointestinal tract, is highly acetylated in the blood and urine, and binds firmly to plasma proteins (Papastephanou and Frantz, 1978). The structure of a 1 : 1 complex between sulfadimidine and salicylic acid was recently determined (Patel *et al.*, 1988).

[1]Department of Chemistry, University of Cape Town, Private Bag, Rondebosch, 7700, South Africa.

No systematic X-ray structural characterization of sulfadimidine complexes has been reported. The present study was undertaken to elucidate the structures of complexes between the drug and variously substituted aromatic carboxylic acids. The preparation and X-ray crystal structures of 1 : 1 complexes of sulfadimidine with 2-aminobenzoic acid (anthranilic acid) and 4-aminobenzoic acid are reported below. Both the 2- and 4-aminobenzoic acid isomers are biologically-active. The former is active as vitamin L_1 (Merck Index, 1989; Nakahara *et al.*, 1945). The interaction between sulfadimidine and 4-aminobenzoic acid (PABA) is of particular interest since PABA plays a central role as an essential metabolite in dihydrofolic acid synthesis, the process which is competitively inhibited by sulfonamides (Williams and Kruk, 1981).

Experimental

Colorless crystals of **I** were obtained by slow evaporation of a solution of sulfadimidine and 2-aminobenzoic acid in 1 : 1 ratio in acetonitrile. Crystals of **II** were

0277-8068/91/1000-0641$06.50/0 © 1991 Plenum Publishing Corporation

UM00013058
NOVARTIS EXHIBIT 1017
Novartis v. Regents, IPR2023-01346
Page 1804 of 4460

yellow and grew from a solution of sulfadimidine and 4-aminobenzoic acid in 1:1 ratio in 96% ethanol. In both cases, the best crystals were isolated after a period of 1 to 2 weeks. Elemental analyses confirmed the 1:1 stoichiometry for both complexes. Preliminary unit-cell and space-group data were deduced from precession photographs. Intensity data were measured at 294 K on an Enraf–Nonius CAD4 diffractometer using graphite-monochromated Mo $K\alpha$ radiation ($\bar{\lambda}$ = 0.71069 Å). Crystal data, data-collection parameters, and details of the structural analyses appear in Table 1. Accurate cell dimensions were obtained by a least-squares refinement of 24 accurately measured reflections with $32° \leq 2\theta \leq 34°$. Data in the range $1° \leq \theta \leq 25°$ were collected in the ω–2θ mode with a variable scan speed depending on I and σ(I) with a minimum recording time of 40 s per reflection. Intensity control was performed every hour and orientation control every 200 reflections. All data were corrected for *Lp*-effects and for absorption (North *et al.*, 1968) using program EAC of the Enraf–Nonius Structure Determination Package (1982).

The structures were solved by Patterson and Fourier methods and refined by full-matrix least-squares in which all nonhydrogen atoms were treated anisotropically and $\Sigma w||F_o| - |F_c||^2$ was minimized. All H atoms were found in difference Fourier syntheses. Phenyl and methyl H atoms were added in idealized positions (C—H = 1.00 Å) with common variable U_{iso} values for different rings. The remaining H atoms were allowed to refine with variable positions and U_{iso} parameters. Complex neutral atomic scattering factors (*International Tables for X-Ray Crystallography*, 1974) were

Table 1. Crystal data, data-collection parameters and details of the structural analyses

	I	II
Formula	$C_{12}H_{14}N_4O_2S \cdot 2{-}NH_2C_6H_4COOH$	$C_{12}H_{14}N_4O_2S \cdot 4{-}NH_2C_6H_4COOH$
M_r	415.5	415.5
Space group	$P2_1/c$	$P\bar{1}$
a/Å	9.455(2)	8.398(1)
b/Å	15.118(2)	9.375(2)
c/Å	14.391(1)	13.979(1)
α/deg	90.0	109.18(1)
β/deg	108.12(1)	91.26(1)
γ/deg	90.0	107.24(2)
V/Å^3	1955.0(5)	984.1(3)
Z	4	2
D_x/g cm^{-3}	1.412	1.402
μ (Mo $K\alpha$)/cm^{-1}	1.93	1.93
F(000)	872	436
Crystal size/mm	0.19 × 0.31 × 0.41	0.28 × 0.34 × 0.34
Index range	−11, 11; 0, 18; 0, 17	−10, 10; −11, 11; 0, 16
Standard reflections	721; $\bar{2}$ 11 4; $\bar{4}$ 1 11	$\bar{6}$ $\bar{1}$ 4; 4 $\bar{7}$ 3; 1 $\bar{3}$ 11
Intensity variation/%	−2.3	+0.9
Scan width in ω/deg	0.85 + 0.35 tan θ	0.85 + 0.35 tan θ
Vertical aperture/mm	4	4
Aperture width/mm	1.12 + 1.05 tan θ	1.12 + 1.05 tan θ
Reflections measured	3729	3601
Unique reflections	3022	3247
R_{int}	0.014	0.015
Absorption corrections: min, max, mean	0.9902, 0.9995, 0.9935	0.9912, 0.9996, 0.9949
Observed reflections, $I > 2\sigma(I)$	2528	2927
Parameters refined	291	291
R	0.039	0.037
R_w	0.038	0.037
S	2.34	3.01
w	$[\sigma^2(F_o)]^{-1}$	$[\sigma^2(F_o)]^{-1}$
Max Δ/σ for non-H atoms	0.15	0.13
$\Delta\rho$: max, min/e Å^{-3}	0.23, −0.27	0.27, −0.31

NOVARTIS EXHIBIT 1017
Novartis v. Regents, IPR2023-01346
Page 1805 of 4460

Table 8. Hydrogen bond data

D—H···A	D—H/Å	D···A/Å	H···A/Å	D—H···A/deg
		Complex I		
N(11)—H(11)···O(28)	0.85(3)	2.838(2)	2.00(3)	171(3)
O(27)—H(27)···N(17)	1.05(4)	2.663(2)	1.63(4)	171(4)
N(29)—H(291)···O(28)	0.88(3)	2.717(3)	2.11(3)	126(3)
N(7)—H(71)···O(9)^{i}	0.92(3)	3.153(3)	2.34(3)	147(3)
N(7)—H(72)···N(29)^{ii}	0.82(4)	3.211(5)	2.64(4)	128(3)
N(7)—H(72)···O(28)^{ii}	0.82(4)	3.395(4)	2.62(4)	157(3)
N(29)—H(291)···N(7)^{iii}	0.88(3)	3.164(4)	2.56(3)	127(2)
(i) $= 1-x, -\frac{1}{2}+y, \frac{1}{2}-z$ (ii) $= x, 1\frac{1}{2}-y, -\frac{1}{2}+z$ (iii) $= 1-x, \frac{1}{2}+y, \frac{1}{2}-z$				
		Complex II		
N(11)—H(11)···O(28)	1.01(4)	2.811(2)	1.81(4)	173(3)
O(27)—H(27)···N(17)	1.09(4)	2.676(2)	1.59(4)	176(3)
N(7)—H(71)···O(10)^{i}	0.90(2)	3.157(3)	2.55(3)	125(2)
N(7)—H(72)···O(9)^{ii}	0.88(3)	3.247(3)	2.38(3)	170(2)
N(29)—H(291)···O(10)^{iii}	0.89(2)	3.258(3)	2.39(2)	164(2)
N(29)—H(292)···N(7)^{iv}	0.91(3)	3.377(5)	2.52(3)	158(2)
(i) $= -x, -y, -z$ (ii) $= -1+x, y, z$ (iii) $= 2-x, 1-y, 1-z$ (iv) $= 1-x, -y, 1-z$				

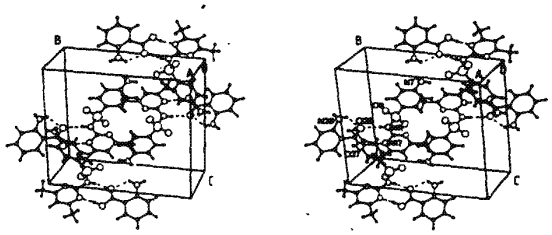


Fig. 3. Stereoview of the molecular packing in the unit cell of I.

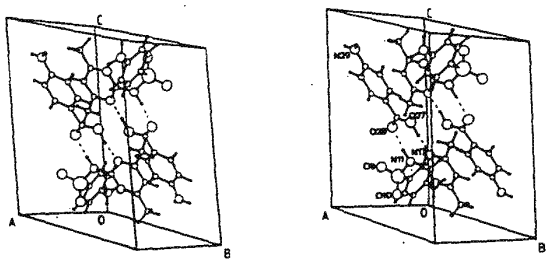


Fig. 4. Stereoview of the molecular packing in the unit cell of II.

Acknowledgments

Financial assistance from the FRD, Pretoria, and the University of Cape Town are gratefully acknowledged. Thanks are also due to Dr. M. L. Niven, the Computing Center at UCT and Prof. A. P. Lötter of the Research Institute for Industrial Pharmacy, PUCHO, for providing the sulfadimidine.

References

Basak, A. K., Mazumdar, S. K., and Chaudhuri, S. (1983). *Acta Crystallogr.* C**39**, 492–494.

CRC Handbook of Chemistry and Physics (1985–1986). R. C. Weast (ed.) (CRC Press, Cleveland, Ohio).

Ghose, S., Chakrabarti, C., and Dattagupta, J. K. (1987). *J. Crystallogr. Spectrosc. Res.* **17**, 197–206.

Ghose, S., Chakrabarti, C., Dattagupta, J. K., Le Page, Y., and Trotter, J. (1988). *Acta Crystallogr.* C**44**, 1810–1813.

Ghosh, M., Basak, A. K., Mazumdar, S. K., and Sheldrick, B. (1989). *J. Crystallogr. Spectrosc. Res.* **19**, 289–298.

Grahame-Smith, D. G., and Aronson, J. K. (1985). In *The Oxford textbook of clinical pharmacology and drug therapy*. (Oxford University Press, Oxford OX2 6DP), p. 755.

International Tables for X-Ray Crystallography (1974). Vol. IV. (Kynoch Press, Birmingham) (Present distributor: Reidel, D., Dordrecht).

Kálmán, A., Czugler, M., and Argay, G. (1981). *Acta Crystallogr.* B**37**, 868–877.

Lai, T. F., and Marsh, R. E. (1967). *Acta Crystallogr.* B**22**, 885–893.

Merck Index, 11th Edition (1989). 434. S. Budavari (ed.) (Merck & Co., Inc. Rahway, N. J.).

Motherwell, S. (1979). PLUTO, *A Program for plotting molecular and crystal structures* (University of Cambridge, England).

Nagai, K., Takayama, K., and Nanbu, N. (1979). (Yamanouchi Pharmaceutical Co., Ltd.) Jpn. Kokai Tokkyo Koho, Patent 79 16,494.

UM00013060
NOVARTIS EXHIBIT 1017
Novartis v. Regents, IPR2023-01346
Page 1806 of 4460

Nakahara, W., Inukai, F., Ugami, S., and Nagata, Y. (1945). *Sci. Papers Inst. Phys. Chem. Res.* **39**, 39–44.
Nardelli, M. (1983). *Comput. Chem.* **7**(3), 95–98.
North, A. C. T., Philips, D. C., and Scott Mathews, F. (1968). *Acta Crystallogr. A***24**, 351–359.
Papastephanou, C., and Frantz, M. (1978). In *Analytical Profiles of Drug Substances*, Vol. 7 K. Florey. (ed.) (Academic Press, New York), p. 414.
Patel, U., Haridas, M., and Singh, T. P. (1988). *Acta Crystallogr. C***44**, 1264–1267.
Rambaud, J., Maury, L., Pauvert, B., Audran, M., Lasserre, Y., Berge, G., and Declercq, J. P. (1985). *Acta Crystallogr. C***41**, 133–134.
Shefter, E., and Sackman, P. (1971). *J. Pharm. Sci.* **60**, 282–286.
Sheldrick, G. M. (1976). SHELX, *A System of Computer Programs for X-Ray Structure Determination* (University of Cambridge, England).
Simonov, Y., Battaglia, L. P., Corradi, A. B., Ianelli, S., Pelosi, G., Ganin, E., and Lukjanenko, N. (1990). *J. Incl. Phenom.* **9**, 181–194.
Structure Determination Package (1982). B. A. Frenz and Associates Inc., College Station, Texas 77840.
Takazawa, H., Ohba, S., and Saito, Y. (1986). *Acta Crystallogr. C***42**, 1880–1881.
Tiwari, R. K., Haridas, M., and Singh, T. P. (1984). *Acta Crystallogr. C***40**, 655–657.
Williams, R. A. D., and Kruk, Z. L. (1981). In *The Biochemistry and Pharmacology of Antibacterial Agents*. (Croom Helm biology in medicine series, London), pp. 24–28.

Structure factor data have been deposited with the British Library, Boston Spa, Wetherby, West Yorkshire, UK as supplementary publication No. 60750 (46 pages).

UM00013061
NOVARTIS EXHIBIT 1017
Novartis v. Regents, IPR2023-01346
Page 1807 of 4460

This Page is Inserted by IFW Indexing and Scanning Operations and is not part of the Official Record

BEST AVAILABLE IMAGES

Defective images within this document are accurate representations of the original documents submitted by the applicant.

Defects in the images include but are not limited to the items checked:

- ☐ BLACK BORDERS
- ☐ IMAGE CUT OFF AT TOP, BOTTOM OR SIDES
- ☐ FADED TEXT OR DRAWING
- ☐ BLURRED OR ILLEGIBLE TEXT OR DRAWING
- ☐ SKEWED/SLANTED IMAGES
- ☐ COLOR OR BLACK AND WHITE PHOTOGRAPHS
- ☐ GRAY SCALE DOCUMENTS
- ☐ LINES OR MARKS ON ORIGINAL DOCUMENT
- ☐ REFERENCE(S) OR EXHIBIT(S) SUBMITTED ARE POOR QUALITY
- ☐ OTHER: _____

IMAGES ARE BEST AVAILABLE COPY.
As rescanning these documents will not correct the image problems checked, please do not report these problems to the IFW Image Problem Mailbox.

Journal of Crystallographic and Spectroscopic Research, Vol. 22, No. 2, 1992

Molecular complexes of sulfonamides. 2. 1:1 complexes between drug molecules: sulfadimidine–acetylsalicylic acid and sulfadimidine–4-aminosalicylic acid

Mino R. Caira[1]

Received July 15, 1991; accepted August 5, 1991

The preparation and crystal structures of the 1 : 1 complexes sulfadimidine–acetylsalicylic acid (**I**) and sulfadimidine–4-aminosalicylic acid (**II**) are described. Each complex unit is maintained by two intermolecular hydrogen bonds, namely N—H · · · O=C and N · · · H—O, involving the N atom of the sulfonamide group and one pyrimidine N atom of the sulfonamide and the carboxylic group of the acid. Molecular parameters for protonated complexed aspirin, as found in **I**, are reported for the first time and reveal a significantly different conformation from that of the uncomplexed aspirin molecule. The structure of the 4-aminosalicylic acid molecule does not change significantly on complexation with sulfadimidine. Variation in the hydrogen bonded N · · · O distances in these complexes and their analogs is discussed.

Introduction

The first article in this series (Caira, 1991) outlined the relevance of molecular complexes of sulfonamides and reported the preparation and crystal structures of the 1 : 1 complexes between sulfadimidine [4-amino-N-(4,6-dimethyl-2-pyrimidinyl)benzenesulfonamide] and 2- and 4-aminobenzoic acids, respectively. An earlier report on the structure of the 1 : 1 sulfadimidine–salicylic acid complex (Patel *et al.*, 1988) prompted the present study in which two pharmacologically-active salicylic acid derivatives, acetylsalicylic acid (aspirin) and 4-aminosalicylic acid (PAS), were found to form analogous complexes with sulfadimidine.

The important therapeutic properties of these acids, namely analgesic, anti-inflammatory and antipyretic for aspirin, and tuberculostatic for PAS are well known. Both PAS and sulfonamides inhibit bacterial folic acid synthesis as analogues of p-aminobenzoic acid (PABA), but the binding sites for PABA on the enzyme dihydropteroate synthetase are quite specific. Thus, sulfonamides are ineffective against tubercle bacilli while PAS is ineffective against most bacteria (Jawetz, 1984; Williams and Kruk, 1981). Complex formation between different drug molecules continues to receive attention because the resultant species may display synergism and could therefore be clinically useful. Representative examples of complexes containing sulfonamides which have recently been studied in the solid state include trimethoprim-sulfamethoxazole (Nakai *et al.*, 1984), various antipyrine-sulfonamide complexes (Jeanjean *et al.*, 1985) and aminacrine-sulfadimidine (Ghose *et al.*, 1988). Although structural data for metal complexes or salts containing the anionic acetylsalicylato- and p-aminosalicylato-species have been published (e.g., Bandoli and Clemente, 1981; Greenaway *et al.*, 1984; Nishioka *et al.*, 1984; Sabirov *et al.*, 1982; Sequeira *et al.*, 1968), no crystallographic results for molecular complexes containing aspirin or PAS in their unionized forms have hitherto appeared in the literature (Cambridge Structural Database, 1991).

Experimental

Colorless single crystals of **I** grew within 2 days from a mixture of sulfadimidine and acetylsalicylic acid

[1] Department of Chemistry, Private Bag, Rondebosch 7700, South Africa.

0277-8068/92/0400-0193$06.50/0 © 1992 Plenum Publishing Corporation

UM00013063
NOVARTIS EXHIBIT 1017
Novartis v. Regents, IPR2023-01346
Page 1809 of 4460

in 1 : 1 molar ratio in acetonitrile. Brown prismatic crystals of **II** were obtained after 3 weeks from a mixture of sulfadimidine and *p*-aminosalicylic acid in 1 : 1 molar ratio in ethanol. Elemental analyses confirmed the 1 : 1 stoichiometry of both complexes. Preliminary unit-cell dimensions and space group data were obtained from precession photographs. Intensity data were collected at 294K in the ω-2θ mode on an Enraf–Nonius CAD4 diffractometer with Mo $K\alpha$-radiation (λ = 0.71069 Å). Accurate cell parameters were in each case determined by least-squares analysis of accurate setting angles in the range $16° \leq \theta \leq 17°$. Reflections in the range $1° \leq \theta \leq 25°$ were collected using a variable scan speed depending on I and $\sigma(I)$ with a minimum recording time of 40 s per reflection. Intensity control was performed every hour and orientation control every 200 measured reflections. Both data sets were corrected for Lp-effects and for absorption (North *et al.*, 1968) using the program EAC of the Enraf–Nonius Structure Determination Package (Frenz *et al.*, 1982). Data-collection parameters and details of structure refinements are listed in Table 1. The structures were solved by Patterson and Fourier methods. For **II**, the Patterson-derived S atom position was nearly identical to that in the 1 : 1 complex between sulfadimidine and PABA (Caira, 1991) whose unit-cell dimensions agreed with those for **II** within 2%. The nearly isomorphous relationship between the complexes allowed the atoms of the PABA complex to be successfully used as a trial model for **II**, atom O(30) of the PAS molecule being subsequently located from a difference Fourier synthesis. Refinement by full-matrix least-squares using the program SHELX76 (Sheldrick, 1976) involved minimization of $\Sigma\, w(|F_o| - |kF_c|)^2$ with anisotropic thermal parameters assigned to all nonhydrogen atoms. H-atoms were located in difference Fourier syntheses but were generally included in idealised positions (C—H = 1.00 Å). H-atoms which were refined included those of the amino, phenolic, and carboxylic groups and that attached to the N atom of the sulfonamide group. Location and refinement of H atoms in the latter two categories were deemed essential to establish unequivocally the tautomeric form of sulfadimidine present and the charged or protonated state of the complexing acid components. Complex neutral atomic scattering factors (*International Tables for X-Ray Crystallography*, 1974) were used. Other programs used were PARST (Nardelli, 1983) and PLUTO (Motherwell, 1979). Fractional atomic coordinates and equivalent isotropic thermal parameters ($U_{eq} = (\frac{1}{3})\, \Sigma_i \Sigma_j\, U_{ij} a_i^* a_j^* a_i \cdot a_j$) for nonhydrogen atoms are listed in Tables 2 and 3. H-atom coordinates are listed in Table 4. Structure factors, U_{ij} values, torsion angles and mean-plane data have been deposited.

Results and discussion

Perspective views of the structures of the complexes **I** and **II** are shown in Figs. 1 and 2, respectively. In each complex unit, molecular association occurs through hydrogen bonding involving the carboxylic group of the acid component and two N atoms (one pyrimidine N atom and the N atom of the sulfonamide group) of sulfadimidine. The aspirin and PAS molecules are in their unionized forms. The specific arrangement of C=O · · · H—N and O—H · · · N hydrogen bonds shown in Figs. 1 and 2 results in an eight-membered ring which occurs invariably, having now been observed in seven complexes between sulfadimidine and substituted aromatic carboxylic acids (Caira, 1991; Patel *et al.*, 1988), including p-chlorobenzoic acid and *o*-phthalic acid (Caira, 1992).

Sulfadimidine conformation

Interatomic distances and bond angles in sulfadimidine (Tables 5 and 6) are in the expected range. The sulfadimidine molecule adopts significantly different conformations in **I** and **II**. The values of the torsion angles τ_1–τ_3 (Table 7) for **I** are within a few degrees of those previously found in sulfadimidine–2-aminobenzoic acid. Those for **II** resemble closely the corresponding torsion angles in sulfadimidine–4-aminobenzoic acid, as expected for nearly isomorphous structures. The occurrence of both conformations with equal frequency in these complexes suggests that they are energetically similar, which accords with the finding (Kàlmàn *et al.*, 1981) that rotation about the S—C bond is not hindered in N-substituted aryl-sulfonamides. The conformation in which the plane of the phenyl ring approximately bisects the O—S—O angle (as in **II**, $\tau_1 \approx 160°$) is nevertheless unusual since the reported clustering range for τ_1 is 70–120°.

Aspirin and PAS structures

Because of their chemical significance, the crystal and molecular structures of both aspirin (Kim *et al.*, 1985; Wheatley, 1964) and PAS (Bertinotti *et al.*, 1954;

UM00013064
NOVARTIS EXHIBIT 1017
Novartis v. Regents, IPR2023-01346
Page 1810 of 4460

Table 1. Crystal data, data-collection parameters, and details of the structural analyses

	I	II
Formula	$C_{12}H_{14}N_4O_2S \cdot C_9H_8O_4$	$C_{12}H_{14}N_4O_2S \cdot C_7H_7NO_3$
M_r	458.4	431.5
Space group	$P2_1/c$	$P\bar{1}$
a/Å	7.696(1)	8.205(6)
b/Å	21.988(7)	9.449(3)
c/Å	13.432(2)	14.161(2)
α/deg	90	107.02(2)
β/deg	102.66(1)	92.29(4)
γ/deg	90	105.85(4)
V/Å^3	2218.1(8)	1001.3(9)
Z	4	2
D_x/g cm^{-3}	1.373	1.431
μ(Mo $K\alpha$)/cm^{-1}	1.82	1.94
F(000)	960	452
Crystal size/mm	0.38 × .44 × .44	0.13 × .33 × .43
Index range	−9, 9; 0, 26; 0, 16	−9, 9; −11, 11; 0, 16
Standard reflections	$\bar{6}$ 4 3, $\bar{2}$ 7 10, $\bar{1}$ 16 5	1 1 10, 6 $\bar{4}$ 2, $\bar{2}$ 7 1
Intensity variation/%	+2.4	−0.5
Scan width in ω/deg	0.85 + 0.35 tan θ	0.85 + 0.35 tan θ
Vertical aperture/mm	4	4
Aperture width/mm	1.12 + 1.05 tan θ	1.12 + 1.05 tan θ
Reflections measured	4185	3667
Unique reflections	3485	3179
R_{int}	0.013	0.021
Absorption corrections:		
min.	0.9887	0.9741
max.	1.0000	0.9997
mean	0.9959	0.9848
Observed reflections $I > 2\sigma(I)$	2933	2679
Parameters refined	316	302
R	0.040	0.051
R_w	0.040	0.055
S	2.859	1.703
w	$[\sigma^2(F_o)]^{-1}$	$[\sigma^2(F_o) + 1.545 \times 10^{-3}F_o^2]^{-1}$
Max Δ/σ for non-H atoms	0.16	0.21
$\Delta\rho$/e Å^{-3}		
min.	−0.28	−0.60
max.	0.18	0.53

UM00013065
NOVARTIS EXHIBIT 1017
Novartis v. Regents, IPR2023-01346
Page 1811 of 4460

Table 2. Fractional atomic coordinates ($\times 10^4$) and thermal parameters ($Å^2 \times 10^3$) with esd's in parentheses for Complex I

Atom	x/a	y/b	z/c	U_{eq}
C(1)	700(3)	2823(1)	4772(2)	40(1)
C(2)	−1005(3)	2904(1)	4940(2)	48(1)
C(3)	−2467(3)	2694(1)	4243(2)	55(1)
C(4)	−2249(3)	2395(1)	3368(2)	53(1)
C(5)	−543(4)	2307(1)	3218(2)	53(1)
C(6)	919(3)	2525(1)	3902(2)	47(1)
N(7)	−3696(4)	2173(2)	2673(2)	83(1)
S(8)	2523(1)	3097(0)	5664(0)	47(0)
O(9)	2164(2)	3040(1)	6664(1)	59(1)
O(10)	4109(2)	2831(1)	5475(1)	62(1)
N(11)	2557(3)	3837(1)	5502(2)	53(1)
C(12)	2833(3)	4133(1)	4642(2)	46(1)
N(13)	3255(3)	3802(1)	3905(2)	51(1)
C(14)	3547(3)	4111(1)	3093(2)	54(1)
C(15)	3392(4)	4740(1)	3043(2)	60(1)
C(16)	2940(3)	5043(1)	3844(2)	56(1)
N(17)	2653(3)	4742(1)	4661(2)	49(1)
C(18)	4059(4)	3746(1)	2264(2)	75(1)
C(19)	2719(4)	5725(1)	3844(3)	74(1)
C(20)	1465(3)	5505(1)	7866(2)	50(1)
C(21)	1637(3)	5271(1)	8845(2)	53(1)
C(22)	1309(4)	5622(1)	9641(2)	63(1)
C(23)	818(4)	6220(1)	9456(3)	70(1)
C(24)	666(4)	6467(1)	8498(3)	70(1)
C(25)	996(3)	6115(1)	7712(2)	58(1)
C(26)	1728(3)	5127(1)	6995(2)	54(1)
O(27)	1938(3)	5437(1)	6202(2)	69(1)
O(28)	1717(3)	4573(1)	7012(1)	74(1)
O(29)	2075(3)	4662(1)	9083(1)	60(1)
C(30)	3741(4)	4475(1)	9027(2)	57(1)
O(31)	4837(3)	4812(1)	8840(2)	68(1)
C(32)	3957(5)	3810(1)	9229(3)	82(2)

Table 3. Fractional atomic coordinates ($\times 10^4$) and thermal parameters ($Å^2 \times 10^3$) with esd's in parentheses for Complex II

Atom	x/a	y/b	z/c	U_{eq}
C(1)	2492(3)	370(3)	1502(2)	32(1)
C(2)	1377(4)	622(3)	2200(2)	40(1)
C(3)	−343(4)	−155(3)	1944(2)	41(1)
C(4)	−971(3)	−1189(3)	1002(2)	38(1)
C(5)	165(3)	−1474(3)	317(2)	40(1)
C(6)	1886(3)	−686(3)	564(2)	36(1)
N(7)	−2706(3)	−1982(3)	747(3)	49(1)
S(8)	4682(1)	1318(1)	1788(1)	33(0)
O(9)	5502(3)	407(2)	2178(2)	49(1)
O(10)	5292(2)	1718(2)	945(1)	42(1)
N(11)	4908(3)	2866(2)	2728(2)	35(1)
C(12)	4738(3)	4268(3)	2665(2)	30(1)
N(13)	3824(3)	4252(2)	1872(2)	34(1)
C(14)	3740(4)	5644(3)	1852(2)	37(1)
C(15)	4563(4)	6976(3)	2615(2)	45(1)
C(16)	5482(4)	6889(3)	3414(2)	40(1)
N(17)	5557(3)	5491(2)	3443(2)	34(1)
C(18)	2749(5)	5687(4)	961(3)	55(2)
C(19)	6447(5)	8268(4)	4266(3)	60(1)
C(20)	8759(3)	4479(3)	5981(2)	38(1)
C(21)	9685(4)	5911(3)	6637(2)	40(1)
C(22)	10733(4)	6053(4)	7458(2)	43(1)
C(23)	10898(4)	4720(3)	7646(2)	40(1)
C(24)	10002(4)	3283(4)	6995(2)	49(1)
C(25)	8950(4)	3145(3)	6168(2)	45(1)
C(26)	7625(4)	4349(3)	5126(2)	40(1)
O(27)	7491(3)	5661(3)	5053(2)	53(1)
O(28)	6822(3)	3089(3)	4511(2)	53(1)
N(29)	11924(4)	4869(4)	8475(2)	55(1)
O(30)	8125(4)	1729(3)	5567(2)	80(1)

Lin *et al.*, 1978) have been studied in some detail. Further reference to either of these compounds here cites data from the more recent structure redetermination. Crystals of both aspirin and PAS contain centrosymmetric dimers hydrogen bonded through their carboxylic groups. In aspirin, the carbonyl group of the —COOH function is *anti*-periplanar to the acetoxy group. For aspirin complexed to sulfadimidine in **I**, the relationship is *syn*-periplanar with the torsion angle O(28)—C(26)—C(20)—C(21) 16.7(4)° compared with −178.8(1)° in uncomplexed aspirin. The acetoxy groups in uncomplexed and complexed aspirin have a high degree of planarity but conform differently. In complex **I**, the acetoxy group is folded towards the carboxylic group with C(20)—C(21)—O(29)—C(30) 67.2(3)°, while in free aspirin the corresponding torsion angle is 85.2(2)°, i.e., a nearly perpendicular relationship between the phenyl ring and acetoxy group mean planes in the latter case. This conformational difference may be traced to participation by keto oxygen atom O(31) of **I** in a weak intermolecular hydrogen bond to sulfadimidine, $O(31)^{ii} \cdots H(15)—C(15)$ (Table 8). The corresponding O atom in uncomplexed aspirin is not hydrogen bonded. Distances and angles for aspirin in the two environments are generally in excellent agreement, the largest difference being that for C(26)—O(28), which is 1.218(3) Å in **I** and 1.239(2) Å in uncomplexed aspirin. Since the carboxylic acid groups are engaged in different hydrogen bonding patterns in the two cases, a difference of this magnitude is not unexpected. Accurate parameters for protonated aspirin hydrogen bonded to a molecule other than itself, as in complex **I**, have not been reported previously. Aspirin molecules included as guests in β-cyclodextrin are probably present as carboxylate anions (Nishioka *et al.*, 1984).

UM00013066
NOVARTIS EXHIBIT 1017
Novartis v. Regents, IPR2023-01346
Page 1812 of 4460

Table 4. Fractional atomic coordinates ($\times 10^4$ for idealised H atoms, $\times 10^3$ for refined H atoms) and isotropic thermal parameters ($Å^2 \times 10^3$) in Complexes I and II with esd's in parentheses

Atom	x/a	y/b	z/c	U_{iso}
Complex I				
H(2)	−1173	3119	5570	69(4)
H(3)	−3689	2757	4367	69(4)
H(5)	−372	2081	2600	69(4)
H(6)	2139	2468	3771	69(4)
H(71)	−371(5)	213(2)	205(3)	132(11)
H(72)	−474(5)	232(2)	277(3)	132(11)
H(11)	219(4)	404(1)	598(2)	83(11)
H(15)	3605	4968	2436	128(5)
H(181)	4221	4005	1679	128(5)
H(182)	3217	3407	2004	128(5)
H(183)	5235	3574	2617	128(5)
H(191)	3102	5888	3230	128(5)
H(192)	3477	5905	4474	128(5)
H(193)	1445	5835	3805	128(5)
H(22)	1426	5443	10338	104(5)
H(23)	569	6478	10022	104(5)
H(24)	316	6903	8373	104(5)
H(25)	897	6299	7021	104(5)
H(27)	211(5)	514(2)	565(3)	155(17)
H(321)	5234	3687	9321	104(5)
H(322)	3225	3585	8636	104(5)
H(323)	3528	3709	9860	104(5)
Complex II				
H(2)	1819	1363	2886	54(4)
H(3)	−1147	31	2447	54(4)
H(5)	−268	−2254	−358	54(4)
H(6)	2693	−879	64	54(4)
H(71)	−298(5)	−231(4)	13(3)	54(4)
H(72)	−323(5)	−157(4)	114(3)	54(4)
H(11)	549(4)	292(4)	327(2)	43(9)
H(15)	4491	8003	2587	110(6)
H(181)	2865	6807	1069	110(6)
H(182)	1516	5100	908	110(6)
H(183)	3211	5256	333	110(6)
H(191)	6230	9212	4171	110(6)
H(192)	7695	8380	4285	110(6)
H(193)	6063	8148	4907	110(6)
H(21)	9586	6871	6508	63(4)
H(22)	11375	7103	7924	63(4)
H(24)	10118	2327	7124	63(4)
H(27)	686(5)	557(4)	444(3)	63(4)
H(291)	1255(5)	571(5)	876(3)	63(4)
H(292)	1201(5)	406(5)	856(3)	63(4)
H(30)	747(5)	192(4)	503(3)	63(4)

Molecular dimensions for PAS in complex II are very similar to those in uncomplexed PAS. The only noteworthy difference is in the bond length C(25)—O(30), which is 1.329(2) Å in II vs 1.361(2) Å in uncomplexed PAS. In both cases, the intramolecular O—H · · · O hydrogen bond locks the phenyl and carboxy planes into near coplanarity. The least-squares planes through these sets of atoms intersect at 1.5° in PAS and 2.9(2)° in II. Complexation with sulfadimidine thus has no remarkable effect on the dimensions or conformation of the PAS molecule.

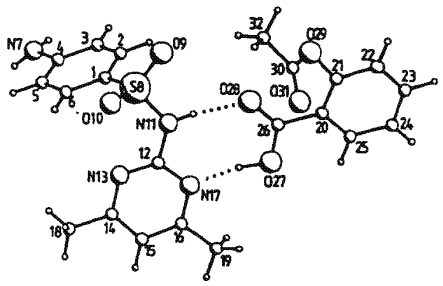


Fig. 1. Molecular structure of I. C atoms are labeled with numerals only. Dotted lines indicate hydrogen bonds.

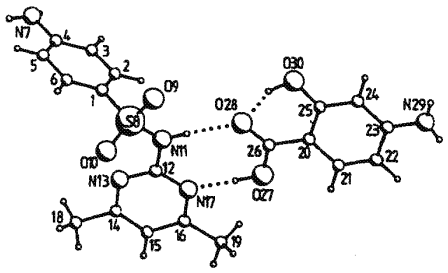


Fig. 2. Molecular structure of II. C atoms are labeled with numerals only. Dotted lines indicate hydrogen bonds.

Hydrogen bonding and crystal packing

Hydrogen bond data are listed in Table 8. One objective in investigating the series of 1:1 complexes between sulfadimidine and variously substituted aromatic carboxylic acids was to seek possible correlations between the N · · · O distances for the hydrogen bonds N—H · · · O and N · · · H—O and the acid p*K*a values. The former distance parameters may be taken as a measure of the strength of molecular association between sulfadimidine and the carboxylic acid and might therefore be expected to depend on acid strength. Significant variations in the distances N(11) · · · O(28) and N(17) · · · O(27) do occur in this series. The respective ranges are 2.779(3)–2.841(4) Å and 2.639(3)–2.724(4) Å for

UM00013067
NOVARTIS EXHIBIT 1017
Novartis v. Regents, IPR2023-01346
Page 1813 of 4460

Table 5. Bond lengths (Å) with esd's in parentheses for Complexes I and II

(a) Sulfadimidine	I	II	(b) Acetylsalicyclic acid	(I)
C(1)–C(2)	1.392(4)	1.387(4)	C(20)–C(26)	1.484(4)
C(1)–C(6)	1.382(4)	1.382(3)	C(21)–C(22)	1.386(4)
C(1)–S(8)	1.742(2)	1.745(3)	C(21)–O(29)	1.401(3)
C(2)–C(3)	1.377(3)	1.378(4)	C(22)–C(23)	1.376(3)
C(3)–C(4)	1.389(4)	1.381(3)	C(23)–C(24)	1.378(5)
C(4)–C(5)	1.385(4)	1.392(4)	C(24)–C(25)	1.377(5)
C(4)–N(7)	1.377(4)	1.392(3)	C(26)–O(27)	1.304(4)
C(5)–C(6)	1.374(3)	1.380(3)	C(26)–O(28)	1.218(3)
S(8)–O(9)	1.436(2)	1.437(3)	O(29)–C(30)	1.365(4)
S(8)–O(10)	1.425(2)	1.424(2)	C(30)–O(31)	1.189(4)
S(8)–N(11)	1.643(2)	1.624(2)	C(30)–C(32)	1.490(3)
N(11)–C(12)	1.382(4)	1.397(4)		
C(12)–N(13)	1.325(4)	1.319(4)	(c) *p*-Aminosalicyclic acid	(II)
C(12)–N(17)	1.347(3)	1.331(3)		
N(13)–C(14)	1.345(4)	1.345(4)	C(20)–C(21)	1.385(3)
C(14)–C(15)	1.389(3)	1.373(3)	C(20)–C(25)	1.408(5)
C(14)–C(18)	1.494(4)	1.491(6)	C(20)–C(26)	1.452(4)
C(15)–C(16)	1.373(4)	1.370(5)	C(21)–C(22)	1.370(4)
C(16)–N(17)	1.341(4)	1.351(4)	C(22)–C(23)	1.400(5)
C(16)–C(19)	1.509(3)	1.490(4)	C(23)–C(24)	1.379(4)
			C(23)–N(29)	1.366(4)
(b) Acetylsalicyclic acid	(I)		C(24)–C(25)	1.379(5)
			C(25)–O(30)	1.329(3)
C(20)–C(21)	1.391(4)		C(26)–O(27)	1.307(5)
C(20)–C(25)	1.393(3)		C(26)–O(28)	1.236(3)

Table 6. Bond angles (°) with esd's in parentheses for Complexes I and II

(a) Sulfadimidine	I	II	(b) Acetylsalicyclic acid	(I)
C(6)–C(1)–S(8)	121.1(2)	118.3(3)	C(21)–C(20)–C(25)	117.7(2)
C(2)–C(1)–S(8)	119.4(2)	121.6(2)	C(20)–C(21)–O(29)	122.5(2)
C(2)–C(1)–C(6)	119.5(2)	120.1(4)	C(20)–C(21)–C(22)	121.9(2)
C(1)–C(2)–C(3)	120.4(2)	119.7(3)	C(22)–C(21)–O(29)	115.6(2)
C(2)–C(3)–C(4)	120.2(2)	120.8(4)	C(21)–C(22)–C(23)	118.8(3)
C(3)–C(4)–N(7)	120.8(3)	120.8(3)	C(22)–C(23)–C(24)	120.6(3)
C(3)–C(4)–C(5)	118.9(2)	119.1(3)	C(23)–C(24)–C(25)	120.2(2)
C(5)–C(4)–N(7)	120.3(2)	120.1(3)	C(20)–C(25)–C(24)	120.9(3)
C(4)–C(5)–C(6)	121.2(3)	120.4(3)	C(20)–C(26)–O(28)	122.8(2)
C(1)–C(6)–C(5)	119.8(2)	119.9(3)	C(20)–C(26)–O(27)	114.4(2)
C(1)–S(8)–N(11)	106.6(1)	106.3(2)	O(27)–C(26)–O(28)	122.7(3)
C(1)–S(8)–O(10)	109.2(1)	108.6(2)	C(21)–O(29)–C(30)	117.2(2)
C(1)–S(8)–O(9)	108.9(1)	109.3(2)	O(29)–C(30)–C(32)	110.7(3)
O(10)–S(8)–N(11)	110.1(1)	110.7(2)	O(29)–C(30)–O(31)	122.8(3)
O(9)–S(8)–N(11)	102.9(1)	104.0(2)	O(31)–C(30)–C(32)	126.5(3)
O(9)–S(8)–O(10)	118.6(1)	117.4(3)		
S(8)–N(11)–C(12)	125.9(2)	125.3(2)		
N(11)–C(12)–N(17)	114.7(2)	113.8(3)	(c) p-Aminosalicyclic acid	(II)
N(11)–C(12)–N(13)	118.3(2)	118.6(3)		
N(13)–C(12)–N(17)	127.1(3)	127.6(3)	C(25)–C(20)–C(26)	120.8(3)
C(12)–N(13)–C(14)	116.1(2)	115.4(3)	C(21)–C(20)–C(26)	121.3(3)
N(13)–C(14)–C(18)	116.8(2)	117.3(3)	C(21)–C(20)–C(25)	117.9(3)
N(13)–C(14)–C(15)	121.0(2)	121.3(3)	C(20)–C(21)–C(22)	122.0(3)
C(15)–C(14)–C(18)	122.2(2)	121.4(3)	C(21)–C(22)–C(23)	119.7(3)
C(14)–C(15)–C(16)	118.6(2)	119.6(3)	C(22)–C(23)–N(29)	119.4(3)
C(15)–C(16)–C(19)	122.0(2)	123.6(3)	C(22)–C(23)–C(24)	119.2(3)
C(15)–C(16)–N(17)	121.1(2)	119.4(3)	C(24)–C(23)–N(29)	121.4(3)
N(17)–C(16)–C(19)	116.9(2)	117.0(3)	C(23)–C(24)–C(25)	121.0(3)
C(12)–N(17)–C(16)	116.1(2)	116.7(3)	C(20)–C(25)–C(24)	120.2(3)
			C(24)–C(25)–O(30)	118.1(3)
(b) Acetylsalicyclic acid	(I)		C(20)–C(25)–O(30)	121.6(3)
			C(20)–C(26)–O(28)	122.8(3)
C(25)–C(20)–C(26)	119.9(2)		C(20)–C(26)–O(27)	115.4(3)
C(21)–C(20)–C(26)	122.5(2)		O(27)–C(26)–O(28)	121.9(3)

UM00013068
NOVARTIS EXHIBIT 1017
Novartis v. Regents, IPR2023-01346
Page 1814 of 4460

Table 7. Selected torsion angles (°) with esd's in parentheses for Complexes I and II

		I	II
τ_1	C(6)−C(1)−S(8)−N(11)	104.2(2)	159.8(3)
τ_2	C(1)−S(8)−N(11)−C(12)	−64.7(3)	−82.8(4)
τ_3	S(8)−N(11)−C(12)−N(13)	−5.9(4)	23.0(5)
	C(21)−C(20)−C(26)−O(27)	−164.5(3)	−3.0(5)
	C(21)−C(20)−C(26)−O(28)	16.7(4)	177.7(4)
	C(20)−C(21)−O(29)−C(30)	67.2(3)	—
	C(21)−O(29)−C(30)−O(31)	4.0(4)	—

Table 8. Hydrogen bond data

D−H ··· A	D-H (Å)	D ··· A (Å)	H ··· A (Å)	D−H ··· A (°)
Complex I				
N(11)−H(11) ··· O(28)	0.88(3)	2.779(3)	1.91(3)	171(3)
O(27)−H(27) ··· N(17)	1.02(4)	2.724(4)	1.72(4)	169(4)
N(7)−H(71) ··· O(10)^{i}	0.84(4)	3.065(3)	2.40(3)	137(3)
C(15)−H(15) ··· O(31)^{ii}	1.00(4)	3.276(4)	2.35(4)	154(3)
(i) = $-1+x, 0.5-y, -0.5+z$ (ii) = $1-x, 1-y, 1-z$				
Complex II				
N(11)−H(11) ··· O(28)	0.87(4)	2.842(4)	1.97(4)	179(3)
O(27)−H(27) ··· N(17)	0.97(4)	2.664(4)	1.71(4)	172(4)
O(30)−H(30) ··· O(28)	1.00(5)	2.603(5)	1.68(5)	153(4)
N(7)−H(72) ··· O(9)^{i}	0.79(4)	3.277(4)	2.51(4)	163(4)
N(29)−H(291) ··· O(10)^{ii}	0.79(3)	3.251(4)	2.49(4)	160(4)
(i) = $-1+x, y, z$ (ii) = $2-x, 1-y, 1-z$				

seven complexes, with acid p*K*a values spanning the range 2.89–6.97. When all the available data are considered, however, no systematic change in either of the N ··· O distances with p*K*a is found. It is concluded that any subtle variations in N ··· O distance that may arise from differences in acid strength are overshadowed by the requirements of crystal packing. This was recently confirmed by the finding (Caira, 1992) that in the 1 : 1 complex sulfadimidine-p-chlorobenzoic acid (space group $P2_1/c$, $Z = 8$), the crystallographically independent but chemically equivalent N ··· O distances in the N−H ··· O hydrogen bonds differ by as much as 8σ, compared with a difference of 12σ for the observed distance range quoted above.

Figures 3 and 4 are stereoscopic views illustrating the molecular packing in I and II. For clarity, the hydrogen bonds indicated include only the N−H ··· O and N ··· H−O bonds referred to above, the C−H

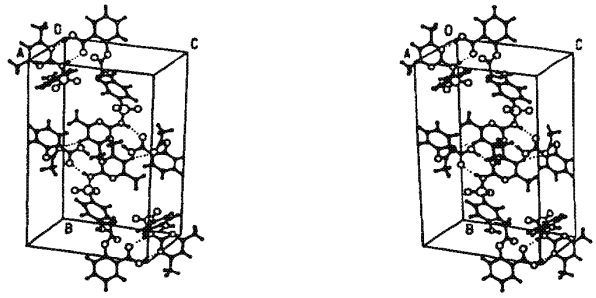


Fig. 3. Stereoview of the molecular packing and principal hydrogen bonds in I.

UM00013069
NOVARTIS EXHIBIT 1017
Novartis v. Regents, IPR2023-01346
Page 1815 of 4460

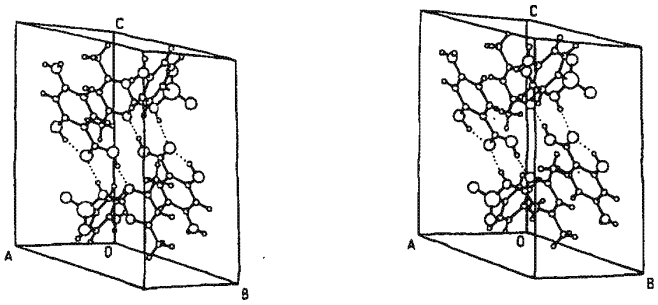


Fig. 4. Stereoview of the molecular packing and principal hydrogen bonds in **II**.

· · · O bond which stabilizes the conformation of the acetoxy group of aspirin in **I**, and the intramolecular O—H · · · O bond of PAS in **II**. There are additional weaker intermolecular N—H · · · O (sulfonyl) hydrogen bonds involving the $-NH_2$ functions in both complexes (Table 8).

Acknowledgments

Financial assistance from the FRD, Pretoria, and the University of Cape Town are gratefully acknowledged. Thanks are also due to Dr. M. L. Niven, the Computing Centre at UCT and Professor A. P. Lötter of the Research Institute for Industrial Pharmacy, PUCHO, for providing the sulfadimidine.

References

Bandoli, G., and Clemente, D. A. (1981) *J. Inorg. Nucl. Chem.* **43**, 2843–2846.

Bertinotti, F., Giacomello, G., and Liquori, A. M. (1954) *Acta Crystallogr.* **7**, 808–812.

Caira, M. R. (1991) *J. Crystallogr. Spectrosc. Res.* **21**, 641.

Caira, M. R. (1992) In preparation.

Cambridge Structural Database. (1991) Version 4.4. Cambridge Crystallographic Data Centre, University Chemical Laboratory, Cambridge.

Frenz, B. A., and Associates Inc. (1982) Structure Determination Package (College Station, Texas).

Ghose, S., Chakrabarti, C., Dattagupta, J. K., Le Page, Y., and Trotter, J. (1988) *Acta Crystallogr. C***44**, 1810–1813.

Greenaway, F. T. Pezeshk, A., Cordes, A. W., Noble, M. C., and Sorenson, J. R. J. (1984) *Inorg. Chim. Acta* **93**, 67–71.

International Tables for X-Ray Crystallography (1974) Vol. IV (Birmingham: Kynoch Press) (Present distributor: Reidel, D., Dordrecht).

Jawetz, E. (1984) In *Basic and Clinical Pharmacology*. (second edition) B. G. Katzung (ed.) (Lange Medical Publications, Los Altos, California).

Jeanjean, B., Alberola, S., Rambaud, J., and Sabon, F. (1985) *Ann. Pharm. Fr.* **42(6)**, 561–568.

Kàlmàn, A., Czugler, M., and Argay, G. (1981) *Acta Crystallogr. B***37**, 868–877.

Kim, Y., Machida, K., Taga, T., and Osaki, K. (1985) *Chem. Pharm. Bull.* **33(7)**, 2641–2647.

Lin, C., Siew, P., and Byrn, S. R. (1978) *J. Chem. Soc. Perkin* **2**, 957–962.

Motherwell, S. (1979) *PLUTO, A program for plotting molecular and crystal structures* (University of Cambridge, England).

Nakai, H., Takasuka, M., and Shiro, M. (1984) *J. Chem. Soc. Perkin Trans* **2**, 9, 1459–1464.

Nardelli, M. (1983) *Comput. Chem.* **7(3)**, 95–98.

Nishioka, F., Nakanashi, I., Fujiwara, T., and Tomita, K. (1984) *J. Incl. Phenom.* **2**, 701–714.

North, A. C. T., Philips, D. C., and Scott Mathews, F. (1968) *Acta Crystallogr. A***24**, 351–359.

Patel, U., Haridas, M., and Singh, T. P. (1988) *Acta Crystallogr. C***44**, 1264–1267.

Sabirov, V. Kh., Azizov, M. A., Shabilalov, A. A., Struchkov, Yu. T., and Aleksandrov, G. G. (1982) *Koord. Khim.* **8**, 245–250.

Sequeira, A., Berkebile, C. A., and Hamilton, W. C. (1968) *J. Mol. Struct.* **1**, 283–294.

Sheldrick, G. M. (1976) *SHELX, A system of computer programs for x-ray structure determination* (University of Cambridge, England).

Wheatley, P. J. (1964) *J. Chem. Soc.* 6036–6048.

Williams, R. A. D., and Kruk, Z. L. (1981) In *The Biochemistry and Pharmacology of Antibacterial Agents*, p. 29. (Croom Helm biology in medicine series, London).

Anisotropic thermal parameters, torsion angles, weighted least-squares planes and structure factor data have been deposited with the British Library, Boston Spa, Wetherby, West Yorkshire, UK, as supplementary publication No. 63165 (45 pages).

UM00013070
NOVARTIS EXHIBIT 1017
Novartis v. Regents, IPR2023-01346
Page 1816 of 4460

Journal of Chemical Crystallography, Vol. 24, No. 10, 1994

Molecular complexes of sulfonamides. 3. Structure of 5-methoxysulfadiazine (Form II) and its 1:1 complex with acetylsalicylic acid

Mino R. Caira[1]

Received August 11, 1994

The X-ray structure of the biologically most active polymorph (Form II) of 5-methoxysulfadiazine (**1**) and that of the 1 : 1 complex between this sulfonamide and acetylsalicylic acid (**2**) are reported. The polymorph **1** is monoclinic, space group $P2_1/c$ with $a = 13.086(2)$ Å, $b = 5.583(1)$ Å, $c = 17.222(3)$ Å, $\beta = 99.98(1)°$, $Z = 4$ and occurs as centrosymmetric hydrogen bonded (N—H···N) dimers in the crystal. This arrangement differs from that observed in other polymorphs of the drug. Complex **2** is triclinic, $P\bar{1}$, $a = 8.102(1)$ Å, $b = 12.033(1)$ Å, $c = 12.170(2)$ Å, $\alpha = 111.67(1)°$, $\beta = 93.77(1)°$, $\gamma = 103.82(1)°$, $Z = 2$. Complexation involves linear intermolecular hydrogen bonds, N—H···O=C and N···O—H, between the amide group and pyrimidinyl N atom of the sulfonamide and the carboxylic group of the acetylsalicylic acid. On complexation to form **2**, neither molecular component undergoes any major structural change.

KEY WORDS: Key Words: Molecular complexes, sulfonamides, acetylsalicylic acid.

Introduction

In earlier parts of this series we described the structures of 1 : 1 complexes between sulfadimidine [4-amino-N-(4,6-dimethyl-2-pyrimidinyl)benzenesulfonamide] and various aromatic carboxylic acid derivatives including 2- and 4-aminobenzoic acids,[1] 4-aminosalicylic acid (p-aminosalicylic acid or PAS) and acetylsalicylic acid (aspirin).[2] These studies have been extended to an investigation of the complexing behaviour of the related drug 5-methoxysulfadiazine [4-amino-N-(5-methoxy-2-pyrimidinyl)benzeneulfonamide] (hereinafter SMD). Only one molecular complex containing SMD has been structurally characterized.[3] Various aspects of the polymorphism of this drug have also been reported during the last 25 years, including the identification of various polymorphs,[4-7] their interconversion,[8,9] and the X-ray crystal structures of two polymorphs designated Forms I and III.[10]

Reaction between SMD and aspirin produces a 1 : 1 molecular complex, analogous to that formed between sulfadimidine and aspirin. However, in our attempt to obtain a complex between SMD and PAS, large single crystals of a polymorph of SMD were obtained instead. We identified these as Form II, the biologically most active form of the sulfonamide,[8] which when prepared by the usual method involving recrystallization from ethanol by rapid cooling to −12°C, is obtained as small particles with little or no geometrical form.[5] This probably accounts for the fact that the crystal structure of this important polymorphic species has not hitherto been determined.

We report here the crystal structures of (**1**) SMD Form II and (**2**) the 1 : 1 complex between SMD and aspirin. The results allow several useful comparisons: the conformation and hydrogen bonding scheme for SMD in Form II with corresponding features in Forms I and III, the conformations of uncomplexed SMD and SMD complexed with aspirin, and finally the structures of the SMD-aspirin complex and its sulfadimidine analog. A possible reason for the crystallization of SMD Form II during the attempted preparation of a SMD–PAS complex is also discussed.

[1]Department of Chemistry, University of Cape Town, Rondebosch 7700, South Africa.

1074-1542/94/1000-0695$07.00/0 © 1994 Plenum Publishing Corporation

UM00013071
NOVARTIS EXHIBIT 1017
Novartis v. Regents, IPR2023-01346
Page 1817 of 4460

Experimental

Crystal preparation

SMD was purchased from Aldrich-Chemie, Steinheim. X-ray powder diffraction analysis of the unground material matched the published pattern for Form I.[5] A solution containing 0.05 g of SMD in 6 cm^3 CH_3CN was mixed with a solution containing 0.027 g PAS in 2 cm^3 CH_3CN and the mixture heated to 323K with stirring for 10 min. On evaporation, the residue consisted of unreacted PAS and several large columnar crystals. The latter were tentatively identified as SMD Form II from the resemblance between the unit cell data obtained photographically with those reported in the literature.[5] Confirmation of this assignment was obtained after the single crystal X-ray analysis had been performed, by calculating the XRD pattern and finding that it corresponded with that published for Form II.[5] A solution made by mixing 0.05 g SMD in 6 cm^3 CH_3CN and 0.032 g aspirin in 1.5 cm^3 CH_3CN and heating to 323K with stirring for ten minutes yielded, after slow evaporation, yellow prismatic crystals of (2) the 1 : 1 SMD-aspirin complex. Preliminary unit cell data for 2 differed from those reported for the starting materials, confirming that a compound had been formed. The 1 : 1 complex stoichiometry was confirmed by single crystal X-ray analysis.

Single crystal X-ray analyses

Analogous procedures were used for the crystal structure determinations. Preliminary unit cell dimensions and space group data were obtained from precession photographs. Intensity data were collected on an Enraf-Nonius CAD4 diffractometer with MoKα-radiation (λ = 0.71069 Å). Accurate cell parameters were determined by the least-squares analysis of accurate setting angles in the θ-range 16–17°. Reflections in the θ-range 1–25° were collected by the ω-2θ scan mode using a variable scan speed depending on I and $\sigma(I)$ with a maximum time of 40 s per reflection. A variable scan width ω of (0.85 + 0.35 tan θ)° and a variable aperture width of (1.12 + 1.05 tan θ) mm were used. Intensity control was performed every hour and orientation control every 200 measured reflections. Both data sets were corrected for Lp-effects and for absorption[11] using the program EAC of the Enraf-Nonius Structure Determination Package.[12] Data-collection parameters and details of structure refinements are listed in Table 1. Intensity statistics indicated that $P\bar{1}$ is the correct space group for the complex 2. The structures were solved by direct methods using program SHELX86[13] and refined by full-matrix least-squares using SHELX76[14] and minimizing $\Sigma w(|F_o| - |kF_c|)^2$. All H atoms were located in difference Fourier maps. Those attached to O or N atoms were allowed to refine freely while the rest were added in idealized positions with C—H 1.00 Å. Anisotropic thermal parameters were employed for non-H atoms and common variable U_{iso} values were assigned to H atoms in different chemical groups. The latter refined in the ranges 0.046–0.090 $Å^2$ and 0.054–0.103 $Å^2$ for 1 and 2, respectively. Complex neutral atomic scattering factors[15] were used. Program PARST[16] was used for geometrical calculations and PLUTO[17] for molecular drawings. Fractional atomic coordinates and equivalent isotropic thermal parameters (U_{eq} = (1/3)$\Sigma_i\Sigma_j U_{ij} a_i^* a_j^* a_i \cdot a_j$) for nonhydrogen atoms are listed in Tables 2 and 3. Hydrogen atom positions, U_{ij} values, torsion angles and structure factor tables have been submitted to this journal.

Table 1. Crystal data, details of data-collection and refinement

	1	2
Formula	$C_{11}H_{12}N_4O_3S$	$C_{11}H_{12}N_4O_3S \cdot C_9H_8O_4$
M/g mol^{-1}	280.3	460.5
a/Å	13.086(2)	8.102(1)
b/Å	5.583(1)	12.033(1)
c/Å	17.222(3)	12.170(2)
α/°	90.0	111.67(1)
β/°	99.98(1)	93.77(1)
γ/°	90.0	103.82(1)
V/Å^3	1239.2(4)	1055.0(3)
Z	4	2
Space group	$P2_1/c$	$P\bar{1}$
μ(MoKα)/cm^{-1}	2.59	1.94
F(000)	584	480
D_c/g cm^{-3}	1.502	1.450
Crystal size/mm	0.28 × 0.34 × 0.41	0.28 × 0.34 × 0.34
Index range	−15, 15; 0, 6; 0, 20	−9, 9; −14, 14; 0, 14
Standard intensity variation/%	+0.5	+1.4
Absorption correction factor range	0.9899, 1.0000	0.9934, 0.9992
Reflections measured	2519	3896
Unique reflections	2064	3391
R_{int}	0.015	0.033
Observed reflections, $I > 2\sigma(I)$	1905	2971
L S variables	188	315
Mean shift/error	0.01	0.01
Weighting scheme	$[\sigma^2(F_o)]^{-1}$	$[\sigma^2(F_o)]^{-1}$
R	0.041	0.037
R_w	0.041	0.038
S	3.918	2.764
Final $\Delta\rho$/e Å^{-3}, min, max	−0.42, 0.27	−0.34, 0.20

UM00013072
NOVARTIS EXHIBIT 1017
Novartis v. Regents, IPR2023-01346
Page 1818 of 4460

Table 2. Fractional atomic coordinates ($\times 10^4$, $\times 10^5$ for S) and equivalent isotropic thermal parameters ($Å^2 \times 10^3$) with esd's in parentheses for 1

Atom	x/a	y/b	z/c	U_{eq}
S(1)	25849(5)	15494(13)	53683(4)	32(0)
O(1)	2719(1)	−309(4)	5956(1)	41(1)
O(2)	2815(1)	3961(4)	5618(1)	42(1)
O(3)	−929(2)	7023(5)	2829(2)	91(1)
N(1)	1366(2)	1251(5)	4966(1)	38(1)
N(2)	1266(2)	4468(5)	4087(1)	45(1)
N(3)	−230(2)	2321(4)	4293(1)	36(1)
N(4)	5198(2)	−813(5)	2997(2)	43(1)
C(1)	3314(2)	862(5)	4639(1)	29(1)
C(2)	3182(2)	−1305(5)	4242(2)	35(1)
C(3)	3802(2)	−1851(5)	3695(2)	36(1)
C(4)	4581(2)	−293(5)	3559(1)	33(1)
C(5)	4718(2)	1858(5)	3970(2)	35(1)
C(6)	4086(2)	2441(5)	4506(2)	33(1)
C(7)	783(2)	2775(5)	4425(2)	33(1)
C(8)	655(2)	5834(6)	3570(2)	56(1)
C(9)	−401(2)	5520(6)	3380(2)	48(1)
C(10)	−820(2)	3714(6)	3759(2)	42(1)
C(11)	−1984(2)	6628(8)	2570(2)	63(1)

Results and discussion

Bond lengths and bond angles for **1** and **2** are listed in Tables 4 and 5; hydrogen bond data appear in Table 6.

Table 3. Fractional atomic coordinates ($\times 10^4$) and equivalent isotropic thermal parameters ($Å^2 \times 10^3$) with esd's in parentheses for 2

Atom	x/a	y/b	z/c	U_{eq}
S(1)	4639(1)	6152(1)	7383(1)	41(0)
O(1)	5298(2)	5604(1)	8117(2)	58(1)
O(2)	5398(2)	6082(2)	6334(2)	54(1)
O(3)	4496(2)	11363(2)	7004(2)	63(1)
O(4)	7540(2)	8323(1)	10275(2)	60(1)
O(5)	8275(2)	10339(2)	10656(2)	53(1)
O(6)	8774(2)	7613(1)	11933(1)	46(1)
O(7)	10542(2)	7135(2)	10606(2)	69(1)
N(1)	4967(2)	7608(2)	8311(2)	40(1)
N(2)	3853(2)	8292(2)	6936(2)	42(1)
N(3)	5859(2)	9694(2)	8688(2)	36(1)
N(4)	−2830(3)	3783(2)	5784(2)	55(1)
C(1)	2413(3)	5522(2)	6949(2)	37(1)
C(2)	1249(3)	5968(2)	7648(2)	43(1)
C(3)	−485(3)	5384(2)	7267(2)	47(1)
C(4)	−1096(3)	4349(2)	6181(2)	41(1)
C(5)	99(3)	3893(2)	5508(2)	44(1)
C(6)	1826(3)	4477(2)	5878(2)	43(1)
C(7)	4886(3)	8568(2)	7950(2)	34(1)

Table 3. Continued

Atom	x/a	y/b	z/c	U_{eq}
C(8)	3779(3)	9253(2)	6664(2)	49(1)
C(9)	4702(3)	10468(2)	7372(2)	42(1)
C(10)	5761(3)	10652(2)	8398(2)	39(1)
C(11)	5323(4)	12623(2)	7795(3)	65(1)
C(12)	9642(3)	9713(2)	11990(2)	39(1)
C(13)	9810(3)	8844(2)	12460(2)	42(1)
C(14)	10914(3)	9184(3)	13510(2)	54(1)
C(15)	11906(3)	10401(3)	14102(2)	60(1)
C(16)	11796(3)	11278(2)	13653(2)	52(1)
C(17)	10668(3)	10944(2)	12607(2)	46(1)
C(18)	8400(3)	9374(2)	10887(2)	41(1)
C(19)	9230(3)	6832(2)	10946(2)	46(1)
C(20)	7886(3)	5605(2)	10391(3)	58(1)

Table 4. Bond lengths (Å) with esd's in parentheses

	1	2
S(1)−O(1)	1.439(2)	1.435(3)
S(1)−O(2)	1.430(2)	1.437(3)
S(1)−N(1)	1.634(2)	1.641(2)
S(1)−C(1)	1.746(2)	1.741(2)
O(3)−C(9)	1.362(4)	1.349(4)
O(3)−C(11)	1.393(4)	1.424(3)
N(1)−C(7)	1.388(4)	1.392(4)
N(2)−C(7)	1.326(4)	1.329(3)
N(2)−C(8)	1.329(4)	1.327(4)
N(3)−C(7)	1.330(4)	1.327(3)
N(3)−C(10)	1.342(4)	1.342(4)
N(4)−C(4)	1.394(4)	1.372(3)
C(1)−C(2)	1.386(4)	1.383(4)
C(1)−C(6)	1.389(4)	1.389(3)
C(2)−C(3)	1.381(5)	1.373(3)
C(3)−C(4)	1.390(4)	1.395(3)
C(4)−C(5)	1.390(4)	1.391(4)
C(5)−C(6)	1.381(5)	1.367(3)
C(8)−C(9)	1.375(4)	1.379(3)
C(9)−C(10)	1.367(5)	1.382(4)
Acetylsalicylic acid moiety in 2		
O(4)−C(18)		1.206(2)
O(5)−C(18)		1.316(4)
O(6)−C(13)		1.394(2)
O(6)−C(19)		1.361(3)
O(7)−C(19)		1.191(3)
C(12)−C(13)		1.392(4)
C(12)−C(17)		1.399(3)
C(12)−C(18)		1.484(3)
C(13)−C(14)		1.374(3)
C(14)−C(15)		1.376(4)
C(15)−C(16)		1.373(5)
C(16)−C(17)		1.382(3)
C(19)−C(20)		1.490(3)

UM00013073
NOVARTIS EXHIBIT 1017
Novartis v. Regents, IPR2023-01346
Page 1819 of 4460

Table 5. Bond angles (°) with esd's in parentheses

	1	2		1	2
N(1)−S(1)−C(1)	106.7(1)	106.3(1)	O(3)−C(9)−C(8)	117.1(3)	117.6(2)
O(2)−S(1)−C(1)	108.1(1)	108.6(1)	C(8)−C(9)−C(10)	116.8(3)	116.4(2)
O(2)−S(1)−N(1)	111.3(1)	110.8(2)	O(3)−C(9)−C(10)	126.2(3)	126.1(2)
O(1)−S(1)−C(1)	109.4(1)	110.5(1)	N(3)−C(10)−C(9)	121.6(3)	121.3(2)
O(1)−S(1)−N(1)	102.5(1)	103.4(1)			
O(1)−S(1)−O(2)	118.3(1)	116.7(1)	**Acetylsalicylic acid moiety in 2**		
C(9)−O(3)−C(11)	118.7(3)	117.1(2)			
S(1)−N(1)−C(7)	127.2(2)	124.1(2)	C(13)−O(6)−C(19)	117.1(2)	
C(7)−N(2)−C(8)	115.2(3)	115.7(2)	C(17)−C(12)−C(18)	120.1(2)	
C(7)−N(3)−C(10)	116.4(3)	117.0(2)	C(13)−C(12)−C(18)	122.1(2)	
S(1)−C(1)−C(6)	118.9(2)	116.8(2)	C(13)−C(12)−C(17)	117.8(2)	
S(1)−C(1)−C(2)	120.6(2)	123.1(2)	O(6)−C(13)−C(12)	121.3(2)	
C(2)−C(1)−C(6)	120.3(2)	119.9(2)	C(12)−C(13)−C(14)	121.4(3)	
C(1)−C(2)−C(3)	119.5(3)	119.6(2)	O(6)−C(13)−C(14)	117.1(2)	
C(2)−C(3)−C(4)	120.8(3)	121.1(2)	C(13)−C(14)−C(15)	119.7(3)	
N(4)−C(4)−C(3)	121.1(2)	121.2(2)	C(14)−C(15)−C(16)	120.4(2)	
C(3)−C(4)−C(5)	119.3(2)	118.4(2)	C(15)−C(16)−C(17)	120.0(2)	
N(4)−C(4)−C(5)	119.6(2)	120.5(2)	C(12)−C(17)−C(16)	120.6(2)	
C(4)−C(5)−C(6)	120.3(3)	120.7(2)	O(5)−C(18)−C(12)	113.6(2)	
C(1)−C(6)−C(5)	119.8(3)	120.2(2)	O(4)−C(18)−C(12)	123.8(2)	
N(2)−C(7)−N(3)	126.7(3)	126.3(3)	O(4)−C(18)−O(5)	122.6(2)	
N(1)−C(7)−N(3)	114.4(3)	115.2(2)	O(6)−C(19)−O(7)	122.3(2)	
N(1)−C(7)−N(2)	118.9(3)	118.5(2)	O(7)−C(19)−C(20)	126.9(3)	
N(2)−C(8)−C(9)	123.3(3)	123.4(2)	O(6)−C(19)−C(20)	110.9(2)	

Table 6. Hydrogen bond data with esd's in parentheses

D−H···A	D−H(Å)	D···A(Å)	H···A(Å)	D−H···A(°)
Compound 1				
N(1)−H(1)···N(3)^{i}	0.86(3)	2.911(4)	2.05(3)	176(3)
N(4)−H(41)···N(4)^{ii}	0.85(4)	3.269(4)	2.48(4)	156(3)
N(4)−H(42)···O(1)^{iii}	0.92(3)	3.061(3)	2.22(3)	152(3)
(i) = $-x, -y, 1-z$; (ii) = $1-x, -1/2+y, 1/2-z$; (iii) = $1-x, -y, 1-z$				
Compound 2				
O(5)−H(51)···N(3)	0.86(3)	2.730(3)	1.87(3)	178(3)
N(1)−H(1)···O(4)	0.92(2)	2.787(3)	1.87(2)	178(2)
N(4)−H(41)···O(2)^{i}	0.91(3)	3.290(4)	2.48(3)	149(2)
N(4)−H(42)···O(2)^{ii}	0.88(3)	3.281(4)	2.72(3)	123(2)
N(4)−H(42)···N(2)^{ii}	0.88(3)	3.230(3)	2.38(2)	162(3)
(i) = $-1+x, y, z$; (ii) = $-x, 1-y, 1-z$				

Polymorphism of SMD

The nomenclature used here to designate different polymorphs of SMD is that of Bettinetti *et al.*[5] The molecular conformation adopted in **1** (SMD Form II) is shown in Fig. 1. Bond lengths and bond angles for **1** (Tables 4 and 5) are generally in excellent agreement with those reported for SMD Forms I and III.[10] The overall conformation of **1** is described by the torsion angles τ_1 C(6)−C(1)−S(1)−N(1) 130.1(2)°, τ_2 C(1)−S(1)−N(1)−C(7) − 73.5(3)°, and τ_3 S(1)−N(1)−C(7)−N(2) 11.6(4)°, which differ signif-

UM00013074
NOVARTIS EXHIBIT 1017
Novartis v. Regents, IPR2023-01346
Page 1820 of 4460

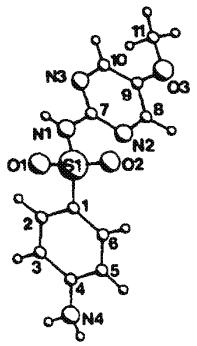


Fig. 1. Conformation of the SMD molecule in 1, (SMD Form II).

icantly from those observed in the other known polymorphs of SMD. This is due to the different hydrogen bonding arrangements occurring in Forms I, II, and III. In each polymorph, SMD forms dimeric hydrogen bonded motifs (non-centrosymmetric in Form I, centrosymmetric in Forms II and III). These motifs, shown schematically in Fig. 2, involve different combinations of N—H···O and N—H···N hydrogen bonds. It has long been recognized that the tendency for sulfonamides to form polymorphs is due to the variety of hydrogen bonding possibilities afforded by the presence of the sulfonyl (S=O), amide (N—H) and pyrimidinyl (N) functions.[18,19] The SMD dimer reported here for **1** contains two identical N—H···N hydrogen bonds and also occurs in three solvates of SMD.[20] The crystal packing in **1** is shown in Fig. 3. A distinctive feature for this polymorph is the formation of a hydrogen bond N(4)—H···N(4′) which links the amino groups of screw-related molecules. Repetition of this interaction by the 2_1-axis (parallel to the short unit cell *b*-axis) generates an infinite chain (···N—H···N—H···) in which each N atom is both hydrogen bond donor and acceptor. There is significant pyramidization at N(4) as a result of this interaction (Fig. 1).

We have confirmed by X-ray powder diffractometry that the raw material used in our experiments is SMD Form I. We have also noted that when this form is recrystallized from acetonitrile, the same form results. However, in attempting to prepare a complex between SMD and PAS in acetonitrile, no complexation occurred and the unreacted SMD consisted of Form II, whose structure is described above. These observations do not explain the failure of SMD and PAS to complex under the conditions described, but it can be inferred that the presence of PAS induces crystallization of SMD Form II rather than Form I. A possible explanation is that the growth of nuclei of Form I are inhibited by pref-

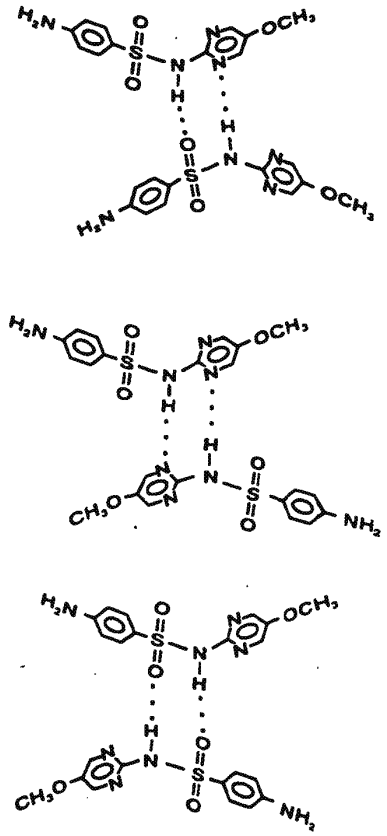


Fig. 2. Hydrogen bonded dimers in SMD polymorphs. Top: Form I[10]; Middle: Form II (present study), Bottom: Form III.[10]

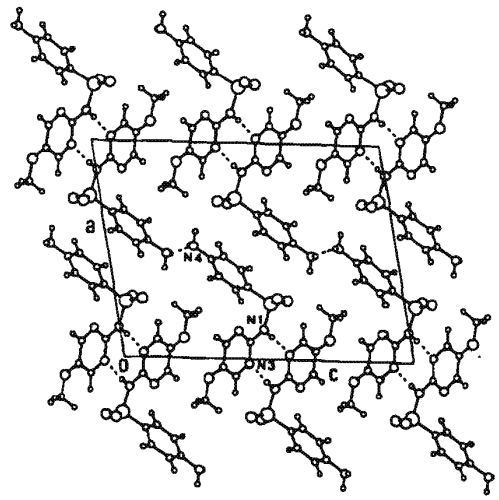


Fig. 3. [010] projection of the structure of **1** showing principal hydrogen bonds (dashed lines).

UM00013075
NOVARTIS EXHIBIT 1017
Novartis v. Regents, IPR2023-01346
Page 1821 of 4460

erential surface adsorption of PAS, thus favoring the crystallization of a different polymorph. Further experiments are necessary to confirm this hypothesis. Such a mechanism is likely, however, since Ebian *et al.*,[9] who studied the effect of additives on the interconversion of SMD crystal forms, have shown that molecules which are structurally related to SMD (e.g., p-aminobenzoic acid) retard the transformation of Form II to Form III in aqueous suspension by their ability to fit onto growing sites on nuclei of Form III. Attempts are being made to obtain a complex between SMD and PAS using different conditions from those described above.

Structure of the complex 2

The structure of complex **2** is shown in Fig. 4. The carboxylic acid group of the aspirin molecule engages in complementary hydrogen bonding with the SMD amide group and pyrimidinyl N atom. This mode of complexation is identical to that previously reported for complexes of the related drug sulfadimidine with substituted aromatic acids, and in particular, with acetylsalicylic acid.[2] There are no significant changes in bond lengths and bond angles in SMD upon complexation (Tables 4 and 5). The torsion angles for SMD (defined above) in the complex are τ_1 157.9(2)°, τ_2 − 78.4(2)°, and τ_3 28.9(3)°. Molecular parameters for the aspirin molecule are identical to those for aspirin in its 1 : 1 complex with sulfadimidine[2] and the carbonyl group of the −COOH function is again syn-planar to the acetoxy group. The intramolecular N−H···O and N···H−O hydrogen bonds in **2** are identical in length to those in the sulfadimidine complex but are more linear in **2**. Table 6 lists these and other hydrogen bond data for **2**.

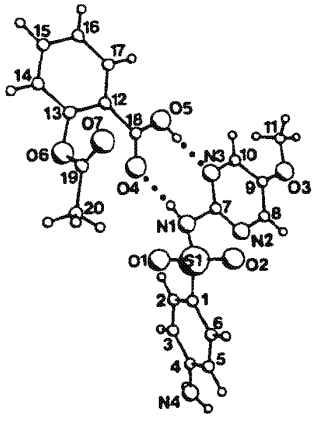


Fig. 4. Structure of the complex **2**.

Complexation by solid–solid reaction

Thus far, all of the 1 : 1 sulfonamide–aromatic carboxylic acid complexes reported in this series have been recovered from reactions occurring in solution, using either acetonitrile or ethanol as common solvent for the reacting components. However, we have recently obtained evidence for complex formation on co-grinding the solid reactants in a 1 : 1 molar ratio. These results will be published shortly.

Appendix

Hydrogen atom positions, anisotropic thermal parameters, torsion angles and structure factor tables for: **1** 5-methoxysulfadiazine (polymorphic Form II) and **2** 1 : 1 complex between 5-methoxysulfadiazine and acetylsalicylic acid.

Acknowledgments

Financial assistance from the FRD, Pretoria, and the University of Cape Town are gratefully acknowledged.

References

1. Caira, M.R. *J. Crystallogr. Spectr. Res.* **1991**, *21*, 641.
2. Caira, M.R. *J. Crystallogr. Spectr. Res.* **1992**, *22*, 193.
3. Caira, M.R.; Mohamed, R. *Acta Cryst.* **1993**, *B49*, 760.
4. Rambaud, J.; Alberola, S.; Grignon, H.; Masse, J.; Sabon, F. *Trav. Soc. Pharm. Montpellier* **1974**, *34*, 293.
5. Bettinetti, G.P.; Giordano, F.; La Manna, A.; Giuseppetti, G. *Il Farmaco-Ed.Pr.* **1974**, *29*, 493.
6. Yokoyama, T., Umeda, T., Kuroda, K., Watanabe, A. *Chem. Pharm. Bull.* **1978**, *26*, 1044.
7. Burger, A.; Ramberger, R.; Schulte, K. *Arch. Pharm. (Weinheim)* **1980**, *313*, 1020.
8. Moustafa, M.A.; Khalil, S.A.; Ebian, A.R.; Motawi, M.M. *J. Pharm. Pharmac.* **1972**, *24*, 921.
9. Ebian, A.R.; Moustafa, M.F.; Khalil, S.A.; Motawi, M.M. *J. Pharm. Pharmac.* **1973**, *25*, 13.
10. Giuseppetti, G.; Tadini, C.; Bettinetti, G.P.; Giordano, F. *Cryst. Struct. Comm.* **1977**, *6*, 263.
11. North, A.C.T.; Philips, D.C.; Scott Mathews, F. *Acta Crystallogr.* **1968**, *A24*, 351.
12. Frenz, B.A.; Associates Inc. (1982) *Structure Determination Package*, College Station: Texas.
13. Sheldrick, G.M. SHELXS86. In *Crystallographic Computing* 3,

UM00013076
NOVARTIS EXHIBIT 1017
Novartis v. Regents, IPR2023-01346
Page 1822 of 4460

Sheldrick, G.M., Kruger, C., and Goddard, R. Eds.; p. 175; Oxford University Press, 1985.
14. Sheldrick, G.M. SHELX. A system of computer programs for X-ray structure determination; England, University of Cambridge: 1976.
15. *International Tables for X-Ray Crystallography* Vol. IV, **1974**, Kynoch Press, Birmingham; (Present distributor: Reidel, D., Dordrecht).
16. Nardelli, M. *Comput. Chem.* **1983**, *7*, 95.
17. Motherwell, S. PLUTO. A program for plotting molecular and crystal structures; University of Cambridge: England, **1979**.
18. Byrn, S.R. *Solid-State Chemistry of Drugs*, Academic Press: London; 1982, p. 103.
19. Yang, S.S., Guillory, J.K. *J. Pharm. Sci.* **1972**, *61*, 26.
20. Caira, M.R.; Mohamed, R. *Supramolec. Chem.* **1993**, *2*, 201.

UM00013077
NOVARTIS EXHIBIT 1017
Novartis v. Regents, IPR2023-01346
Page 1823 of 4460